Order Number 8822811

The Aspen Grove landslide, Ephraim Canyon, central Utah

Baum, Rex Lee, Ph.D.

University of Cincinnati, 1988

U·M·I
300 N. Zeeb Rd.
Ann Arbor, MI 48106

THE ASPEN GROVE LANDSLIDE,

EPHRAIM CANYON, CENTRAL UTAH

A thesis submitted to the

Division of Graduate Education and Research
of the University of Cincinnati

in partial fulfillment of the
requirements for the degree of

DOCTOR OF PHILOSOPHY

in the Department of Geology

of the College of Arts and Sciences

1988

by

Rex Lee Baum

B.U.S., University of New Mexico, 1981

M.S., University of Cincinnati, 1983

UNIVERSITY OF CINCINNATI

January 22 19 88

I hereby recommend that the thesis prepared under my supervision by Rex Lee Baum

entitled The Aspen Grove Landslide, Ephriam Canyon, Central Utah

be accepted as fulfilling this part of the requirements for the degree of Doctor of Philosophy

Approved by:

David M. Johnson

Andrew Bodocsi

David B. Nash

THE ASPEN GROVE LANDSLIDE, EPHRAIM CANYON, CENTRAL UTAH

Rex Lee Baum

ABSTRACT

Scores of landslides and debris flows occurred in Ephraim Canyon, central Utah during May and June of 1983 as a snowpack containing 75 to 100 cm of water melted. About 80 percent of the landslides occurred in surficial deposits, and about 20 percent occurred in bedrock. Most of the debris flows occurred in thin residuum and colluvium in ground sloping 25 to 34°.

The Aspen Grove landslide occurred in older landslide debris that consists of medium to high-plasticity clays and silty or sandy clays. The debris is about 6 to 15(?) m thick. Persistent landslide structures, including feet, hollows and flank ridges, in the older landslide debris outline dimly preserved landslide masses.

The landslide was about 600 m long and 25 to 50 m wide in 1983. It enlarged to 1000 m long and 25 to 100 m wide in 1984 and 1985.

The head of the landslide was defined by crescent-shaped tension cracks. Segmented strike-slip faults formed the flanks of the landslide. The terminus was poorly defined. Cracks, domes, anticlines, flank ridges, scarps and other structures formed at the surface of the landslide as movement progressed.

The landslide mass is wide at the head and foot, and narrow at midlength. The upper 200 m is 50 to 60 m wide. The width of the next 250 m tapers from 50 to 25 m. Below is a steep section, 25 m wide and

100 m long. Farther from the head, 550 to 690 m, the landslide widens to 90 m. A large internal foot, 100 m wide, is between 690 and 750 m from the head. Two sets of en echelon cracks, 70 to 100 m apart, define the flanks of a 250-m-long extension of the landslide below the internal foot.

Annual displacements in 1984, 1985, and 1986 were 0.1 to 4.5 m in the upper part of the landslide, 4.5 to 8.8 m near midlength, and 0.1 to 2.5 m in the lower 400 m of the landslide.

Movement began each spring as the landslide became saturated with snow-meltwater. The landslide became active when the water table was 0.5 to 1.0 m below the ground surface. The landslide accelerated as the water table rose to the ground surface, and reached a maximum velocity of 20 cm per day. The landslide slowed as the water table fell during the summer, and stopped in July or August.

Slow movement of the landslide might be explained by a theory for resistance to sliding on uneven surfaces. The flanks and basal slip surface of the Aspen Grove landslide are uneven. Sliding resistance caused by the redistribution of pore water as the landslide deforms at asperities on the slip surface can control the velocity of the landslide. The velocity is proportional to the resistance to sliding offered by the deformation and to the permeability of the landslide. The low velocity of the landslide is consistent with the low permeability of the clayey landslide debris.

ACKNOWLEDGEMENTS

This dissertation is based on work I have done together with Robert W. Fleming and Arvid M. Johnson since I joined the U.S. Geological Survey in 1984. The advice, encouragement, and assistance of my supervisor, Robert Fleming, has been invaluable. He began study of the Aspen Grove Landslide in 1983, and suggested many of the topics addressed here.

Arvid Johnson, the chairman of my dissertation committee, has given valuable advice and assistance. He suggested that I try to determine what controls the velocity of slow landslides, suggested a way of approaching the problem, and shared insights along the way. He also shared his knowledge of the geometry and structure of the Aspen Grove landslide.

Plane-table maps by Fleming and Johnson are reproduced in many of the figures as an aid in describing features of the landslide. Observations and data they collected have been of great value.

Colleagues and technicians at the U.S. Geological Survey have provided services and assistance. Roger Nichols and his staff at the U.S.G.S. Engineering Laboratory in Golden, Colorado provided drilling, sampling and soil mechanics testing. Robert Fleming, Robert Schuster, Richard Madole, Alan Chleborad, Steve Obermier, and David Keefer reviewed parts of the manuscript. Roger Nichols and Lee Ann Chandler helped with field work.

Roger Johnson and Gary Jorgensen, both of Ephraim, Utah, shared information about the landslide and its surroundings. Ben Black, the district forest ranger at Ephraim, Utah shared observations and helped with some logistical problems. Chan Parry of Ephraim, Utah and Douglas Robins of Gunnison, Utah helped with measurements in 1983.

Members of my dissertation committee, professors David Nash and Andrew Bodocsi, reviewed the manuscript.

My wife, Carol, showed patience, love, encouragement, and support as I finished this work. I thank Joan Braaten and my stepmother, Barbara Baum, for typing the final manuscript.

TABLE OF CONTENTS

LIST OF FIGURES

FIGURE PAGE

FIGURE PAGE

FIGURE PAGE

FIGURE | PAGE

FIGURE PAGE

FIGURE PAGE

LIST OF TABLES

LIST OF PLATES

LIST OF SYMBOLS

CHAPTER IV

$\underline{A}$	area of the basal slip surface
$\underline{B}$	resisting force on the basal slip surface
$\underline{C}$	resisting force due to convergence
$\underline{C}^*$	part of resisting force due to convergence not included in passive resistance
$\underline{D}$	driving force
$\underline{F}$	resisting force due to friction at flanks of the landslide
$\underline{L}$	length of the flank
$\underline{P}$	resistance due to passive failure
$\underline{w}$	width of the landslide
$\underline{t}$	thickness of the landslide
γ_b	buoyant unit weight of soil
γ_t	total unit weight of soil
ι	slope angle of the slip surface
σ_n	effective normal stress on the slip surface
τ	shear strength

CHAPTER V

$\underline{A}$	cross-sectional area of landslide in plane normal to the axis
$\underline{A}_{\underline{f}}$	final area of a strain gauge
$\underline{A}_{\underline{o}}$	initial area of a strain gauge
$\underline{B}$	arbitrary constant
$\underline{c}$	a constant
$\underline{L}_{\underline{f}}$	final length of a line segment

$\underline{L}_{\underline{o}}$	initial length of a line segment
$\underline{r}$	a radius measured from the apex of a converging channel
$\underline{S}$	stretch
$\underline{S}_1, \underline{S}_2, \underline{S}_3$	principal stretches
$\underline{S}_{\underline{o}}$	an omnidirectional stretch causing pure area change
$\underline{S}_{\underline{x}}$	stretch parallel to $\underline{x}$
$\underline{S}_{\underline{y}}$	stretch parallel to $\underline{y}$
$\underline{v}$	velocity
$\underline{v}_{\underline{r}}$	velocity parallel to a radius in a converging channel
$\underline{x}, \underline{y}$	cartesian coordinates, $\underline{x}$ parallel to displacement of the landslide
β	counterclockwise angle measured from $\underline{x}$ to $\underline{S}_1$
γ_{max}	maximum finite sheer strain
θ	angle between the axis of a converging channel and a radial line from the apex of the channel
θ_d	counterclockwise angle between direction of displacement and the flank of landslide
ρ	density of landslide debris
ψ	angle between algebraically greatest principal stress and a radial slip line in a converging channel
ψ_y	angle of simple shear

CHAPTER VI

$\underline{a}$, $\underline{b}$, $\underline{c}$	arbitrary constants
$\underline{A}$, $\underline{B}$, $\underline{C}$, $\underline{D}$	corners of a quadrilateral
$\underline{d}$	area strain
$\underline{L}$	length of a line segment
$\underline{p}$	plunge angle of the displacement vector

$\underline{S}$	stretch
$\underline{S}_1, \underline{S}_2$	major and minor principal stretches
$\underline{U}$	magnitude of the displacement vector
$\underline{u}_1$	horizontal displacement component parallel to the reference line and the $\underline{x}$ axis
$\underline{u}_2$	horizontal displacement component perpendicular to $\underline{u}_1$
$\underline{u}_3$	vertical displacement component
$\underline{w}$	error of closure, an angle
$\underline{x}$, $\underline{y}$, $\underline{z}$	cartesian coordinates, $\underline{z}$ is vertical
α	angle between $\underline{S}_1$ and a reference direction, ζ, in the deformed state
β_i	angle between $\underline{S}_1$ and a line in the deformed state
γ	finite shear strain
δ	dip angle of a plane
ζ	direction of a reference line (usually a diagonal of the quadrilateral) used in computing the direction of the major principal stretch.
$\theta_{\underline{i}}$	angles between a side and a diagonal of the quadrilateral
λ	angle between the reference line and the horizontal component of displacement
$\xi_{\underline{i}}$	an arbitrary direction in the $\underline{x}$-$\underline{y}$ plane (usually the trend of a side or a diagonal of a quadrilateral)
$\phi_{\underline{i}}$	horizontal projections of the angles $\theta_{\underline{i}}$
$\omega_{\underline{i}}$	angle between $\xi_{\underline{i}}$ and the positive $\underline{x}$ direction
$\omega_{\underline{max}}$	dip direction of a plane tangent to the ground surface
ϵ	linear strain, $\underline{S}$-1

Primes denote positions or values in the deformed state

CHAPTER VII

$\underline{A}$	amplitude of sine wave
$\underline{B}$	Skempton's pore-pressure coefficient
$\underline{c}$	diffusion coefficient
$\underline{c}_1,\ldots,\underline{c}_5$	constants
$\underline{C}_\alpha$	a constant
$\underline{C}_\beta$	a constant
$\underline{D}_{\underline{xx}}$, etc.	deformation rate components
$\underline{E}_{\underline{xx}}$, etc.	strain components
$\underline{G}$	elastic shear modulus
$\underline{h}$	height of the water table
$\underline{k}$	plastic yield strength
$\underline{k}_{\underline{r}}$	shear strength of the slip surface
$\underline{K}$	hydraulic conductivity
$\underline{K}$*	hydraulic conductivity of Rice and Cleary
ℓ	wave number ($2\pi/L$)
$\underline{L}$	wavelength
$\underline{M}$	a stress variable
$\underline{n}$	porosity
$\underline{n}$, $\underline{s}$	coordinates normal and tangential to a surface
$\underline{p}$	pressure (negative of mean stress)
$\underline{P}$	pore pressure
$\underline{q}_{\underline{x}}$, $\underline{q}_{\underline{z}}$	specific discharge components
$\underline{t}$	time
$\underline{T}$	thickness of a landslide
$\underline{T}_{\underline{xx}}$, etc.	stress components

$\underline{u}_{\underline{x}}$, $\underline{u}_{\underline{z}}$	displacement components
$\underline{v}_{\underline{x}}$, $\underline{v}_{\underline{z}}$	velocity components
$\underline{x}$, $\underline{z}$	Cartesian coordinates
$\underline{z}_{\underline{o}}$	the wavy slip surface
α,β	characteristics or slip lines
β	compressibility of water
γ_t	unit weight of saturated soil
γ_w	unit weight of water
η	viscosity of glacier ice
Θ	time, in quasi-static coordinate system
θ	an angle
ι	slope angle
κ	intrinsic permeability
μ	viscosity of water
ν	Poisson's ratio (drained)
$\nu_{\underline{u}}$	Poisson's ratio (undrained)
ξ	$x - \bar{v}_x t$, a coordinate parallel to $\underline{x}$
ρ	density
τ	drag
ϕ	Airy's stress function
ϕ'	friction angle of a soil in effective stress
Φ	counterclockwise angle from $\underline{x}$ to an α-line
∇	the divergence operator, $(\partial/\partial\underline{x}) + (\partial/\partial\underline{z})$
∇^2	the Laplacian operator, $\partial^2/\partial\underline{x}^2 + \partial^2/\partial\underline{z}^2$
∇^4	the biharmonic operator, $\partial^4/\partial\underline{x}^4 + 2\partial^4/\partial\underline{x}^2\partial\underline{z}^2 + \partial^4/\partial\underline{z}$

CHAPTER I

INTRODUCTION

Landslides, debris flows, and floods ravaged parts of central Utah during 1983 and 1984 (Anderson and others, 1984). The Thistle landslide (Fig. 1.1) formed a dam in 1983, the lake behind which flooded Thistle, Utah, and threatened communities downstream. Construction of outlet works and relocation of a highway at Thistle were costly (Duncan and others, 1986, p. 1). A huge debris flow in Twelvemile Canyon (Fig. 1.1) choked Twelvemile Creek. The Twin Lake landslide, also in Twelvemile Canyon, threatened to dam Twelvemile Creek (Robert W. Fleming, oral commun., 1984). Debris flows destroyed homes and killed two people at Clear Creek, Utah (Robert L. Schuster, oral commun., 1984). Landslides and debris flows in canyons on the west side of the Wasatch Plateau (Fig. 1.1) destroyed facilities of the U.S. Forest Service and damaged roads, aqueducts, and power lines serving towns in the Sanpete Valley (Ben Black, District Ranger, USFS, Ephraim, Utah, oral commun., 1984).

Among landslides in central Utah, the Aspen Grove landslide, near Ephraim, Utah (Fig. 1.1), was outstanding because it had straight boundaries and minor internal deformation (Robert W. Fleming, oral commun., 1987).

Gary Jorgensen (USFS) and Roger Johnson (USAF, ret.), both of Ephraim, Utah, discovered the Aspen Grove landslide on May 31, 1983. At

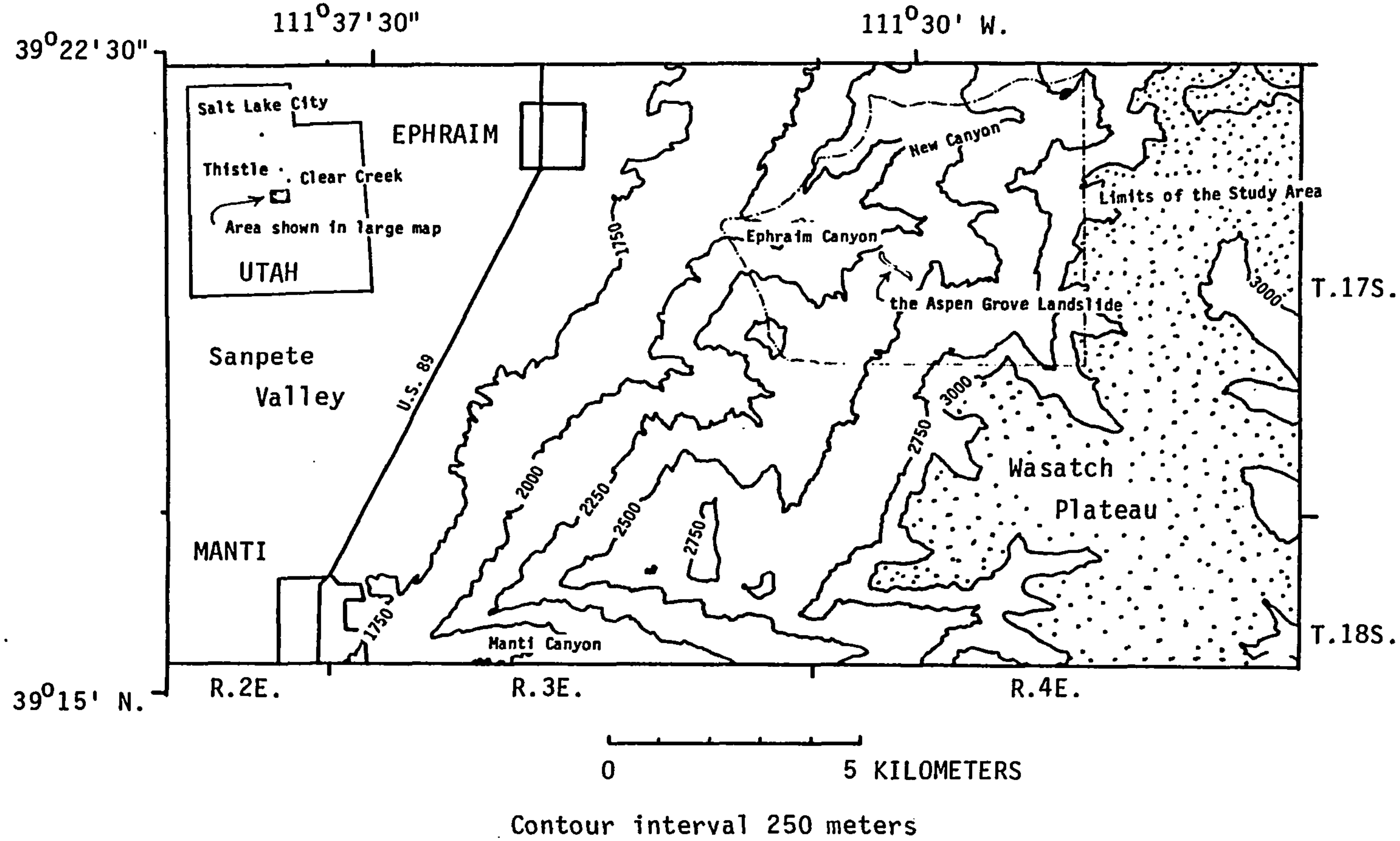

FIGURE 1.1 Map showing location of the study area. The stippled area represents the summit of the Wasatch Plateau. Contour interval is 250 m.

that time the landslide was about 600 m long, 25 to 50 m wide and 6 m thick.

Robert W. Fleming and Arvid M. Johnson visited the Aspen Grove landslide on June 8, 1983. Fleming and David J. Varnes established measurement stations on the landslide during mid-June 1983, in order to determine displacement along boundaries of the landslide. Chad Parry of Ephraim, Utah, and Douglas Robins of Gunnison, Utah made measurements during June and July 1983. Fleming and Johnson returned in August 1984 to map parts of the landslide.

I joined the project in March 1984. I helped with measurements and began to study the hydrology of the landslide and the geologic setting of landslides in Ephraim Canyon, Utah. Incidentally, upon the suggestion of Arvid Johnson, I began investigating why landslides in clayey soils, such as the Aspen Grove landslide, move slowly, and how roughness of the failure surfaces of landslides might increase resistance to sliding.

Fleming, Johnson, and I studied the Aspen Grove landslide for several weeks each spring and summer during 1984, 1985 and 1986. Fleming and Johnson made a structural-topographic map during August 1984, and remapped the upper part of the landslide during 1985 and 1986. I made a geologic map of part of Ephraim Canyon, a structural map of a landslide complex at Majors Flat in Ephraim Canyon, and a surficial geologic map of the area of the Aspen Grove landslide during that period.

A crew from the USGS Engineering Laboratory in Golden, Colorado (Roger Nichols, supervisor) drilled several holes in the landslide during 1984 and 1985 to collect samples and install instruments. Robert Fleming installed recording extensiometers and numerous lines and quadrilaterals of survey stakes to monitor movement of the landslide.

This dissertation describes the results of our collaborative study of the Aspen Grove landslide. Chapters II, III and VII are largely my work alone. Chapter II describes landslides and debris flows in Ephraim Canyon in the context of the geology of the canyon. Chapter III describes weather-related events that preceded the landslides and debris flows. Chapters IV, V and VI are based partly on my work on the Aspen Grove landslide. Chapter IV describes the geology, geometry, structure, evolution, hydrology and mechanics, and Chapter V describes the kinematics of the Aspen Grove landslide. Chapter VI describes a new method for measuring displacement and strain that was originated by David J. Varnes and Robert W. Fleming. The final Chapter, VII, describes preliminary analyses for the effect of roughness of slip surfaces on the velocity of landslides, and resistance to sliding.

CHAPTER II

LANDSLIDING IN EPHRAIM CANYON, CENTRAL UTAH

Introduction

This chapter focuses on landslides, rockslides, and debris flows that occurred in Ephraim Canyon, on the west side of the Wasatch Plateau, central Utah, during 1983-1986 (Fig. 1.1). The landslides and debris flows are studied in the context of the geology of Ephraim Canyon, which is similar to the geology of other canyons on the west side of the Wasatch Plateau. This chapter also contains background information relevant to detailed investigations of the Aspen Grove landslide in Ephraim Canyon.

Relations between landslides and debris flows that occurred from 1983 to 1986 and the bedrock and surficial geology of Ephraim Canyon are shown in Plate 1. The outlines of landslides and debris flows that had been active in 1983 and 1984 were transferred from air photographs taken on June 16, 1984, directly to the base map, by means of a stereo plotter. Contacts between other map units (including landslides that occurred in 1985 and 1986) were mapped in the field. Units older than the landslides and debris flows of 1983 were mapped in less detail and less accurately than the landslides of 1983 and 1984, because the contacts between older deposits are generally poorly expressed and faults in the bedrock are exposed well at only a few locations.

Ephraim Canyon is on the west side of the Wasatch Plateau of central Utah; the mouth of the canyon is at about 1,850 m elevation and is about 3 km southeast of the town of Ephraim (Fig. 1.1). The canyon is about 5 km long and heads in the Wasatch Plateau, which is a slightly dissected, nearly horizontal surface at about 3,050 to 3,200 m altitude.

Much of the geomorphic expression of Ephraim Canyon can be related to geologic structure. Slopes that are subparallel to the dip direction generally are northwest- and west-facing slopes, and tend to be flatter than slopes that cut across bedding. Slopes that cut across bedding generally are east- and south-facing. Hogbacks (Fig. 1.1) that stand at either side of the canyon mouth are held up by westward-dipping beds of the Wasatch monocline (Spieker, 1949). The steep, east-facing sides of the hobgbacks are fault-line scarps. North-trending fault-line scarps form steps on the broad, blunt tops of canyon walls. An escarpment, 300 m high and west facing, along the west edge of the plateau, is probably a fault-line scarp.

Geology of Ephraim Canyon

Bedrock Geology

The bedrock exposed in Ephraim Canyon consists of bedded sedimentary rocks that are divided into three formations (Spieker, 1946; Bonar, 1948; Witkind and others, 1982). Lowest stratigraphically is the Upper Cretaceous and Paleocene North Horn Formation, an orange to buff unit (Fig. 2.1) that consists dominantly of cemented sandstones interbedded with variegated shales. Conformably overlying the North

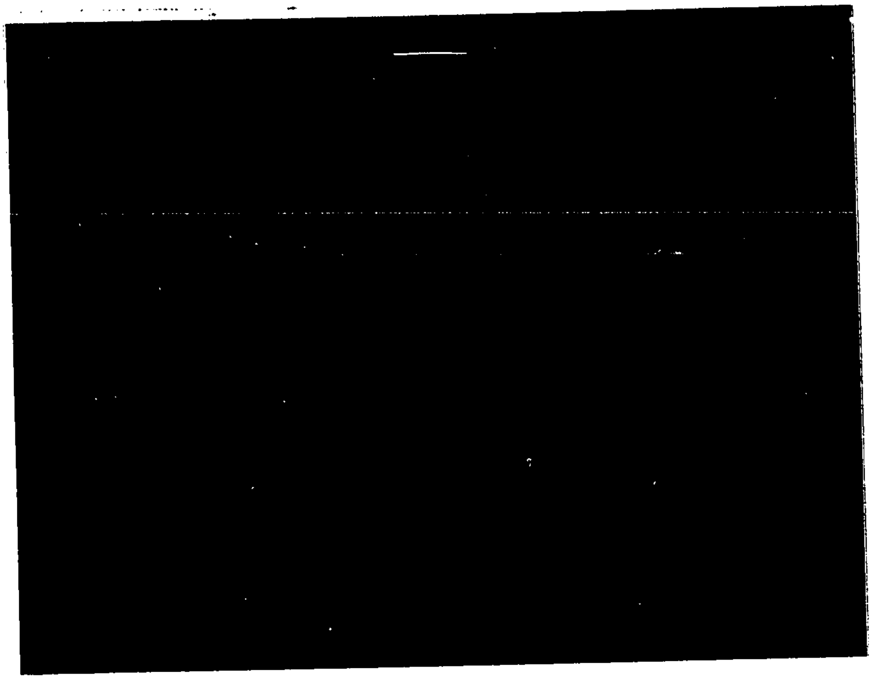

FIGURE 2.1. Photograph showing exposures of the North Horn Formation (TKn) and the Flagstaff Limestone (Tf) on the north side of Ephraim Canyon (looking north from Bald Mountain, fig. 1). A rockslide (Ql) on the north side of Ephraim Creek is shown near the right-hand edge of the photograph.

Horn Formation is the Paleocene and Eocene Flagstaff Limestone, a whiteto buff unit, about 275 m thick (Fig. 2.1) that consists of limestone interbedded with gray, green, and black shales (LaRocque, 1960; Stanley and Collinson, 1979). The Eocene Colton Formation overlies and intertongues with the Flagstaff Limestone (Zawiskie and others, 1982). Beds of the Colton Formation that are exposed in Ephraim Canyon consist of lenticular sandstone, limestone, and reddish-brown shale.

Steep, north-trending faults (Plate 1) break the rocks of the central part of the canyon into a series of elongate blocks. The blocks have been rotated so that bedding dips toward the west (Bonar, 1948; Spieker, 1949). The dips increase westward from horizontal at the rim of the Wasatch Plateau (at the eastern edge of the area) to about 25 to 40° in the hogbacks that flank the mouth of the canyon (Plate 1). Stratigraphic offsets on several faults range between 100 m and 360 m (Plate 1). Displacement across some of the faults and rotation of some of the blocks are large enough that locally the North Horn Formation is topographically higher than the Flagstaff Limestone.

Surficial Geology

The surficial deposits constitute a veneer that covers the faulted, tilted, sedimentary bedrock of the canyon. The distribution of bedrock and surficial deposits at the ground surface is shown on the geologic map (Plate 1). The mapped area extends from the mouth of the canyon eastward to the rim of the Wasatch Plateau and a few kilometers north and south from the Aspen Grove landslide.

In addition to deposits of landslides and debris flows that occurred between 1983 and 1986, four kinds of surficial deposits are recognized in the area: (1) alluvium, (2) older debris-flow deposits, (3) older landslide deposits, and (4) undifferentiated surficial materials that include colluvium, slope wash, and locally, alluvium, bedrock, and residuum. In the text, these undifferentiated materials will be referred to as slope deposits and they correspond to the map unit (Qc, plate 1) called colluvium, residuum, and slope wash undifferentiated.

Alluvium is limited to channels of Ephraim Creek and its tributaries, Maple Creek, Cottonwood Creek, and New Creek. It consists of locally derived gravel, laminated sands or silts, and clay. Older alluvium (that is, terrace deposits) occurs along the banks of Ephraim Creek and New Creek.

Deposits of debris flows were recognized on the basis of their morphology and recognizable deposits are of limited extent. They consist of angular cobbles and boulders of limestone and sandstone in a poorly sorted matrix of sandy clay. The debris-flow deposits are probably less than 2 m thick. Thin soil is developed in the tops of the debris-flow deposits.

Older landslide deposits consist of unsorted, unstratified mixtures of limestone and sandstone boulders, cobbles, and pebbles in a sandy clay matrix. Older landslide deposits might be as much as 40 m thick. Topsoils up to several decimeters thick have developed on most older landslide deposits.

Slope deposits consist of unsorted, unstratified, or poorly stratified mixtures of limestone or sandstone boulders, cobbles, pebbles, sand, silt, and clay. Most slope deposits are probably less than 5 m thick, but locally might be as much as 25 m thick. Slope deposits typically have topsoils that are several decimeters thick and dark brown.

Bedrock crops out on steep slopes and in cliffs. Bedrock in the area is exposed primarily in south-facing slopes of New Canyon and Cottonwood Creek, in cliffs along the edge of the plateau at White Ledge and the Great Basin Experiment Station, in the area between Maple Creek and Cottonwood Creek, and in the rims of the hogbacks (Plate 1, Fig. 2.1).

The remainder of the areas mapped as bedrock formations are covered by a thin layer of residual material that has formed in place as a result of mechanical and chemical weathering. The residual material is not considered to be mass-wasting material. Residual material weathered from the North Horn Formation consists of clasts of yellow or gray sandstone in a matrix of orange or tan sandy clay. Residual material derived from the Flagstaff Limestone is characterized by clasts of white or light gray limestone in a matrix of white, gray, or brown clay. White limy sandstone, silicified limestone, and chert are locally abundant in residual material of the Flagstaff Limestone. The clasts are boulder, cobble, and pebble sized.

The map shows three classes of pre-1983 mass-wasting deposits: older landslide deposits, older debris-flow deposits, and slope deposits (colluvium, residuum, and slope wash, undifferentiated). In parts of the study area weathered material has moved downslope by sliding, flowing, creeping, toppling, rolling, or other processes to form mass-wasting deposits. Deposits formed by sliding or flowing have distinctive surface morphologies that can be used to recognize individual landslide or debris-flow deposits. However, deposits formed by other processes including slope wash and possibly some deposits formed by sliding or flowing could not be distinguished on the basis of their surface morphologies; thus, they were lumped together as slope deposits.

Slope Deposits--Slope deposits, which include colluvium, residuum, and sheet-wash deposits, are particularly common on north- and west-facing slopes that are subparallel to dip of the bedrock (Plate 1). Slope deposits are on the south side of New Canyon, on Dusterburgs Hill, and in the area between Maple Creek and Cottonwood Creek. Steep slopes along the west edge of the Wasatch Plateau are covered by deposits of colluvium 0.5 to 1.0 m thick. The surfaces of slope deposits typically slope smoothly or undulate gently; however, hummocks, ridges or closed depressions occur in isolated locations on the deposits. Slope deposits are perhaps as thick as 15 m and occur on slopes as steep as 27°.

Slope deposits are derived from bedrock in Ephraim Canyon. The lithology of clasts in the deposits match the lithology of the underlying bedrock at some places; however, the lithology of the clasts is exotic elsewhere. Slope deposits on the northwest side of Dusterburgs Hill (S1/2 sec. 7, T. 17 S., R. 4 E., Plate 1) contain only limestone derived from the Flagstaff Limestone that underlies the deposits. Slope deposits along the dirt road between Cottonwood Creek and Maple Creek (SE1/4 sec. 18 and NE1/4 sec. 19, T. 17 S., R. 4 E., Plate 1) contain 0.5 to 1.5 m boulders of cross-bedded, well-indurated sandstone derived from the North Horn Formation. The Flagstaff Limestone lies under these deposits also (Plate 1). The source of the sandstone is apparently beds of the North Horn Formation east of a fault that passes through sec. 17 and crops out near the east boundary of sec. 19 (Plate 1).

Older Landslide Deposits.--Older landslide deposits cover about one quarter of the study area. Several deposits are on north- and west-facing slopes in New Canyon, and a large deposit occupies the head of New Canyon. Other large deposits are between White Ledge and the Great Basin Experiment Station, and in the area south of Maple Creek (Plate 1). Individual deposits range in area from about 1 to 240 square hectometers (hm^2), in thickness from a few meters to perhaps 50 m. Their surfaces generally slope about 7 to 13°; however, the surfaces of a few slope as much as 26° and local slopes are as great as 33°. Hummocks, closed depressions, benches, arcuate troughs, lateral ridges, and lobate toes adorn the surfaces of the deposits. Some deposits are elongate, others are wide at the head and narrow gradually toward the toe, and still others are roughly equidimensional.

Several of the larger landslides involved material from the North Horn Formation, and occur at the base of steep cliffs along the rim of the plateau. As an example of an older landslide deposit of this type, consider the deposit mapped between the Great Basin Experiment Station and Cottonwood Creek (sections 16, 17, 20, and 21, T. 17 S., R. 4 E.). The southern end of the deposit represents the head of the old landslide; a steep cliff exposing horizontally layered bedrock towers above the southern end of the deposit. The outline of the head is roughly arcuate. A curving, transverse ridge about 300 m north of the base of the cliff is a distinctive topographic feature at the surface of the deposit. (Similar ridges have been observed at the heads of other large landslides in the area.) Downslope from the head area, the surface of the deposit slopes about 8° toward the north-northwest, and the deposit narrows gradually. Closed depressions, which were expressed on the June 1984 airphotos as ponds, are common between the head and Cottonwood Creek. At Cottonwood Creek, the deposit turns to the west and narrows. Along both sides of Cottonwood Creek, remnants of the deposit form a terrace that slopes downstream and can be traced to the vicinity of Cottonwood Spring (NE1/4 sec. 18, T. 17 S., R. 4 E.).

Older Debris-Flow Deposits.--Individual debris-flow deposits are difficult to recognise in the area. However, on a south-facing slope in New Canyon (SW1/4 sec. 7, T. 17 S., R. 4 E.) and on a north-facing slope near Bluebell Flat (sec. 21, T. 17 S., R. 4 E.) it is possible to distinguish single older debris-flow deposits. The New Canyon deposit covers about 2.5 hm^2, and the Bluebell Flat deposit covers about 4.0 hm^2. The deposits are elongate, have bulbous terminations, and lie in and adjacent to channels that slope about 17 to 26°. The surfaces of the deposits are littered with angular rock fragments and are partly covered with vegetation.

Debris Flows of 1983-1986

In May 1983, surficial materials on slopes in Ephraim Canyon became water saturated, and in many places failed and moved downslope either as landslides or as debris flows. Bedrock also became saturated in places, failed and moved downslope as rockslides. In general, the debris flows and landslides of 1983 coincided with rapid melting of the snowpack. In the Wasatch Plateau and other parts of Utah, debris flows were observed to mobilize from parts of large landslides and from thin colluvium on steep hillslopes. The large landslides typically began to move before the snowpack was gone and movement fractured the snow into intricate patterns. Mobilization of colluvium seemed to coincide with most rapid melting. After the snow line receded above any given elevation point, no new debris flows occurred below that elevation. A few debris flows occurred during intense thunderstorms in 1984 and 1985.

Landslide movement that began in early spring of 1983 typically ended during July or August 1983, and apparently did not begin again until the spring of 1984. This pattern of movement has been documented for other reactivations of large landslides in similar materials (Fleming and others, in press).

Debris flows were active in the study area during the springs of 1983, 1984, 1985, and 1986. Many of the debris flows occurred on steep (25 to 34°), colluvium-covered slopes in the eastern part of the area. The remainder mobilized from landslide deposits distributed throughout the area or from loose, weathered bedrock exposed on the north walls of New Canyon and the canyon occupied by Cottonwood Creek. Debris flows occurred on slopes ranging from 13 to 34°. Altogether, the debris flows covered about 26 hm^2, or about 0.8 percent of the study area. The debris-flow scars and deposits appear as long, narrow strips and irregular blobs on the map. Most are between 10 and 50 m wide and 60 to 600 m long. Typically, the scars are less than 1 m deep and the deposits are less than 3 m thick. The long, narrow debris flows were channelized; they flowed in preexisting swales or gullies. At several locations, neighboring debris flows coalesced to produce the irregular shapes shown on the map. Some of the debris flows had sheetlike geometries and were unchannelized. Such debris flows occurred on smooth, ungullied slopes.

Cobbles, large boulders, broken trees, and light brown mud, a few centimeters to a few decimeters thick, covered the surfaces of the debris-flow deposits. The smooth, light brown mud contrasted with the dark brown, vegetated topsoil on adjacent ground. The boulders and broken trees were arranged in heaps so that parts of the deposits had jagged surface topography.

The debris flow that occurred in 1986 at Cottonwood Spring (Fig. 2.2) was notably different from debris flows that occurred at other localities in Ephraim Canyon during 1983. The 1986 debris flow began as a first-time failure in bedrock on a dip slope. We observed a few widely spaced cracks were observed on the upper part of the dip slope in 1984 or 1985, but a slope failure was unexpected because many of the landslides that had been active in 1983 or 1984 had stopped by 1985. However, movement started on about April 15, 1986, and continued for several days. Material slid down the dip slope, gradually being

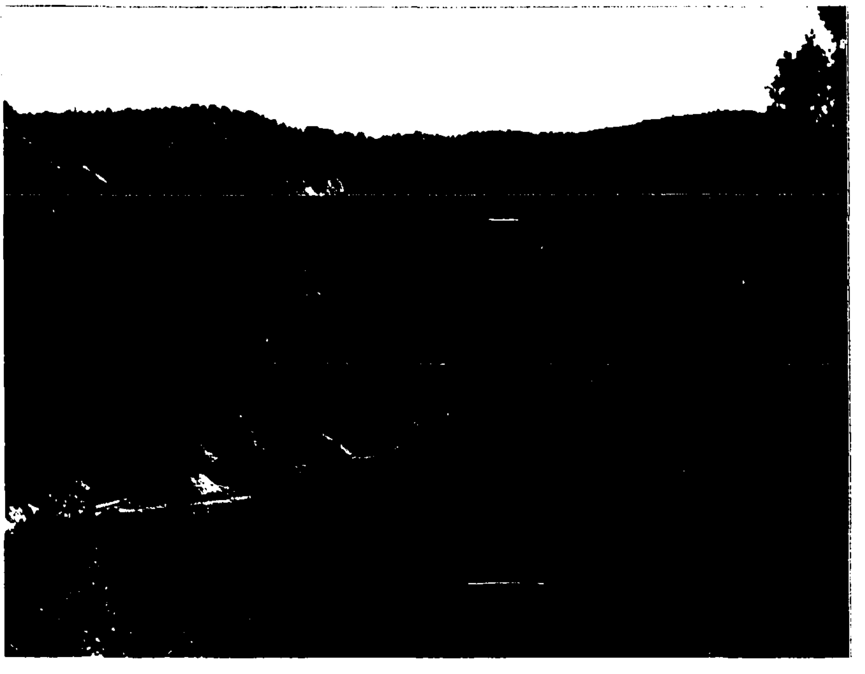

FIGURE 2.2. Photograph showing the Cottonwood Spring debris flow of 1986. (Photograph by Arvid Johnson).

remolded until it began flowing, and then cascaded over steep slopes toward Ephraim Creek. The flow partially dammed and diverted the creek, and covered an intake structure for a power plant at the mouth of Ephraim Canyon. In the bottom of the canyon, the flow moved a few meters per hour (Roger Johnson, oral commun., 1986).

The Cottonwood Spring debris flow differed from typical debris flows in Ephraim Canyon in that it developed slowly for one or two years before it failed abruptly in 1986. It moved more slowly than other debris flows, was active for several days, and was mobilized from a layer of weathered bedrock several meters thick rather than colluvium.

Landslides of 1983-1986

Many spectacular landslides occurred in 1983 and 1984 and movement in some of the landslides was renewed during 1984, 1985, and 1986. The landslides are distributed throughout the area and their deposits covered about 166 hm^2, or about 4.7 percent of the study area. About 94 hm^2 (57 percent) were reactivations of old landslide debris, 39 hm^2 occurred in slope deposits, and 33 hm^2 (20 percent) occurred in bedrock.

Shapes, sizes, and slopes of the landslides varied widely. Areas ranged from about 0.1 to 28 hm^2, and thicknesses ranged up to perhaps 25 m. The average surface slopes of individual landslides ranged from about 11 to 30°. Some landslides, as the Aspen Grove landslide, were long and narrow. Others, such as those along the banks of Cottonwood Creek, were short and wide. Many others were equidimensional, and a few had irregular shapes.

In general, the heads were flat or gently sloping, the bodies of the landslides sloped more or less uniformly, and the toes were relatively steep. In order to illustrate the settings and general features of the landslides, we describe representative examples.

The Rockslide at Cottonwood Spring

Many distinguishing features of bedrock landslides (that is, rockslides) are illustrated by a landslide in the fault zone upslope from Cottonwood Spring, SE1/4 sec. 7, T. 17 S., R. 4 E. (Fig. 2.3). The rockslide is about 170 m long, its head is about 45 m wide, but the landslide tapers gradually so that the toe is about 5 m wide. The thickness ranges between 1 and perhaps 8 m and the average is perhaps 4 m. The volume of the landslide is approximately 1.8 x 10^4 m^3. The slope of the ground surface where the landslide occurred was about 30^o.

The head scarp exposes fractured limestone bedrock of the Cove Mountain Member of the Flagstaff Limestone. The head of the slide slopes a few degrees toward the south. It is covered with porous, white limestone blocks. The body and toe of the landslide consist of an unsorted mixture of silty clay with angular fragments and blocks of limestone. Dead trees lying in various positions dot the surface of the slide (Fig. 2.3).

Geometry of the landslide suggests that failure originated in the head. Because the head of the slide is the largest displaced mass, I speculate that water moved downward along cracks in the vicinity of the head and caused the the jointed rock to fail first. Subsequently, loose

FIGURE 2.3. Photograph showing a rockslide near Cottonwood Spring. Faulted, thickly bedded limestone is exposed in the head scarp. Arrows indicate locations of faults.

material slid down the surface of the slope to form the thinner and narrower deposits near the toe.

The rockslide at Cottonwood Spring is typical of the rockslides on the north wall of New Canyon and the north wall of the canyon occupied by Cottonwood Creek (Plate 1). Thickly bedded, fractured, faulted limestone is exposed in the head scarps. The heads are wide relative to the bodies of the landslides. The distal ends or toes of some rockslides had a high proportion of fine-grained material and a lobate morphology.

Nearly all rockslides on the north walls of New Canyon and the canyon occupied by Cottonwood Creek occurred in fault zones (plate 1). The head scarps of the rockslides expose beds of thick, jointed and faulted limestone or sandstone. The faults and joints presumably weakened the rock and facilitated the movement of ground water. Wet spots were observed in fault gouge exposed in the head scarps of several of the bedrock landslides. A spring was observed on the right side of a large bedrock landslide located in New Canyon (SW1/4 sec. 5). Cottonwood Spring, which has been developed for water supply, flows from the same fault zone that is exposed in the head of the rockslide just described.

The Aspen Grove Landslide

The Aspen Grove landslide occurred in older landslide debris on a northwest-facing slope between Cottonwood Creek and Maple Creek (SW1/4 sec. 17 and SE1/4 sec. 18, plate 1). The landslide is about 1 km long, and its width ranges between about 30 and 100 m. Its thickness is 6 m near the proximal end and probably ranges from about 4 to 15 m with an average thickness of about 6 m. The volume of the landslide is about 3.6×10^5 m^3. The average slope of the landslide surface is about 12°.

The landslide surface is covered with trees, grasses, and shrubs, most of which have survived several meters of displacement. Gaping cracks define the head, well-developed shear zones mark the lateral boundaries, and small toes separated by apparently undeformed ground define the presumed distal boundary of the landslide. Cracks, thrusts, and other deformational features occurred on the surface of the landslide. Longitudinal ridges at the lateral boundaries and a large lobate toe about 300 m upslope from the present distal boundary of the landslide are remnants from a previous episode of movement. Much of the landslide is slightly higher than the neighboring ground.

The landslide debris contains large sandstone boulders derived from the North Horn Formation. Similar boulders are present on the slopes adjacent to the landslide, but outcrops near the landslide are Flagstaff Limestone. The North Horn Formation crops out a few hundred meters upslope from the head of the Aspen Grove landslide, thus the debris has moved hundreds of meters downslope from its source.

The landslide became active in May 1983 and moved a few millimeters to a few centimeters per day until it stopped moving in mid-July 1983. Movement started again in April or May 1984 and continued until August 1984. Similar patterns of movement were repeated in 1985 and 1986. Although some parts of the landslide have been broken or remolded, the material has flowed very little. During 1984 and 1985 the landslide damaged the road (Utah highway 29) in two places, making it impassable to vehicles until grading equipment filled holes and smoothed bumps where the landslide crossed the road.

Meltwater infiltrating from the surface was probably the main source of water responsible for reactivating the Aspen Grove landslide. However, there was probably some contribution from subsurface water, because springs were observed near the head of the landslide and near its toe, downslope from the pipeline.

The Dusterburgs Hill Landslide

The Dusterburgs Hill landslide is another example of a long and narrow slope failure that originated in older landslide and slope deposits. It is located on Dusterburgs Hill, near the middle of sec. 8 (Plate 1). The landslide is about 1 km long, and its width ranges between 35 and 120 m. The landslide is probably between 4 and 8 m thick with an average thickness of perhaps 6 m. Its volume is about 3.8×10^5 m^3. The upper half of the landslide slopes toward the northwest; about midway between the head and toe, the landslide turns abruptly toward the west (Fig. 2.4). The average slope of the surface is about 13°. The dominant mode of movement was sliding; only a small amount of the material flowed.

The geometry of the Dusterbergs Hill landslide differs in some details from that of the Aspen Grove landslide. An arcuate head scarp, 2 to 3 m high, defines the proximal boundary of the landslide. The surface of the upper half of the landslide is slightly lower than neighboring ground. Well-developed shear zones mark the lateral boundaries, and a steep toe, 1.5 to 2.0 m high, marks the distal boundary. The surface of the landslide was strongly deformed and is broken by many cracks. Most trees and shrubs growing on the landslide were killed by its movement (Fig. 2.4).

The sharp bend in the landslide is an unique feature. Most landslide debris slid out of the bend leaving a bowl-like depression about 3 to 4 m deep (Fig. 2.4). Red shale, probably of the Colton Formation, is exposed in the bottom of the depression. During the summer of 1985, two small springs were observed near the margins of the depression.

Unlike debris in the Aspen Grove landslide, the debris in the Dusterburgs Hill landslide appears to be derived from bedrock in the immediate vicinity of the landslide. Boulders and cobbles in the landslide and on the adjacent slopes are limestone and limy sandstone derived from the Flagstaff Limestone and the Colton Formation, both of which underlie the landslide.

The landslide probably was active only during 1983 and 1984. Dead trees and shrubs on the surface of the landslide already looked dry and brown in June 1984. Features on the surface of the landslide were displaced only a few meters to perhaps 20 m.

The Majors Flat Landslide

The Majors Flat landslide is a relatively large, irregularly shaped failure in colluvium overlying bedrock (sec. 13, T. 17 S., R. 3 E., and sec. 18, T. 17 S., R. 4 E., Plate 1). The landslide is about 590 m long; its upper part is about 320 m wide, and its lower part is about 190 m wide. Its thickness ranges from about 1 to perhaps 20 m.

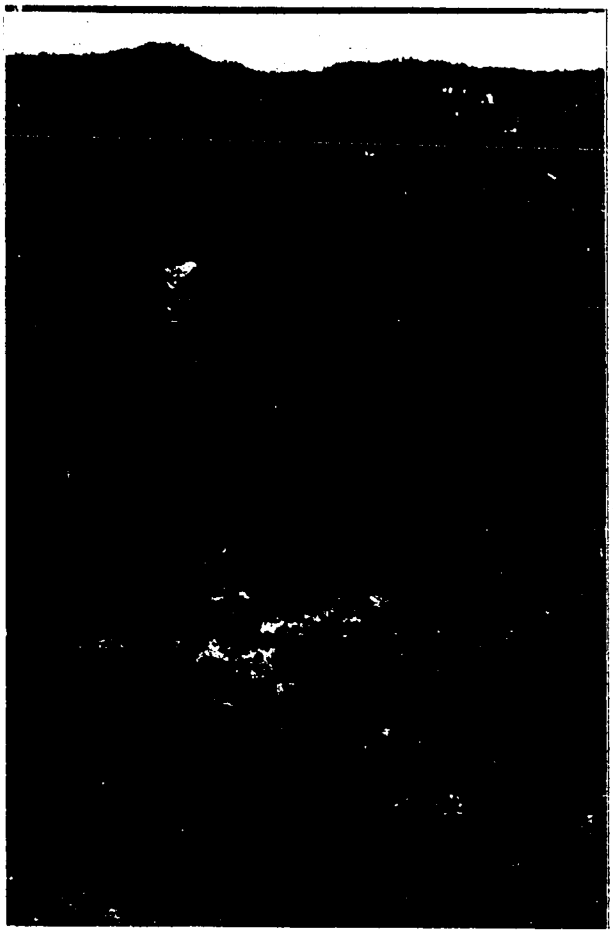

FIGURE 2.4. Photograph of the Dusterburgs Hill landslide, looking east from the northwest rim of New Canyon.

Assuming an average thickness of 10 m, its volume is approximately 9.6×10^6 m^3. The average slope of the landslide surface is 10 to 11° (Fig. 2.5a). In plan view, the landslide is shaped about like Africa, with the head of the landslide corresponding to the north coast of Africa, and the toe of the landslide to the Cape of Good Hope (Figs. 2.5b).

Deformation due to movement occurred mainly around the edges of the landslide; the central part is relatively uncracked and undeformed (Fig. 2.5b). The head scarp of the landslide is jagged and irregular, and stands about 1 to 3 m high. A region immediately below the head scarp, about 30 to 60 m long and extending the full width of the landslide, is broken into long, narrow blocks bounded by transverse cracks and scarps. En echelon cracks and segmented faults (Fig. 2.5b) define the flanks of the landslide. A slightly sinuous toe, 1 to 2 m high, connects the right flank of the wide upper half of the landslide to the right flank of the narrower, lower half of the landslide (Fig. 2.5b). Imbricated thrust sheets occur in the foot of the landslide; the edges of the thrust sheets are defined by steep, sinuous ridges, 0.5 to 1.5 m high.

Debris in the landslide consists of boulder-, cobble-, and pebble-size clasts of limestone and sandstone in a sandy clay matrix. The debris is derived from the Flagstaff Limestone, which underlies the steep slope along the east margin of the landslide, and the North Horn Formation which underlies the body of the landslide.

The landslide started moving during the spring of 1983 and was active for several weeks until mid-summer 1983. The landslide started

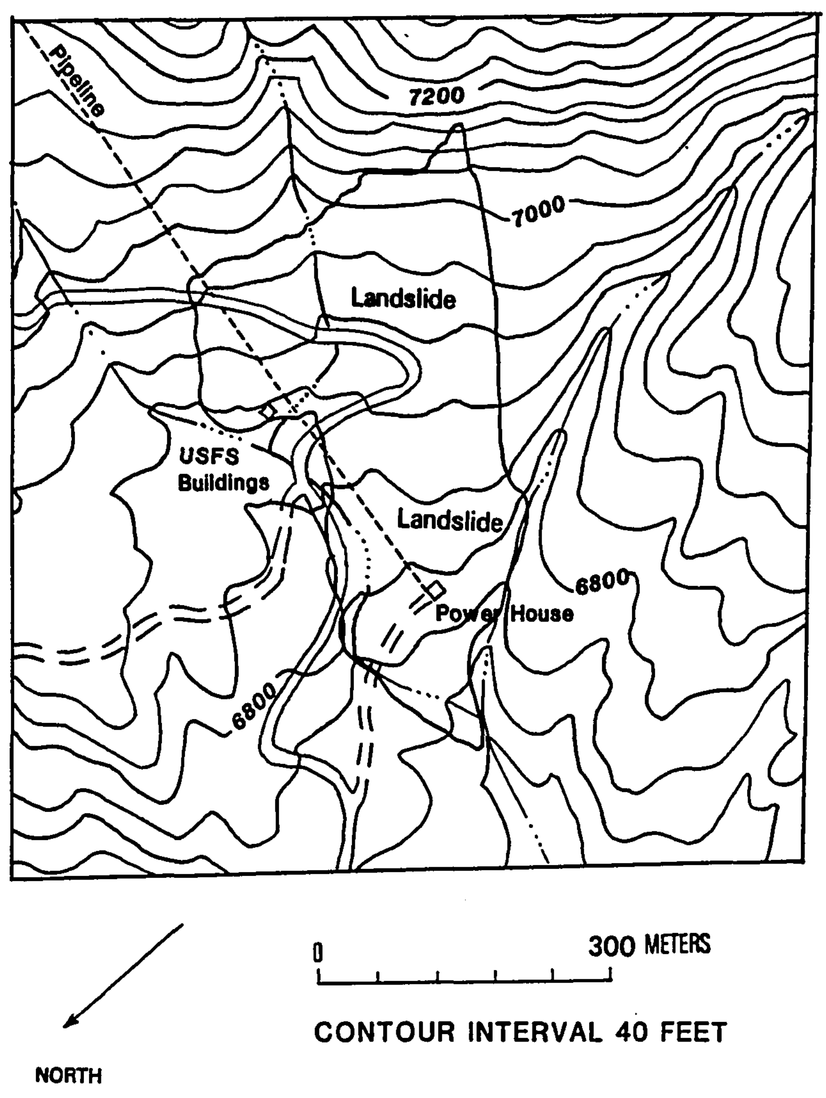

FIGURE 2.5. Map showing the Majors Flat landslide. (A) Topographic map redrafted from Ephraim 7-1/2-minute quadrangle (USGS.); (B) map showing features at the surface of the landslide.

FIGURE 2.5b. Map showing features at the surface of the landslide.

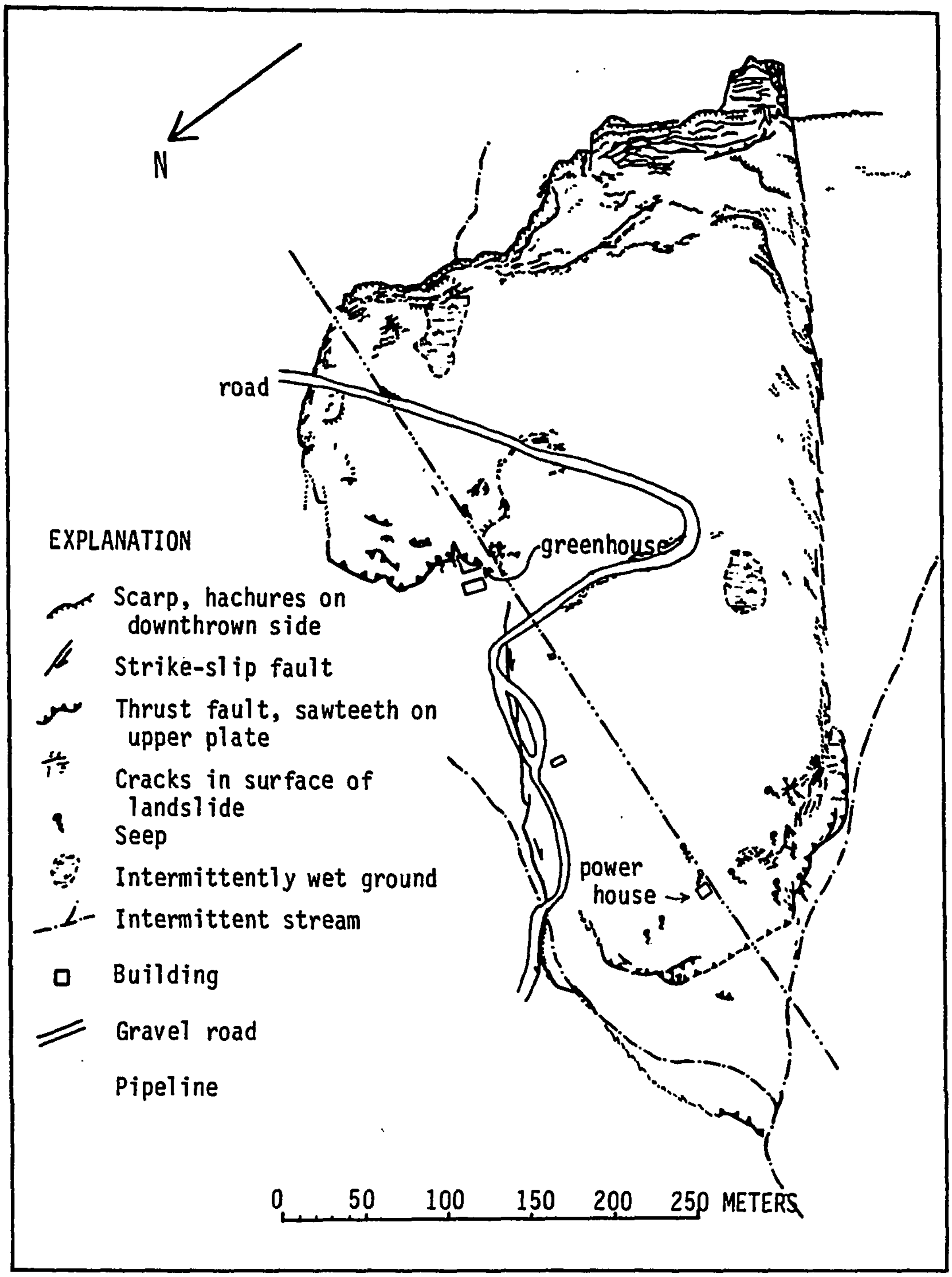
N
road
greenhouse
power house
EXPLANATION
Scarp, hachures on downthrown side
Strike-slip fault
Thrust fault, sawteeth on upper plate
Cracks in surface of landslide
Seep
Intermittently wet ground
Intermittent stream
Building
Gravel road
Pipeline
0 50 100 150 200 250 METERS

moving again in the spring of 1984, when it broke a water line that supplied the City of Ephraim and destroyed some buildings belonging to the U.S. Forest Service. Measurements made by Roger Johnson (oral commun., 1984) showed that the landslide was moving a few centimeters per day in May 1984. The landslide gradually slowed to a stop sometime in June or July 1984.

Seeps observed at several places on the surface of the landslide indicate that subsurface water played a role in sustaining movement. Several seeps occurred along the trace of the pipeline, which suggests that they probably were fed by leaks in the pipe. Other seeps occurred in the toe that could not be directly attributed to any man-made source of water. Surface water from a spring east of the landslide spilled onto the surface and soaked into the ground at the head of the landslide. It seems probable that infiltrating meltwater and spring water triggered the landslide, and that water leaking from the broken pipeline helped sustain the movement.

The Aspen Grove, Dusterburgs Hill, and Majors Flat landslides are typical of landslides in unconsolidated deposits in the study area, regardless of shape and size. The debris consists of a bouldery, sandy clay. The landslides moved by translation at rates of a few millimeters to a few centimeters per day. Tension cracks and scarps 1 to 3 m high characterized the landslide heads. The lateral boundaries were well marked by shear zones. The surfaces of the landslides were only slightly cracked and deformed.

Discussion and Conclusion

Much of Ephraim Canyon is covered by older landslide debris, including parts of areas labeled slope deposits on the map. Many of the older landslide masses are much larger than the landslides of 1983-86. The abundance of large landslide deposits in the area indicates that the 1983 event is not unique and may have been overshadowed by past events.

About 80 percent of the area involved in recent landslides was underlain by old landslide deposits and slope deposits, 57 percent in older landslide deposits plus 23 percent in slope deposits. The colluvium and older landslide deposits are derived from similar parent materials and have similar textures, and together the deposits cover perhaps 70 to 80 percent of Ephraim Canyon. Because the deposits are so widespread, we cannot reach any conclusions about the stability of these deposits compared to others.

Nearly all rockslides during 1983-84 occurred in fault zones. Rockslides constituted about 20 percent of the area of recent landslides. The rockslides occurred only on barren, south-facing slopes in New Canyon and Cottonwood Canyon.

Of the landslides and debris flows that were active in Ephraim Canyon during 1983-1986, relatively few were first-time failures; the overwhelming majority of landslides and debris flows involved in previously failed materials.

Ten or eleven rockslides that occurred on the north sides of Cottonwood Canyon and New Canyon constitute the majority of first-time failures. A few small landslides and debris flows that resulted from failure of loose, weathered-bedrock on the north sides of the canyon occupied by Cottonwood Creek and New Canyon constitute the remainder of the first-time failures.[1]

The locations of only some of the first-time failures might have been predicted. It was noted that rockslides occurred in fault zones on south-facing slopes. Thus, in hindsight, sites of possible rockslides could have been predicted by identifying fault zones on south-facing slopes.

The debris flow of 1986 at Cottonwood Spring was less predictable than the rockslides. During 1984 or 1985, a few cracks were noticed on the dip slope where the flow originated, but the cracks did not obvoiusly outline a landslide. Many other landslides had dried out and stopped moving in 1983 or 1984. The snowfall during 1985 and 1986 was less than in 1983 and 1984, and the cracks were on a south-facing slope. South-facing slopes in the area are dry, especially compared to north-facing slopes. Thus, I was surprised when the material on the dip slope failed and started flowing during the spring thaw in April 1986.

---

[1]First-time failures are indicated on the map (Plate 1).

CHAPTER III

MELTING SNOW: THE TRIGGER FOR LANDSLIDES AND DEBRIS FLOWS IN EPHRAIM CANYON

Introduction

The Aspen Grove landslide and other landslides in Ephraim Canyon, central Utah (Fig. 3.1) became active after two years of heavy snowfall there. Data collected by the U.S. Forest Service (Gary Jorgensen, unpub. data) document the long-term pattern of precipitation in Ephraim Canyon, and the precipitation events that preceded the landslides. Heavier than average snowfall accumulated during the winter of 1981-82, unusually large amounts of rain and snow fell during September 1982, and record-breaking snowfall accumulated during the winter of 1982-83. Finally, a belated spring thaw brought rapid melting of the snow. The meltwater saturated the slopes in the canyon and caused numerous landslides and debris flows. The purpose of this chapter is to briefly describe the hydrologic condition before and during the spring of 1983.

Precipitation, Evapotranspiration and Snowmelt

Precipitation in Ephraim Canyon is primarily orographic. It increases according to elevation as shown by the records of five weather stations in Ephraim Canyon (Figs. 3.1 and 3.2). For the 33-year record common to all five stations (1951 to 1983), the mean annual

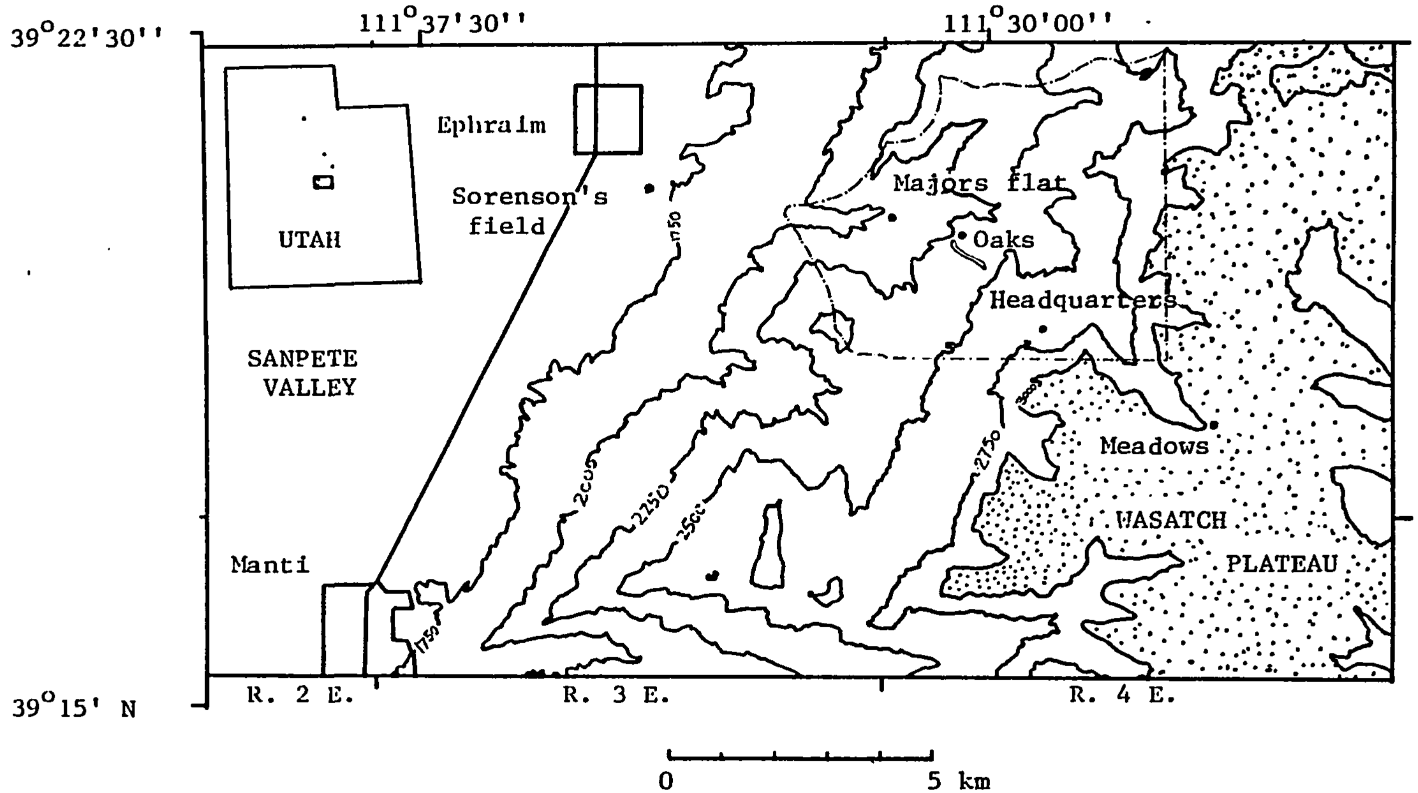

FIGURE 3.1. Map showing locations of weather stations in Ephraim Canyon. Contour interval is 250 m. The stippled area represents the top of the Wasatch Plateau.

precipitation is 28 cm at Sorensens Field (Ephraim, elev. 1725 m), 48 cm at Majors Flat (elev. 2097 m), 58 cm at the Oaks (elev. 2274 m), 80 cm at Headquarters (elev. 2682 m) and 94 cm at the Meadows (elev. 3042 m), near the top of the plateau. Thus, the precipitation at the top of the plateau is about 3 times that at Ephraim.

Seasonal variations occur in the precipitation at each station. Most precipitation falls as snow during the months of October through May. The summers are relatively dry; however, several centimeters of rain falls each summer as a result of thunderstorms.

Annual variations affect precipitation throughout the canyon, and are superimposed on the differences due to elevation. Figure 3.2 shows that the annual precipitation at Headquarters always exceeds that at the Oaks and Majors Flat, which are lower in elevation. Also, local maxima and minima in the plots (Fig. 3.2) occurred during the same years at each station.

The landslides occurred after two years of heavy precipitation. The greatest annual precipitation that has been recorded occurred in 1983 at all three stations (Fig. 3.2). Precipitation for a few centimeters less than the 1983 maximum accumulated in 1982. During 1952 and 1965, precipitation at each of the three stations nearly equaled the 1983 precipitation. However, 1952 and 1965 were preceded by years of average or below average precipitation. To our knowledge, the Aspen Grove landslide was not active, nor did other landslides occur in Ephraim Canyon during 1952 or 1965.

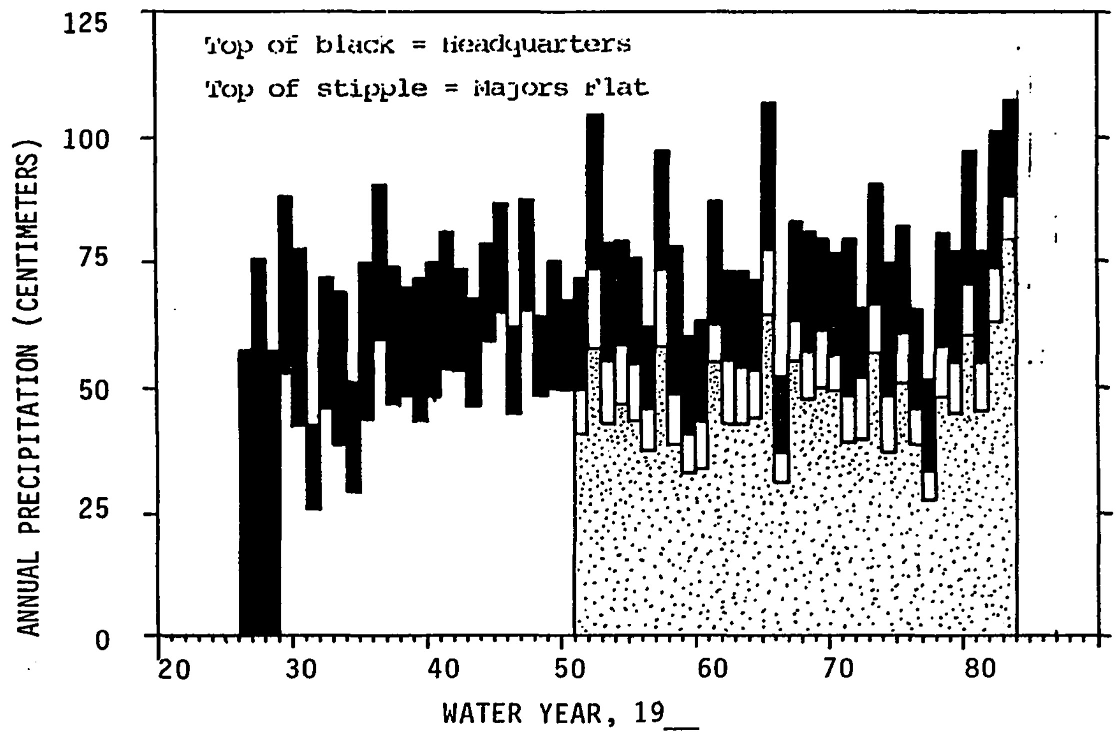

FIGURE 3.2 Bar graph showing annual precipitation at Majors Flat, the Oaks and Headquarters. Measurements began at Headquarters in 1926, at the Oaks in 1929 and at Majors Flat in 1951.

Part of the annual precipitation is evaporated or used by plant life; however, the remainder produces runoff or becomes stored as soil moisture or ground water. In Ephraim Canyon, the summer precipitation (June through September) is transpired in the same season that it falls; additional water, derived from the precipitation in October through May, is also transpired (Grover and others, 1970). During the period October through May, about 30 to 40 cm of precipitation that falls at higher elevations remains after transpiration to produce runoff or enter storage as soil moisture or ground water.

The precipitation during October through May 1982 was 10 to 12 percent above average, so that soil moisture probably was relatively high during the summer and even in September 1982. The average precipitation in October through May (1951 through 1983) at the Oaks was 45.1 cm and at Headquarters was 66.6 cm (Gary Jorgensen, USFS, unpub. data). The annual water usage by Aspen and related vegetation that grow in much of the canyon is 36.4 cm (Grover and others, 1970). Thus, even during average years, the precipitation at this elevation is sufficient to produce runoff and recharge the groundwater reservoirs. During 1982, the October through May precipitation was 50.9 cm at the Oaks and 73.1 cm at Headquarters (Gary Jorgensen, USFS, unpub. data). Therefore, precipitation remaining after evapotranspiration during the summer of 1982 was 5 to 6 cm more than average. Much of this might have been stored as soil moisture.

A severe storm occurred in Ephraim Canyon during September 1982. About 16.1 cm of rain fell at the Oaks station, and snow having a water content of 20.8 cm fell at Headquarters that month (Gary Jorgensen, USFS, unpub. data). Part of the rain probably soaked into the ground to increase the moisture content of the soil. Most of the snow that fell at high elevations stayed on the ground and contributed to the snowpack that accumulated during the fall and winter of 1983.

The depth and water content of the snowpack that accumulated in Ephraim Canyon during 1983 broke all previous records there. The precipitation in October through May was about 73.5 cm at the Oaks station and about 90.4 cm at Headquarters (Gary Jorgensen, USFS, unpub. data).

Much of the snow stayed on the ground at Headquarters until at least the first of May, when the last snow course measurements were made (Gary Jorgensen, USFS, unpub. data). Snow course data at the Headquarters station indicate that snow equivalent to 71.4 cm of water was present on May 1, which was about 95 percent of the 74.7 cm that had fallen since October 1, or 75 percent of the 95.5 cm of precipitation that had fallen since September 1.

The snowpack did not melt significantly until late May and early June 1983. Significant melting probably started around the last week of May. Local residents report that extensive melting of the snow pack with resultant flooding occurred in late May. These reports agree with observations and official temperature measurements at Manti (Lee J. Anderson, written commun., 1987), about 12 km south of Ephraim. The temperatures in Manti rose rapidly after May 20 and local flooding was observed in Manti about May 30 (Fig. 3.3).

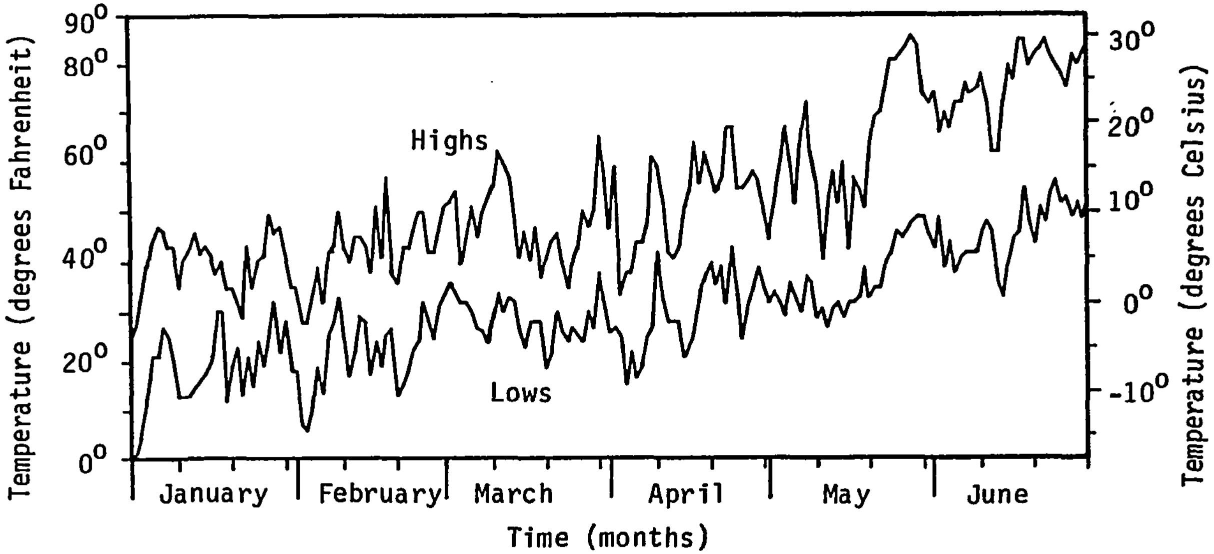

FIGURE 3.3 Graph showing daily high and low temperatures at Manti, Utah, January through June 1983. (Data courtesy of Lee J. Anderson, Manti, Utah.)

Melting probably was finished by the end of June. Anderson and others (1984) report that the snow pack in much of Utah had melted by about June 25.

Nearly all of the meltwater could have soaked into the ground as rapidly as it was produced. Steady-state infiltration rates of soils in Manti Canyon, which are similar to soils in Ephraim Canyon, are about 0.7 to 9.1 cm/hr (Orr, 1957, and Meeuwig, 1965). These rates exceed the rate of melting that probably occurred during May and June 1983. The average rate of melting was 0.13 cm/hr, assuming that the snow pack produced 90 cm of water over a period of 30 days.

The moisture content of the soil prior to melting, combined with the water derived from the 1983 snowpack was more than adequate to trigger the Aspen Grove landslide and other landslides in Ephraim Canyon. The Aspen Grove landslide started moving on or before May 31, 1983, which was shortly after the start of rapid melting (Gary Jorgensen, USFS, personal commun., 1983). The White Ledge landslide (also in Ephraim Canyon) was moving in early June but was still covered with a thick blanket of snow (Robert W. Fleming, oral commun., 1987).

Discussion and Conclusion

The precipitation that fell during 1982 and 1983 triggered the Aspen Grove landslide and other landslides that became active in Ephraim Canyon during May and June 1983. Combined precipitation that fell during 1982 and 1983 was the greatest for any two successive years on record prior to 1983. According to long time residents of Ephraim, landslides have never been as numerous in Ephraim Canyon as they were in

1983. No changes that affect slope stability other than heavy precipitation are known to have occurred in the canyon during 1982 and 1983.

We have debated whether the melt water that triggered the landslides moved primarily in the shallow subsurface layers of the soil, or in deep layers of bedrock. Evidence was found to support both possibilities.

Two lines of evidence suggest that water circulating within a few meters of the ground surface triggered shallow landslides. First, many of the landslides that occurred during 1983 were relatively shallow; most were only a few meters deep. This suggests that shallow, perched water tables formed in the soil and activated the shallow landslides. Second, the majority of landslides and debris flows were active while snow was melting, which indicates that the meltwater was able to raise the pore pressures rapidly. I would expect a time lag of weeks between melting and response of deep groundwater (Robinson, 1971), especially if the melt water needed to percolate through an unsaturated zone.

Other lines of evidence support the idea that deep groundwater played a role in triggering rockslides in fault zones. First, springs and seeps are common on the Wasatch Plateau (Robinson, 1971) and several springs in Ephraim Canyon have been developed for water supply. Second, groundwater flows through the westward tilted rocks on the west side of the Wasatch Plateau toward the Sanpete Valley (Robinson, 1971, p. 28). Third, springs were observed in porous rocks exposed in the headscarps of several rockslides.

The evidence indicates that most shallow landslides, including shallow slides that were mobilized into debris flows, were triggered by meltwater that was percolating downward through the shallow layers of soil to perched water table. Most rockslides were triggered by groundwater percolating through fault zones in the bedrock. The source of water that triggered thick (thicker than 2 to 3 m) landslides in surficial deposits is unclear.

CHAPTER IV

THE ASPEN GROVE LANDSLIDE

Introduction

Dozens of landslides in the vicinity of Salt Lake City along the Wasatch Front in northern Utah and hundreds of landslides east of the Sanpete Valley along the western edge of the Wasatch Plateau in south-central Utah began moving during May and June of 1983 as a result of extraordinarily rapid melting of deep snow cover. Some of the landslides mobilized into debris flows that invaded and damaged communities built on alluvial fans, particularly in the vicinity of Salt Lake City. Others broke water mains or dammed creeks that drain the western edge of the Wasatch Plateau, or disrupted mountain roads that connect small towns in the Sanpete Valley to coal mines on the Wasatch Plateau to the east.

The landslides appeared in an astonishing array of sizes and shapes as shown, for example, in my geologic map of Ephraim Canyon (Plate 1). Some are thin slips that headed small debris-flow tongues a few decimeters thick and several tens or hundreds of meters long. Some others are massive slide blocks one or more kilometers wide and long, and 40 to 60 m thick. An example is the Twin Lake landslide complex, described by Fleming and Johnson (unpub. manuscript). Several are long, narrow, and thin, like debris flows, but moved as more-or-less rigid bodies, like slide blocks. An example of one of these, the Aspen Grove landslide, is the subject of this chapter.

The Aspen Grove landslide is about 7 km east-southeast of Ephraim, Utah, on a northwest-facing slope within Ephraim Canyon (Fig. 1.1). The landslide was discovered by Gary Jorgensen (U.S. Forest Service) and Roger Johnson (USAF pilot, ret.) on May 31, 1983, as they were driving along a gravel road (State Highway 29) in Ephraim Canyon looking for signs of damage to water lines that supply the town of Ephraim. They observed sets of cracks in two arms of a switchback of the road (Fig. 4.1) on the hillside above a water main, and Roger Johnson followed discontinuous cracks from the upper arm, down the hillside, across the lower arm, and about 10 m below the lower arm, some 300 m above the water main.

At that time, the Aspen Grove landslide was about 600 m long and 25 to 50 m wide; its volume was on the order of 120,000 m^3.

During 1984, the Aspen Grove landslide enlarged, adding about 20 m to its head and 300 m to its toe, so that its total length increased about 50 percent, to about 900 m, and its volume increased 50 to 100 percent, to between 200,000 and 300,000 m^3. The addition to the toe area is wider and appears to be deeper than the rest of the landslide.

The landslide maintained roughly the same overall shape during 1985 and 1986; changes were largely evident in development of internal structures.

The Aspen Grove landslide is unusually long for its width; its length-to-width ratio generally ranges from 20 to 40. A result is that the flanks of the landslide are largely defined by strike-slip faults

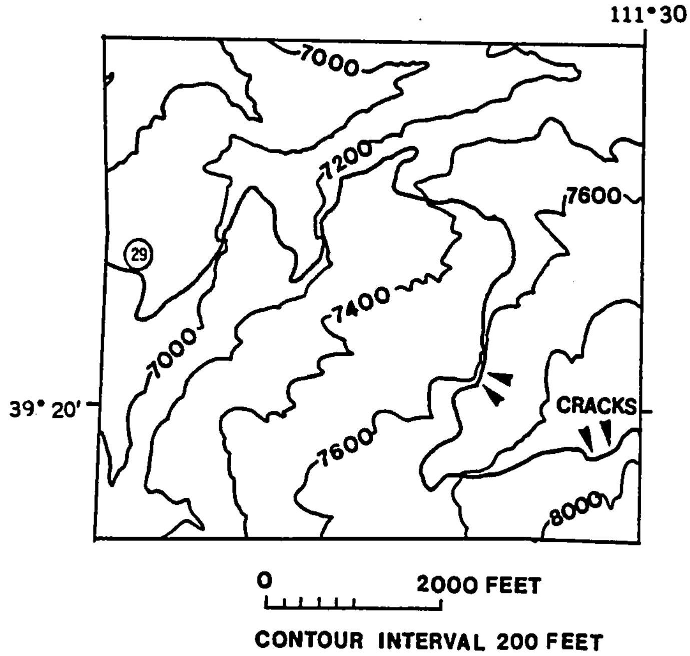

FIGURE 4.1. Map showing approximate locations of crack in the road near Aspen Grove, May, 1983 (sec. 17 and 18, T. 17 S., R. 4. E., Ephraim 7-1/2 minute quadrangle, U.S.G.S.).

and fault zones (Plate 2). Many well-developed and preserved features provide an unusual opportunity to study the development, behavior, and relationship of strike-slip faulting to the movement of the landslide.

The Aspen Grove landslide is a reactivation of previously failed landslide debris. In part, the boundaries of the landslide followed recognizable margins of previous movements. However, the area of previously failed material is two to three times larger than the landslide that reactivated in 1983.

Starting in June 1983, and ending in the summer of 1986, Robert Fleming, Arvid Johnson and I have spent 3 to 6 weeks each spring and summer monitoring and mapping the Aspen Grove landslide. This chapter describes the landslide, its setting, and its evolution during those four years.

Setting of Landslide

The head of the Aspen Grove landslide is at about 2,423 m (about 7,950 ft) altitude in an assemblage of spruce, fir, aspen, and maple (Plate 3). The toe is at about 2,240 m (about 7,350 ft) altitude in an assemblage of scrub oak and sage brush. Grasses and shrubs cover the ground surface, and boulders of sandstone jut out of the ground.

The slope of the ground in the vicinity of the landslide ranges from 0 to 31° and averages perhaps 11°. The ground slopes generally toward the west.

Superimposed on the westerly slope of the area are plunging ridges and troughs in the ground surface that trend west or northwest (Plate 3). The ridges are 100 to 200 m wide and hundreds of meters long. The troughs are of the same length, but are about half as wide as the ridges. Relief on the troughs and ridges is about 10 to 50 m. The troughs and ridges result from relief on the surface of the bedrock, because bedrock crops out at the crests of many of the ridges. The trend of the troughs and ridges is oblique to the strike of the bedrock.

Bedrock

Bedrock in the area consists of bedded limestone, limy sandstone, and shale of the Cove Mountain and Musina Peak Members of the Flagstaff Limestone (Stanley and Collinson, 1979), and sandstones and shales of the North Horn Formation. The distribution of bedrock formations is shown in Figure 4.2. The Flagstaff Limestone underlies ground in the vicinity of the Aspen Grove landslide, and the North Horn Formation underlies an escarpment east of the landslide.

Limestone of the Cove Mountain Member of the Flagstaff Limestone is white or gray, porous, and lacks fossils. Some brown chert occurs with the limestone. Limestone of the Musina Peak Member contains abundant mollusk fossils and is white or gray and fine-grained. Some of the limestone is silicified.

Sandstone occurs only in the Cove Mountain Member; it is white or light gray and moderately indurated. The sandstone consists of fine- to medium-grained, pink and white quartz sand with calcite cement.

Shale in both members is compact and gray, white, brown, or red claystone.

The North Horn Formation southeast of the landslide consists of 1- to 3-m-thick beds of ledge-forming sandstone, alternating with beds of

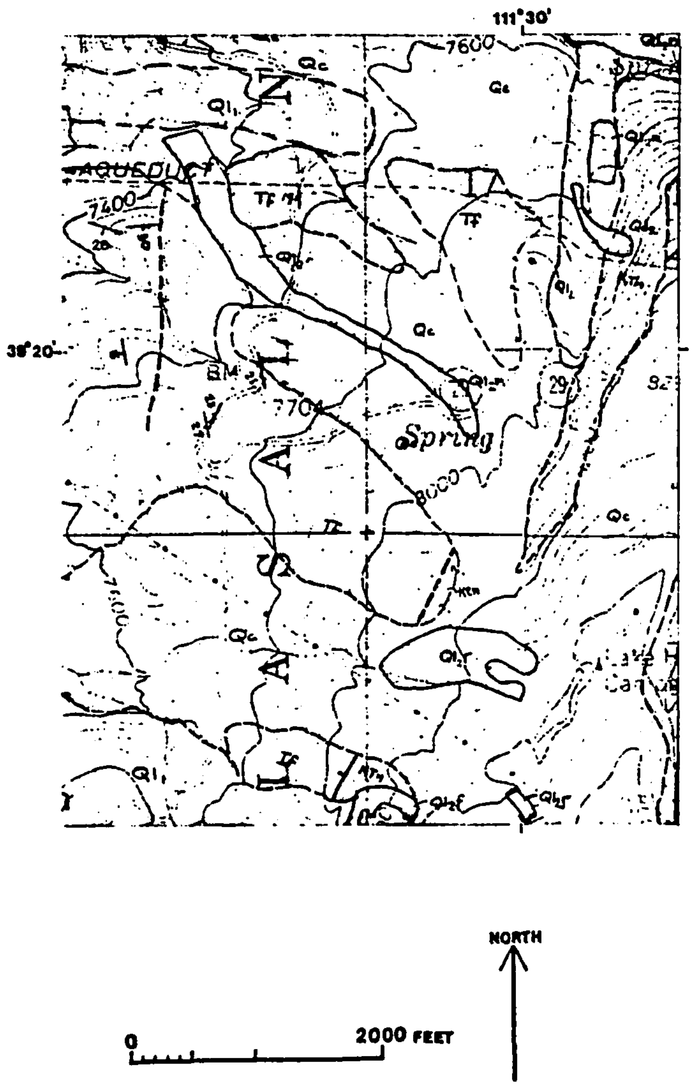

FIGURE 4.2. Geologic map of part of Ephraim Canyon, reduced from Plate 1.

claystone and a few 0.1- to 0.3-m-thick beds of limestone. The sandstone is light gray or light yellow, massive or cross laminated, and consists of quartz sand mixed with a few chert granules and cemented by silica. The claystones are red, brown, orange, or gray, massive and silty. The limestone is medium- to dark-gray, and fossiliferous.

The source area of the landslide debris at Aspen Grove must be about 200 to 300 m east-southeast of the head of the Aspen Grove landslide (Fig. 4.2).

The bedding in the Flagstaff Formation, which underlies the area of Aspen Grove landslide, dips about 20° toward the west. The structures in the area include a fault at the foot of the escarpment (east of Aspen Grove, Fig. 4.2). The fault dips steeply toward the west and trends about N. 10° E. Beds of the Flagstaff Limestone, west of the fault, are down relative to beds of the North Horn Formation, east of the fault. The North Horn beds are about horizontal. Another fault is in Flagstaff Limestone, near the presumed terminus of the Aspen Grove landslide. The fault trends about due north and dips steeply or is vertical. Beds are down on the east side of the fault.

Residuum

The area of the Aspen Grove landslide is blanketed by residuum in some places and by landslide debris in others. The residuum is material derived from the underlying bedrock of the Flagstaff Limestone by weathering essentially in place. It is generally 0.5 to 2 m thick. The residuum is predominantly clay, and contains abundant pebble-, cobble-, and boulder-sized clasts. The clasts include white or gray limestone; white, silicified, fossiliferous limestone; white or gray limy sandstone; and light gray, red, or green claystone.[1]

Landslide Debris

The matrix of the landslide debris in the area of the Aspen Grove landslide consists of yellow or brown, sandy clay and contains abundant boulders and blocks of cross-laminated yellow and light-gray sandstone derived from the North Horn Formation (Fig. 4.3). It also contains some clasts of limestone and claystone derived from the Flagstaff Limestone. The landslide debris is 6 to 8 m thick in the upper half of the landslide and may be thicker in the foot area below the lower road crossing.

The sandstone boulders and blocks in the landslide debris consist of fine- to medium-grained, moderately sorted quartz sand with granules and pebbles of white chert. The sandstone has silica cement and does not effervesce in acid as does the limy sandstone found in the residuum.

[1]South of Aspen Grove, the residuum contains clasts of claystone and white or gray limestone. Fine- to medium-grained, white, limy sandstone clasts occur with the limestone and claystone clasts.

Upslope from the upper crossing of the road (locations E-7, F-7, Plate 3), clasts of white, limy sandstone and silicified limestone are especially common.

In the triangular deposit of residuum north of the modern landslide (D-3, E-3, F-4), white or light-gray limestone is present with only minor amounts of white, limy sandstone and greenish-gray claystone clasts.

In the northeastern corner of the map area (G-4, H-5), the residuum contains white, fine- to medium-grained, limy sandstone and light-gray claystone with small amounts of limestone.

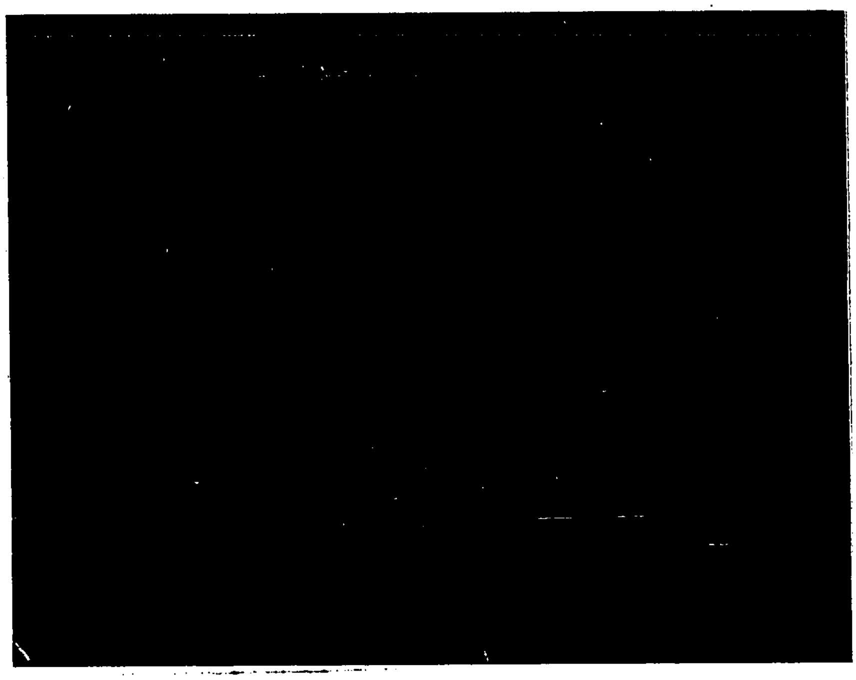

FIGURE 4.3. Photograph of a boulder derived from the North Horn Formation in landslide debris near the Aspen Grove landslide.

Distribution of Landslide Debris and Residuum

The distribution of residuum and landslide deposits closely correlates with topographic position at the site. A thin, discontinuous mantle of residuum covers large, north-trending ridges and some minor troughs. Bedrock crops out at few locations, mainly on ridge crests and

in road cuts. Landslide debris occupies the main trough through the center, the branch trough in the northeast, and the low-lying, marshy ground in the northwest corner of the area (Plate 3).

Stratigraphy of Landslide Debris

During August 1984, five holes were drilled in the upper part of the landslide with a truck-mounted drill rig operated by the U.S.G.S. Geotechnical Laboratory, Golden, Colorado (Roger Nichols, Supervisor). One was drilled in ground adjacent to the landslide (borehole B4, Station 160, Plate 2). Another was drilled through the right flank of the landslide (B3), and three others were drilled near midwidth (B1 at Station 160 and B2 and B2A at Station 270). During July 1985, two new holes (B5 and B6, Plate 1) were drilled at Station 160, near B1. Three undisturbed samples were collected near the bottom of hole B6 for laboratory testing.

The stratigraphy of the debris in the upper part of the Aspen Grove landslide was determined by examination of the cuttings and detailed description of cores.

The log of one boring (B4, Plate 4) shows the older landslide debris about 30 m northeast of the modern Aspen Grove landslide. The others (B1, ..., B6, Plate 4, and Figs. 4.4, 4.5) show the debris involved in the upper part of the landslide.

Details of each profile are different, of course, but three layers can be identified in each profile. From the top downward they are: (1) top soil; 1 to 2 m of black to dark brown, organic, sandy clay containing sandstone boulders; (2) landslide debris; 4 to 6 m of brown or yellow-brown, plastic, sandy clay containing sandstone boulders; (3) bedrock of Flagstaff Limestone; green, gray, and tan claystone interbedded with white, cherty limestone. The failure surface is above or at the top of bedrock.

Tube samples collected in borehole B6, in the upper part of the Aspen Grove landslide, were extruded and examined in the laboratory.

Several intervals (C; Fig. 4.6) of the tube samples are thinly laminated, plastic clay, like that shown in Figure 4.7. Alternating intervals are massive plastic clay or silty clay (SC).

Study of the tube sample suggests that the failure zone or slip surface of the landslide passed through the laminated clay at depths of 6.15 or 6.52 m (Fig. 4.6). A crack and some poorly developed slickensides that dipped about 15^{o} were observed at a contact between silty clay and laminated clay at a depth of 6.15 m. There was a disturbed zone at the base of the tube sample in greenish-gray, waxy shale at a depth of 6.52. m, but much of the disturbance was due to drilling, because the most obvious structures were slickensides with circumferential striations.

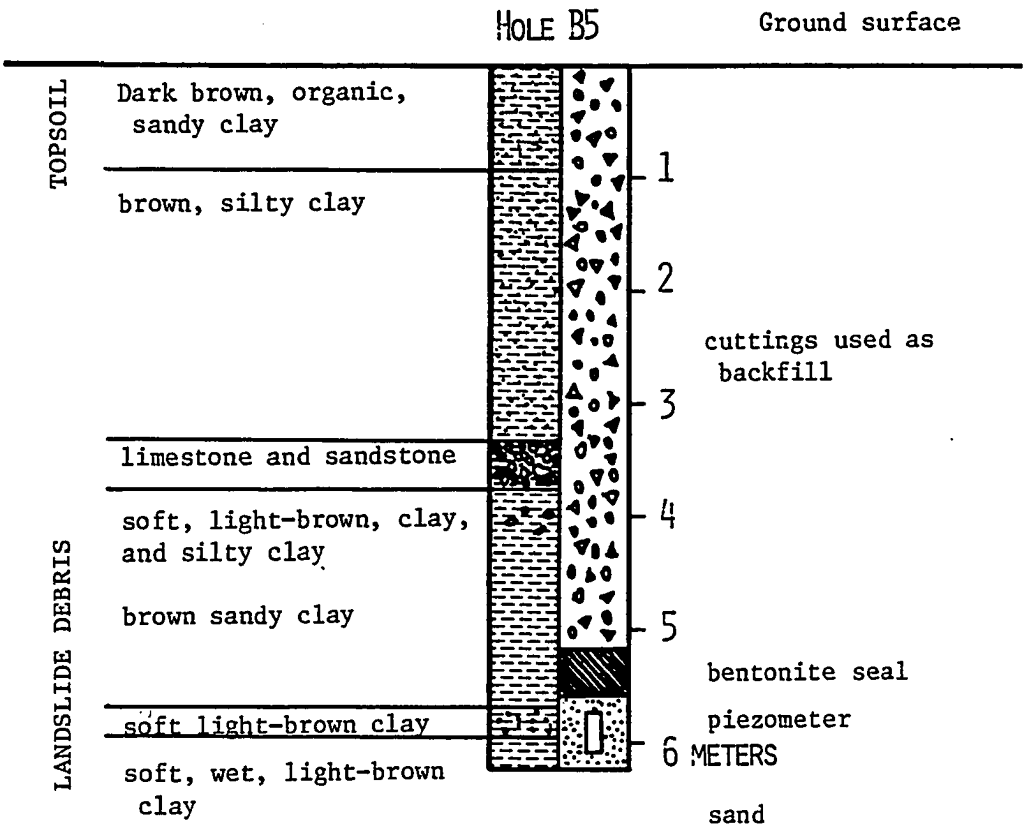

FIGURE 4.4. Log of hole B5. See Plate 2 for location.

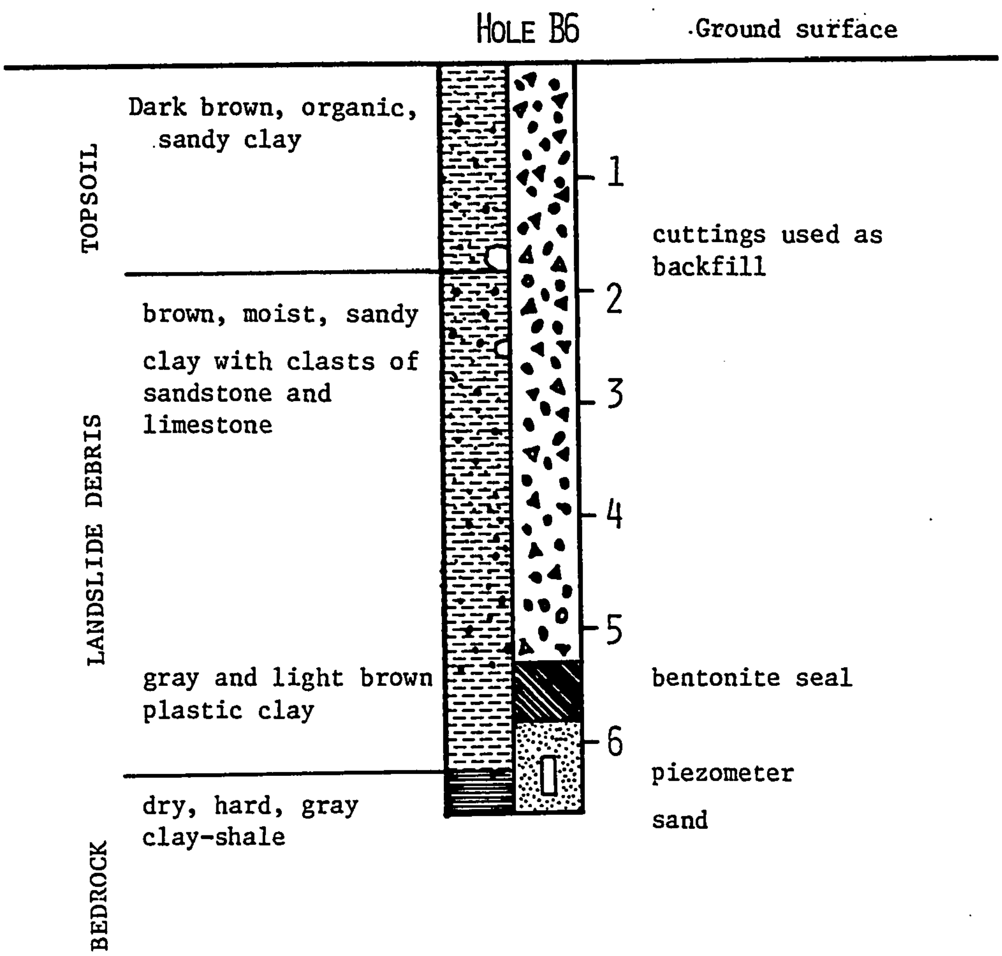

FIGURE 4.5. Log of hole B6. See Plate 2 for location.

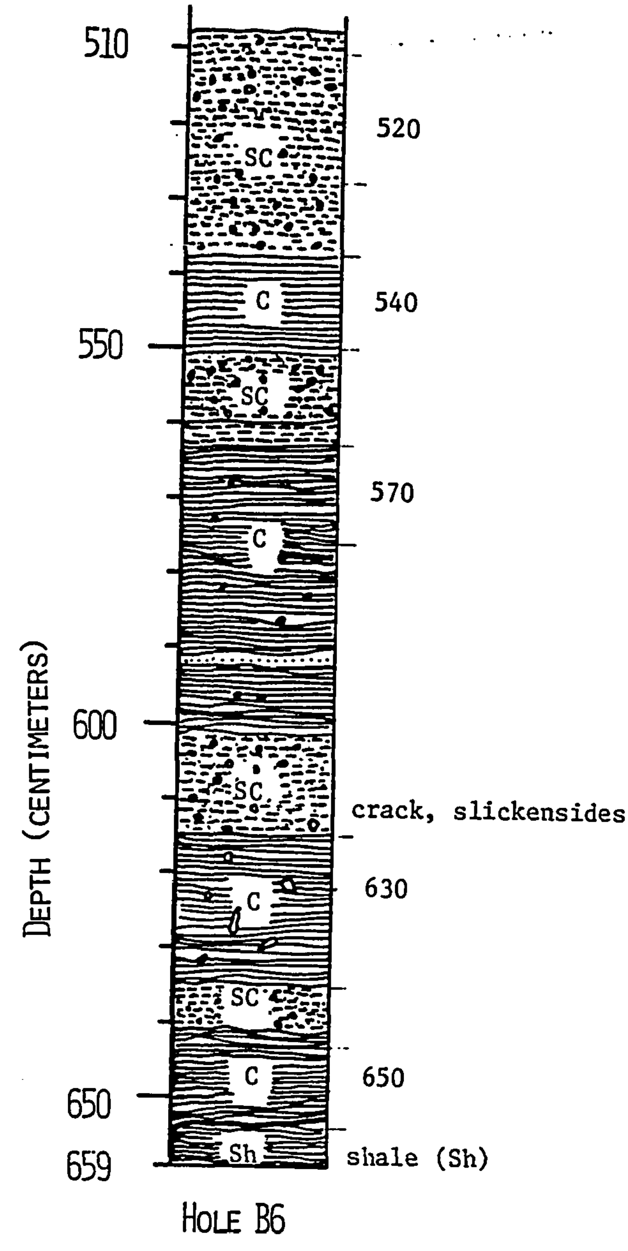

FIGURE 4.6. Detailed log of the lower 1.5 m of hole B6. Limits of samples taken for laboratory testing are shown on the right-hand side of the log; the sample number corresponds to the approximate depth in centimeters.

Geotechnical Properties

Samples for determination of standard physical properties were collected from various units within the tube samples taken in borehole B6 in 1985. The samples are identified by the depth in centimeters near the middle of the sample (Fig. 4.6).

Particle-size distributions and Atterberg limits for the samples are given in Table 4.1 as functions of depth below the ground surface. The table shows that materials identified as clay or silty clay in the log (Fig. 4.6) indeed are dominantly clay or silty clay. In the bottom 1.5 m of borehole B6, the clay content ranges from 44 to 74 percent, the plastic limit (PL) ranges from 12 to 19 percent, and the plasticity index (PI) ranges from 26 to 49 percent. A sample of green shale collected about a decimeter above the bedrock has a relatively high clay content of 58 percent and a low PI of 28. Microscopic examination of the sand fraction indicates that 95 percent of the sand in the sample is actually calcite-cemented claystone fragments. Cementation of the clay particles in the shale might be responsible for the low PI.

Three of the samples have high liquid limits (LL > 50) and all samples plot well above the A-line (Fig. 4.8), so all the samples are medium- to high-plasticity clays, which are supposed to have low shear strengths and low permeabilities (Lambe and Whitman, 1969, p. 35-38).

The strength of one sample was determined in the U.S.G.S. Geotechnical Laboratory in Golden, Colorado. An undisturbed sample was tested in order to estimate peak strength and residual strength. The tests were done in a direct-shear apparatus under slow, drained

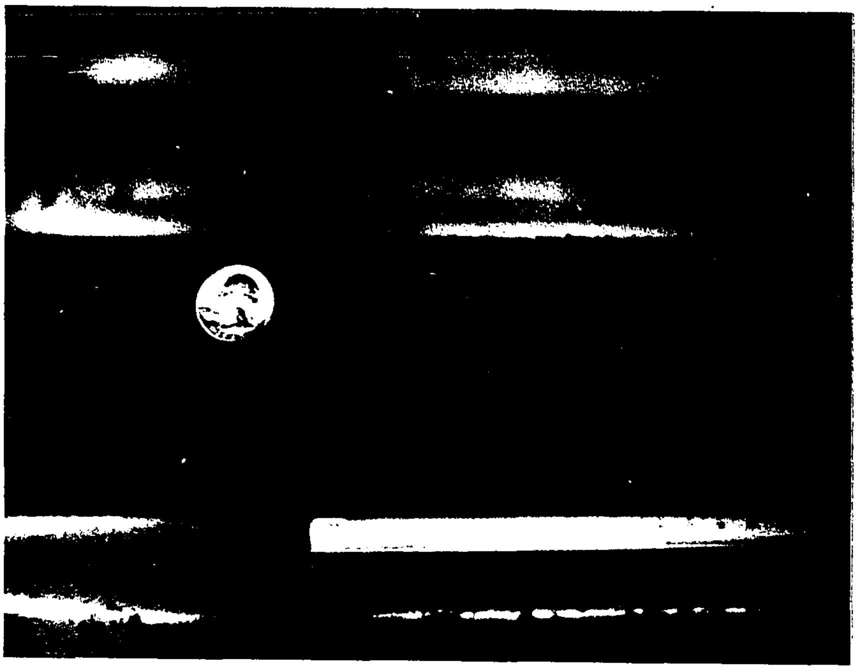

FIGURE 4.7. Photograph of laminated clay (C) from hole B6. Coin is 2.5 cm in diameter.

conditions. Specimens were cut from the tube sample in the interval from 6.15 to 6.35 m (sample 630, Fig. 4.6) and trimmed to fit the shear box of the direct shear device (6.4 cm in diameter and 2.08 cm thick). Water content of each specimen before the test was determined from trimmings, and water content after the test was determined from a piece of the specimen. The first specimen was placed in the shear box of the direct shear apparatus and consolidated under a normal stress of 34.5 kPa (kN/m^2). The specimen was then sheared at a rate of 0.0240 mm/min. (approximately 35 mm/ day). until displacement totaled 9 mm. The second and third specimens were consolidated under stresses of 138 and 414 kPa, respectively and sheared in the same manner as the first.

The stress-displacement diagrams are shown in Figure 4.9. The specimen tested under a normal stress of 34.5 kPa reached its peak strength, 42.4 kPa, after about 1 mm of displacement (Fig. 4.9). The strength decreased rapidly during the next 2 to 3 mm of displacement and then more gradually to 21.5 kPa.

The specimen swelled and took on water during consolidation and during the shear test. During consolidation its thickness increased from 2.08 cm to 2.16 cm, about four percent. During the first 2.5 mm of displacement of the shearing test, thickness of the specimen gradually increased to its maximum thickness of 2.19 cm. During the last 6.5 mm of displacement, the thickness of the specimen decreased to a final thickness of 2.15 cm.

TABLE 4.1 PHYSICAL PROPERTIES OF SAMPLES FROM HOLE B6

Sample Depth	Particle Size Distribution (ASTM classification)				Atterberg Limits (water content, percent of weight of solids)			Grain density (g/cm^3)
	gravel 4.76 mm	sand 4.76-0.075 mm	silt 0.075-0.005 mm	clay <0.005 mm	LL	PL	PI	
520	0	27	29	44	38	12	26	2.76
540	1	11	29	59	68	19	49	2.75
570	1	14	31	54	52	16	36	2.81
630	2	6	18	74	59	16	43	2.68
650	0	17	25	58	46	18	28	2.76

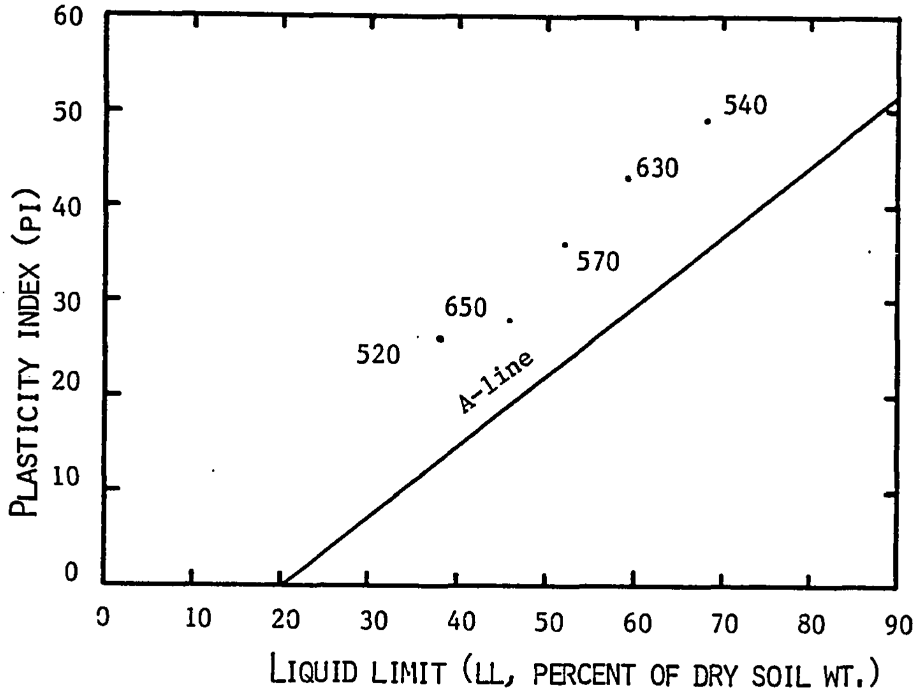

FIGURE 4.8. Plasticity chart showing plasticity index and liquid limits of each sample from hole B6.

The water content[2] before the test was 19 percent and the water content at the end of the test was 25.7 percent, so the water content increased by seven percent.

The second specimen, tested under a normal stress of 138 kPa, had a marked peak strength and took on water as did the first. The specimen reached its peak strength, 76.7 kPa, after 1.2 mm of displacement (Fig. 4.9). The shear strength decreased gradually during the remainder of the test, and the strength after 9 mm of displacement was 43.2 kPa.

The specimen swelled from a thickness of 2.08 cm to 2.09 cm during consolidation, but gradually decreased in thickness as material was extruded from the shear box during the shear test. The water content of the specimen increased from 19.2 percent before the test to 23.9 percent at the end of the test, so the water content increased by about five percent.

Swelling of the first two specimens suggests that the relatively high peak strengths (about twice the "residual" strengths) results from overconsolidation of the sample.

The peak and residual strengths of the third specimen were about equal. The specimen tested under a normal stress of 414 kPa reached its peak strength, 122 kPa after 5.4 mm of displacement (Fig. 4.9). The strength decreased almost imperceptibly during the remainder of the test to 117 kPa after 8.8 mm of displacement. The stress-displacement curve for this specimen is similar to that of a normally consolidated soil (Lambe and Whitman, 1969, p. 312).

---

[2]The water content is defined as the weight of water divided by the weight of solids in the soil, multiplied by 100 percent.

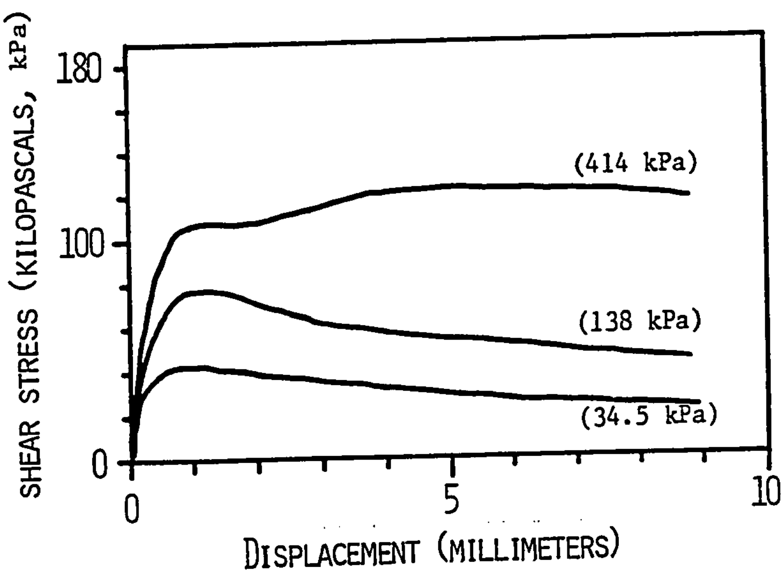

FIGURE 4.9. Stress-displacement diagrams for direct shear tests on sample 630 from hole B6. Curves are identified by the normal stress (in kiloPascals) applied during the test.

The specimen decreased in thickness during consolidation from 2.08 cm to 2.04 cm, and decreased in thickness during the shear test. However, the specimen took on water during the test, because its water content increased from 20.7 percent at the beginning of the test to 23.2 percent at the end of the test, a net increase of 2.5 percent.

The strengths of the specimens are plotted as a function of normal stress in Figure 4.10. The peak strength defines a segmented failure envelope. The intercept is about 31 kPa and the segment defining peak strengths at lower normal stresses slopes about 18°. The segment defining peak strengths at higher normal stresses slopes about 9°.

Upper- and lower-bound estimates of the residual strength are also shown in Figure 4.10. The upper-bound estimate uses the strength at the end of each direct-shear test. The upper-bound failure envelope has an intercept of 10.8 kPa and slopes 14.3°. The lower-bound estimate uses the residual strength determined for the specimen tested under a normal stress of 414 kPa, and extrapolates through the origin. Slopes of the stress-displacement diagrams (Fig. 4.9) indicate that the specimen tested under a normal stress of 414 kPa was the only one of the three that attained its residual strength after 9 mm of shearing. The lower-bound estimate has an intercept of 0 kPa and slopes 15.8°.

The residual strength of the sample is consistent with residual strength of similar soils. Skempton (1964) found that soils having clay contents[3] of 60 to 70 percent have residual friction angle of about 9° to 18°. Our sample had a clay content of 66 percent.

---

[3]Clay content defined as weight of particles smaller than 2 microns divided by weight of solids, multiplied by 100 percent.

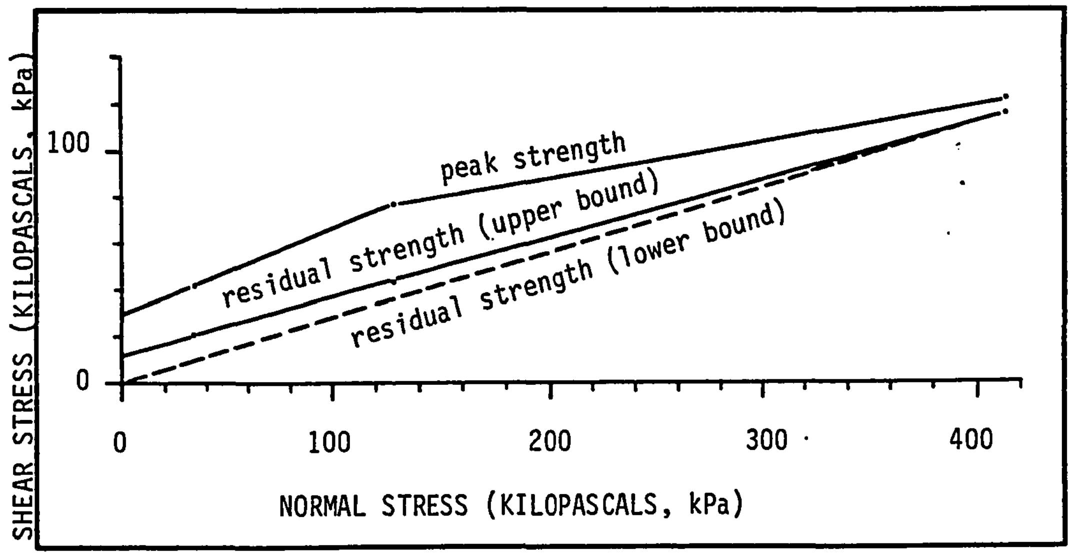

FIGURE 4.10. Peak and residual shear strength as a function of normal stress for the sample 630 from hole B6.

Approximate Boundaries of Ancient Landslides

A few characteristic features of landslides are preserved for long times and, in some places, mapping of these features allows one to map dimly preserved landslide masses. The persistent features I mapped in the area of the Aspen Grove landslide are hollows, feet, and flank ridges.

The contacts between landslide debris and residuum, shown in Plate 3, are presumably defined by boundaries of ancient landslides. However, the contacts are necessarily compound boundaries and they need not define shapes of individual landslide bodies. The boundaries of the modern Aspen Grove landslide, for example, in most places do not correspond to contacts between landslide debris and residuum (Plate 3).

Persistent Structures--Hollows, Feet, and Ridges

Landslide hollows are half-bowl-shaped or trough-shaped depressions in landslide debris that remain where landslide debris has pulled away from a headscarp.

A distinctive hollow occurs near the left flank of the Aspen Grove landslide (locations E-5 and E-6, Plate 3). The hollow is about 70 m wide and 100 m long. A smaller hollow, about 30 to 35 m wide, is adjacent to the right flank of the landslide (F-5, Plate 3).

Landslide feet are defined by Varnes (1978) as lobate masses in distal terminations of landslides. A landslide foot has a steep (20 to 30°), rounded, fan-like, distal slope. In plan, a foot has a distinctive tongue- or teardrop-shape.

A large remnant landslide foot occurs within the Aspen Grove landslide below the lower road crossing (D-4, Plate 3). Two less prominent feet are adjacent to the large hollow (E-5 and E-6, Plate 3).

Landslide flank ridges have been defined by Fleming and Johnson (in press) as doubly-plunging domes of landslide debris that develop adjacent to strike-slip faults bounding landslide elements. The long axes of the flank ridges are subparallel to the traces of the bounding strike-slip faults. The flank ridges at Aspen Grove can be recognized by abundant boulders at their surfaces. Also, the layer of top soil is typically thinner on ridge crests than on adjacent ground.

The contrast in soil thickness was displayed vividly in cracks and scarps formed in the upper part of the Aspen Grove landslide, near the 7,875 ft contour (Plate 3). In 1986, the crest of the ridge was crosscut by scarps, exposing soil that was medium brown and bouldery. In contrast, the soil was dark brown, rich in organics, and contained relatively few boulders on the flanks of the ridge.

Most of the features identified as flank ridges in the area of the Aspen Grove landslide are along the flanks of the modern (i.e. 1983) landslide, but some occur where a trough trending northwest branches off the main trough (F-5 and G-5, Plate 3). Some of the ridges in this area are parallel to the Aspen Grove landslide, and others are more nearly parallel to the branch trough.

Two long flank ridges occur downslope from the large foot (D-3, D-4 and C-3, Plate 3). When the modern landslide lengthened in the foot area in 1985, the flanks followed the axes of these two ridges.

Several flank ridges in and adjacent to the Aspen Grove landslide are shown in Plate 2. Some others that occur within old landslide debris at Aspen Grove are shown in Plate 3.

The old ridges are assumed to mark locations of flanks of former landslides.

Boundaries of Older Landslides at Aspen Grove

The boundaries of the modern Aspen Grove landslide and the inferred boundaries of four ancestral landslides are shown in Figure 4.11. The longest landslide mass, on the right-hand side, and the relatively short and wide landslide mass on the left-hand side, appear to have been crosscut by two younger landslides near the center in the view of the map (nos. II and III, Fig. 4.11). The landslide feet of nos. II and III appear to encroach on the hollow of the older landslide (no. I) on the left. The foot of no. III appears to encroach on the left flank of no. II.

These relationships are the bases for the relative ages, I through III assigned to older landslides, the approximate boundaries of which are shown in Figure 4.11.

The modern Aspen Grove landslide is, of course, younger than all the others shown in Figure 4.11.

The five landslides (Fig. 4.11) do not account for all the landslide debris in the area of Aspen Grove. However, all the older, distinct landslides that I could recognize by mapping persistent landslide features are indicated in Figure 4.11.

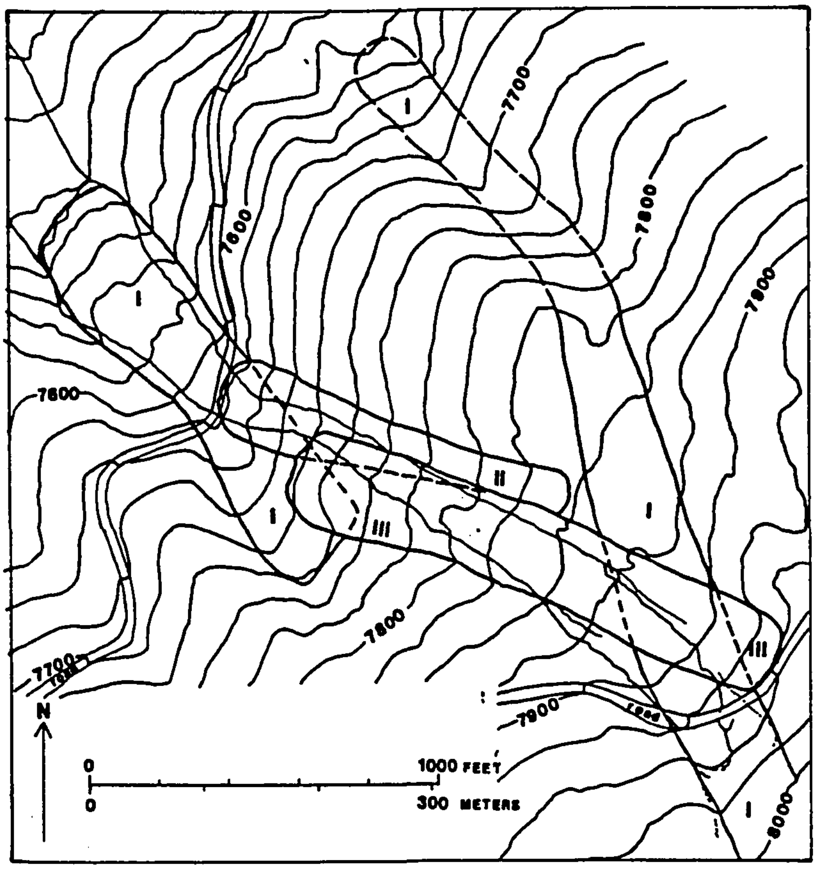

FIGURE 4.11. Map showing possible ancestral landslides of the Aspen Grove landslide.

Probable Antiquity of Form of Even the Modern Landslide

Some observations suggest that the Aspen Grove landslide has moved with a configuration similar to its present one for a long time. The distinctive foot within the modern landslide and the distinctive ridges along its flanks formed almost entirely during previous episodes of movement. One ridge that we monitored has a height of about 1 m, and its height grew only about 0.1 m during the present episode of movement. The large foot is 3 or 4 m high and it grew less than 0.1 m during the present episode.

Using purely linear extrapolation, Arvid Johnson (written commun., 1987) estimates that the flank ridge we monitored grew during five or ten previous episodes of landslide activity, and that the old foot developed during ten to thirty previous episodes of landslide activity.

In any case, it is conceivable that the ancestral and modern Aspen Grove landslides may have been active intermittently for thousands of years.

The Aspen Grove Landslide in 1984

The structures of the Aspen Grove landslide during August 1984 are shown in Plate 2, which is a reduced composite of nine plane-table sheets mapped by Fleming and Johnson (in press). Here we describe the landslide as it existed at that time.

The Head Area

The head of the landslide is in a grove of aspen, about 40 m above the upper road crossing (Plate 2). The head is about 35 m wide. The ground slopes at an angle of 9 to 10^{o} toward the northwest. Rather than a distinctive, bounding headscarp, the upper boundary of the landslide is marked by discontinous, sinuous, and arched gashes.

The traces of the gashes tend to be concave downslope. Some of them opened in mode I, normal to crack[4] faces and are up to 1 to 2 dm wide. Others accommodated both mode I and mode II, and are thus combinations of tension cracks and normal faults. Some of these are offset vertically 1 to 2 dm and in a few places up to 1 m.

Nearly the entire lengths of the flanks in the head area, above the upper crossing of the road, are marked by through-going, strike-slip faults[5] (Fig. 4.12). The left uppermost part of the left flank,

---

[4]Cracks are open breaks (fissures or gashes) in the ground surface. Motion on the crack is primarily normal to the crack surfaces and thus a crack is generally a mode I fracture (Lawn, B.R., and Wilshaw, T.R., 1975. Fracture of brittle solids. Cambridge Univ. Press, 204 pages.) In plan, cracks are widest near midlength and narrow toward wedge-shaped to somewhat rounded terminations. The lengths of cracks range from a few centimeters to several meters in the Aspen Grove landslide. Their widths range from nearly zero up to a few decimeters.

[5]Strike-slip fault is a term used here to describe surfaces or narrow zones across which differential shearing displacement has occurred. Such features are mode II or mode III fractures (Lawn and Wilshaw, 1975).

Figure 4.12 shows the plan view of a right-lateral fault in the Aspen Grove landslide that accommodated 4 m of differential shearing displacement. A furrow, about 1 dm wide and 3 cm deep, marks the trace of the fault. Open cracks, parallel to the bottom of the fault, occur in the bottom of the furrow.

(continued...)

however, is a zone of echelon tension cracks (Plate 2). The trace of the left flank curves through an arc of about 20° from the head to within a few meters of the upper road crossing. At the distal end of the curved flank fault, a few meters above the road, the left flank steps 3 m to the right. The stepping segments of the flank fault are connected by a thrust fault.[6]

The right flank of the head area is a more nearly straight strike-slip fault. There is a left step of about 1 m, connected by a thrust fault, about 10 m above the road.

Thus, a block in the head area is bounded by flank faults that diverge. The next block below is bounded by diverging flank faults as well. At the boundary between the two blocks, the flank faults step inward, on both flanks, toward the center of the landslide. Thus, the flank faults bounding the second block telescope into the flank faults bounding the first.

---

[5](...continued)
Characteristics common to strike-slip faults in the Aspen Grove landslide include: (1) The faults dip at angles between 80 and 90°. (2) Shearing offsets are subparallel to the ground surface, and striations generally plunge at or near the average slope angle of the ground. (3) The faults are segmented, and traces of adjacent segments step or have different orientations. In general, segments step right in left-lateral and step left in right-lateral fault zones. (4) The faults commonly produce scarps by juxtaposition of ground with different heights relative to the slip surface of the landslide.

[6]Thrust faults are horizontal or gently dipping surfaces or zones of shear. They occur within the Aspen Grove landslide at toes of landslide blocks or in some places on flanks where strike-slip faults step. In plan, the traces of thrust faults are broadly curved or sinuous.

FIGURE 4.12. Photograph of a strike-slip fault on the Aspen Grove landslide (by Arvid Johnson, Univ. of Cincinnati).

There is a small landslide mass within the large landslide, in the left side of the head area, between the upper road crossing and the zone of gashes at the head. It consists of blocks of intact soil of irregular plan shape, ranging from 0.5 m to 1 m in height, separated by a striated slip surface. Its toe is marked by a small thrust fault a few meters above the road. Other thrust faults, a few meters to 10 m below the road, may also be toes of the small, internal landslide.

The right flank both above and below the upper road crossing is relatively complicated. There is a landslide block bounded on its left side by the right flank fault of the main landslide and on its right by a variety of structures. Where the right flank fault of the block steps left, a set of en echelon cracks mark an incipient head and a right step of about 6 m. Below the road there is another head scarp, a right flank fault, and a set of en echelon cracks that define the right side of the block. The flank fault merges distally with a thrust fault, which curves to join the flank fault of the main landslide mass 25 to 30 m below the road.

Northeast of the head area of the main landslide, a new head was developing in 1984. The new head is bounded by a set of en echelon cracks that form an inverted "J" pattern. The orientations of the cracks within the en echelon pattern are consistent with right-lateral shearing. The hook of the "J" starts about 30 m east of the head in the bowl-shaped depression (at Station 0, Plate 2). Widely spaced cracks trace the contours of the bowl for a short distance and then follow a straight course for 70 m downslope in a direction of about N. 45° W. The trend of the en echelon cracks projects into an abrupt turn in the right flank fault of the main landslide at an altitude of about 2,405 m (near Station 100, Plate 2).

The Pond Area

The pond area of the Aspen Grove landslide is the upper part of the landslide where the bounding flank faults have nearly parallel traces. The pond area is about 120 m long and uniformly about 50 m wide, between Stations 100 and about 220 (Plate 2).

The pond area is characterized by strong flank ridges and by two of the largest steps in the flank faults. Also, it contains a peculiar low on the right side, which is opposed by a peculiar high on the left side. An intermittent pond forms in the low area.

The steps are associated with pairs of flank faults on each side, the younger in each case appearing on the right of the older. Thus, the most actively moving part of the landslide, in effect, has shifted toward the right by 5 to 10 m.

The right step in the right flank developed in 1983 and in 1984 (Fig. 4.13a and 4.13b). The one in the left step did too.

As shown in Plate 2, the right step in the right flank was being removed by the formation of a new, through-going flank fault sometime in 1984. In contrast, the left step in the left flank, near Station 220, produced a dog-leg in the left flank, and partly immobilized the relatively straight, through-going, outer flank fault.

The landslide is largely devoid of fractures in the upper part of the pond area, between Stations 90 and 140.

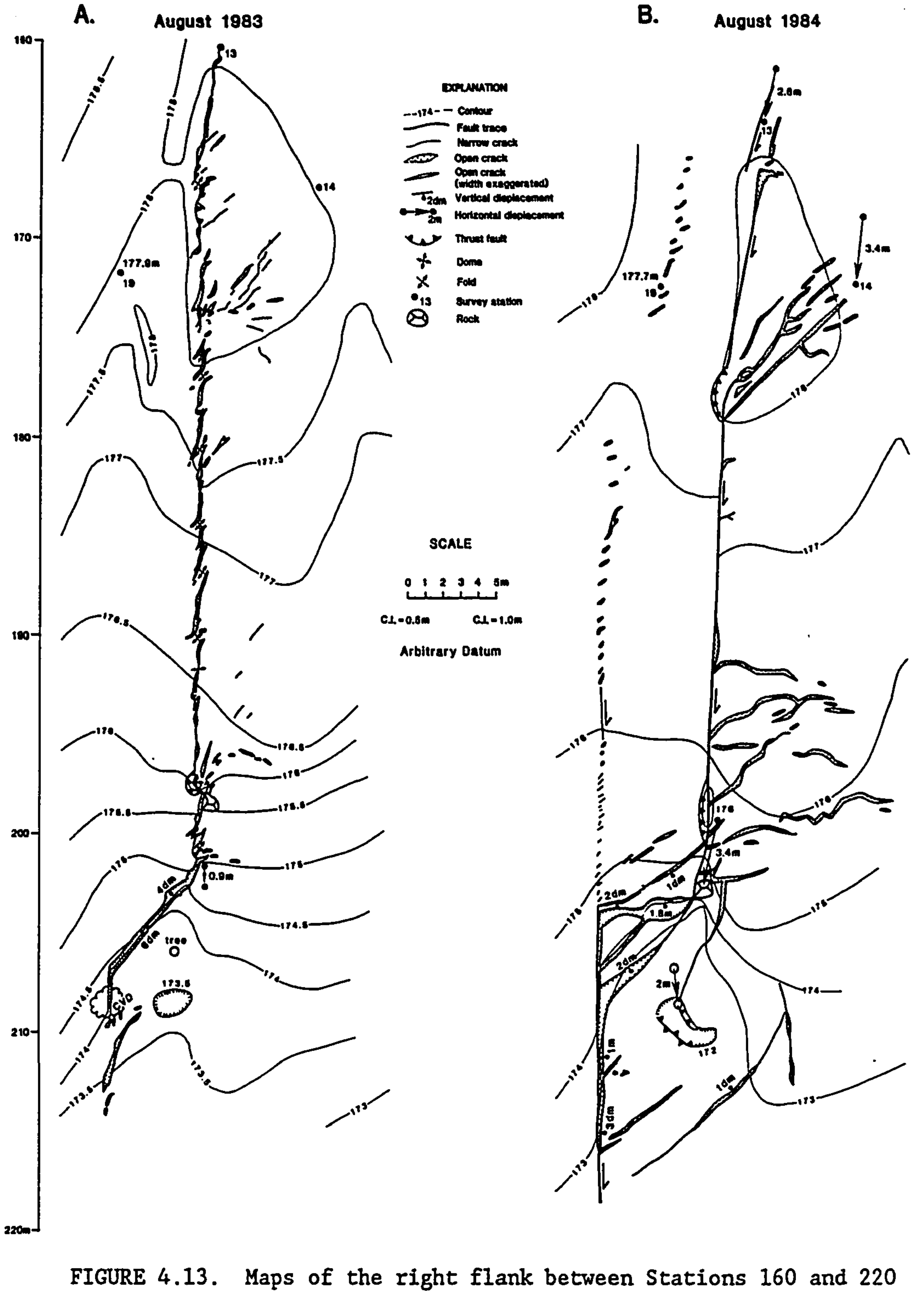

FIGURE 4.13. Maps of the right flank between Stations 160 and 220 (by Robert W. Fleming (RWF) and Arvid M. Johnson (AMJ)). (a) 1983. (b) 1984.

In this area, ground in the central part of the landslide is on the order of 2 m higher than ground near the flank faults. The flank faults are in troughs.

Cracks subparallel to the right flank fault near Station 150 are associated with a growing flank ridge, as documented elsewhere (Fleming and Johnson, in press). The flank ridge is 2 to 4 m wide, about 50 m long, and 0.5 to 1.2 m high. Narrow troughs occur on either side of the ridge. The right side of the ridge is truncated abruptly by the flank fault, forming a scarp several decimeters high. The downslope termination of the ridge occurs in a shallow pond (Station 150). In the pond, soft sediment folds 1 to 2 dm high and 5 to 15 m long are oriented circumferentially with respect to the base of the ridge.

Cracks with a similar orientation near the offset fence, Station 120, in the left flank appear to be near the crest of a younger ridge, growing inside the left flank. Offset of the fence indicates that the landslide had moved about 4.8 m at the time the map was made (Plate 2).

The flank fault in that area is a scarp; ground outside the landslide is up to 1 m higher than ground inside the landslide.

A thrust fault at Station 130 in the left flank appears to represent a right step in the left flank, where part of the differential displacement across the flank fault steps to the newer flank fault that is clearly visible near the end of the water trough.

At the water trough, the left flank fault makes a small left step of about 1 m and forms a small pull-apart basin.

Downslope from the water trough, between Stations 175 to about 220, the left flank fault consists of fault segments 5 to 15 m long.

The segments are consistently oriented counterclockwise, 5 to 10°, with respect to the general trend of the flank fault.

The same kinds of fault segments occur along much of the length of the right flank of the lake area of the landslide, between Stations 120 and 190. The segments of the right flank fault, though, are oriented clockwise 5 to 10° with respect to the gross trend of the right flank. Fleming and Johnson (in press) have described these and other features of the segments elsewhere.

A landslide element of rectangular shape, about 75 m long and 10 m wide, adjacent to the left flank, is bounded on each side by strike-slip faults, at its distal end by a combination of tension cracks and an oblique fault, and at its proximal end, apparently, by a thrust fault. The element was moving more slowly than the main part of the landslide; offset of a split tree adjacent to the element, at Station 175, indicates that the element had moved about 3 m, whereas the main body of the landslide nearby had moved about 6 m by the time the map was made.

A spectacular pull-apart basin occurs in the right flank near Station 210 (Plate 2). The basin is about 4 m wide, 6 to 8 m long, and between 1 and 2 m deep. The basin occurs where the right-lateral flank fault steps about 6 m to the right. The two fault segments are connected by a group of fractures and faults, the traces of which trend about 45° clockwise with respect to the trend of the flank faults. The major connecting fracture is an oblique fault, on which azimuths of striations parallel the trends of the flank faults. Ground in the main part of the landslide near the pull-apart basin has drifted downslope about twice as much as ground within the pull-apart basin. The ground in the basin has subsided nearly 2 m. During late winter and early spring, the basin is filled with water.

The Wedge Area

The part of the landslide between Station 220 and 430 is the wedge, so named because the flank faults generally converge downslope. The landslide narrows, remarkably uniformly, from a width of 55 m at Station 225 to 37 m at Station 325 to 30 m at Station 420.

The wedge area is characterized by superelevation of landslide debris relative to the surface of stable ground on either side of the landslide, a trough form for the landslide surface, and long, rather sharp-crested ridges on each flank.

Upslope from the wedge, the topographic contours indicate that the ground surface falls, generally, as one approaches the landslide from ground on either side. Within the wedge, the contours indicate that the ground rises. Thus, upslope from the wedge, the landslide debris appears to be contained, in effect, by a channel, whereas within the wedge the landslide debris forms its own channel as well as its own moving levees.

The differential elevation between landslide debris and adjacent ground culminates in the left flank near Station 345, where the landslide debris rises nearly vertically 2 to 3 m (Plate 2, Fig. 4.14).

The Fall Area

The fall area is a relatively short part of the Aspen Grove landslide, between Stations 420 and 530. The fall area is where the landslide is narrowest and the ground slope is steepest. The landslide

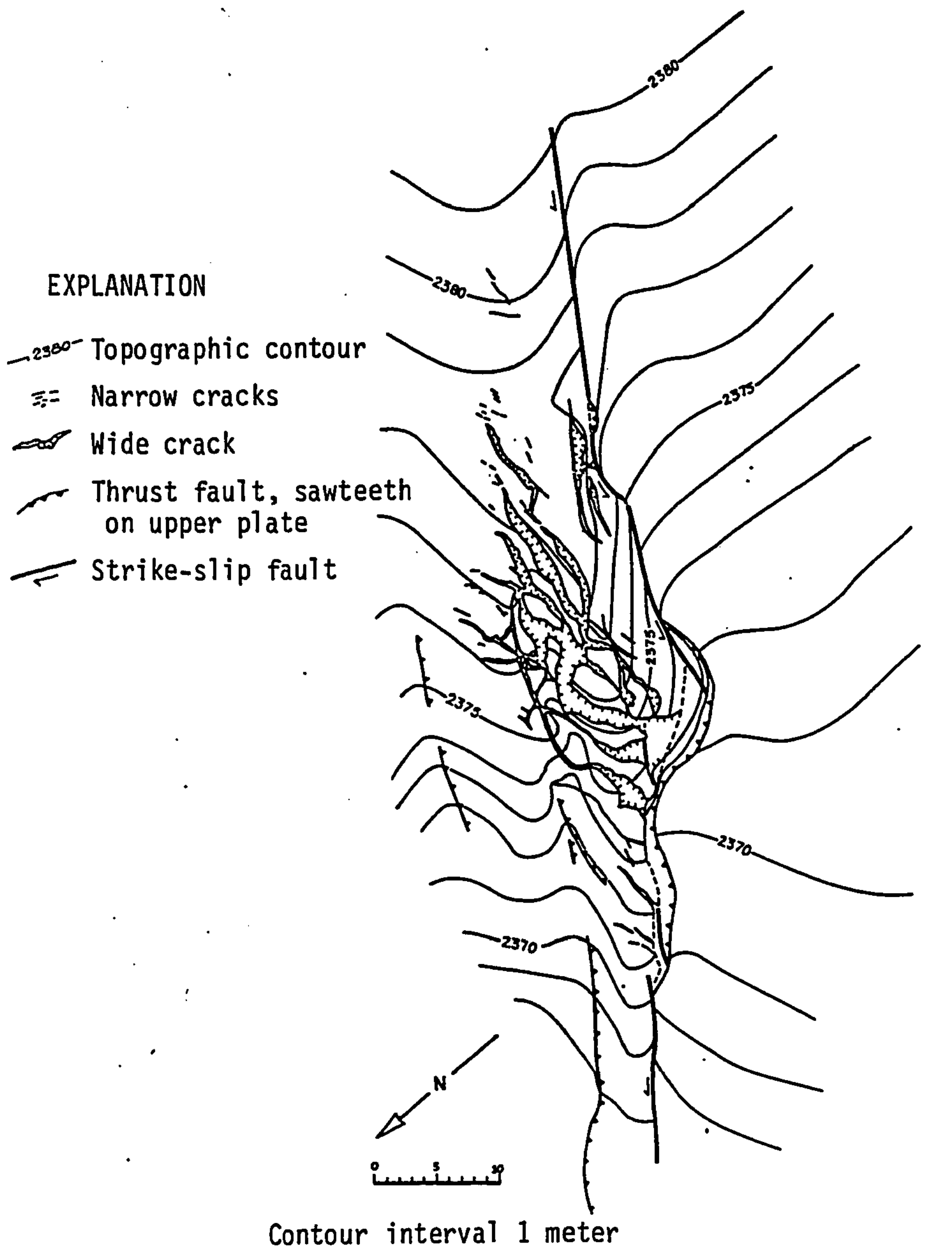

FIGURE 4.14. Map of the elevated, fractured area on the left flank, near Station 340. (by RWF and AMJ, September 1986).

surface is broken by many tension cracks. The fall area begins with a tension crack that extends nearly across the width of the landslide at Station 420, and it ends with thrust faults in the vicinity of Stations 520 and 530, about 30 m above the lower road crossing (Plate 2).

The Flare Area

Between the lower road crossing, near Station 540, and the beginning of the internal foot area, near Station 700, is the flare area, where the flank faults diverge markedly and the width of the landslide more than doubles, from about 35 to 80 m. Most of the flare area was inactive in 1983, so most of the structures shown in the flare area in Plate 2 formed in 1984, the summer the map was made. The structures are restricted to flank faults, which are partly through-going, strike-slip faults with minor steps, partly segmented faults, and locally en echelon tension cracks.

The Internal Foot

One of the most spectacular structures within the landslide is the old foot area of the landslide. The toe of the old foot is defined on three sides by segmented thrust faults, but the differential movement across the thrusts in the toe is small, on the order of a few decimeters in 1984, and the active landslide continues for two or three hundred m below the old foot area.

Thus, even though the topography of the old foot area bespeaks of termination of landslide movement, it bespeaks more strongly of landslide movement at some previous time. The topography of the foot has changed insignificantly during the current episode of landslide activity at Aspen Grove.

Within the right third of the foot area is a small internal landslide that heads near the top of the steep ground on the instep of the foot.

Undefined Terminus

The actual toe of the active Aspen Grove landslide is unknown. Displacements appear to gradually decrease distally and to provide no visible record beyond 200 m below the old toe in 1984, the time the map in Plate 2 was made. Even then, only the flank faults are marked, and these are marked very faintly by occasional cracks, some of which are shown in Plate 2.

Thus, the landslide just fizzled at its end in 1984.

In 1985 and 1986, the picture was scarcely clearer. Fleming, Johnson and I found clear evidence of sliding at least as far as the swampy area, about 100 m below the pipeline road shown in plate 2. However, Fleming and Johnson also found evidence of reactivation far below the swamp, in roadcuts along the main gravel road to Aspen Grove (Fleming and Johnson, in press).

Evolution of the Landslide from 1983 to 1987

Fleming and Johnson first examined the Aspen Grove landslide on June 8, 1983. It apparently started moving late in May; it was discovered on May 31 by Roger Johnson and Gary Jorgensen, of Ephraim. In early June the surface of the landslide was almost entirely unbroken by cracks, except immediately along the flank faults. Scattered tension cracks defined the head. There were a few cracks near midwidth at Station 250.

They were immediately struck by the facts that the flank faults maintained remarkably straight traces, diagonally over ridges and valleys, through depressions and over domes, and that the flank faults extended for great distances compared to their separation; that the landslide was unusually long and narrow, but apparently deep (Arvid Johnson, written commun., 1987).

During 1983, the landslide extended from the head area, between Stations 0 and 60 (Plate 2) to a terminus in the vicinity of Station 600. There were well-defined, strike-slip faults developed through the road near Station 575, but, below the road, between Stations 575 and 600, the flanks were defined by a few cracks, some of which were arranged en echelon.

The following year, in 1984, Roger Nichols and I first visited the landslide in mid-May. On May 17, I observed a few cracks at the crown of the landslide, suggesting movement of several centimeters at the head. However, Roger Nichols noted that the pull-apart basin at the large right step in the right flank, at Station 200 (Plate 2), had enlarged and deepened since 1983.

By May 18, new flanks had formed between Stations 580 and 750, below the lower road crossing. On May 22, I first visited the pipeline road, near Station 900 (Plate 2), and observed en echelon cracks on the right flank at the road, indicating that, by that time, all the ground between Stations 0 and at least 900 was moving. Roger Johnson, from

Ephraim, had already sometime earlier flagged the cracks in the pipeline road, so the cracks probably had already formed by the 17th to perhaps as late as the 21st of May.

Between May 17 and May 21, the head of the landslide had evolved dramatically. On May 21, the surface of the road at the upper crossing had dropped about 1 m at the left flank of the landslide (Fig. 4.15a). Diagonal cracks near the right flank broke the road into a series of narrow blocks (Fig. 4.15b, 4.15c). Ground between the road and the crown contained gaping tension cracks 1 to 5 dm wide and up to 5 dm deep. By May 25, the toe of the small landslide within the head at the left flank had extended to the northwest edge of the roadbed (Fig 4.15a).

A few cracks were observed on May 29 in the right flank, at Station 655, between the internal foot and the pipeline road. At that time, a measuring station was established for monitoring differential displacement across the right flank fault. On June 1, I observed cracks on the left flank, at Stations 780 and 800.

On June 2, Arvid Johnson observed fresh cracking and small wrinkles in soft mud in the pond at Station 150, which appeared to be evidence that the ridge between Stations 120 and 150 was growing. Early results of the measurements that document the growth of the ridge have been reported by Fleming and Johnson (in press), and all are reported in another chapter in this Dissertation (please see Chapter V).

About June 6, thrust faults in the internal toe, at Station 755, were making small bulges on the surface of the toe.

Arvid Johnson (written commun., 1987) estimates that three or fewer decimeters of strike-slip movement occurred to produce cracks at Station 580 in the right flank below the lower road crossing in 1983. Most of the movement had occurred before systematic measurements were started there. Between early May and June 2, 1984, there was an additional 0.62 m of differential displacement across the right flank fault at Station 580. Between June 2 and August 4, there was an additional 0.84 m of movement, so the total differential displacement in 1984, at the time the map shown in Plate 2 was made in August 1984, was 1.5 to 1.8 m. About 1.5 m of displacement transformed the right flank fault at Station 580 from a series of widely spaced cracks to a through-going, strike-slip fault surface.

Sliding during late April and early May 1984 lengthened the Aspen Grove landslide between Stations 600 and 900. By May 15, the flanks of the landslide could be traced continuously between the lower road crossing, near Station 570, to the old toe, near Station 740. Between Stations 740 and 900, the flanks were defined merely by a few cracks, such as those shown on the left flank between Stations 740 and 800 in Plate 2.

Measurements of differential displacement across the right flank at Station 790, between May 18 and August 4, 1984, indicate 7 to 8 cm of differential displacement, so the total amount of differential displacement responsible for the minor cracking was between 1 cm and 1 dm. Clearly, a few centimeters to a few decimeters of differential shearing displacement occur across a flank before there are obvious signs that a strike-slip fault is developing at depth. By the time the

FIGURE 4.15. Photographs of head area of the Aspen Grove landslide on May 25, 1984. (a) View to south, showing scarp where left flank crosses the road. Toe of the small internal landslide in foreground. (b) View to north, diagonal cracks in the road near the right flank. (c) View to west, diagonal cracks in the road near the right flank.

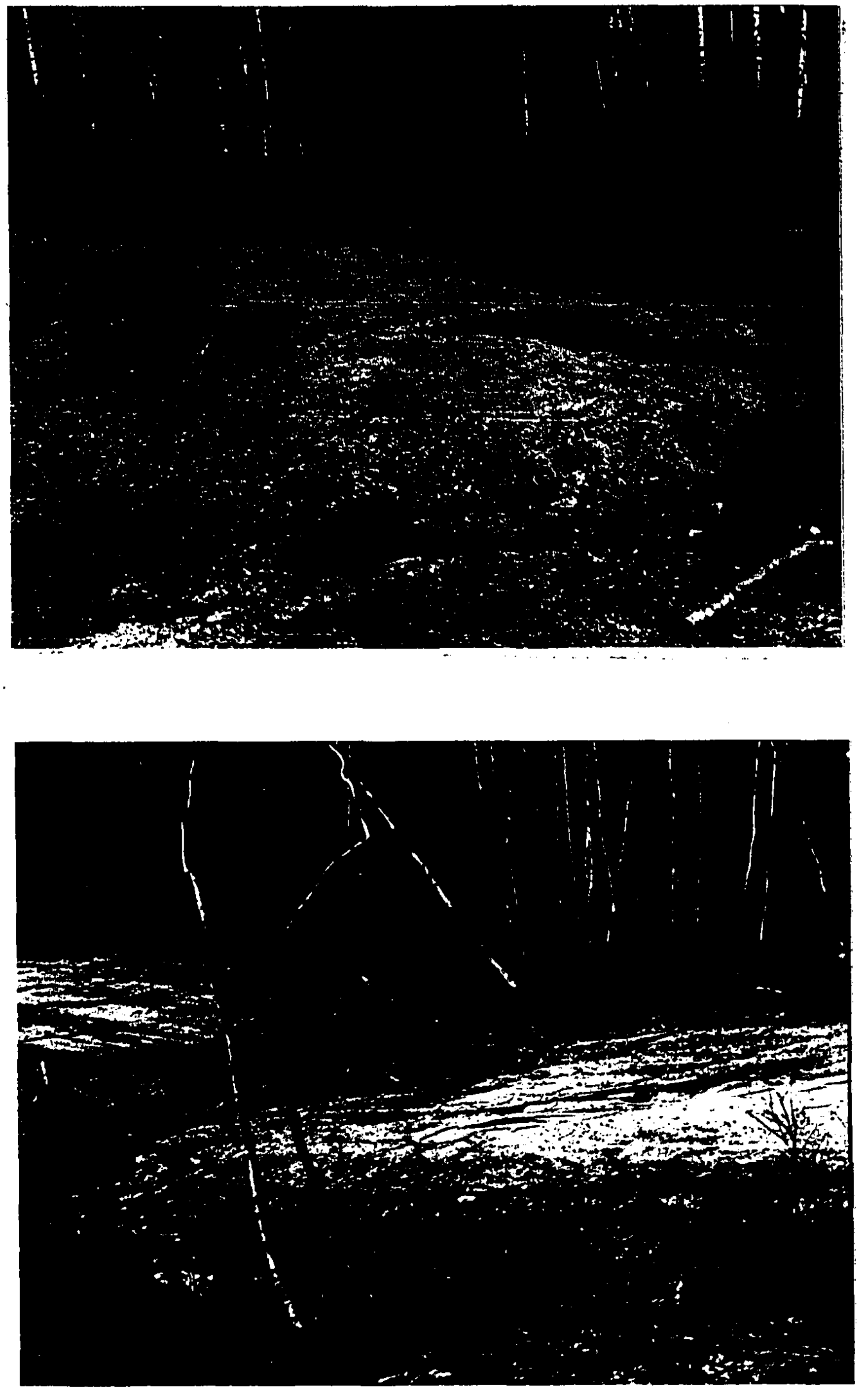

FIGURE 4.15b and 4.15c

map shown in Plate 2 was made, in August 1984, there had already been about 1 dm of differential shearing displacement.

More than a meter of differential shearing across flanks was required to transform crack arrays into through-going strike-slip faults in the flare area near the old foot. Both the left and right flanks of the landslide between Stations 600 and 700 (Plate 2) were represented by arrays of fractures in 1984. Some of the fractures were arranged en echelon and others were subparallel but misaligned fault segments, with associated tension cracks and small thrusts as described by Fleming and Johnson (in press). The amount of differential shear displacement measured across the left flank at Station 695 between May 19 and August 4, 1984, was about 2.7 dm. Sliding started earlier, and the total displacement probably was on the order of 4 dm. The amount of differential shear displacement across the right flank at Station 650 during the same time was 7 dm, so the total probably was 8 to 10 dm at the time the map was made (Plate 2). Thus, perhaps more than a meter of differential shearing was required to produce through-going fault surfaces in this part of the landslide.

Changes in the right flank fault in the pond area of Aspen Grove landslide between 1983 and 1984 are shown in Figure 4.13. The differential shearing across the right flank was about 1 m at the time the map for August 1983 (Fig. 4.13a) was made, whereas it was about 4 m at the time the map for 1984 (Fig. 4.13b) was made. The traces of fault segments, which defined the right flank in 1983, were misoriented 5 to 15° clockwise relative to the average trend of the right flank. The through-going fault surface which developed subsequently in 1984 was nearly straight, markedly simplifying the trace of the flank fault. Folds and thrusts formed at steps between fault segments in 1983 were severed in 1984 (Fleming and Johnson, in press, Fig. 25).

Similar simplification of flanks is shown in Figure 4.16, maps of the Aspen Grove landslide between Stations 330 and 430, at the distal end of the wedge area. The landslide had moved about 2 m in 1983 (Fig. 4.16a) and about 6 m in 1984 (Fig. 4.16b). In 1983, the right flank consisted of a series of long, left-stepping, subparallel, fault segments. Where the fault segments overlapped, thrusts and domes had formed. By August 1984, the right flank was a single shear break at the ground surface, except for major discontinuities at Stations 345 and 422, which persisted and grew.

The landslide was dormant between early August and mid-spring 1984-85 (see Chapter V, Kinematics of the Aspen Grove Landslide, for details of movement). During the early summer of 1985, several features of the landslide evolved. The shear zone on the right flank between Stations 100 and 200, which appeared at the ground surface in 1984 (Fig. 4.17a) as en echelon cracks and a few fault segments, became, in early 1985, a through-going flank fault (Fig. 4.17b). Where there had been gaps in the en echelon cracks and fault segments, pull-apart basins developed (Fig. 4.17a and 4.17b). Thus, even details of the flank fault were predetermined very early in its development.

The pull-apart basin at the large step at Station 200 deepened and more cracks formed around its perimeter. Also, a thrust fault began to form as an extension of the inner strike-slip fault, between the end of the strike-slip fault and the bottom of the pond (Fig. 4.17b).

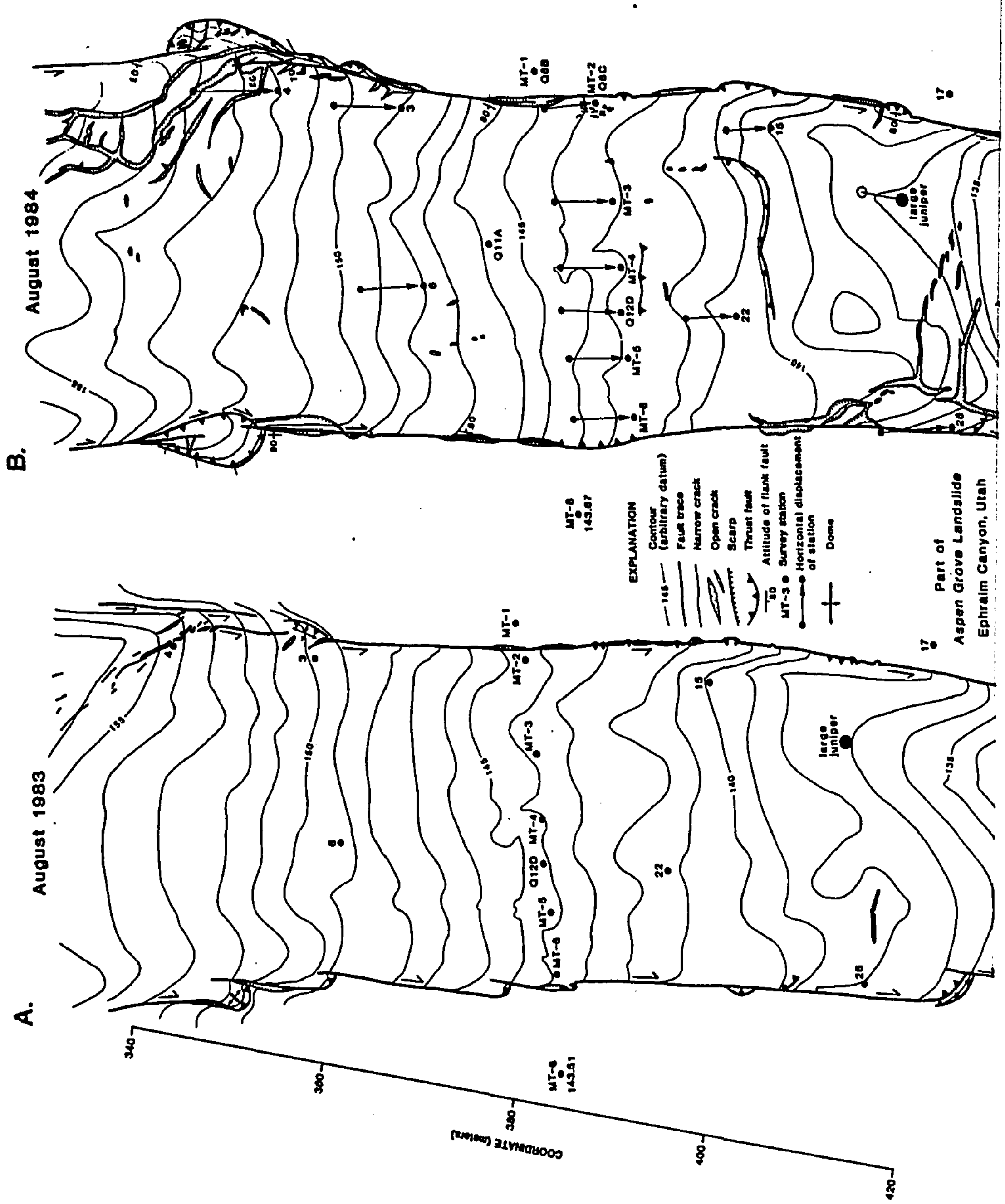

FIGURE 4.16. Maps of the wedge area between Stations 340 and 420 (by RWF and AMJ). (a) August 1983. (b) August 1984.

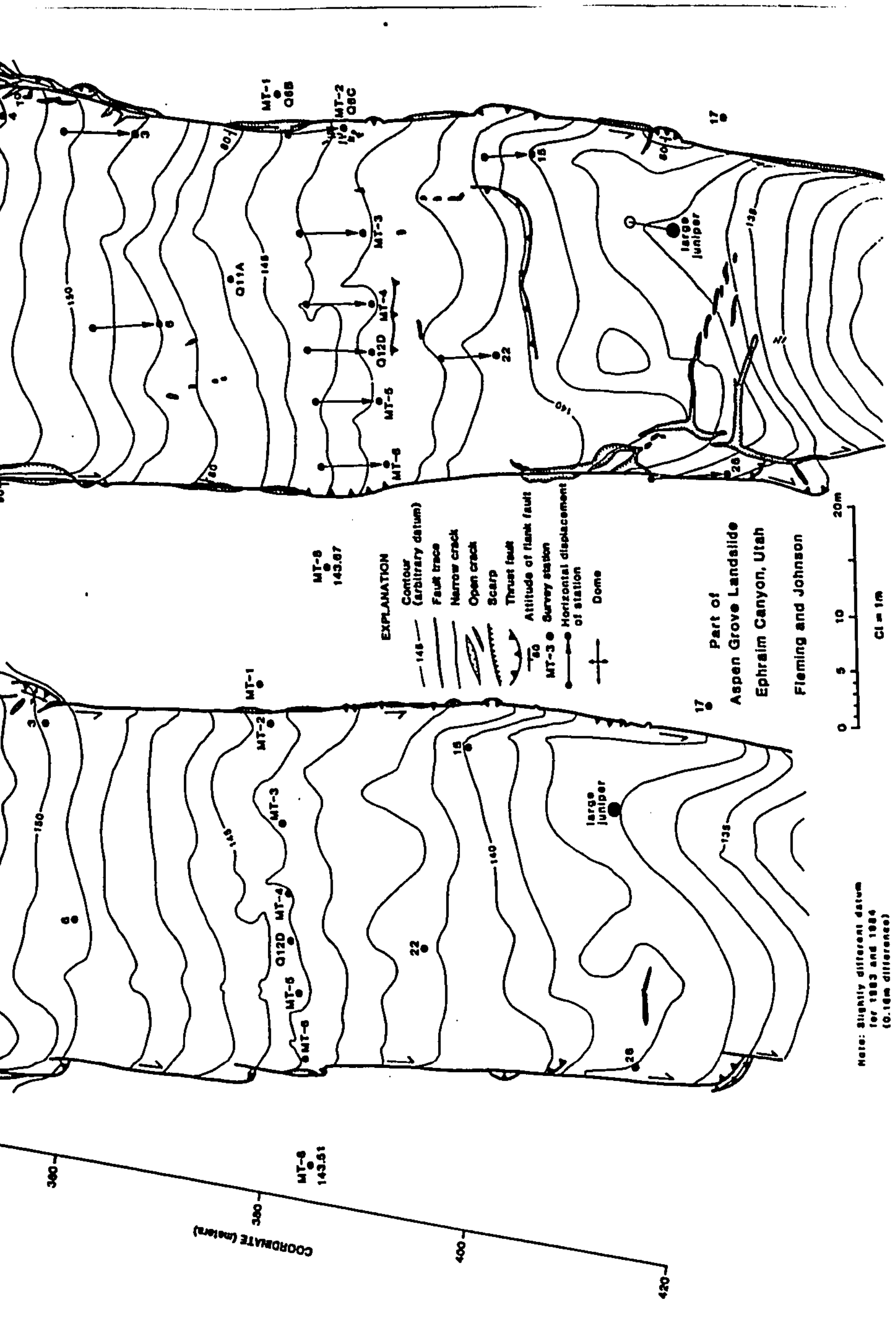

f the wedge area between Stations 340 and 420

gust 1983. (b) August 1984.

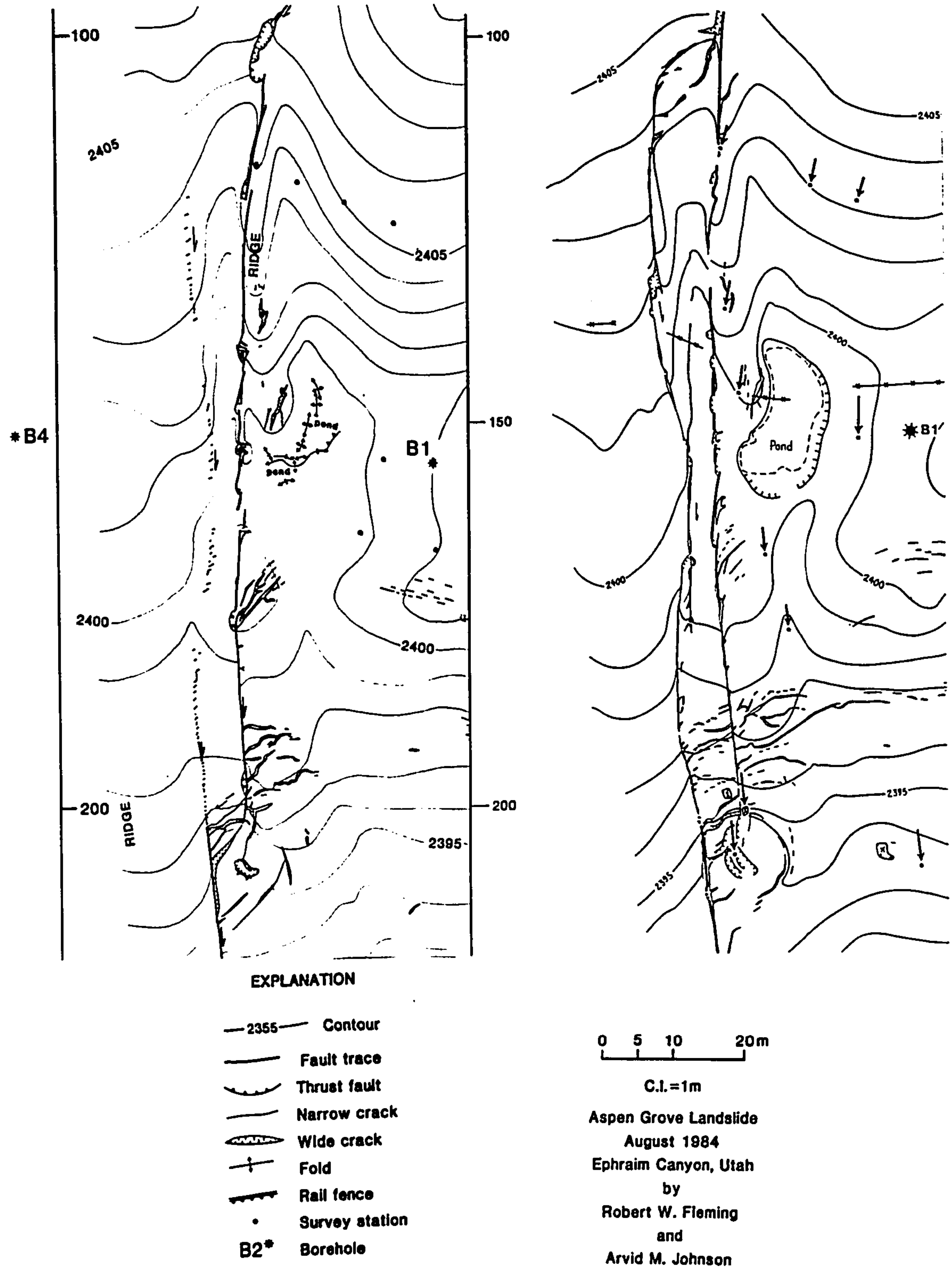

FIGURE 4.17. Maps of the right flank between Stations 80 and 220 (by RWF and AMJ). (a) August 1984. (b) August 1985.

Some other features formed that were not documented with maps but they are shown schematically in Plate 5. A set of echelon cracks formed an extension of the left flank fault into ground above the crown that existed in 1984. Thus, the head lengthened by about 50 m in 1985. The landslide also grew distally. Sets of echelon cracks formed and extended the right and left flanks of the landslide to points well beyond the pipeline road, and into the marshy area at location C-2, Plate 3, and increased the length of the landslide by about 100 to 200m. Discontinous toes formed in the marsh (location C-2 Plate 3).

In 1986, the landslide began moving even earlier than in previous years; it began moving in late March of 1986. A graben formed between the inner flank faults on the left and right sides near Station 175 (Fig. 4.18). Tension cracks were mapped in this area in 1984 (Fig. 4.19a) and some of them had subsequently become normal faults in 1985 (Fig. 4.19b). But the graben developed into a spectacular structure in 1986 (Fig. 4.20).

The landslide moved very little in 1987. It appears to be dormant now.

Inferences About Geometry of Basal Slip Surface

Nowhere along the length of the Aspen Grove landslide is the basal slip surface exposed. Nevertheless, we have been able to infer some gross geometrical properties of the slip surface by studying changes in structures at the ground surface and by some minor subsurface exploration.

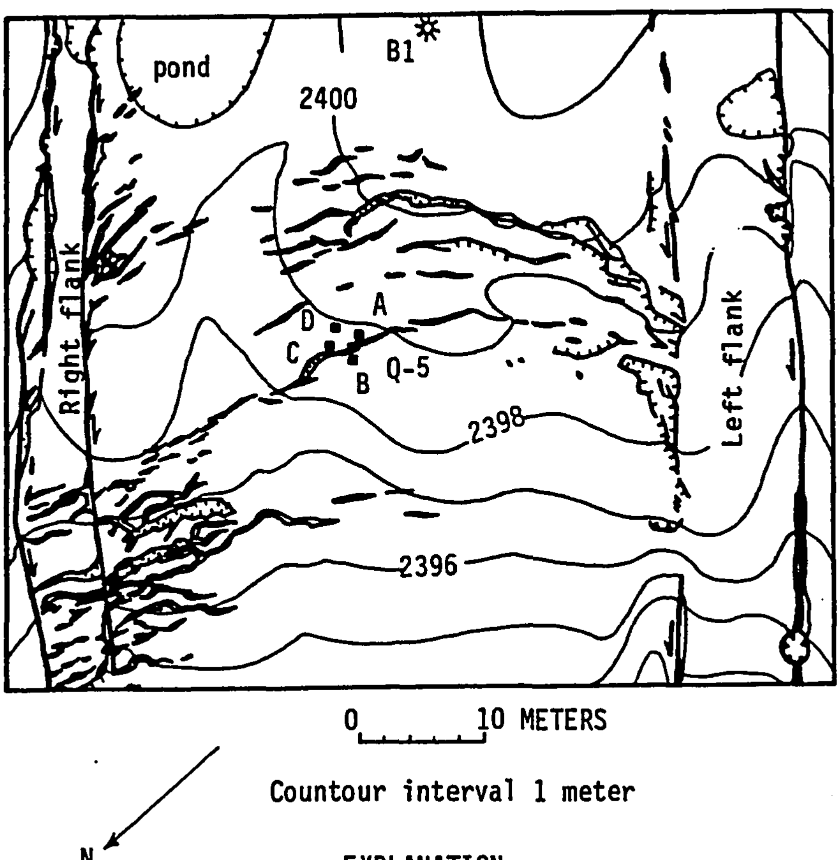

Countour interval 1 meter

EXPLANATION

2400 Topographic contour

Strike-slip fault

Scarp, hachures on downdropped side

Cracks

Thrust fault, sawteeth on upper plate

B1 Borehole

A Survey station (wooden stake)

FIGURE 4.18. Map of the graben near Station 170 in September 1986 (by RWF and AMJ).

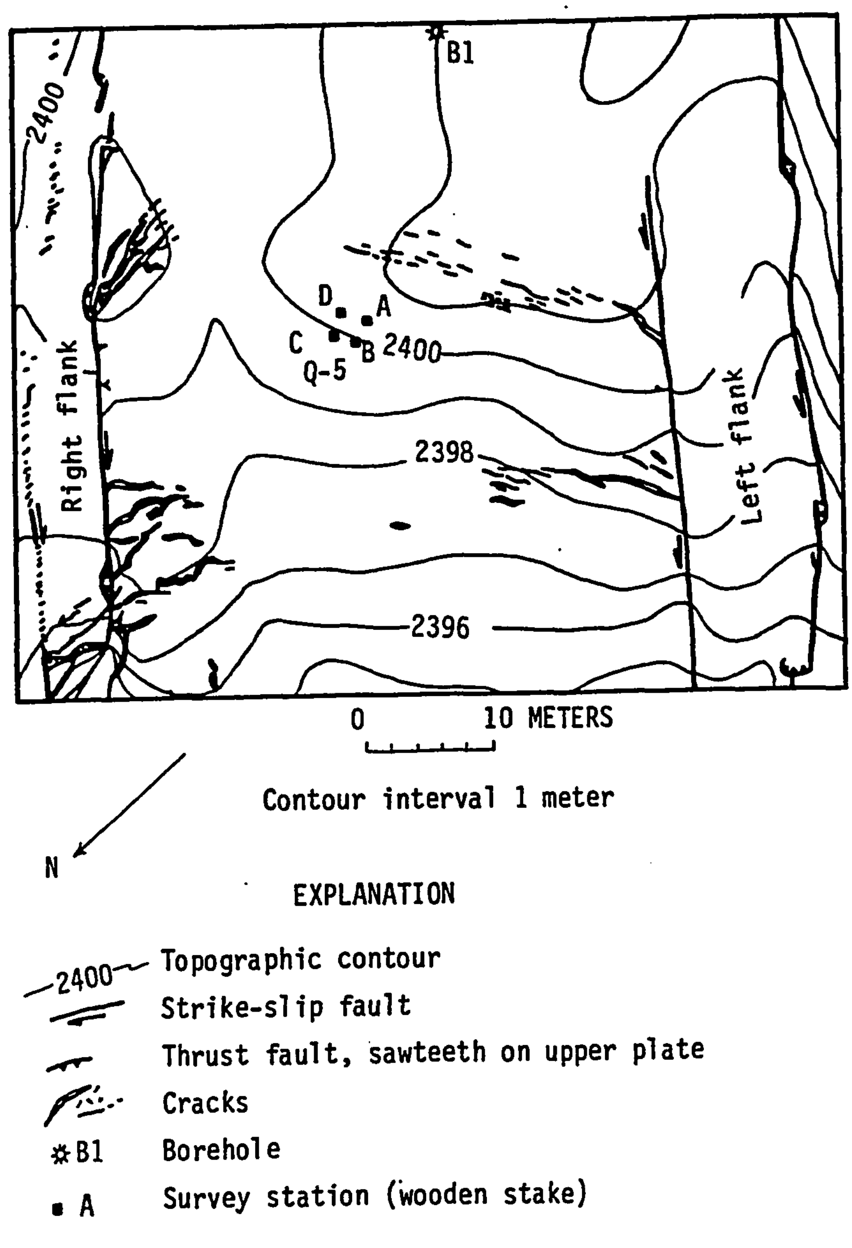

FIGURE 4.19. Maps of the area near Station 170 (by RWF and AMJ).

(a) August 1984, cracks are present where scarps later formed.

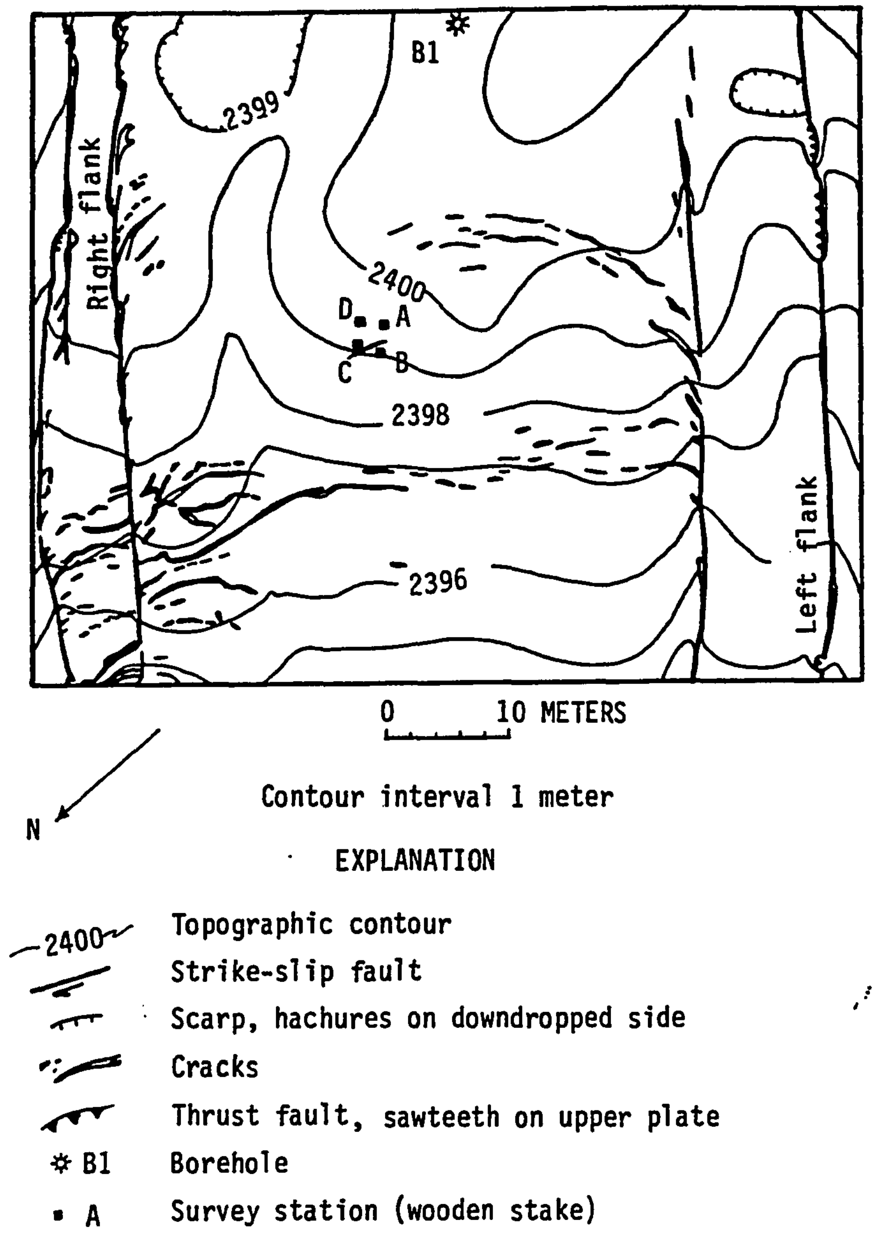

FIGURE 4.19 (b) August 1985, cracks and small scarps are present.

FIGURE 4.20. Photograph of the scarps on the proximal side of the graben at Station 170. (Photograph by Robert W. Fleming).

Our observations suggest that the failure surface resembles a long, shallow, sloping trough with a rectangular or broad U-shape cross section. The sides are steep to nearly vertical and undulate gently. The basal slip surface slopes approximately parallel to the ground surface (Fig. 4.21).

Depth to Basal Slip Surface

The thickness of the Aspen Grove landslide is known in only a few places. At Station 160, near midwidth (boreholes B1, B5, B6), the landslide is about 6 m deep.[7] The landslide is 55 to 60 m wide there, so the width-to-thickness ratio is about ten.

At midwidth in the landslide at Station 270, the basal slip surface is poorly known, only that it occurs at a depth of between 3.1 and 6.5 m.

One to two meters inside the right flank, at Station 245 (borehole B3, Plate 2), the failure surface is about 2.5 m deep. It is unclear, here, whether the failure surface is the flank fault or the basal shear

[7]Cables were anchored at various depths in holes B1 and B3 to locate approximately the depth of the failure surface. Cables anchored below the failure surface are pulled down the hole as the landslide moves downslope; consequently, their length above ground shortens. Cables anchored in ground above the failure surface are not pulled down the hole and, thus, their length above ground is unchanged by movement.

The idea for the use of cables in this way arose from comments in the Ph.D. dissertation of Karl Vonder Linden (1972), that movement of the upper part of the Portuguese Bend Landslide in Los Angeles was measured by a cable anchored below the slip surface that was pulled below ground as the landslide moved.

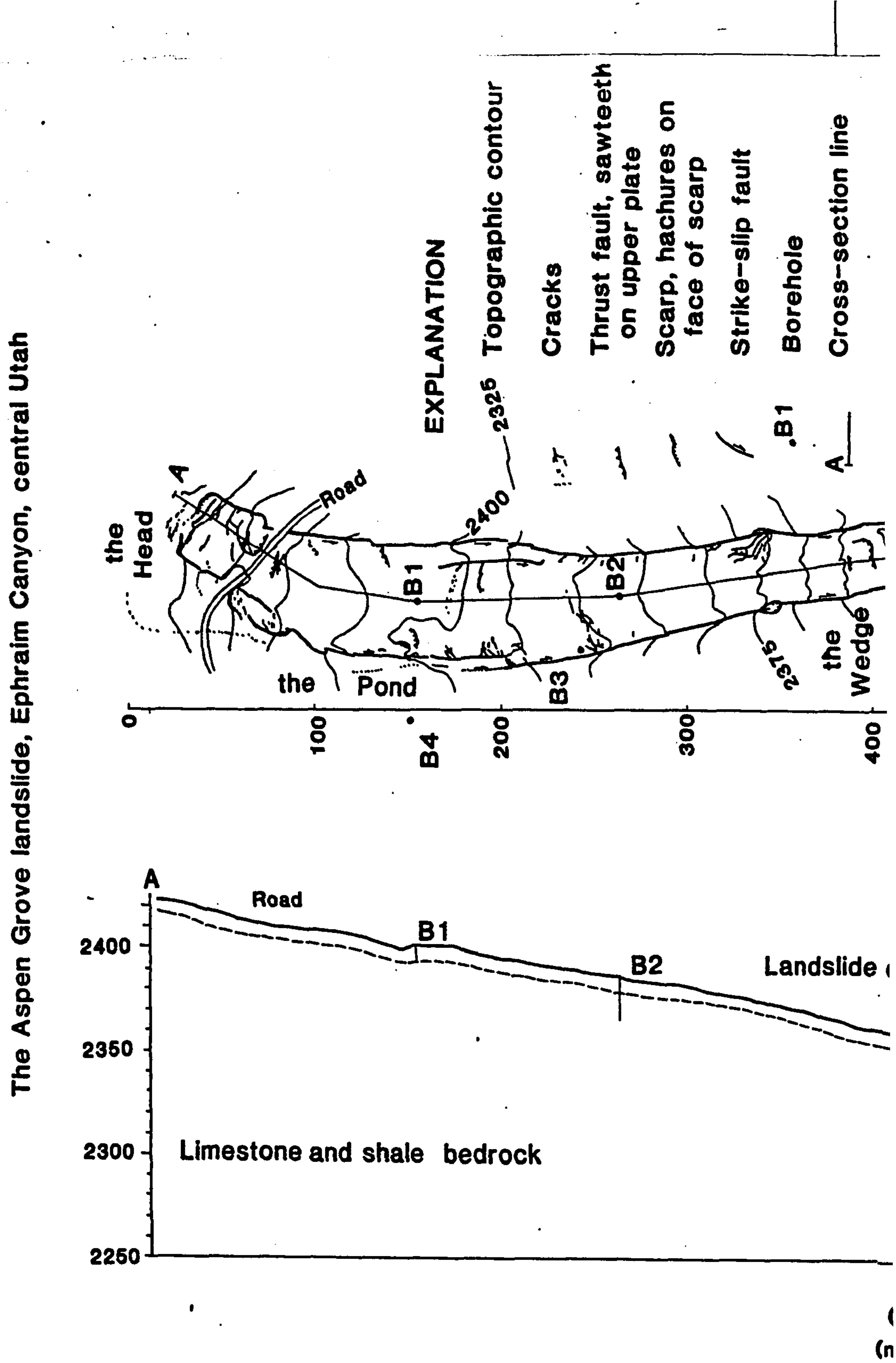

FIGURE 4.21. Map and cross section showing the approximate position of the slip surface of the Aspen Grove landslide. (map simplified from original by RWF and AMJ).

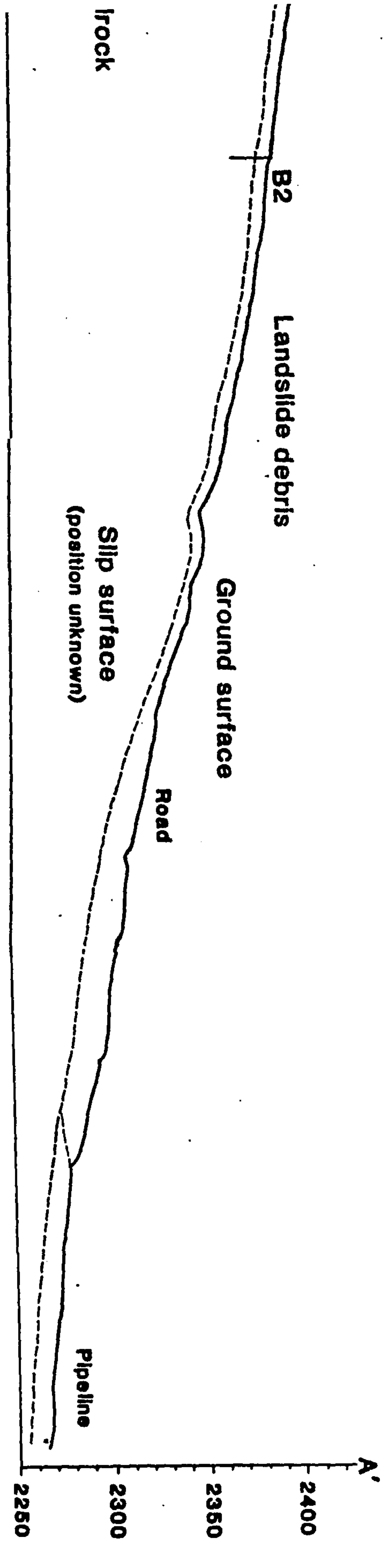
Cross section A-A'
Landslide debris
B2
Ground surface
Slip surface
(position unknown)
Road
Pipeline
A'
2250
2300
2350
2400
Elevation (meters)

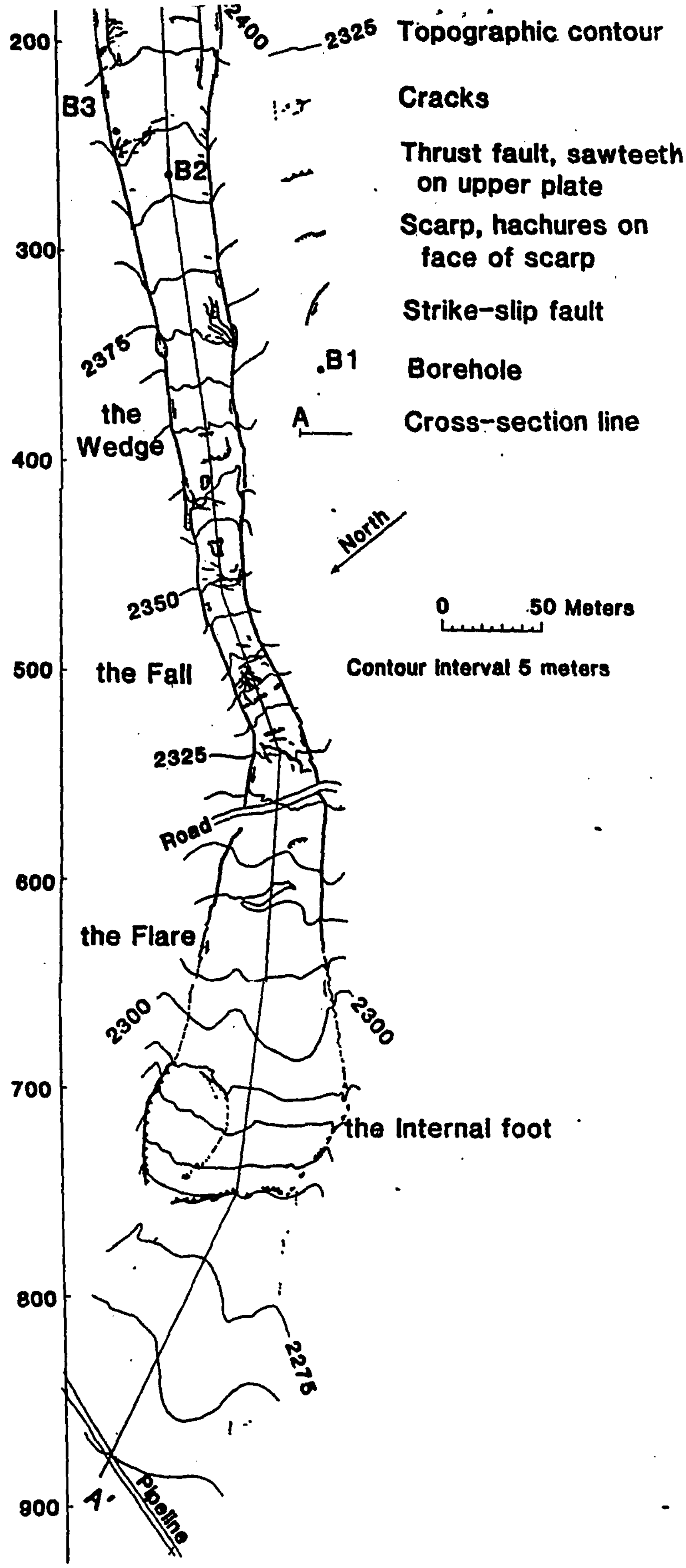
2325 Topographic contour
Cracks
Thrust fault, sawteeth on upper plate
Scarp, hachures on face of scarp
Strike-slip fault
.B1 Borehole
A Cross-section line
North
0 50 Meters
Contour interval 5 meters
B3
B2
2400
2375
2350
2325
2300
2275
the Wedge
the Fall
Road
the Flare
the Internal foot
Pipeline
A'
200
300
400
500
600
700
800
900
August 1984 by A.M. Johnson and R.W. Fleming

surface; I suspect it is the flank fault, in which case the average dip of the flank fault would be on the order of 45 to 60°.

Depths to the failure surface in the boreholes were determined by measuring the changes in lengths of cables in holes B1 and B3, knowing the depths of piezometers that were damaged by landslide movement, or by measuring the depths of observation wells disrupted by the landslide.

For example, consider B1. Five cables were anchored at different depths, (D1 through D5, Plate 4). Cables D1, D2, D3 and D4 were pulled down the borehole and their length above ground shortened by 2.7 m between August 1984 and July 1985, indicating that these cables were anchored below the failure surface. Cable D4 was anchored at a depth of 11 m. The others (D1, D2, and D3) were deeper. Cable D5 was not pulled down the hole, and was anchored at a depth of 4.9 m. Monitoring of the cables, therefore, indicated that the failure surface is at a depth between 4.9 (D5) and 11 m (D4).

Now, at B1 we also had an observation well of PVC pipe for measuring water levels. It was open to 12.5 m depth in August 1984. In April 1985, the pipe had been sheared and one could probe it to a depth of only 5.95 m. On this basis, I infer that the failure surface is between 6 and 11 m deep; I assume that it is 6 m deep.

Undulations in Basal Slip Surface

Some undulations on the basal failure surface are reflected in topographic features at the surface of the landslide. These features are characterized by the fact that they remain in place as the landslide debris moves by. Examples are the pond along the right flank, at

Station 160; the dome on the right flank and the locus of tension cracks that extend from the left flank to midwidth at Station 175; the dome or ridge along the right flank at Station 260; the thrust faults on the right flank and the tension cracks and stepping flank fault on the left flank at Station 350; and the depression in the center of the landslide at Station 440.

In contrast is the pull-apart basin at coordinate 200 on the right flank, which, during 1984 through 1986, moved distally with the landslide. It almost certainly is a result of a temporary step in the flank fault in the right side of the landslide (Fleming and Johnson, in press).

Bob Fleming (oral commun., 1984) noted, especially, that the locus of the pond at Station 160 is essentially fixed. Each year, black soil from the bottom of the pond and water-loving grass from the edge of the pond migrated a few meters downslope with the landslide mass. He infered that the pond represents a low in the failure surface.

Analysis of displacements of stakes, indeed, suggests that there is a trough in the failure surface trending diagonally roughly N-S from near the pond across to the left flank of the landslide. It suggests a ridge immediately downslope, trending in the same direction (Robert Fleming and Arvid Johnson, unpublished data).

Similarly, the dome and tension cracks on the right flank at Station 250 appear to represent a half-dome on the basal failure surface that extends across about one third of the landslide. The pattern of tilting of aspen trees on the dome is consistent with movement of the slide mass over a half-dome (Chapter V).

Ground-water Levels in Upper Part of Landslide

Snow meltwater infiltrating at the surface of the landslide is almost certainly the main source of water in the landslide. When we visited the landslide in May 1984, snow was still melting on the surface of the landslide. Meltwater flowed everywhere across the surface of the landslide, in numerous rivulets. Shallow holes, about 1 m deep, dug into the internal toe and at the lower road crossing, to emplace pressure cells, quickly filled with water flowing from the walls of the holes. Cracks and hollows contained ponded water.

A few observations suggest that the landslide is a conduit for ground water, and this may be a reason the entire landslide mobilizes essentially simultaneously[8] in spite of the fact that its length is two orders of magnitude greater than its thickness and more than an order of magnitude greater than its width. Just as the walls of the landslide channelize the landslide, the walls and the trough-like topography on the surface of the landslide channelize the meltwater from the head to the foot. Surface channels drain away from the landslide only in the area of the old foot. Even there, channels bring the water back onto the sliding ground beyond the internal toe (Plate 3).

Timing of the landslide activity suggests that water derived from the surface controlled the activity of the landslide. The beginning of movement coincided approximately with the spring thaw, which suggests that infiltration of surface water through cracks in the landslide

[8]Actually, the main body of the landslide started moving a few days or a few weeks before the foot of the landslide, and the foot generally stopped moving weeks before the the main body (please see Chapter V).

surface was the primary cause of pore pressure increases at the basal failure surface that enabled movement to start in 1984, 1985 and 1986. The end of movement coincided approximately with the drying up of ponds on the surface of the landslide.

Water-level measurements during parts of 1985 and 1986 in six boreholes, B1 through B6, are shown in Figures 4.23 - 4.28. Water levels were measured directly in boreholes B1, B2 and B3, and water levels were calculated from piezometric measurements made in boreholes B4, B5 and B6.

The measurements show that, at three locations within the upper part of the landslide, between Stations 150 and 260, the water level was always within 3 m of the ground surface during April through August 1985 and during February through September 1986 (Figs. 4.23, 4.24, and 4.25).

The best record exists for B1, at Station 160, where water level fell 1.2 m from a maximum height of about 0.3 m below the ground surface during May to about 1.5 m below the ground surface when movement stopped in 1985.

It is interesting to note that sliding started in April 1985 when the water level in B1 was relatively low, at a depth of 2.5 m below the ground surface (Fig. 4.23). Thus, water level was lower when sliding started than when it stopped (Fig. 4.24).

According to the scant data, the water level was at a depth of about 1 m when movement began in 1986. Again, the water level appears to have reached a maximum during May (Fig. 4.23).

FIGURE 4.22. Photograph of leaning trees on the dome (view to north).

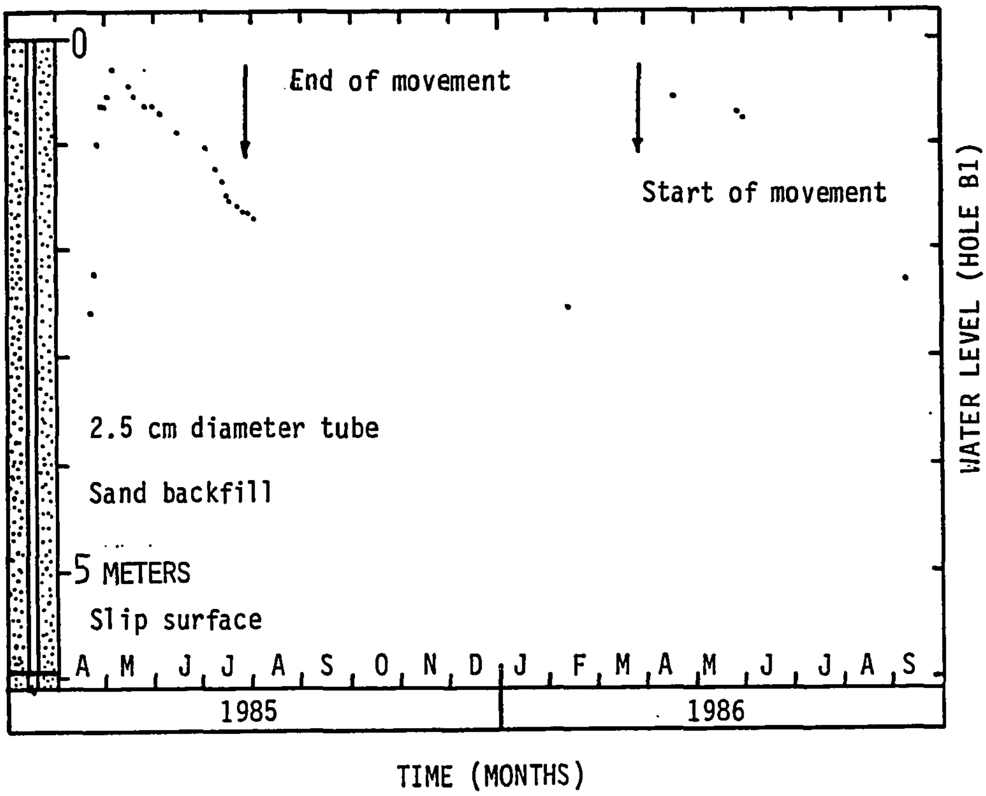

FIGURE 4.23. Water levels observed in hole B1.

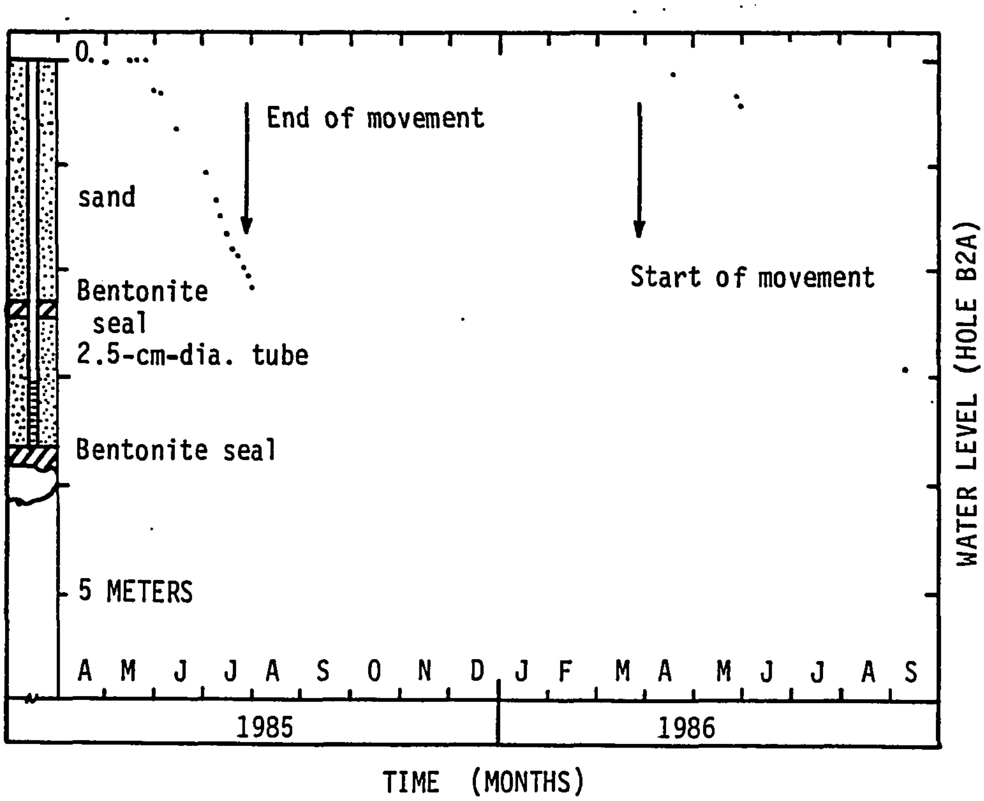

FIGURE 4.24. Water levels observed in hole B2A.

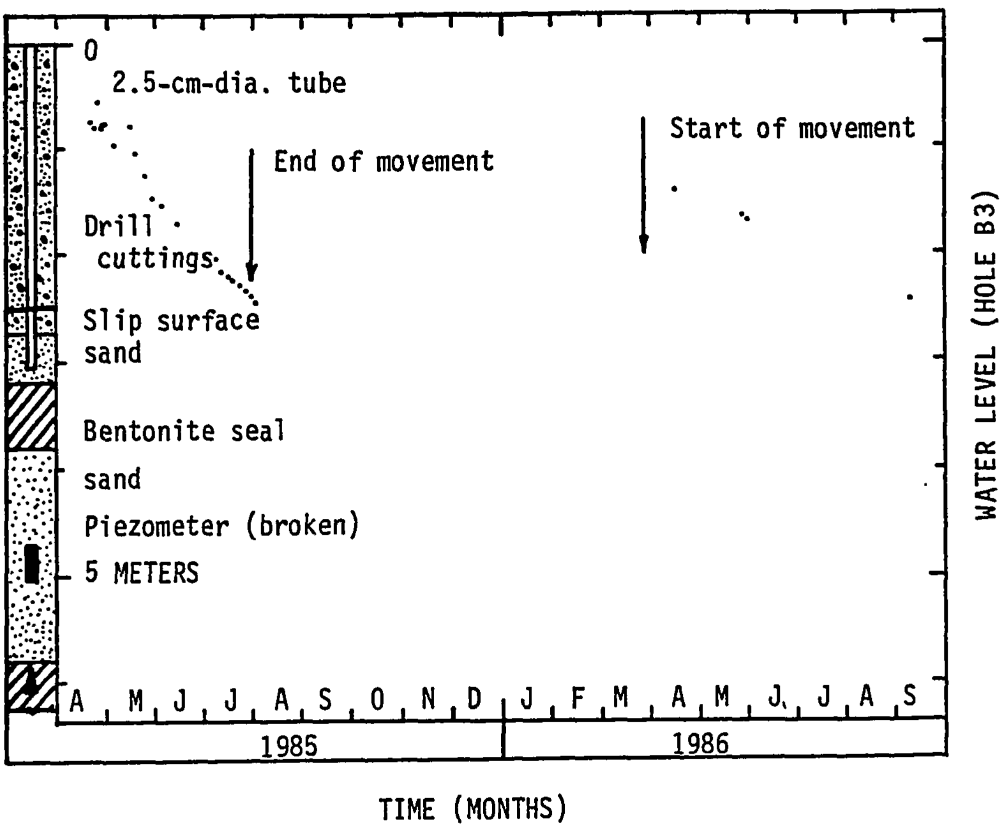

FIGURE 4.25. Water levels observed in hole B3.

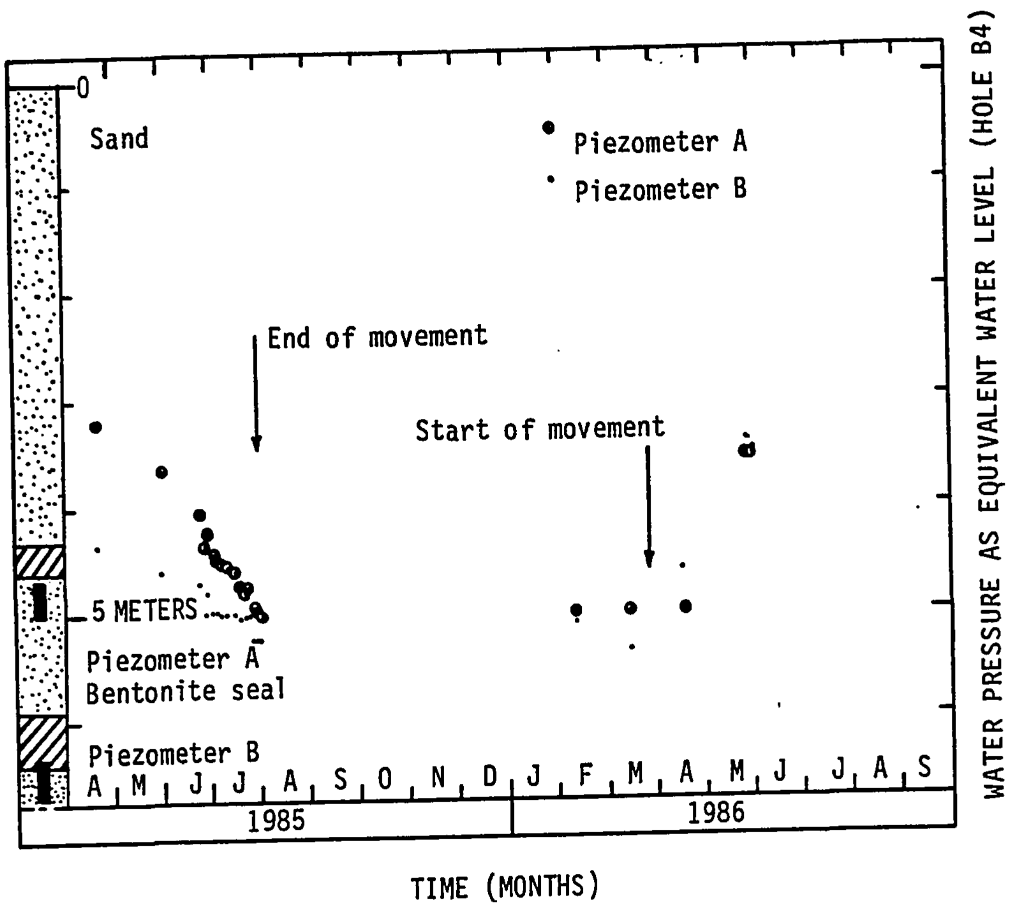

FIGURE 4.26. Water levels computed from pore-pressure measurements in hole B4.

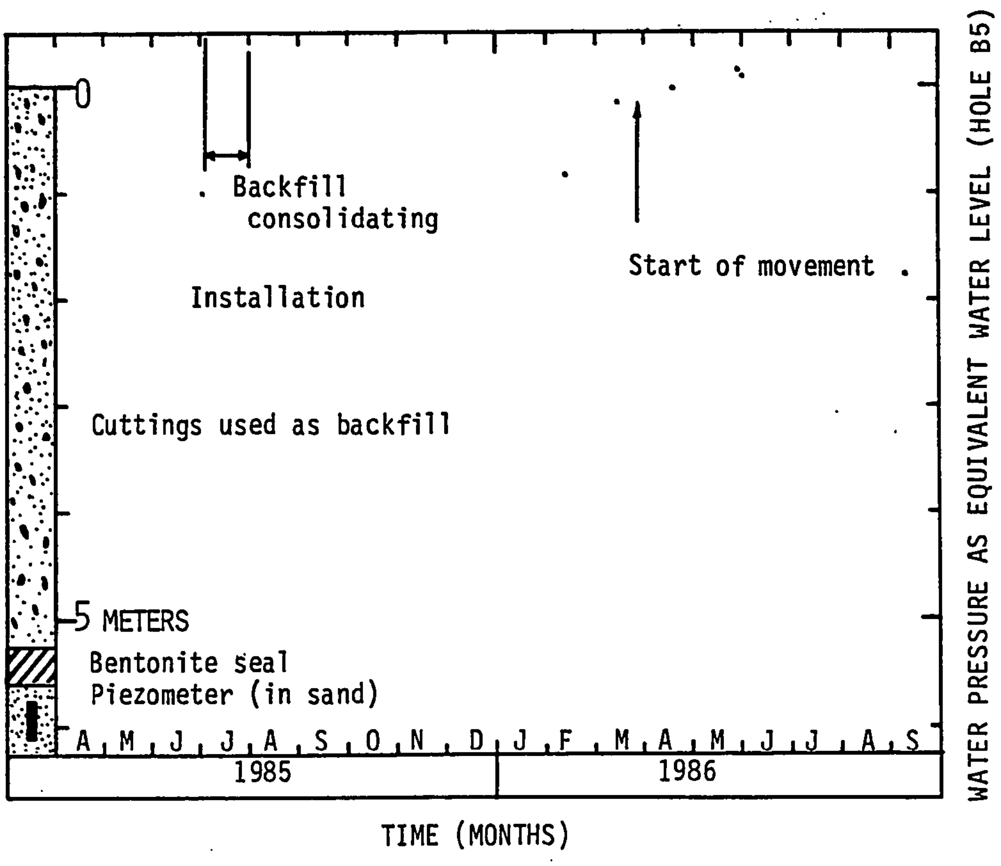

FIGURE 4.27. Water levels computed from pore-pressure measurements in hole B5.

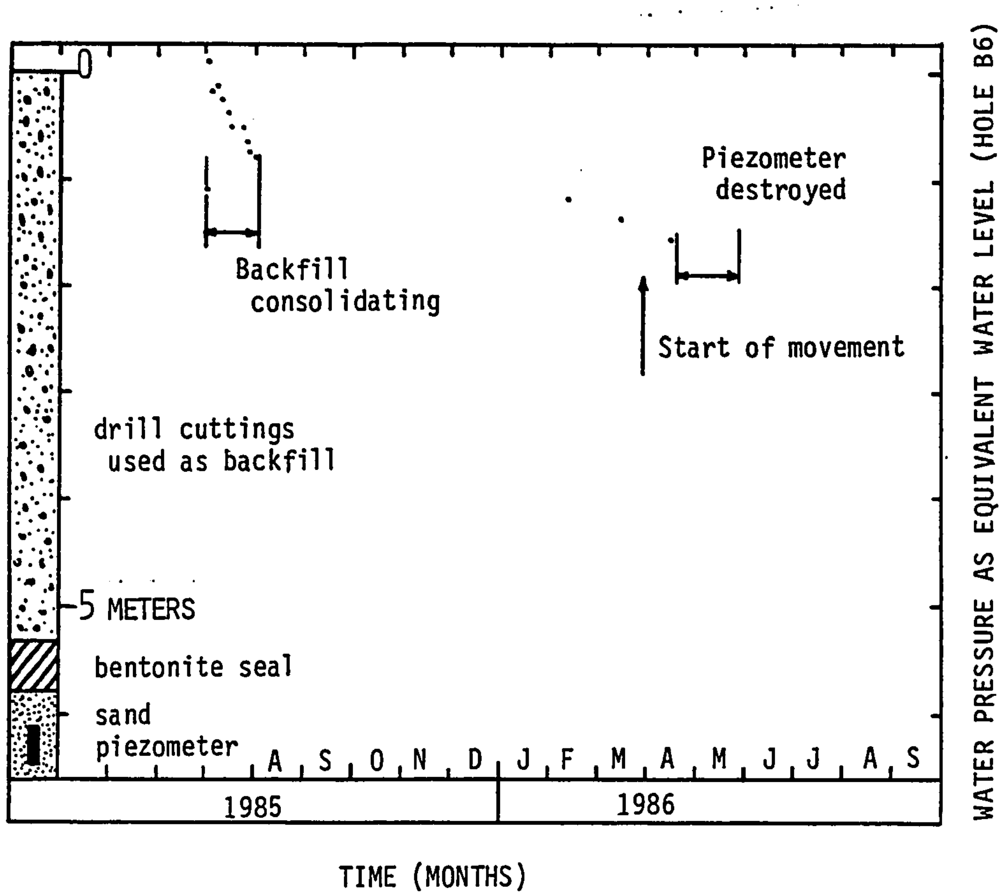

FIGURE 4.28. Water levels computed from pore-pressure measurements in hole B6.

In contrast, the water level in the one borehole in stable ground outside the landslide, B4 (Fig. 4.26), was always low, at depths greater than 3 m below the ground surface. Water levels ranged from 3 to 5 m below the ground surface during the period of measurement (Fig. 4.26).

Figure 4.29 shows a cross section of the inferred water level in ground on either side and within the upper part of the Aspen Grove landslide while the landslide was active, according to the measurements.

The average velocity of the Aspen Grove landslide increased and decreased with the water level in the landslide debris. Figure 4.30a shows average velocity determined by measuring the change in length of a cable anchored in bedrock beneath the landslide at borehole B1, Station 160. The average velocity peaked at about 10 cm per day in early May, when the water level peaked at a depth of about 0.2 dm below the ground surface. The water level was much lower when the landslide started moving, in April, than it was when the landslide stopped moving, in June.

Figure 4.30b shows velocities, determined nearly continuously with an extensiometer across the right flank of the landslide at Station 270, and water levels determined in borehole B2A, nearby. Again, the times of high velocities generally correlate with times of high water levels. There are, however, many variations in velocity that occurred when the water level was at the ground surface, during April and May.

Similar relations between water levels and velocities have been reported by others (Terzaghi, 1950, p. 120; Rybar, 1968, p. 140; and Japan Society of Landslide, 1980, p. 9).

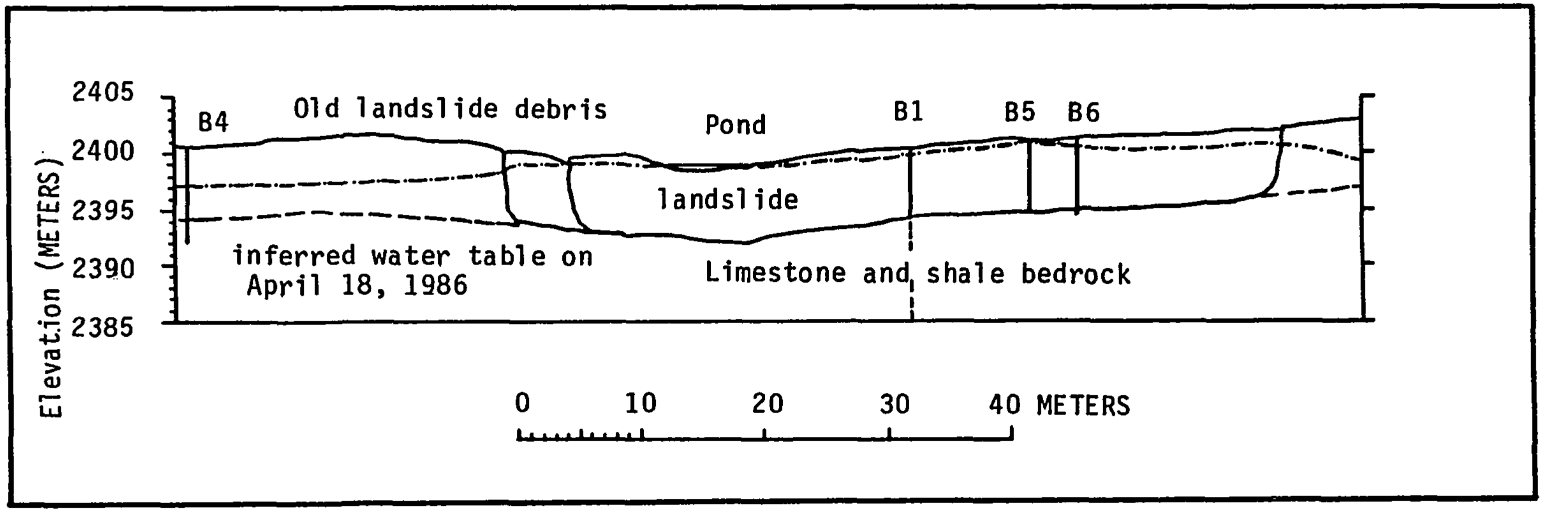

FIGURE 4.29. Transverse cross section through the Aspen Grove landslide along a line connecting holes B4, B1, and B5. Approximate water level on April 18, 1986 in the landslide, and in ground outside the landslide is indicated by the dashed and dotted line.

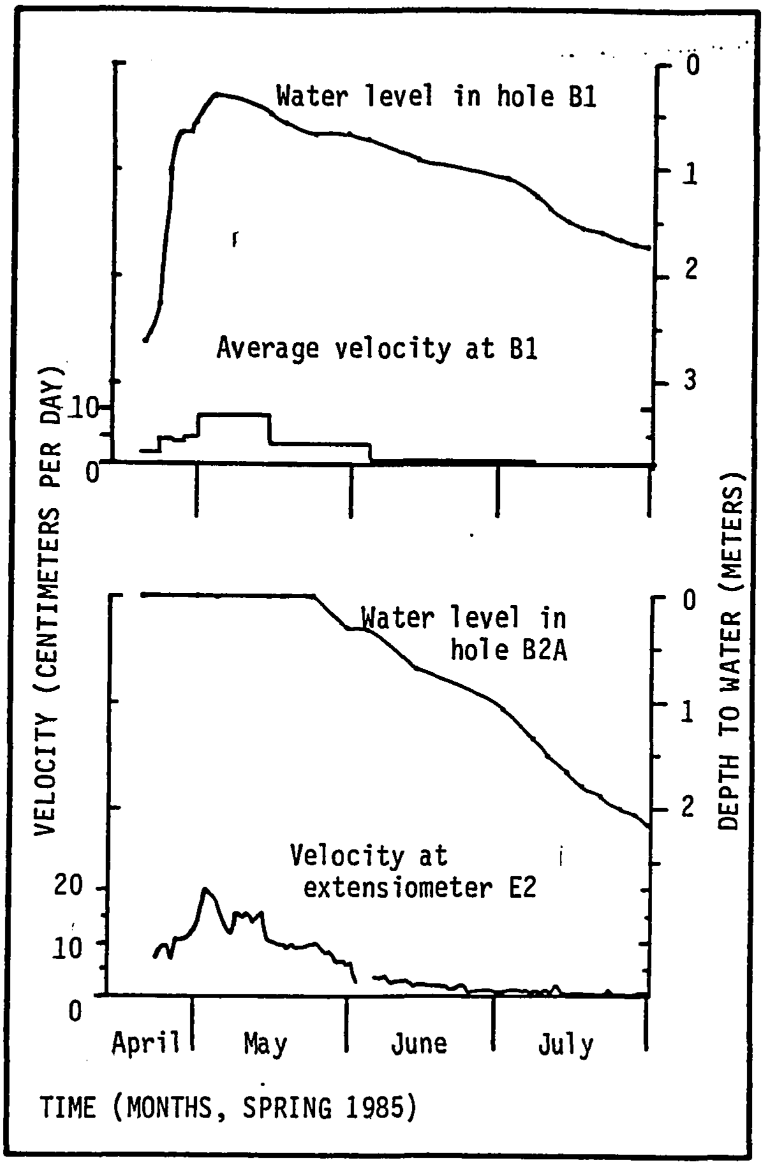

FIGURE 4.30. Graphs comparing water levels in the landslide to velocity of the landslide. (a) Water level in hole B1 and average velocity of the landslide as determined from the change in length of cables anchored below the slip surface in hole B1. (b) Water level at hole B2 and daily velocity at a recording extensiometer nearby.

A possible explanation for the relationship between velocity and water level in the landslide might be found in a theory for the movement of landslides on uneven slip surfaces (Chapter VII). The theory indicates that a resisting force that helps keep the landslide from accelerating to catastrophic speeds results from rate-dependent deformation of the landslide debris above the slip surface. The rate dependent resisting force is a function of the velocity of the landslide.

Stability Analysis

For the upper part of the Aspen Grove landslide, I have some information about the strengths of the landslide debris, the water pressures at the times of sliding, and about the subsurface geometry of the landslide. I can use this information to analyze, in an elementary way, the instability of the landslide.

The upper part of the landslide is divided into blocks for the analysis (Fig. 4.31) and boundaries of the blocks are determined by the geometry and structure of the landslide. Boundaries between blocks were chosen where the slope of the slip surface (as inferred from the slope of the ground surface along section A-A', Fig. 4.21) changes noticeably. The boundaries between blocks are perpendicular to the axis of the landslide, except the distal boundaries of blocks 3 and 4 (Fig. 4.31) which are parallel to a ridge and trough inferred to exist on the slip surface.

Structural features coincide with many of the boundaries between blocks. Tension cracks define the proximal boundary of block 1.

Tension cracks, which later developed into scarps occurred at the distal boundary of block 4 (Fig. 4.31). Thrust faults occur at the distal boundaries of blocks 1, 3, and 7. A strike-slip fault and a tension crack bound a landslide element on the left flank between Stations 180 and 240 that was excluded from block 5, because it was apparently uncoupled from block 5, by the fault and crack.

The upper part of the landslide (Stations 0 to 400) was analyzed in two sections assumed to be uncoupled from each other. The first section included the head and pond areas (blocks 1, 2, 3, and 4, Fig. 4.31). Normal stress on the distal edge of block 4 was assumed to be zero because of the presence of tension cracks. The second section was the wedge (blocks 5, 6 and 7, Fig. 4.31). Normal stress at the distal edge of block 7 was assumed equal to the major principal stress in the passive state, because internal thrust faults formed there.

The following assumptions were made in order to calculate the driving and resisting forces in the blocks. Blocks 1, 2, 3, and 4, have an average thickness, $\underline{t}$, of 6 m, and blocks 5, 6, and 7, have an average thickness of 5 m. Flank faults are vertical. The basal slip surface is parallel to the average slope of the ground surface in each block, as determined from profile A-A' (Plate 2). The water table is at the ground surface, with flow parallel to the slope. The saturated unit weight of the soil, γ_t, is 20.5 kN/m^3 and the buoyant unit weight, γ_b, is 10.7 kN/m^3 (average of three laboratory determinations on sample 630).

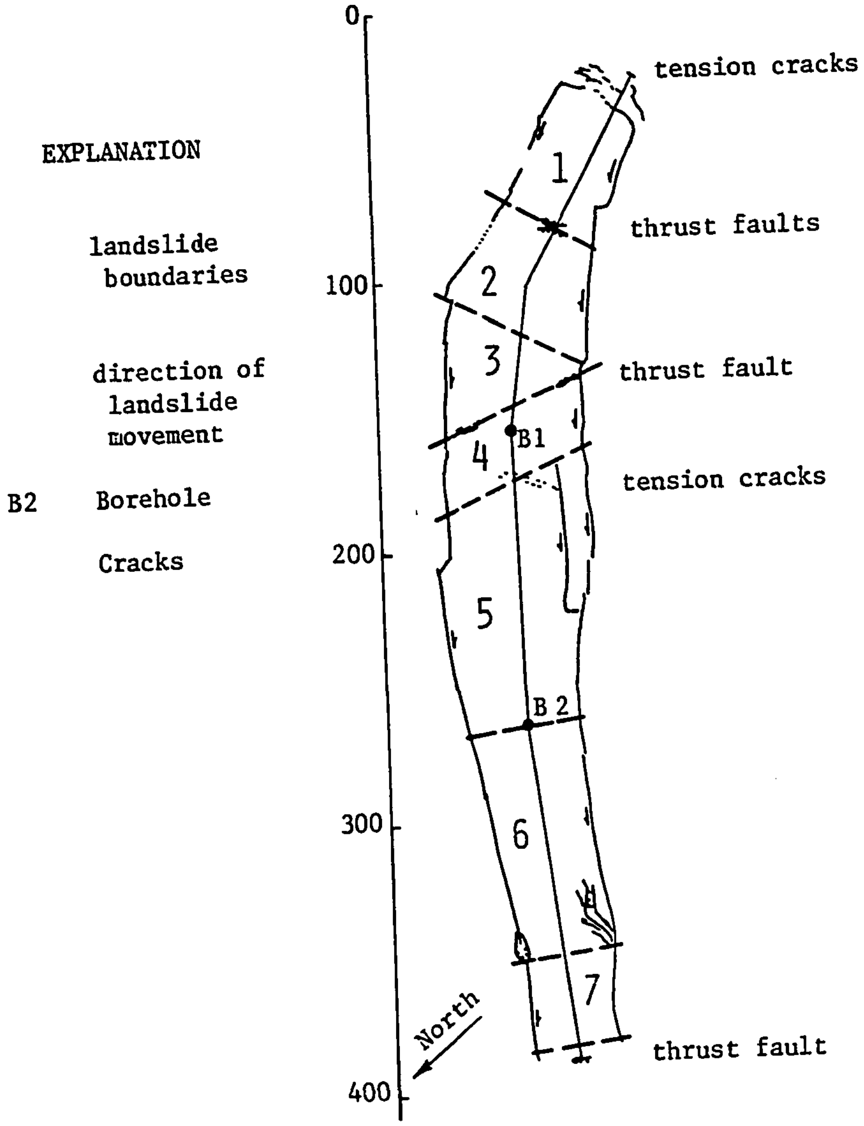

FIGURE 4.31. Map showing boundaries of blocks used in stability analysis of the upper and middle parts of the Aspen Grove landslide.

The shear strength, τ, is related to the effective normal stress, σ_n, by the formula

$$\tau = 0.282\ \sigma_n, \tag{4.1}$$

which is the equation describing the lower bound estimate of the residual shear strength of the soil (Fig. 4.10).

The driving force of each block, D, is the component of the weight of the block that is parallel to the slip surface,

$$D = t\gamma_t A \sin(\iota) \tag{4.2}$$

In equation 4.2, A is the area of the basal slip surface, and ι is the slope angle of the slip surface.

The resisting force on the basal slip surface, B, is the product of the shear strength and the area of the slip surface,

$$B = 0.282\ t\gamma_b A \cos(\iota). \tag{4.3}$$

The resisting force on the flanks, F, is the product of the average shear strength and the area of the flank.

$$F = (1/2)\ t^2\gamma_b L \cos(\iota). \tag{4.4}$$

In equation 4, L is the length of the flank.

The resisting force, P, due to the the passive failure, (distal end of block 7, Fig. 4.31) is approximately equal to the vertical normal stress plus twice the shear strength of the soil,

$$P = ((1/2)\ t\gamma_b + 0.282\ t\gamma_b)\ tw. \tag{4.5}$$

The width of the landslide is denoted by w in equation 4.5.

Resisting force due to convergence of the channel in the wedge is approximately the product of the mean stress with the area at the distal boundary of block 7. In a plastic solid being forced through a channel that converges by a few degrees, with the shear stress at the boundaries equal to the shear strength (Hill, 1950) the slip lines and the maximum shear stress trajectories are approximately parallel and perpendicular to the axis of the channel. Consequently the normal stress parallel to the axis of the channel is equal to the mean stress. The difference in the normal force at two cross sections of the channel is the resisting force offered by convergence of the channel. The normal stress on the proximal end of the wedge is assumed zero, consequently the resisting force due to convergence is the product of the mean stress with the area of the distal end of block 7.

The resisting force due to convergence, C, is computed by assuming that the mean stress in the soil is equal to the vertical normal total stress. However, part of the total stress is accounted for in the passive resistance (equation 4.5). The remainder of the resisting force, C*, is accounted for by the difference in the total stress and the effective stress. Thus,

$$C^* = (1/2)\ (\gamma_t - \gamma_b)\ t^2 w \tag{4.6}$$

Results of the analysis on the head and pond area are listed in Table 4.2. The total resisting forces are about 25 percent greater than the driving forces, which suggests that the residual strength estimated by the direct shear tests is about 25 percent too high. A friction coefficient of approximately 0.222 is consistent with the results of the analysis.

The analysis (Table 4.2) indicates that blocks 1 and 3 drive blocks 2 and 4. Blocks 1 and 3 have excess driving force, and blocks 2 and 4 have excess resisting force. Resisting force in block 4 is so great that it buttresses blocks 1, 2 and 3. The presence of compressional features (thrust faults) at the distal edges of blocks 1 and 3 are consistent with the inference that they drive blocks 2 and 4.

The results of the analysis of the wedge (blocks 5, 6, and 7) are summarized in Table 4.3. The driving forces are about 5 percent less than the resisting forces in the wedge, which is an acceptable level of error.

The analysis indicates that block 5 drives block 6, and that block 7 drives material distal to it. Blocks 5 and 7 have excess driving force (Table 4.3). Excess resisting force in block 6 and resisting force at the distal end of block 7 due to the passive failure and convergence of the flanks balance the excess driving forces of blocks 5 and 7.

TABLE 4.2 Stability Analysis of Upper Part of Landslide

Element	Slope angle		area (m^2)	thickness (m)	Driving force (kN)	Shear strength (kPa)	Resisting force (kN)
1	12°		2068	6	52,885	17.71	36,624
2	5.5°		2155	6	25,405	18.02	38,833
3	12°		1073	6	27,440	17.71	19,003
		flank	237			9.05	2,146
4	-4°		1212	6	-10,399	18.06	21,891
		flanks	263			9.03	2,375
TOTAL					95,331		120,872

Resisting forces contributed by the flanks are small compared to the resistance on the basal slip surface. The flanks in the head and pond area contributed only about 4 percent of the resisting force (Table 4.2). The flanks in blocks 1 and 2 contributed no resisting force because the flanks in the head area of the landslide diverge. The flanks in the wedge area contributed about 10 percent of the resisting force (Table 4.3). A few percent of the total resisting force are also contributed by convergence of the flanks in the wedge area.

The uneven distribution of driving and resisting forces in the upper part of the landslide suggests that failure might have occurred at several locations and spread laterally. Steeper parts of the landslide might have become active first. After displacement of a few millimeters, steeper parts began pushing on flatter parts of the landslide.

The entire landslide could have mobilized in a few days at the end of May, 1983. Flank faults of the Manti landslide, near Manti Utah, lengthened at rates of a few meters per hour (Robert Fleming, pers. comm. 1987). If four to five steeper parts of the landslide became active at about the same time and failure spread at 1 to 2 m per hour, then the failures could spread and link to form the 600 m long landslide in about three days.

Mobilization of the residual strength might have occurred by at least two different mechanisms. The apparent antiquity of the landslide suggests that preexisting slip surfaces might have been reactivated. Skempton and Petley (1967) determined the shear strength of slip surfaces presumed to be dormant for hundreds of years was only slightly

TABLE 4.3 Stability Analysis of Middle Part of Landslide

Element	Slope angle		area (m^2)	thickness (m)	Driving force (kN)	Shear strength (kPa)	Resisting force (kN)
5	9.4°		4477	5	74,949	14.9	66,707
		flanks	921		---	7.4	6,815
6	8.3°		3395	5	50,234	14.9	50,585
		flanks	851		---	7.5	6,383
7	14.7°		1064	5	27,675	14.6	15,534
		flanks	307		---	7.3	2,241
		distal end	167			7.3	10,964
TOTAL					152,858		159,229

greater than residual and that displacements of 1 to 2 mm reduced the shear strength to the residual strength. Progressive failure (Bjerrum, 1967), the process of forming slip surfaces in previously unfailed material, can also account for the failure. Calculations using a simple model similar to that derived by Palmer and Rice (1973), and assuming soil having stress-displacement relations of sample 630 (Fig. 10) indicate slip surfaces as short as 7 m could grow spontaneously on slopes of 12°, slip surfaces about 40 m long could grow on slopes of 9° and slip surfaces could not grow spontaneously on slopes flatter than 8.4°.

CHAPTER V

KINEMATICS OF THE ASPEN GROVE LANDSLIDE

Introduction

By monitoring displacements, strains and velocities of parts of a landslide, one can describe the way the landslide moves and how the landslide debris is deforming; in short, the kinematics of the landslide. Here I describe the kinematics of the Aspen Grove landslide in Ephraim Canyon, Utah the dimensions, features, and setting of which I have described in previous chapters of this dissertation.

Velocities, calculated from the measurements of displacement of points every fifteen minutes, were determined with three extensometers in the lower end of the pond segment of the landslide and the upper part of the wedge segment and with one in the foot segment of the Aspen Grove landslide (Plate 3, Chapter VI) during 1985 and 1986. A purpose of the measurements was to determine whether the landslide moves uniformly (Keefer and Johnson, 1983) or in surges (Hutchinson, 1970; Hutchinson and others, 1974; Prior and Stephens, 1972).

Relative altitudes and horizontal distances between stakes in lines were measured in the upper, middle and lower parts of the landslide. Changes in spacing of stakes aligned axially in the upper part of the landslide reflect stretching and tension cracking there.

Three transverse lines of stakes show the distribution of displacements across the width of the landslide. Several short lines of stakes on a lateral ridge and a half dome provide insights into gross deformation of the landslide debris within these structures, and thus provide clues as to the mechanisms that might be responsible for their formation.

Finally, repetitive measurements of quadrilaterals (please see Chapter VI) provide detailed information about local deformation associated with gross structures within the landslide. In one place in the pond segment of the Aspen Grove landslide, for example, deformation within a small quadrilateral indicated highly localized, fault-like and crack-like displacements within an area two years before that area became part of a large graben structure.

Figure 5.1 shows when different types of measurements were made and when the landslide was active during the period 1983-86.

Timing of Landslide Activity

Each year between 1983 and 1986, the Aspen Grove landslide was active for about 3 to 5 months, between about April and August (Fig. 5.1). A few observations and data are available to specifically constrain the beginning and end of movement episodes.

In 1983, the landslide started moving near the end of May and stopped moving during mid July. En echelon cracks defining the boundaries of the landslide were first observed on May 31, so movement probably started a few days before May 31. Measurements of quadrilaterals Q-2, and Q-6, (please see Fig. 5.2 for locations) show insignificant changes after July 15 and July 23, respectively. Movement

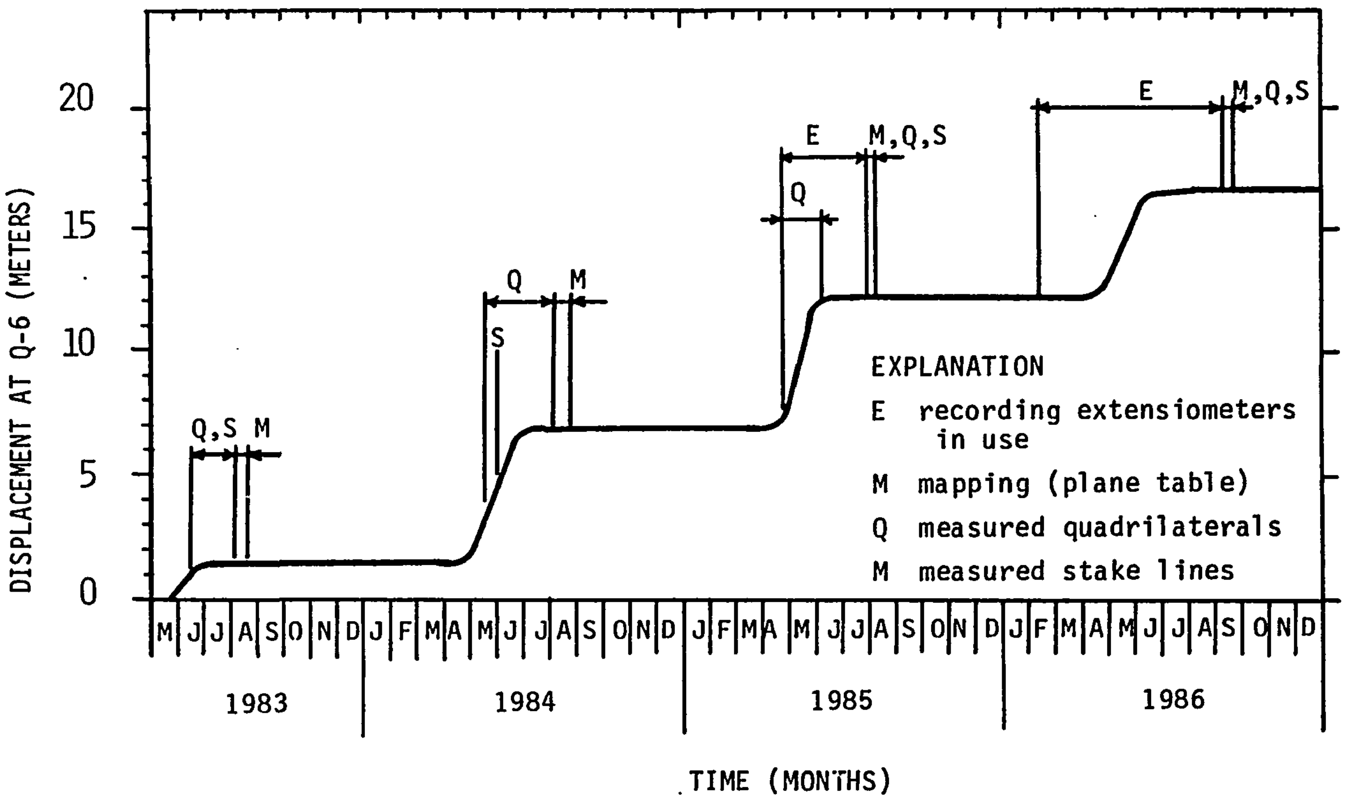

FIGURE 5.1. Graph showing the timing of measurements in relation to the activity of the landslide.

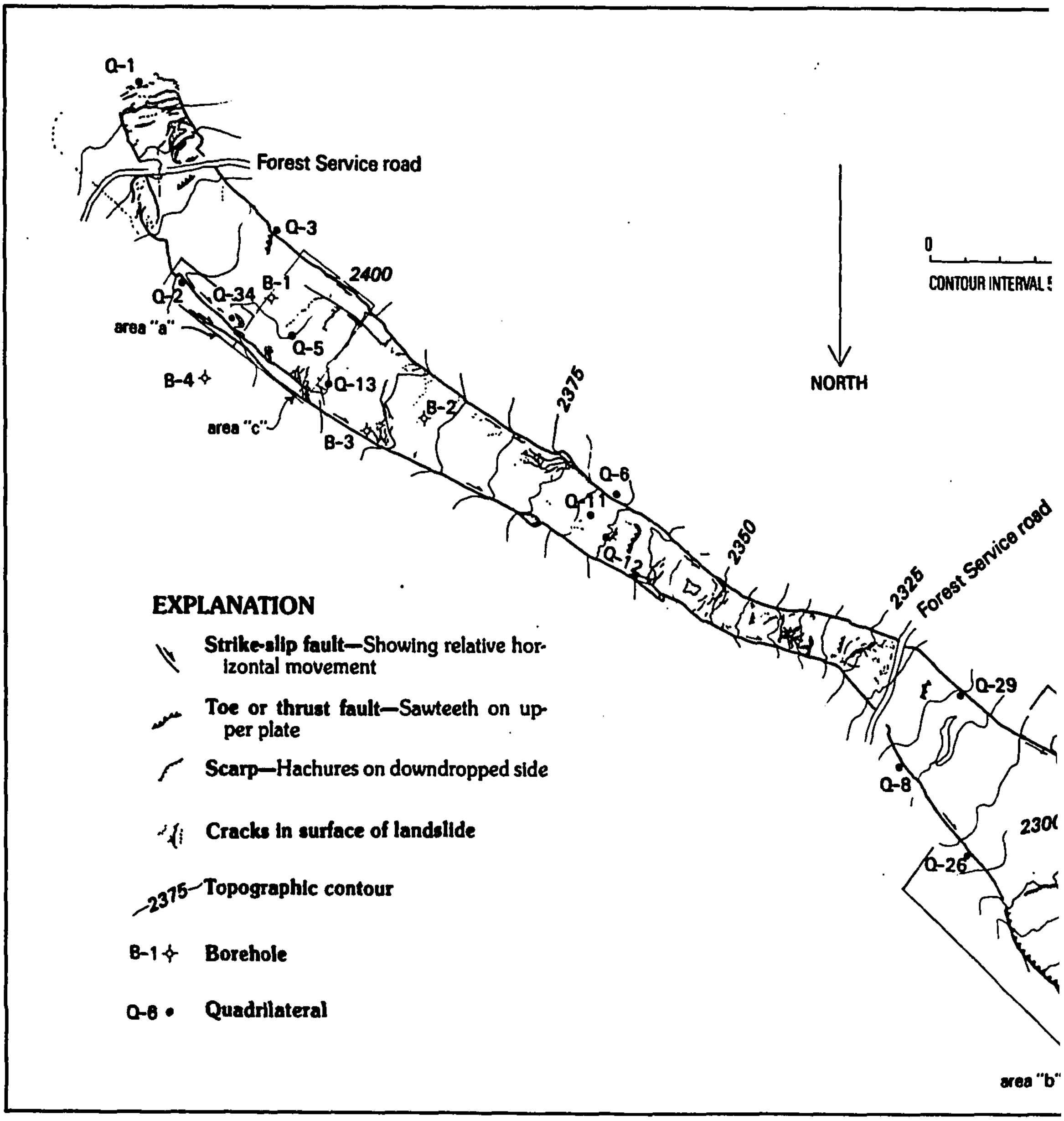

FIGURE 5.2. Map showing the Aspen Grove landslide. August 1984.

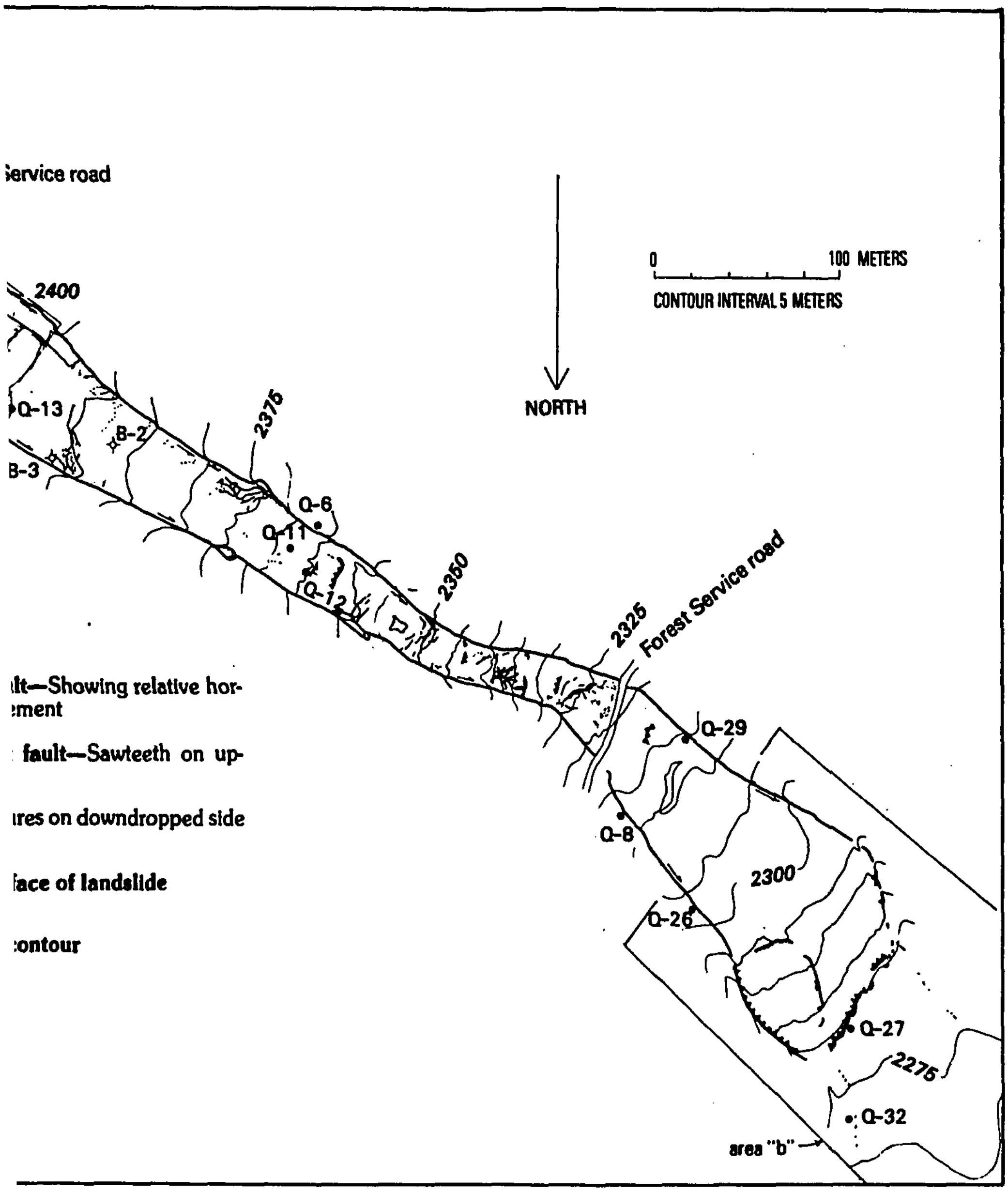

the Aspen Grove landslide. August 1984.

stopped during mid July, and the landslide was dormant until spring 1984.

Sliding began earlier and lasted longer in 1984 than in 1983. The landslide started moving between mid April and early May, and it stopped during August. By the time of our first visit to the landslide on May 16, the landslide had already moved several centimeters at some locations and perhaps a few decimeters near the middle (Station 390, Plate 5) Therefore movement probably had started by May 1 or perhaps mid April. In August, the landslide was still moving slowly because small en echelon cracks were observed in fresh mud that had collected in furrows at the flanks. However, movement appears to have stopped by mid to late August 1984.

In 1985, the landslide started moving even earlier. On April 23, 1985 the landslide was already moving several centimeters per day and the displacement at Q-2 since the end of movement in 1984 totaled 0.3 m. Thus, the landslide had probably started moving several weeks earlier, perhaps at the end of March or beginning of April.

The foot of the landslide stopped moving about a month before the main body of the landslide in 1985. Movement at extensometer E6, (please see Plate 5 for locations of extensometers) in the distal part, stopped about June 25, 1985; however, movement at E2, in the main body, stopped July 31, and movement at E3, also in the main body of the landslide, stopped on July 29, 1985. Thus movement at E6 stopped about 1 month before it stopped at E2 and E3. Movement ended slightly earlier in 1985 than it had in 1984.

The first movement in the main body of the landslide was well documented in 1986. Extensometer E1 (Fig. 5.3) operated until March 31, and the readings were stable (no changes) until about March 19, when minor fluctuations began. The first movement began on March 26 (Fig. 5.3).

The distal part of the landslide started moving at least a day later and probably two weeks later than the main body in 1986 (Fig. 5.4). The clock that controlled extensometer E6, at the distal part of the landslide, worked between February 12 and March 27. However, the extensometer continued to work, so all movement that occurred between March 27 and April 18 was registered when the clock was reactivated on April 18. Only 5 cm of displacement occurred between March 27 and April 18. Extrapolation of the steep part of the extensometer curve (Fig. 4.4) suggests that movement started about April 11.

Approximate Rate of Movement

The Aspen Grove landslide moved slowly, and its velocity rarely changed by more than a few centimeters per day per day. During the initial movements in June 1983, the average velocities in the upper part of the main body (estimated from offsets in lines of sticks near Q-2 and Q-3, Fig. 5.2) ranged from 0.8 to 2.5 cm/d (centimeters per day). By June 16, the landslide had reached its peak velocity and had started slowing down (Fig. 5.5).

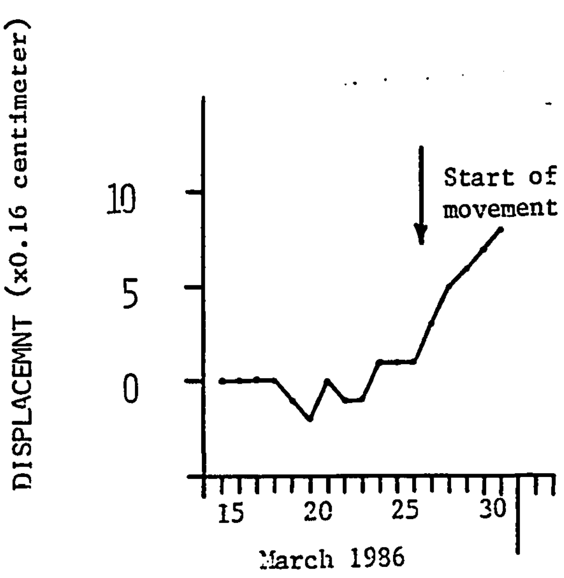

FIGURE 5.3. Record of displacement at E1 in March 1986 showing the beginning of movement.

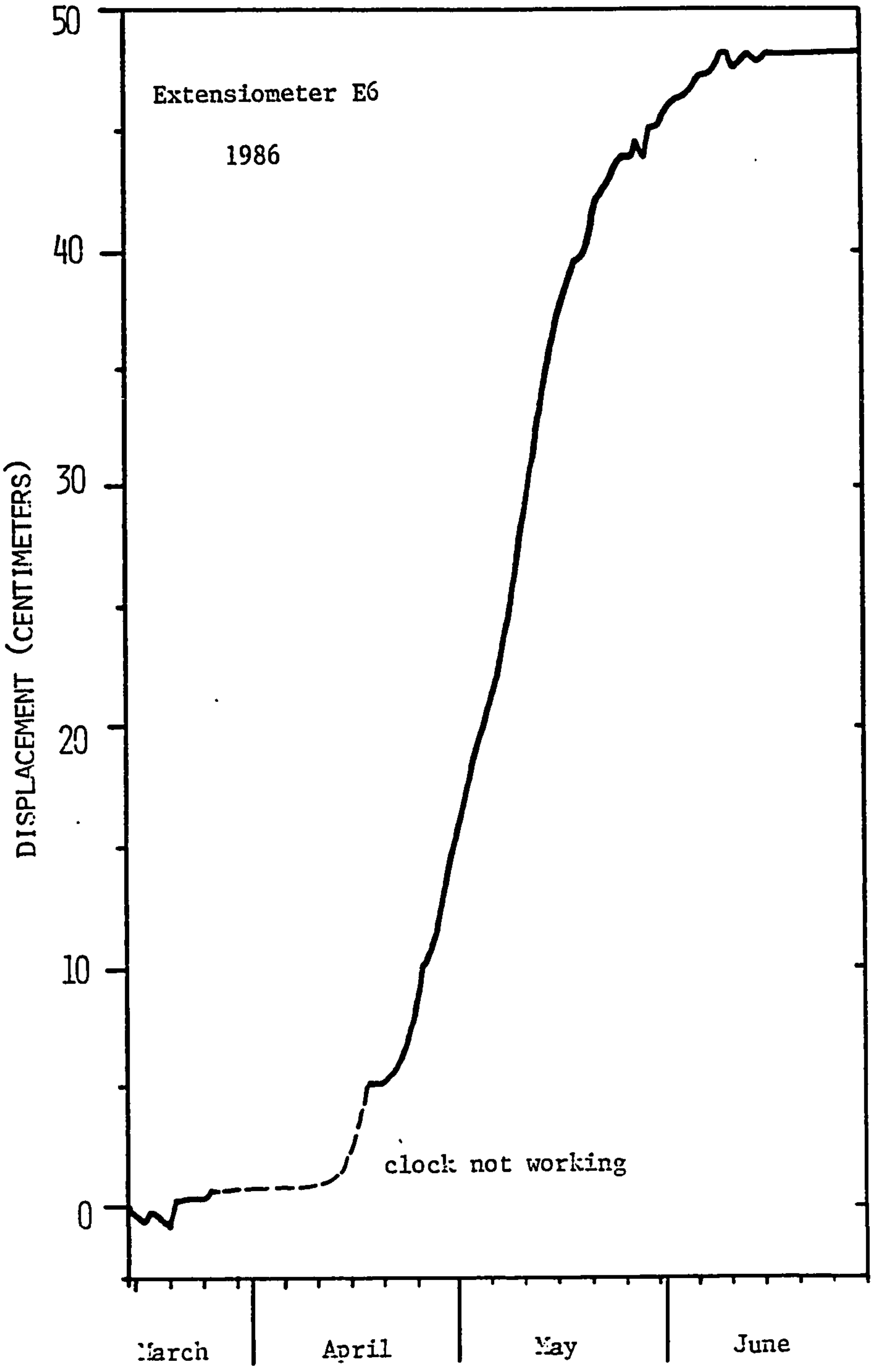

FIGURE 5.4. Record of displacements at extensometer E6 during 1986. Clock stopped working at the end of March; movement began before clock was replaced on April 18. Movement began between March 27 and April 18, (probably about April 10) and movement ended about June 11.

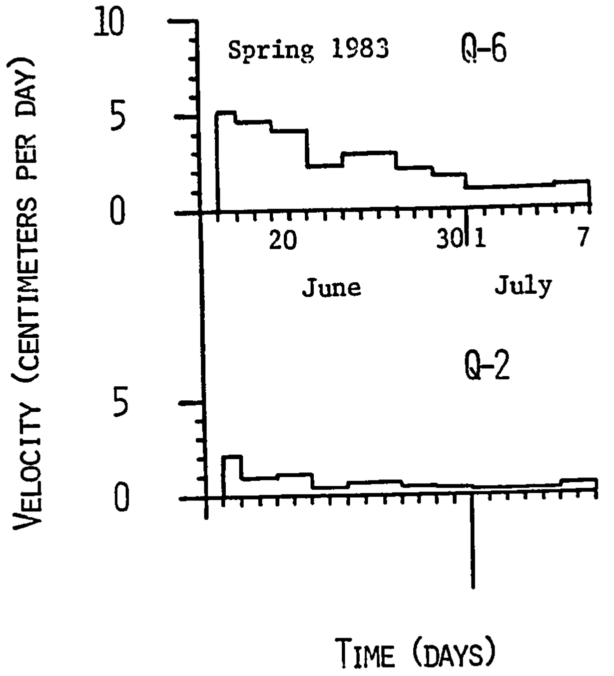

FIGURE 5.5. Average velocities at quadrilaterals Q-2 and Q-6 during part of 1983.

The velocity at Q-6 exceeded that at Q-2 during 1983. On June 16 and 17, the velocity at Q-2 was 2 cm/d. The velocity near mid length, at Q-6, was 5 cm/d. By July 7, the velocity at Q-2 had slowed to 0.5 cm/d and the velocity at Q-6 had slowed to 1 cm/d.

Changes in velocity at the two quadrilaterals occurred at approximately the same time (Fig. 5.5).

In 1984 the motion of the landslide became more complicated. Rapid movement occurred at the head causing the road to drop 1 m between May 17 and 21. The velocity was still relatively high, 17 cm/d, from May 23 to May 25 at quadrilateral Q-2 (Fig. 5.6). At the same time, relatively rapid movement also occurred at the split tree and at Q-6.

The average velocity at Q-2 slowed by 10 cm/d^2 between about May 25 and May 26, and then more gradually (0 to 2 cm/d^2) through June 7. Rapid movement followed by abrupt slowing also occurred at Q-6 and the split tree. At Q-29, far downslope from the head, movement was relatively steady, at rates between 2 and 4 cm/d (Fig. 5.6).

Motion of the landslide between Q-2 and Q-6 was less unified by June 1984 than it had been in 1983. Early in June, the velocity at Q-6, Q-29 and the split tree increased slightly, but the velocity decreased at Q-2 (Fig. 5.6).

Generally Steady Movement in Main Body

During much of the spring of 1985, we were able to observe the rate of movement in greater detail than in 1983 and 1984, by means of three extensometers (Appendix A). The extensometers were on the right flank in the wedge segment of the Aspen Grove landslide (Fig. 5.7).

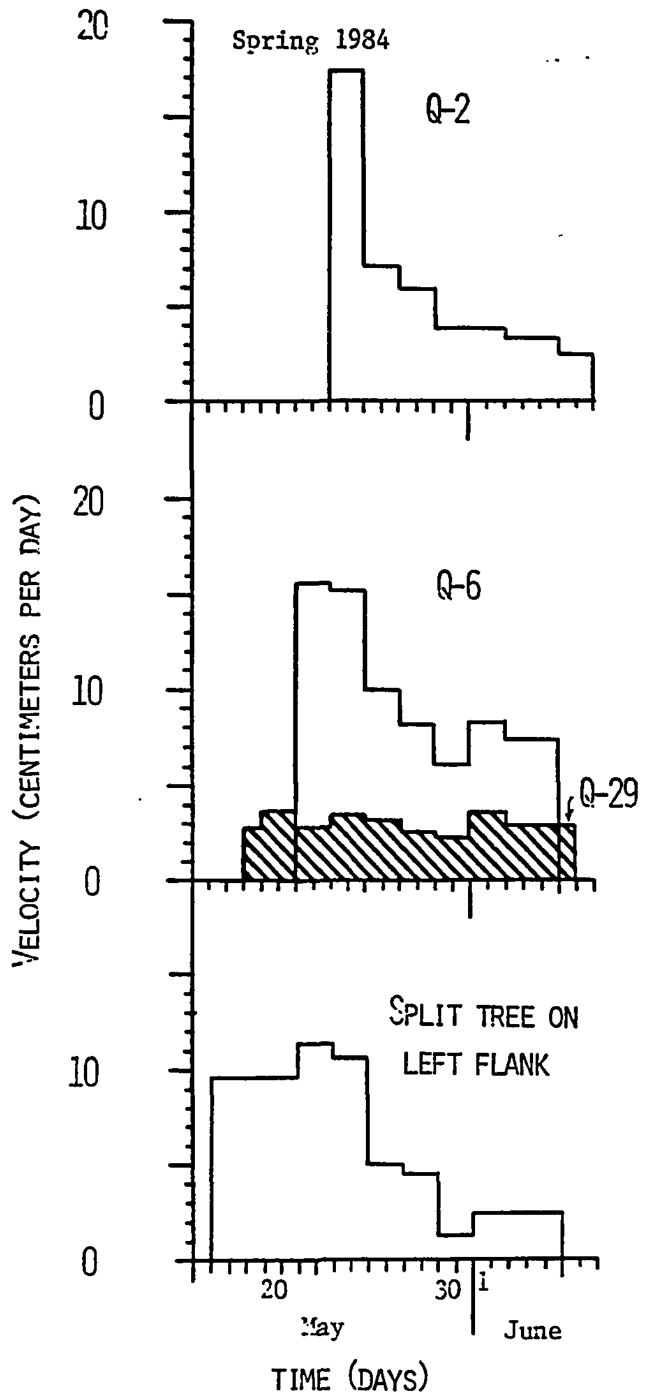

FIGURE 5.6. Average velocities at quadrilaterals Q-2, Q-6, and Q-29, and at the split tree on the left flank, during part of 1984.

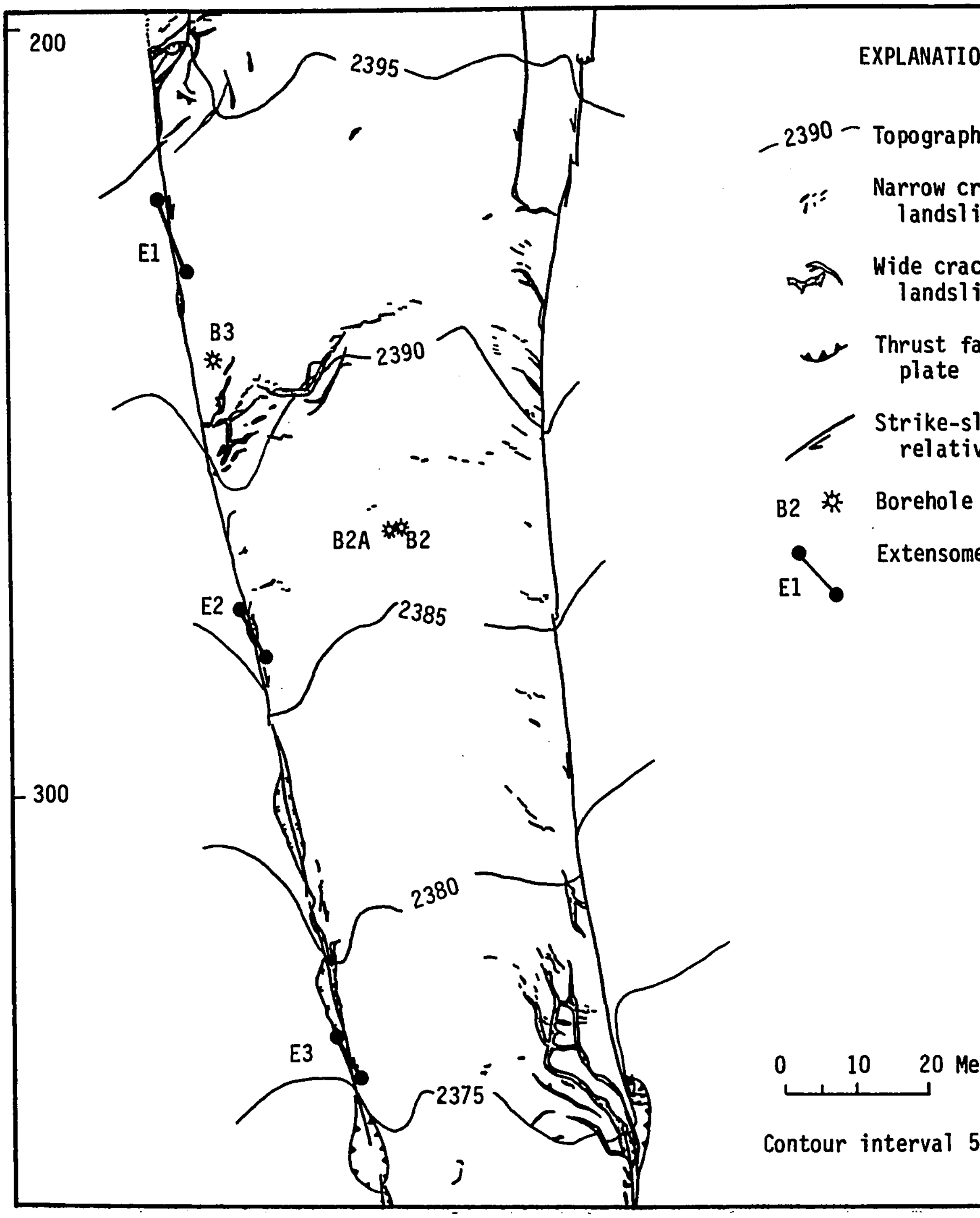

FIGURE 5.7. Map showing locations and settings of extensometers E1, E2, and E3.

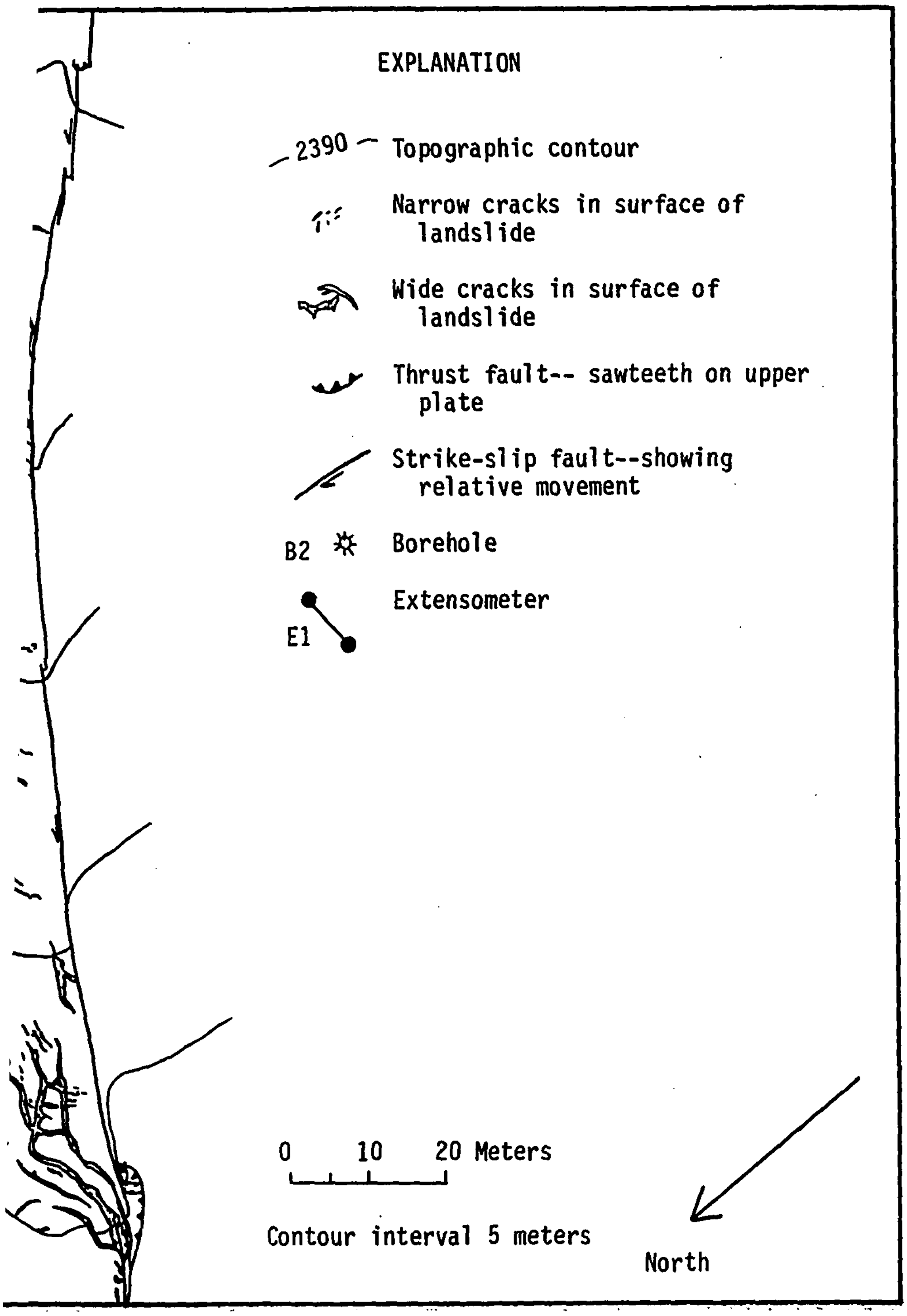

:ings of extensometers

The extensometer records show that sudden movements were uncommon, and that the landslide usually accelerated and decelerated gradually (Fig. 5.8). Smooth acceleration is also indicated in 1986 by the record of extensometer E6, which was on the right flank in the toe of the landslide. (Fig. 5.4).

The displacement curves are relatively smooth, even during the period of most rapid movement (Fig. 5.8). Most of the small bumps on the curve result from the incremental record of the extensometers. The extensometers register changes of displacement in increments of 0.070 in. (0.18 cm), and they record displacement at intervals of 15 minutes. A few of the larger bumps on the curve apparently resulted from rapid movements amounting to about 1-3 cm in fifteen minutes or one half hour.

At a scale of days, the landslide accelerated gradually as shown in Figure 5.9, which shows graphs of the daily average velocity at E1, E2 and E3 derived from the extensometer records.

Figure 5.9 shows that the landslide gradually accelerated to a peak velocity of 16.5-20 cm/d on May 4, and then gradually slowed during May, June and July. Changes in the daily average velocity were as great as 5 cm/d^2, but commonly were less than 1.5 cm/d^2. The general pattern of gradual acceleration to a peak velocity followed by gradual slowing appears to have been followed each year.

Figure 5.9 indicates that the velocity at E1 was always less than the velocity at E2 or E3, and that the velocity at E2 was usually less than the velocity at E3. This trend of increasing velocities from E1 to E3 is consistent with the gradual decrease in width from E1 to E3.

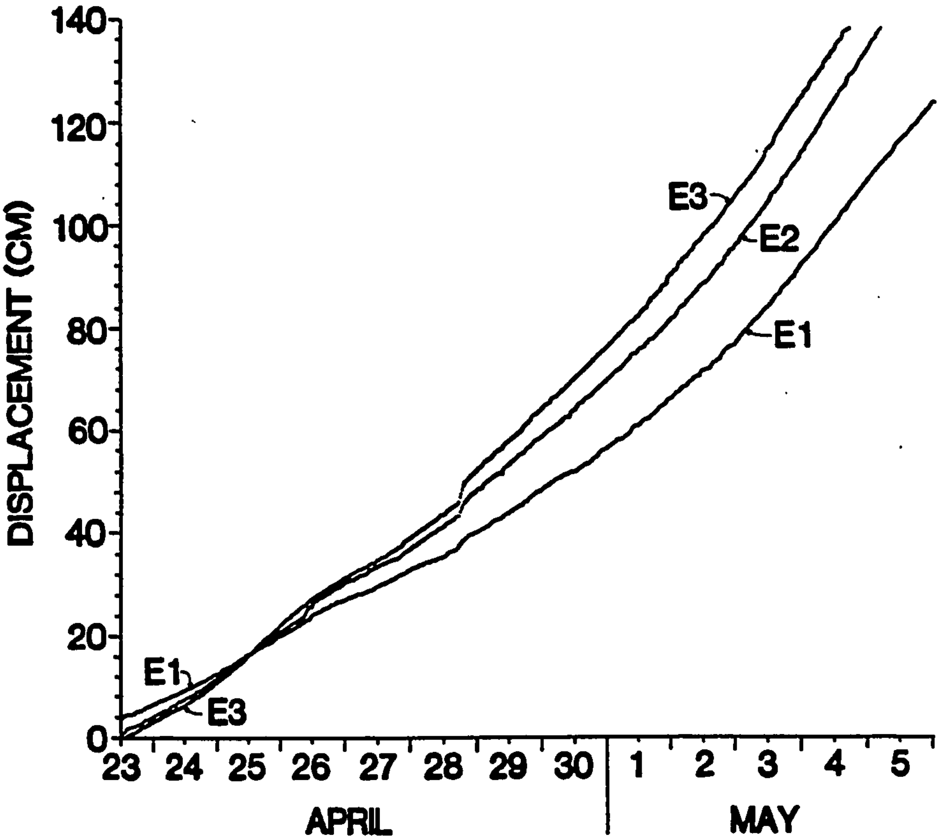

FIGURE 5.8. Displacements measured by extensometers E1, E2, and E3 during late April and early May 1985.

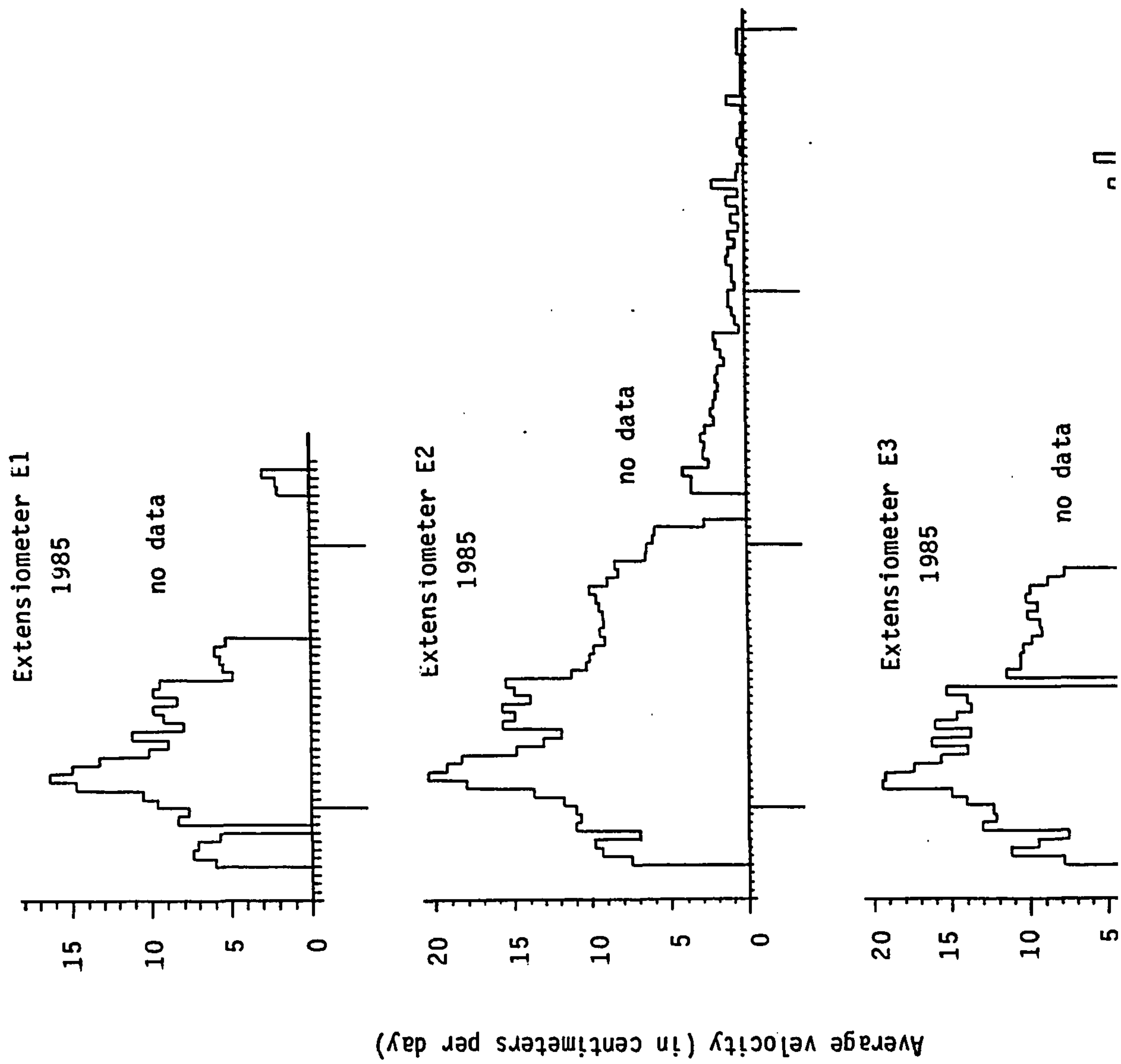

FIGURE 5.9. Average daily velocity at extensometers E1, E2, and E3 during 1985. Average daily velocity is equal to the displacement measured between 12:00 midnight at the start of the day and 12:00 midnight at the start of the next day.

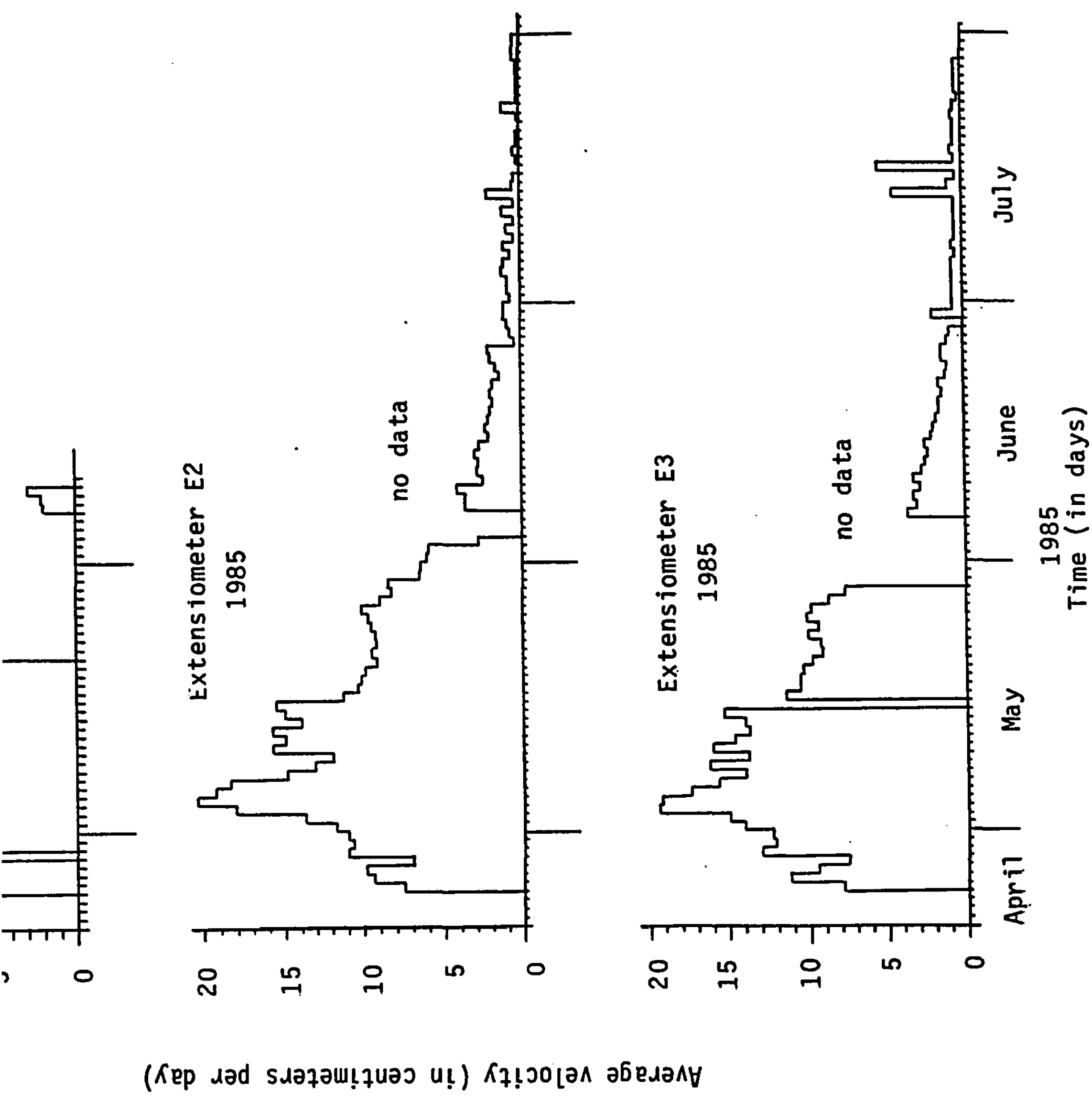

verage daily velocity at extensometers E1, E2, and
age daily velocity is equal to the displacement
0 midnight at the start of the day and 12:00
of the next day.

Most local maxima and minima occurred on about the same day at the three extensometers (Fig. 5.10). However, maxima or minima at E2 (between E1 and E3) were sometimes out of phase with corresponding maxima or minima that occurred simultaneously at E1 and E3.

One example of a surge is suggested by the extensometer records (Fig. 5.11). On the evening of July 13, 1985 a sudden movement of 1.6 cm was registered at E2 between 7:15 and 7:30 p.m. Later, between 8:45 and 9:00 p.m. a sudden movement of 4.0 cm was registered at E3, about 60-70 m downslope from E2. Sudden movement was not recorded at E1 because it was not working during July. Each event happened during less time than the extensometers can resolve, thus their occurrence is questionable. However, if the two incidents reflect wavelike propagation of a surge, then a zone of rapid movement propagated down the slope from E2 to E3, at a speed of about 34-56 meters per hour.

The landslide was in static equilibrium throughout its period of activity. Although the velocity fluctuated from hour to hour and day to day, the acceleration of the landslide was negligible when compared to the acceleration due to gravity. Except for the supposed surges, the greatest acceleration indicated by the extensometer data occurred during late April 1985. The acceleration was approximately, $1.6 \times 10^{-7} cm/s^2$, which is about $10^{-9} g \sin(\theta)$, where $g \sin(\theta)$ is the component of the acceleration due to gravity that is tangent to the slope, assuming $\theta = 12^{\circ}$. Acceleration of about $0.12\ cm/s^2$ ($6 \times 10^{-4}\ g \sin(\theta)$) might have occurred during the supposed surge, assuming that the event (including acceleration and slowing to the original velocity) lasted about 10 s.

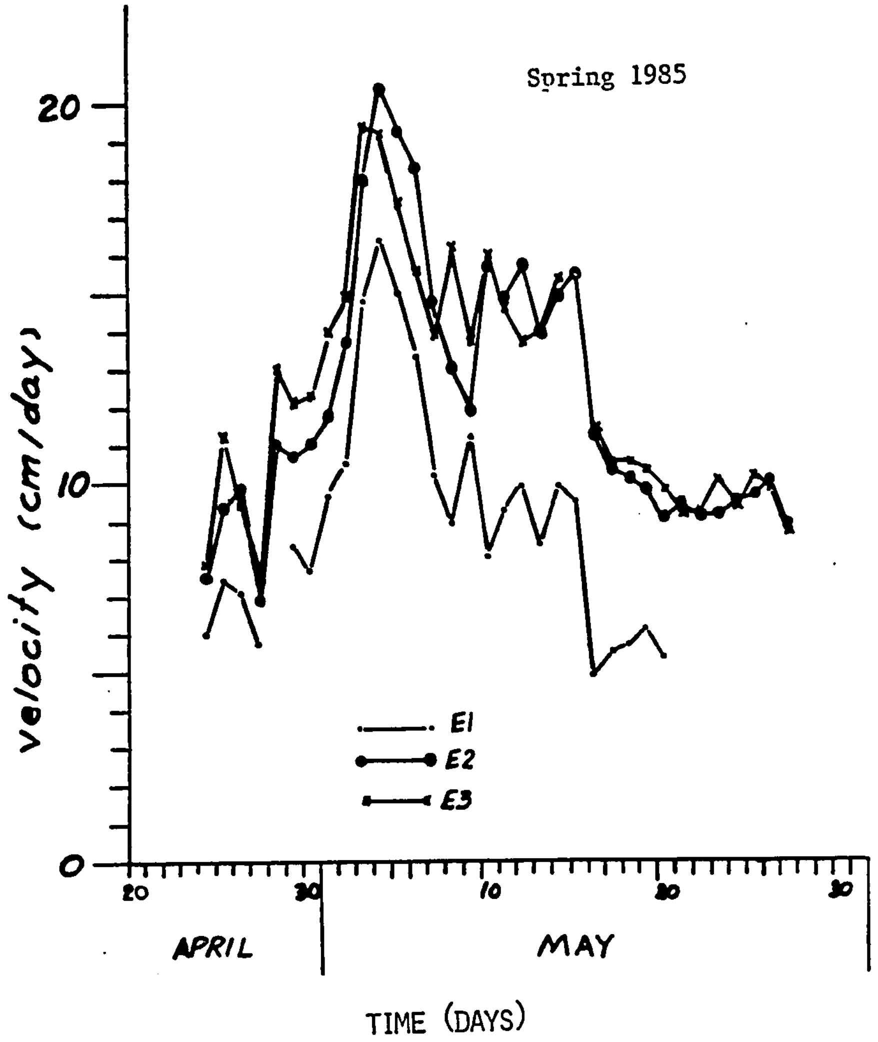

FIGURE 5.10. Graph comparing average daily velocities at extensometers E1, E2, and E3 during part of 1985.

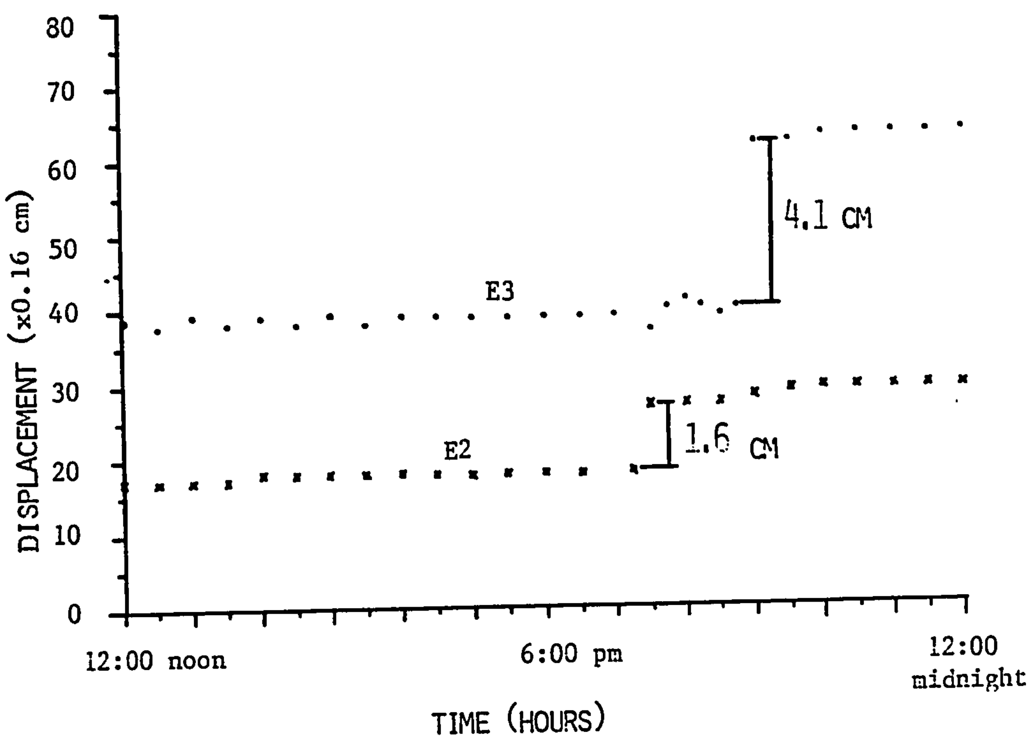

FIGURE 5.11. Displacements measured by extensometers E2 and E3 on July 13, 1985. The landslide was creeping along at a few millimeters per day except for the surges that are recorded in the evening.

Gross Displacements

In order to describe the spatial and temporal pattern of movement the displacements of many points on the surface of the landslide were measured. Displacement measurements were obtained by repeated measurement of lines of stakes and quadrilaterals, and by repeated mapping of survey stakes on the surface of the landslide. The methods and precision of the measurements are described briefly in Appendix A, and Chapter VI.

Points on the surface of the landslide moved as much as 150 cm during 1983. Offset in the impression a piece of plywood made in the ground and an animal trail indicate that the landslide had already moved about 40 cm on the left flank at Station 110 (Plate 5) and about 100 cm on the left flank at Station 390 by June 16, 1983, when measurements at quadrilaterals began. These estimated displacements were added to the displacements measured at the quadrilaterals from June 16 to August 4 to determine the total displacements of points during 1983: At the head (Station 30, Plate 5), 4 cm; at Station 115 on the right flank 60 cm; at Station 130 on the left flank 58 cm; where the impression of the wood crossed the left flank (near Station 110) 62 cm; at Station 390, 150 cm; and at Station 600, less than 10 cm (Plate 5).

During 1983, the displacements followed a general pattern of increasing from a small value at the head to a maximum value somewhere near midlength of the landslide and decreasing to a small value at the terminus. A similar pattern was repeated each year following 1983.

During 1984, a pattern of displacement consistent with that observed in 1983 was documented by a large set of measurements (Plate 5). Displacements at the head increased from 0 cm to 310 cm over the 46 m length of the C-line[9] (between Stations 0 and 40, Plate 5), and displacement was greatest in the lower 20 m of the C-line. Between 100 and 200 m downslope from the head (in the vicinity of the U-line) displacements ranged from 240 to 380 cm. The maximum displacement, 880 cm, occurred near Station 350 m, which is 40 m upslope from the M-line. Displacements decreased gradually over a distance of 70 m from the maximum, 880 cm, to 450 cm at a point about 30 m downslope from the M-line (Plate 5). Displacements decreased further toward the toe; at the L-line, 600 m downslope from the head, displacements ranged between 120 and 170 cm.

Displacements also decreased downslope from Station 600. Measurement of displacement below the Station 600 began on May 18, a few weeks after the landslide had started moving; thus, displacements below the Station 600 can be compared only to each other. Over a distance of about 250 to 280 m the displacements decreased between Station 600 and the pipeline. Displacement was 142 cm at Station 600 about 70 cm at Q-26 (Station 650) 30 cm at Q-27 (Station 760) and Q-28 (Station 680), 10 cm at Q-32 (Station 785) and probably a few centimeters at the pipeline

[9]The C-line is a line of stakes along the axis of the landslide that extends from the crown across the head. The U-line, M-line and the L-line are lines of stakes that are transverse to the landslide in its upper, middle and lower parts, respectively. The U-line is at station 120, the M-line is at station 390, and the L-line is at station 600.

(Plate 5). Hairline cracks were observed at the pipeline, but no cracks were observed downslope from the pipeline in June 1984.

During 1985, the displacement of points in the upper half of the landslide was generally less than displacement of the same points in 1984 (Plate 5). The displacement of points in the head ranged from zero at the crown to 88 cm at the distal end of the C-line. Points in the C-line moved about one fourth the distance they had moved during 1984. Displacement of points about 100 to 200 m below the head ranged from 250 to 540 cm. Although stakes in the U-line were displaced 250 to 320 cm, about 10 to 60 cm less than in 1984, points downslope from the U-line were were displaced 320 to 560 cm, which was from 20 to 240 cm greater than in 1984. Displacements at the M-line ranged from 530 to 610 cm and were about 20 to 90 cm less than displacements of the same points during 1984.

In contrast to points in the upper half of the landslide, points in the lower half of the landslide moved farther during 1985 than they had during 1984. Displacements at the L-line ranged between 230 and 300 cm, about twice the value of the displacements for 1984. Displacement of points downslope from the L-line were 2 to 4 times greater than in 1984: At Q-26 the displacement was 131 cm. At Q-28 the displacement was 580 cm and at Q-27 the displacement was 86 cm.[10] Displacements below the toe equaled 42 cm at Q-32 and Q-87. Cracks and fault segments

[10]The 44 cm value shown on the map (Plate 5) at Q-27 is the displacement across the thrust faults in the toe; the total displacement at Q-27 is 44 cm plus the 42 cm of movement on a deeper failure surface registered at Q-32 and Q-87.

could be traced about 100 m below the pipeline to small toes that were apparently the downslope limit of displacement. The cracks and small toes probably represent 20-30 cm of displacement.

The pattern of displacements for 1985 was approximately repeated in 1986, except that the displacements were less everywhere than in 1985 (Plate 5). Displacements at the head were less than 20 cm at all stakes in the C-line. points between Stations 100 and 180 were displaced 95-200 cm, or about 150 cm less than the same points had moved in 1985. These points were all upslope from a graben that formed in 1986 (Plate 5).

Points immediately downslope from the graben (Stations 200-270) were displaced 300-470 cm, about twice that of points upslope from the graben. However, the 1986 displacements of points downslope from the graben were 100 to 140 cm less than those measured in 1985.

At the M-line (Station 390, Plate 5) displacements for 1986 ranged from 430 to 460 cm, which was about 100-150 cm less than displacements in 1985.

Points in the L-line (Station 600) and points between the Station 600 and the internal toe (Station 760, Plate 5) also moved slightly less than they had in 1985. Points at the L-line moved 110-240 cm, (0-190 cm less, and averaging 90 cm less than in 1985). Displacements at points at the internal toe were about 80-90 cm at Q-26, 56 cm at Q-27, and about 30-40 cm at Q-28. These points moved 20-50 cm less than they had in 1985.

Points below the toe, at Q-32 (Station 785) and Q-87 (Station 770), moved approximately the same distance in 1986 as in 1985. At Q-32 the displacement was 39 cm, (42 cm in 1985) and at Q-87 it was 43 cm (42 cm in 1985). At E6, about 50 m downslope from the pipeline on the right flank, the displacement was 48 cm (30 cm estimated for 1985).

During 1987, the landslide was inactive (Robert W. Fleming, pers. commun., 1987).

Gross Strains

The pattern of displacements on the surface of the landslide (Plate 5) define the pattern of gross deformation of the landslide mass. Gross strains computed from the displacements are listed in Table 5.1. Gross axial stretching (elongation parallel to the axis of the landslide) occurred in the landslide between Stations 0 and 350, because displacements increased downslope between the head and Station 350, where the maximum displacement occurred. Gross axial shortening occurred in the lower parts of the landslide, between Stations 350 and 425 and between Stations 590 and 900 because the displacements decreased downslope in these areas. We have no data for displacements between Stations 425 and 590. The same general pattern of displacement was observed in 1984, 1985 and 1986; thus, the cumulative longitudinal strains have increased each year.

The gross strains suggest that a pulse of extension migrated downslope between the head and midlength of the landslide during 1984-1986 (Table 5.1). Extension at the head was 13 percent in 1984, but it decreased to 0.4 in 1986. Extension in the upper part of the landslide, between Station 40 and the U-line (Station 110) attained a maximum of +2.5 percent during 1985. Extension downslope from the U-line, between

TABLE 5.1

Gross Axial Strains in the Aspen Grove Landslide

Location	percent stain 1984	1985	1986
C-line	+13	+2.9	+0.4
C-line to U-line	+0.6	+2.5	+1.5
U-line to Sta. 270	----	+1.7	+2.2
U-line to Sta. 350	+2.9	----	----
Sta. 270 to M-line	----	+0.4	-0.1
Sta. 350 to Sta. 425	-6.4	----	----
L-line to large toe (Sta. 760)	-0.9	-1.2	-1.4

Stations 110 and 270 was greater during 1986 than during 1985 (Table 5.1).

The gross strains indicate that shortening increased in the flare and internal toe segments of the landslide (between Stations 600 and 760) from 1984 to 1986 (Table 5.1). Axial shortening between the L-line and Q-27 (Station 760) increased from -0.9 in 1984 to -1.4 in 1986.

<u>Analysis of Pattern of Gross Axial Strain</u>

Within some segments of the landslide (between the U-line[11] and the M-line, and between the L-line and the toe) an inverse relationship between width and displacement is evident (Plate 5). The law of conservation of mass can be applied to the motion of the landslide to explain the observed relationship between width and displacement. For simplicity I assume that the landslide maintained a steady profile (constant thickness) and that motion of individual particles was dominantly parallel to the axis of the landslide. The continuity equation, which expresses the law of conservation of mass, then takes the form:

$$\rho_1 v_1 A_1 = \rho_2 v_2 A_2 \qquad (5.1)$$

In equation 5.1, ρ is the density of the landslide debris, $\underline{v}$ is the mean velocity of the landslide, and $\underline{A}$ is the cross-sectional area measured in

[11]The stake lines are named as follows: The C-line is an axial line across the crown and head. The U-line, M-line and L-lines are transverse lines in the upper, middle and lower parts of the landslide, respectively. Please see Plate 5 for locations of the lines.

a plane normal to the axis of the landslide; the subscripts refer to stations along the axis of the landslide.

Changes in the density of the debris can be assumed negligible except where many gaping tension cracks reduce the bulk density of the landslide debris. The landslide remained mostly intact, so changes in density were probably negligible during 1983 and 1984.

Where changes in the density are negligible, equation 5.1 simplifies because ρ is a constant, and changes in the velocity (or displacement) are inversely related to changes in width, because the area, $\underline{A}$, is proportional to the width. For example, if the width gradually decreases distally from one station to another, the mean velocity must increase distally and the debris must elongate parallel to the direction of movement in order to maintain a constant volume flux of landslide debris.

The general pattern of displacements (Plate 5) is consistent with the requirements of the continuity equation. Displacements were greatest near the narrowest part of the landslide, and displacements were smaller upslope and downslope where the landslide was wider.

Local Strains not Predictable from Gross Axial Strains

Strains at quadrilaterals along the axis of the landslide suggest that alternating zones of axial extension and axial shortening exist within zones of gross extension and zones of gross shortening. Axial shortening occurred in a zone of gross axial extension at a quadrilateral (Q-4) on the U-line (Station 120). Axial strains at Q-4 were 0.0 to -0.4 percent in 1984, -1 to -4 percent in 1985 and 0 to +0.1

percent in 1986. Axial extension at another quadrilateral in the main body of the landslide, Q-14 (Station 205) exceeded the gross axial extension by 1.7 percent. Axial extension at Q-14 was +4.6 percent in 1984, compared to gross axial extension in this section of the landslide of +2.9 percent (between Stations 110 and 270, Plate 5).

Two segments of a line of stakes on the axis of the landslide elongated, while other segments of the line shortened (Fig. 5.12). Cumulative strains of 1.5 to 11 percent occurred in segments of the line between 1983 and 1985, but the overall cumulative strain in the line was negligible, only about -0.2 percent.

Distributed Shear Within the Landslide Debris

Gross strains in three areas are also reflected in deformation of transverse lines of stakes (Fig. 5.13). The stakes within each line moved at different rates relative to their neighbors, and patterns of differential movement developed gradually. Thus, the pattern of differential movement was more obvious at the end of 1986 than in previous years.

At the M-line, stakes near the middle moved farther than points near either flank, and stakes near the right flank moved farther than those at the left flank. Stakes near the middle of the L-line moved farther than stakes at either flank, and stakes near the left flank moved farther than stakes near the right flank.

The pattern of displacements in the M-line might result from bending about a vertical axis outside the left flank of the landslide

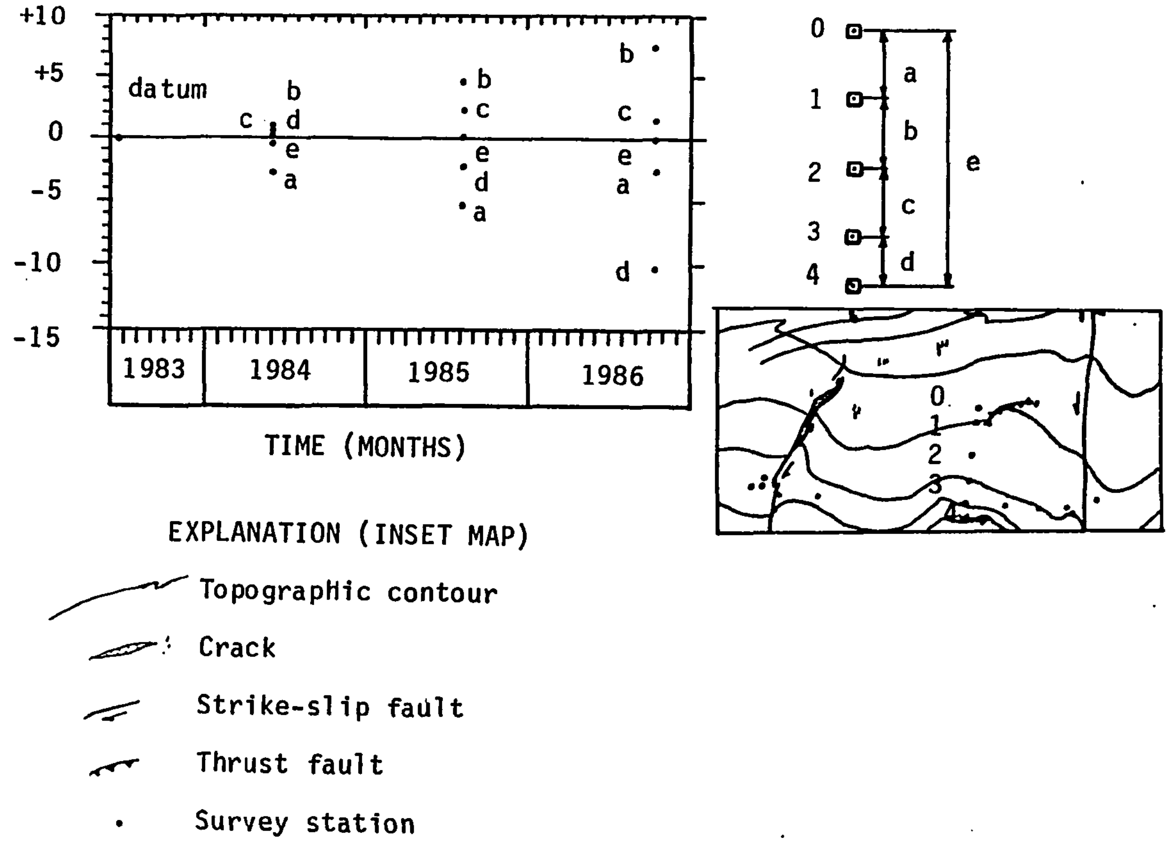

FIGURE 5.12. Graph showing strain in a longitudinal stake line near Station 600.

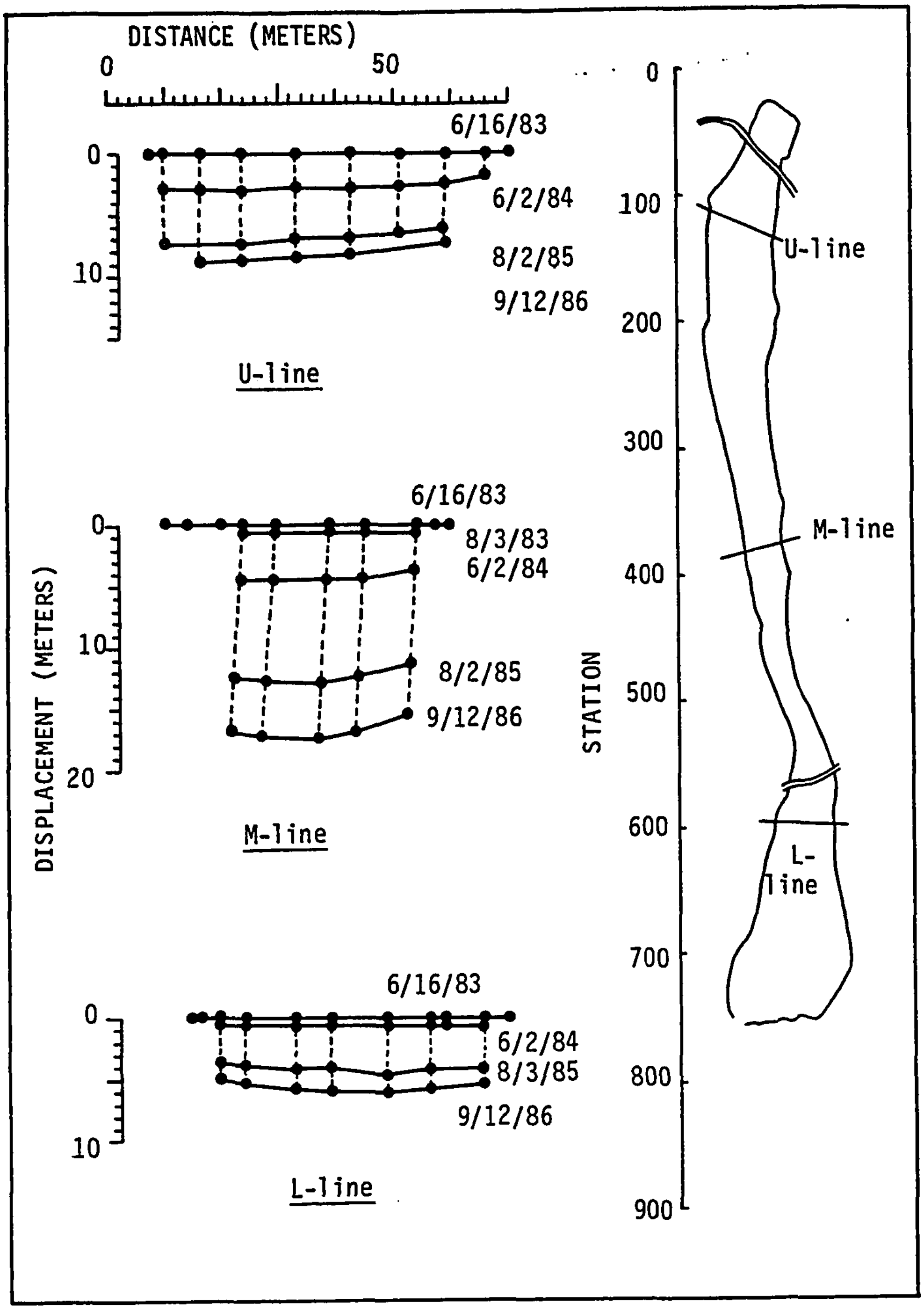

FIGURE 5.13. Graphs showing displacement of transverse stake lines in the upper, middle and lower parts of the Aspen Grove landslide.

superimposed on plastic flow in a converging channel with friction at the boundaries (Hill, 1950, p. 208-212). The boundaries of the landslide converge upslope and downslope from the M-line, making angles of about 3.2° with the axis of the landslide. The left flank curves near the M-line, causing the landslide to turn a few degrees to its left.

The velocity distribution for plastic flow in a straight, converging channel is determined by the following formulas (Hill, 1950, p. 211)

$$v_r = B/\{r\ (c - \cos 2\psi)\}. \tag{5.2}$$

In equation 5.2, $\underline{v_r}$ is the radial component of velocity, $\underline{B}$ is a positive constant, ψ is the angle between the algebraically greatest principal stress and a radial slip line, $\underline{r}$ is the radius measured from the apex of the channel, and $\underline{c}$ is a positive constant (greater than unity) that satisfies the following equation:

$$c/(c^2 - 1)^{1/2} \tan^{-1}\{[(c + 1)/(c - 1]^{1/2}\} = \alpha + \pi/4 \tag{5.3}$$

In equation 5.3, α is one half the angle between the sides of the converging channel (Fig. 5.14).

The angle θ between a line bisecting the channel and a radial line in the channel is related to $\underline{c}$ and ψ by the following (Fig. 5.14)

$$\theta = -\psi + c/(c^2 - 1)^{1/2} \tan^{-1}\{[(c + 1)/(c - 1)]^{1/2} \tan \psi\}$$

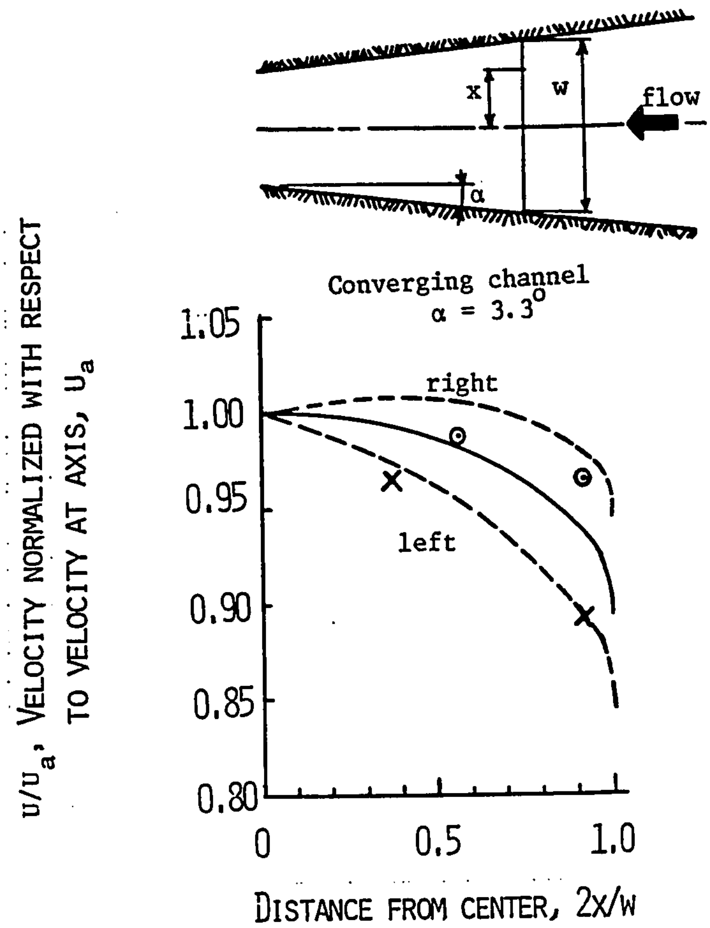

FIGURE 5.14. Graph comparing observed deformation at the M-line to theoretical plastic deformation in a converging channel. of the axis of the channel and diminishes velocities of points to the left of the axis.

Figure 5.14 compares the velocities predicted by plasticity theory for a straight, converging channel (solid curve, Fig. 5.14) with the displacements of points in the M-line (x's and circles, Fig. 5.14) between 1983 and 1986. Points to the right of the axis plot above the theoretical velocity profile for plastic flow in a straight, converging channel, and points to the left plot below the curve.

When a velocity profile consistent with bending is superimposed on velocity profile due to plastic flow, the data plot near the modified theoretical curves (dashed curves, Fig. 14). Bending of a few degrees is assumed to cause a linear gradient in the velocities of points across the channel. The gradient augments velocities of particles to the right

We expected the pattern of displacements in the L-line to be consistent with bending about an axis outside the right flank superimposed on plastic flow in a diverging channel with friction at the boundaries, because the greatest velocity occurs at the axis of the channel, and the velocity decreases toward the boundaries of the channel. Curiously however, Hill's (1950) theory for flow in a diverging channel predicts that the maximum velocity occurs at the edges of the channel, and that the velocity decreases to its minimum value at the axis, because the velocity is determined by the following equation:

$$v_r = B/[r\ (c + \cos 2\psi)]. \tag{5.4}$$

At the U-line, stakes near the right flank moved farther than stakes in the middle, and stakes in the middle moved farther than those near the left flank (Fig. 5.13). Thus, left-lateral shearing parallel to the direction of movement and distributed across the entire width of the landslide could account for the observed gradient in displacement. Bending of the landslide about a vertical axis outside the left flank could also account for the observed gradient.

I cannot determine which style of deformation occurred. Bending would cause compression near the left flank and elongation near the right flank, but presumably, distributed shearing would not produce such compression and elongation. Although a thrust fault, which suggests compression, is mapped next to left flank near the U-line, no corresponding evidence of extension was found at along the right flank near the U-line.

Localized Deformation

Gross strains in the landslide are relatively small, amounting to only a few percent (Table 5.1). However, strains are larger where deformational structures have formed at the surface of the landslide.

Deformation associated with structures on the surface of the landslide was documented by a combination of mapping structures by plane-table methods and repeating measurements of quadrilaterals and stake lines. Parts of the landslide were mapped each year during August to record visible changes in the structures. Strain and tilt was computed from the quadrilateral measurements and strain was computed from stake line measurements.

Finite (large) strain theory was used to study the deformation, because strains greater than 0.010 (one percent) were observed on the surface of the landslide. One of the most convenient quantities for describing large strains is the stretch (Malvern, 1969; A.M. Johnson, unpub. data). The stretch, $\underline{S}$, is defined as the ratio of the final (deformed) length, $\underline{L}_f$, to the initial length, $\underline{L}_o$, of a line segment:

$$S = L_f/L_o. \tag{5.5}$$

According to the definition of stretch, a stretch greater than one indicates that the line segment has elongated; whereas a stretch less than one indicates that the line segment has shortened.

The major principal stretch is denoted by $\underline{S}_1$ and the minor principal stretch is denoted by $\underline{S}_2$. Computation of the principal stretches is described in Chapter VI. The principal stretches squared are equal to the principal values of the Green Deformation Tensor (Malvern, 1969, p. 164-165).

Area change is measured by the ratio of the final area to the initial area; the ratio of the final area to the initial area is equal to the product of the major and minor principal stretches:

$$A_f/A_o = S_1S_2. \tag{5.6}$$

In equation 5.6, $\underline{A}_f$, is the final area of the quadrilateral strain gauge, and A_o is the initial area of the strain gauge.

Where the density of the landslide debris is essentially constant, the product $\underline{S}_1\underline{S}_2$ can be used to determine whether the landslide is thickening or thinning beneath a quadrilateral. In three dimensions, the ratio of the final to the initial volume of an element of material that deforms with constant density is given by

$$S_1S_2S_3 = 1. \tag{5.7}$$

In equation 5.7, S_3 is the principal stretch perpendicular to the surface of the landslide. If

$$S_1S_2 > 1,$$

then,

$$S_3 < 1.$$

Therefore, the landslide must be thinning where $S_1S_2 > 1$, and the landslide must be thickening where $S_1S_2 < 1$.

Deformation in Ground Being Extended

The sequence of deformations that occur in ground being extended was observed at two places in the Aspen Grove landslide. The head of the landslide began to develop in 1983 but evolved rapidly during 1984; only late stages of its development were recorded.

A group of scarps formed in the upper part of the main body of the landslide between 1984 and 1986. The group developed slowly over three seasons and early stages of its development were observed and documented. In order to describe the sequence of deformations that occur in ground that is being extended, the development of the scarps is described first, followed by the late stage development of the head.

The scarps.--The scarps area is in the upper part of the landslide, near Station 160 (Plate 2). This part of the landslide was about 64 m wide and strike-slip faults parallel to the flanks divided the landslide into three elements. The central element, which hosted the scarps, was 46 m wide. Ground on the distal side of the group of scarps sloped about 12° toward the northwest. Ground on the proximal side of the group had a back slope of about 6° toward the north-northeast.

During 1983 and the early part of 1984, the ground at the site of the scarps was undeformed. No cracks occurred there, and insignificant changes occurred in quadrilateral Q-5, which was at the site. (Fig. 5.15a).[12]

By the end of 1984, a few cracks had appeared at the site. A group of cracks formed in the left half of the central landslide element, in and near a diagonal ridge that separated ground sloping toward the northwest from ground sloping toward the north-northeast. The cracks were a few centimeters to a few meters long and were open a few centimeters wide (Fig. 5.15a). Another group of cracks, parallel to the first group and about 10 to 15 m downslope from the first group occurred in the left one-third of the central element.

[12]Contraction of Q-5 indicated by the strains measured between August 1983 and May 1984 was due to accidental tilting of stake B during the winter.

Deformation at Q-5 during 1984 showed that the ground was extending parallel to diagonal BD (i.e. N. 81° W.), and that stake B was dropping. Between May 23 and August 3, 1984, stake B pulled away slightly from stakes A, C, and D, however the positions of stakes A, C, and D relative to each other were practically unchanged (Table 5.2). Between May 23 and August 3, 1984, the dip of triangle ABC increased from 9.9° to 10.7° while the dip of triangle ACD remained between 7.1° and 7.4° (Table 5.3).

During 1985, the cracks that had formed in 1984 enlarged, and new cracks appeared (Fig. 5.15b). The group of cracks in the ridge occupied about the same position as in 1984, but the cracks were larger and the group defined a crescent. The group of cracks below the ridge extended across the entire width of the central landslide element.

The style of deformation at Q-5 during 1985 was identical to that during 1984 (Table 5.2). As a result of the deformation, a crack formed within Q-5 between stake B and line AC during August 1985 (Fig. 5.15b).

By September 1986, scarps had formed in the left half of the central landslide element. The crescent-shaped group of cracks in the ridge evolved into a family of normal faults (Fig. 5.15c), which formed the group of scarps. New cracks formed and older cracks enlarged. Ground distal to the normal faults was down relative to ground proximal to the faults.

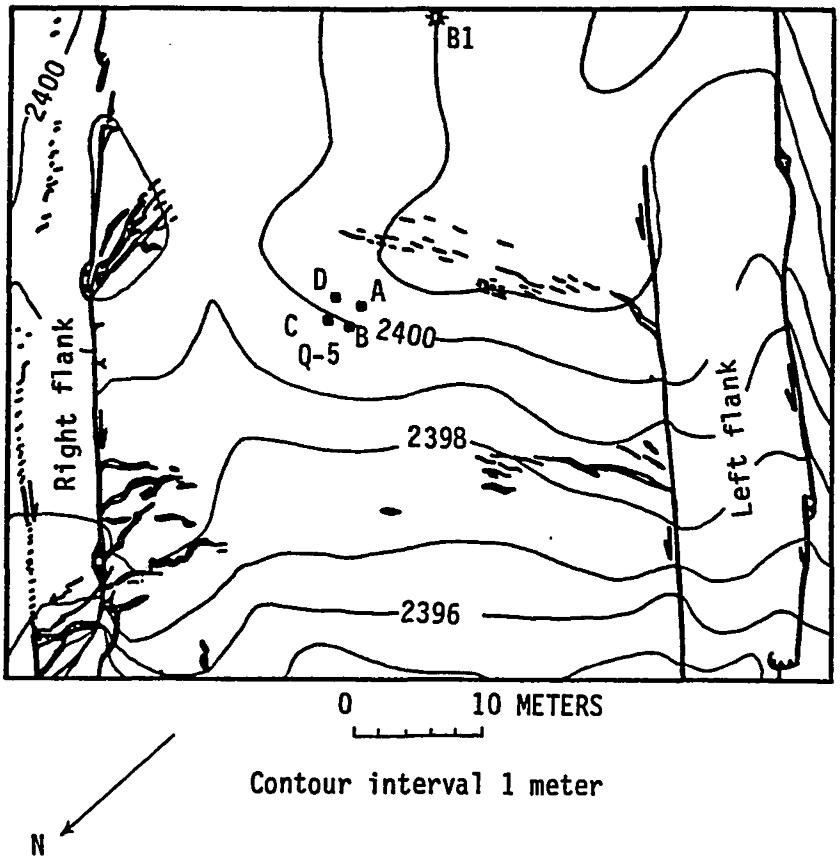

EXPLANATION

- 2400 Topographic contour
- Strike-slip fault
- Thrust fault, sawteeth on upper plate
- Cracks
- B1 Borehole
- A Survey station (wooden stake)

FIGURE 5.15. Plane-table maps of the landslide near Station 170 showing the development of a graben. (a) August 1984 (b) August 1985 (c) September 1986.

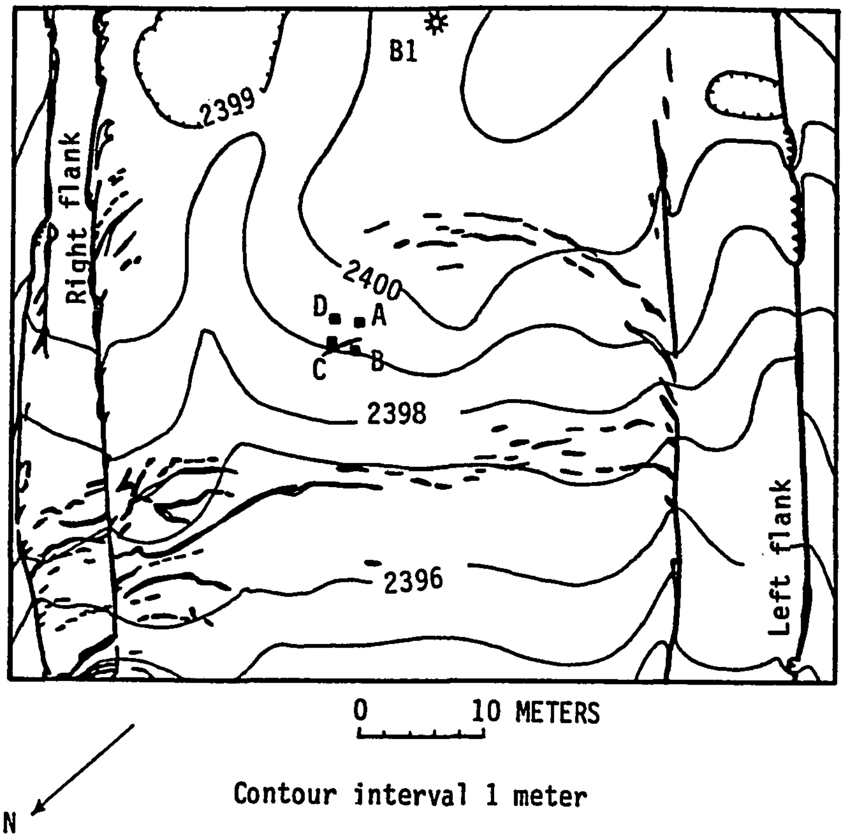

Contour interval 1 meter

EXPLANATION

2400	Topographic contour
	Strike-slip fault
	Scarp, hachures on downdropped side
	Cracks
	Thrust fault, sawteeth on upper plate
B1	Borehole
A	Survey station (wooden stake)

FIGURE 5.15b

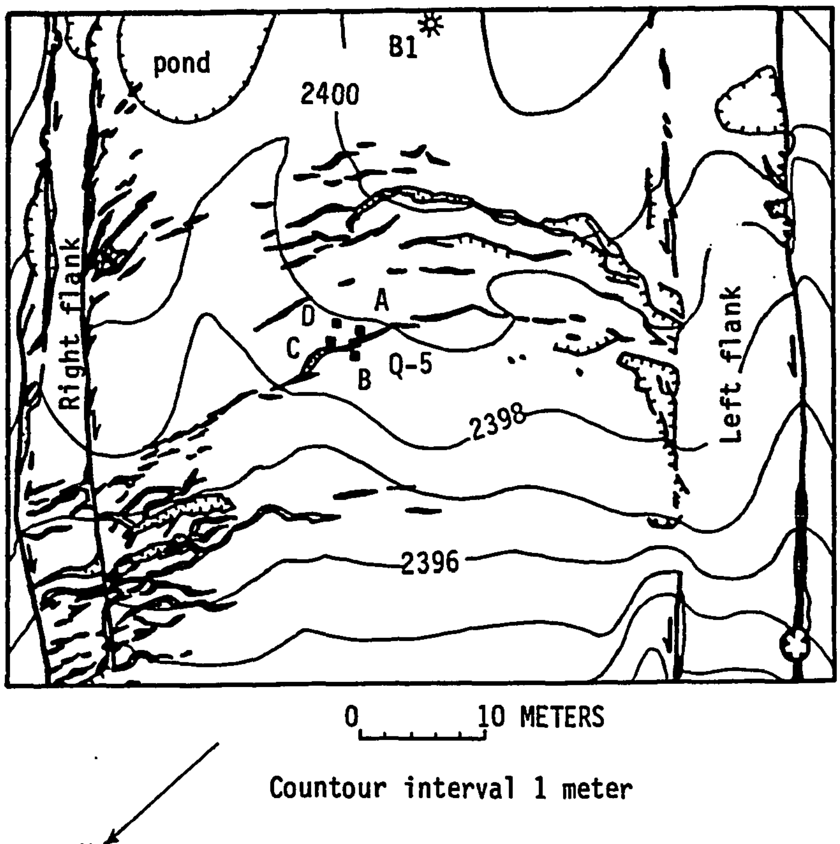

EXPLANATION

2400	Topographic contour
	Strike-slip fault
	Scarp, hachures on downdropped side
	Cracks
	Thrust fault, sawteeth on upper plate
✲ B1	Borehole
▪ A	Survey station (wooden stake)

FIGURE 5.15c.

TABLE 5.2

Strains in Quadrilateral Q-5

Beginning Date	Ending Date	Strain between corners of the quadrilteral (percent) AB	BC	CD	DA	AC	BD
6/16/83	8/04/83	0.0	+0.1	+0.1	-0.2	-0.1	+0.1
8/04/83	5/23/84	-1.4	-0.7	+0.9	+0.7	-0.3	0.0
5/23/84	8/03/84	+0.3	+0.3	-0.2	+0.2	-0.3	+0.6
8/03/84	6/04/85	+2.5	+0.6	+0.1	+0.2	-0.8	+2.1

TABLE 5.3

Tilt of triangles ABC and ACD of Q-5

Date	ABC	ACD
6/15/83	8.5°	7.2°
5/23/84	9.9°	7.1°
8/03/84	10.7°	7.4°
6/04/85	12.2°	7.2°
8/02/85	12.7°	7.1°

A normal fault with a vertical offset of about 10 to 15 cm was formed between stake B and line AC of Q-5, where the crack had been in 1985 (Fig. 5.15c). Displacement of point B was 13.0 cm down vertically relative to stake A, and stake B moved laterally 1.0 cm parallel to line AD.

Deformation of Q-5 suggests that faults in the landslide form at depth and propagate to the surface. Stake B was moving away from triangle ACD in a manner consistent with displacement on a fault, about two years before the fault could be recognized, and one year before a crack formed in the quadrilateral.

The head.--A few small cracks defined the head of the landslide in June of 1983. The cracks were oriented about N. 60° E. and the highest cracks were at about the 2420 m contour (Fig. 5.2). The flanks in the head area were marked by small en echelon cracks. Measurements at a quadrilateral indicate that ground at the head accommodated at least 3 percent elongation before cracks appeared.

The head evolved rapidly between May 17 and May 21, 1984. On May 17, the head was concealed by several inches of snow, and the road across the landslide was still intact. On May 21, most of the snow had melted and gaping cracks had appeared. Displacement at the uppermost crack in the head was 0.3 m and displacement increased distally in the head region. The cracks were about 1 m deep, and separated the head into a group of irregular blocks (Fig. 5.16). The flanks of the landslide had evolved into strike-slip faults, and the road was offset about 1 m vertically on the left flank. Striations on the scarp at the

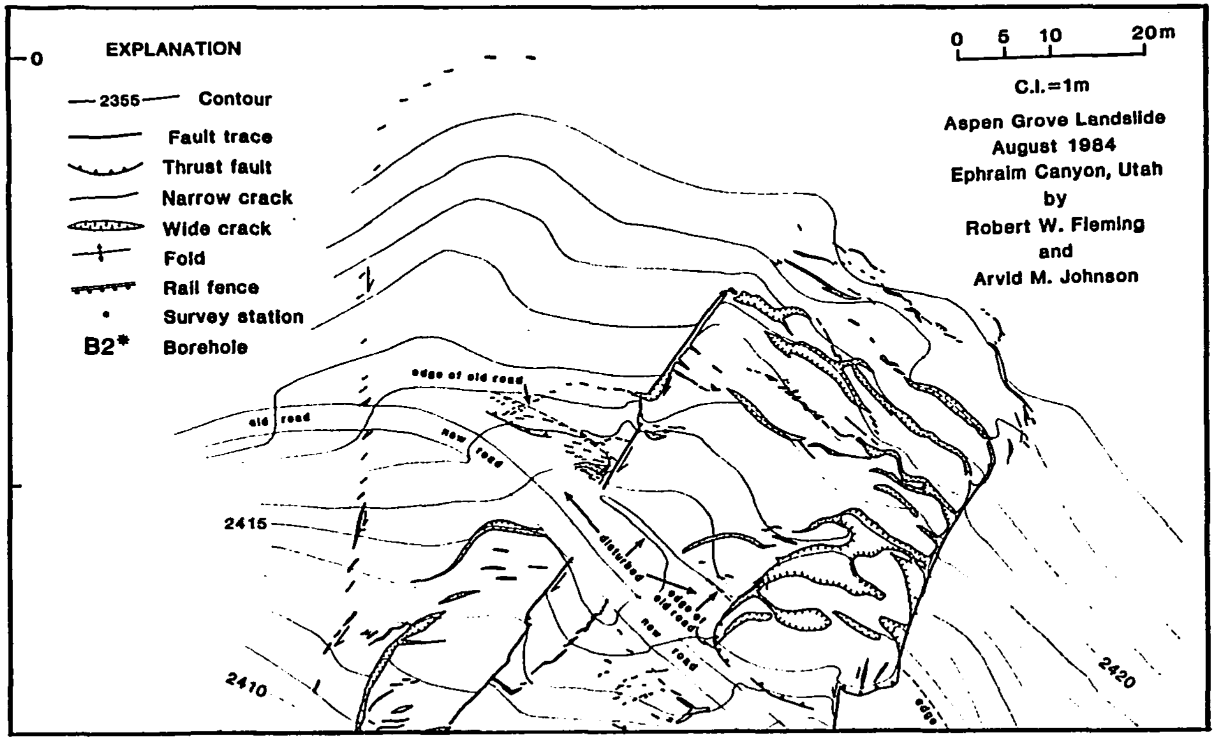

FIGURE 5.16. Map showing the head of the Aspen Grove landslide, August 1984.

road crossing plunged 40°; thus, the offset of the road resulted from 1.6 m of net slip.

The head slowly enlarged during the remainder of 1984 and during 1985. A group of en echelon cracks that outline an inverted J formed east of the head during late May of 1984 (Fig. 5.16). En echelon cracks constituting an upslope extension of the left flank formed during 1985 (Fig. 5.16). The line of cracks was oriented about N. 14° W. Axial strain of +0.6 percent (elongation) occurring in ground upslope from the head during 1984 was a precursor to formation of the cracks during 1985. Additional axial strain of +0.8 percent during 1985 accompanied formation of the en echelon cracks.

Deformation in Ground Being Shortened

Detailed measurements of quadrilaterals documented the deformation of two areas that shortened axially. These areas are the vicinity of the M-line, between Stations 370 and 400, and the large internal foot, between Stations 600 and 760. Measurements indicate that ground in the vicinity of the M-line thickened. The internal foot thickened and grew in height.

Thickening between Stations 370 and 400.--The surface of the landslide was elevated relative to ground neighboring the landslide between Stations 220 and 420 in August 1984 (Fig. 5.17), and the landslide became more elevated along the left flank between 1984 and 1986. This entire section of the landslide also narrows uniformly from 55 m at Station 225 to 40 m at Station 420. Scarps 1-2 m high defined the right flank and scarps 0.5-1.0 m high defined the left flank in

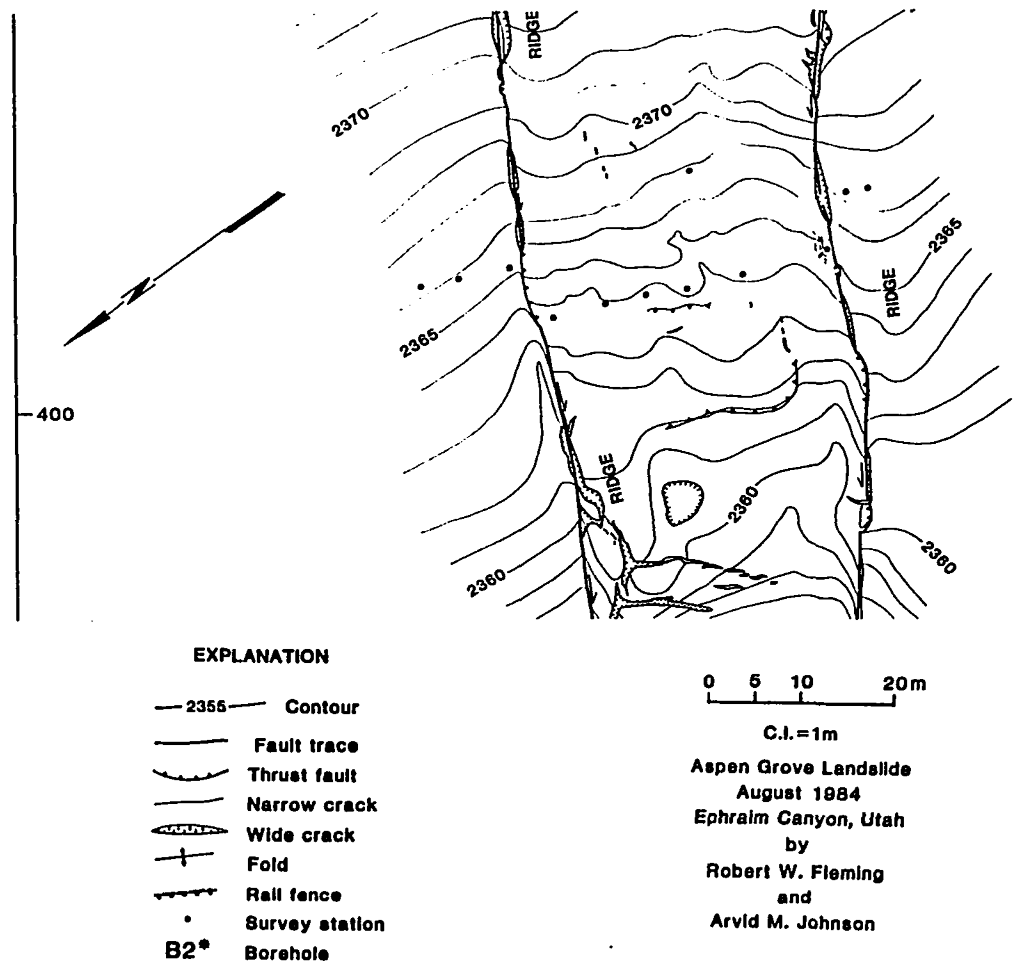

FIGURE 5.17. Map showing the topography and structures near Station 400 (August 1984).

1984. Scarps at the right flank were 1.5-2.0 m high, but scarps at the left flank were 1.0-1.5 m high in 1986.

Deformation of quadrilaterals near the M-line indicates that the landslide thickened at midlength between 1983 and 1986. Quadrilateral Q-11 contracted 15.2 to 18.8 percent, and triangle BCD of Q-12 contracted 23.8 percent between June 1983 and September 1986. Contraction of the quadrilaterals indicates that the landslide thickened 18 to 23 percent beneath Q-11 and 31 percent beneath Q-12, assuming that the bulk density of the landslide was constant. Thickening was nonuniform.

Thickening can explain the formation of scarps along the flanks of the landslide. If the original thickness of the landslide was 5 m, then the final thickness was between 5.9 and 6.5 m. The difference in the final and the original thicknesses of the landslide, 0.9 to 1.5 m, is consistent with the heights of the scarps. However, displacement of the landslide can also account for part the height of the scarps if the original thickness varied along the length of the landslide.

Distal flattening of the slip surface and nonuniform thickening might account for flattening of the ground surface near the center of the M-line. Quadrilateral Q-12 consistently flattened, and the net flattening from May 1984 to September 1986 was 9.2-12.4°. The ground surface of the landslide slopes about 15° between Stations 360 and 390 and about 10° between Stations 390 and 405. In August 1984, the quadrilateral was near Station 390, where the ground slopes 15°. The quadrilateral was displaced about 14 m between May 1984 and September 1986 to ground that sloped 10° in 1984. Displacement of the quadrilateral can account for only 5° of flattening if we assume that the slip surface was approximately parallel to the ground surface in 1984. I assume that the remainder of the flattening of the slope observed at Q-12 (4-7°) resulted from nonuniform thickening, which is evident in the formation of thrust faults between Stations 390 and 420 (Fig. 5.17).

Deformation of the internal toe.--The internal toe is one of the most conspicuous features on the surface of the landslide (Figs. 5.2, 5.18). The distal end of the toe is steep, about 24°; however, the surface of the toe flattens to about 18° some 40 m upslope from the tip of the toe. Overall, the toe is about 7 m high. The average slope of the surface is about 12° above the toe and about 7° below the toe. At its maximum, the toe is about 100 m wide. However, the landslide is narrower both upslope and downslope from the toe (Fig. 5.18). From its narrowest part, near contour 2340 (Station 500), far above the toe, the landslide gradually widens to about 80 m at the proximal end of the toe (near contour 2310, or Station 610). Downslope from the toe, two sets of en echelon cracks marking the lateral boundaries of the landslide are about 70 m apart.

The surface morphology of the internal toe of the landslide suggests that it formed by the accumulation of debris from previous movement of the landslide. Further downslope movement of the debris might have been hindered because the slope flattens from about 12° to about 7°. Debris hindered in its forward movement apparently spread out laterally to form the bulbous shape of the toe.

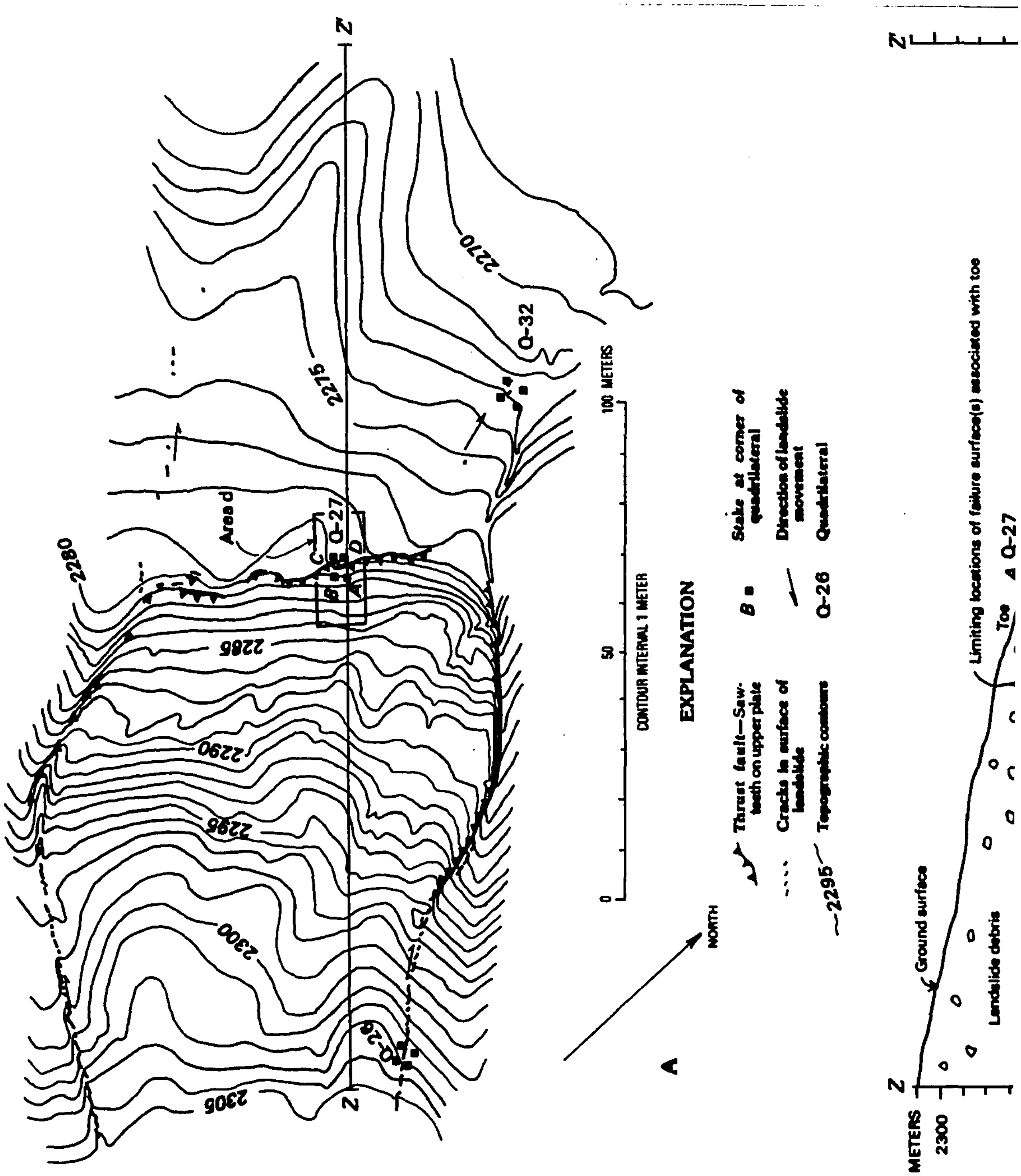

FIGURE 5.18. Map showing the internal toe of the landslide (August 1984 by A.M. Johnson and R.W. Fleming).

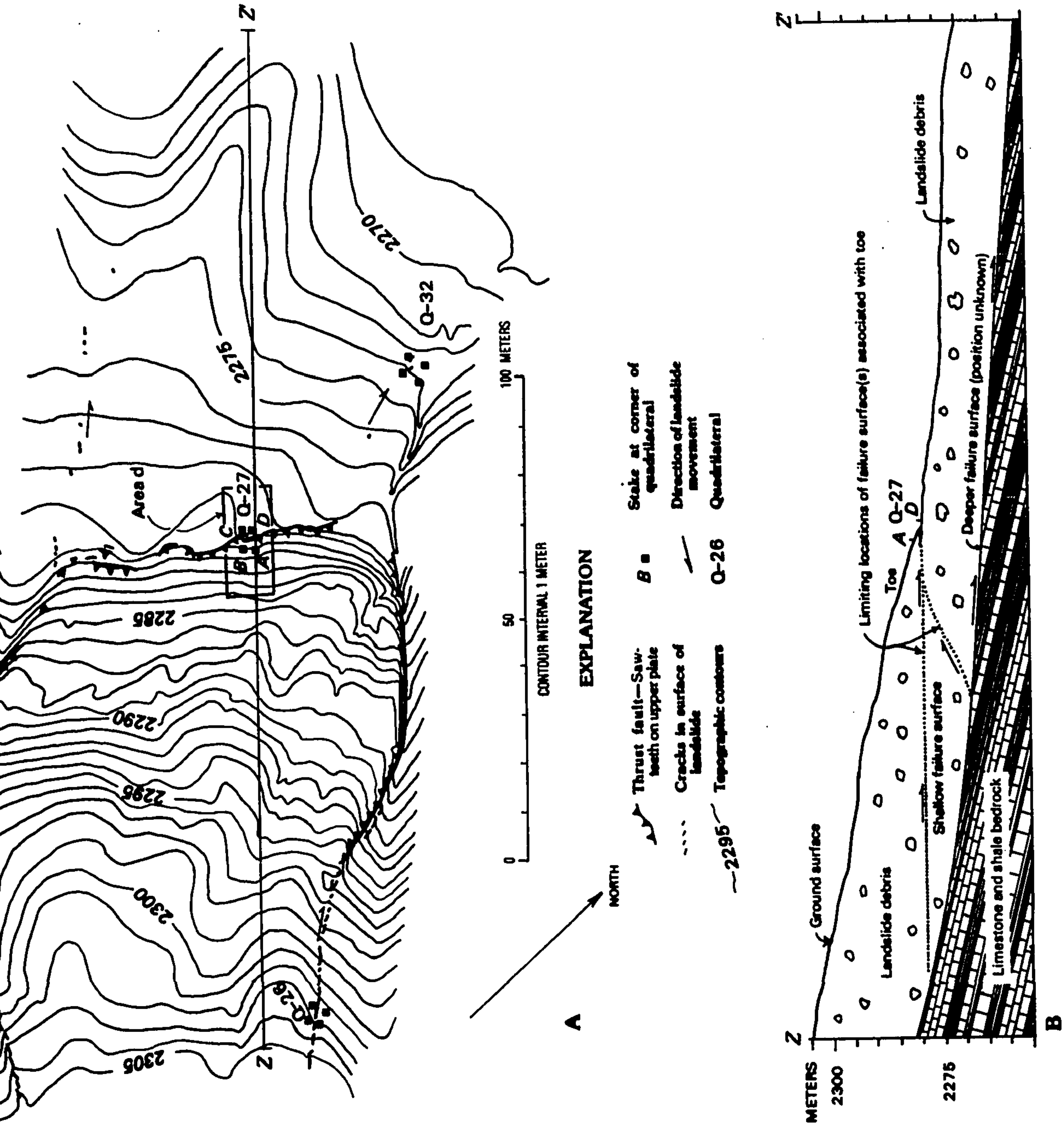

.18. Map showing the internal toe of the landslide

y A.M. Johnson and R.W. Fleming).

The internal toe, at Station 750, did not move during 1983, but began to move during the spring of 1984. Cracks were not observed downslope from Station 600 (Plate 5) during 1983. En echelon cracks appeared along the flanks of the internal toe during May of 1984. Quadrilateral Q-27 on the toe (Fig. 5.18) shortened as the internal toe moved forward, apparently on a shallow failure surface (<1.5 m deep). A narrow band of cracks appeared where the failure surface intersects the surface of the toe about June 6, 1984. En echelon cracks appeared downslope from the toe toward the end of May 1984 as ground distal to the internal foot moved on a deeper failure surface.

The toe grew in height as it moved forward. Stakes on the toe were displaced 70 cm toward N. 40° W., parallel to the axis of the toe, between May 18, 1984 and August 3, 1985. Net displacement of the stakes was about horizontal or 1° upward (Fig. 5.19). Consequently, the stakes were displaced about 7 to 8° upward relative to the sloping surface of ground distal to the toe, and the ground thus thickened in the toe.

Also, the central part of the toe shortened transversely, because the distance between stakes <u>A</u> and <u>B</u> on the toe shortened about 2.0 percent between May 1984 and August 1985.

Deformation at a Flank Ridge

Flank ridges are low ridges having rounded profiles that form within moving landslide debris on the flanks of landslides. The ridges are tens of meters long, several meters wide at the base and from 1 to 4 m high. Flank ridges might be formed by several different processes including deposition and several styles of deformation (Robert W.

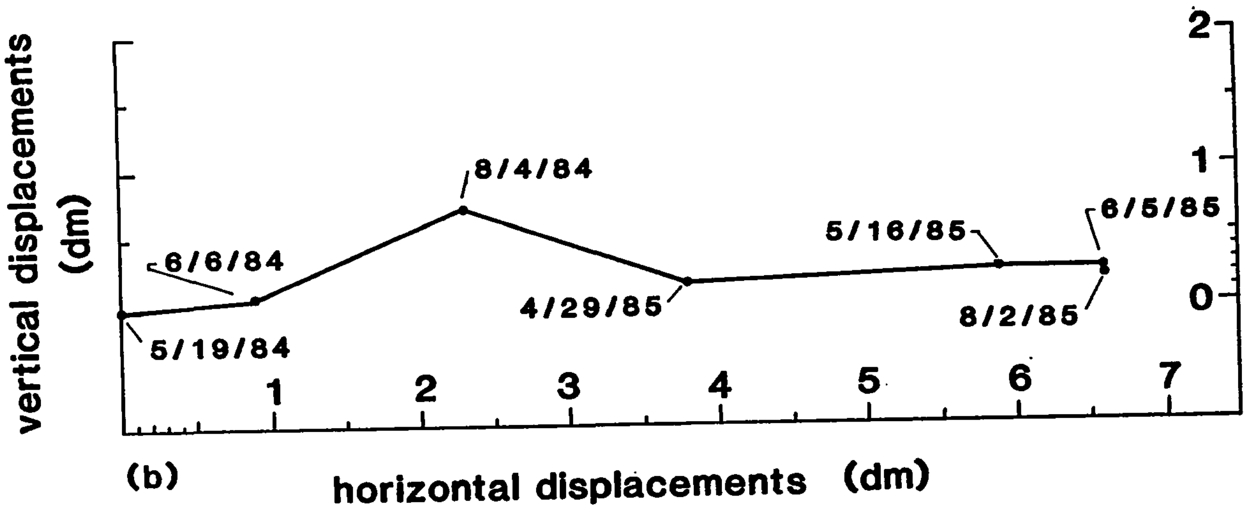

FIGURE 5.19. Graph showing of displacement of stake A of quadrilateral Q-27 at the internal toe.

Fleming, oral commun., 1986). The kinematics of one ridge is described here.

Observations made in June 1984 of a flank ridge on the right flank the of Aspen Grove landslide, in the vicinity of the 2400 m contour (Fig. 5.2) indicated that the ridge might be growing: Cracks were present in the top of the ridge (Fig. 5.20). The trunk of a dead tree had been lifted out of the indentation made by the tree on the surface of the ridge.

On the strength of these observations, quadrilaterals (Q-33 and Q-34) and transverse lines of stakes (R1-line, and R2-line) were placed on the ridge early in June 1984 to determine whether it would grow during the summer of 1984 (see Fig. 5.20 for locations of stake lines and quadrilaterals).

The differential vertical displacements of each stake in lines R1, and R2, between June and August 1984, showed that the ridge was indeed growing in height (Figs. 5.21, and 5.22) Stakes near the crest of the ridge were displaced downward less than stakes on the sides of the ridge. Even though all stakes were moving downward, because the landslide itself was moving downslope, stakes on the crest of the ridge moved upward relative to stakes on the sides of the ridge.

During August 1984, Fleming and Johnson mapped the ridge (Fig. 5.20). In April 1985 they put in more measurement Stations (R3-line), and continued monitoring during spring and summer 1985. The ridge continued growing during 1985 (Figs. 5.21, 5.22, and 5.23).

The greatest growth in height did not occur at the topographic axis of the ridge. A dashed line connecting the stakes having the least

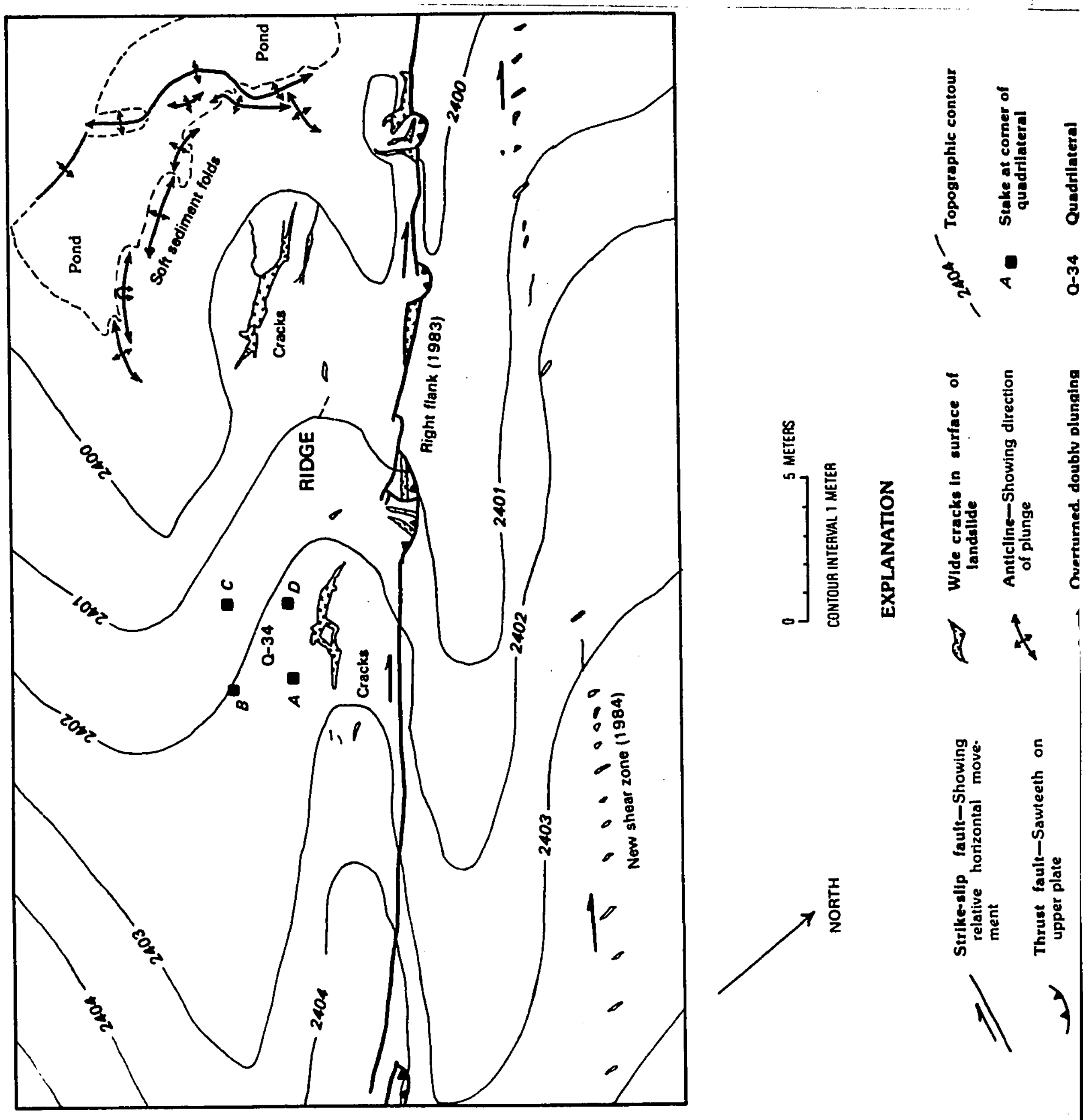

FIGURE 5.20. Map showing the topography, cracks and positions of stakes on the ridge in August 1984. (by R.W. Fleming and A.M. Johnson).

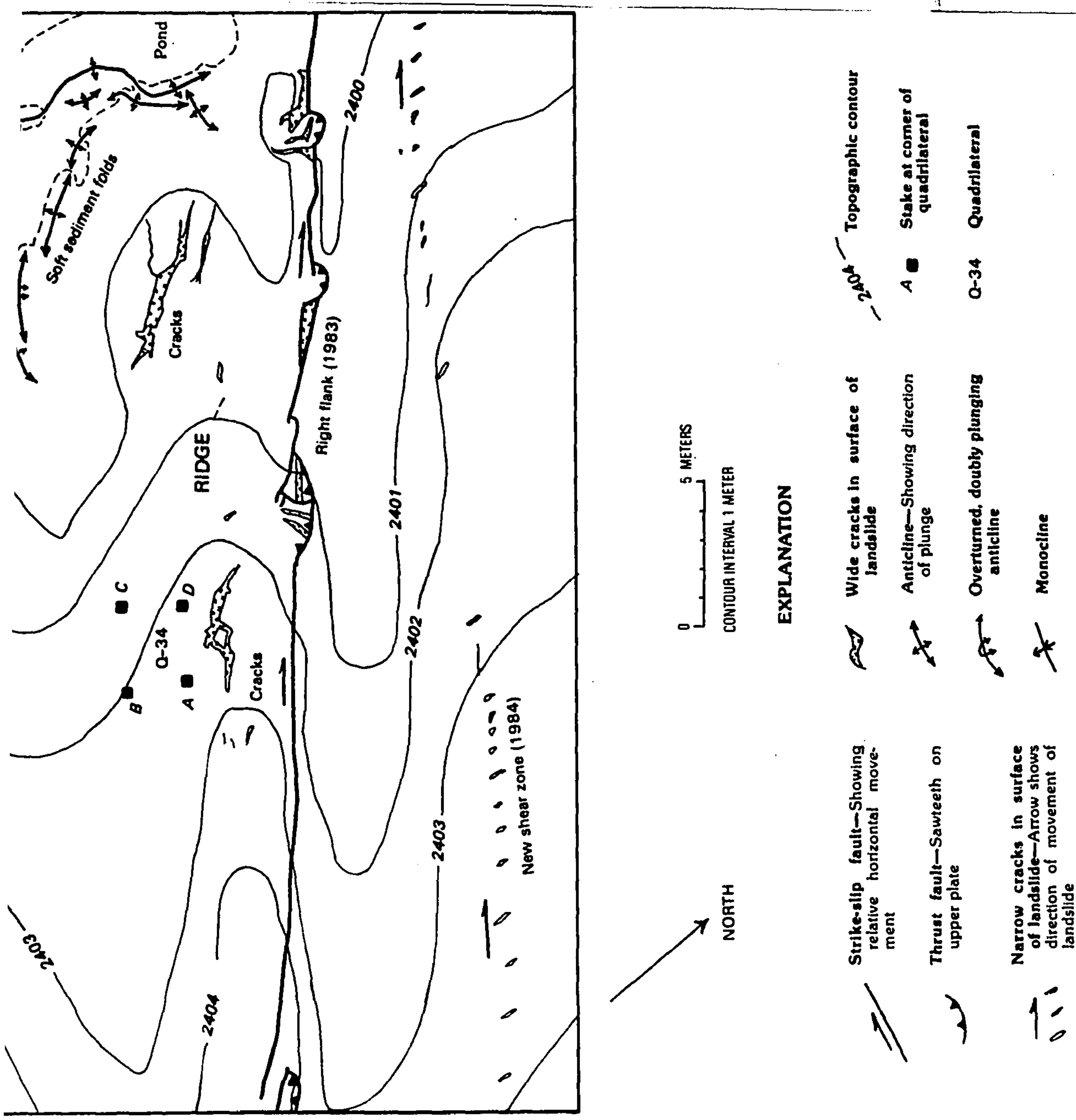

RE 5.20. Map showing the topography, cracks and positions of the ridge in August 1984. (by R.W. Fleming and A.M. Johnson).

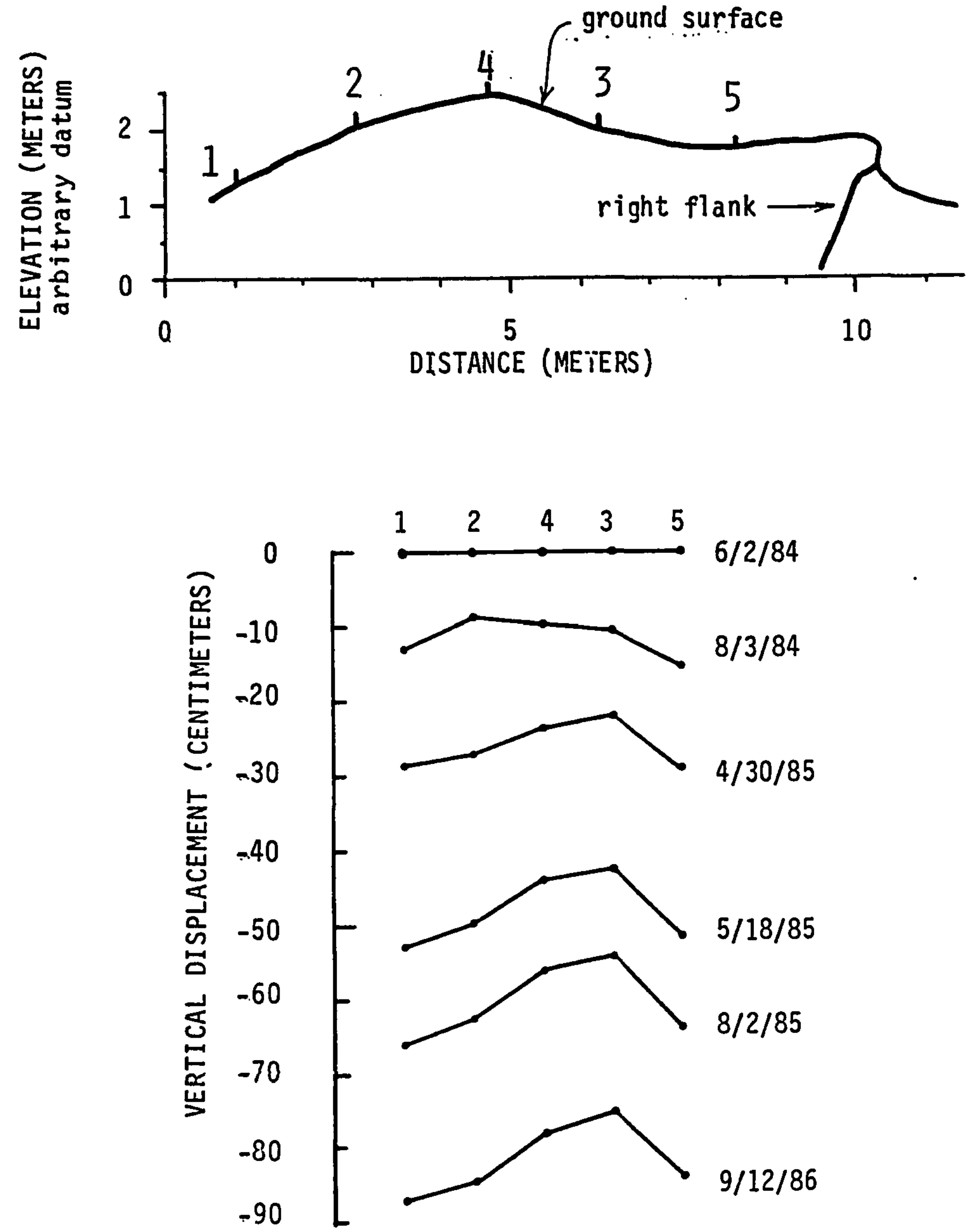

FIGURE 5.21. Profile of the R1-line and graph showing vertical displacements of the stakes in the line.

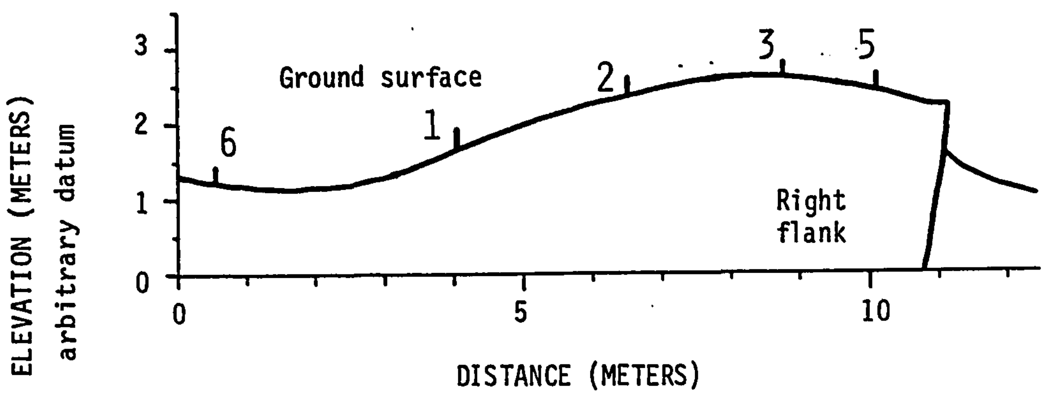

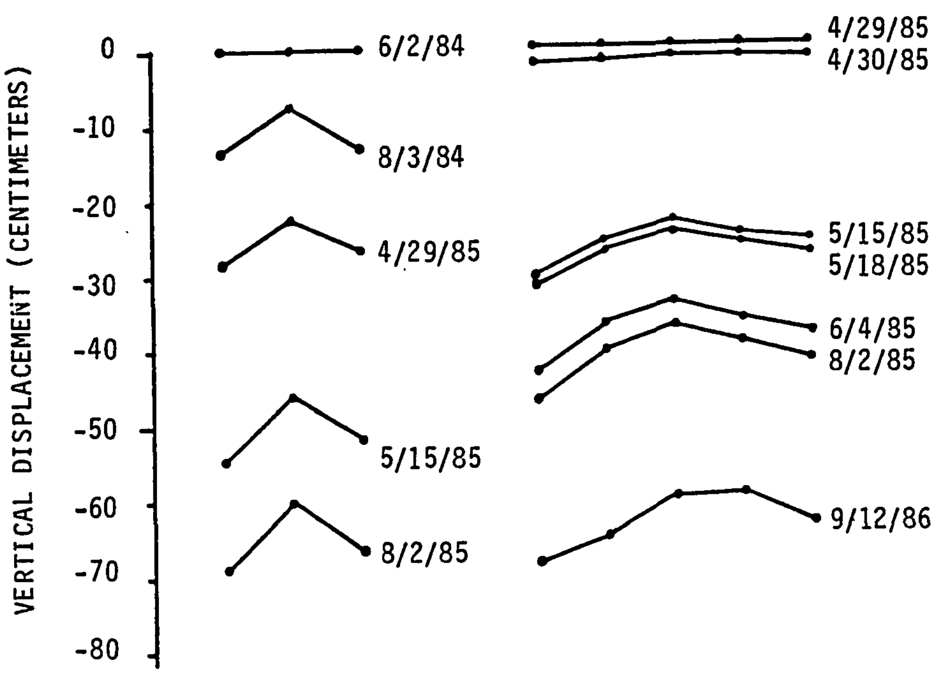

FIGURE 5.22. Profile of the R2-line and graph showing vertical displacements of stakes in the line.

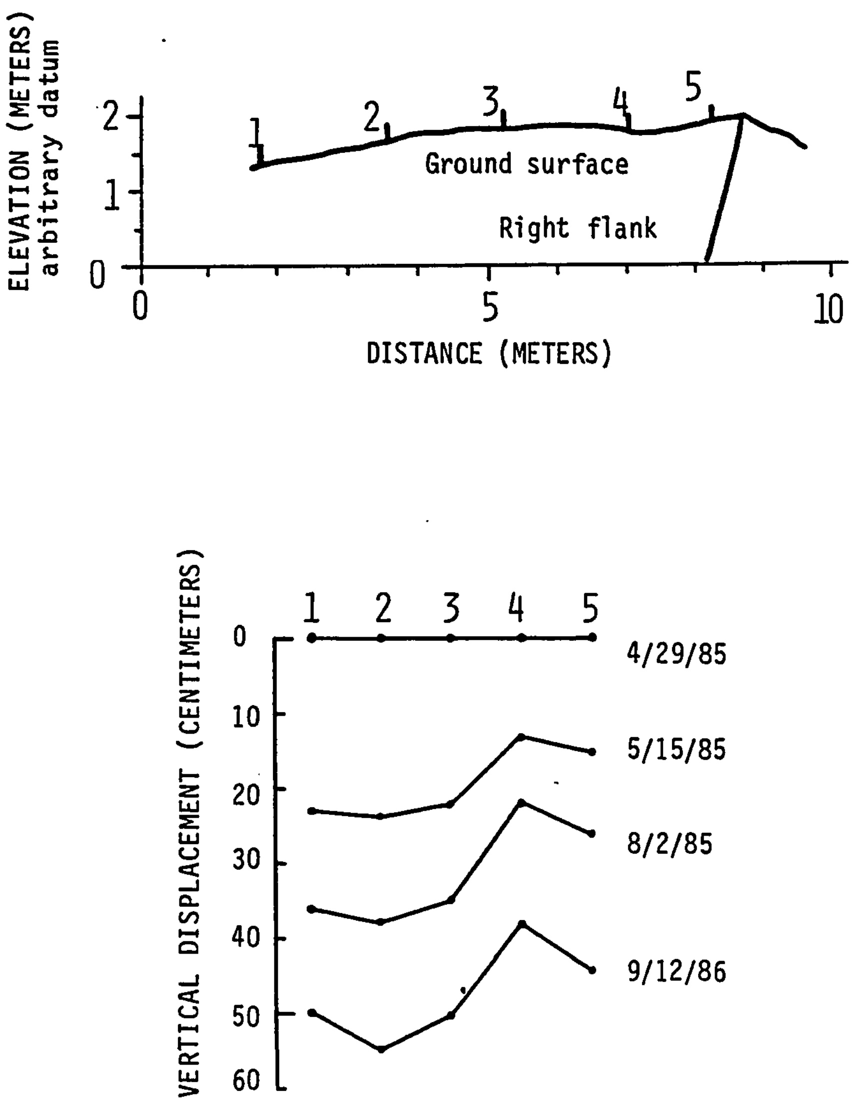

FIGURE 5.23. Profile of the R3-line and graph showing vertical displacements of stakes in the line.

downward displacement from lines R1, R2, and R3 is oblique to the axis of the ridge (Fig. 5.24a).

Tilt of the quadrilaterals was consistent with growth in height of the ridge. The ground surface at quadrilateral Q-34, on the left side of the ridge next to the R2-line (Fig. 5.24a), steepened about 2° between June 2, 1984 and August 2, 1985. The ground surface at Q-33, on the right side of the ridge steepened 0.0 to 1.7° between April and June 1985.

Strains transverse to the axis of the ridge indicate that the axial part of the ridge generally expanded or widened and the sides of the ridge contracted. Strain approximately perpendicular to the axis of the ridge is shown by changes in the <u>horizontal</u> distances between neighboring stakes of lines R1, R2, and R3 (Fig. 5.25). Horizontal lengths of the two outer segments of the R1-line consistently shortened. The area of Q-33, which was on the right-hand end of the R1-line decreased by 2.4-7.4 percent between April and June 1985. The horizontal lengths of the two inner segments of the R1-line consistently lengthened. Similar strain occurred at the R2-line during 1985 (Fig. 5.25). The area of Q-34, on an elongating inner segment of the R2-line increased by 2.8 to 7.3 percent between June 1984 and August 1985. Most segments of the R3-line shortened (Fig. 5.25).

Displacement vectors of stakes on the ridge make counterclockwise angles of several degrees with the trend of the strike-slip fault that defines the original right flank of the landslide (Fig. 5.24b). The trend of the fault is N. 51 W. next to the ridge. Stakes that were mapped by plane table methods in August 1984 and remapped in August 1985

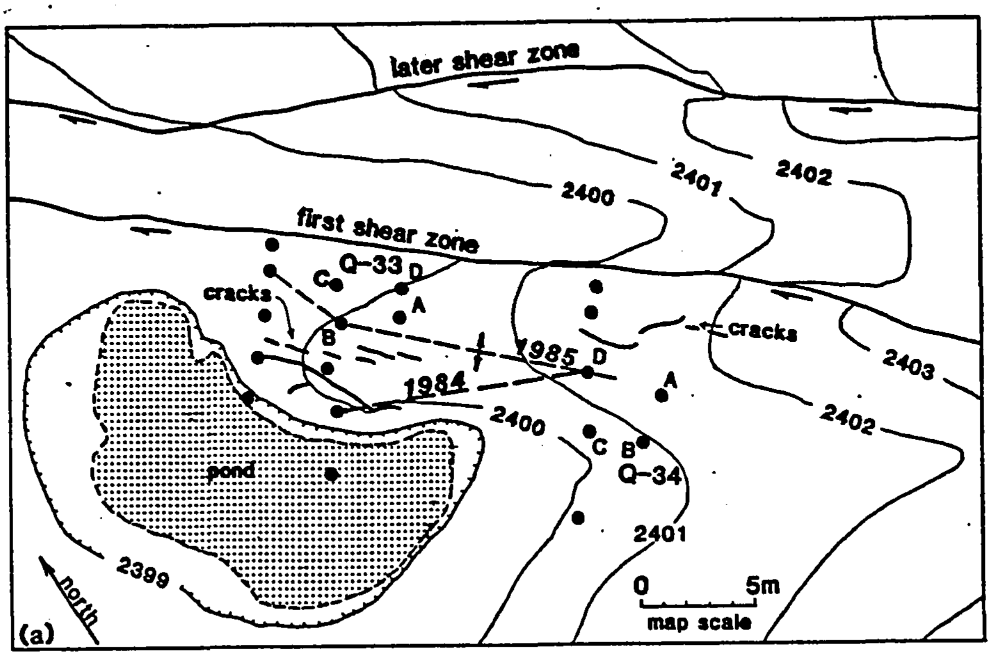

FIGURE 5.24. Map showing the topography, cracks, and positions of stakes on the flank ridge in August 1985. (a) Light lines are topographic contours; the contour interval is 1 m. Large dots are locations of stakes in August 1985. Heavy dashed lines connect the stakes heaving the smallest downward displacements in 1984 and 1985.

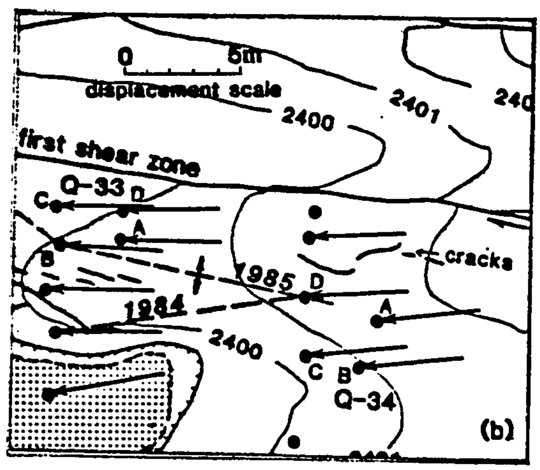

FIGURE 5.24b. Arrows are displacement vectors showing the displacement between August 1984 and August 1985. Stakes without arrows were installed in April 1985. (by R.W. Fleming and A.M. Johnson).

were displaced about 4.5 m toward the N. 61° W (trajectories of the stakes range from N. 56° W. to N. 68° W.). Displacement vectors of stakes A and B of quadrilateral Q-2, farther upslope on the ridge, made counterclockwise angles (ϕ_d in Table 5.4) of 4.5-31° with the trend of the fault. The net displacement of stake A between 1983 and 1986 made an angle of about 10° with the trend of the fault.

Orientation of the displacement vectors are consistent with dilation of the the fault. However, the fault did not dilate, because we observed that the fault surfaces remained in contact with each other at the ground surface.

The form of the ridge resembles the form of a fold. However, the overall change in horizontal length of each line was small; the expansion about the axis of the ridge was compensated by contraction on its sides (Fig. 5.25). The ridge did not form as result of buckling, because net shortening across the ridge at the stake lines was insignificant when compared to the growth in height of the ridge (Figs. 5.21, 5.22, 5.23, and 5.25).

Orientation of the displacement vectors and the growth in height of the ridge are consistent with helical flow that occurs in some non-Newtonian fluids (Truesdell, 1964; Rivlin, 1964; McTigue and others, 1985). If particles in a growing ridge move along helical paths, we would expect the particles to circulate in a counterclockwise sense on the right flank, with respect to an observer standing at the crown of the landslide and looking downslope. Particles following such paths would move up next to the fault and subsequently move toward the axis of

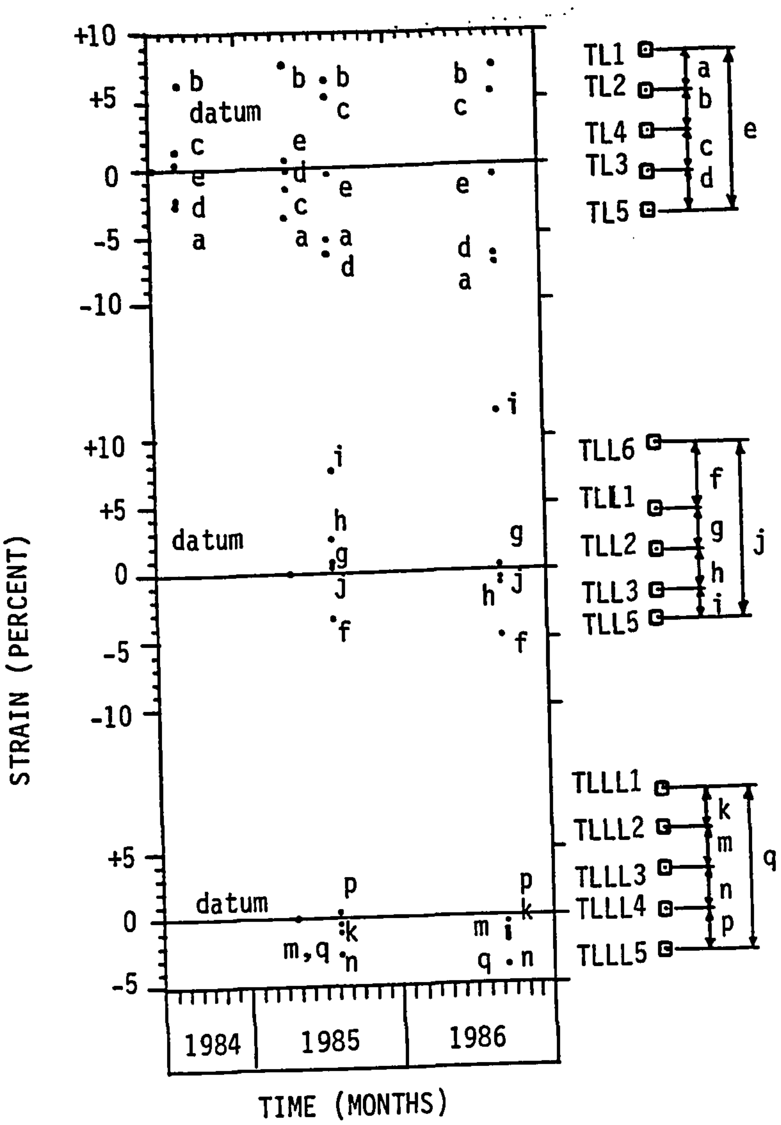

FIGURE 5.25. Graph showing horizontal strain in the stake lines (R1-, R2-, and R3-lines) on the ridge.

TABLE 5.4

Displacement of stakes on the Ridge

Beginning Date	Ending Date	Stake Q-2A θ_d	Stake Q-2A Displacement cm	Stake Q-2B θ_d	Stake Q-2B Displacement cm
6/15/83	8/04/83	10.2°	14	11.4°	16
8/04/83	5/23/84	5.4°	222	7.2°	216
5/23/84	8/03/84	13.0°	159	11.8°	160
8/03/84	4/28/85	24.5°	29	31.2°	30
4/28/85	8/02/85	9.6°	108	8.0°	106
8/02/85	9/12/86	15.4°	32	4.6°	33
6/15/83	9/12/86	10.2°	564		

the landslide, where particles would be moving down toward the slip surface (Fig. 5.26).

Deformation of the quadrilaterals suggests that material in the ridge was sheared and elongated parallel to the direction of displacement. Components of deformation such as shearing or elongation parallel to a given direction can be extracted from the principal stretches by applying successive deformations (Appendix B). I assume that deformation of the quadrilaterals can be treated as a three step process (Fig. 5.27). The quadrilateral contracts or dilates in step one (pure area change). The quadrilateral elongates parallel to the direction of average displacement and shortens a corresponding amount perpendicular to that direction is step two (pure shear). The quadrilateral is deformed into a rhomboidal shape by right lateral shearing in step three (simple shear).

A single parameter determines the magnitude of each component of the deformation (Appendix B). An omnidirectional stretch, $\underline{S}_o$, determines the degree of dilation or contraction. A stretch parallel to the direction of displacement, $\underline{S}_x$, determines the component of pure shear. The angle of simple shear, ψ_y determines the component of right lateral shearing. These parameters have been computed for quadrilaterals Q-33 and Q-34 (Table 5.5). The area change has been discussed in connection with horizontal deformation of the stake lines. The parameter $\underline{S}_x$ indicates that the ridge changed shape by elongating parallel to the direction of displacement, because all values of $\underline{S}_x$ in Table 5.5 are greater than one. The parameter ψ_y indicates that the ridge also was deformed by right lateral shearing parallel to the

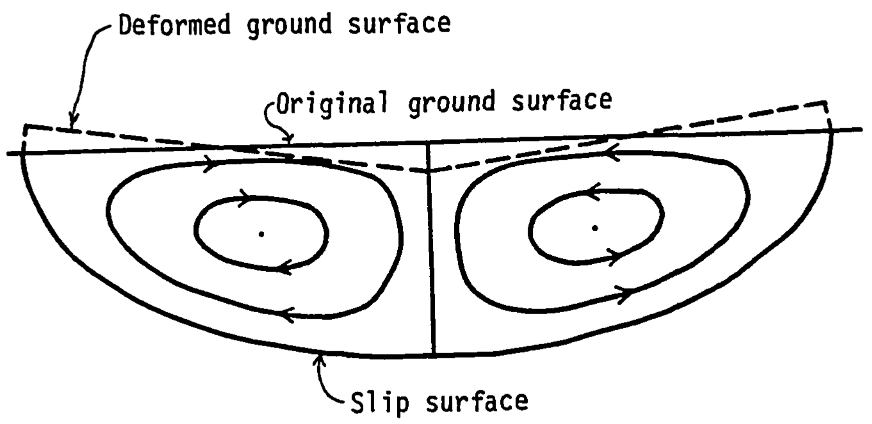

FIGURE 5.26. Schematic diagram showing helical flow pattern suggested by displacement of points on the surface of the ridge (modified from Rivlin, 1964).

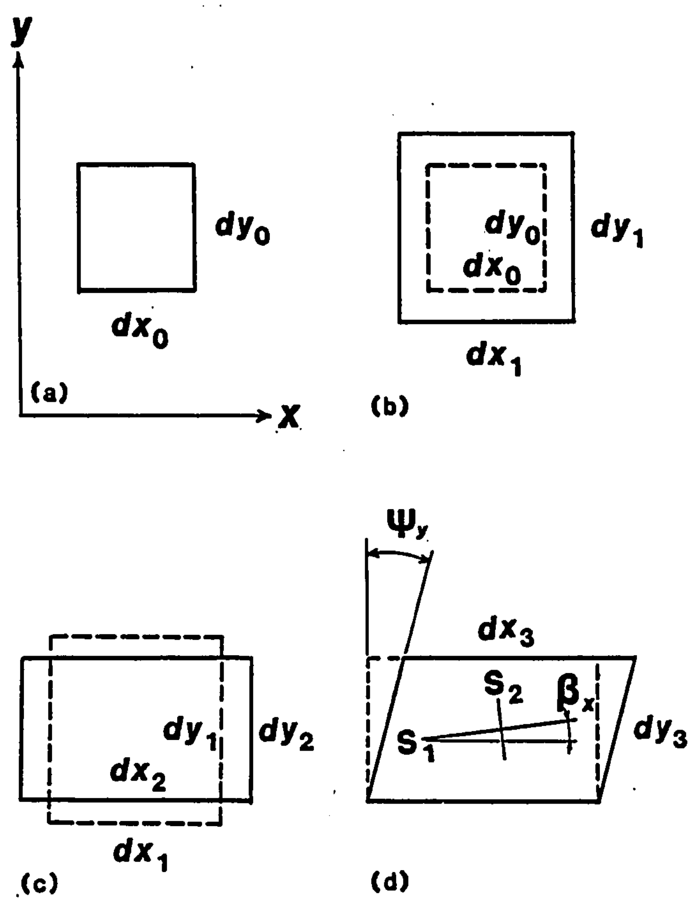

FIGURE 5.27. Schematic diagram showing three successive deformations. (a) coordinate system, and an undeformed element; (b) pure dilation $dx_1/dx_o = dy_1/dy_o = S_o$; (c) pure shear $dx_2/dx_1 = S_x$, $dy_2/dy_1 = 1/S_x$; and (d) simple shear. Angle of simple shear is ψ_y; β_x is angle between S_1 and x-axis.

direction of displacement, because values of ψ_y in Table 5.5 range between 0.0 and +3.53°.

I do not know whether elongation and shearing are characteristics of deformation at landslide flanks, or merely coincidental, but the evidence suggests that shearing and elongation parallel to the direction of displacement does not occur adjacent to every part of the landslide flanks. For example, deformation at Q-7, on the left flank at the L-line, resulted in shortening parallel to the direction of displacement. The minor principal stretch was oriented parallel to the direction of displacement and $\underline{S}_0$ was less than one (Table 5.6).

Deformation over a Bump in the Failure Surface

A bump in the ground surface that is shaped like half a dome is on the right flank of the Aspen Grove landslide near the 2390 m contour (Figs. 5.2, 5.28). This bump is referred to as the dome henceforth. The dome is about 30 m long, 15 m wide and 1.5 m high. Several field observations suggested that the dome was growing or deforming. Trees tilted away from the center of the dome (Fig. 5.29) and tension cracks shattered the surface of the dome.

A quadrilateral (Q-86) and two lines of stakes were set up on the dome (Fig. 5.28) to observe its growth.

Points crossing the top of the dome rose in absolute elevation during 1985 (Fig. 5.30). Point BH3, near the apex of the dome, rose 0.3 m relative to stable ground. Points on the inside flank of the dome went down about 0.3 m.

TABLE 5.5

Stretches and tilts at the ridge

	Q-34 (6/84 - 8/85)				Q-33 (4/85 - 6/85)			
	ΔABC	ΔBCD	ΔCDA	ΔDAB	ΔABC	ΔBCD	ΔCDA	ΔDAB
S_1	1.059	1.068	1.046	1.037	1.023	1.004	0.971	1.002
S_2	0.981	1.005	1.008	0.991	0.954	0.951	0.954	0.950
S_1S_2	1.039	1.073	1.055	1.028	0.976	0.955	0.926	0.952
γ_{max}	0.0767	0.0612	0.0370	0.0459	0.0698	0.0539	0.0179	0.0530
β_x	6°	22°	19°	0°	31°	38°	12°	7°
ψ_y	0.91°	2.43°	1.30°	0.00°	3.53°	2.99°	0.42°	0.74°
S_o	1.019	1.036	1.027	1.014	0.988	0.977	0.962	0.976
S_x	1.038	1.023	1.015	1.023	1.017	1.007	1.008	1.026
Tilt[1]	2.8°s	0.4°s	1.9°s	4.2°s	1.4°s	1.7°s	0.1°s	---

[1] s = steepen

TABLE 5.6

Stretches at the left flank Q-7 (8/84 - 8/85)

	ΔABC	ΔBCD	ΔCDA	ΔADC
$\underline{S}_1$	1.027	1.007	0.988	1.008
$\underline{S}_2$	0.931	0.928	0.931	0.932
$\underline{S}_1,\underline{S}_2$	0.956	0.935	0.920	0.940
β_x	$+1^o$	-5^o	-2^o	$+7^o$
S_o	0.978	0.967	0.959	0.970

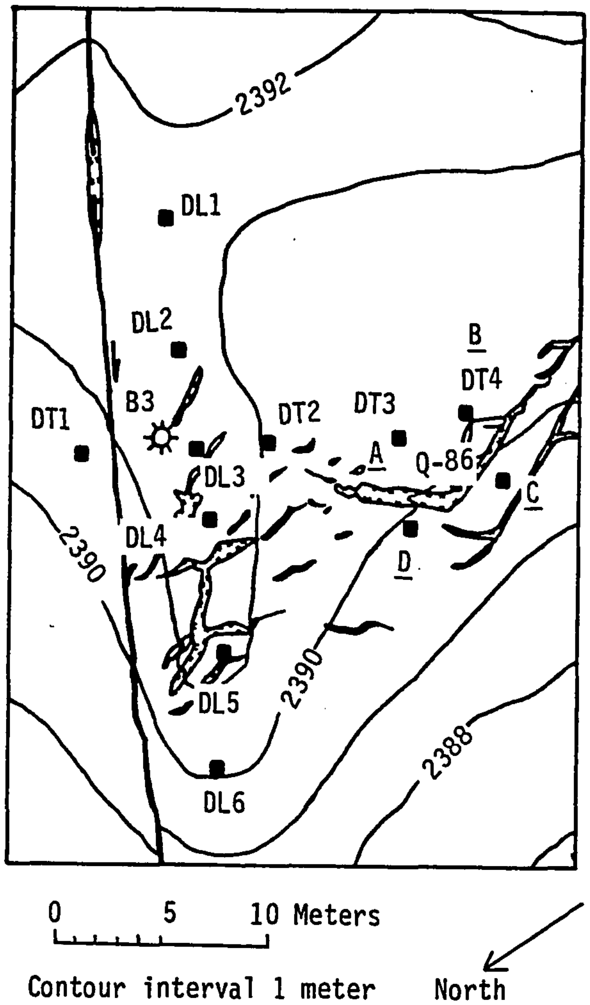

EXPLANATION

2390 — Topographic contour

Strike-slip fault--showing relative movement

Wide cracks in surface of landslide

Narrow cracks in surface of landslide

B3 — Borehole

TL2 — Survey station

Q-86 — Quadrilateral

FIGURE 5.28. Map showing topography, cracks and positions of stakes on the dome at the beginning of movement in 1985. Topography and cracks mapped August 1984 (by Robert Fleming and Arvid Johnson).

FIGURE 5.29. Photograph of leaning trees on the dome in July 1985. Trees upslope (right in photograph) from the dome lean to the right; those downslope lean to the left. Trees in foreground (on the side of the dome) lean toward the observer.

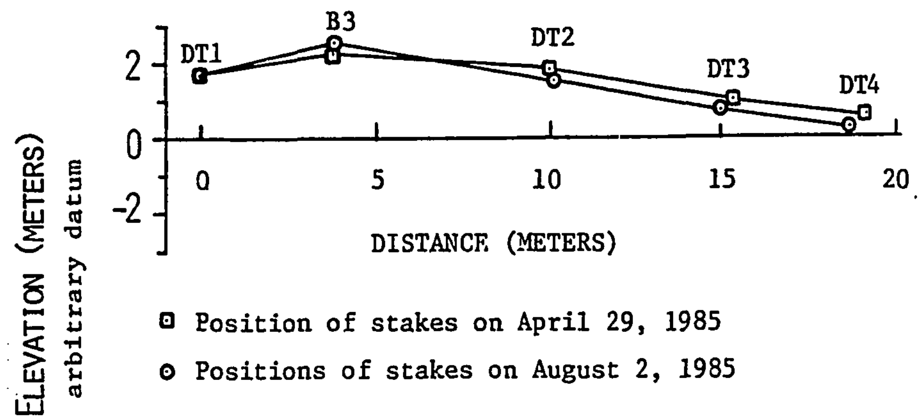

FIGURE 5.30. Profiles of DT-line showing vertical and lateral displacement of stakes in the line during the summer of 1985.

The measurements indicate that the dome is a topographic feature that remains in a fixed location and that the landslide debris passes through it. Figure 5.31 shows the positions of stakes along a longitudinal line across the dome, that is, a line parallel to the flank (Fig. 5.28). in April and August 1985. The elevations of the stakes are relative to a station off the landslide. The average displacement near the dome during this time was about 3 m, so the horizontal position of the first stake for August 1985 is displaced 3 m downslope (to the right) from its earlier position. The relative positions of all the stakes are maintained (Fig. 5.28). The longitudinal profile of the dome is well preserved, except for minor thickening at the downslope end of the survey line.

Deformation of the soil on the dome from April to June 1985 was consistent with deformation that might occur as landslide debris slides over a rounded bump in the basal slip surface. Paths of particles at the surface of the landslide would trace the profile of the bump on the slip surface, except that ground crossing the apex of the bump might dilate and ground on the sides of the bump might slide laterally, causing shortening perpendicular to the topographic contours.

The ground surface at Q-86 on the side of the dome steepened by 2.6-4.3° and the slope direction rotated 12-18° clockwise about a vertical axis. The quadrilateral contracted 0.9-2.0 percent. Ground on the side of the dome shortened, but ground near the crest of the dome elongated (Fig. 5.31). The major principal stretch at Q-86 was 1.003-1.014 and oriented about parallel to the contours, from N 30° W. to N.

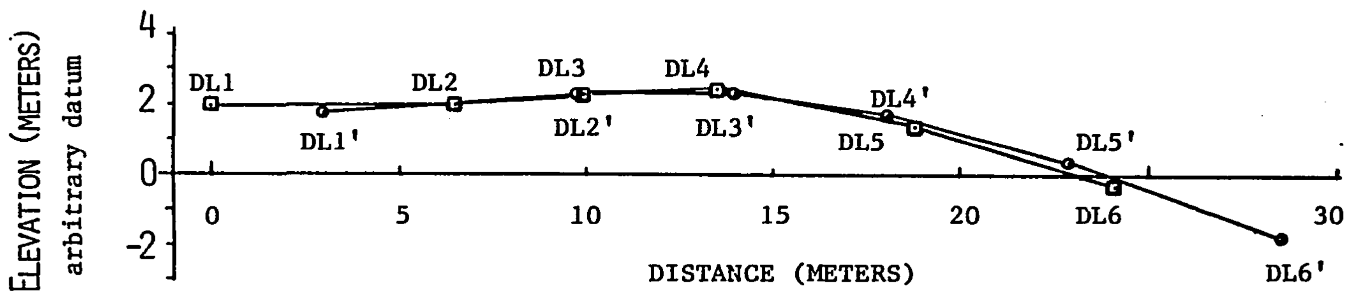

Positions of stakes on April 29, 1985

Positions of stakes on August 2, 1985

FIGURE 5.31. Profiles of the DL-line showing changes during the summer of 1985. Profiles of the DL-line with the later (August 2, 1985) profile displaced 3 m to the right of the earlier profile.

42° W. The minor principal stretch was 0.972-0.978 and about perpendicular to the contours.

A simple two dimensional model shows how trees that are initially vertical might be tilted as the landslide moves over a bump on the basal slip surface (Fig. 5.32). Trees initially upslope from the bump and on the distal side of the bump (trees 1 and 3, Fig. 5.32) tilt in such a way that they plunge parallel to the direction of displacement. Trees initially on the proximal side of the bump (tree 2, Fig. 5.32) tilt in the opposite direction, which is antiparallel to the direction of displacement. Trees distal to the bump (tree 4, Fig. 5.32) are of course untilted.

The pattern of tilting of aspen trees near the right flank (Fig. 5.33) is similar to the pattern predicted by the model (Fig 32). Trees proximal to the crest of the dome (between the 2390 and 2391 contours) plunge 63° to 77° toward the west, roughly parallel to the direction of displacement. Trees distal to the crest of the dome (between the 2389 and 2390 contours) plunge 51° to 73° toward the east, roughly antiparallel to the direction of displacement. Trees opposite hole B2, distal to the dome, plunge 73° to 84° toward the west or southwest, roughly parallel to the direction of displacement.

Other features on the surface of the landslide also appeared to result from deformation over undulations in the basal failure surface. In particular, we observed that the pond next to the ridge (Figs. 5.2, 5.20) and the pond between the 2350 and the 2355 m contours (Fig. 5.2) maintained their positions between 1983 and 1986. The former edges and bottoms of the ponds were observed downslope from the ponds, and trees

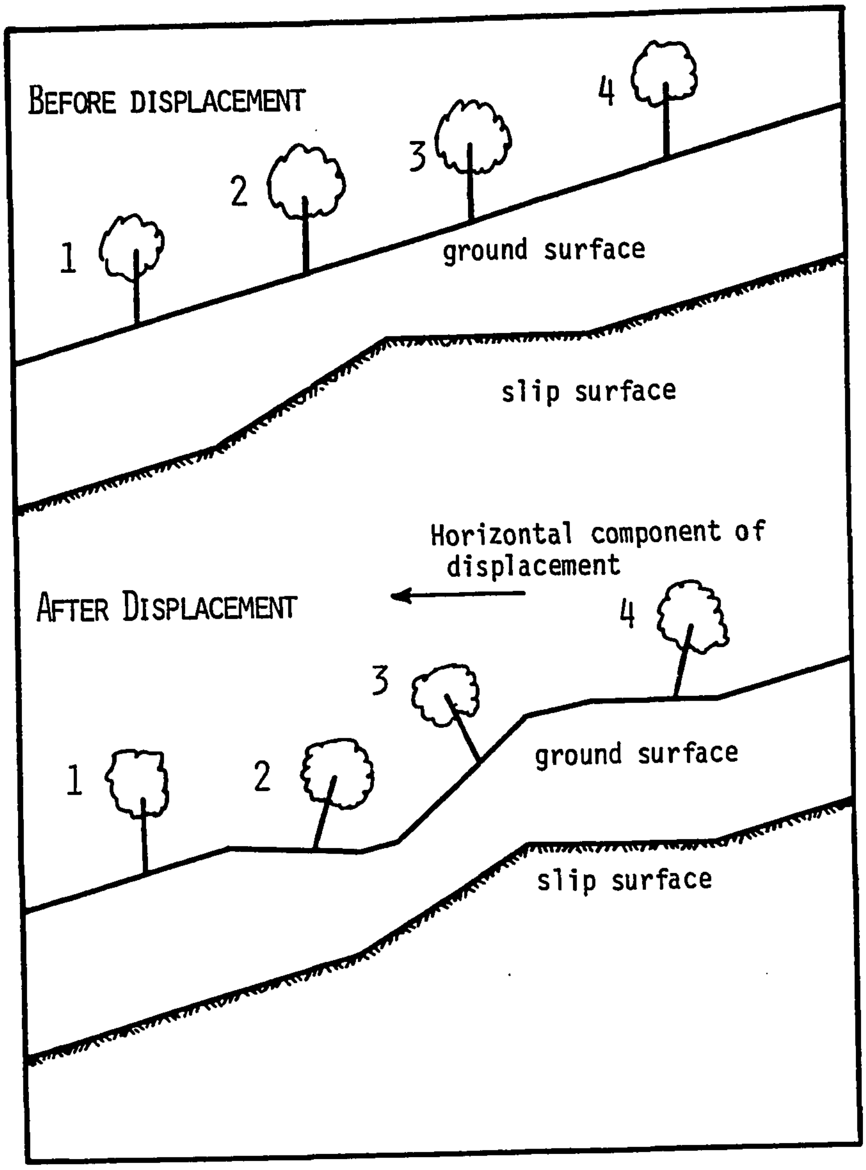

FIGURE 5.32. Diagram showing how trees that were initially vertical are tilted as the landslide moves over a bump on the slip surface.

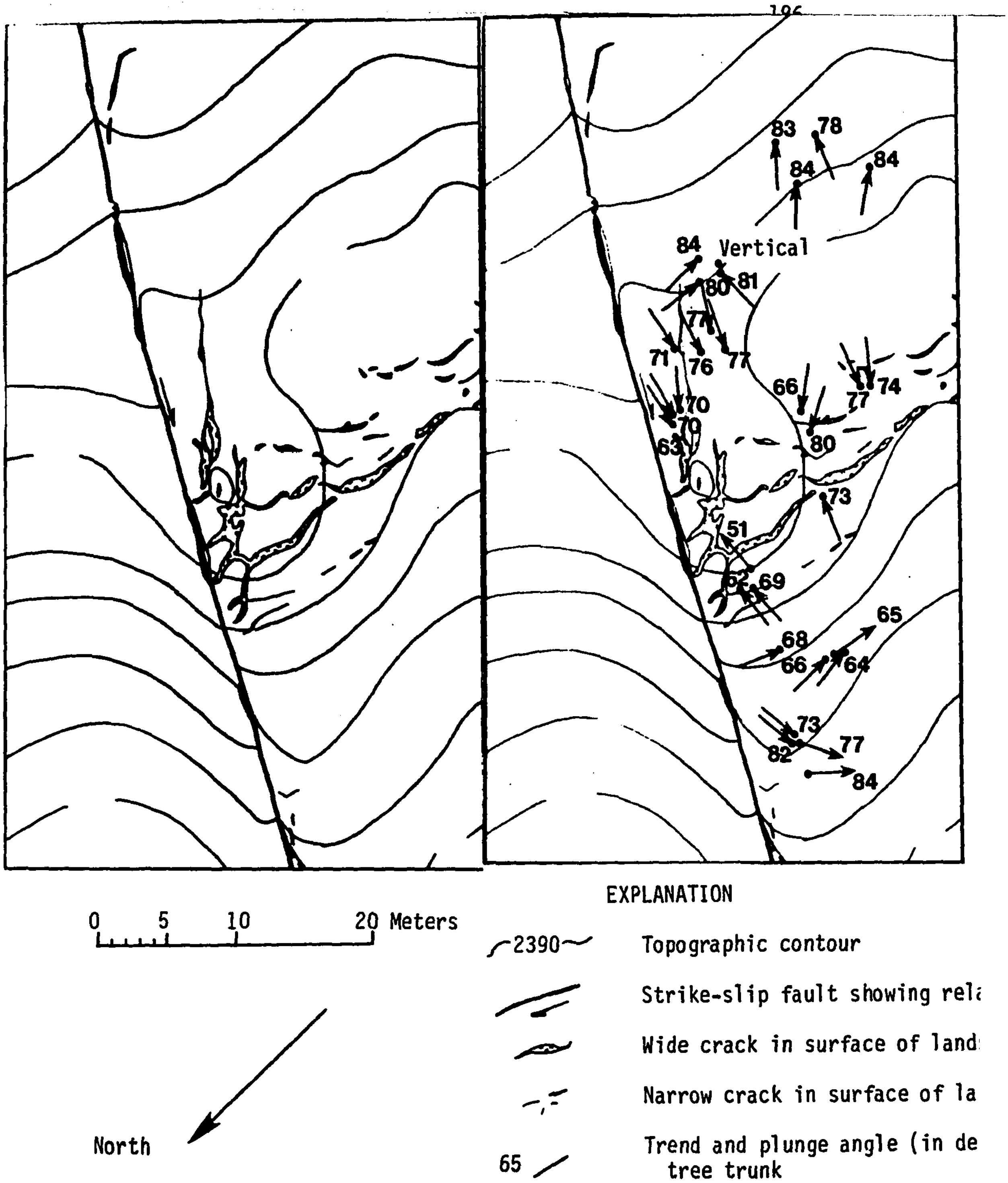

FIGURE 5.33. Map showing trend and plunge angle of tree trunks near the dome (August 1985).

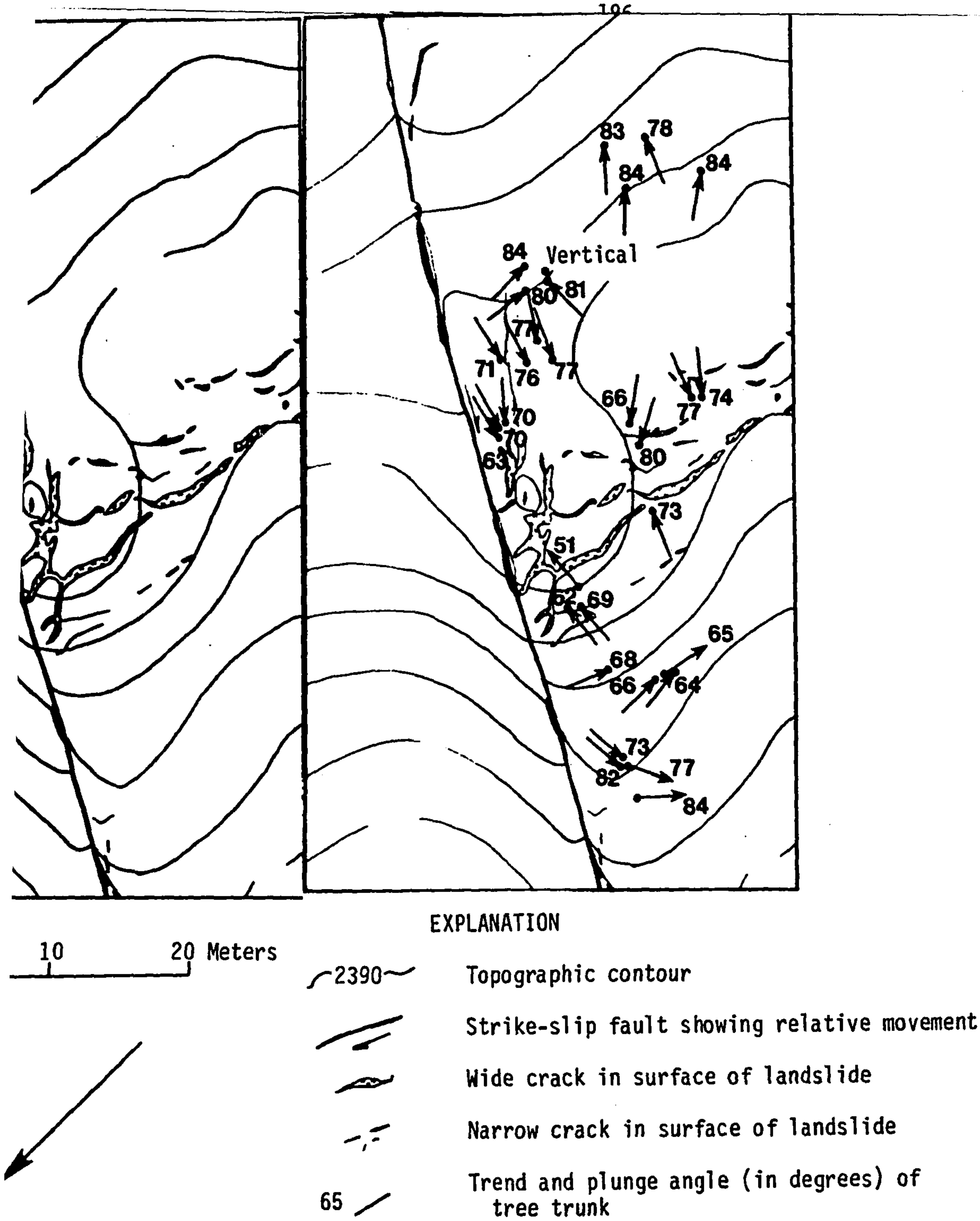

Map showing trend and plunge angle of tree trunks
ıst 1985).

that started out being upslope from the ponds later occupied the bottoms of the ponds.

Discussion

Some general conclusions about the motion and mechanics of the Aspen Grove landslide follow from analysis of our data and observations. The landslide moved uniformly rather than in surges. Movement occurred almost simulatneously throughout the landslide. Much localized deformation occurred near uneven boundaries and some localized deformation might have occurred as a result of nonlinear behavior of the landslide debris.

Presumably each part of the landslide responded to movements elsewhere in the landslide, but the timing of the responses varied. Ground in the lowest part of the landslide started moving at least a day and perhaps two weeks after movement started in the main body (Figs. 5.3 and 5.4). Movement stopped in the lower part of the landslide several weeks before movement stopped in the main body of the landslide. Within the main body of the landslide, maxima and minima in the daily velocity observed at three extensometers usually occurred on the same day (Fig. 5.10). During 1983 and the first part of 1984, the upper (Q-2) and middle (Q-6) parts of the landslide accelerated at about the same time (Figs. 5.5, 5.6). The gross pattern of displacements (Plate 5) and the distribution of velocities at the extensometers (Fig. 5.9) are consistent with the distribution of velocities predicted by a simple form of the continuity equation (equation 5.1).

Much deformation observed in the landslide can be attributed to geometry of the landslide boundaries. The landslide debris stretches axially and shortens transversely as it slides between converging flanks, and it shortens axially as it slides between diverging flanks (Table 5.1). Features at the surface of the landslide, such as the ponds at Station 150 (Plate 2) and Station 430 and the dome, near Station 250, mimic depressions and a bump on the basal slip surface. Transverse gradients in the velocity occur where the landslide is forced to bend at turns in the flanks, or to squeeze between converging flanks (Figs. 5.13 and 5.14).

Some deformation apparently results from the rheology of the landslide material. The flank ridge that was monitored in detail might result from a type of circulation or secondary deformation that occurs in materials having nonlinear rheologies (Fig. 5.26).

Overall, the landslide was in equilibrium during the time it was active. Acceleration of the landslide was negligible during the time that displacement was monitored by recording devices. The velocity varied through time between 0 and about 20 cm per day, and surging occurred rarely or not at all. Although thickness, slope angle and other factors that determine the stability of a slope vary over the extent of the landslide, the parts of the landslide interacted to allow the whole to slide in a stable, or steady fashion characteristic of landslides in fine grained soils (Keefer and Johnson, 1983). The velocity varied through time between 0 and about 20 cm per day, which suggests that rate dependent processes contribute a stabilizing force that prevents the Aspen Grove landslide from accelerating to high velocities.

CHAPTER VI

MEASUREMENT OF SLOPE DEFORMATION USING QUADRILATERALS

Introduction

Displacements and strains have been used in many studies of slope behavior. Such data are useful for studying landslide kinematics and dynamics (Keefer and Johnson, 1983; Iverson, 1984; Lantz, 1984), monitoring stability of slopes and safety of structures during and after construction (Hanna, 1985), planning and evaluating landslide stabilization schemes (Ter-Stepanian, 1984), measuring near-surface stresses in slopes (Zaruba and Mencl, 1982), and estimating the geometry of slip surfaces (Carter and Bentley, 1985; Cruden, 1986). These applications have in common an attempt to use surface measurements to infer conditions at depth.

In order to understand and possibly predict some aspects of landslide behavior by means of surface measurements, Robert Fleming began monitoring the Aspen Grove landslide in 1983. Quadrilaterals were installed at several places on the landslide, at the suggestion of David Varnes (U.S. Geological Survey). Arvid Johnson derived equations for computing displacement, strain and tilt from quadrilateral measurements and wrote computer progams for calculating these quantities. I have checked these equations and programs and made corrections. Such a technique was also proposed by Brunsden (1984, p. 393, 396), who indicated that no published accounts exist of the use of quadrilaterals in studying landslides.

In surveying, a quadrilateral is a four-sided, plane figure defined by the survey stations (stakes or monuments) at its four corners (Ingram, 1972; Brinker and Wolf, 1977; Laurila, 1983). Brinker and Wolf (1977, p. 372) noted that the quadrilateral is the simplest geometric figure that permits rigorous closure checks and adjustment of measurement errors. Errors of closure can be determined because a redundant measurement is made whenever the lengths of all four sides and both diagonals of the quadrilateral are measured. Various methods are used to distribute the error (Laurila, 1983).

In addition to the fact that the measurements of quadrilaterals can be checked and adjusted rigorously, quadrilaterals have several features that make them useful for measuring strains and displacements. Quadrilaterals permit measurement of strain in several directions at one location because the sides and diagonals trend in as many as six different compass directions. Because quadrilaterals are defined by survey stations at their four corners, soil within a quadrilateral can undergo large deformations without the quadrilateral affecting soil movement. This is a distinct advantage over some types of soil strain gages (Hanna, 1985, p. 296-300). Quadrilaterals can be measured with a variety of instruments, such as a steel tape, a tape extensiometer, or a sophisticated electronic device. Thus, they can be used to make measurements at levels of precision needed for a wide variety of landslide studies.

Experience with the use of quadrilaterals during the last few years has convinced me that the method has significant potential for studying landslide kinematics. I have learned, by trial and error, how quadrilaterals can be expected to function in field situations. This paper explains the theory behind the use of quadrilaterals and describes how quadrilaterals were used in the field. The use of the data for describing the kinematics of the landslide is discussed in Chapter V of this dissertation. Raw quadrilateral measurements are listed in Appendix C, and displacements computed from quadrilaterals are listed in Appendix D.

Method

Here I discuss the theory behind the use of quadrilaterals and some practical details that apply to all quadrilaterals: the fundamentals of computing displacements, strains, and tilts (derivations of the equations for finite strain are in Appendix E); the optimum range of size, shape, and frequency of measurement of the quadrilaterals; and detecting and dealing with the measurement errors.

Computational Methods

In the field, a quadrilateral is marked by stakes or permanent markers at its four corners (Fig. 6.1). Measurements of the lengths of the sides and diagonals are repeated to observe deformation of the quadrilateral through time.

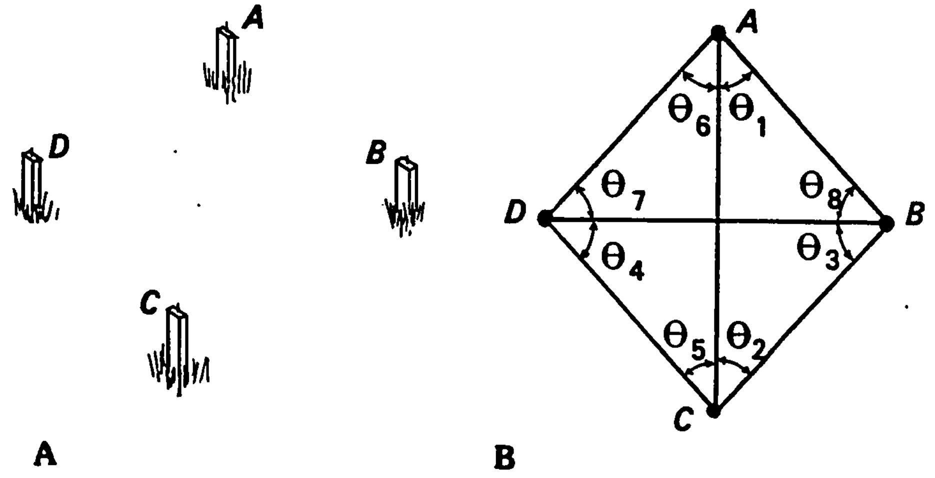

FIGURE 6.1. Typical quadrilateral. (A) Isometric view, (B) Normal view. Stakes are labeled A through D in clockwise rotation, with stake A having the highest elevation. Slope lengths of the four sides and two diagonals and the vertical distances (elevation differences) between A and the other three corners are measured. Angles $\theta_1, \ldots, \theta_8$ are computed from the slope lengths of the sides and diagonals of the quadrilateral, by the law of cosines.

If the quadrilateral straddles an outer edge of the landslide, then the data are used to compute landslide displacements relative to the stable ground along the boundary. If the quadrilateral is within the landslide, then the data are used to compute strains and tilts within the landslide mass.

Errors.--Detailed theories for checking closure and adjusting measurement errors in quadrilaterals are in the surveying literature (Ingram, 1972; Brinker and Wolf, 1977; Laurila, 1983; and others).

We compute the error of closure by projecting the quadrilateral onto a horizontal plane. Angles $\phi_1, \ldots, \phi_8$, the horizontal projections of angles $\theta_1, \ldots, \theta_8$, shown in Figure 6.1, are computed by means of the law of cosines. The angular error of closure is determined by using the following equation (Laurila, 1983, p. 43):

$$w = \left(\sum_{i=1}^{8} \phi_i\right) - 360^\circ. \tag{6.1}$$

Displacement.--Displacement across a landslide boundary is computed from the original and final positions of a corner of the quadrilateral (Fig. 6.2). The x-y plane is horizontal, with the positive x-axis being the horizontal projection of side AD of the quadrilateral (Figs. 6.1b, 6.2a). Angle ϕ (Fig. 6.2b) for the initial position of corner B of the quadrilateral is computed from the horizontal components of AB, BD, and DA by means of the law of cosines. Similarly, angle ϕ', for the final position of corner B, is computed from the horizontal components of AB', B'D, and DA. The x and y

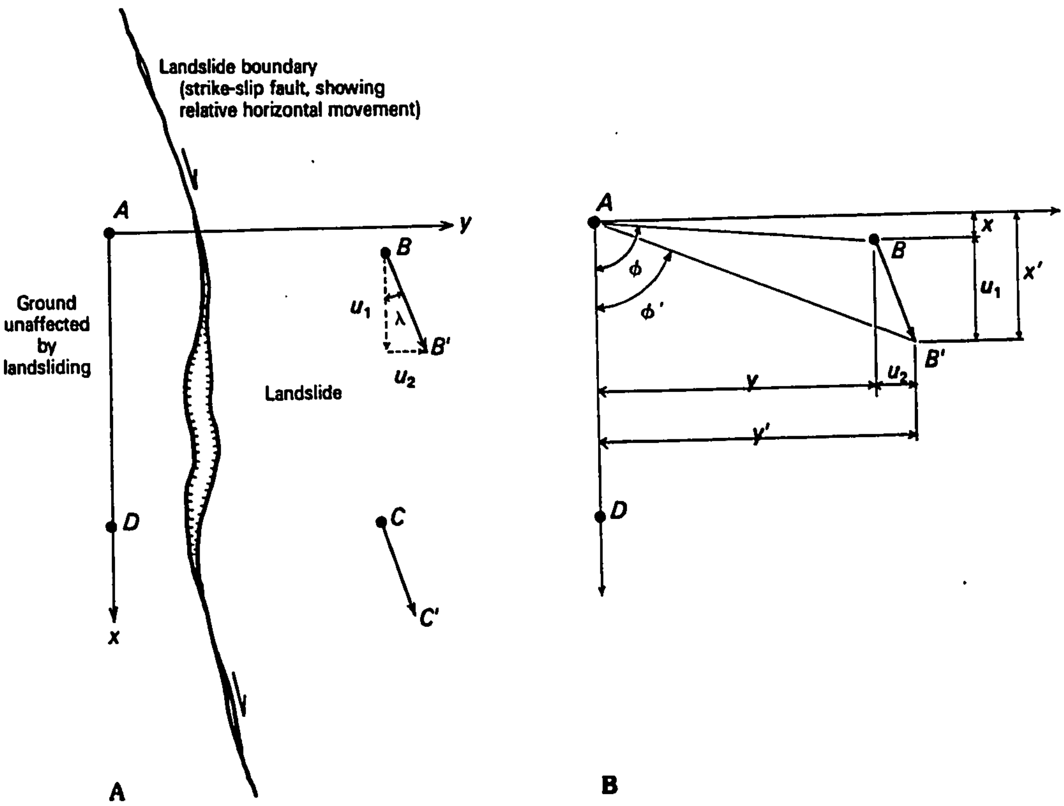

FIGURE 6.2. Sketch of reference system for computing displacements across a discontinuity or landslide boundary. The $\underline{x}$-$\underline{y}$ plane is horizontal; the origin is at point $\underline{A}$ and the positive $\underline{x}$ direction coincides with the direction of line $\underline{AD}$. (a) Displacement component $\underline{u}_1$ is parallel to $\underline{x}$, $\underline{u}_3$ (not shown) is vertical, and $\underline{u}_2$ is parallel to $\underline{y}$. The angle between the horizontal projection of the total displacement and the $\underline{x}$ axis is λ. (b) Initial position of point $\underline{B}$ is given by coordinates $\underline{x}$, $\underline{y}$; its final position, $\underline{B}'$, by coordinates $\underline{x}'$, $\underline{y}'$. The projection of angle $\underline{DAB}$ onto the $\underline{x}$-$\underline{y}$ plane is ϕ; that of angle $\underline{DAB}'$ is ϕ'.

components of line AB and the x and y components of line AB' are computed by means of standard trigonometric formulas. The x and y components of displacement, u_1 and u_2, (Fig. 6.2) are determined by:

$$u_1 = x' - x, \tag{6.2a}$$

and,

$$u_2 = y' - y. \tag{6.2b}$$

The vertical component of displacement, u_3, is the elevation difference between B and B'. Total displacement (net slip), U, is determined by the Pythagorean theorem:

$$U = (u_1^2 + u_2^2 + u_3^2)^{1/2}. \tag{6.3}$$

The counterclockwise angle λ between the positive x-axis and the horizontal component of displacement of corner B is:

$$\lambda = \tan^{-1} (u_2/u_1). \tag{6.4}$$

Plunge, p, of the displacement is determined by:

$$p = \tan^{-1} (u_3/(u_1^2 + u_2^2)^{1/2}). \tag{6.5}$$

In this way, one determines the magnitude, azimuth, and plunge of displacements at a point on the landslide. Similar calculations are performed to compute displacements of the second point, C.

Strains.--The differences in displacement of corners B and C of the quadrilateral, used to measure displacement at a landslide boundary

(Fig. 6.2a), define the strain between the corners. Also, by comparing the original length of line BC to its final length, B'C', stretch parallel to B'C' can be determined.

At a quadrilateral on the surface of the landslide, more detailed information about the strain can be obtained. If all four corners of the quadrilateral are coplanar and remain so during deformation, then one set of principal strains for the quadrilateral can be computed by the method of least squares (Appendix E). However, the corners seldom are coplanar. Therefore, a set of principal strains is computed, in the plane of the triangle, for each of the four triangles making the quadrilateral (Fig. 6.1), ΔABC, ΔBCD, ΔCDA, ΔDAB. Each set of strains comprises the major and minor principal strains and the angle between the major principal strain and a reference direction for the quadrilateral.

Strains larger than 0.01 (1.0 percent) are treated as finite strains. A convenient measure of finite strain is the stretch[13], S (Malvern, 1969; A.M. Johnson, unpub. data, 1981), which is the ratio of the final length, L_f, to the initial length, L_o, of a line segment:

$$S = L_f/L_o.$$

The linear strain is ϵ,

$$\epsilon = S-1.$$

---

[13]The quadratic elongation or quadratic extension, widely used in structural geology, is equal to the stretch squared (S^2). For elongation, S is greater than 1, and for shortening, S is less than 1. Of course, the principal values of the right Cauchy-Green tensor are $S_1{}^2$ and $S_2{}^2$.

In two dimensions, the stretch can be described by an ellipse as in figure 3 (Ramsay, 1967; Ragan, 1973; A.M. Johnson, unpub. data, 1981).

$$1 = (x_1/S_1)^2 + (x_2/S_2)^2. \tag{6.6}$$

In equation 6.6, the major and minor principal stretches are $\underline{S}_1$ and $\underline{S}_2$, respectively. The clockwise angle between $\underline{S}_1$ and a given side of the triangle is α (Fig. 6.3). The nondimensional coordinate $\underline{x}_1$ is parallel to $\underline{S}_1$, and $\underline{x}_2$ is parallel to $\underline{S}_2$. The radius of the circle deformed into the ellipse is equal to one.

The stretches within each triangular strain gauge (that is, each group of three stakes in the quadrilateral) are fully determined because values of stretch, $\underline{S}$, are known in three directions. In each triangle, $\underline{S}_1$, $\underline{S}_2$, and α constitute three unknowns that can be determined by solving three equations relating the unknowns to the three stretches (see Appendix E for solution of the equations).

Once $\underline{S}_1$, $\underline{S}_2$, and α are known, they may be used to compute the area strain, the finite shear strain, γ, and the stretch, $\underline{S}$, in any direction (Jaeger, 1962; Ramsay, 1967; Ragan, 1973; A.M. Johnson, unpub. data, 1981). The area strain is $\underline{d}$:

$$d = S_1 S_2 - 1.$$

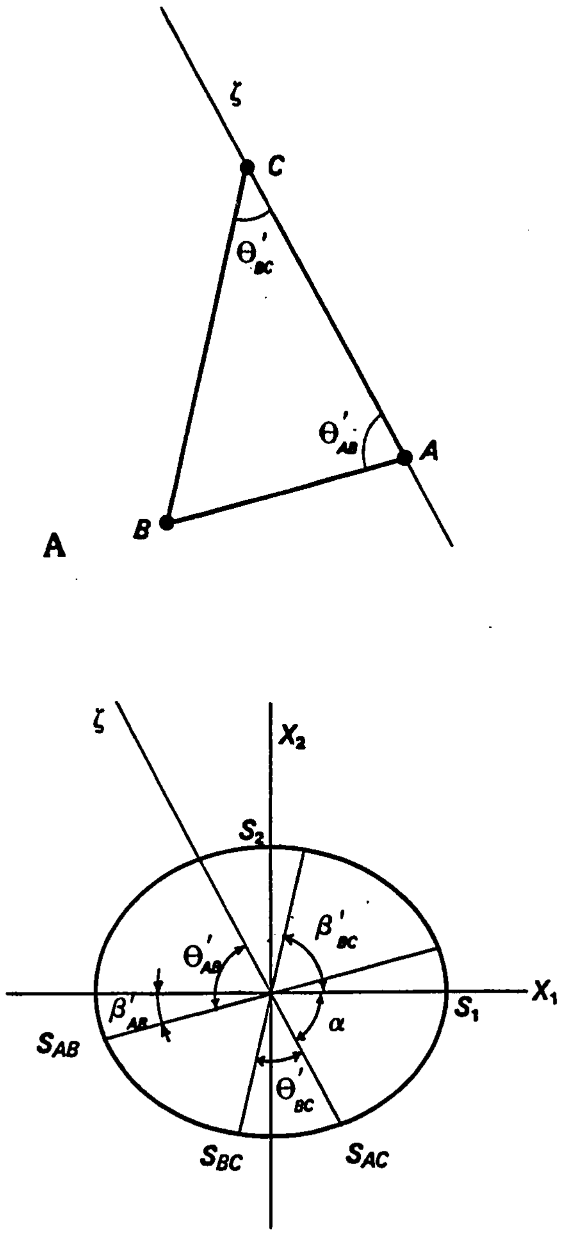

B

FIGURE 6.3. Geometrical relationships between a deformed triangle and its stretch ellipse. (a) Triangle <u>ABC</u> in its final state. Angle θ'_{AB} is angle <u>CAB</u>; angle θ'_{BC} is angle <u>BCA</u>. (b) The stretch ellipse. $\underline{S}_1$ and $\underline{S}_2$ are the principal stretches and are parallel to the $\underline{x}_1$ and $\underline{x}_2$ coordinates. $\underline{S}_{AB}$, $\underline{S}_{AC}$, and $\underline{S}_{BC}$ are the components of stretch parallel to lines <u>AB</u>, <u>AC</u>, and <u>BC</u>, respectively. The angle α ($= \beta'_{AC}$) is the acute angle between line <u>AC</u> and $\underline{x}_1$; $\beta'_{AB} = \theta'_{AB} - \alpha$; $\beta'_{BC} = \alpha + \theta'_{BC}$.

The maximum finite shear strain is γ_{max}:

$$\gamma_{max} = (S_1^2 - S_2^2)/(2S_1S_2).$$

Tilt.--Tilt is the difference between the initial and final amount of dip of any triangle in the quadrilateral. Similarly, change in dip direction is defined as the angle between the initial and final dip direction of a triangle. Both are useful in interpreting strain data. Tilt shows whether the ground is steepening or flattening, and it is related to differences in the rate of thickening from one side of the quadrilateral to the other. Changes in the dip direction relate the tilt to changes in the shape of surface features.

The amount of dip and the dip direction of a triangle are computed as follows: The sides of a triangle correspond to coordinate directions ξ_i in the x-y plane, and the azimuths of those directions are ω_i (Fig. 6.4). The slope $(\partial z/\partial \xi_i)$ and the azimuth (ω_i) of each side of the triangle are computed from field data. The slope of a line in any arbitrary direction ξ_i within a plane is computed by differentiating the equation of a plane,

$$z = ax + by,$$

with respect to ξ_i and making the substitutions

$$\cos(\omega_i) = (\partial x/\partial \xi_i), \text{ and } \sin(\omega_i) = (\partial y/\partial \xi_i):$$

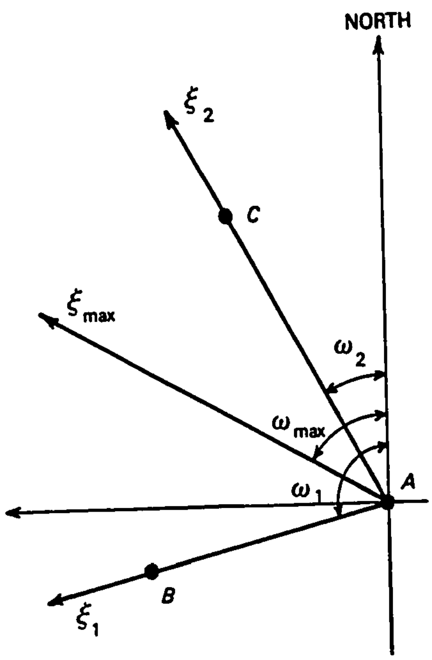

Figure 6.4. Dip direction and dip of triangle ABC; point A has the highest elevation. The positive x direction is due north. Line AB parallels coordinate direction ξ_1, its bearing is ω_1. Line AC parallels coordinate direction ξ_2, and its bearing is ω_2. The dip direction parallels coordinate direction ξ_{max}, and its bearing is ω_{max}.

$$(\partial z/\partial \xi_1) = \underline{a}\cos(\omega_1) + \underline{b}\sin(\omega_1); \tag{6.7a}$$

$$(\partial z/\partial \xi_2) = \underline{a}\cos(\omega_2) + \underline{b}\sin(\omega_2); \tag{6.7b}$$

In these equations, $\underline{a}$ and $\underline{b}$ are constants describing the slope of the plane in the $\underline{x}$ and $\underline{y}$ directions, respectively. Using the slopes of two sides of the triangle, one solves the set of equations, 6.7a and 6.7b, simultaneously for $\underline{a}$ and $\underline{b}$. The azimuth of the dip direction, which is the direction of maximum slope, is found by differentiating equation 6.7 with respect to ω, letting the derivative of equation 6.7 equal zero, and solving for ω_{max}:

$$\omega_{max} = \tan^{-1}(b/a). \tag{6.8}$$

The tangent of the dip angle, δ, is derived by substituting the azimuth of the dip direction, ω_{max}, back into equation 6.7 and solving for $(\partial z/\partial \xi_{max})$, the tangent.

$$\tan(\delta) = \underline{a}\cos(\omega_{max}) + \underline{b}\sin(\omega_{max}),$$

and

$$\delta = \tan^{-1}[\underline{a}\cos(\omega_{max}) + \underline{b}\sin(\omega_{max})].$$

Repeating these calculations for each triangle in its initial and final state and determining the differences gives four values of tilt and four values for the change in dip direction.

Computation.--The data for computing the errors of closure, displacements, strains, and tilts are the (slope) distances and elevation differences between corners of the quadrilateral. The formulas for computing these quantities, given previously, were chosen to simplify the task of programming.

Separate programs are used for computing displacement or strain and tilt, and each program reads the data from files stored on a diskette. A file exists for each quadrilateral; each set of raw measurements in a file is identified by the date on which it was collected. Documentation and BASIC computer programs for creating the files and performing the computations are available from the U.S. Geological Survey (Johnson and Baum, 1987) and in Appendix F.

Field Technique

At each site selected for strain or displacement measurement, we drove four wooden stakes in the ground to mark the corners of a quadrilateral, and put a small finishing nail in the top of each stake (Fig. 6.1).

We used a steel tape to measure distances between nails, hooking the end of the tape on one nail and reading the tape at the center of each of the other nails. The elevation of the top of each stake was obtained by taking backsights with a precision level. The azimuth of a reference line (diagonal AC) was measured with a Brunton compass so that strain and displacement data could be oriented.

No provisions were made to determine rigid body rotations of the quadrilaterals; where such data are of interest, accurate measurement of the azimuth of a reference line would be needed each time the length and elevation measurements were repeated. If the azimuth were known, additional computations would determine the rotation of a line that becomes parallel to the principal stretch.

We encountered three major difficulties in using the quadrilateral method: (1) Some of the stakes became tilted, loose, or broken, either by animals or heavy winter snow. (2) Repetition of length measurements showed that measurement errors of 3 mm were common and that errors of 5-6 mm sometimes occurred. (3) Errors of 0.5 mm were fairly common in the elevation measurements, apparently because many stakes were tilted. However, errors were small in comparison to displacement.

In order to minimize the errors, we discounted results from stakes that were loose or greatly tilted. Also, we used the theory of quadrilaterals to detect errors of measurement of length.

We tried quadrilaterals of various shapes; however, most were approximately square (that is, equidimensional). Squares worked well because it was difficult to anticipate the direction of maximum strain at most locations on the landslide. The advantage of using a shape that is approximately square is that strain measurements are distributed throughout the four quadrants, whereas an elongate quadrilateral tends to concentrate strain measurements in two opposite quadrants.

Squares also worked well for displacement measurements. However, as quadrilaterals were distorted into diamond shapes, measurement errors increased. Thus, it was necessary to put new stakes in the ground from time to time to restore the original square shape of some of the quadrilaterals.

The quadrilaterals that we used ranged from 1.5 to 10 m in width, but quadrilaterals that were from 1.5 to 4 m wide seemed to work best for strain measurements. The larger quadrilaterals (from 6 to 10 m wide) were sensitive to inhomogeneous strain. Quadrilaterals smaller than 1.5 m would be too sensitive to measurement error.

Experience indicated that displacement measurements were needed more often, whereas strain measurements were needed less often than we made them. During June and July 1983, and May 1984, the quadrilaterals were measured once every two or three days. Displacements averaged a few millimeters per day in 1983 and a few centimeters per day in 1984. By measuring every few days, a discontinuous record of displacements was obtained. However, the strain accumulating from a few days of movement was often too small to measure.

In order to satisfactorily measure displacement and strain in 1985, we measured the quadrilaterals once every three or four weeks and supplemented the quadrilaterals with three recording extensiometers along a flank of the landslide in order to obtain more nearly continuous displacement data. From the quadrilateral measurements, I computed the long-term (weeks or months) displacements at many points on the boundaries and long-term strains at points on the surface of the landslide. The combination of measurements used in 1985 worked well for describing the kinematics of the landslide, except that erroneous measurements of strains were more difficult to detect.

Errors and Sensitivity

Detection and distribution of errors.--When quadrilaterals were measured frequently (once every two to three days, or several times a day) many inaccurate data sets could be eliminated by inspection. Measurements that differed significantly from a series of otherwise constant values or a steady trend were regarded as inaccurate and were discarded. From the remaining sets of measurements, those having the smallest errors of closure were used for strain computations.

Errors of closure were computed by means of equation 6.1, as an aid in detecting inaccurate data sets. Arvid Johnson and I tried a simple method for distributing the errors, described by Laurila (1983, p. 41-45). In order to apply this method, we assumed that the length of one side of each quadrilateral, AB, was known accurately; however, we had no independent check on the length of AB or any other length. Thus, if AB happened to be measured inaccurately, then using it to distribute the errors might make the adjusted measurements less accurate than the original measurements. Therefore, I decided to use the raw measurements, and to eliminate sets of measurements that had errors of closure larger than 0.3°.[14] By inspecting the raw measurements and checking the magnitude of w, I eliminated data sets having closure errors larger than a few millimeters.

---

[14]By computing the error of closure for a square quadrilateral having sides exactly 2 m long, I found that an error of 6 mm in the measured length of one side caused an error of closure equal to approximately 0.3°.

Sensitivity of measurements.--When we measured quadrilaterals and then remeasured them a few minutes later, we found that our measurements could differ by as much as 5-6 mm, which is equivalent to a strain of 0.003 in a quadrilateral with sides of 2 m length. Errors of 5-6 mm occurred in 10-20 percent of our measurements. Consequently, the smallest strains that could be detected confidently by our measurements with a steel tape were 0.003 (0.3 percent strain). As a result, the smallest strain that could be computed with an error less than 10 percent was 0.030 (3.0 percent strain). We sometimes used measurements where the strains were less than 0.030, especially if they were internally consistent and the orientations of the principal stretches for the four triangles were oriented in about the same direction.

The measurements were adequate for observing long-term strains. Strains of +0.080 (+8.0 percent) to -0.180 (-18.0 percent) accumulated at many quadrilaterals during weeks and months of landslide movement. Thus, long-term strains were large compared to errors in the measurements.

Because boundary displacements of many decimeters accumulated as a result of days or weeks of landslide movement, measurement errors were small enough to disregard when computing displacements.

Examples of Quadrilateral Measurements

In order to illustrate how quadrilaterals have been used in the field to measure displacement, strain, and tilt, several examples from the Aspen Grove landslide in central Utah are cited: (1) the measurement of displacement at a landslide flank (strike-slip fault),

(2) the measurement of displacement at a landslide toe (thrust fault), (3) the measurement of tilt and strain on a ridge, and (4) the measurement of strain at a place that unexpectedly became a normal fault. Before describing the history of the quadrilateral sites, I briefly describe the landslide.

The Aspen Grove Landslide

The Aspen Grove landslide, on a northwest-facing, forested slope in Ephraim Canyon, central Utah (Fg. 6.5), involves old landslide debris that consists of sandstone boulders in a sandy clay matrix. The slope angle of the landslide surface averages 11° and locally ranges from 0° to 31°. From drilling and mapping in the vicinity of the landslide, I infer that the landslide debris occupies a trough in the surface of the bedrock.

The landslide debris upslope from a road that crosses the lower part of the landslide (Fig. 6.6) is probably less than 10 m thick. At boreholes B1, B2 and B3, in the upper part of the landslide, the debris is 6 m thick. Downslope from the lower road crossing, the debris may be as thick as 15-20 m beneath the large internal toe (between quadrilaterals Q-26 and Q-27, Fig. 6.6).

The boundaries of the landslide curve. The landslide is 1 km long and its width changes gradually throughout its length. From the head (quadrilateral Q-1, Fig. 6.6) to the vicinity of B1, the width is from 50 to 55 m. Downslope from B1, the width decreases to a minimum of 20 m near the 2340 m contour and then increases farther downslope to a maximum of 100 m on the internal toe. Downslope from the internal toe,

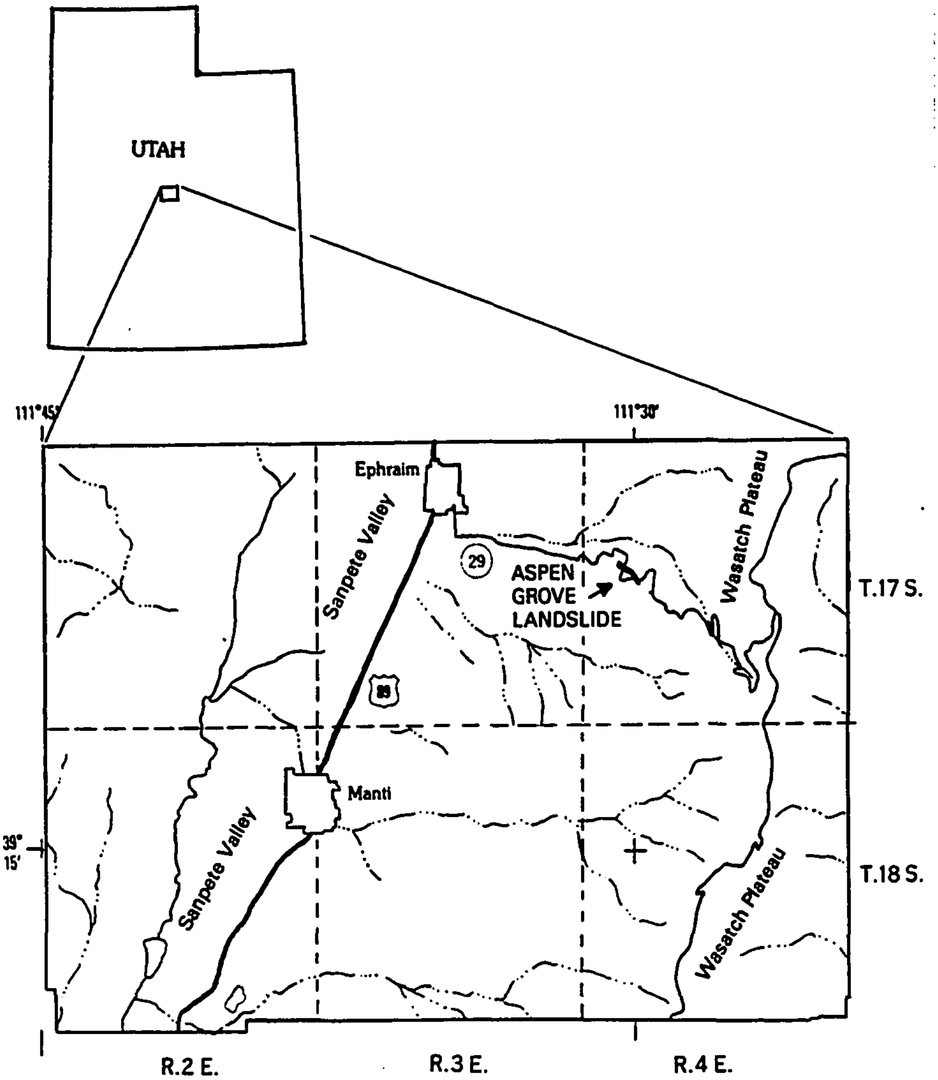

FIGURE 6.5. Map showing location of the Aspen Grove landslide, central Utah.

the landslide is 70 m wide near quadrilateral Q-32, but beyond the edge of the mapped area, its width increases again to about 100 m.

Sliding at Aspen Grove began late in May 1983 when a record snowpack containing from 75 to 100 cm of water melted in a few weeks. Discontinuous ground cracks marking the boundaries of the landslide were first discovered on May 31, 1983, and sliding continued for several weeks, until mid-July or early August. During this time, the landslide extended from the head at quadrilateral Q-1 (Fig. 6.6) to the vicinity of quadrilaterals Q-8 and Q-29. The landslide was dormant from late summer 1983 until approximately mid-April 1984, when sliding was renewed in all parts of the landslide that had been active in 1983. Features at the surface of the landslide evolved dramatically. Many of the tension cracks in the head region opened wide, as the thin debris at the head slid downslope. A graben, near quadrilateral Q-13, and the flank ridge, at quadrilateral Q-2, enlarged. Flanks defined by en echelon cracks and fault segments in 1983 were defined by continuous strike-slip faults in 1984. The flanks of the landslide propagated farther downslope than in 1983. By the time I saw the landslide in mid-May, cracks had appeared at the 2,280 m contour on the internal toe. By the end of May, scattered cracks were visible downslope from the internal toe (near quadrilateral Q-32, Fig. 6.6). In August 1984, Fleming, Johnson, and I observed a new shear zone that had started to form on the right flank,[15] between quadrilateral Q-2 and quadrilateral Q-13.

[15]The right flank is to the right of an observer standing at the crown and looking downslope. By this convention, right-lateral shearing occurs on the right flank.

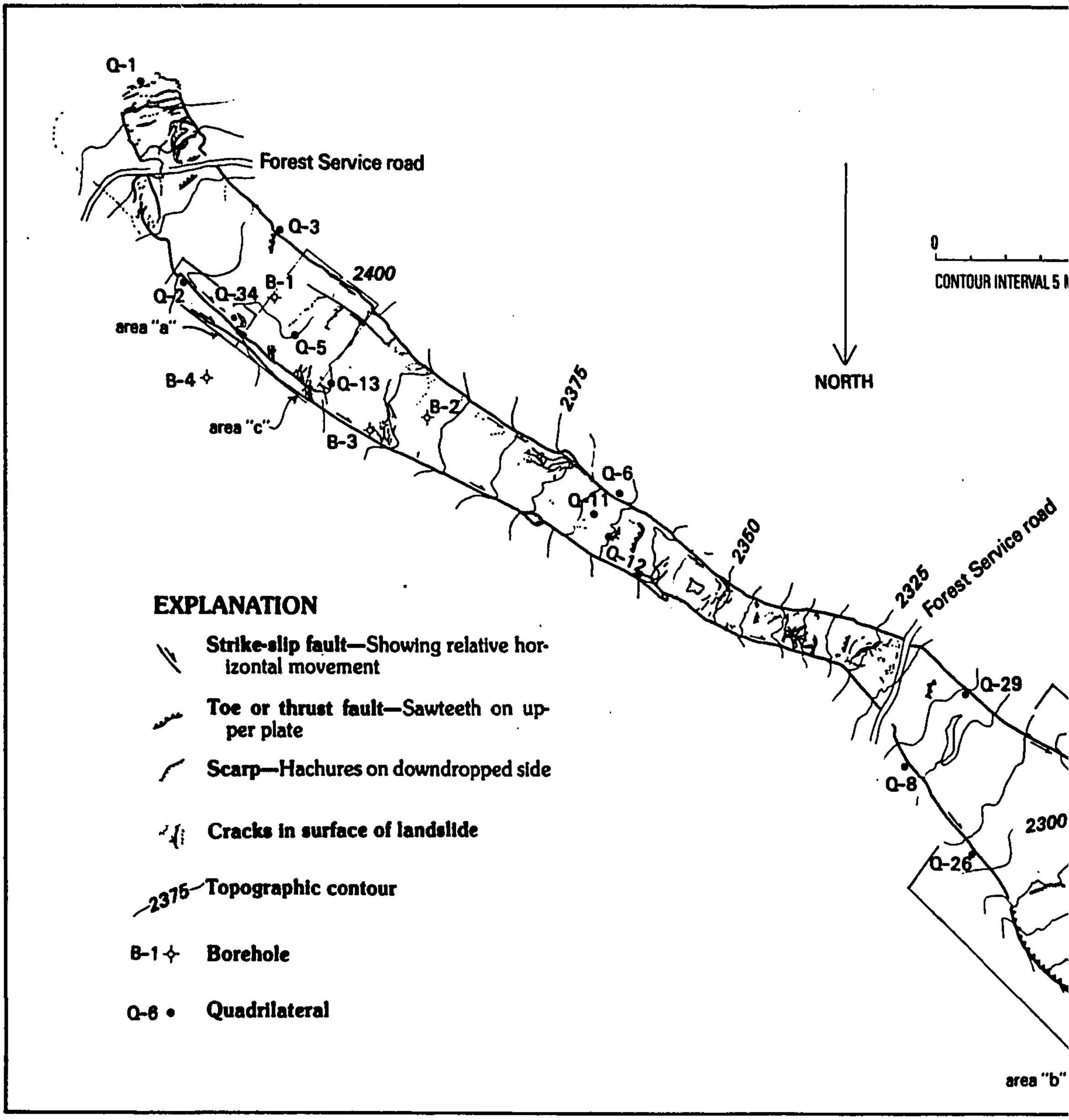

FIGURE 6.6. Map showing the Aspen Grove landslide, August 1984.

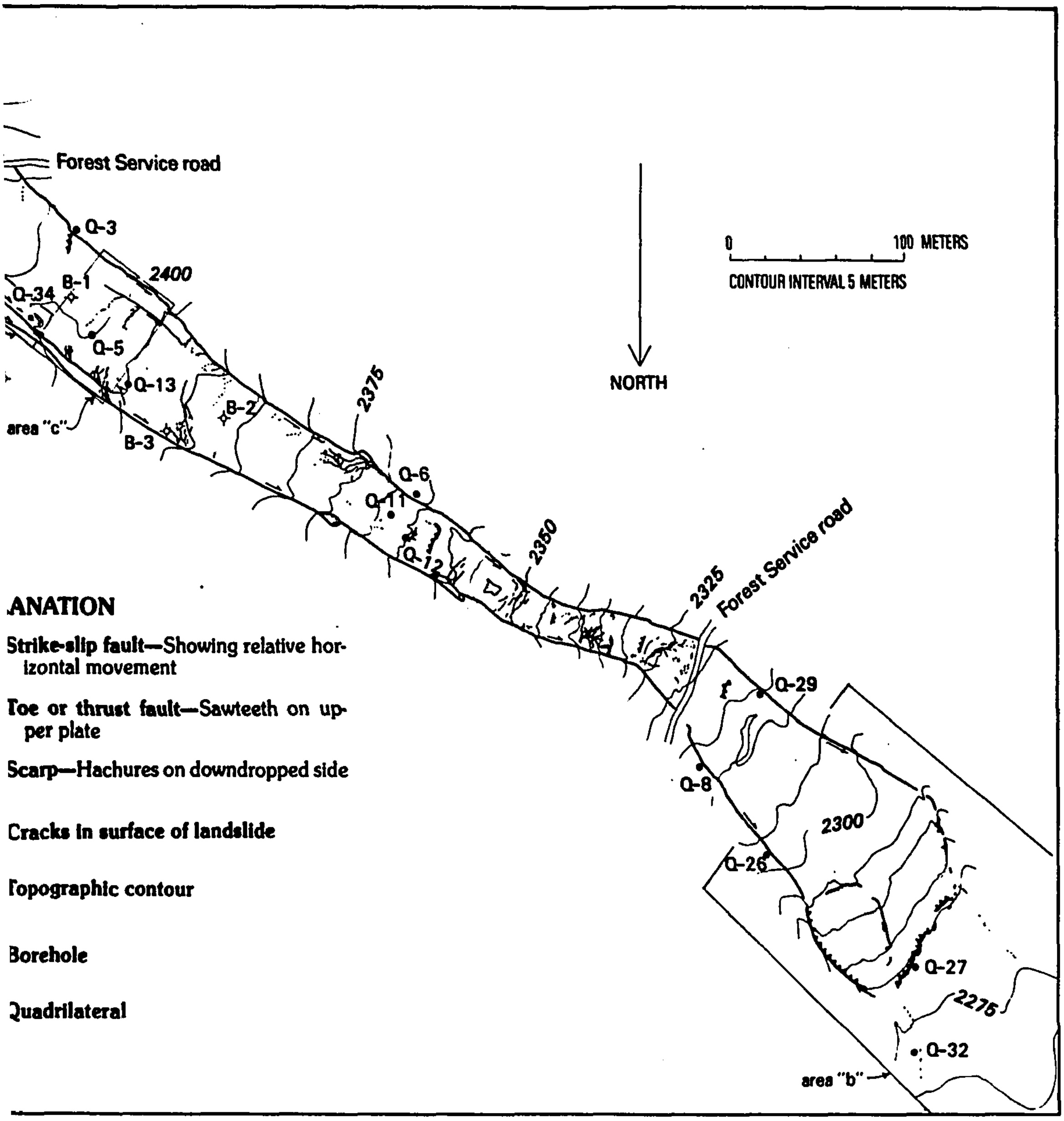

p showing the Aspen Grove landslide, August 1984.

Measurement of Displacement on a Landslide Flank

The flanks of the Aspen Grove landslide were characterized by strike-slip faults or shear zones. The faults were from a few centimeters to a few decimeters wide, so that small quadrilaterals worked well to measure displacement on the faults and strain parallel to the faults. The installation and history of quadrilateral Q-2 is described as an example of using a quadrilateral to measure displacement on a landslide flank.

Quadrilateral Q-2 was installed on the right flank, in the upper one-third of the Aspen Grove landslide, on June 15, 1983 (Fig. 6.6). It was primarily intended to provide a sensitive measure of displacement on the right flank. Also, the two stakes of Q-2 on moving ground could be used to measure one-dimensional strain adjacent to the strike-slip fault on the right flank.

A perspective sketch (Fig. 6.7), based on a photograph, shows the site as it appeared on the day the stakes were installed. Two cracks marked the location of a right-lateral shear zone. The shear zone was parallel to the axis of a low ridge, from 50 to 80 cm high, and passed through the northeast flank of the ridge.

Small swales with axes parallel to the shear zone occurred on each side of the ridge. The one on the outer side of the ridge, on stationary ground, is shown in the foreground in Figure 6.7. It was about 2 m wide and 1 m deep; it had a smooth, roughly semicircular profile. The swale on moving ground was subtle; it was marked by a small furrow at the boundary between the ridge and the slightly arched,

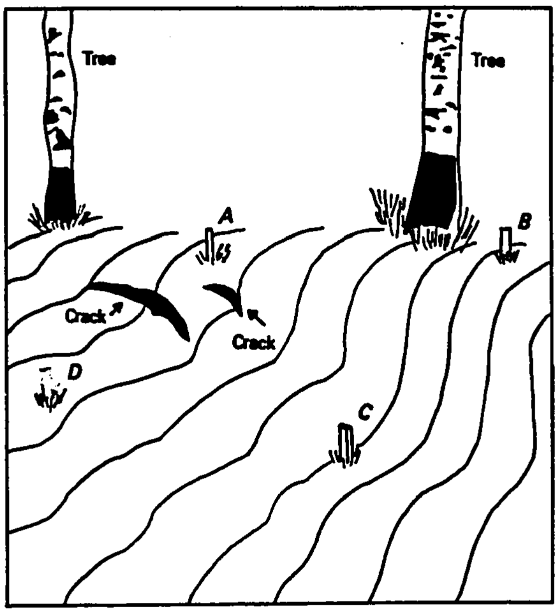

FIGURE 6.7. Sketch of the site of Q-2 (part of area "a", shown in Fig. 6.6) made from polaroid photograph taken by R.W. Fleming on June 15, 1983. Ground surface depicted by means of serial profiles in perspective view.

convex surface of the landslide. Twenty meters farther downslope, both swales became more prominent and the ridge became a conspicuous topographic feature.

Stakes C and D were placed on stationary ground northeast of the ridge so that line DC was parallel to the shear zone, which had a trend of N. 41° W. Stakes A and B were placed on the crest of the ridge, on moving ground, a few decimeters southeast of the shear zone (opposite stakes C and D).

The size, orientation, and shape of the quadrilateral were determined mainly by the geometry of the site. The quadrilateral needed to be large enough to straddle the shear zone and allow clearance for the measuring tape to stretch between the tops of the stakes. Had stakes A and B been located off the crest of the ridge, clearance might have been a problem. The reference line (line CD, the line defined by stakes on stationary ground) was approximately parallel to the shear zone so that the largest component of displacement would be parallel to the reference line. This orientation was chosen for convenience in making the measurements and in orienting the displacement vectors. The trapezoidal shape was a result of trying to fit the quadrilateral to the site.

During part of June and July 1983, the quadrilateral was measured once every two or three days, and displacement on the shear zone was computed for the period from June 15 to August 4. Movement on the shear zone amounted to 14 cm between June 15 and July 10, when movement ended. The azimuth of the displacement was N. 49° W., or 8° counterclockwise from the trend of the shear zone. Thus, the stakes were displaced toward the center of the landslide, away from the shear zone. The quadrilateral functioned very well. The strike-slip displacements were much larger than the measurement errors.

Renewed movement began in the spring of 1984, and displacement of 2.2 m, nearly parallel to the trend of the fault zone, occurred between August 4, 1983, and May 23, 1984. As a result of the displacement, the shear zone defined by en echelon cracks in 1983 was replaced by a through-going fault in 1984 (Fig. 6.8). Moist, light-brown, slickensided clay was exposed at the ground surface on either side of the fault, and vegetation was disrupted in a strip, from 10 to 20 cm wide, along the fault.

Shortening of 1.2 percent occurred between stakes A and B on the low ridge within the landslide between August 1983 and May 23, 1984. Shortening was surprising because the maximum rate of displacement was occurring approximately 230 m downslope from Q-2, and we had measured progressively less displacement in several places between this point of maximum displacement and Q-2. Thus, we expected the strain at Q-2 to be extensional.

As a result of the movement during the spring of 1984, stake B had moved into a position where the tape was deflected by the ground surface when measuring between stake B and stake C or D. Therefore, the movement of stake B was overestimated in our calculations. No action was taken to correct this situation during 1984, because we were able to measure to point A without difficulty.

The landslide was active through June and July and stopped moving sometime during August 1984. We measured Q-2 once every two or three

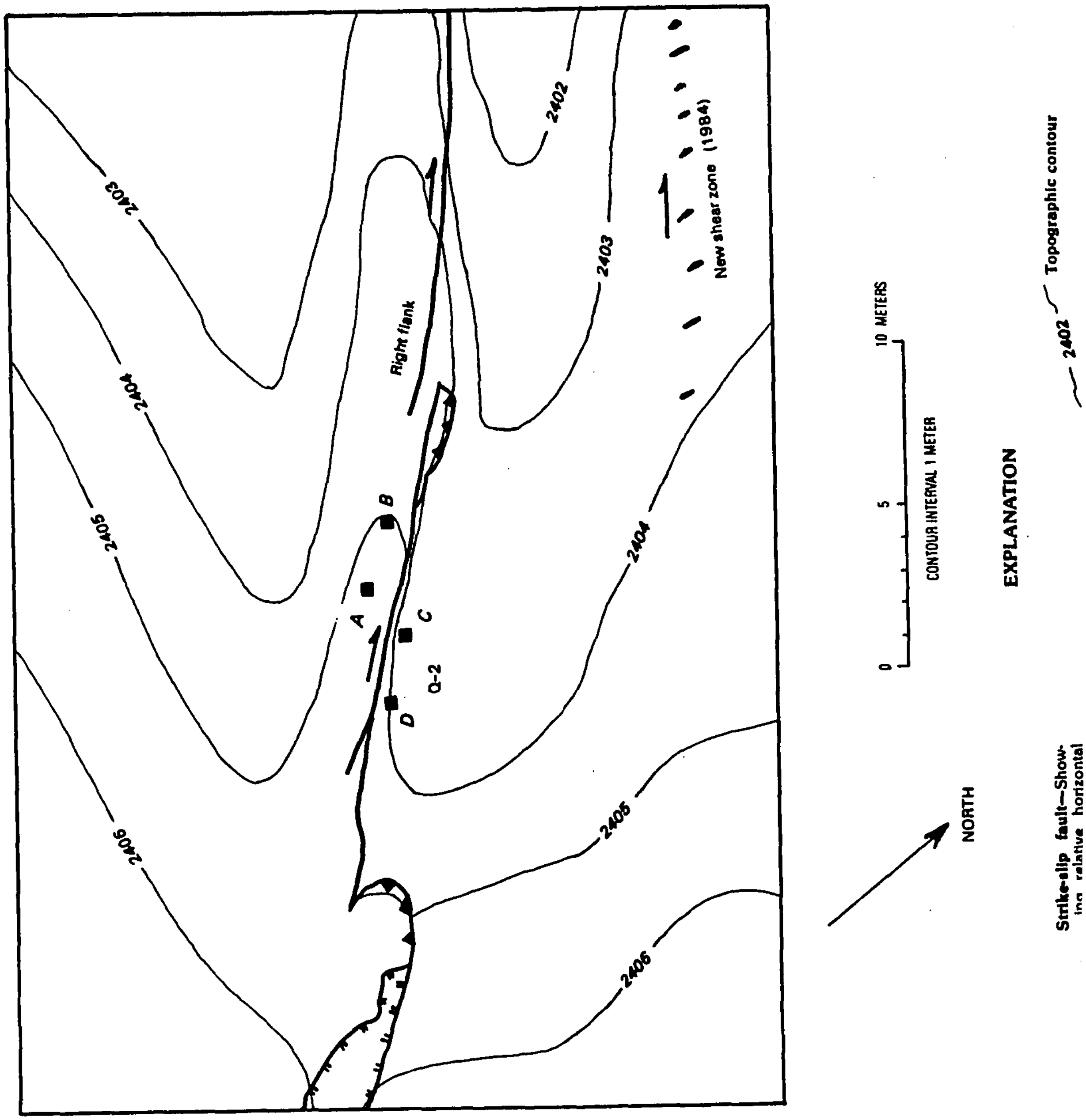

FIGURE 6.8. Map showing part of the Aspen Grove landslide in vicinity of quadrilateral Q-2 during August 1984 (part of area "a", shown in Fig. 6.6).

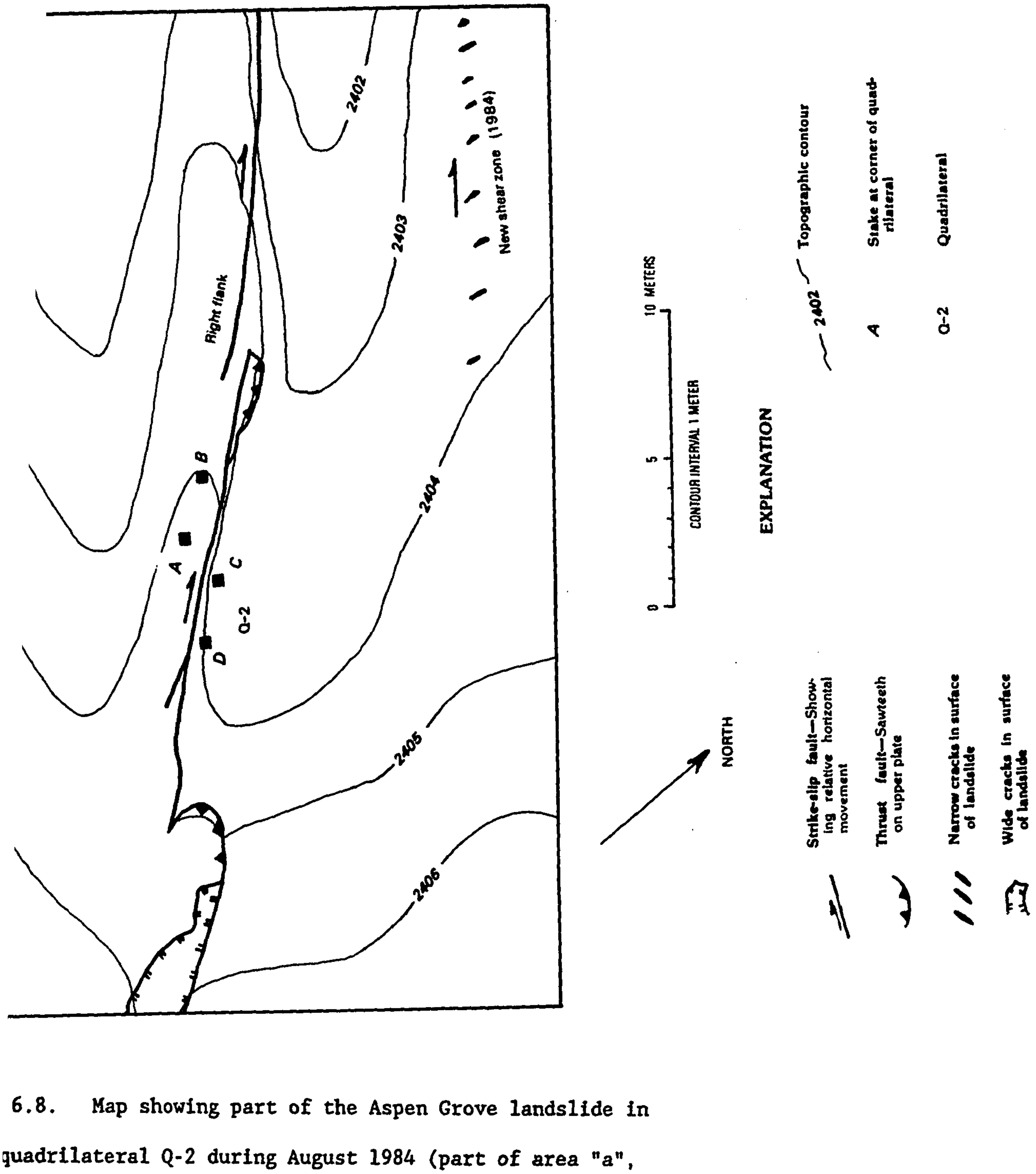

6.8. Map showing part of the Aspen Grove landslide in
quadrilateral Q-2 during August 1984 (part of area "a",
. 6.6).

days between May 23 and June 7, and once on August 3. Between May 23 and August 3, 1.6 m of displacement occurred on the fault.

Displacement was oriented 11° counterclockwise from the trace of the fault and plunged only 1.5°. The shallow plunge was interesting because one might expect the movement to be roughly parallel to the ground surface, which sloped 10°. The nonzero component of displacement of stakes normal to the fault, toward the center of the landslide, was also interesting because we observed no evidence of dilation near the fault. Both of these, though, might reflect a secondary flow of the landslide debris, which Arvid Johnson and I associate with the construction of lateral ridges.

By April 1985, quadrilateral Q-2 had been deformed into a diamond-shaped figure. Therefore, after measuring the distances between all of the stakes, stakes A and B were removed and replaced with new stakes in positions that were across the shear zone and opposite stakes C and D.

During the period that quadrilateral Q-2 was in use, the site changed. The shear zone evolved from a set of en echelon cracks to a through-going strike-slip fault.

The quadrilateral measured displacement of several meters, with sensitivity of several millimeters. Even though the quadrilateral was small, 2 m by 2 m, it was able to measure displacements amounting to a few meters before stakes A and B had to be replaced in order to restore the original shape of the quadrilateral.

Measurement of Displacement at a Landslide Toe

In May 1984, I observed that the Aspen Grove landslide was enlarging distally. Cracks were appearing farther downslope, toward a large internal toe of the landslide that had formed during a previous episode of movement (near quadrilateral Q-27, fig. 6). I expected the internal toe to be reactivated and become the toe of the modern Aspen Grove landslide; I wanted to observe the early stages of movement as the toe became reactivated. Quadrilateral Q-27 was installed about halfway across the width of the toe on May 18, 1984, in order to accomplish this.

The internal toe was one of the most conspicuous features of the landslide surface (Fig. 6.9a). The slope angle of the profile of the distal end of the toe was about 24°, and the angle gradually reduced to 16° about 40 m upslope (Fig. 6.9b). The toe was about 7 m high, and its maximum width was about 100 m. However, the landslide was narrower upslope from the toe (Fig. 6.6).

A site for a quadrilateral midway across the toe was chosen in an area relatively clear of vegetation that would interfere with measurement. Movement was expected to be greatest in this area; therefore, it was the optimum place to detect small movements. Also, the toe was well defined topographically near its middle, so it seemed possible to estimate within a meter or two where the failure surface would intersect the ground surface.

The quadrilateral was oblong, from 2.2 to 2.8 m wide and 4.4 m long, and its long dimension was parallel to the axis of the landslide.

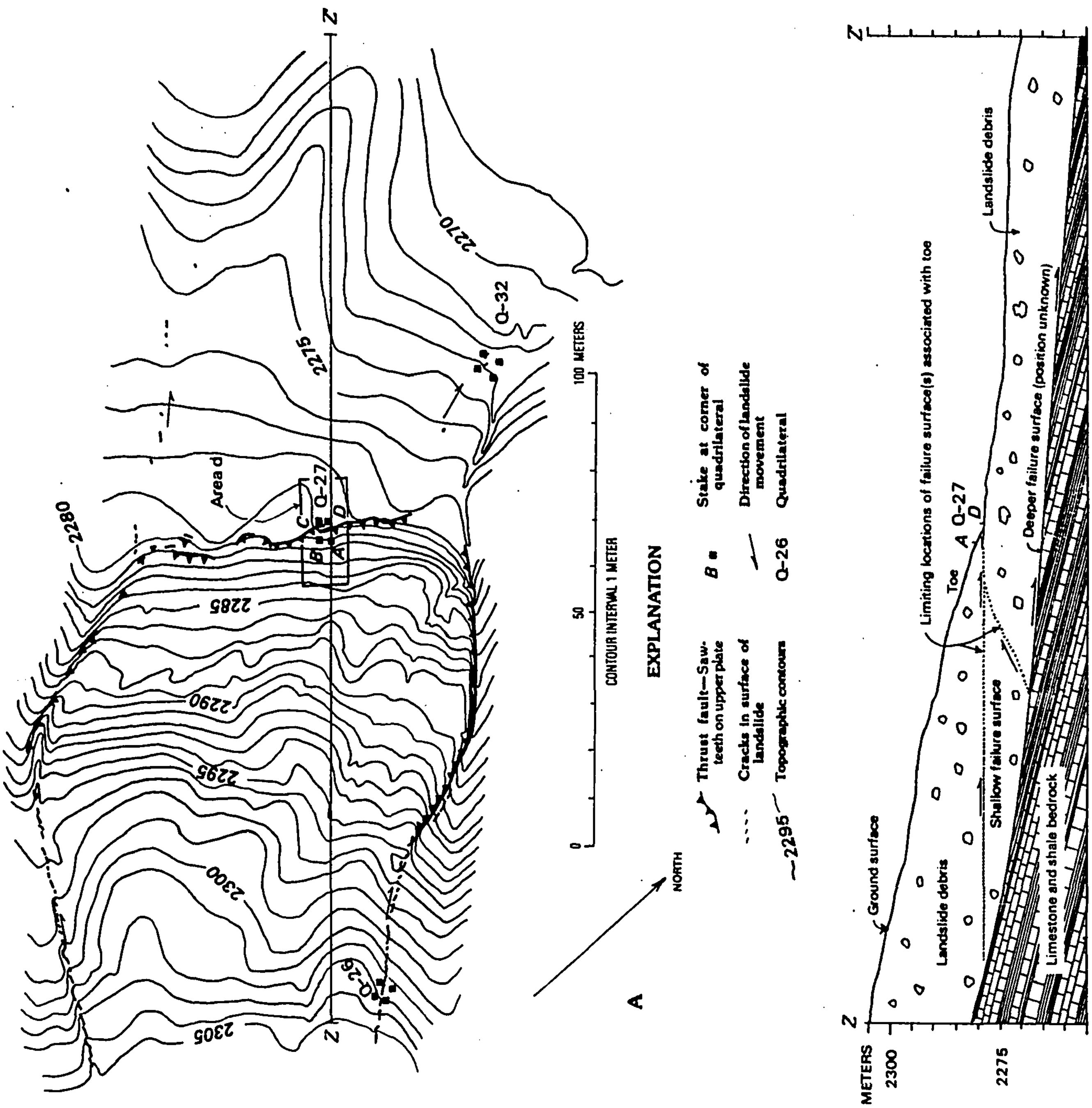

FIGURE 6.9. Map and cross section showing internal toe of the Aspen Grove landslide (area "b", shown in Fig. 6.6). (A) Map view, August 1984. (B) Cross section Z-Z'.

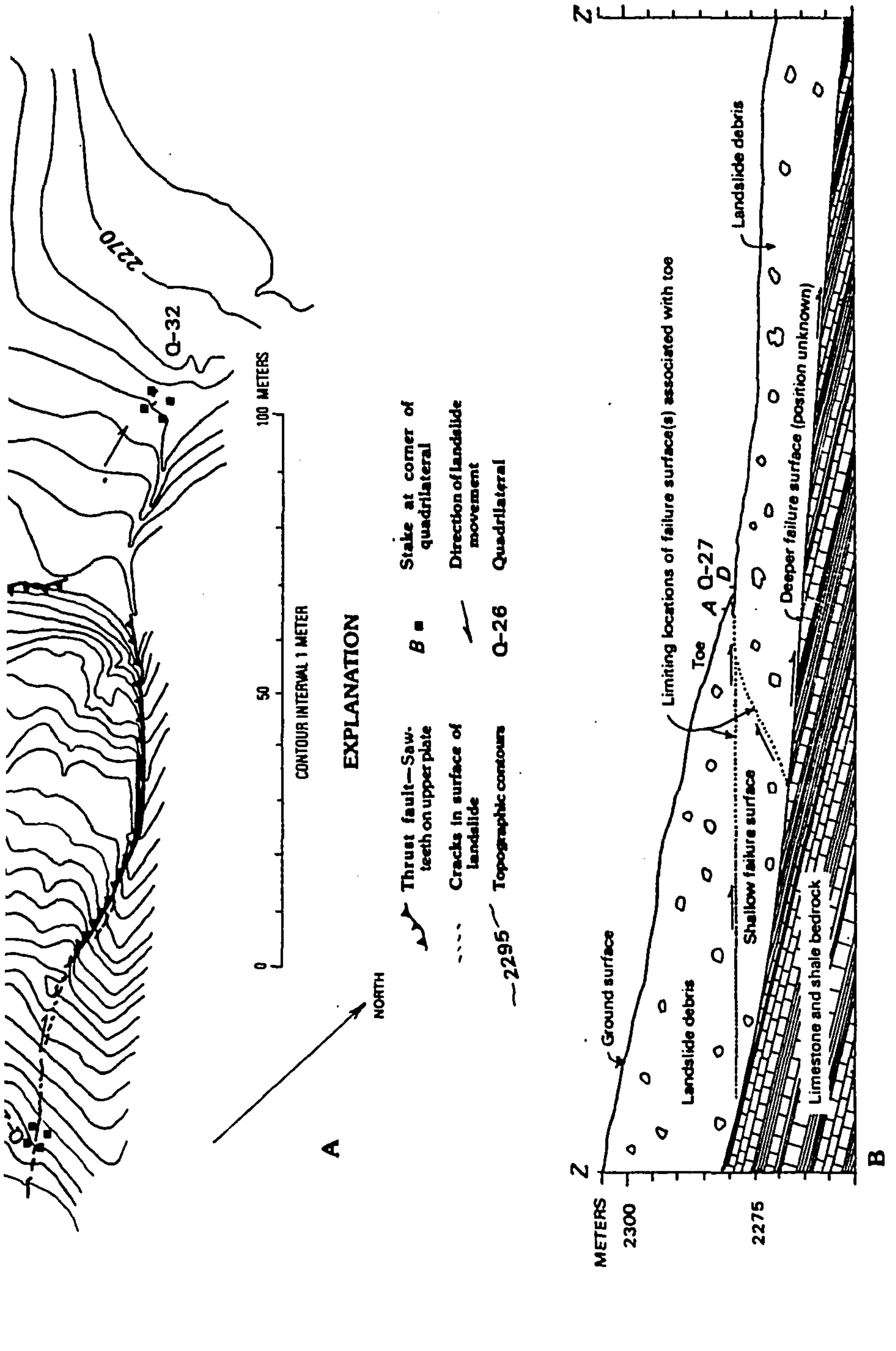

and cross section showing internal toe of the

rea "b", shown in Fig. 6.6). (A) Map view,

section Z-Z'.

Line CD was installed on gently sloping ground, downslope from the toe (Fig. 6.9). Points C and D were a meter downslope from where the thrust was expected to intersect the ground surface. I tried to make line CD parallel to the local trend of the toe, so that motion would be approximately perpendicular to line CD. Points A and B were 4.3 m upslope from line CD, and were 1 m higher in elevation than stakes C and D.

Within the quadrilateral, the ground surface sloped gently (a few degrees) for 1 m upslope from stakes C and D. The slope then increased abruptly to 20°. The slope was relatively smooth, but pebbles, cobbles, and small undulations made the slope locally rough.

In order to document differential movement occurring in the toe, we measured Q-27 every few days from May 18 to June 6, 1984. The computed displacements for stake A are shown in Figure 10. Although we measured displacements of 6 cm between May 18 and June 2, no physical changes could be observed in the site.

When Robert Fleming and I returned to the site on June 6, we observed a band of cracked soil on the face of the toe, just northeast of line AD. The displacement between May 18 and June 6 was 9 cm. I do not know how much movement occurred in the toe before measurements were started at Q-27, but I do know that displacement of at least 6 to 9 cm was needed before the ground cracks became visible.

In August 1984, the cracks observed in June were no longer visible, but other thrust features appeared along the toe. Robert Fleming observed and mapped three branches of the thrust fault within the boundaries of the quadrilateral (Fig. 6.11). These changes were associated with 22 cm of displacement between May 18 and August 4, 1984.

Points A and B, which were on the toe upslope from the thrust features, moved approximately parallel to the axis of the landslide. During May 1984, displacement of point A was nearly horizontal. The ground surface of the landslide below Q-27 slopes about 7°, so the displacement at Q-27 has an upward component relative to the ground surface. Later displacements, occurring between June 6 and August 4, had a vertical upward component (Fig. 6.10).

These movements were relative to stakes C and D, which themselves were moving on a landslide element that was downslope from the internal toe. Thus, the magnitude and direction of movement of stakes A and B relative to nonmoving ground is unknown.

Measurement of Strain and Tilt on a Ridge

In June 1984, Arvid Johnson and Robert Fleming observed that the ridge near Q-2, on the right flank of the landslide, was deforming. Q-2 was at the upslope end of the ridge. Most evidence for growth of the ridge was 15 to 20 m farther downslope. Thus, stakes were installed there to measure and document the deformation that was occurring. Several quadrilaterals were installed on the ridge, one of which (Q-34) is described here.

In 1983, very few cracks were present within the boundaries of the Aspen Grove landslide. On June 2, 1984, near the beginning of the second season of movement, cracks were observed in the crest of the small ridge on the right flank of the landslide, near Q-2. Large

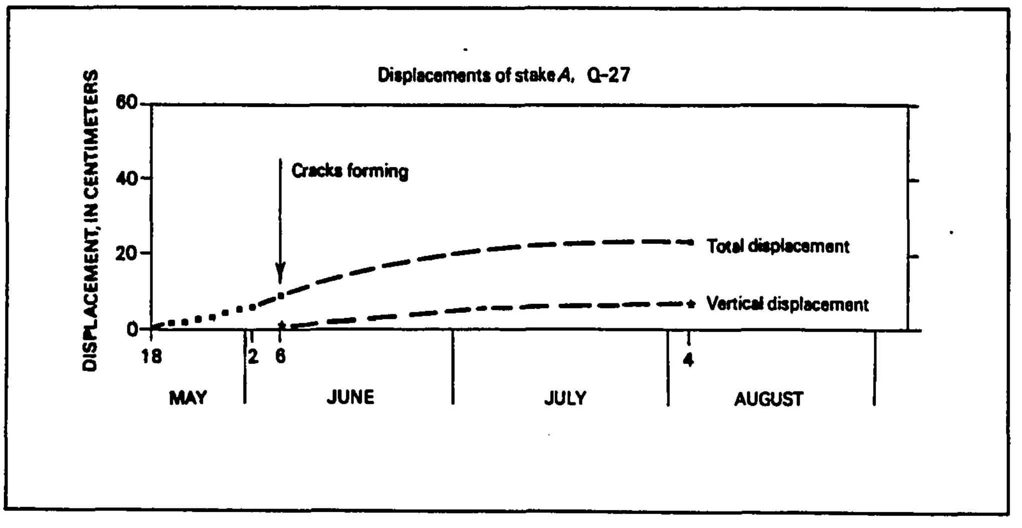

FIGURE 6.10. Graph showing displacements of stake A at Q-27 from May 18 to August 4, 1984.

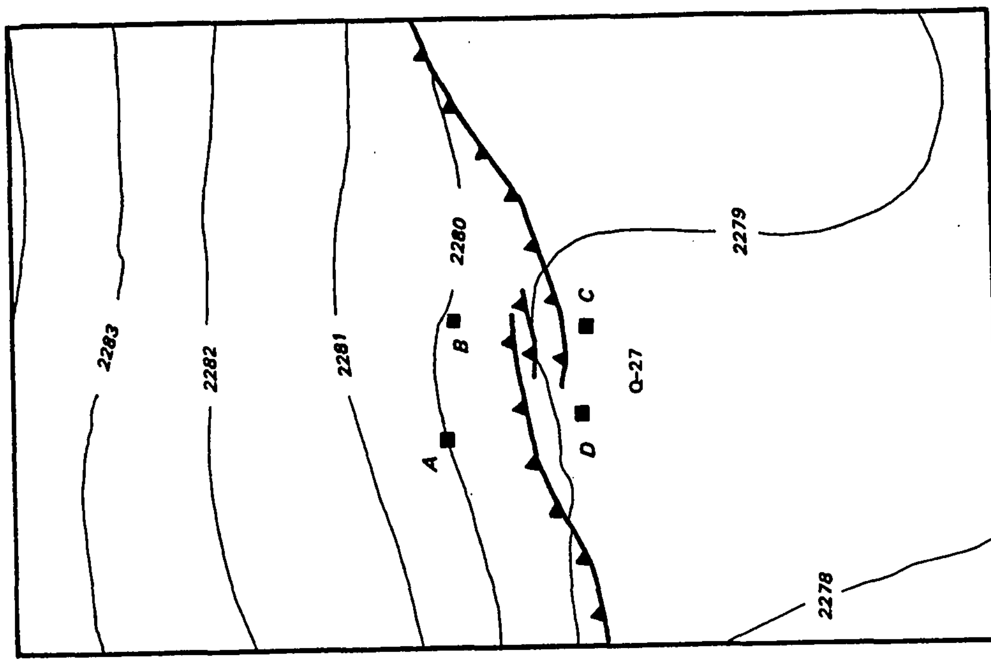

FIGURE 6.11. Enlarged view of area "d", shown in Figure 6.9. Three thrust faults were noted within the boundaries of quadrilateral Q-2 in August 1984.

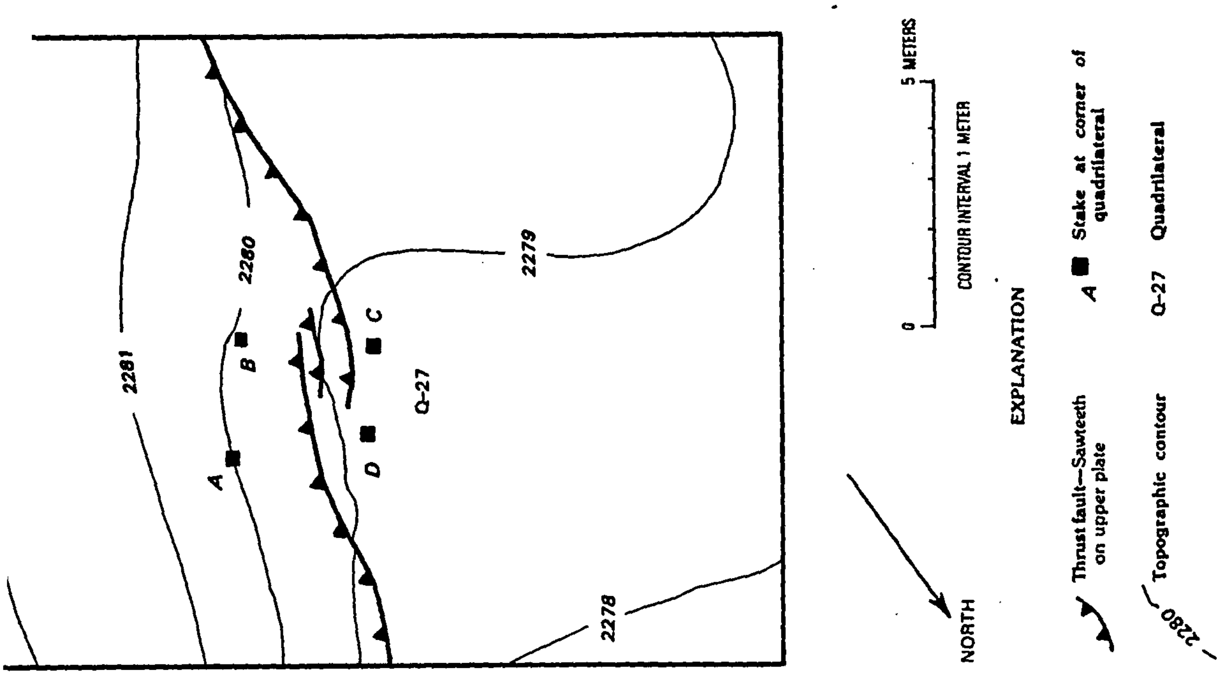

d view of area "d", shown in Figure 6.9.

ted within the boundaries of quadrilateral Q-tension cracks, oblique to the axis of the ridge, were observed at several places along the ridge crest. A fallen tree trunk lying on the south flank of the ridge had been lifted out of a depression it had formed in the ground surface.

The ridge itself was approximately 1-1.2 m high, 3 m wide, and 20 m long (Fig. 6.6; Fig. 6.12). In cross section, the ridge was rounded and slightly asymmetric. The north side of the ridge, which was parallel to the strike-slip fault, was steeper and higher than the south side of the ridge. The surface of the ridge was covered with boulders and had a thin layer of top soil.

Quadrilateral Q-34 was one of several points of measurement intended to document the growth and deformation of the ridge. One longitudinal and two transverse lines of stakes were surveyed on the ridge and across to stable ground. Also, two quadrilaterals were placed on different parts of the ridge. Quadrilateral Q-34 was intended to monitor a simple, relatively smooth section of the inside flank of the ridge. Two of the stakes, C and D, were also part of a transverse stake line across the ridge. The transverse line provided data on ridge growth, and Q-34 provided data for computation of strain and tilt. Stakes A and B also provided a check on the results from stakes C and D. They (Fleming and Johnson) did not assume that growth of a ridge is two-dimensional (Robert Fleming, written commun., 1987).

Stakes A and D were installed near the crest of the ridge so that line AD was nearly parallel to the axis of the ridge. Stakes B and C were installed downslope from stakes A and D, near the base of the south side of the ridge, so that the four stakes defined the corners of

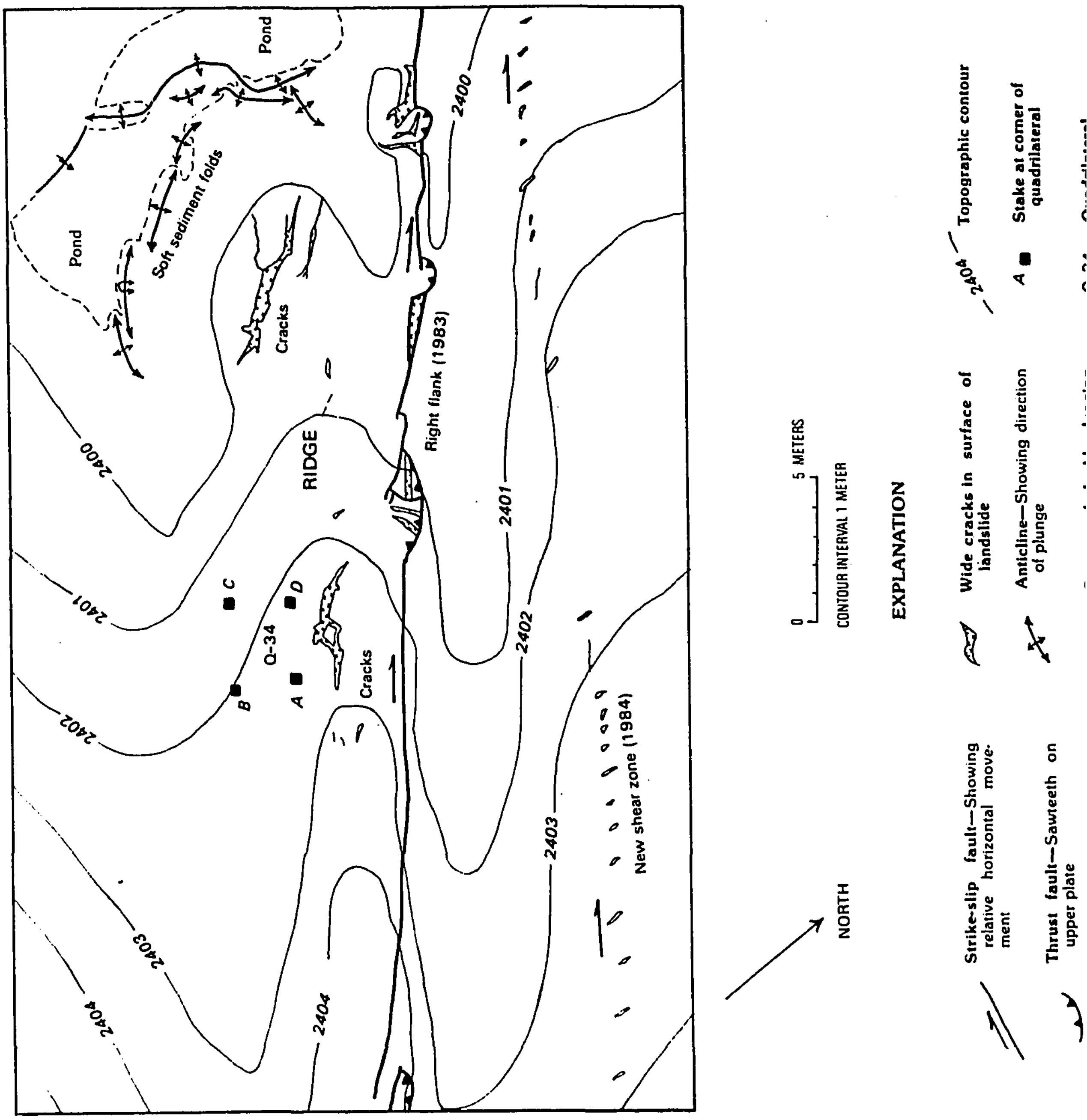

FIGURE 6.12. Map showing ridge on the right flank of the Aspen Grove landslide (part of area "a", shown in Fig. 6.6) (August 1984). Quadrilateral Q-34 was located on the southwest side of the ridge, on upper part of the landslide.

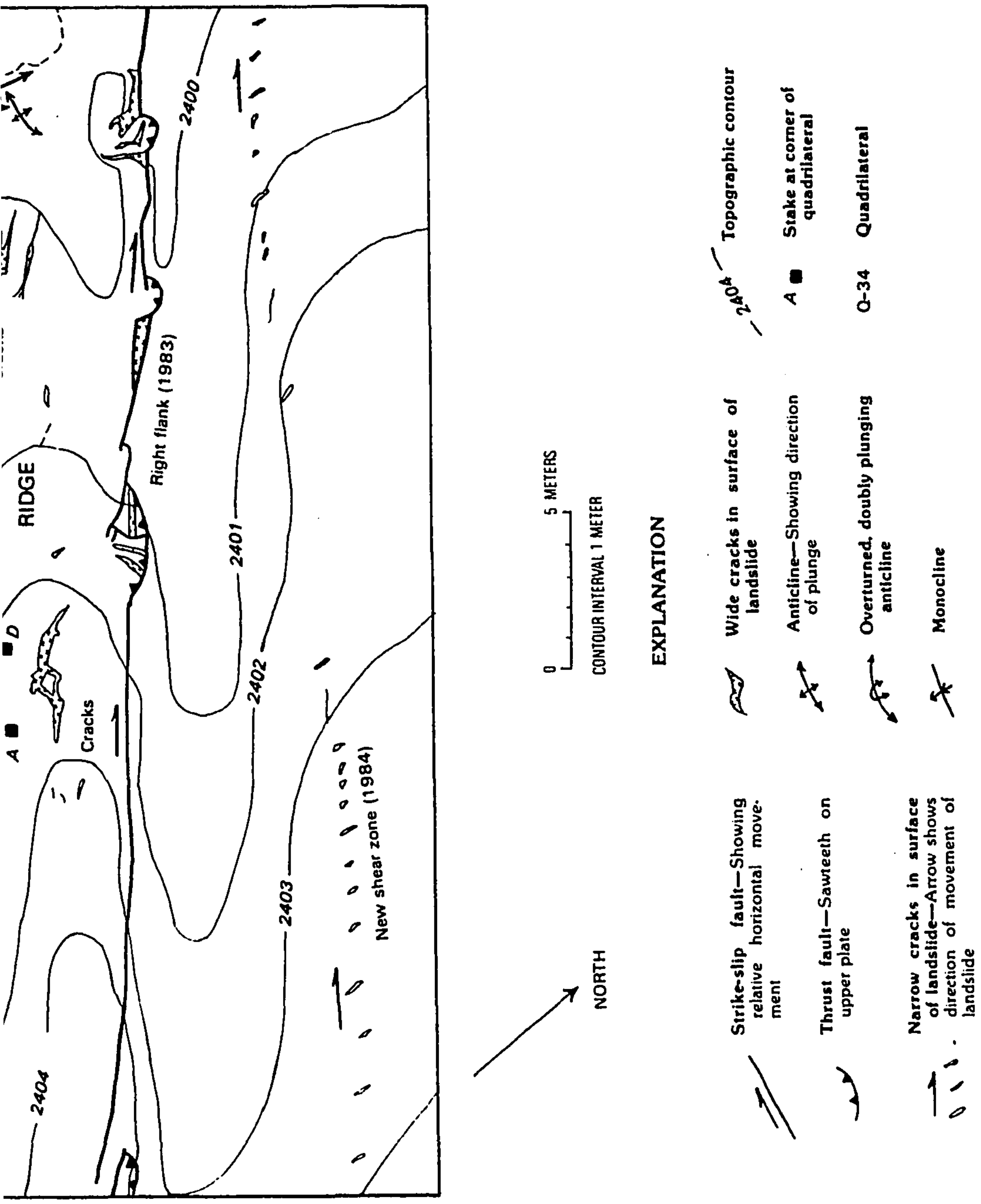

showing ridge on the right flank of the Aspen

: area "a", shown in Fig. 6.6) (August 1984).

Located on the southwest side of the ridge, on

.ide.

a trapezoid (Fig. 6.12). The quadrilateral was 3.3 m long and 2.6 m wide, and side AD was 0.5 m higher than side BC.

Measurements were made on June 2, June 5, June 7, and August 3, 1984. Strain and tilt from June 2 to June 7 were small, and displacement along the right flank at Q-2 was only 0.15 m. However, the magnitudes and directions of the strains were consistent among the four triangles in the quadrilateral. The maximum principal strain had a small positive value and was oriented toward the west or northwest. The minor principal strain indicated small amounts of shortening or elongation. Minor amounts of tilt, oriented toward the south, also occurred.

Considerably more deformation had occurred at Q-34 by August 3. The ridge was displaced 0.68 m between June 7 and August 3 (measured at Q-2), making a total displacement of 0.83 m since measurements started on June 2. The major principal strain at Q-34 for the period June 2 to August 3 was oriented toward the west-northwest and was between +1.3 and +2.5 percent (Table 6.1). The minor principal strain was from -0.3 to -0.8 percent. Continued tilting toward the south-southwest resulted in the southwest side of the ridge being 1.0-1.5° steeper than it had been on June 2 (Fig. 6.13). The site of the quadrilateral looked about the same as it had before, except that the cracks just upslope from Q-34 were slightly wider than they had been on June 2.

During 1985, deformation of the ridge continued. The principal strains for the period June 2, 1984 to August 2, 1985, indicate that elongation in a west or west-northwest direction continued. A small amount of shortening occurred in triangles ABC and DAB and elongation

TABLE 6.1

Principal strains at Q-34

Beginning Date	Final Date	Triangle	Major Principal Strain (percent)	Azimuth - Major Principal Strain	Minor Principal Strain (percent)
6/2/84	8/3/84	ABC	+1.58	N. 81° W.	-0.76
		BCD	+1.30	N. 63° W.	-0.32
		CDA	+2.31	N. 62° W.	-0.33
		DAB	+2.51	N. 73° W.	-0.55
6/2/84	8/2/85	ABC	+5.91	N. 73° W.	-1.91
		BCD	+6.82	N. 89° W.	+0.48
		CDA	+4.62	N. 86° W.	+0.82
		DAB	+3.74	N. 66° W.	-0.91

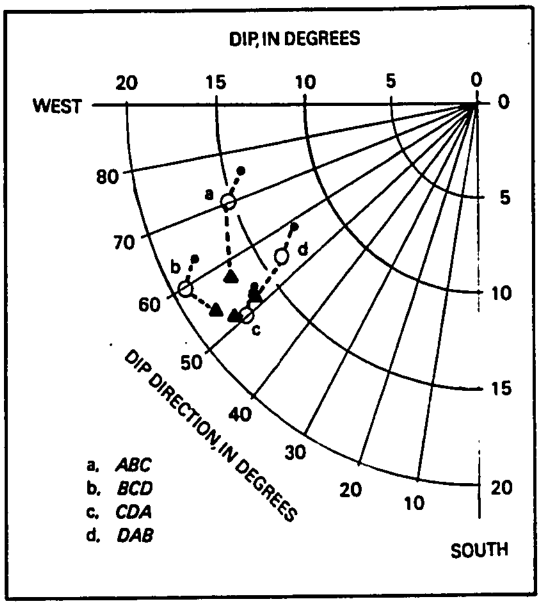

FIGURE 6.13. Polar plot showing attitude (dip and dip directions) of the four triangles in quadrilateral Q-34. Solid dots, attitudes on June 2, 1984; open circles, attitudes on August 3, 1984; and solid triangles, attitudes on August 2, 1985.

occurred in triangles BCD and CDA in a north or north-northeast direction (Table 1). Tilt increased at three of the triangles and decreased slightly at one (Fig. 6.13). The 1985 deformation resulted from 1.36 m of displacement on the old flank fault (2.19 m for 1984 and 1985 combined) and 1.95 m of displacement on the new flank fault.

The measurements of the quadrilateral showed that the ridge was, in fact, growing in height while the landslide was moving during 1984 and 1985. Steepening of the side of the ridge, as documented by the increasing tilt of the quadrilateral, showed that the ridge was growing in height relative to the neighboring ground. Although shortening of the quadrilateral perpendicular to the ridge axis would have produced similar results, the leveling data show that the vertical distance between line AD and line BC actually increased. For example, the height differences between stakes A and B increased from 0.48 m on June 2, 1984 to 0.54 m on August 4, 1984.

The ridge elongated approximately parallel to its axis. Deformation perpendicular to the axis of the ridge was small, and shortening occurred in some triangles but elongation occurred in others. Area strain was positive (increasing area) throughout the period of activity; however, no tension cracks formed within the quadrilateral. Positive area strain is normally associated with thinning of the landslide debris.[16] However, positive area strain in Q-34 was associated with growth in the height of the ridge.

Measurement of Strain and Tilt in an Area of Developing Normal Faults Within the Landslide

During early June 1983, only a few cracks were the sole evidence of deformation anywhere within the boundaries of the Aspen Grove landslide. Quadrilateral Q-5 was set on a topographic high point near the axis (midway between the two flanks) of the landslide, at a high point along a prominent change in slope. East of Q-5, the surface of the landslide had a backslope of a few degrees toward the northeast (Fig. 6.6). West of Q-5, the surface of the landslide sloped toward the northwest, roughly parallel to the direction of sliding, but the ground was locally steepened.

Robert Fleming (written commun., 1987) expected purely extensional strains at Q-5 because the most rapidly moving part of the landslide was 170 m downslope from Q-5. Although he wanted to observe these strains, he was perhaps more interested in monitoring changes in what was initially a high point in the surface of the landslide.

Quadrilateral Q-5 was 1.8 m wide, 2 m long, and roughly rectangular. The long dimension of the quadrilateral was oriented N. 50° E. and the short dimension was oriented N. 30° W. Thus, the

[16] If it is assumed that the density of the debris is constant, then the ratio of the final volume to the initial volume, $\underline{S}_1\underline{S}_2\underline{S}_3$, must equal unity. Thus, if $\underline{S}_1\underline{S}_2 > 1$, then $\underline{S}_3$, which is oriented perpendicular to the surface of the landslide, must be less than 1, and $\underline{S}_3 < 1$ indicates thinning of the landslide.

sides of the quadrilateral were slightly oblique to the axis of the landslide, which was oriented N. 55° W. The quadrilateral sloped gently (about 8°) toward the north-northwest.

During 1983, quadrilateral Q-5 remained unchanged. The computed strains were of the same size as those that would result from the expected errors in the measurements (Table 6.2) and the principal strains showed inconsistent orientations among the four triangles. Thus, any deformation that occurred during 1983 was too small to be detected by our measurements.

During 1984, it was apparent that Q-5 no longer stood on the high point of the landslide. The highest point in the area was now upslope from Q-5 and closer to the left flank (Fig. 6.14). Tilt of quadrilateral Q-5 increased from August 4, 1983 to May 23, 1984. From May 23 to August 3, 1984, the slope of line AB increased while the slope of line AC remained unchanged and the slope of line AD decreased. Thus, the quadrilateral sloped from 10° to 11° toward the north-northwest by August 3, 1984.

Strains were relatively small in 1984 and the principal strains were difficult to interpret; however, the deformation can be understood by looking at the relative motions of the four stakes (Table 6.2). For the period from August 4, 1983 to May 23, 1984, the strains in individual stake lines show that stakes A and C moved toward stake B. Between May 23 and August 3, 1984, stakes A, C, and D maintained their positions relative to one another, but stake B moved away from the other three.

TABLE 6.2

Strains in Quadrilateral Q-5

Beginning Date	Final Date	Strain in lines (percent) AB	BC	CD	DA	AC	BD
6/16/83	8/3/83	0.0	+0.1	+0.1	-0.2	-0.1	+0.1
8/4/83	5/23/84	-1.4	-0.7	+0.9	+0.7	-0.3	0.0
5/23/84	8/3/84	+0.3	+0.3	-0.2	+0.2	-0.3	+0.6
8/3/84	8/2/85	+4.5	+1.1	-0.1	-0.1	-0.5	+3.5

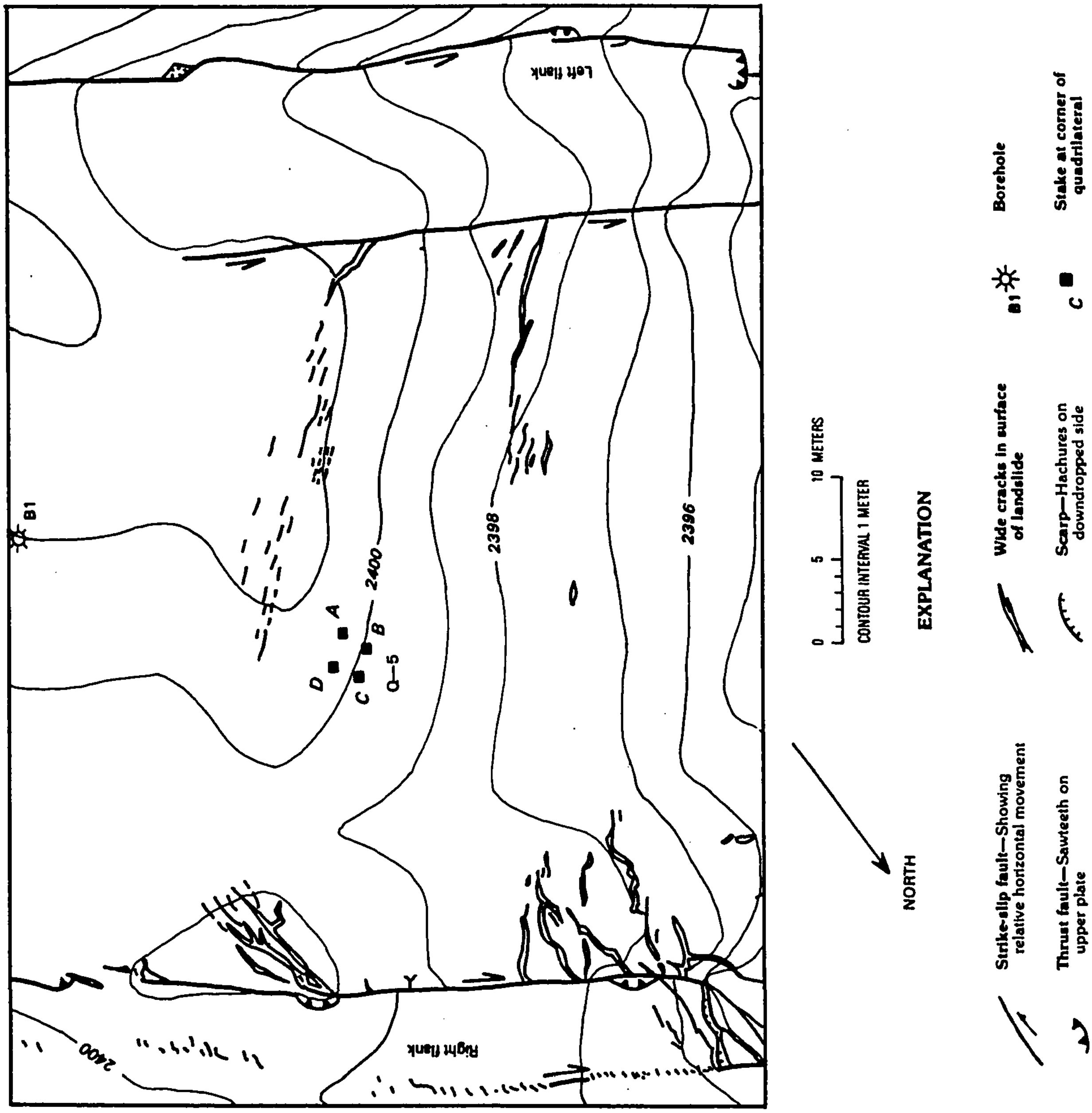

FIGURE 6.14. Map showing part of the Aspen Grove landslide in the vicinity of Q-5 during August 1984 (area "c", shown in Fig. 6.6).

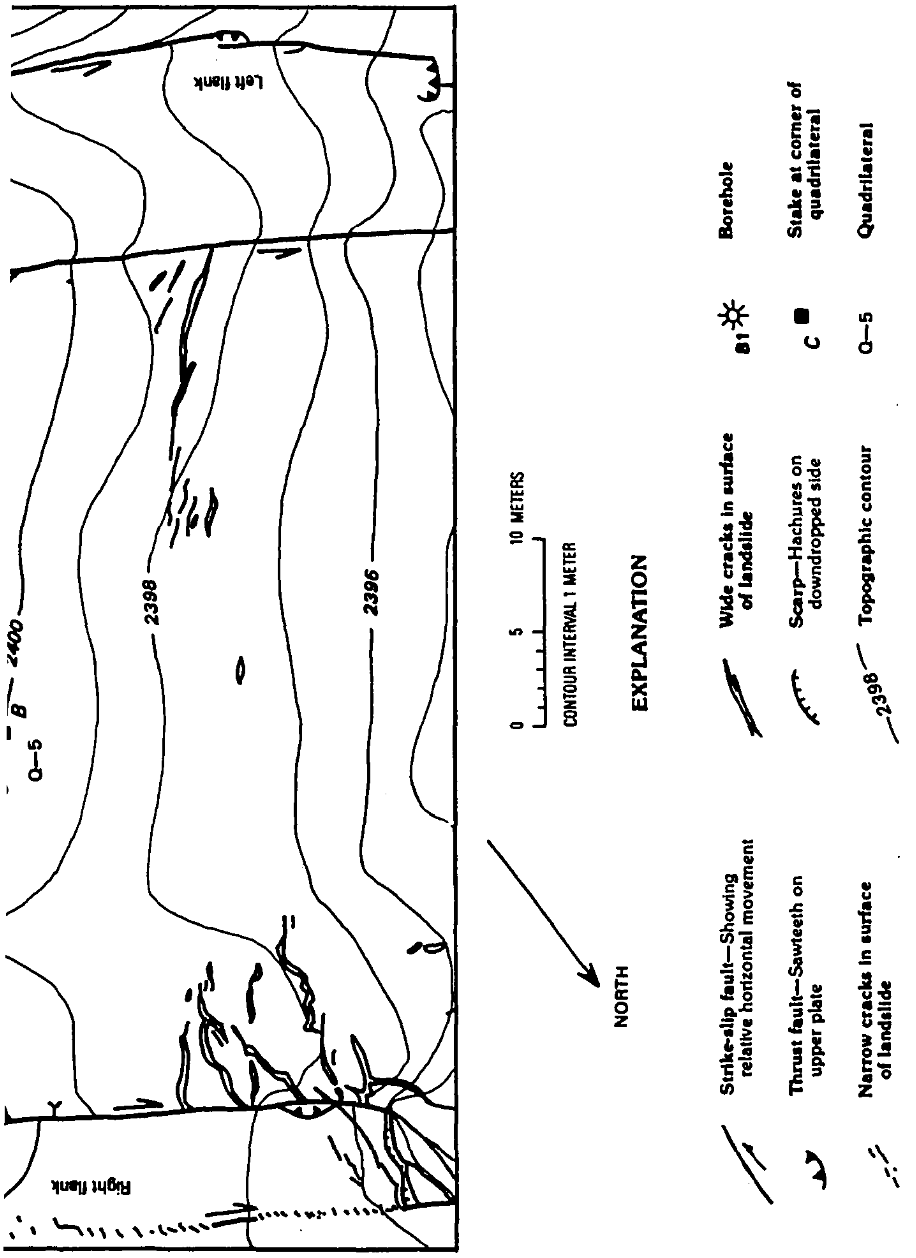

ng part of the Aspen Grove landslide in the

1984 (area "c", shown in Fig. 6.6).

In 1985, the difference in topographic form became even more pronounced than it had been in 1984 (Fig. 6.15). Tension cracks that had been noted near the left flank in 1984 appeared upslope from and within quadrilateral Q-5. By this time, Q-5 had changed from a gently sloping quadrilateral on a high point to a steeply sloping quadrilateral downslope from a high point. The quadrilateral sloped from 11° to 12° toward the northwest or north-northwest. Line AB continued to steepen during 1985, while lines AC and AD became flatter.

During the period from August 3, 1984 to August 4, 1985, the major principal strain was oriented between west and northwest, or roughly parallel to line BD. The minor principal strain indicated a small amount of contraction normal to that direction. As in the latter part of 1984, the relative motions of individual stakes indicated that triangle ACD remained relatively undeformed, while stake B moved away from it (Table 6.2). Such motion is consistent with the appearance of cracks between stake B and triangle ACD during 1985.

In 1986, cracks that appeared during 1985 developed into a normal fault (Fig. 6.16) that dropped stake B 13 cm relative to stake A between August 2, 1985 and September 12, 1986. The fault scarp appeared to be between 10 and 15 cm high and nearly vertical. Horizontal displacement of stake B relative to line AD amounted to only one centimeter during the same period; thus, movement was roughly parallel to the fault surface exposed in the scarp. Stakes C and D moved upward relative to stake A so that triangle ACD was relatively flat in September 1986.

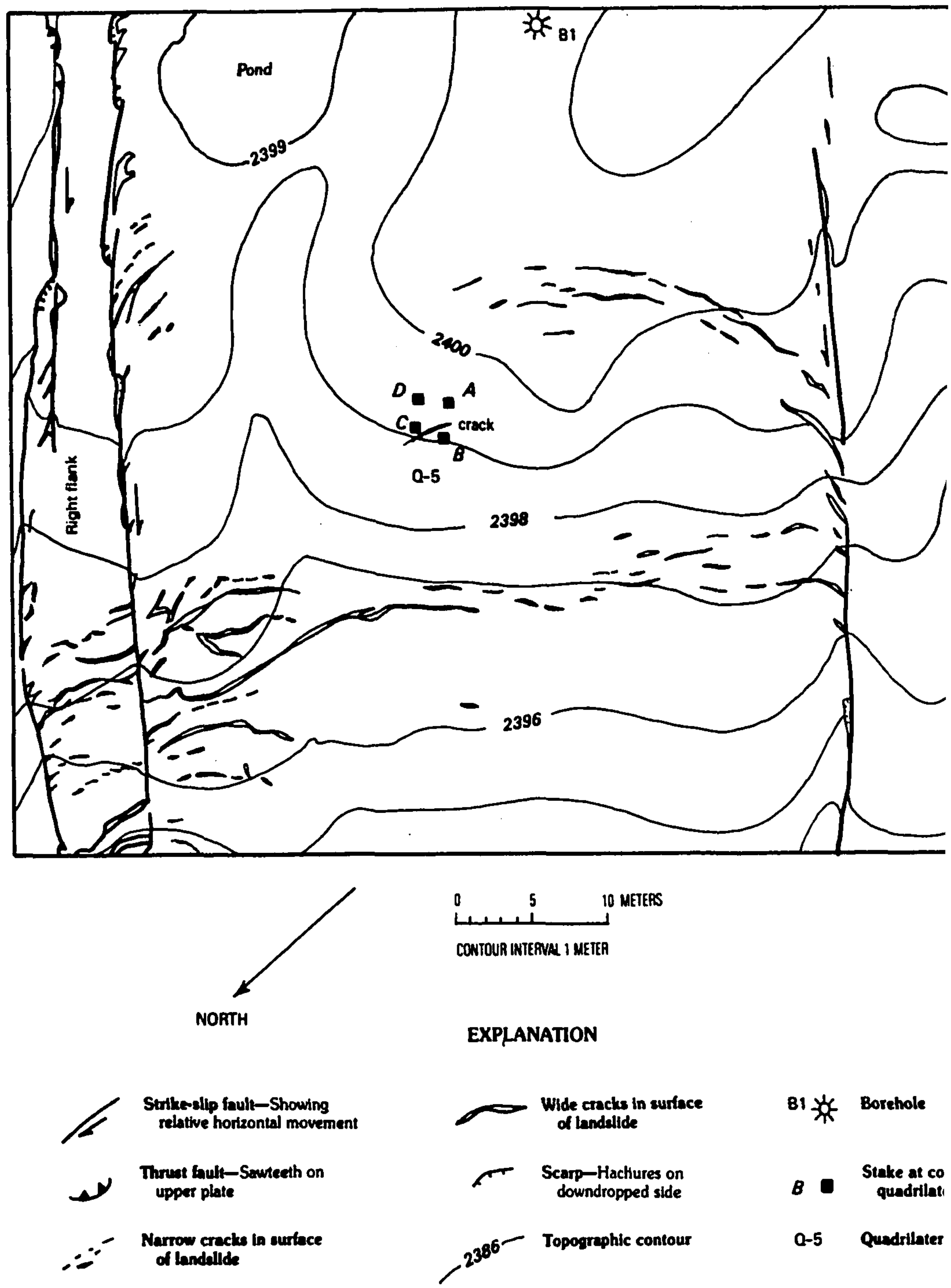

FIGURE 6.15. Map showing part of the Aspen Grove landslide in the vicinity of Q-5 during August 1985 (area "c", shown in Fig. 6.6).

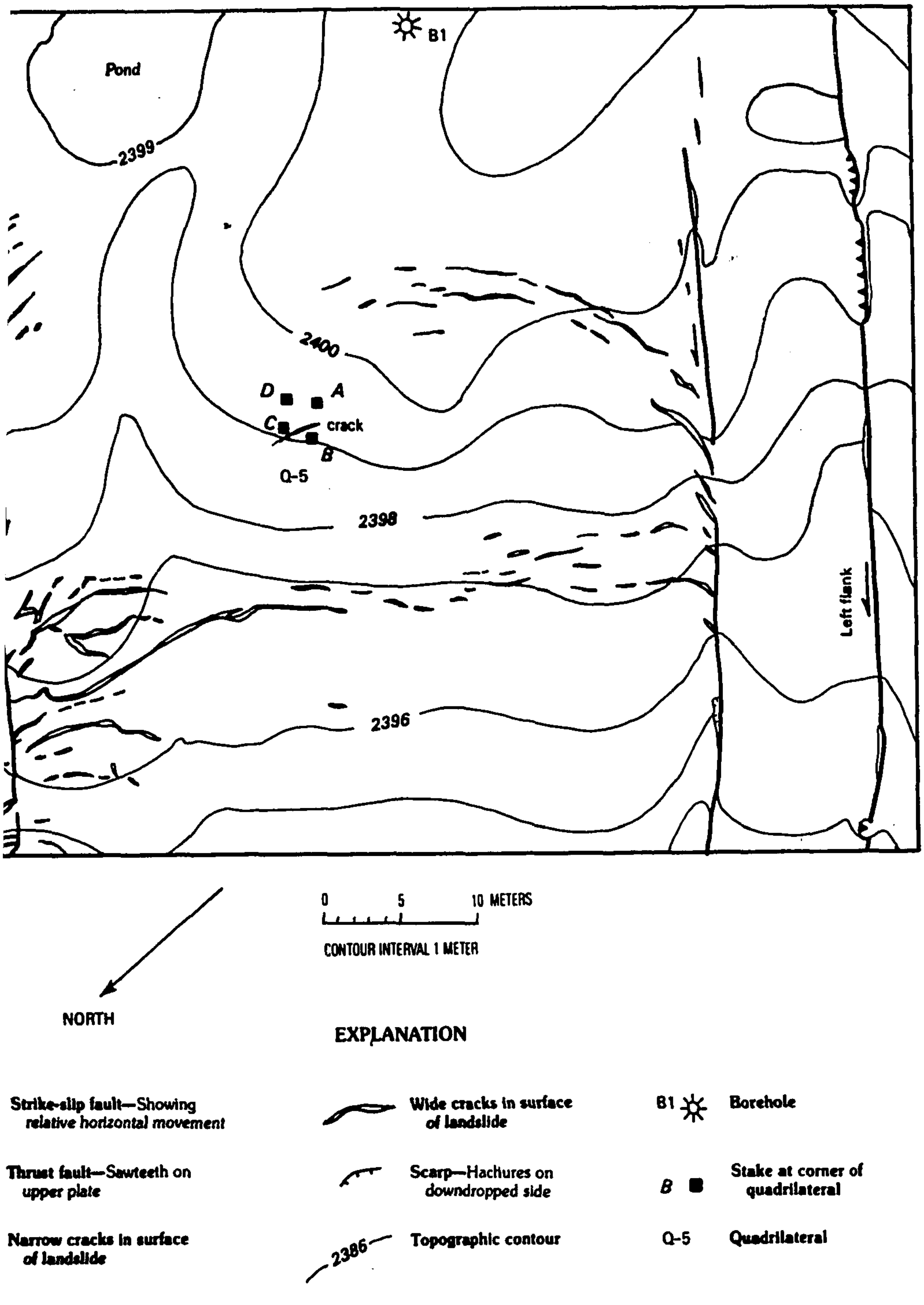

showing part of the Aspen Grove landslide in the

ugust 1985 (area "c", shown in Fig. 6.6).

Deformation at quadrilateral Q-5 was surprising. While the first few meters of movement occurred, the quadrilateral deformed very little but steepened as it seemingly moved off a high point in the slip surface of the landslide. Crack-like deformation began during 1984 as stake B moved away from triangle ACD, well before cracks appeared within the quadrilateral during 1985. What appeared to be simple tilting of the quadrilateral during 1984 and 1985, apparently was a precursor of the movement on the normal fault that occurred in 1986. Thus, had I recognized the style of deformation evident in the data, I could have predicted the formation of a normal fault passing through Q-5 long before the fault could be observed in the field.

Discussion and Conclusion

I have described a method for measuring the displacements, strains, and tilts at the surface of a landslide and have illustrated the field technique by means of examples.

The method is practical and can be easily done along with field mapping and other data-collection activities. The field technique is simple and the required measurements can be made rapidly. In the heavily wooded terrain of the Aspen Grove landslide, 28 quadrilaterals and eight stake lines could be measured by two people in one working day.

The equations provided in the text have general application because they treat three-dimensional displacements and large strains. Thus, the equations are more useful than graphical methods (Ragan, 1973; Ter-Stepanian and Ter-Stepanian, 1974). BASIC computer programs are

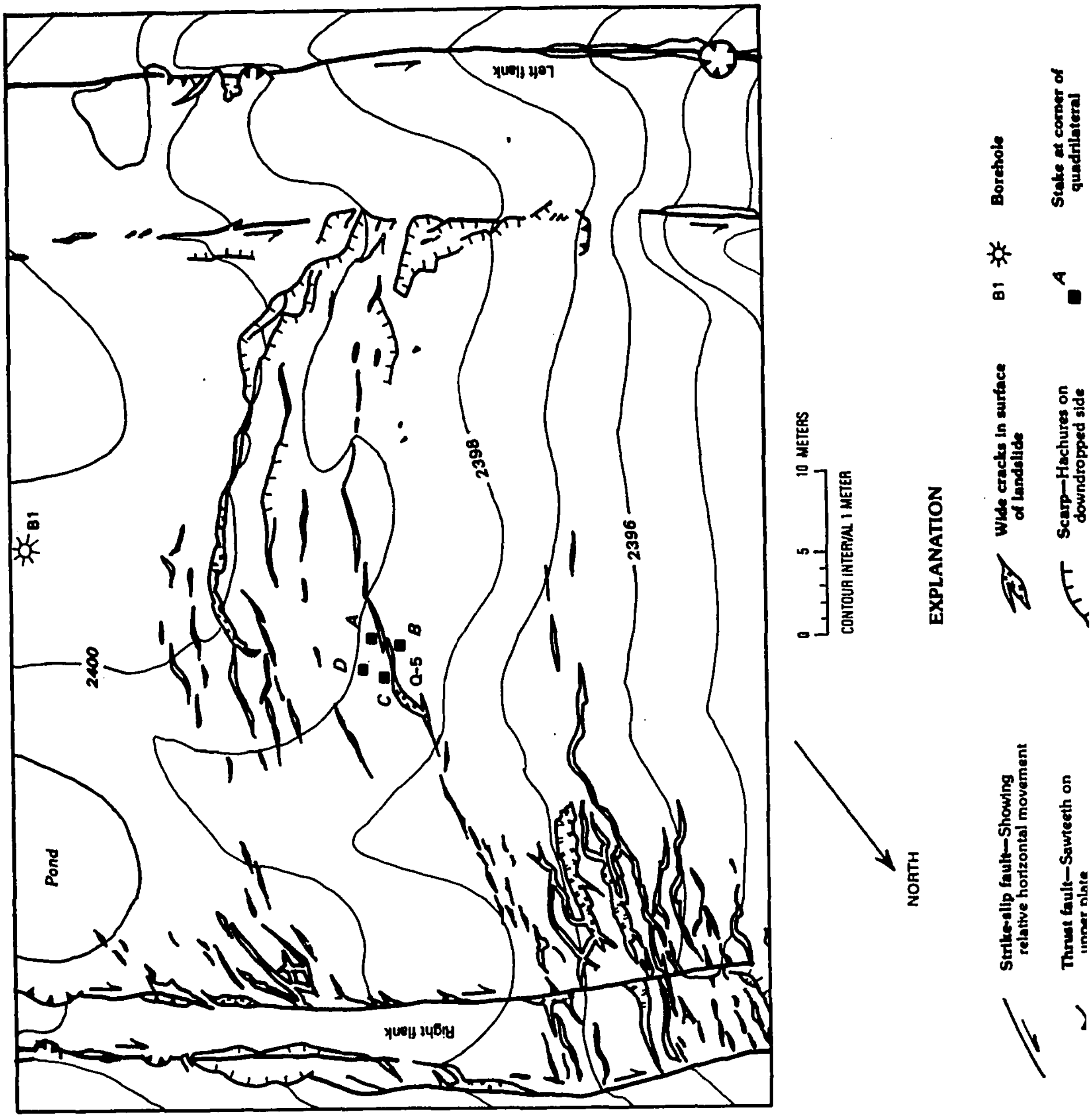

FIGURE 6.16. Map showing part of the Aspen Grove landslide in the vicinity of Q-5 during September 1986 (area "c", shown in Fig. 6.6).

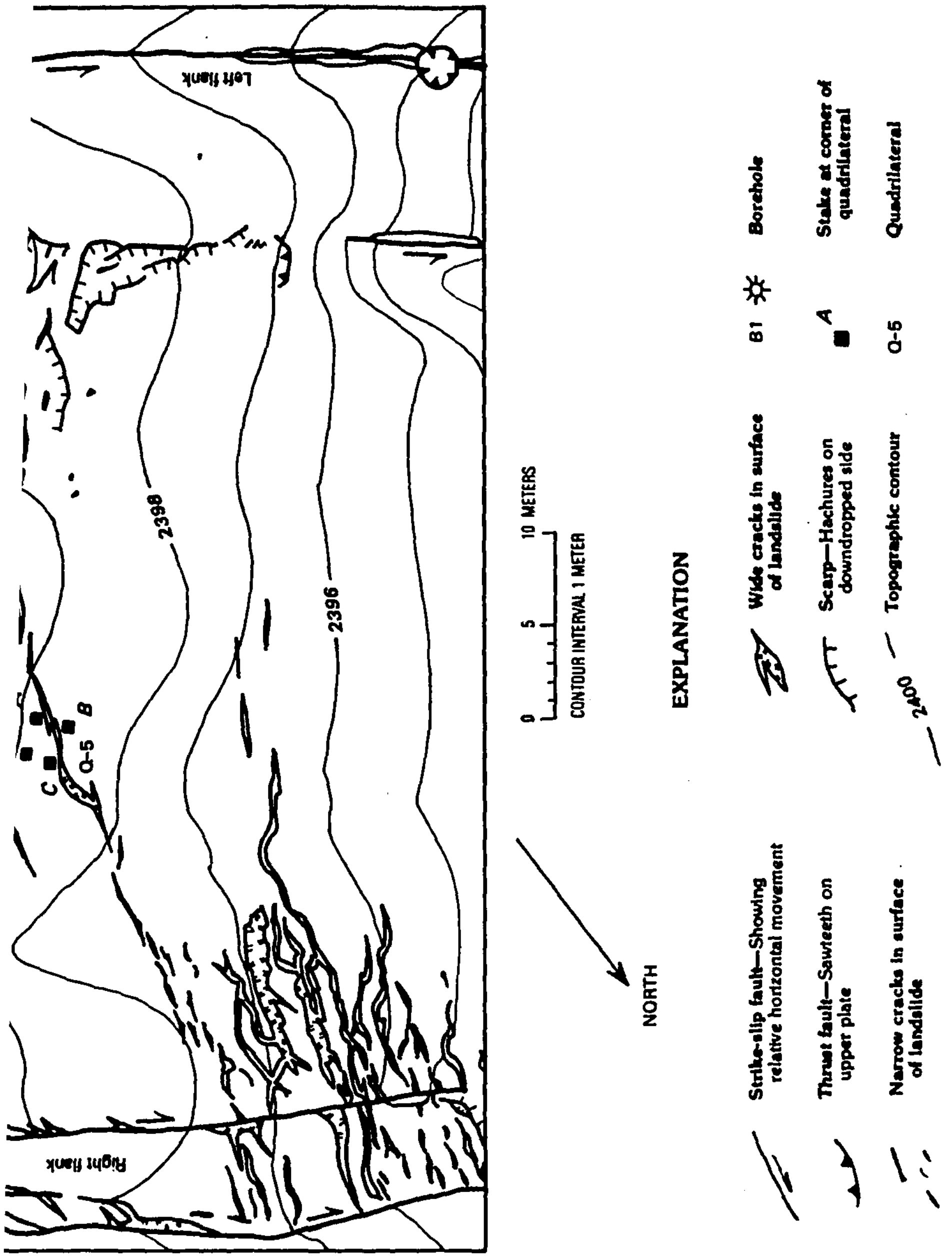

ng part of the Aspen Grove landslide in the

ber 1986 (area "c", shown in Fig. 6.6).

available for processing the data (Appendix F, and Johnson and Baum, 1987).

When David Varnes and Robert Fleming installed the first few quadrilaterals, they hoped to measure strains and displacements in a simple way (Robert Fleming, oral commun., 1987). As data accumulated, it was obvious that strains and displacements could be measured, and we began asking questions that required more data and better precision in the measurements. A few simple improvements would have resulted in a better data set.

First, we should have used something sturdier than 13 by 40 mm (nominal 1" by 2") wooden stakes and should have used metal tags with numbers stamped into them to identify the stakes. Several alternatives are available, from sturdier wooden stakes to elaborate concrete and metal stakes having machined heads that accept tape or rod extensiometers.

During years when the landslide was visited infrequently, we should have replicated measurements during each visit in order to eliminate large errors that resulted from careless mistakes. Measurements were made with a tape that was marked in feet and inches, thus it was easy to make mistakes when reading the tape or recording the measurement. Errors in measurements caused by such mistakes were frequently large enough to interfere with strain computations; thus, repeated measurements would have improved the quality of our data sets.

Replication of measurements and application of tension and temperature corrections to measurements made with a steel tape would have improved sensitivity to small strains. Greater accuracy and sensitivity could have been achieved by making measurements with a tape extensiometer or rod extensiometer (Franklin, 1984; Hanna, 1985) so that strains as small as 0.0001 (0.01 percent strain) could be computed accurately. Quadrilateral measurements obtained by such means would be amenable to correction by least squares (Laurila, 1983) or Ingram's (1972) method of angular value weighting.

We should have replaced the stakes on moving ground next to strike-slip faults at the end of each season to keep the quadrilaterals as nearly equidimensional as possible, because measurement errors increased when the quadrilaterals became stretched into narrow diamond-shaped figures.

We should have taken photographs, and made sketches and detailed maps to show how some of the sites changed through time. The magnitudes of strains and displacements that result in visible changes to the ground surface are poorly known. Carefully drawn sketches and large-scale maps of the quadrilateral sites might have been even more useful than the photographs, because they would have insured that we studied the sites carefully and thoughtfully.

Planning is an important aspect of the field technique. We tried to view each quadrilateral as an experiment that had at least one specific question to be answered. Observations made during a visit to the site usually prompted questions. Quadrilaterals were then designed and surveyed in order to answer these questions. In some cases, we may not have asked significant questions, but we always learned something from the quadrilaterals as we measured and observed changes in them.

Once we had questions in mind, we tried to position and configure the quadrilaterals so that they would give optimum response to the deformations. Thus, quadrilaterals used to measure displacements were positioned at several locations on the boundaries and they were configured so that two sides were approximately parallel to the discontinuity at the boundary. Likewise, quadrilaterals used to measure strain and tilt were positioned on deformational features that were poorly understood or in uncomplicated areas where the background pattern of deformation could be observed. Quadrilaterals used to measure strain and tilt were configured and sized to fit the feature being measured.

During the course of measuring and observing the quadrilaterals, our understanding of the landslide increased and new questions presented themselves. As these questions arose, we evaluated the adequacy of our quadrilaterals to answer the new questions. In some cases, the new questions could be answered with more quadrilaterals; in other cases, the questions could be answered only by other types of measurements or observations.

CHAPTER VII

EFFECTS OF UNEVEN SLIP SURFACES ON THE STABILITY AND VELOCITY OF LANDSLIDES IN SOIL

Introduction

Surface roughness has been recognized as a source of sliding resistance in rock slopes (Patton, 1966), glaciers (Kamb, 1970) and faults (Byerlee, 1970). However, surface roughness has not previously been recognized as a source of significant sliding resistance for landslides in soils. The basal and lateral slip surfaces of landslides in soils are uneven. The unevenness of these surfaces might retard landslide movement so as to increase the stability of landslides and control their velocities.

Observations show that many landslides move for weeks, months or even longer at rates ranging from less than a millimeter per day to a few meters per day. Keefer and Johnson (1983, p. 45, 46) compiled data from many sources on the minimum and average velocities of landslides in soils. The average velocities range between 10^{-5} and 10 m/d (meters per day), and the maximum velocities range from 10^{-3} to 10^4 m/d (maximum velocities in the range from 10^2 to 10^4 m/d occurred during surges).

Landslides commonly move at constant rates for periods of several days. These periods are interrupted by shorter periods of acceleration and deceleration. However, sustained acceleration resulting in very rapid movement generally does not occur (Keefer and Johnson, 1983, p. 46-48).

Slow, steady movement of landslides cannot be explained in terms of slope stability theory, which predicts that a landslide will accelerate as soon as the driving forces exceed the frictional and cohesive resisting forces on the slip surface (Keefer and Johnson 1983, p. 48, 49). For example, a slight increase of pore-water pressure in a landslide at equilibrium ought to cause the landslide to accelerate.

Field measurements show that velocities of landslides increase gradually with increasing pore-water pressures. Terzaghi (1950, p. 120) observed a linear relationship between water level and velocity in a landslide that was about 40 m deep. The velocity increased from about 60 mm/d when the water level was 3.0 m below the ground surface to about 200 mm/d when the water level was only 1.0 m below the ground surface. Rybar (1968, p. 140) observed that the velocity of a landslide 5.4 m deep increased from about zero to about 8 mm/d as water levels increased by 1 m. The velocity of a landslide in Japan increased from about 1 mm/d to 13 mm/d as the water level in a bore hole rose about 2 to 2.5 m (Japan Society of Landslide, 1980, p. 9). Similar findings were reported by Iverson (1986).

A popular model used to explain the slow movement of landslides is inconsistent with field observations (Fig. 7.1). In the model, the velocity at the basal boundary of the landslide is assumed to be zero, and flow is assumed to occur in a layer of material above the basal boundary (Yen, 1969; Keefer, 1977; Suhayda and Prior, 1978; Craig, 1981;

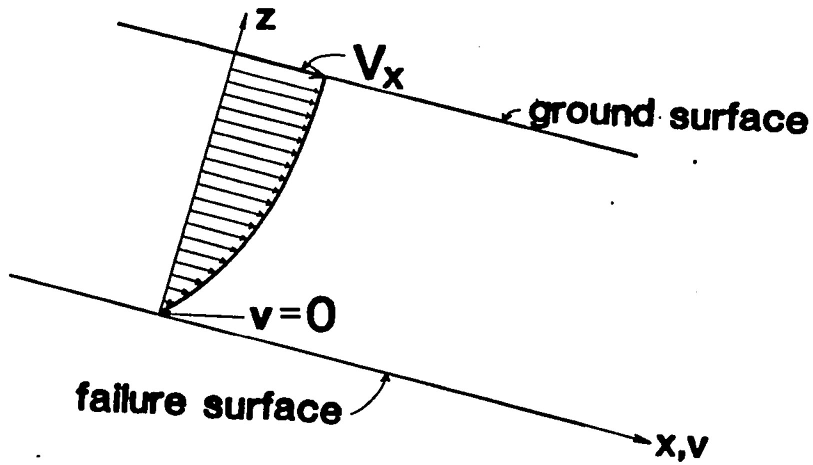

FIGURE 7.1. Schematic diagram showing the zero-velocity boundary condition assumed in other theories of landslide motion.

Savage and Chleborad, 1982; Iverson, 1986; and others). However, field observations (Keefer and Johnson, 1983; Hutchinson, 1970; Prior and Stephens, 1972) indicate that movement occurs primarily by block gliding. The velocity at the basal slip surface nearly equals the velocity at the ground surface, and deformation is concentrated at the slip surface.

A possible explanation for the slow movement of landslides in soils is that strength of material at the slip surface is velocity dependent, although this explanation is discounted by several investigators. Keefer and Johnson (1983) determined that the shear strength of a sample of slip surface of a landslide increased linearly with the log of the velocity so that the strength of the material tested increased only 2.5 percent for each 10 fold increase in velocity. They concluded that such an increase is too small to account for the slow movement of landslides. Similar results were obtained by Kenney (1967) and Ramiah and Purushothamaraj (1971), and Mitchell (1976, p. 292) who indicates that shear strength of soils generally increases 5 to 10 percent for each 10 fold increase in rate of deformation.

Superficial similarities between the movement of glaciers and the movement of landslides in soils suggest that the mechanics of sliding of glaciers and of landslides might be analogous (Keefer and Johnson, 1983). Both glaciers and landslides move slowly and steadily, and temperate glaciers are known to move by block gliding over uneven bedrock surfaces. Surface roughness (i.e. unevenness of the bedrock surface) has been shown to retard movement of temperate glaciers by causing regelation and plastic deformation of the ice (Kamb and LaChapelle, 1964; Kamb, 1970).

Similarly, surface roughness might retard movement of landslides by causing movement of pore fluid (due to consolidation and swelling) and plastic deformation of landslide debris. These are the models investigated here.

Slip Surfaces in Landslides

An analogy between the mechanics of landslides and the mechanics of temperate glaciers is reasonable only if landslides move by gliding over uneven surfaces as do the glaciers. We describe slip surfaces of landslides in soils in order to document the ubiquity of slip surfaces in landslides, to show that most landslides move by block gliding on slip surfaces and that some slip surfaces could be sufficiently uneven to retard landslide movement.

Slip surfaces are thin layers of parallel clay particles where deformation has been concentrated. Hutchinson (1983, p 243) noted that slip surfaces are often paper thin, making them difficult to locate in samples and exploratory trenches. Mary Riestenberg (oral comm., 1987) observed that the slip surfaces of landslides in Cincinnati are paper thin. Observations made by means of polarizing microscope (Skempton and Petley, 1967; Morganstern and Tchalenko, 1967) indicate that slip surfaces are 100- to 500-micron-thick layers of strongly oriented clay particles. Typically the clay within a few centimeters of the slip surfaces is deformed or remolded, but deformation is concentrated on the slip surfaces.

The existence of slip surfaces in landslides has been recognized for more than a century. Collin (1846) was the first to document and accurately describe slip surfaces of landslides that occurred in clay embankments and cuttings in clay slopes. During the course of repairing the landslides, the debris was cleared away, exposing the basal slip surfaces. They were "smooth, slippery and soapy" surfaces.

Summarizing observations of many landslides, Skempton and Petley (1967, p. 33) indicated that slip surfaces occur in the majority of landslides:

"In most landslides . . . large movements have taken place, chiefly concentrated on 'principal slip surfaces.' Typically these surfaces are polished and subplanar, with striations in the direction of movement, and they may extend over considerable areas."

Observations and measurements indicate that landslides move primarily by block gliding on their slip surfaces. Collin (1846, p. 36, 37) was able to show that the basal slip surfaces formed as a result of landslide movement and that movement occurred primarily by sliding on the basal slip surface. He observed that the bedding or layering was tilted and offset across the basal slip surface of a landslide.

In a landslide near Beltinge, England at least 89 to 95 percent of total displacement occurred on or within 20 cm of the basal shear surface (Hutchinson, 1970). A bore hole inclinometer was used to measure deformation at depth that accompanied displacement observed at the surface. The lowest point of measurement in the borehole, about 20 cm above the basal slip surface, moved only a few cm less than the top of the borehole during about 0.8 m of movement.

At a shallow earthflow in California, experiment showed that displacement was concentrated on the basal slip surface (Keefer and Johnson 1983, p. 31, 32). A stack of wooden disks, shaped like poker chips, was placed in a borehole that penetrated the basal slip surface. After the landslide had moved about 0.4 m, the disks were recovered by digging a trench next to the borehole, and the positions of the disks were mapped. At least 94 percent of the movement occurred within 1.3 cm (the thickness of one disk) of the basal slip surface. Little evidence of deformation outside the slip surface was observed.

Displacement at the lateral boundaries of landslides also occurs on slip surfaces. Strike-slip faults having slickensided surfaces constituted the lateral boundaries of the Aspen Grove landslide in central Utah. Displacement measurements at three transverse lines of stakes on the landslide show that displacement at the boundaries was 85 to 95 percent of the displacement at the axis of the landslide. (See Chapter V.)

Several investigators have reported that some deep landslides move on "thick kneaded zones" (Zaruba and Mencl, 1982, p. 161; Goold, 1960; Brunsden, 1984). However, even the kneaded zones are bounded by or contain slip surfaces that accommodate most of the displacement. At the toe of the Twin Lake landslide, near Mayfield, Utah, a layer of plastic clay; 1 m thick, thinly laminated and shistose; was divided into almond-shaped pieces by a family of anastomosing, subhorizontal slip surfaces. A layer of "kneaded" clay exposed in the south bank of Ephraim Creek, near Ephraim, Utah was bounded at its top by slip surfaces (Fig. 7.2). Several meters away at another exposure, polished

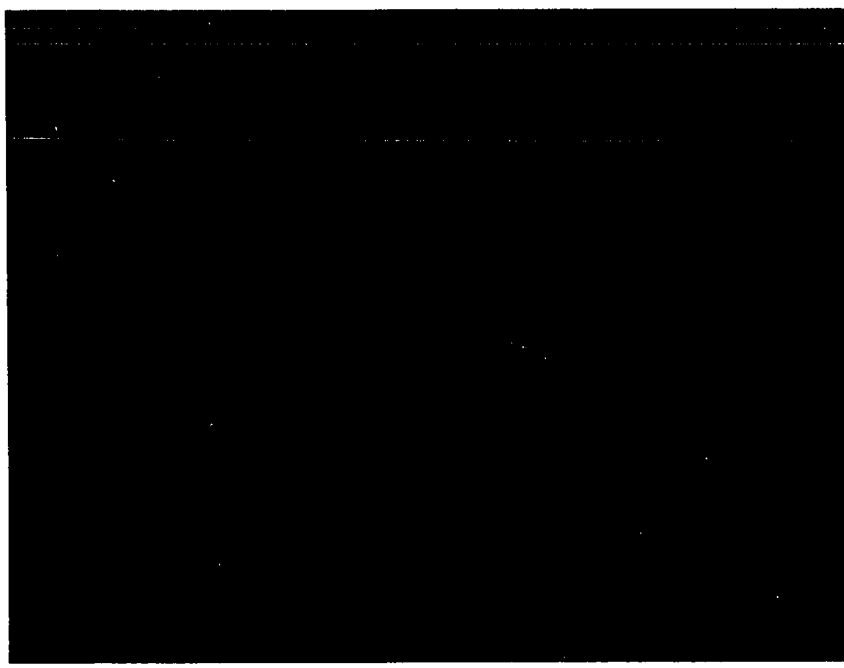

FIGURE 7.2. Cross-sectional view of a shear zone or kneaded zone exposed in bank of Ephraim Creek, near Ephraim, Utah. Dark lens-shaped area is part of a slip surface exposed in an overhang.

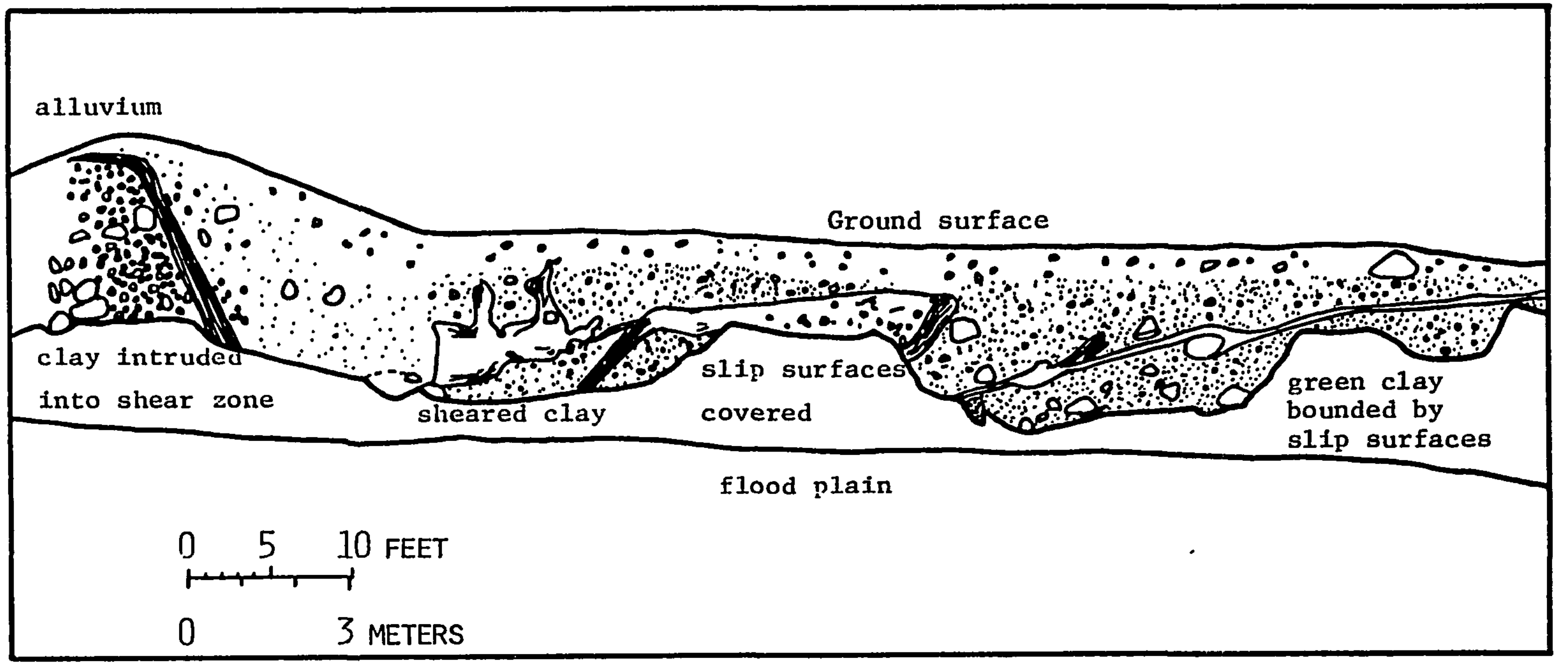

FIGURE 7.3. Shear zones and intruded layers of clay exposed in the bank of Ephraim Creek.
(a) Sketch.

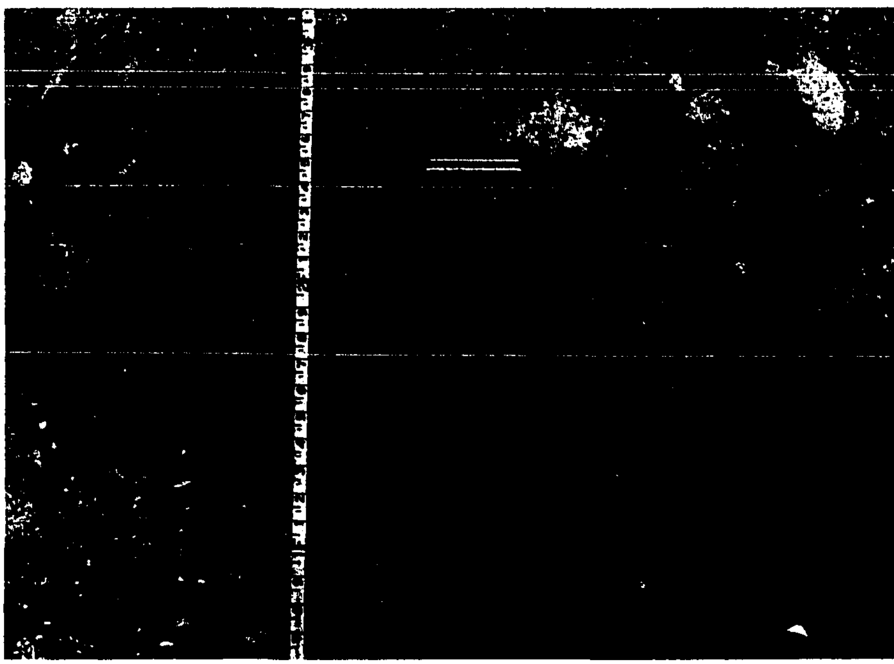

FIGURE 7.3. Shear zones and intruded layers of clay exposed in the bank of Ephraim Creek. (b) Close-up photograph of clay layer shown in 7.3a. Layer is bounded both above and below by slip surfaces, which are marked by scale (15 cm long) and trowel handle. Approximate location shown by star near center of 7.3a.

slip surfaces formed the boundaries between layers of plastic clay and the gravel-rich colluvium that they had intruded (Figs. 7.3a and 7.3b). Thus, movement by gliding on slip surfaces appears to be almost universal in landslides.

Slip surfaces deviate from the idealized cylindrical or planar shapes assumed in stability analysis. Steps, bumps, depressions, grooves, striations and other irregularities have been observed on slip surfaces of landslides in California, Utah, Ohio, France, and Norway.

Striations and grooves are commonly observed on slip surfaces (Fig. 7.4). They form as a result of deformation at small irregularities in the slip surface that might retard landslide movement slightly. Striations and grooves are parallel to the direction of movement of the landslide, so they themselves cannot cause significant deformation of the landslide debris, rather they merely increase the area of the slip surface.

Steps, depressions and bumps are other types of irregularities on a slip surface and they can obstruct movement. Such irregularities are termed asperities. Asperities are oblique to the direction of movement so that they can cause interlocking or deformation of the landslide debris.

Slip surfaces of some landslides in France had streamlined bumps that caused them to deviate from idealized cycloidal shapes (Collin, 1846, plates VI, VII, VIII and others). Accurate surveys showed that the bumps were a few meters long and a few decimeters high.

The slip surfaces of two landslides in California had steps that consisted of rounded treads (flats) and risers (ramps) Stout (1971).

FIGURE 7.4. Slip surface on a thrust fault within the Thistle landslide, Thistle, Utah. The slip surface is covered with grooves and striations. (Photo by Irving J. Witkind, U.S. Geological Survey).

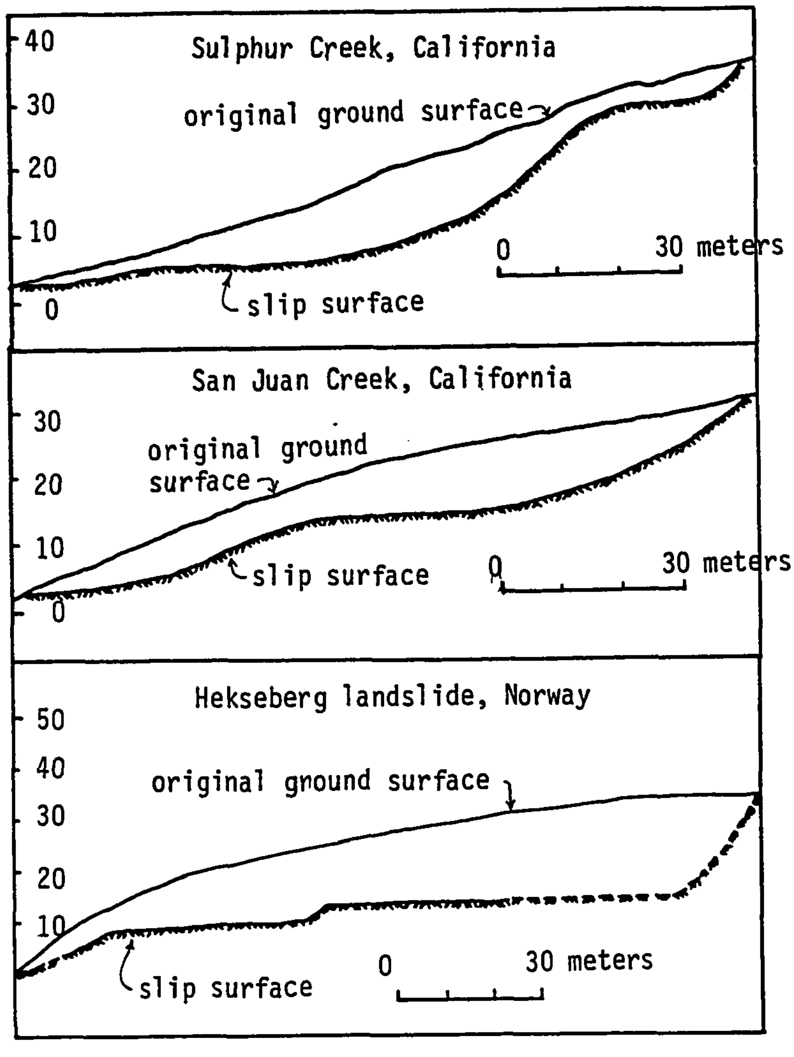

FIGURE 7.5. Sketch showing profiles of stepped slip surfaces of landslides (modified from Stout, 1971). (a) Profile of a slip surface in California. (b) Profile of a second slip surface in California. (c) Profile of a slip surface in Norway.

The treads had slopes as low as 4°, and the risers had slopes as steep as 41°. The average slope of each slip surface was about 14°. Measured relative to a smoothly curving, average slip surface, the steps were about 3 to 6 m high, and tens of meters long (Fig. 7.5a, 7.5b).

Steps were also observed in the basal slip surface of a quick-clay landslide in Norway (Stout, 1971). About one third of the slip surface was exposed, including parts of the steps. The steps had rounded noses that separated broad, gently sloping treads from steep risers (Fig. 7.5c). The treads sloped about 0.5 to 2.0°, and the risers sloped as steeply as 50°. The risers were about 5 to 7 m high, and the average slope of the slip surface (not including the headscarp) was about 5°.

The slip surface of a landslide at Delhi Pike, in Cincinnati, Ohio has a series of steps, and the landslide debris near the steps contains deformational structures (Fig. 7.6). The steps are several meters long and several decimeters high. Some of the steps are markedly asymmetrical such that the distal sides sloped steeply, and the proximal sides sloped gently with respect to the average slope of the slip surface. Listric faults formed on the distal sides of the steps and other deformational structures, such as tension cracks and segments of slip surfaces, also formed in the debris near the steps.

Streamlined bumps are common on the slip surface of the Indianola landslide in central Utah. The slip surface is roughly a U-shaped (Fig. 7.7a) or V-shaped (Fig. 7.7b), slightly sinuous channel. Grooves and striations on the sides of the channel are approximately parallel to the channel bottom (Figs. 7.7a, 7.7b). Larger bumps on the sides of the

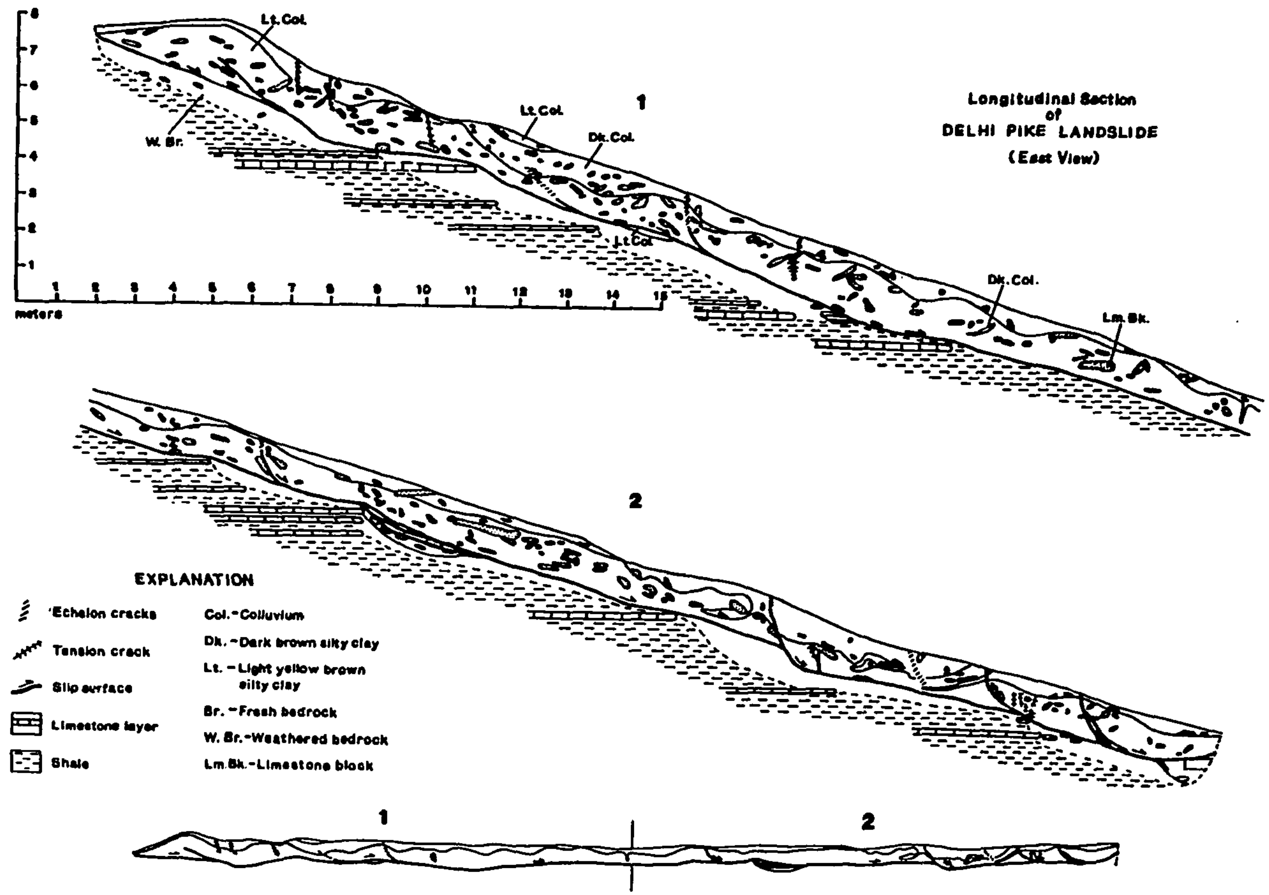

FIGURE 7.6. Cross section of the Delhi Pike landslide near Cincinnati, Ohio (by Robert W. Fleming and A. Onder Gokce, summer 1982; courtesy of Robert W. Fleming).

channel are a few meters long and small bumps, each less than a meter long are superimposed on the larger bumps (Fig. 7.7a). Many of the smaller bumps are relatively narrow features oriented approximately parallel to the direction of movement.

Elongate, asymmetrical bumps resembling roches moutonnees are exposed in a lateral slip surface of a landslide at Cottonwood Spring in Ephraim Canyon, Utah (Fig. 7.8). All are 15 to 40 cm long, 5 to 15 cm wide and a few centimeters high, and are superimposed on a larger bump that is about 1 to 1.5 m long. Other larger bumps are nearby.

To summarize, several general observations can be made about slip surfaces of landslides. Landslides commonly move by block gliding on a single slip surface consisting of thin (usually less than 1 mm thick) layers of strongly oriented clay particles. At least 90 to 95 percent of the displacement observed at the ground surface occurs on the basal slip surface; minor deformation occurs in the ground adjacent to the slip surface.

Slip surfaces are uneven. Asperities on slip surfaces comprise bumps that resemble flattened domes or roches moutonnees, broad steps having steep risers and gently sloping treads, and perhaps other forms. Lengths of asperities range from meters to tens of meters. Generally, the amplitudes or heights are small compared to the lengths of the asperities. Asperities tend to be asymmetrical; distal slopes are generally steeper than proximal slopes.

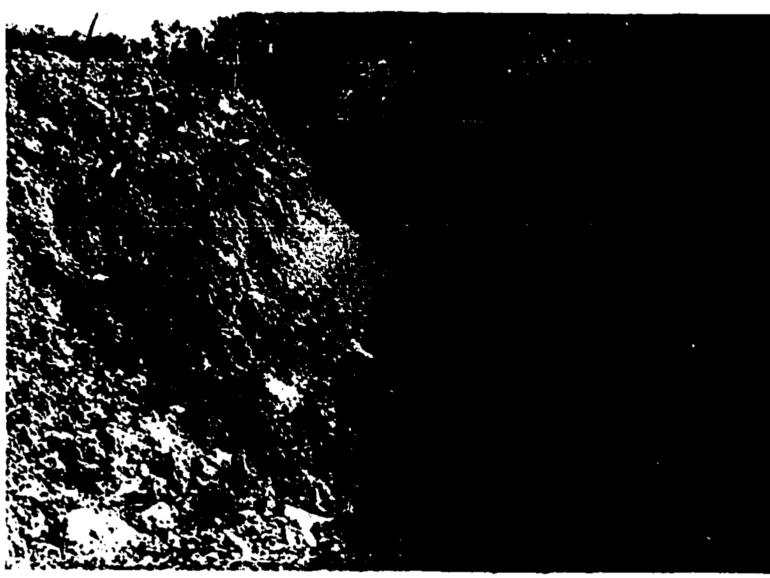

FIGURE 7.7. Photographs of a slip surface of a landslide near Indianola, Utah. (a) The landslide occupied a V-shaped channel or trough. Striations on channel wall are parallel to the transport direction. Streamlined bumps are transverse to direction of movement.

FIGURE 7.7(b). Curvature of channel and streamlined shapes of bumps on the slip surface are evident in this view. (Both photographs by Arvid M. Johnson, University of Cincinnati.)

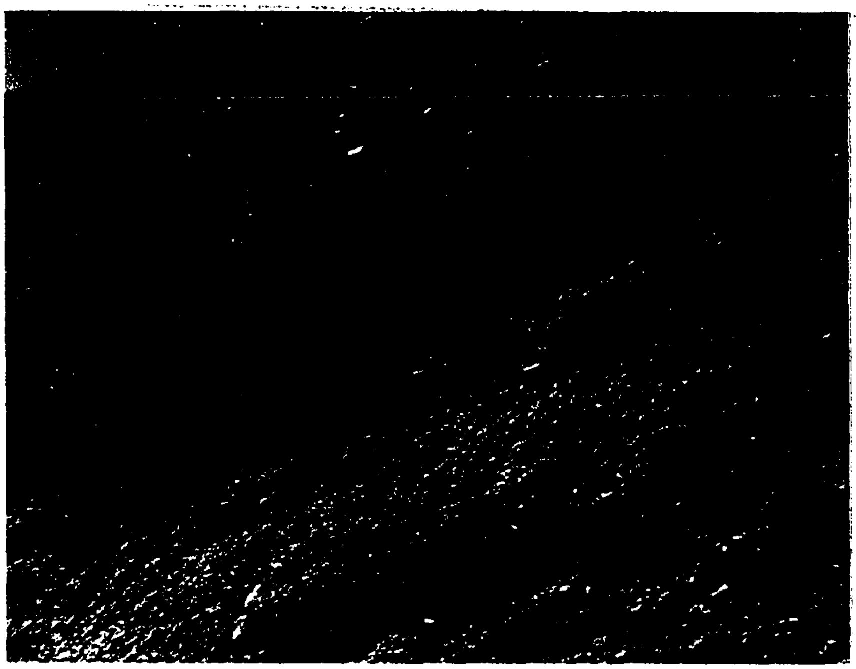

FIGURE 7.8. Photograph of a lateral slip surface of the Cottonwood Spring landslide, Ephraim Canyon, Utah. Features resembling roches moutonnees are visible near center of photography, lens cap is about 5 cm in diameter.

Preliminary Analyses of the Effect of Surface Roughness On the Movement of Landslides

Block gliding of landslides on uneven slip surfaces appears to be analogous to block gliding of temperate glaciers on uneven bedrock surfaces. I postulate that asperities retard landslide movement much as they retard glacier movement (Keefer and Johnson, 1983, p. 53).

As a temperate glacier slides over an uneven bedrock surface, it deforms in order to move over asperities. Deformation occurs by at least two processes: regelation and plastic deformation (Lliboutry, 1968; Budd, 1970; Kamb, 1970; Nye, 1969, 1970; Morland, 1976a, 1976b). In regelation, water moves around asperities by melting of ice at the proximal sides and refreezing at the distal sides of asperities. The rate of regelation is controlled by the rate of heat transfer in the ice and in the bedrock. In plastic deformation, solid ice flows around the asperity. The rate of plastic deformation is controlled by the rheological properties of the ice.

Similarly, as a landslide moves over its slip surface, the landslide must deform in order to move over asperities. I suspect that landslides also deform by two processes as they move over asperities: consolidation/swelling and plastic deformation. Consolidation at the proximal sides and swelling at the distal sides of asperities might play a role corresponding to that of regelation in glaciers. The rate of consolidation and swelling is controlled by the movement of water, which is related to the permeability of the soil. Henceforth, this mechanism is called <u>forced circulation</u>, because volume change of the soil forces water to circulate from places of high pressure to places of low pressure. Plastic deformation around the obstacles might be distributed as plastic flow, or localized on slip surfaces that form within the landslide debris. In either case, plastic deformation will resist sliding.

As a result of the plastic deformation, I would expect to see a deformed zone near the basal slip surface that is roughly the same thickness as the height of asperities on the slip surface. I am unsure what would determine the rate of plastic deformation.

A landslide is modeled as a deformable body that slides at a constant velocity past a rigid body (Fig. 7.9). The boundary (i.e. interface) between the bodies undulates. It is assumed that variation of stresses generated by acceleration and body forces is negligible near the interface and that no cavitation occurs at the interface. The undulations are assumed to be wide, symmetrical, low-amplitude steps. Movement is assumed parallel to the x-axis, and the undulations are assumed to be periodic in x, and independent of y. Consequently, plane deformation is assumed to occur.

Resistance to sliding is determined by the stresses acting on the slip surface. In the following derivations I separate sliding resistance that is expressed as a shear stress, T_{ns}, and as a normal stress, T_{nn}, on an uneven slip surface. In the first derivation, I assume that $T_{ns} = 0$. Yet, the normal stress that acts on the uneven slip surface can oppose sliding. Integration of this normal stress over a wavelength of the uneven surface determines the resistance to sliding.

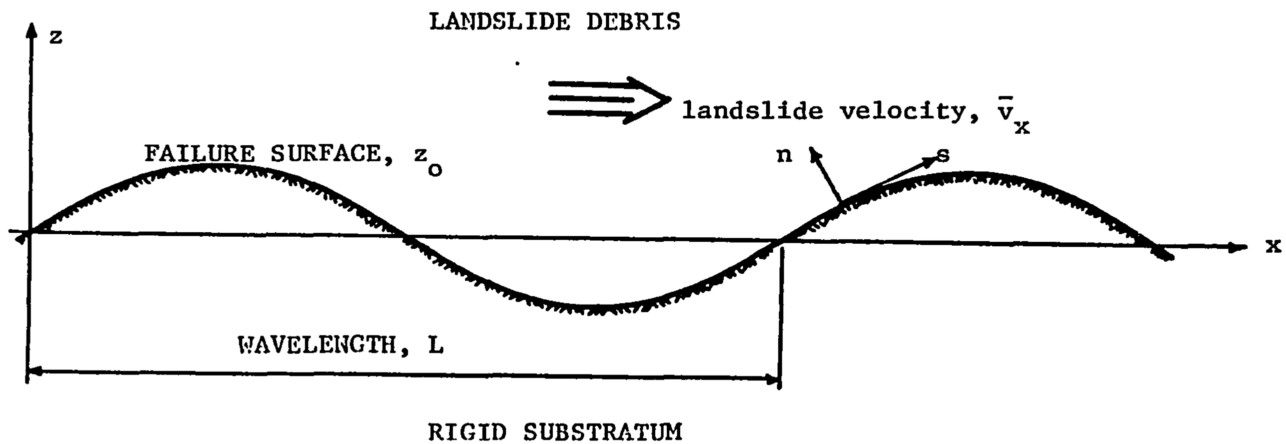

FIGURE 7.9. Sketch showing the problem domain for analysis of resistance to sliding.

Analysis of Plastic Deformation

Zero adhesion.--In order to investigate the normal stress generated by plastic deformation of landslide debris, I assume that the debris behaves like a perfectly plastic material (Hill, 1950). Arvid Johnson suggested this analysis to me in the spring of 1987, and heobtained an approximte solution. Subsequently I obtained an exact solution to the problem for zero adhesion. Deformation of perfectly plastic materials is rate independent; therefore, resistance to sliding computed for such a material is independent of the velocity of sliding.

Deformation of the plastic material and the resulting resistance to sliding is computed most easily if the undulations on the interface take the form of sawteeth (Fig. 7.10). Faces of the sawteeth make angles of $\pm\theta$ with the x-axis. A series of low-amplitude, symmetrical sawteeth is similar to a sine wave.

Hill (1950, chapter 6) lists the basic equations for large plastic deformations when the elastic deformations can be ignored. When elastic deformations are ignored, the hypothetical material is known as a rigid plastic. The governing equations for plane plastic deformation are the equilibrium equations, the continuity equation, the yield criterion,

$$k^2 = (T_{xx} - T_{zz})^2/4 + T_{xz}^2 \tag{7.1}$$

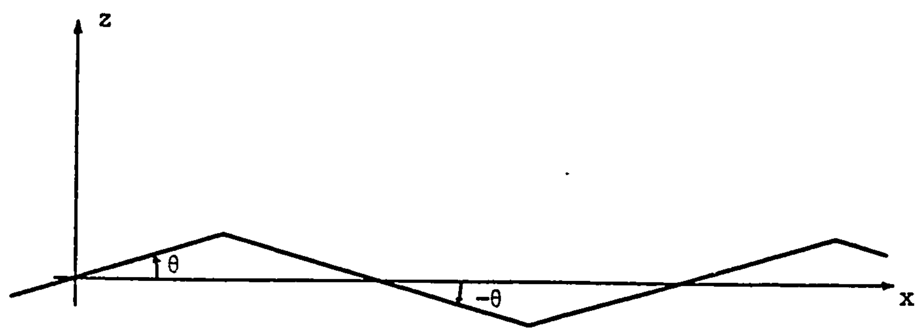

FIGURE 7.10. Sketch showing the sawtooth boundary used to analyze the resistance to sliding of a plastic solid.

and an expression that insures that the principal axes of stress and deformation rate coincide,

$$(2T_{xz})/(T_{xx} - T_{zz}) = (2D_{xz})/(D_{xx} - D_{zz}). \qquad (7.2)$$

In equations 7.1 and 7.2, $\underline{k}$ is the yield stress; $\underline{T}_{xx}$, $\underline{T}_{xz}$, and $\underline{T}_{zz}$ are components of the stress tensor (notation of Malvern, 1969); $\underline{x}$ is the coordinate parallel to the direction of landslide motion, and $\underline{z}$ is the vertical coordinate; and $\underline{D}_{xx}$, $\underline{D}_{xz}$, and $\underline{D}_{zz}$ are components of the deformation rate tensor.

These equations constitute a system of hyperbolic partial differential equations for the stresses and velocities in the plastic region (Hill, 1950, p. 132-134). The hyperbolic equations can be solved most easily by the method of characteristics, which is also known as the method of slip lines.

The characteristics constitute two orthogonal families of curves, one family called α-lines and the other family called β-lines. By convention, the line of action of the algebraically greatest principal stress lies in the first and third quadrants of the α-β coordinate system; stresses are assumed positive in tension. Physically, the characteristics coincide with the directions of maximum shearing stress and the directions of maximum shearing deformation. Following the notation of Hill (1950, p. 135), I define Φ as the angle measured counterclockwise from the $\underline{x}$-axis to an α-line in physical space. In stress space 2Φ is the clockwise angle measured from the point representing $\underline{x}$ on the Mohr circle to the point representing α.

The following relationships exist between the stresses, the pressure, p, and Φ:

$$T_{xx} = -p - k\sin(2\Phi); \tag{7.3a}$$

$$T_{zz} = -p + k\sin(2\Phi); \tag{7.3b}$$

$$T_{xz} = k\cos(2\Phi). \tag{7.3c}$$

The following relationships hold on the characteristics (Hill, 1950, p. 135):

on an α-line,

$$p + 2k\Phi = C_\alpha, \tag{7.4a}$$

$$dv_\alpha - v_\beta d\Phi = 0; \tag{7.4b}$$

and on a β-line,

$$p - 2k\Phi = C_\beta, \tag{7.5a}$$

$$dv_\beta + v_\alpha d\Phi = 0, \tag{7.5b}$$

where,

$$v_x = v_\alpha\cos(\Phi) - v_\beta\sin(\Phi), \tag{7.6a}$$

$$v_z = v_\alpha \sin(\Phi) + v_\beta \cos(\Phi). \tag{7.6b}$$

In equations 7.6, $\underline{v}_z$ and $\underline{v}_x$ are components of velocity parallel to $\underline{z}$ and $\underline{x}$ respectively.

The assumption that no cavitation occurs at the interface requires that

$$v_z = v_x \tan(\theta) \tag{7.7a}$$

on line $\underline{AB}$ (Fig. 7.10), and that

$$v_z = v_x \tan(-\theta) \tag{7.7b}$$

on line $\underline{BC}$.

Shearing stress tangent to the interface is assumed to be zero, i.e.

$$[T_{ns}]_{z_o} = 0.$$

The orientation of the slip lines at the boundary is deduced from a Mohr circle representation of the state of stress there (Fig. 7.11). The normal stresses acting parallel and perpendicular to the boundaries are the principal stresses, because the shearing stress tangent to the boundary is zero. On line segment $\underline{AB}$ (Fig. 7.10) the normal stress acting perpendicular to the boundary, $\underline{T}_{nn}$, is more highly negative than

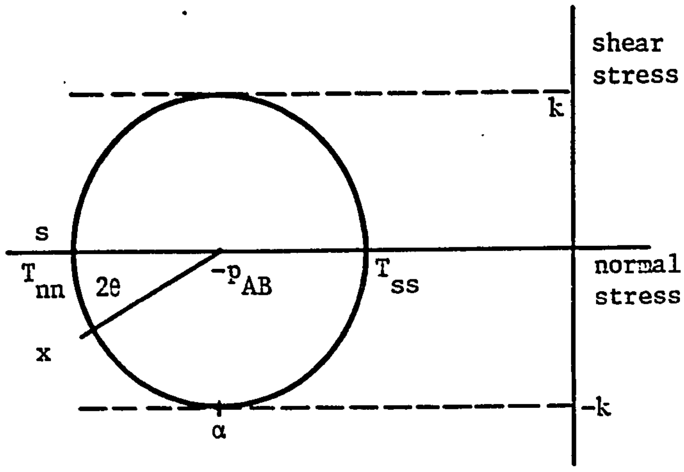

A.

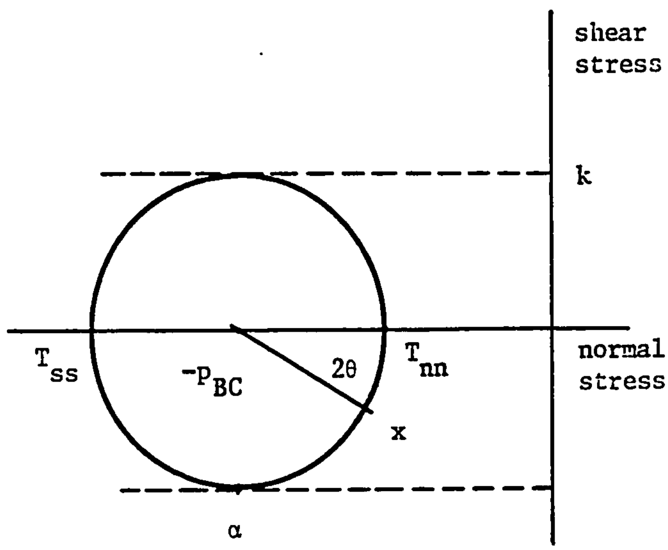

B.

FIGURE 7.11. Mohr's circle representation of the state of stress on the boundary for zero adhesion. Shear stress tangent to the boundary is zero. (a) State of stress on AB. (b) State of stress on BC.

the normal stress, T_{nn}, acting perpendicular to line BC, and the normal stress acting parallel to line AB, T_{ss}. For this state of stress (Fig. 7.11a), the clockwise angle between the point representing s, the direction tangent to line AB, and the point representing α, is $3\pi/2$. Thus, in physical space, the counterclockwise angle between line AB and an α-line is $3\pi/4$.

Similarly, the angle between an α-line and line BC is $\pi/4$ (Fig. 7.11b).

On AB,

$$\Phi = 3\pi/4 + \theta, \qquad (7.8a)$$

and on BC,

$$\Phi = \pi/4 - \theta. \qquad (7.8b)$$

A slip line field that is consistent with the stress boundary conditions is shown in Figure 7.12. Triangular regions of constant state, ABF and BDC occur on the slopes of the sawteeth. The regions of constant state are connected by fans centered on the crests (region BDEF) and troughs (region AFGH) of the sawteeth.

The solution is valid for sawteeth having sides that slope less than 45° (that is, $\pi/4$). When the sides are steeper than 45°, plastic deformation will occur by some other mechanism.

The slip line pattern satisfies the velocity boundary conditions. Velocities on α-lines in centered fan BDEF must be zero, because material above arc DEF is not deforming (Fig. 7.12). For the same reason, velocities on β-lines in centered fan AFGH must be zero. Substitution of equations 7.6a, 7.6b, and 7.8a into equation 7.7a shows that the velocities along the slip lines where they intersect AB are equal,

$$v_\alpha = v_\beta. \tag{7.9}$$

Substitution of equations 7.6a, 7.6b and 7.8b into equation 7.7b shows that equation 7.9 also holds on BC.

In the regions of constant state,

$$d\Phi = 0.$$

Consequently, equations 7.4b and 7.5b simplify so that v_α and v_β are constants in regions ABF and BDC. The velocities are proportional to the loading rate.

The slip line pattern can now be used to compute the stresses in the plastic region, to within an arbitrary constant, p_{BC}. Line AFEDC is a β-line. Two expressions for C_β can be computed by substituting appropriate values of p and Φ into equation 7.5a. At A,

$$C_\beta = p_{AB} - 2k(3\pi/4 + \theta), \tag{7.10a}$$

and at C,

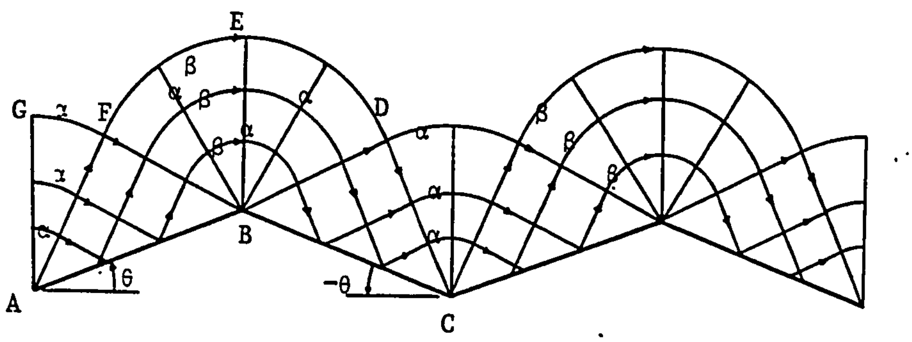

FIGURE 7.12. Slip-line field for deformation of a plastic solid sliding past a sawtooth boundary without adhesion. Shear stress tangent to the boundary is zero. Arrows on the slip lines indicate the direction of particle motion.

$$C_\beta = p_{BC} - 2k(\pi/4 - \theta), \tag{7.10a}$$

I compute the pressure on AB by substituting equation 7.10a into equation 7.10b and solving for p_{AB},

$$p_{AB} = p_{BC} + 4k(\pi/4 + \theta). \tag{7.11}$$

The force on any segment, δx, of the interface, AB, that acts parallel to the direction of sliding, x, is $T_{nn}\ \delta x\ \tan(\theta)$, because T_{ns} = 0. T_{nn} is a principal stress, on AB, T_{nn} is determined by (Fig. 7.11a)

$$[T_{nn}]_{AB} = -p_{AB} - k. \tag{7.12a}$$

Or, if equation 7.11 is substituted into equation 7.12a, then the expression for T_{nn} becomes

$$[T_{nn}]_{AB} = -p_{BC} - 4k(\pi/4 + \theta) - k. \tag{7.12b}$$

Likewise, T_{nn} on BC is determined by (Fig. 7.11b):

$$[T_{nn}]_{BC} = -\ p_{BC} + k. \tag{7.12c}$$

The resistance to sliding, τ, is the integral of the forces on one wavelength of the interface, divided by the wavelength. The integral turns out to be a simple algebraic expression, because the normal stress on each segment of the uneven slip surface is a constant (equations 7.12b and 7.12c)

$$\tau = ([T_{nn}]_{AB} - [T_{nn}]_{BC}) \tan(\theta). \tag{7.13}$$

Substituting equations 7.12b and 7.12c into equation 7.13, yields an expression for τ,

$$\tau = 2k(1 + \pi/2 + 2\theta) \tan(\theta). \tag{7.14}$$

Equation 7.14 shows that the absolute value of the resistance to sliding, τ, caused by deformation around the sawteeth, increases with the slope of the sawteeth, θ. For small angles, the resistance is approximately proportional to θ (Fig. 7.13).

Adhesion and drag.--I now solve a more general problem where the shear stress tangent to the interface is allowed to take on a constant value, k_r, between zero and the yield stress, k,

$$0 \leq |k_r| \leq k.$$

For example, k_r might be the residual strength of the soil developed on the failure surface after several millimeters or centimeters of displacement, and k might be the peak strength of the soil near the slip surface.

The states of stress on $\underline{AB}$ and $\underline{BC}$ are shown in Figure 7.14. The clockwise angle between the point representing the $\underline{s}$-direction and α in

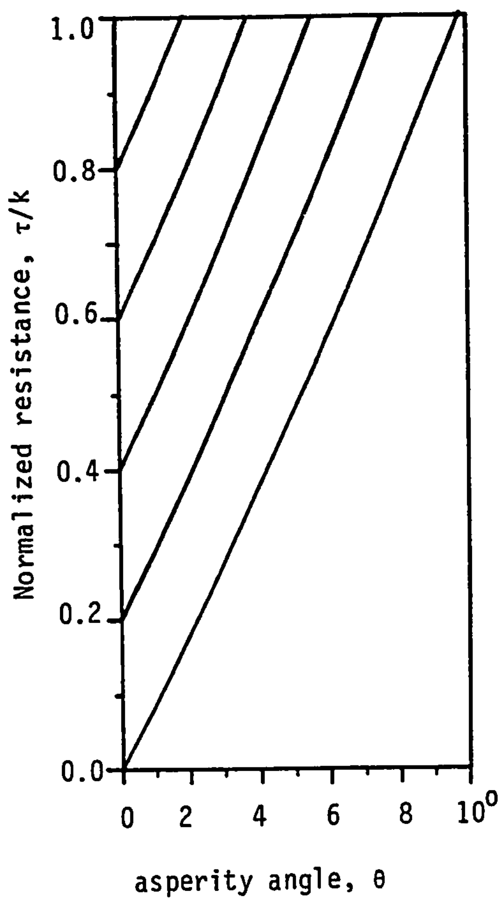

FIGURE 7.13. Resistance to sliding as a function of slope of the sawtooth, θ and the ratio of the shear strength (adhesion) of the boundary to $\underline{k}_{\underline{r}}$, to the shear strength of the plastic, $\underline{k}$.

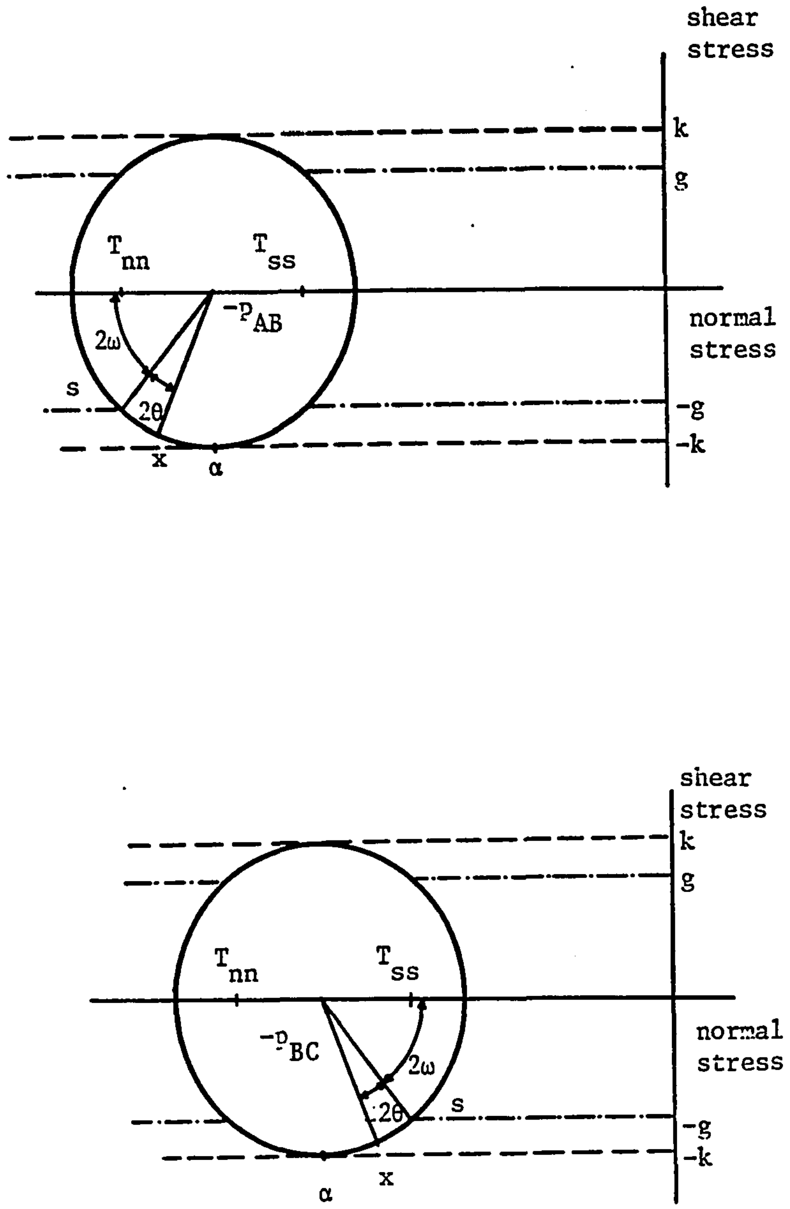

FIGURE 7.14. Mohr's circle representation of the state of stress on the boundary with adhesion. Shear stress tangent to the boundary is equal to $\underline{k_r}$. (a) State of stress on <u>AB</u>. (b) State of stress on <u>BC</u>.

stress space is designated 2ρ. On <u>AB</u> the following relationships hold between $\underline{k}_r$, $\underline{k}$, and 2ρ (Fig. 7.14)

$$\cos(2\rho) = k_r/k, \tag{7.15a}$$

and

$$\sin(2\rho) = -[1 - (k_r/k)^2]^{(1/2)};\ k \geq k_r \tag{7.15b}$$

For convenience, the angle ω is introduced, it is the angle between the least algebraic principal stress and $\underline{T}_{\underline{nn}}$ on <u>AB</u> or the algebraically greatest principal stress on <u>BC</u>, and it is determined by

$$\omega = (1/2)\sin^{-1}(k_r/k).$$

The orientations of the α-lines in terms of ω are

$$\rho = 3\pi/4 + \omega,$$

or

$$\Phi = 3\pi/4 + \omega + \theta, \tag{7.16a}$$

on <u>AB</u>, and

$$\rho = \pi/4 - \omega,$$

or

$$\Phi = \pi/4 - \omega - \theta \tag{7.16b}$$

on <u>BC</u>.

A slip line field can be constructed using the orientations of the α-lines determined by equations 7.16a and 7.16b (Fig. 7.15) The slip line field is similar to that shown in Figure 7.12, except that the α-lines have lower slopes in Figure 7.15 than in Figure 7.12.

Because the shearing stress tangent to the interface is nonzero, the solution is valid only for sawteeth having slopes less than 45°. The limiting slope of the sawteeth depends on $\underline{k}_r$, and therefore on ω. Examination of equations 7.16a and 7.16b shows that the limit of the solution occurs where

$$\omega + \theta = \pi/4. \tag{7.17}$$

Because ω increases as $\underline{k}_r/\underline{k}$, the limiting value of θ (equation 7.17) approaches zero as $\underline{k}_r/\underline{k}$ approaches one. This indicates that the strength of material above an uneven slip surface must exceed the adhesional strength of the slip surface. If $\underline{k}_r$ equals $\underline{k}$, the slip surface must be planar in order for sliding to occur, according to the mechanism considered here.

The velocity solution for the slip line pattern shown in Figure 7.15 is similar to that shown in Figure 7.11, except that the following relationship between $\underline{v}_\alpha$ and $\underline{v}_\beta$ replaces equation 7.9,

$$v_\alpha = v_\beta\{[1 - \tan(\theta)]\cos(\omega + \theta) + [1 + \tan(\theta)]\sin(\omega + \theta)\}$$

$$/\{[1 + \tan(\theta)]\cos(\omega + \theta) - [1 - \tan(\theta)]\sin(\omega + \theta)\}$$

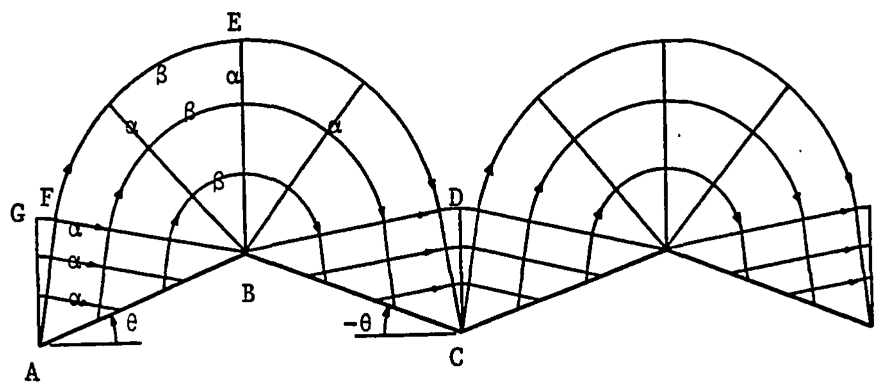

FIGURE 7.15. Slip-line field for deformation of a plastic solid sliding past a sawtooth boundary with adhesion. Shear stress tangent to the boundary is $\underline{k}_{\underline{r}}$.

The resistance to sliding caused by the sawteeth is computed by the procedure outlined previously. The resistance contributed by the sawteeth is added to the x-component of the shear stress tangent to the interface.

$$\tau = 2k\{1 + \pi/2 + 2\omega + 2\theta - 2\sin^2(\omega)\} \tan(\theta) + k_r \quad (7.18a)$$

$$\omega = (1/2) \sin^{-1} (k_r/k) \quad (7.18b)$$

The resistance to sliding is approximately 5.14 tan (θ) + k_r, for small θ. Consequently, the resistance to sliding can equal the peak strength of the soil, k, even when θ is as small as a few degrees (Fig. 7.13), and this mechanism can operate only when roughness is low. For example, if k_r/k is 0.4, the resistance to sliding equals k when $\theta \approx 5.5^\circ$, or in the limiting case when k_r is zero, resistance to sliding equals k when $\theta \approx 9.5^\circ$.

The resistance to sliding will not exceed k, the peak strength, even though the limiting value of θ for the slip-line solution is greater than the value of θ where the resistance equals k. If the slip surface were so rough that the resistance to sliding exceeded k, the landslide would form a new slip surface with lower roughness that would have resistance less than or equal to k, or yield by some other mechanism.

Furthermore, the resistance to sliding exceeds k_r, the residual strength, if θ is greater than zero.

Analysis of Forced Circulation

In order to investigate the resistance to sliding generated by forced circulation of pore water in a landslide, and the effect of that resistance on the velocity of the landslide, I assume that the landslide debris behaves like a fluid-infiltrated porous-elastic solid (Biot, 1941; Rice and Cleary, 1976). I have chosen such a model for material behavior because the movement of pore water is considered the primary cause of time-dependent effects in fine-grained soils (Terzaghi, 1925; Wroth and Houlsby, 1985, p. 6). In analogy to deformation of fine-grained soil, deformation of a porous-elastic solid is rate dependent because volume change in the porous solid is coupled to diffusion of the pore fluid.

I have made several assumptions in setting up a boundary value problem that describes forced circulation of water around bumps in a wavy slip surface as the landslide moves over its slip surface. The landslide is represented as a half space bounded by the x-y plane and moving parallel to the x-coordinate with a mean velocity of $\bar{v}_x$ (Fig. 7.8). The basal slip surface, z_o, is a sinusoidal perturbation of the x-y plane:

$$z_o = A \sin(\ell x) \qquad (7.19a)$$

For z_o having small amplitude, A, I can solve the problem on the planar boundary, subject to boundary conditions on z_o. The small amplitude also insures that small strains occur, as required by the constitutive model.

The boundary conditions on $\underline{z}_o$ are that sliding is tangential to $\underline{z}_o$,

$$v_n = 0,$$

thus

$$[v_z]_{z_o} = [v_x]_{z_o} \tan(\theta); \qquad (7.19b)$$

$$\tan(\theta) = dz_o/dx.$$

I assume zero adhesional drag at the slip surface, so shear stress tangential to z_o is zero,

$$[\bar{T}_{ns}]_{z_o} = 0, \qquad (7.19c)$$

For the flow problem, I assume that the slip surface is impermeable to water, so that

$$[q_n]_{z_o} = 0. \qquad (7.19d)$$

The boundary is nonlinear, therefore first-order approximations to the boundary conditions are used so that the problem can be solved analytically; however, restrictions apply to the results obtained by using first order approximations. Let the roughness of the slip surface be, $\underline{A}\ell$, the maximum local slope. Then $(\underline{A}\ell)^2$ must be small compared to $\underline{A}\ell$.

First-order approximations are designated by a $\tilde{}$ (squiggle) and zero order quantities are designated by a - (bar). The first order approximation of the velocity boundary condition (equation 7.19b) is:

$$[\tilde{v}_z]_{z_o} = \bar{v}_x A\ell \cos(\ell x) \qquad (7.20)$$

where:

$$v_x = \bar{v}_x + \tilde{v}_x, \text{ and } v_z = \tilde{v}_z$$

and the first order approximation of the zero shear stress boundary condition (equation 7.19c) is:

$$[\tilde{T}_{xz}]_{z_o} = 0 \qquad (7.21)$$

Equations 7.20 and 7.21 were derived by Johnson (1984).

The constitutive equations, equilibrium equations, and compatibility equations that govern the behavior of the porous-elastic solid are listed in Rice and Cleary (1976).

I have assumed that the soil particles are incompressible, so that the pore-pressure coefficient $\underline{B}$ (Skempton, 1954; Lambe and Whitman, 1969) is equal to one, and Poisson's ratio for undrained loading, ν_u, is 0.5. For this assumption, the constitutive equations of Rice and Cleary (1976, p. 229) simplify to the following:

$$2GE_{xx} = T_{xx} - \nu(T_{xx} + T_{zz}) + (1 - 2\nu) P \qquad (7.25a)$$

$$2GE_{xz} = T_{xz} \qquad (7.25b)$$

$$2GE_{zz} = T_{zz} - \nu(T_{xx} + T_{zz}) + (1 - 2\nu) P \qquad (7.25c)$$

The field equation for stress diffusion is

$$c\nabla^2 M = \partial M/\partial t; \qquad (7.25d)$$

$$M = T_{xx} + T_{zz} + 2P.$$

In equations 7.25a, 7.25b, 7.25c, and 7.25d, $\underline{G}$ is the shear modulus of the soil, $\underline{P}$ is the pore-fluid pressure, $\underline{M}$ is twice the effective mean stress, and ν is Poisson's ratio for drained loading. The diffusion constant, $\underline{c}$, in equation 7.25d is determined by

$$c = (\kappa/\mu)[2G(1-\nu)/(1-2\nu)],$$

where κ is the intrinsic permeability, and μ is the viscosity of water.

The diffusion equation (equation 7.25d) makes the problem time dependent; however, the assumption that the landslide moves at a constant rate allows the problem to be solved independently of time. This is accomplished by introducing a new set of coordinates that put the problem in a quasi-steady state[17] (Rosenthal, 1946). Only two

---

[17]Shames (1962) describes a quasi-steady state by using an analogy with a torpedo moving at a constant velocity through still water. An observer riding on the torpedo sees the same pattern of flow surrounding the torpedo as it travels through the water; this is the quasi-steady (continued...)

independent variables, ξ and $\underline{z}$, remain after transforming the coordinates. Let

$$\xi = x - \bar{v}_x t,$$

and

$$\theta = t,$$

then,

$$\partial/\partial x = \partial/\partial \xi,$$

and

$$\partial/\partial t = -\bar{v}_x(\partial/\partial \xi) + \partial/\partial \theta,$$

but

$$\partial/\partial \theta = 0,$$

because in the new coordinate system the frame of reference is fixed to the rigid boundary, and one sees a constant or steady state of deformation in the porous solid as it moves by.

---

[17](...continued)
state. An observer at a stationary point in the water sees the pattern of flow change (an unsteady state) as the torpedo approaches, passes and then leaves.

The diffusion equation is transformed to the following:

$$\nabla^2 M = (-\bar{v}_x/c)\partial M/\partial \xi .$$

For slow moving landslides where $\underline{\bar{v}}_x \leq 10$ cm per day, and the debris has typical values for $\underline{G}$, ν, κ and μ ($\underline{G} = 10^7$ N/m^2, $\nu = 0.3$, Lambe and Whitman, 1969; and $\kappa > 2 \times 10^{-13}$ cm^2, $\mu = 1.124 \times 10^{-3}$ Ns/m^2, Freeze and Cherry, 1979); the term $|\underline{\bar{v}}_x/\underline{c}| \leq 0.02$. To a good approximation, the diffusion equation can be replaced by Laplace's equation:

$$\nabla^2 M = 0. \tag{7.26}$$

Equation 7.26, together with the compatibility equation, the equilibrium equations, the constitutive equations and the boundary conditions govern the problem in the new coordinate system.

The compatibility equation, in terms of stresses and the new coordinates is

$$\nabla^2 [T_{\xi\xi} + T_{zz} + ((1 - 2\nu)/(1 - \nu))P] = 0. \tag{7.27}$$

As a result of transforming the coordinates, the velocity of the landslide enters the problem through the boundary condition governing fluid flow at the interface (equation 7.19d). The first order approximation of the boundary condition for the flow problem is (please see Appendix G for its derivation):

$$[\partial^2\tilde{P}/\partial\xi^2]_{z_o} = (-\bar{v}_x/K^*)[\partial\tilde{e}/\partial\xi]_{z_o}. \qquad (7.28)$$

In equation 7.28,

$$\tilde{e} = \tilde{E}_{\xi\xi} + \tilde{E}_{zz},$$

and

$$K^* = \kappa/\mu.$$

K* is the hydraulic conductivity of Rice and Cleary (1976), it can be converted to the familiar or standard hydraulic conductivity, K, (Freeze and Cherry, 1979) by multiplying by the unit weight of water, γ_w,

$$K = K^*\gamma_w.$$

Airy's stress function (Malvern, 1969) facilitates solution of this problem. The stress function automatically satisfies the equilibrium equations; the following relationships hold between the stress components and the stress function:

$$\partial^2\phi/\partial z^2 = T_{\xi\xi}, \qquad (7.29a)$$

$$\partial^2\phi/\partial\xi^2 = T_{zz}, \qquad (7.29b)$$

and

and

$$\partial^2\phi/\partial\xi\partial z = -T_{\xi z}. \tag{7.29c}$$

When the stress function is substituted into the simplified diffusion equation (equation 7.26) and the compatibility equation (equation 7.27), two equations relating the stress function and the pore-pressure function are obtained.

$$\nabla^2[\nabla^2\phi + 2P] = 0 \tag{7.30}$$

and

$$\nabla^2[\nabla^2\phi + ((1-2\nu)/(1-\nu))P] = 0 \tag{7.31}$$

The Laplacian, ∇^2, is a linear operator and the quantities in square brackets in equations 7.30 and 7.31 satisfy Laplace's equation; therefore, any linear combination of these quantities also satisfy Laplace's equation. Equations 7.30 and 7.31 can be combined algebraically to show that P satisfies Laplace's equation and ϕ satisfies the biharmonic equation:

$$\nabla^2 P = 0, \tag{7.32}$$

$$\nabla^4\phi = 0. \tag{7.33}$$

Having simplified the problem to the solution of two well known equations I use the first-order boundary conditions to guess the form of the pore-pressure function, $\underline{\tilde{P}}$, and the stress function, $\bar{\phi}$,

$$\bar{P} = \exp(-\ell z)[c_1\cos(\ell x) + c_2\sin(\ell x)], \tag{7.34}$$

and

$$\bar{\phi} = (c_3 + c_4\ell z)\exp(-\ell z)[c_5\cos(\ell x) + c_6\sin(\ell x)]. \tag{7.35}$$

Equations 7.34 and 7.35 are solved for the velocities, stresses and the pore-pressure (Appendix G). The resistance to sliding is computed from the solution for the stresses and pore pressure.

The resistance to sliding is the average shear stress acting parallel to $\underline{x}$ on the boundary, $\underline{z}_0$ (Nye, 1969). The resistance is a second order quantity, and it can be computed in two different ways: One way is to do a second order perturbation analysis for the stresses and velocities and then compute the average shear stress on the boundary from second order terms. A simpler way that gives equivalent results (Nye, 1969, p. 452, 453) is to take advantage of the fact that the pressure, $\bar{\underline{p}}$ (the opposite of the mean stress), on the upstream sides of the bumps is greater than on the downstream sides. The pressure is a first order quantity and its integral over the basal slip surface also gives the resistance to sliding. A first order analysis is used to solve for the pressure. Then the infinitesimal forces acting parallel to $\underline{x}$ on $\underline{z}_0$ are summed to compute the resistance to sliding. These forces are determined by

$$dF = \bar{p}(dS)\sin(\theta),$$

where θ is the angle between $\underline{z}_o$ and the $\underline{x}$-axis. The forces are also determined by

$$dF = \tilde{p}(dz_o/dx)dx$$

(Kamb, 1970, p. 690).

Thus the resistance to sliding, τ, is:

$$\tau = (1/L)\int_0^L [p]_z (dz_o/dx)dx. \tag{7.36a}$$

On the boundary, the pressure is given by

$$\tilde{p} = -\ell^2[c_5\cos(\ell\xi) + c_6\sin(\ell\xi)]. \tag{7.36b}$$

Equation 7.36b is substituted into equation 7.36a to compute τ:

$$\tau = -(A\ell^3 c_5)/2, \tag{7.37}$$

Subsequently, the boundary conditions are used to solve for the constants, $\underline{c}_1,\ldots,\underline{c}_6$ (Appendix G). The constant $\underline{c}_5$ is determined by

$$\begin{aligned} c_5 = {} & [A\bar{v}_x(1-2\nu)/K^*(1-\nu)]/\{[2\ell^2(1-\nu)/(1-2\nu)] \\ & - [\bar{v}_x(1-2\nu)/(K^*G)]^2\cdot[1 - 2(1-\nu)/(1-2\nu)] \\ & \cdot[1 - (1-2\nu)/(2(1-\nu))]\}. \end{aligned} \tag{7.38}$$

The expression for drag can now be written out fully by substituting equation 7.38 into 7.37:

$$\tau = -(A\ell)^2\ell\bar{v}_x(1-2\nu)/\{2K^*(1-\nu)\{[2\ell^2(1-\nu)/(1-2\nu)] \\ -[\bar{v}_x(1-2\nu)/K^*G)]^2\cdot[1-2(1-\nu)/(1-2\nu)] \\ \cdot[1-(1-2\nu)/(2(1-\nu))]\}\} \qquad (7.39)$$

In equation 7.39, the term

$$[\bar{v}_x(1-2\nu)/K^*G]^2 = [2\bar{v}_x(1-\nu)/c]^2.$$

For combinations of $\bar{v}_x$, G and K^* typical for silty and clayey soils and consistent with the earlier assumption that

$$|\bar{v}_x/c| \leq 0.02,$$

the denominator of equation 7.39 is dominated by the first term, $[2\ell^2(1-\nu)/1-2\nu)]$, which goes as ℓ^2. The resistance is approximately

$$\tau = -(A\ell)^2\bar{v}_x(1-2\nu)^2/[4K^*(1-\nu)^2\ell]. \qquad (7.40a)$$

By making the substitution $K^*=K/\gamma_w$, equation 40a is transformed to

$$\tau = -(A\ell)^2\bar{v}_x\gamma_w\,(1-2\nu)^2/[4K\ell(1-\nu)^2]. \qquad (7.40b)$$

The corresponding expression for viscous drag (Kamb, 1970), is

$$\tau = -(1/2)\bar{v}_x(A\ell)^2\ell\eta \qquad (7.41)$$

In equation 7.41, η is the viscosity of glacier ice. The negative sign in the right hand side of equations 7.39, 7.40a, 7.40b and 7.41 are a result of the sign convention used in computing the stresses.

For short wavelengths, the resistance due to forced circulation is small, and it increases with increasing wavelength, so that forced circulation will occur at short wavelength bumps on the slip surface. This result is consistent with the fact that diffusion becomes more difficult as the path length, which is proportional to the wavelength, L, increases. At sufficiently long wavelengths, the resistance to sliding caused by forced circulation might become so great that some other mechanism of deformation becomes active near the slip surface, in much the same way that regelation gives way to viscous drag as the wavelength increases. In glaciers, viscous drag is active at long wavelengths, because the drag decreases with increasing wavelength (equation 7.41). I do not know what mechanism in landslides might correspond to viscous drag in glaciers.

Equations 7.39 and 7.40 were derived for the case where the boundary is impermeable. If the boundary is permeable, pore-fluid diffusion is active at asperities having longer wavelengths (other things being equal), because a greater volume of soil conducts the water. A permeable boundary has the same effect on the resistance to sliding or the velocity of the landslide as increasing the permeability of the soil above the slip surface.

Discussion and Conclusion

Roughness of slip surfaces can affect equilbrium (stability) of slopes and velocity of landslides. Initial stability of a slope can be markedly affected by bumps and asperities on the slip surface. Plastic deformation of landslide debris that is displaced around an asperity can augment resistance to sliding at the slip surface. I show that forced circulation of water caused by movement around asperities can control the velocity of a landslide. Forced circulation provides a plausible explanation for the low velocities of landslides in soils.

Plastic deformation at asperities offers a possible explanation for the stability of thin layers of clayey colluvium on steep slopes, for example, the residual shear strength of colluvium on natural slopes in the Cincinnati area is too small to account for stability of the slopes (Robert Fleming, oral commun., 1983). However, the slip surfaces of landslides in colluvium of the Cincinnati area have steps and bumps that can contribute to the stability of the slopes (Fig. 7.6).

The colluvium at Delhi Pike, 15 km west of Cincinnati, Ohio, is about 1.5 m thick and rests on a slope of about 19° (Fig. 7.6). The best estimate of the angle of residual friction of the colluvium is 17°, and the residual cohesion is about 3.3 kPa. When the water table is at the ground surface, the factor of safety is 0.92. If the shear strength on the slip surface, $\underline{k}_r$, is about 0.6 times the strength of the soil above the slip surface, $\underline{k}$, then the resistance needed for equilibrium is about 0.65k. According to Figure 7.13, an asperity angle of about 0.4° is sufficient for stability. Steps on the slip surface form angles of about 2° to 6° with the average slope of the slip surface (Fig. 7.6), thus they are more than adequate to account for the stability of the slope and are too large for plastic deformation to operate by the mechanism analyzed here.

The asperity angles at which the resistance to sliding, τ, equals the yield strength of the landslide debris are so small (Fig. 7.13) that the mechanism of plastic deformation analyzed here can operate in landslides having only minor undulations on their basal slip surfaces. For example if the residual strength, $\underline{k}_r$, at the slip surface is 40 percent of the yield strength, $\underline{k}$, of the soil above the slip surface, then θ can be no greater than 5.5°. Yielding can occur by this mechanism for $\theta = 5.5^{\circ}$ when the driving stresses equal $\underline{k}$. However, if the driving stresses are only slightly greater than the residual strength, $\underline{k}_r$, as in many natural slopes underlain by colluvium, then yielding can occur only if $\theta < 1^{\circ}$.

In landslides having basal slip surfaces with relatively large undulations, as the Delhi Pike landslide, other mechanisms of plastic deformation might operate. Listric faults, cracks and other deformational structures are associated with the bumps and steps on the slip surface of the Delhi Pike landslide (Fig. 7.6). The formation of such structures suggests that faulting might be another mechanism by which landslides deform in order to slide over obstacles on slip surfaces. Consumption of energy by faulting in dilatant soils can also retard the movement landslides (Rice, 1973).

Forced circulation of water around asperities is a plausible mechanism for the slow movement of landslides in clayey soils because most rate-dependent properties of soils have been attributed to the movement of pore water. In particular, consolidation is considered the primary cause of time dependent effects in fine-grained soils (Terzaghi, 1925; Wroth and Houlsby, 1985, p. 6). This suggests that movement of pore water might play an important role in controlling the velocities of landslides.

The mechanism of forced circulation is consistent with the observed linear relationship between landslide velocity and height of the water table (Terzaghi, 1950). In a landslide where the water table is unconfined and parallel to the ground surface, τ is proportional to the height of the water table, h. The velocity dependent resistance to sliding, τ, needed to maintain equilibrium is determined by

$$\tau = T\gamma\{\sin(\iota) - [1 - (h\gamma_w/T\gamma_t)]\cos(\iota)\tan(\phi')\}. \qquad (7.42)$$

In equation 7.42, $\underline{T}$ is the thickness of the landslide, ι is the inclination of the slope, ϕ' is the angle of residual friction, γ_t is the unit weight of the landslide debris and γ_w is the unit weight of water.

Equation 7.42 indicates that as the water table rises, the shear strength due to friction on the slip surface decreases in proportion to the change in the height of the water table, but the driving forces remain constant. Consequently, τ increases linearly as the water table rises in order to provide enough resistance at the slip surface to balance the driving forces acting on the landslide. This increase in τ causes a corresponding increase in the velocity of the landslide.

For the mechanism of forced circulation analyzed here, the velocity of the landslide, $\bar{v}_x$, is proportional to τ. Rearranging equation 7.40b yields

$$\bar{v}_x = 4K\tau\ell\ (1 - \nu)^2/((A\ell)^2\gamma_w(1 - 2\nu)^2). \tag{7.43}$$

Thus, according to the mechanism of forced circulation (equations 7.42 and 7.43) the velocity increases linearly with the height of the water table. Furthermore, equations 7.42 and 7.43 suggest that the maximum velocity of a given landslide is determined by the maximum height attained by the water table.

The large range of velocities of landslides might also be explained by the mechanism of forced circulation. The velocity of the landslide is proportional to the hydraulic conductivity of the soil (equation 7.43). The permeability of fine-grained soils ranges over several orders of magnitude, from 10^{-15} to 10^{-8} cm^2 (Freeze and Cherry, 1979, p. 29). The average velocities of landslides in fine-grained soils also range over several orders of magnitude, from 10^{-5} to 50 m/d (Keefer and Johnson, 1983). Observations indicate that landslides in clay soils, which have very low permeability, move slowly. For example, debris of the Aspen Grove landslide, near Ephraim, Utah, was clay and silty clay that presumably had a low permeability. The peak velocity of the landslide, which occurred when the water table was at the ground surface, was only 20 cm/d. The peak velocity of the Thistle landslide (Duncan and others, 1986, p. 11) was 48 m/d. Of landslides in clayey soils that were active in central Utah during 1983 and 1984, the Thistle landslide moved faster than any others I know of and the Aspen Grove landslide moved at a speed I consider typical of the landslides in central Utah.

I do not have enough field data to verify the mechanism of forced circulation, but I know of one landslide where the hydraulic conductivity is known well enough to use equation 7.43 to compute the velocity. The Minor Creek landslide in northern California has an average hydraulic conductivity, $\underline{K}$, of 5×10^{-8} m/s (Iverson and Major, 1987) and a maximum velocity of a few decimeters per month (Iverson, 1986) or from about 4×10^{-8} to 2×10^{-7} m/s. Using data from a stability analysis by Iverson and Major (1987) I calculate that τ equals 0.13 kPa when the landslide is moving at its maximum velocity. Using this value for τ, and assuming that the wavelength, $\underline{L}$, is 1 m, the roughness, $\underline{A\ell}$, is 0.1, and ν is 0.3, I calculate a maximum velocity for the Minor Creek landslide of 5×10^{-6} m/s (about 13 m/month). My calculated velocity is from 1 to 2 orders of magnitude higher than the maximum velocity observed by Iverson and Major (1987). However, the wavelength and roughness are too poorly known to refine my calculation or to speculate about the cause for the difference between the observed and calculated velocities.

My model for forced circulation applies to landslides that fail in a ductile manner (without sudden loss of strength) such as landslides on natural slopes that fail by a gradual rise of the water table.

BIBLIOGRAPHY

Anderson, L.R., Keaton, J.R., Saarinen, T.F., and Wells, W.G., II, 1984, The Utah landslides, debris flows, and floods of May and June 1983: Washington, D.C., National Research Council, National Academy Press, 96 p.

Biot, M.A., 1941, General theory of three-dimensional consolidation: Journal of Applied Physics, v. 12, p. 155-164.

Bjerrum, L., 1967, Progressive failure in overconsolidated clays and clay shales: Journal of the Soil Mechanics and Foundations Division of the American Society of Civil Engineers, vol. 93, no. SM5, p. 3-49.

Bonar, C.M., 1948, Geology of Ephraim area, Utah: Columbus, Ohio, Ohio State University, M.S. thesis, 124 p.

Brinker, R.C., and Wolf, P.R., 1977, Elementary surveying, in the collection The IEP series in civil engineering, 6th edition: New York, Thomas Y. Crowell Co., 568 p.

Brunsden, D., 1984, Mudslides, in Brunsden, D. and Prior, D.B., eds., Slope instability: New York, John Wiley, p. 363-418.

Budd, W.F., 1970, Ice flow over bedrock perturbations: Journal of Glaciolgy, v. 9, no. 55, p. 29-48.

Byerlee, J.D., 1970, The mechanics of stick slip: Tectonophysics, v. 19, p. 475-486.

Carter, M., and Bentley, S.P., 1985, The geometry of slip surfaces beneath landslides--Predictions from surface measurements: Canadian Geotechnical Journal, v. 22, p. 234-238.

Collin, A., 1846, Landslides in Clays, translated from Recherches Experimentales sur les Glissements Spontanes des terrains argileux translated by Schriever W.R., 1956, Toronto, University of Toronto Press, 160 p.

Craig, D., 1981, Mudslide plugflow within channels: Engineering Geology, v. 17, p. 273-281.

Cruden, D.M., 1986, The geometry of slip surfaces beneath landslides--Predictions from surface measurements--Discussion: Canadian Geotechnical Journal, v. 23, p. 94.

Duncan, J.M., Fleming, R.W., and Patton, F.D., 1986, Report of the Thistle Slide Committee to State of Utah Department of Natural Resources Division of Water Rights: U.S. Geological Survey Open-File Report 86-505, 95 p.

Fleming, R.W., and Johnson, A.M., (in press) Structures associated with strike-slip boundaries in landslides. In Johnson, A.M., ed., Richard H. Jahns memorial volume: New York, Elsevier.

Fleming, R.W., Johnson, R.B., and Schuster, R.L., in press, The reactivation of the Manti landslide, Utah, in Fleming and others, The Manti, Utah, Landslide: U.S. Geological Survey Professional Paper 1311.

Franklin, J.A., 1984, Slope instrumentation and monitoring, in Brunsden, D., and Prior, D.B., eds., Slope instability: New York, John Wiley, p. 143-170.

Freeze, R.A. and Cherry, J.A., 1979, Groundwater: Englewood Cliffs, New Jersey, Prentice Hall, 604 p.

Goold, J.P., 1960, A study of shear failure of certain Tertiary marine sediments, in Research conference on shear strength of cohesive soils, at Boulder, Colorado: New York, American Society of Civil Engineers, p. 615-641.

Grover, B.L., Campbell, C.B., and Campbell, M.D., 1970, a prediction equation for vegetation effects on water yield from watersheds in arid areas: Soil Science Society of America, Proceedings, v. 34, p. 669-673.

Hanna, T.H., 1985, Field instrumentation in geotechnical engineering, in Series on Rock and Soil Mechanics, v. 10: Rockport, Maine, Trans Tech Publications, 843 p.

Hansen, W.R., 1965. Effects of the earthquake of March 27, 1964, at Anchorage, Alaska: U.S. Geological Survey Professional Paper 542-A. 68 p.

Hill, R., 1950, The mathematical theory of plasticity: London, Oxford University Press, 356 p.

Hutchinson, J.N., 1970, A coastal mudflow on the London clay cliffs at Beltinge, north Kent [England]: Geotechnique, v. 20, no. 3, p. 412-438.

Hutchinson, J.N., 1983, Methods of locating slip surfaces in landslides: Bulletin of the Association of Engineering Geologists, v. 20, no. 3, p. 235-252.

Hutchinson, J.N., Prior, D.B., and Stephens, N., 1974, Potentially dangerous surges in an Antrim [Ireland] mudslide: Quarterly Journal of Engineering Geology, v. 7, no. 4, p. 363-376.

Ingram, F.L., 1972, The Ingram method of angular value weighting in trilateration: Surveying and Mapping, v. 32, p. 509-515.

Iverson, R.M., 1984, Unsteady, nonuniform landslide motion--Theory and measurement: Stanford, Calif., Stanford University, Ph.D. thesis, 303 p.

Iverson, R.M., 1986, Dynamics of slow landslides: A theory for time-dependent behavior, in Abrahams, A.D., ed., Hillslope processes: Winchester Massachussets, Allen & Unwin, p. 297-317.

Iverson, R.M., and Major, J.J., 1987, Rainfall, groundwater flow, and seasonal movement at Minor Creek landslide, northwestern California--Physical interpretation of empirical relations: Geological Society of America Bulletin, v. 99, p. 579-594.

Jaeger, J.C., 1962, Elasticity, fracture, and flow, 2nd edition: London, Methuen, and New York, John Wiley, 208 p.

Jakobson, B., 1952, The landslide at Surte on the Gota River: Proceedings of the Royal Swedish Geotechnical Institute. v.5, p. 1-121.

Japan Society of Landslide, 1980, Landslides in Japan: Tokyo, The Japan Society of Landslide National Conference on Landslide Control, 44 p.

Johnson, A.M., 1965, A model for debris flow: University Park, Pennsylvania, The Pennsylvania State University, Ph.D. dissertation, 248 p.

Johnson, A.M., 1970, Physical processes in geology: San Francisco, Freeman, Cooper and Co. 577 p.

Johnson, A.M., 1981, Theory and application of finite strain. Cincinnati, Ohio, University of Cincinnati, Unpublished manuscript. 137 p.

Johnson, A.M., 1984, Final report to Earth Sciences Division, Geology program of the National Science Foundation for grant #EAR 80-00053, v. II, chapter III.

Johnson, A.M., and Baum, R.L., 1987, BASIC programs for computing displacements, strains, and tilts from quadrilateral measurements: U.S. Geological Survey Open-File Report 87-343, 19 p.

Kamb, B., 1970, Sliding motion of glaciers -- theory and observation: Reviews of Geophysics and Space Physics, v. 8, no. 4, p. 673-728.

Kamb, B., and LaChapelle, E., 1964, Direct observation of the mechanism of glacier sliding over bedrock: Journal of Glaciology, v. 5, no. 38, p. 159-172.

Keefer, D.K., and Johnson, A.M., 1983, Earth flows--morphology, mobilization and movement: U.S. Geological Survey Professional Paper 1264, 56p.

Kenney, T. C., 1967, The influence of mineral composition on the residual strength of natural soils: Oslo, Norway, Proceedings of the Geotechnical Conference, v. 1, p. 123-129.

Lambe, T.W., and Whitman, R.V., 1969, Soil Mechanics: New York, Wiley, 553 p.

Lantz, J.R., 1984, Geology and kinematics of a clay-rich landslide with an undulatory slip surface: College Station, Texas, Texas A & M University M.S. thesis, 132 p.

LaRocque, A., 1960, Molluscan faunas of the Flagstaff Formation of central Utah: Geological Society of America Memoir 78, 100 p.

Laurila, S.H., 1983, Electronic surveying in practice: New York, John Wiley, 388 p.

Lawn, B.R. and Wilshaw T.R., 1975, Fracture of brittle solids. London, Cambridge University Press, 204 p.

Lliboutry, L., 1968, General theory of subglacial cavitation and sliding of temperate glaciers: Journal of Glaciology, v. 7, no. 49, p. 21-58.

Malvern, L.E., 1969, An Introduction to the Mechanics of a Continuous Medium: Englewood Cliffs, New Jersey, Prentice Hall, 713 p.

McTigue, D.F., Passman, S.L., and Jones, S.F., 1985, Normal stress effects in the creep of ice: Journal of Glaciology, v. 31, no. 108, p. 120-126.

Meeuwig, R.O., 1965, Effects of seeding and grazing on infiltration capacity and soil stability of a subalpine range in central Utah: Journal of Range Management, v. 18, no. 4, p. 173-180.

Mitchell, J.K., 1976, Fundamentals of soil behavior: New York, Wiley, 422 p.

Morganstern, N.R., and Tchalenko, J.S., 1967, Microstructural observations on shear zones from slips in natural clays, in Proceedings of the Geotechnical Conference: Oslo, Norway, v. 1, p. 147-152.

Morland, L.W., 1976a, Glacier sliding down an inclined wavy bed: Journal of Glaciolgy, v. 17, no. 77, p. 447-462.

Morland, L.W., 1976b, Glacier sliding down an inclined wavy bed with friction: Journal of Glaciology, v. 17, no. 77, p 463-477.

Nye, J.F., 1969, A calculation on the sliding of ice over a wavy surface using a Newtonian viscous approximation: Proceedings of the Royal Society of London, series A, v. 311, p. 445-467.

Nye, J.F., 1970, Glacier Sliding without cavitation in a linear viscous approximation: Proceedings of the Royal Society of London, series A, v. 315, p. 381-403.

Orr, H.R., 1957, Effects of plowing and seeding on some forage production and hydrologic characteristics of a subalpine range in central Utah: Journal of Range Management, v. 18, no. 4, p. 173-180.

Palmer, A.C., and Rice, J.R., 1973, The growth of slip surfaces in the progressive failure of over-consolidated clay: Proceedings of the Royal Society of London, series A, v. 232, p. 527-548.

Patton, F.D., 1966, Multiple modes of shear failure in rock and related materials: Urbana, University of Illinois, Ph.D. thesis, 293 p.

Prior, D.B., and Stephens, N., 1972, Some movement patterns of temperate mudflows--examples from northeastern Ireland: Geological Society of America Bulletin, v. 38, no. 8, p. 2533-2543.

Ragan, D.M., 1973, Structural geology, an introduction to geometrical techniques: New York, John Wiley, 208 p.

Ramiah, B.K., and Purushothamaraj, P., 1971, Influence of strain rate on the residual strength of a kaolinitic clay: Geotechnical Engineering, v. 2, no. 2, p. 151-158.

Ramsay, J.G., 1967, Folding and fracturing of rocks: New York, McGraw-Hill, 568 p.

Rice, J.R., 1973, Initiation and growth of shear bands, in Palmer, A.C., ed., Plasticity and Soil Mechanics: Cambridge, England, Cambridge University Engineering Department, p. 263-274.

Rice, J.R. and Cleary, M.P., 1976, Some basic stress diffusion solutions for fluid saturated elastic porous media with compressible constituents: Reviews of Geophysics and Space Physics, v. 14, no. 2, p. 227-241.

Rivlin, R.S., 1964, Second and higher order theories for the flow of a viscoelastic fluid in a noncircular pipe, in, Proceedings of the International Symposium on Second Order Effects, International Union of Theoretical and Applied Mechanics, Hafia, Israel, 1962: New York, Macmillan Co., p. 668-677.

Robinson, G.B., Jr., 1971, Groundwater hydrology of the San Pitch River drainage basin, Sanpete County, Utah: U.S. Geological Survey Water-Supply Paper 1896, 80 p.

Rosenthal, D., 1946, The theory of moving sources of heat and its application to metal treatments: Transactions of the American Society of Mechanical Engineers, v. 68, p 849-866.

Rybar, J., 1968, Ein Beispiel von Bewegsungsmessungen an Rutschungen: Zeitschrift fur angewandte Geologie, v. 14, p. 138-141.

Savage, W.Z., and Chleborad, A.F., 1982, A model for creeping flow in landslides: Bulletin of the Association of Engineering Geology. v. 19, p. 333-338.

Shames, I.H., 1962, Mechanics of fluids: New York, McGraw-Hill, 558 p.

Skempton, A.W., 1954, The pore-pressure coefficients A and B: Geotechnique, v. 4, p. 143-147.

Skempton, A.W., and Petley, D.J., 1967, The strength along structural discontinuities in stiff clays, in Proceedings of the Geotechnical Conference: Oslo, Norway, v. 2, p. 29-48.

Spieker, E.M., 1949, The transition between the Colorado plateaus and the Great Basin in central Utah: Utah Geological Society Guidebook 4, 106 p.

Spieker, E.M., 1946, Late Mesozoic and early Cenozoic history of central Utah: U.S. Geological Survey Professional Paper 205D, p. 117-161.

Stanley K.O., and Collinson, J.W., 1979, Depositional history of Paleocene-lower Eocene Flagstaff Limestone and coeval rocks, central Utah: American Association of Petroleum Geologists Bulletin, v. 63, no. 3, p. 311-323.

Stout, M.L., 1971, Slip surface geometry in landslides, southern California and Norway: Bulletin of the Association of Engineering Geologists. v. 8, no. 1, p. 59-78.

Suhayda, J.N., and Prior, D.B., 1978, Explanation of submarine landslide morphology by stability analysis and rheological models, in Proceedings of the 10th Annual Offshore Technology Conference: Houston, Texas, v. 2, p. 31-73.

Ter-Stepanian, G., 1984, Analysis of slope deformation for determining the landslide mechanism, in Proceedings of the Fourth International Symposium on Landslides, v. 2: Downview, Ontario, Canada, University of Toronto Press, p. 499-504.

Ter-Stepanian, G., and Ter-Stepanian, H., 1974, Determination of deformed state of a sliding body by creep hodographs, in Proceedings of the Second International Congress of the International Association of Engineering Geology: Sao Paulo, Brazil, v. II, p. V23.1-V23.5.

Terzaghi, K.V., 1925, Erdbaumechanik auf Bodenphysicalischer Grundlage: Vienna, Franz Deuticke, 399 p.

Terzaghi, K.V., 1950, Mechanism of Landslides, in Engineering Geology (Berkey) volume: The Geological Society of America, p. 83-123.

Truesdell, C., 1964, Second-order effects in the mechanics of materials, in, Proceedings of the International Symposium on Second Order Effects, International Union of Theoretical and Applied Mechanics, Hafia, Israel, 1962: New York, MacMillian Co. p. 1-47.

Varnes, D.J., 1978, Slope movement types and processes, chap. 2 in Schuster, R.L., and Krizek, R.S., eds., Landslides: Analysis and control: U.S. National Academy of Sciences, Transportation Research Board Special Report 176, p. 11-33.

Vonder Linden, Karl, 1972, An analysis of the Portugese Bend landslide, Palos Verdes Hills, California: Stanford, California, Stanford University, Ph.D. dissertation, 405 p.

Witkind, I.J., Weiss, M.P., and Brown, T.L., 1982, Preliminary geologic map of the Manti 30′ x 60′ quadrangle, Carbon, Emery, Juab, Sanpete, and Sevier Counties, Utah: U.S. Geological Survey Open-File Report 82-0654, 1 sheet, 1:100,000 scale.

Wroth, C.P. and Houlsby, G.T., 1985, Soil mechanics--property characterization and analysis procedures, in Proceedings of the Eleventh International Conference on Soil Mechanics and Foundation Engineering, San Francisco, v. 1, p. 1-55.

Yen, B.C., 1969, Stability of Slopes undergoing creep deformation, Journal of the Soil Mechanics and Foundations Division, American Society of Civil Engineers, v. 95, no. SM4, p. 1075-1096.

Zaruba, Q., and Mencl, V., 1982, Landslides and their control, 2nd revised edition: New York, Elsevier, 324 p.

Zawiskie, J., Chapman, D., and Alley, R., 1982, Depositional history of the Paleocene-Eocene Colton Formation, north-central Utah, in Nielson, D.L., ed., Overthrust Belt of Utah: Utah Geological Association Publication 10, p. 273-284.

APPENDICES

Appendix A

METHODS OF DISPLACEMENT MEASUREMENTS

Wooden stakes were used at the corners of quadrilaterals and in stake lines. A small finishing nail was driven into the tops of the stakes to serve as a measuring point. Positions of stakes in transverse stake lines were measured either by holding a string taut between the reference stakes off the landslide, holding a tape perpendicular to the string and measuring to a plumb line positioned over each stake, or by making a plane-table map of the stakes on the landslide and the reference stakes. Longitudinal stake lines and quadrilaterals were measured by hooking a steel tape on one nail and measuring the distance to adjacent stakes. Elevations of the tops of the stakes were measured by taking backsights with a precision level. Details of the use of quadrilaterals are described elsewhere (Chapter VI).

The recording extensiometers were water-level recorders (slightly modified) of the type used by the Water Resources Division of the U.S. Geological Survey. Each recorder was placed in a wooden box attached to a tree just outside the flank of the landslide. One end of a fine stainless steel wire was hooked to another tree just inside the flank of the landslide that was a few meters downslope from the recorder. The other end of the wire was attached to and wrapped around the recorder flywheel. A counterweight, hung from a second wire that was wrapped in the opposite direction around a small hub on the recorder flywheel, kept tension in the stainless steel wire. As the landslide moved, the stainless steel wire uncoiled and caused the flywheel to rotate. A clock activated the recorder every fifteen minutes, causing it to punch a tape. Later, in the office, the data were read from the tape and plotted as time-displacement curves.

The accuracy and precision of the measurements varied with the techniques and instruments used: Measurements made with a steel tape usually could be repeated to within 3 mm; however, errors of 6 mm were sometimes observed and larger errors might exist in some of the measurements. Our average precision in measuring the downslope displacements of stakes in the transverse lines was probably about 5 to 8 cm (2 to 3 in.). Elevations measured with the precision level were repeatable to about 0.5 mm. Displacements of most points amounted to tens or hundreds of centimeters each year; therefore, the accuracy of our measurements was adequate to determine the displacements.

Several factors can affect the accuracy of measurements made by recording extensiometers: (1) Diurnal temperature variations can cause the wire to change length by 1 to 2 mm over the course of a day. (2) Sagging of the wire can introduce errors of a few centimeters over the course of a few meters displacement. (3) Misalignment of 5° between the wire and the direction of displacement causes errors of a few centimeters in measuring a total displacement of 10 m. It is difficult to make corrections for any of these without making additional measurements. However, the accuracy of the extensiometer data was judged adequate because other methods of measuring displacements were subject to errors as large or larger than those in the extensiometer data.

Appendix B

SUCCESSIVE DEFORMATIONS

Where the direction of displacement, and the magnitude and orientation of the principal stretches are known, the deformation can be resolved into components of pure shear, simple shear, and pure area change (Fig. 5.27). The components of pure shear and simple shear are oriented so that the direction of shearing in simple shear and either the major or minor principal axis of pure shear are parallel to the displacement direction. Area change is independent of direction.

The strains are resolved into components of pure shear and simple shear oriented parallel to the direction of displacement because neighboring particles in the landslide generally moved along approximately parallel paths. Thus, simple shear and elongation or shortening in pure shear would be most likely to occur parallel to the direction of landslide motion.

Typically, the principal stretches are oriented at some oblique angle to the direction of movement. Pure shear parallel to the direction of movement would result in principal stretches oriented parallel and perpendicular to the direction of movement. Simple shear parallel to the direction of movement would result in principal stretches oriented between 45° (small deformation) and 0° (infinite deformation) from the direction of movement. A combination of simple shear and pure shear can account for any orientation of the principal axes of stretch. The magnitude the component of pure shear is measured by $\underline{S}_{\underline{x}}$, the major or minor principal stretch of the pure shear component.

The magnitude of the component of simple shear is measured by the angle of simple shear, ψ_y.

Application of successive deformations makes it possible to solve for components of the deformation. Successive deformations are, as the name suggests, a sequence of deformations that together determine the final deformed state. The sequence of deformations assumed to produce the principal stretches computed for quadrilaterals on the ridge is outlined in Figure 5.27, and in the text.

A simple way of treating successive deformations is matrix multiplication (A.M. Johnson, unpub. data). The transformation matrix of each deformation pre-multiplies that of the matrix of the preceding deformation. Thus, for the sequence of deformations described in the text and Figure 5.27, the following expression can be written:

$$\begin{bmatrix} dx_3 \\ dy_3 \end{bmatrix} = \begin{bmatrix} 1 & \tan(\psi_y) \\ 0 & 1 \end{bmatrix} \begin{bmatrix} S_x & 0 \\ 0 & 1/S_x \end{bmatrix} \begin{bmatrix} S_o & 0 \\ 0 & S_o \end{bmatrix} \begin{bmatrix} dx_o \\ dy_o \end{bmatrix}. \qquad \text{(B1)}$$

The initial dimensions of a small element are $\underline{dx_o}$ and $\underline{dy_o}$; the dimensions in the final state are $\underline{dx_3}$ and $\underline{dy_3}$ (Fig. 5.27). Equation B1 simplifies to

$$\begin{bmatrix} dx_3 \\ \\ dy_3 \end{bmatrix} = \begin{bmatrix} S_o S_x & (S_o/S_x) \tan(\psi_y) \\ \\ 0 & S_o/S_x \end{bmatrix} \begin{bmatrix} dx_o \\ \\ dy_o \end{bmatrix}. \qquad \text{(B2)}$$

The square matrix in equation B2 is the deformation gradient, F. The stretch is related to F through the Green deformation tensor, C, where

$$C = F^T \cdot F,$$

and the components of C are:

$$C_{xx} = S_x^2 S_o^2;$$

$$C_{xy} = S_o^2 \tan(\psi_y); \qquad \text{(B3)}$$

$$C_{yy} = (S_o/S_x)^2 (\tan^2\psi_y + 1).$$

The squares of the principal stretches are equal to the principal values of the Green Deformation Tensor (Malvern, 1969; A.M. Johnson, unpub. data):

$$S^2_{1,2} = (C_{xx} + C_{yy})/2 \pm \{((C_{xx} + C_{yy})/2)^2 + C_{xy}^2 - C_{xx}C_{yy}\}^{1/2}. \qquad \text{(B4)}$$

By substituting equations B3 into B4 and using the definition of the maximum finite shear strain, γ_{max},

$$\gamma_{max} = (S_1^2 - S_2^2)/2S_1S_2,$$

I solve for tan ψ_y:

$$\tan^2\psi_y = 2S_x^2\,(\gamma^2_{max} + 1)^{1/2} - S_x^4 - 1. \qquad \text{(B5)}$$

Because pure shear and simple shear are constant volume deformations, $\underline{S}_o$ is the only stretch causing area change; therefore:

$$S_o = (S_1S_2)^{1/2}. \qquad \text{(B6)}$$

Using Equation, B2, I solved for $\underline{S}_y$, the <u>observed</u> stretch normal to the direction of displacement,

$$S_y = S_o/S_x$$

or

$$S_x = S_o/S_y. \tag{B7}$$

The stretch, $\underline{S}_y$, can be computed from the principal stretches by the relationship

$$(1/S_y)^2 = (1/S_1)^2\cos^2(\beta) + (1/S_2)^2\sin^2(\beta), \tag{B8}$$

in which β is the angle between the direction of S_1 and the displacement direction. Therefore, the parameters that represent the three successive deformations can be computed with equations B5, B6, and B7 if $\underline{S}_1$, $\underline{S}_2$, and their orientations relative to the mean displacement direction are known. The expressions I have derived here might only be applicable to small strains (Arvid Johnson, oral commun., 1987); however, the concepts are still useful for understanding the deformation of a landslide.

Appendix C

RAW QUADRILATERAL MEASUREMENTS

Q-1

15 JUNE 1983	85	1.576	1.219	1.434	1.140	1.803	2.011	0.038	0.194	0.248
19 JUNE 1983	85	1.576	1.226	1.437	1.154	1.805	2.021	0.010	0.156	0.197
21 JUNE 1983	85	1.578	1.229	1.430	1.157	1.803	2.026	0.000	0.152	0.189
23 JUNE 1983	85	1.578	1.229	1.430	1.162	1.803	2.027	0.038	0.194	0.248
26 JUNE 1983	85	1.578	1.230	1.429	1.165	1.803	2.030	0.038	0.194	0.248
28 JUNE 1983	85	1.578	1.230	1.429	1.165	1.803	2.030	0.038	0.194	0.248
30 JUNE 1983	85	1.578	1.232	1.429	1.167	1.803	2.030	-0.003	0.149	0.193
7 JULY 1983	85	1.578	1.233	1.426	1.167	1.802	2.032	0.038	0.194	0.248
9 JULY 1983	85	1.578	1.235	1.426	1.165	1.800	2.032	-0.014	0.168	0.206
11 JULY 1983	85	1.580	1.237	1.427	1.165	1.802	2.032	0.038	0.194	0.248
4 AUG 1983	85	1.578	1.230	1.426	1.175	1.802	2.035	0.038	0.194	0.248

Q-2

15 JUNE 1983	-5	2.256	2.546	2.016	1.757	2.470	3.458	0.060	0.854	0.651
28 JUNE 1983	-5	2.262	2.580	2.021	1.797	2.411	3.551	0.073	0.813	0.648
30 JUNE 1983	-5	2.261	2.580	2.019	1.800	2.407	3.558	0.073	0.813	0.629
5 JULY 1983	-5	2.262	2.581	2.011	1.803	2.397	3.567	0.082	0.822	0.632
7 JULY 1983	-5	2.264	2.584	2.019	1.803	2.395	3.578	0.144	0.787	0.621
9 JULY 1983	-5	2.264	2.586	2.021	1.803	2.394	3.574	0.093	0.817	0.627
15 JULY 1983	-5	2.267	2.588	2.019	1.803	2.392	3.577	0.149	0.806	0.625
19 JULY 1983	-5	2.264	2.588	2.024	1.803	2.391	3.575	0.148	0.791	0.619
22 JULY 1983	-5	2.267	2.588	2.019	1.803	2.392	3.575	0.159	0.791	0.613
23 JULY 1983	-5	2.267	2.586	2.018	1.803	2.395	3.577	0.156	0.791	0.622
21 JUNE 1983	-5	2.261	2.567	2.019	1.781	2.435	3.515	0.083	0.818	0.634
23 JUNE 1983	-5	2.261	2.567	2.019	1.786	2.427	3.526	0.069	0.827	0.638
26 JUNE 1983	-5	2.261	2.573	2.019	1.789	2.418	3.542	0.075	0.820	0.637
19 JUNE 1983	-5	2.259	2.562	2.019	1.773	2.454	3.499	0.075	0.825	0.645
4 AUG 1983	-5	2.265	2.586	2.021	1.800	2.388	3.574	0.081	0.822	0.625

Q-3

16 JUNE 1983	-8	2.659	2.234	2.905	2.704	3.566	3.832	0.360	0.619	0.573
17 JUNE 1983	-8	2.658	2.235	2.903	2.699	3.572	3.826	0.364	0.627	0.610
19 JUNE 1983	-8	2.653	2.227	2.907	2.694	3.581	3.812	0.384	0.653	0.601
21 JUNE 1983	-8	2.659	2.227	2.908	2.689	3.594	3.799	0.334	0.601	0.591
26 JUNE 1983	-8	2.658	2.223	2.912	2.685	3.612	3.777	0.338	0.578	0.579
28 JUNE 1983	-8	2.658	2.221	2.913	2.681	3.620	3.772	0.327	0.606	0.543
30 JUNE 1983	-8	2.658	2.219	2.913	2.680	3.623	3.766	0.351	0.610	0.582
5 JULY 1983	-8	2.661	2.219	2.916	2.677	3.632	3.756	0.349	0.568	0.583
7 JULY 1983	-8	2.659	2.216	2.916	2.675	3.634	3.753	0.362	0.606	0.591
9 JULY 1983	-8	2.659	2.216	2.916	2.677	3.636	3.751	0.340	0.619	0.603
17 JULY 1983	-8	2.664	2.216	2.918	2.680	3.637	3.748	0.333	0.591	0.594
4 AUG 1983	-8	2.662	2.210	2.915	2.667	3.637	3.740	0.379	0.650	0.604

Q-1

4 AUG 1983	85	1.578	1.230	1.426	1.175	1.802	2.035	0.038	0.194	0.248
21 MAY 1984	85	1.597	1.297	1.432	1.410	1.794	2.218	0.062	0.300	0.512
23 MAY 1984	85	1.595	1.322	1.426	1.475	1.800	2.262	0.062	0.300	0.512
25 MAY 1984	85	1.594	1.362	1.419	1.519	1.816	2.312	0.062	0.300	0.512
27 MAY 1984	85	1.595	1.373	1.421	1.538	1.827	2.313	0.062	0.300	0.512
29 MAY 1984	85	1.597	1.373	1.413	1.553	1.816	2.324	0.067	0.349	0.558
31 MAY 1984	85	1.597	1.380	1.414	1.556	1.818	2.324	0.067	0.349	0.558
2 JUNE 1984	85	1.599	1.386	1.414	1.568	1.832	2.335	0.067	0.349	0.558
5 JUNE 1984	85	1.599	1.391	1.413	1.576	1.829	2.340	0.069	0.368	0.573
3 AUG 1984	85	1.605	1.421	1.426	1.616	1.838	2.384	0.077	0.391	0.584
30 APR 1985	85	1.605	1.438	1.400	1.619	1.819	2.396	0.077	0.413	0.624
30R APR 1985	85	1.605	2.575	1.438	1.619	2.630	2.396	0.077	0.514	0.624
16 MAY 1985	85	1.603	2.673	1.422	1.695	2.683	2.488	0.087	0.527	0.636
5 JUNE 1985	85	1.602	2.683	1.422	1.707	2.686	2.496	0.090	0.532	0.643
2 AUG 1985	85	1.605	2.684	1.419	1.718	2.692	2.505	0.093	0.539	0.638
12 SEP 1986	85	1.605	2.702	1.407	1.738	2.699	2.519	0.096	0.539	0.641

Q-2

4 AUG 1983	-5	2.265	2.586	2.021	1.800	2.388	3.574	0.081	0.822	0.625
23 MAY 1984	-5	2.238	3.870	2.035	3.304	2.127	5.471	0.087	0.807	0.659
25 MAY 1984	-5	2.234	4.159	2.034	3.613	2.292	5.794	0.087	0.807	0.659
27 MAY 1984	-5	2.234	4.296	2.034	3.758	2.381	5.940	0.087	0.807	0.659
29 MAY 1984	-5	2.232	4.356	2.030	3.835	2.432	6.021	0.111	0.813	0.664
31 MAY 1984	-5	2.232	4.420	2.030	3.902	2.477	6.091	0.114	0.812	0.663
2 JUNE 1984	-5	2.234	4.496	2.030	3.980	2.534	6.172	0.114	0.812	0.660
5 JUNE 1984	-5	2.234	4.566	2.030	4.054	2.577	6.258	0.120	0.812	0.662
7 JUNE 1984	-5	2.235	4.647	2.029	4.158	2.638	6.339	0.123	0.812	0.661
3 AUG 1984	-5	2.223	5.259	2.027	4.797	3.164	7.009	0.154	0.765	0.616
28 APR 1985	-5	2.235	5.544	2.034	5.077	3.391	7.299	0.158	0.735	0.584
28R APR 1985	-5	1.805	2.667	2.034	2.772	3.261	3.396	-0.010	0.721	0.570
30 APR 1985	-5	1.806	2.686	2.037	2.778	3.240	3.426	-0.010	0.723	0.568
15 MAY 1985	-5	1.794	2.873	2.202	3.054	3.048	3.939	0.019	0.711	0.556
5 JUNE 1985	-5	1.781	2.978	2.022	3.186	3.011	4.131	0.032	0.686	0.536
2 AUG 1985	-5	1.775	3.016	2.016	3.239	3.007	4.204	0.037	0.665	0.511
12 SEP 1986	-5	1.754	3.159	2.029	3.434	2.994	4.435	0.042	0.603	0.424

Q-3

4 AUG 1983	-8	2.662	2.210	2.915	2.667	3.637	3.740	0.379	0.650	0.604
5 JUNE 1984	-8	2.675	2.777	2.977	2.972	5.145	2.280	0.392	0.906	0.987
3 AUG 1984	-8	2.672	3.258	2.964	3.377	5.774	2.000	0.389	0.972	1.068
29 APR 1985	-8	2.657	3.689	2.951	3.756	6.255	1.940	0.397	1.041	1.148
16 MAY 1985	0	2.659	4.623	2.915	4.632	7.245	2.302	0.403	1.167	1.280
5 JUNE 1985	0	2.657	5.091	2.902	5.086	7.728	2.629	0.408	1.218	1.341
2 AUG 1985	0	2.664	5.280	2.899	5.275	7.930	2.786	0.402	1.239	1.370
12 SEP 1986	0	2.657	6.123	2.872	6.106	8.777	3.519	0.406	1.325	1.477

Q-4

16 JUNE 1983	-12	2.248	2.251	2.197	2.007	3.050	3.099	0.470	0.345	0.044
19 JUNE 1983	-12	2.245	2.251	2.197	2.005	3.050	3.096	0.470	0.345	0.044
21 JUNE 1983	-12	2.246	2.253	2.199	2.005	3.051	3.097	0.470	0.345	0.044
26 JUNE 1983	-12	2.242	2.253	2.200	2.008	3.050	3.099	0.470	0.345	0.044
30 JUNE 1983	-12	2.240	2.253	2.200	2.010	3.048	3.099	0.470	0.345	0.044
7 JULY 1983	-12	2.237	2.259	2.200	2.010	3.050	3.100	0.470	0.345	0.044
9 JULY 1983	-12	2.237	2.253	2.202	2.010	3.046	3.100	0.470	0.345	0.044
11 JULY 1983	-12	2.235	2.259	2.203	2.011	3.048	3.102	0.470	0.345	0.044
13 JULY 1983	-12	2.235	2.254	2.203	2.011	3.045	3.099	0.470	0.345	0.044
15 JULY 1983	-12	2.235	2.253	2.203	2.013	3.046	3.099	0.470	0.345	0.044
4 AUG 1983	-12	2.234	2.248	2.194	2.004	3.040	3.094	0.481	0.353	-0.021

Q-5

16 JUNE 1983	-16	1.805	1.957	1.797	2.112	2.789	2.642	0.266	0.321	0.118
17 JUNE 1983	-16	1.805	1.959	1.797	2.115	2.789	2.642	0.266	0.321	0.118
19 JUNE 1983	-16	1.805	1.959	1.794	2.116	2.791	2.640	0.266	0.321	0.118
21 JUNE 1983	-16	1.803	1.959	1.794	2.115	2.791	2.640	0.260	0.279	0.108
23 JUNE 1983	-16	1.805	1.959	1.794	2.115	2.791	2.640	0.413	0.290	0.100
26 JUNE 1983	-16	1.805	1.957	1.794	2.115	2.791	2.640	0.260	0.249	0.127
28 JUNE 1983	-16	1.805	1.959	1.794	2.115	2.791	2.640	0.266	0.321	0.118
30 JUNE 1983	-16	1.805	1.959	1.794	2.113	2.791	2.640	0.266	0.321	0.118
5 JULY 1983	-16	1.805	1.959	1.791	2.113	2.789	2.639	0.266	0.321	0.118
7 JULY 1983	-16	1.805	1.959	1.791	2.112	2.789	2.639	0.266	0.321	0.118
9 JULY 1983	-16	1.805	1.959	1.792	2.112	2.791	2.639	0.266	0.321	0.118
4 AUG 1983	-16	1.805	1.959	1.799	2.107	2.786	2.643	0.286	0.330	0.111

Q-6

16 JUNE 1983	17	2.308	3.304	2.411	3.138	3.883	4.091	0.216	0.739	0.256
17 JUNE 1983	20	2.305	3.308	2.410	3.142	3.915	4.067	0.218	0.745	0.271
21 JUNE 1983	20	2.305	3.329	2.408	3.161	4.031	3.983	0.177	0.708	0.267
19 JUNE 1983	20	2.305	3.321	2.408	3.150	3.975	4.017	0.218	0.763	0.283
23 JUNE 1983	20	2.305	3.340	2.408	3.156	4.070	3.958	0.185	0.746	0.240
26 JUNE 1983	20	2.305	3.351	2.403	3.183	4.118	3.924	0.178	0.679	0.256
28 JUNE 1983	20	2.305	3.358	2.402	3.191	4.147	3.909	0.200	0.676	0.283
30 JUNE 1983	20	2.305	3.364	2.402	3.199	4.169	3.896	0.185	0.684	0.280
5 JULY 1983	20	2.308	3.373	2.400	3.213	4.207	3.886	0.210	0.724	0.311
7 JULY 1983	20	2.307	3.377	2.402	3.218	4.218	3.872	0.192	0.761	0.296
9 JULY 1983	20	2.308	3.378	2.400	3.221	4.226	3.867	0.181	0.796	0.289
11 JULY 1983	20	2.307	3.380	2.402	3.224	4.232	3.866	0.192	0.721	0.327
19 JULY 1983	20	2.311	3.386	2.407	3.232	4.251	3.861	0.224	0.778	0.346
23 JULY 1983	20	2.305	3.385	2.400	3.231	4.255	3.859	0.194	0.795	0.290
4 AUG 1983	20	2.305	3.386	2.405	3.234	4.259	3.856	0.226	0.842	0.363

Q-4

4 AUG 1983	-12	2.234	2.248	2.194	2.004	3.040	3.094	0.437	0.343	-0.040
23 MAY 1984	-12	2.142	2.256	2.173	2.021	3.002	3.062	0.437	0.343	-0.040
25 MAY 1984	-12	2.140	2.256	2.173	2.019	3.002	3.062	0.437	0.343	-0.040
27 MAY 1984	-12	2.140	2.256	2.175	2.019	3.002	3.062	0.437	0.343	-0.040
29 MAY 1984	-12	2.142	2.256	2.173	2.016	3.002	3.062	0.451	0.355	-0.034
31 MAY 1984	-12	2.142	2.254	2.172	2.019	3.004	3.064	0.451	0.355	-0.034
2 JUNE 1984	-12	2.143	2.259	2.175	2.018	3.004	3.067	0.451	0.355	-0.034
5 JUNE 1984	-12	2.146	2.256	2.173	2.016	3.005	3.069	0.426	0.360	-0.014
3 AUG 1984	-12	2.132	2.249	2.173	2.024	3.002	3.058	0.453	0.346	-0.041
29 APR 1985	-12	2.124	2.245	2.175	2.026	3.005	3.072	0.451	0.347	-0.048
16 MAY 1985	-12	2.130	2.251	2.169	2.021	3.007	3.046	0.453	0.349	-0.054
5 JUNE 1985	-12	2.124	2.251	2.169	2.022	3.007	3.048	0.458	0.351	-0.056
2 AUG 1985	-12	2.118	2.245	2.167	2.029	2.994	3.048	0.456	0.342	-0.057
12 SEP 1986	-12	2.118	2.238	2.170	2.027	2.991	3.042	0.454	0.336	-0.060

Q-5

9 JULY 1983	-16	1.805	1.959	1.792	2.112	2.791	2.639	0.307	0.341	0.169
21 MAY 1984	-16	1.784	1.948	1.799	2.124	2.783	2.646	0.307	0.341	0.169
23 MAY 1984	-16	1.780	1.945	1.815	2.121	2.777	2.642	0.307	0.341	0.169
25 MAY 1984	-16	1.775	1.942	1.813	2.122	2.775	2.638	0.307	0.341	0.169
27 MAY 1984	-16	1.778	1.946	1.810	2.122	2.777	2.640	0.307	0.341	0.169
29 MAY 1984	-16	1.776	1.945	1.810	2.121	2.777	2.640	0.314	0.350	0.169
31 MAY 1984	-16	1.776	1.946	1.810	2.122	2.777	2.640	0.314	0.350	0.169
5 JUNE 1984	-16	1.776	1.945	1.810	2.122	2.775	2.642	0.312	0.343	0.164
3 AUG 1984	-16	1.786	1.951	1.811	2.126	2.769	2.659	0.331	0.343	0.152
28 APR 1985	-16	1.807	1.957	1.808	2.127	2.767	2.692	0.341	0.342	0.138
15 MAY 1985	-16	1.797	1.957	1.810	2.124	2.750	2.686	0.353	0.322	0.118
4 JUNE 1985	-16	1.830	1.962	1.813	2.130	2.748	2.715	0.377	0.311	0.105
2 AUG 1985	-16	1.867	1.972	1.810	2.124	2.754	2.753	0.397	0.303	0.095
12 SEP 1986	-16	2.135	1.972	1.856	2.116	2.759	2.924	0.528	0.200	0.042

Q-6

4 AUG 1983	17	2.305	3.386	2.405	3.234	4.259	3.856	0.226	0.842	0.363
21 MAY 1984	17	2.196	4.331	2.369	4.170	5.867	3.470	0.244	1.240	0.785
23 MAY 1984	17	2.194	4.521	2.350	4.367	6.112	3.529	0.244	1.240	0.785
25 MAY 1984	17	2.194	4.724	2.329	4.585	6.360	3.616	0.244	1.240	0.785
27 MAY 1984	17	2.194	4.870	2.318	4.737	6.531	3.691	0.244	1.240	0.785
29 MAY 1984	17	2.192	4.969	2.302	4.851	6.655	3.745	0.246	1.325	0.866
31 MAY 1984	17	2.192	5.075	2.305	4.956	6.774	3.807	0.246	1.347	0.885
2 JUNE 1984	17	2.194	5.205	2.292	5.093	6.920	3.888	0.246	1.347	0.885
5 JUNE 1984	17	2.192	5.369	2.283	5.269	7.109	3.997	0.249	1.396	0.939
4 AUG 1984	17	2.188	7.245	2.186	7.242	9.144	5.559	0.254	1.709	1.226
29 APR 1985	17	2.242	8.217	2.035	8.392	10.173	6.525	0.262	1.874	1.409
29R APR 1985	10	1.813	2.103	2.072	2.410	2.784	3.146	0.446	0.723	0.160
15 MAY 1985	10	1.808	2.959	1.978	3.016	4.410	2.350	0.543	1.041	0.536
5 JUNE 1985	10	1.807	4.143	1.918	4.162	5.759	2.861	0.447	1.103	0.641
2 AUG 1985	10	1.813	4.740	1.921	4.732	6.393	3.299	0.455	1.223	0.758
12 SEP 1986	10	1.808	8.976	1.738	9.087	10.697	7.385	0.456	1.998	1.546

Q-7

21 JUNE 1983	47	1.861	1.699	1.556	2.061	2.745	2.297	0.210	0.597	0.452
23 JUNE 1983	47	1.862	1.695	1.557	2.061	2.745	2.297	0.210	0.597	0.452
28 JUNE 1983	47	1.864	1.695	1.556	2.061	2.747	2.296	0.210	0.597	0.452
30 JUNE 1983	47	1.861	1.695	1.556	2.059	2.743	2.297	0.210	0.597	0.452
5 JULY 1983	47	1.861	1.695	1.556	2.057	2.743	2.297	0.210	0.597	0.452
7 JULY 1983	47	1.859	1.697	1.557	2.057	2.743	2.296	0.210	0.597	0.452
9 JULY 1983	47	1.862	1.695	1.553	2.057	2.743	2.297	0.210	0.597	0.452
13 JULY 1983	47	1.861	1.699	1.556	2.057	2.743	2.299	0.210	0.597	0.452
17 JULY 1983	44	1.861	1.699	1.556	2.057	2.743	2.299	0.240	0.541	0.422
19 JULY 1983	47	1.861	1.699	1.556	2.057	2.743	2.299	0.210	0.597	0.452
22 JULY 1983	47	1.861	1.699	1.556	2.057	2.743	2.299	0.209	0.597	0.452
23 JULY 1983	47	1.861	1.699	1.556	2.057	2.743	2.299	0.210	0.597	0.452

Q-8

16 JUNE 1983	88	1.926	2.042	2.305	1.394	2.842	2.551	0.237	0.598	0.327
17 JUNE 1983	92	1.924	2.045	2.299	1.395	2.842	2.550	0.237	0.598	0.327
19 JUNE 1983	92	1.929	2.051	2.299	1.397	2.851	2.550	0.237	0.598	0.327
21 JUNE 1983	92	1.929	2.053	2.299	1.395	2.851	2.548	0.237	0.598	0.327
23 JUNE 1983	92	1.929	2.056	2.297	1.395	2.854	2.548	0.237	0.598	0.327
28 JUNE 1983	92	1.930	2.059	2.299	1.397	2.858	2.548	0.237	0.598	0.327
30 JUNE 1983	92	1.930	2.059	2.297	1.395	2.856	2.548	0.237	0.598	0.327
5 JULY 1983	92	1.930	2.059	2.299	1.395	2.858	2.546	0.237	0.598	0.327
7 JULY 1983	92	1.930	2.057	2.299	1.391	2.854	2.543	0.237	0.598	0.327
13 JULY 1983	92	1.930	2.057	2.299	1.392	2.858	2.543	0.237	0.598	0.327
17 JULY 1983	92	1.930	2.057	2.299	1.394	2.858	2.543	0.237	0.598	0.327
19 JULY 1983	92	1.930	2.057	2.299	1.391	2.858	2.542	0.237	0.598	0.327
22 JULY 1983	92	1.930	2.057	2.299	1.391	2.858	2.540	0.237	0.598	0.327
23 JULY 1983	92	1.930	2.057	2.299	1.391	2.858	2.543	0.237	0.598	0.327
4 AUG 1983	92	1.929	2.062	2.302	1.394	2.864	2.543	0.237	0.598	0.327

Q-9

16 JUNE 1983	84	1.716	1.743	1.868	1.926	2.532	2.588	0.397	0.779	0.490
17 JUNE 1983	90	1.715	1.741	1.867	1.924	2.531	2.586	0.397	0.779	0.490
19 JUNE 1983	90	1.713	1.746	1.865	1.923	2.531	2.589	0.397	0.779	0.490
21 JUNE 1983	90	1.715	1.745	1.865	1.919	2.527	2.588	0.397	0.779	0.490
23 JUNE 1983	90	1.715	1.746	1.864	1.919	2.527	2.589	0.397	0.779	0.490
28 JUNE 1983	90	1.716	1.746	1.864	1.921	2.527	2.591	0.397	0.779	0.490
30 JUNE 1983	90	1.716	1.746	1.865	1.919	2.527	2.588	0.397	0.779	0.401
5 JULY 1983	90	1.715	1.748	1.865	1.919	2.529	2.588	0.397	0.779	0.490
7 JULY 1983	90	1.715	1.746	1.867	1.924	2.534	2.589	0.397	0.779	0.490
9 JULY 1983	90	1.715	1.748	1.864	1.921	2.531	2.589	0.397	0.779	0.490
11 JULY 1983	90	1.715	1.748	1.867	1.924	2.535	2.588	0.397	0.779	0.490
15 JULY 1983	90	1.715	1.750	1.867	1.918	2.534	2.588	0.397	0.779	0.490
17 JULY 1983	90	1.715	1.750	1.867	1.918	2.534	2.588	0.397	0.779	0.490
19 JULY 1983	90	1.715	1.750	1.867	1.924	2.537	2.588	0.397	0.779	0.490
22 JULY 1983	90	1.715	1.750	1.864	1.924	2.534	2.586	0.397	0.779	0.490
23 JULY 1983	90	1.715	1.750	1.864	1.924	2.534	2.588	0.397	0.779	0.490
4 AUG 1983	90	1.716	1.753	1.861	1.923	2.531	2.591	0.397	0.779	0.490

Q-10

19 JUNE 1983	22	2.299	1.691	1.694	2.089	2.837	2.615	0.487	0.765	0.368
21 JUNE 1983	22	2.300	1.691	1.692	2.089	2.832	2.615	0.487	0.765	0.368
23 JUNE 1983	22	2.299	1.689	1.691	2.086	2.832	2.613	0.487	0.765	0.368
26 JUNE 1983	22	2.300	1.686	1.691	2.086	2.831	2.611	0.487	0.765	0.368
30 JUNE 1983	22	2.299	1.686	1.691	2.084	2.829	2.610	0.487	0.765	0.368
5 JULY 1983	22	2.300	1.688	1.692	2.084	2.831	2.611	0.487	0.765	0.368
7 JULY 1983	22	2.300	1.686	1.692	2.086	2.831	2.613	0.487	0.765	0.368
9 JULY 1983	22	2.302	1.684	1.692	2.086	2.832	2.613	0.487	0.765	0.368
11 JULY 1983	22	2.302	1.688	1.691	2.084	2.831	2.611	0.487	0.765	0.368
13 JULY 1983	22	2.300	1.686	1.692	2.086	2.831	2.611	0.487	0.765	0.368
15 JULY 1983	22	2.299	1.688	1.694	2.088	2.832	2.613	0.487	0.765	0.368
19 JULY 1983	22	2.302	1.689	1.689	2.086	2.832	2.613	0.487	0.765	0.368
4 AUG 1983	22	2.300	1.684	1.689	2.084	2.831	2.610	0.487	0.765	0.368

Q-7

23 JULY 1983	47	1.861	1.699	1.556	2.057	2.743	2.299	0.198	0.622	0.480
21 MAY 1984	47	1.819	1.680	1.553	2.022	2.689	2.286	0.198	0.622	0.480
23 MAY 1984	47	1.818	1.681	1.549	2.018	2.688	2.283	0.198	0.622	0.480
25 MAY 1984	47	1.815	1.672	1.545	2.015	2.680	2.281	0.198	0.622	0.480
27 MAY 1984	47	1.816	1.670	1.545	2.016	2.677	2.280	0.198	0.622	0.480
29 MAY 1984	47	1.816	1.675	1.545	2.010	2.673	2.280	0.193	0.622	0.484
31 MAY 1984	47	1.815	1.665	1.541	2.008	2.669	2.278	0.198	0.630	0.491
2 JUNE 1984	47	1.818	1.672	1.538	2.011	2.670	2.280	0.198	0.630	0.491
6 JUNE 1984	47	1.813	1.654	1.537	2.007	2.661	2.275	0.178	0.616	0.496
4 AUG 1984	47	1.800	1.616	1.518	1.975	2.597	2.265	0.164	0.602	0.510
2 AUG 1985	47	1.738	1.584	1.457	1.886	2.419	2.280	0.088	0.460	0.453
12 SEP 1986	47	1.705	1.607	1.435	1.876	2.415	2.259	0.012	0.391	0.422

Q-8

4 AUG 1983	92	1.929	2.062	2.302	1.394	2.864	2.543	0.237	0.598	0.327
2 JUNE 1984	92	1.791	2.359	2.507	1.384	3.318	2.191	0.354	0.791	0.328
6 JUNE 1984	92	1.768	2.369	2.553	1.381	3.400	2.102	0.354	0.791	0.328
4 AUG 1984	92	1.788	2.600	2.913	1.383	3.958	1.732	0.421	1.063	0.343
2 AUG 1985	96	0.000	0.000	4.669	1.381	5.936	0.000	-1.253	1.808	0.340

Q-9

4 AUG 1983	90	1.716	1.753	1.861	1.923	2.531	2.591	0.388	0.733	0.474
21 MAY 1984	90	1.695	1.738	1.830	1.835	2.418	2.592	0.388	0.733	0.474
23 MAY 1984	90	1.683	1.727	1.826	1.829	2.408	2.575	0.388	0.733	0.474
25 MAY 1984	90	1.683	1.724	1.826	1.829	2.402	2.578	0.388	0.733	0.474
27 MAY 1984	90	1.683	1.718	1.819	1.826	2.399	2.575	0.388	0.733	0.474
29 MAY 1984	90	1.688	1.716	1.811	1.826	2.394	2.572	0.384	0.717	0.466
31 MAY 1984	90	1.680	1.713	1.813	1.824	2.391	2.567	0.387	0.715	0.467
2 JUNE 1984	90	1.689	1.718	1.805	1.824	2.392	2.570	0.387	0.715	0.467
6 JUNE 1984	90	1.678	1.710	1.794	1.822	2.375	2.567	0.387	0.694	0.461
4 AUG 1984	90	1.680	1.684	1.727	1.815	2.323	2.545	0.369	0.607	0.428
29 APR 1985	90	1.643	1.670	1.688	1.803	2.269	2.524	0.345	0.546	0.396
15 MAY 1985	90	1.551	1.686	1.607	1.810	2.194	2.496	0.293	0.434	0.340
5 JUNE 1985	90	1.502	1.695	1.572	1.816	2.164	2.480	0.272	0.402	0.311
2 AUG 1985	90	1.511	1.686	1.562	1.816	2.175	2.470	0.259	0.397	0.308
12 SEP 1986	90	1.437	1.699	1.505	1.846	2.149	2.440	0.263	0.391	0.266

Q-10

29R APR 1985	0	1.683	1.505	1.961	1.534	2.372	2.362	0.356	0.434	0.185
16 MAY 1985	0	1.673	1.476	1.913	1.527	2.318	2.351	0.417	0.425	0.040
5 JUNE 1985	0	1.664	1.449	1.868	1.514	2.257	2.350	0.464	0.400	0.008
2 JUNE 1985	0	1.662	1.449	1.856	1.505	2.234	2.356	0.489	0.383	-0.016
2 AUG 1985	0	1.662	1.449	1.856	1.505	2.234	2.356	0.489	0.383	-0.016
12 SEP 1986	27	1.464	1.622	1.791	1.559	2.146	2.367	0.482	0.230	-0.181

Q-11

17 JUNE 1983	43	1.889	1.429	1.743	1.875	2.710	2.148	0.513	0.672	0.267
21 JUNE 1983	43	1.883	1.432	1.736	1.878	2.708	2.145	0.513	0.672	0.267
23 JUNE 1983	43	1.881	1.434	1.735	1.875	2.705	2.145	0.513	0.672	0.267
26 JUNE 1983	43	1.878	1.434	1.734	1.875	2.704	2.145	0.513	0.672	0.267
28 JUNE 1983	43	1.878	1.434	1.734	1.878	2.704	2.145	0.513	0.672	0.267
30 JUNE 1983	43	1.877	1.434	1.734	1.875	2.700	2.145	0.513	0.672	0.267
7 JULY 1983	43	1.873	1.434	1.731	1.875	2.699	2.141	0.513	0.672	0.267
9 JULY 1983	43	1.873	1.434	1.732	1.875	2.699	2.145	0.513	0.672	0.267
11 JULY 1983	43	1.870	1.434	1.732	1.875	2.696	2.145	0.513	0.672	0.267
13 JULY 1983	43	1.873	1.432	1.734	1.877	2.699	2.146	0.513	0.672	0.267
15 JULY 1983	43	1.873	1.434	1.734	1.877	2.699	2.146	0.513	0.672	0.267
17 JULY 1983	46	1.873	1.434	1.734	1.875	2.699	2.145	0.471	0.622	0.235
19 JULY 1983	43	1.873	1.434	1.734	1.877	2.699	2.146	0.513	0.672	0.267
22 JULY 1983	43	1.873	1.435	1.734	1.877	2.699	2.146	0.513	0.672	0.267
23 JULY 1983	43	1.870	1.435	1.735	1.877	2.700	2.146	0.513	0.672	0.267
4 AUG 1983	43	1.870	1.434	1.726	1.877	2.696	2.140	0.513	0.672	0.267

Q-12

19 JUNE 1983	36	2.464	1.878	2.316	1.700	3.173	2.780	0.889	0.821	0.084
21 JUNE 1983	36	2.464	1.878	2.316	1.699	3.170	2.778	0.889	0.821	0.084
23 JUNE 1983	36	2.459	1.878	2.316	1.697	3.169	2.776	0.889	0.820	0.084
26 JUNE 1983	36	2.454	1.878	2.313	1.695	3.162	2.778	0.889	0.821	0.084
5 JULY 1983	36	2.453	1.878	2.316	1.697	3.161	2.780	0.889	0.821	0.084
7 JULY 1983	36	2.453	1.877	2.316	1.694	3.161	2.775	0.889	0.821	0.084
11 JULY 1983	36	2.451	1.877	2.313	1.695	3.161	2.776	0.889	0.821	0.084
22 JULY 1983	36	2.451	1.877	2.318	1.695	3.162	2.775	0.889	0.821	0.084
4 AUG 1983	36	2.445	1.872	2.311	1.692	3.154	2.772	0.889	0.821	0.084

Q-11

4 AUG 1983	43	1.870	1.434	1.726	1.877	2.696	2.140	0.561	0.623	0.258
21 MAY 1984	43	1.826	1.453	1.705	1.902	2.684	2.135	0.561	0.623	0.258
23 MAY 1984	43	1.813	1.449	1.702	1.903	2.681	2.129	0.561	0.623	0.258
25 MAY 1984	43	1.807	1.451	1.700	1.905	2.681	2.126	0.561	0.623	0.258
27 MAY 1984	43	1.807	1.453	1.699	1.910	2.681	2.124	0.561	0.623	0.258
29 MAY 1984	43	1.810	1.451	1.694	1.911	2.683	2.126	0.455	0.630	0.265
31 MAY 1984	43	1.811	1.449	1.694	1.911	2.683	2.124	0.455	0.630	0.265
2 JUNE 1984	43	1.808	1.454	1.697	1.915	2.686	2.122	0.455	0.630	0.265
4 AUG 1984	43	1.789	1.454	1.670	1.919	2.678	2.099	0.447	0.680	0.325
29 APR 1985	43	1.783	1.449	1.661	1.921	2.665	2.099	0.423	0.714	0.365
16 MAY 1985	43	1.751	1.434	1.619	1.910	2.613	2.084	0.471	0.772	0.440
5 JUNE 1985	43	1.718	1.413	1.580	1.899	2.559	2.073	0.457	0.777	0.466
2 AUG 1985	43	1.699	1.407	1.564	1.887	2.534	2.062	0.452	0.771	0.470
12 SEP 1986	43	1.581	1.394	1.445	1.895	2.411	2.008	0.326	0.716	0.528

Q-12

4 AUG 1983	36	2.445	1.872	2.311	1.692	3.154	2.772	0.774	0.686	-0.029
23 MAY 1984	36	2.296	1.853	2.232	1.657	2.953	2.767	0.774	0.686	-0.029
25 MAY 1984	36	2.296	1.849	2.224	1.654	2.943	2.762	0.774	0.686	-0.029
27 MAY 1984	36	2.292	1.849	2.219	1.656	2.942	2.761	0.774	0.686	-0.029
29 MAY 1984	36	2.292	1.846	2.216	1.653	2.938	2.757	0.779	0.683	-0.021
31 MAY 1984	36	2.291	1.846	2.213	1.656	2.942	2.756	0.779	0.683	-0.021
2 JUNE 1984	36	2.288	1.846	2.213	1.654	2.935	2.754	0.779	0.683	-0.021
5 JUNE 1984	36	2.286	1.840	2.207	1.654	2.934	2.750	0.773	0.676	-0.016
4 AUG 1984	36	2.251	1.832	2.148	1.641	2.865	2.727	0.747	0.620	-0.016
29APR 1985	36	2.213	1.803	2.059	1.626	2.718	2.746	0.653	0.470	-0.099
29R APR 1985	36	2.407	1.849	2.059	1.768	2.983	2.746	0.787	0.628	0.059
15 MAY 1985	36	2.286	1.819	1.870	1.753	2.724	2.734	0.670	0.435	0.032
5 JUNE 1985	36	2.219	1.811	1.797	1.756	2.597	2.748	0.559	0.320	0.019
2 AUG 1985	36	2.211	1.822	1.788	1.753	2.569	2.772	0.518	0.283	0.012
12 SEP 1986	36	2.162	1.911	1.803	1.732	2.448	2.892	0.380	0.099	-0.075

Q-13

29R APR 1985	78	1.822	1.446	2.443	1.594	2.381	2.807	0.004	0.253	0.173
16 MAY 1985	78	1.818	1.429	2.423	1.572	2.365	2.778	0.073	0.235	0.060
5 JUNE 1985	78	1.808	1.419	2.413	1.561	2.353	2.762	0.000	0.265	0.192
2 AUG 1985	78	1.797	1.410	2.397	1.546	2.340	2.743	0.001	0.265	0.193
12 SEP 1986	78	1.810	1.395	2.369	1.521	2.346	2.705	0.012	0.257	0.189

Q-13

19 JUNE 1983	78	2.291	1.602	1.732	1.597	2.670	2.432	0.320	0.434	0.254
23 JUNE 1983	78	2.292	1.604	1.734	1.599	2.673	2.434	0.320	0.434	0.254
26 JUNE 1983	78	2.291	1.604	1.737	1.600	2.673	2.435	0.320	0.434	0.254
30 JUNE 1983	78	2.289	1.604	1.737	1.602	2.672	2.437	0.320	0.434	0.254
5 JULY 1983	78	2.288	1.604	1.735	1.600	2.672	2.435	0.320	0.434	0.254
7 JULY 1983	78	2.288	1.604	1.740	1.600	2.678	2.434	0.320	0.434	0.254
9 JULY 1983	78	2.289	1.604	1.738	1.600	2.673	2.437	0.320	0.434	0.254
11 JULY 1983	78	2.292	1.605	1.740	1.600	2.680	2.435	0.320	0.434	0.254
13 JULY 1983	78	2.289	1.604	1.740	1.600	2.673	2.435	0.320	0.434	0.254
15 JULY 1983	78	2.291	1.605	1.740	1.600	2.675	2.435	0.320	0.434	0.254
23 JULY 1983	78	2.299	1.602	1.737	1.597	2.677	2.432	0.378	0.474	0.249

Q-14

19 JUNE 1983	65	1.764	1.759	1.826	1.878	2.800	2.280	0.139	0.335	0.165
21 JUNE 1983	65	1.765	1.759	1.826	1.880	2.802	2.283	0.139	0.335	0.165
23 JUNE 1983	65	1.765	1.760	1.827	1.880	2.804	2.281	0.139	0.317	0.143
28 JUNE 1983	65	1.764	1.760	1.827	1.880	2.804	2.281	0.133	0.308	0.140
30 JUNE 1983	65	1.764	1.760	1.827	1.878	2.802	2.281	0.139	0.335	0.165
5 JULY 1983	65	1.764	1.765	1.826	1.878	2.807	2.280	0.139	0.335	0.165
7 JULY 1983	65	1.765	1.765	1.826	1.878	2.807	2.281	0.139	0.335	0.165
9 JULY 1983	65	1.765	1.762	1.826	1.878	2.807	2.280	0.139	0.335	0.152
4 AUG 1983	65	1.764	1.759	1.824	1.881	2.804	2.278	0.139	0.335	0.165

Q-26

18 MAY 1984	-20	2.789	2.584	3.415	2.230	4.196	3.605	0.788	0.962	0.118
19 MAY 1984	-20	2.788	2.586	3.413	2.234	4.188	3.616	0.788	0.962	0.118
21 MAY 1984	-20	2.791	2.592	3.413	2.245	4.169	3.648	0.788	0.962	0.118
23 MAY 1984	-20	2.784	2.599	3.416	2.256	4.153	3.677	0.788	0.962	0.118
25 MAY 1984	-20	2.780	2.605	3.413	2.269	4.135	3.705	0.793	0.939	0.099
27 MAY 1984	-20	2.778	2.610	3.415	2.280	4.120	3.735	0.793	0.939	0.099
29 MAY 1984	-20	2.777	2.616	3.413	2.291	4.107	3.754	0.794	0.927	0.082
31 MAY 1984	-20	2.778	2.621	3.410	2.302	4.094	3.775	0.793	0.919	0.073
2 JUNE 1984	-20	2.780	2.627	3.410	2.318	4.078	3.808	0.793	0.919	0.073
6 JUNE 1984	-20	2.770	2.643	3.415	2.345	4.040	3.867	0.799	0.902	0.054
4 AUG 1984	-20	2.742	2.757	3.412	2.569	3.850	4.237	0.812	0.794	-0.050
29 APR 1985	-20	2.734	2.861	3.383	2.748	3.720	4.512	0.826	0.735	-0.104
16 MAY 1985	-20	2.654	3.119	3.404	3.245	3.554	5.105	0.835	0.581	-0.255
5 JUNE 1985	-20	2.592	3.378	3.402	3.512	3.477	5.385	0.825	0.493	-0.346
2 AUG 1985	-20	2.578	3.388	3.399	3.550	3.742	5.409	0.816	0.466	-0.371
12 SEP 1986	-20	2.419	3.864	3.400	4.248	3.496	6.061	0.752	0.254	-0.579

Q-27

18 MAY 1984	82	2.800	4.594	2.267	4.582	5.304	5.177	0.139	1.300	1.493
19 MAY 1984	82	2.802	4.591	2.265	4.577	5.301	5.139	0.139	1.300	1.493
21 MAY 1984	82	2.805	4.588	2.267	4.566	5.302	5.132	0.139	1.300	1.493
23 MAY 1984	82	2.802	4.575	2.281	4.559	5.291	5.128	0.139	1.300	1.493
25 MAY 1984	82	2.800	4.556	2.265	4.550	5.286	5.112	0.140	1.299	1.493
27 MAY 1984	82	2.800	4.548	2.267	4.543	5.275	5.105	0.140	1.299	1.493
29 MAY 1984	82	2.800	4.542	2.267	4.537	5.274	5.102	0.141	1.301	1.499
31 MAY 1984	82	2.802	4.542	2.269	4.529	5.266	5.094	0.137	1.298	1.495
2 JUNE 1984	82	2.800	4.526	2.270	4.524	5.256	5.093	0.137	1.298	1.495
6 JUNE 1984	82	2.797	4.496	2.269	4.493	5.223	5.061	0.144	1.305	1.500
4 AUG 1984	82	2.786	4.393	2.269	4.388	5.126	4.977	0.082	1.315	1.566
29 APR 1985	82	2.770	4.247	2.265	4.242	4.983	4.858	0.154	1.314	1.510
16 MAY 1985	82	2.753	4.064	2.265	4.051	4.802	4.712	0.156	1.317	1.519
5 JUNE 1985	82	2.745	3.985	2.267	3.978	4.739	4.645	0.147	1.317	1.511
2 AUG 1985	82	2.743	3.983	2.273	3.979	4.734	4.645	0.149	1.309	1.507
12 SEP 1986	82	2.732	3.826	2.267	3.821	4.593	4.513	0.233	1.292	1.486

Q-28

18 MAY 1984	23	3.177	4.331	2.740	4.278	5.050	5.380	0.381	0.394	0.266
19 MAY 1984	23	3.177	4.337	2.743	4.280	5.050	5.385	0.381	0.394	0.266
21 MAY 1984	23	3.177	4.334	2.742	4.288	5.063	5.374	0.381	0.394	0.266
23 MAY 1984	23	3.172	4.331	2.738	4.228	5.067	5.369	0.381	0.394	0.266
25 MAY 1984	23	3.172	4.332	2.737	4.291	5.077	5.363	0.381	0.391	0.269
27 MAY 1984	23	3.170	4.332	2.734	4.296	5.083	5.359	0.381	0.391	0.269
29 MAY 1984	23	3.173	4.335	2.732	4.299	5.091	5.359	0.380	0.389	0.270
31 MAY 1984	23	3.175	4.342	2.731	4.302	5.097	5.351	0.380	0.389	0.270
2 JUNE 1984	23	3.177	4.343	2.727	4.308	5.110	5.351	0.380	0.389	0.270
6 JUNE 1984	23	3.171	4.347	2.726	4.315	5.126	5.347	0.379	0.386	0.273
4 AUG 1984	23	3.180	4.389	2.705	4.377	5.245	5.301	0.377	0.372	0.278
29 APR 1985	23	3.185	4.443	2.705	4.432	5.382	5.261	0.387	0.358	0.275
5 JUNE 1985	23	3.181	4.578	2.667	4.578	5.663	5.166	0.379	0.341	0.295
2 AUG 1985	23	3.183	4.575	2.675	4.585	5.678	5.133	0.379	0.342	0.296
12 SEP 1986	23	3.185	4.740	2.629	4.794	5.985	5.110	0.372	0.326	0.302

Q-29

18 MAY 1984	-13	1.981	2.310	2.216	2.654	3.172	3.307	0.334	0.738	0.306
19 MAY 1984	-13	1.981	2.311	2.218	2.651	3.191	3.288	0.334	0.738	0.306
21 MAY 1984	-13	1.981	2.307	2.215	2.645	3.229	3.243	0.334	0.738	0.306
23 MAY 1984	-13	1.975	2.310	2.215	2.635	3.264	3.200	0.334	0.738	0.306
25 MAY 1984	-13	1.973	2.310	2.213	2.629	3.304	3.153	0.338	0.768	0.332
27 MAY 1984	-13	1.978	2.316	2.211	2.627	3.345	3.113	0.338	0.768	0.332
29 MAY 1984	-13	1.978	2.319	2.211	2.626	3.377	3.081	0.341	0.797	0.359
31 MAY 1984	-13	1.975	2.329	2.210	2.626	3.410	3.051	0.342	0.807	0.368
2 JUNE 1984	-13	1.984	2.338	2.210	2.630	3.459	3.008	0.342	0.807	0.368
6 JUNE 1984	-13	1.978	2.364	2.210	2.635	3.540	2.929	0.337	0.844	0.393
4 AUG 1984	-13	1.983	2.688	2.210	2.867	4.185	2.535	0.337	1.025	0.545
29 APR 1985	-13	1.964	2.981	2.188	3.121	4.612	2.410	0.347	1.151	0.659
16 MAY 1985	-13	1.692	3.794	2.140	3.921	5.593	2.572	0.354	1.448	0.918
5 JUNE 1985	-13	1.970	4.296	2.086	4.447	6.159	2.886	0.349	1.614	1.081
2 AUG 1985	-13	1.967	4.407	2.076	4.576	6.258	2.988	0.345	1.651	1.121
12 SEP 1986	-13	2.019	5.694	1.969	5.880	7.610	4.102	0.343	2.015	1.557

Q-32

29 MAY 1984	-11	4.661	2.553	4.678	4.724	5.840	5.794	0.724	0.684	-0.092
31 MAY 1984	-11	4.666	2.553	4.678	4.728	5.824	5.798	0.724	0.684	-0.092
2 JUNE 1984	-11	4.669	2.554	4.680	4.731	5.845	5.809	0.724	0.684	-0.092
6 JUNE 1984	-11	4.672	2.551	4.682	4.731	5.834	5.809	0.724	0.686	-0.097
4 AUG 1984	-11	4.674	2.538	4.682	4.721	5.775	5.861	0.732	0.684	-0.109
29 APR 1985	-11	4.672	2.523	4.712	4.715	5.731	5.918	0.732	0.686	-0.126
16 MAY 1985	-11	4.677	2.476	4.785	4.693	5.566	6.074	0.801	0.705	-0.174
5 JUNE 1985	-11	4.662	2.445	4.829	4.686	5.493	6.144	0.794	0.710	-0.212
2 AUG 1985	-11	4.658	2.442	4.826	4.677	5.480	6.144	0.791	0.710	-0.222
12 SEP 1986	-11	4.640	2.346	5.007	4.670	5.223	6.412	0.782	0.747	-0.332

Q-33

2 JUNE 1984	27	2.570	2.061	3.059	1.446	3.454	3.127	0.216	0.718	0.264
5 JUNE 1984	27	2.567	2.057	3.054	1.445	3.448	3.127	0.215	0.723	0.270
7 JUNE 1984	27	2.569	2.056	3.045	1.448	3.437	3.132	0.213	0.728	0.276
3 AUG 1983	27	2.596	2.026	3.004	1.411	3.386	3.148	0.202	0.753	0.286
28 APR 1985	27	2.594	2.015	2.965	1.416	3.343	3.156	0.201	0.770	0.315
28R APR 1985	27	2.594	2.015	2.961	1.387	3.343	3.131	0.201	0.770	0.315
30.APR 1985	27	2.596	2.008	2.954	1.386	3.331	3.131	0.200	0.771	0.313
15 MAY 1995	27	2.591	1.986	2.902	1.359	3.251	3.140	0.189	0.784	0.314
18 MAY 1985	27	2.594	1.984	2.897	1.359	3.245	3.146	0.189	0.785	0.315
4 JUNE 1985	27	2.615	1.975	2.877	1.346	3.219	3.137	0.188	0.787	0.313
2 JUNE 1985	27	2.594	1.965	2.864	1.327	3.210	3.127	0.180	0.779	0.305
12 SEP 1986	27	2.597	1.964	2.848	1.305	3.183	3.127	0.189	0.778	0.298

Q-34

2 JUNE 1984	97	2.326	2.465	2.610	3.340	3.778	3.777	0.481	0.911	0.294
5 JUNE 1984	97	2.326	2.467	2.608	3.353	3.781	3.783	0.488	0.919	0.296
7 JUNE 1984	97	2.319	2.473	2.615	3.354	3.783	3.785	0.495	0.926	0.298
3 AUG 1984	97	2.326	2.497	2.602	3.416	3.831	3.797	0.542	0.974	0.294
28 APR 1985	97	2.315	2.588	2.616	3.426	3.921	3.807	0.545	0.996	0.322
30 APR 1985	97	2.311	2.588	2.623	3.426	3.910	3.808	0.547	1.000	0.321
15 MAY 1985	97	2.324	2.600	2.635	3.448	3.927	3.828	0.578	1.036	0.337
18 MAY 1985	97	2.327	2.597	2.635	3.448	3.927	3.826	0.581	1.036	0.337
4 JUNE 1985	97	2.323	2.602	2.648	3.448	3.937	3.826	0.592	1.046	0.341
2 AUG 1985	97	2.315	2.604	2.642	3.461	3.947	3.826	0.651	1.046	0.339
12 SEP 1986	97	2.308	2.727	2.640	3.464	4.051	3.794	0.595	1.107	0.375

Q-35

2 JUNE 1984	-96.5	10.889	10.117	12.881	10.966	14.091	17.439	1.422	0.843	-0.319
5 JUNE 1984	-96.5	10.889	10.124	12.894	10.971	14.095	17.448	1.433	0.851	-0.321
7 JUNE 1984	-96.5	10.889	10.125	12.897	10.973	14.107	17.448	1.421	0.836	-0.323
3 AUG 1984	-96.5	10.878	10.143	12.913	10.978	14.129	17.450	1.394	0.773	-0.358
28R APR 1985	0	10.470	13.910	12.830	13.814	18.104	18.034	0.354	1.410	1.137
15 MAY 1985	-96.5	10.497	13.891	12.814	13.805	18.097	18.028	0.415	1.412	1.066
4 JUNE 1985	-96.5	10.525	14.176	12.840	13.799	18.110	18.139	0.456	1.431	1.041
2 AUG 1985	-96.5	0.000	0.000	12.865	13.792	18.126	0.000	-1.713	1.575	1.029

Q-85

28 APR 1985	112	2.788	1.975	3.724	2.556	3.931	3.923	0.237	0.433	0.344
30 APR 1985	112	2.804	1.978	3.724	2.559	3.980	3.878	0.249	0.448	0.334
15 MAY 1985	112	3.204	1.959	3.848	2.553	4.696	3.496	0.404	0.626	0.346
18 MAY 1985	112	3.251	1.954	3.872	2.559	4.766	3.477	0.417	0.640	0.343
4 JUNE 1985	112	3.535	1.946	4.023	2.553	5.115	3.391	0.485	0.711	0.335
2 AUG 1985	112	3.673	1.929	4.115	2.556	5.315	3.367	0.543	0.765	0.344
12 SEP 1986	112	4.534	1.899	4.724	2.550	6.271	3.526	0.721	0.933	0.346

Q-86

29 APR 1985	0	3.777	4.494	3.867	4.880	5.415	6.610	0.396	0.660	0.333
16 MAY 1985	0	3.693	4.493	3.858	4.891	5.337	6.618	0.429	0.880	0.567
18 MAY 1985	0	3.696	4.496	3.858	4.889	5.334	6.631	0.431	0.897	0.587
5 JUNE 1985	0	3.699	4.496	3.835	4.915	5.309	6.655	0.449	0.990	0.712
2 AUG 1985	0	3.705	4.509	3.823	4.947	5.312	6.690	0.443	1.029	0.764
12 SEP 1986	102	3.715	4.740	3.769	5.124	5.378	6.896	0.471	1.241	1.033

Q-87

29 APR 1985	0	2.854	4.264	3.021	4.524	5.109	5.448	0.185	0.301	0.201
16 MAY 1985	0	2.791	4.369	3.023	4.588	5.255	5.420	0.196	0.309	0.186
5 JUNE 1985	0	2.780	4.428	3.023	4.645	5.363	5.397	0.199	0.306	0.189
2 AUG 1985	0	2.770	4.443	3.024	4.653	5.386	5.394	0.196	0.303	0.187
12 SEP 1986	0	2.602	4.686	3.023	4.763	5.591	5.394	0.216	0.313	0.212

Q-TL

28 APR 1985	0	3.454	4.970	1.975	6.991	6.947	5.967	-0.287	-1.304	-1.500
30 APR 1985	0	3.443	4.962	1.975	6.972	6.928	5.963	-0.291	-1.305	-1.504
16 MAY 1985	0	3.297	4.858	1.959	6.782	6.655	5.915	-0.362	-1.341	-1.562
18 MAY 1985	0	3.289	4.848	1.956	6.771	6.639	5.906	-0.367	-1.342	-1.565
4 JUNE 1985	0	3.229	4.810	1.949	6.702	6.547	5.882	-0.388	-1.350	-1.576
2 AUG 1985	0	3.207	4.796	1.929	6.679	6.504	5.872	-0.392	-1.347	-1.569
12 SEP 1986	-3	3.051	4.705	1.899	6.534	6.309	5.798	-0.393	-1.379	-1.591

Appendix D

DISPLACEMENTS AT QUADRILATERALS

Displacements at quadrilaterals are reported here as *xyz*-components; *x*, *y* and *z* are determined according to the following conventions. The *xy*-plane is horizontal, and the azimuth of the reference line gives the orientation of the positive *x*-direction. The positive *y*-direction is 90° counterclockwise from *x*. The positive *z*-direction is vertical downward. The *xyz*-coordinates so defined are left-handed.

Displacements are reported in centimeters (cm).

Q-1 azimuth AB = S. 53° W.

Dates	Stake	x	y	z
6/15/83--8/4/83	D	-0.3	3.5	-
	C	-1.0	0.9	-
8/4/83--5/21/84	D	-5.6	16.0	26.4
	C	-5.7	3.9	10.6
5/21/84--8/3/84	D	-4.9	18.8	7.2
	C	-5.4	9.8	9.1
8/3/84--4/30/85	D	-1.1	0.0	4.0
	C	-4.4	-1.4	2.2
4/30/85--8/2/85	D	-6.1	9.3	1.4
	C	-9.0	8.6	2.5
8/2/85--9/12/86	D	-0.8	1.9	0.3
	C	-1.4	1.5	0.0

Q-2 azimuth DC = N. 39° W.

Dates	Stake	x	y	z
6/15/83--8/4/83	A	13.6	2.4	-
	B	14.4	3.0	-

8/4/83--5/23/84	A	220.9	20.9	-
	B	214.1	26.9	-
5/23/84--8/3/84*	A	155.3	36.0	-4.2
	B	156.5	32.7	10.9
8/3/84*--4/28/85	A	26.1	11.9	-3.2
	B	25.4	15.4	3.4
4/28/85--8/2/85	A	106.2	17.9	-5.9
	B	104.3	14.6	10.3
8/2/85--9/12/86	A	29.2	8.1	8.6
	B	32.1	2.6	6.7

Q-3 azimuth AB = N. 31° W.

Dates	Stake	x	y	z
6/16/83--8/4/83	D	10.1	-4.1	-
	C	10.0	-3.3	-
8/4/83--6/5/84*	D	186.6	-46.1	38.3
	C	199.7	-55.5	25.6
6/5/84*--8/3/84	D	76.3	-23.5	8.1
	C	68.4	-21.3	6.6
8/3/84--4/29/85	D	55.5	-17.8	8.0
	C	52.7	-19.1	6.9
4/29/85--8/2/85	D	182.2	-54.3	22.2
	C	175.2	-51.9	19.8
8/2/85--9/12/86	D	90.0	-27.8	10.8
	C	87.1	-37.4	8.7

Q-5 azimuth AD = N. 57° E.

Dates	Stake	x	y	z
8/2/85--9/12/86	B	1.2	0	13.1
	C	-1.4	5.1	-10.3

Q-6 azimuth AB = N. 78° W.

Dates	Stake	x	y	z
6/16/83--8/4/83	D	53.8	10.1	10.8
	C	51.9	7.4	10.3
8/4/83--5/21/84	D	205.5	22.6	42.2
	C	205.2	15.3	39.9
5/21/84--8/4/84	D	370.0	53.7	44.1
	C	348.0	50.9	46.9
8/4/84--4/29/85	D	107.4	43.0	18.3
	C	115.1	5.6	16.5

4/29/85--8/2/85	D	427.8	1.3	59.8
	C	417.4	13.0	50.0
8/2/85--9/12/86	D	441.0	65.8	78.8
	C	434.1	33.7	77.5

Q-8 azimuth AD = N. 37° W.

Dates	Stake	x	y	z
6/16/83--8/4/84	B	2.7	0.5	-
	C	4.4	0.8	-
8/4/83--6/2/84	C	65.3	0.6	19.3
6/2/84--8/4/84	C	83.8	-9.3	27.2
8/4/84--8/2/85	C	215.2	-14.8	74.5
8/2/85--9/12/86	C	40.3	101.7	25.4

Q-26 azimuth CD = N. 13° W.

Dates	Stake	x	y	z
5/18/84--8/4/84	A	61.6	29.6	16.8
	B	56.5	28.7	19.3
8/4/84--4/29/85	A	27.1	11.6	5.4
	B	24.4	10.8	7.2
4/29/85--8/2/85*	A	94.3	45.2	26.7
	B	53.3	45.8	25.9
8/2/85*--9/12/86	A	71.8	34.9	20.8
	B	89.5	21.4	14.8

Q-27 azimuth CD = S. 41° W.

Dates	Stake	x	y	z
5/18/84--8/4/84	A	-8.0	-24.5	-7.3
	B	-3.1	-22.9	-7.2
8/4/84--4/29/85	A	8.0	12.5	5.6
	B	6.1	13.0	7.3
4/29/85--8/2/85	A	5.9	-27.6	0.3
	B	3.9	-27.5	0.0
8/2/85--9/12/86	A	3.3	-16.0	2.0
	B	-0.3	-13.4	10.1

Q-28 azimuth AB = N. 82° W.

Dates	Stake	x	y	z
5/18/84--8/4/84	D	27.5	9.7	1.2
	C	23.8	8.1	-2.3
8/4/84--4/29/85	D	15.7	4.7	-0.3
	C	14.8	6.2	-1.4
4/29/85--8/2/85	D	36.1	11.3	2.1
	C	39.6	12.9	-1.6
8/2/85--9/12/86	D	37.0	14.3	0.7
	C	30.3	14.0	-1.6

Q-29 azmiuth AB = N. 34° W.

Dates	Stake	x	y	z
5/18/84--8/4/84*	D	138.9	-15.8	23.9
	C	139.8	-17.9	28.8
8/4/84*--4/29/85	D	56.3	-9.0	11.4
	C	49.6	-9.1	12.6
4/29/85--8/2/85*	D	196.4	-20.6	46.2
	C	184.4	-41.7	50.0
8/2/85*--9/12/86	D	133.6	8.1	43.6
	C	126.3	29.3	36.4

Q-32 azimuth AB = N. 14° W.

Dates	Stake	x	y	z
5/29/84--8/4/84	D	-7.2	1.4	-1.8
8/4/84--4/29/85	D	-7.0	0.9	-1.7
4/29/85--8/2/85	D	-33.6	1.9	-9.6
8/2/85--9/12/86	D	-37.5	2.5	-11.0

(Stakes A, B, and C are on the landslide, and Stake D is off the landslide.)

Q-85 azimuth AD = N. 45° W.

Dates	Stake	x	y	z
4/28/85--8/2/85	B	190.5	-29.8	30.6
	C	186.1	41.2	33.2
8/2/85--9/12/86	B	112.5	-38.8	17.8
	C	113.1	23.7	16.8

Q-87 azimuth CD = N. 61° W.

Dates	Stake	x	y	z
4/29/85--8/2/85	A	-27.3	15.7	-1.4
	B	-36.4	19.8	0.8
8/2/85--9/12/86	A	-20.3	11.8	-2.5
	B	-36.6	23.2	1.1

Q-TL azimuth CD = N. 81° W.

Dates	Stake	x	y	z
4/29/85--8/2/85	A	40.3	-41.5	-6.9
	B	17.5	-26.9	-6.3
8/2/85--9/12/86	A	18.4	-20.3	2.2
	B	0.5	-12.5	3.2

<u>Appendix E</u>

SOLUTION OF EQUATIONS FOR PRINCIPAL STRETCHES

Because analytic expressions for computing the magnitudes and directions of principal stretches from the stretches in three aribtrary directions are not available in any standard references, I present a brief derivation. These equations were originally derived by Arvid Johnson in 1983; I have checked them and made corrections.

Equaton 6.6 in the text of Chapter VI can be rewritten using the notation of Figure 6.3:

$$(1/\underline{S}_{\underline{AB}}^2) = (1/\underline{S}_1^2)\cos^2(\beta_{\underline{AB}}) + (1/\underline{S}_2^2)\sin^2(\beta_{\underline{AB}}), \qquad \text{(E1a)}$$

$$(1/\underline{S}_{\underline{BC}}^2) = (1/\underline{S}_1^2)\cos^2(\beta_{\underline{BC}}) + (1/\underline{S}_2^2)\sin^2(\beta_{\underline{BC}}), \qquad \text{(E1b)}$$

and

$$(1/\underline{S}_{\underline{AC}}^2) = (1/\underline{S}_1^2)\cos^2(\beta_{\underline{AC}}) + (1/\underline{S}_2^2)\sin^2(\beta_{\underline{AC}}), \qquad \text{(E1c)}$$

Equations E1a, E1b, and E1c can be rewritten by using trigonometric identities that relate $\cos(2\beta)$ to $\cos^2(\beta)$ and $\sin^2(\beta)$, and by making the substitution (Fig. 6.3):

$$\alpha + \theta_{\underline{i}} = \beta_{\underline{i}},$$

$$(1/\underline{S}_{\underline{AB}}^2) = (1/2)\ \{[1/\underline{S}_1^2 + 1/\underline{S}_2^2]$$
$$+ [1/\underline{S}_1^2 - 1/\underline{S}_2^2]\cos 2(\alpha + \theta'_{\underline{AB}})\}, \qquad \text{(E2a)}$$

$$(1/\underline{S}_{\underline{BC}}^2) = (1/2)\ \{[1/\underline{S}_1^2 + 1/\underline{S}_2^2]$$

$$+\ [1/\underline{S}_1\ -\ 1/\underline{S}_2]\ \cos 2(\alpha + \theta'_{\underline{BC}})\}, \tag{E2b}$$

and

$$(1/\underline{S}_{\underline{AC}}^2) = (1/2)\ \{[1/\underline{S}_1^2 + 1/\underline{S}_2^2]$$

$$+\ [1/\underline{S}_1^2\ -\ 1/\underline{S}_2^2]\ \cos (2\alpha)\}, \tag{E2c}$$

Subtracting equations E2b from E2a, and E2c from E2a, yields:

$$1/\underline{S}_{\underline{AB}}^2 - 1/\underline{S}_{\underline{BC}}^2 = (1/\underline{S}_1^2 - 1/\underline{S}_2^2)\ \{\cos 2(\alpha + \theta'_{\underline{AB}})$$

$$-\ \cos 2(\alpha + \theta'_{\underline{BC}})\}; \tag{E3a}$$

$$1/\underline{S}_{\underline{AB}}^2 - 1/\underline{S}_{\underline{AC}}^2 = (1/\underline{S}_1^2 - 1/\underline{S}_2^2)\ \{\cos 2(\alpha + \theta'_{\underline{AB}})$$

$$-\ \cos (2\alpha)\}; \tag{E3b}$$

Dividing equation E3a by E3b yields:

$$\frac{1/\underline{S}_{\underline{AB}}^2 - 1/\underline{S}_{\underline{BC}}^2}{1/\underline{S}_{\underline{AB}}^2 - 1/\underline{S}_{\underline{AC}}^2} = \frac{\cos 2(\alpha + \theta'_{\underline{AB}}) - \cos 2(\alpha + \theta'_{\underline{BC}})}{\cos 2(\alpha + \theta'_{\underline{AB}}) - \cos (2\alpha)} \tag{E4}$$

The angle addition formula for cosines is used to isolate terms containing α and rearrange equation E4 to solve for α. Thus,

$$\alpha = (1/2)\ \tan^{-1}\{[(\cos (2\theta'_{\underline{AB}}) - 1)\ (1/\underline{S}_{\underline{AB}}^2 - 1/\underline{S}_{\underline{BC}}^2)/$$

$$(1/\underline{S}_{\underline{AB}}^2 - 1/\underline{S}_{\underline{AC}}^2) + \cos (2\theta'_{\underline{BC}}) - \cos (2\theta'_{\underline{AB}})]$$

$$/[\sin (2\theta'_{\underline{AB}})\ (1/\underline{S}_{\underline{AB}}^2 - 1/\underline{S}_{\underline{BC}}^2)/(1/\underline{S}_{\underline{AB}}^2 - 1/\underline{S}_{\underline{AC}}^2)$$

$$+ \sin (2\theta'_{\underline{BC}}) - \sin (2'_{\underline{AB}})]\}. \qquad \text{(E5)}$$

Because α is the angle between the final orientation of $\underline{AC}$ and the major principal stretch direction, the angles $\theta'_{\underline{AB}}$ and $\theta'_{\underline{BC}}$ are computed fo rthe final shape of the triangle.

After computing α, we substitute α into equations E3a and E3b and rearrange them to get $\underline{S}_1$ and $\underline{S}_2$:

$$\underline{S}_1 = 1/\{(1/\underline{S}^2_{\underline{AC}}) + (1/\underline{S}^2_{\underline{AB}} - 1/\underline{S}^2_{\underline{BC}})(1 - \cos (2\alpha))$$

$$/((\cos 2(\alpha + \theta'_{\underline{AB}}) - \cos 2(\alpha + \theta'_{\underline{BC}}))\}^{(1/2)}; \qquad \text{(E6)}$$

$$\underline{S}_2 = 1/\{(1/\underline{S}^2_{\underline{AC}}) - (1/\underline{S}^2_{\underline{AB}} - 1/\underline{S}^2_{\underline{BC}})(1 + \cos (2\alpha))$$

$$/(\cos 2(\alpha + \theta'_{\underline{AB}}) - \cos 2(\alpha + \theta'_{\underline{BC}}))\}^{(1/2)}. \qquad \text{(E7)}$$

In the event that all four corners of a quadrilateral are coplanar, a least-squares method can be used to find a single set of best-fit values for $\underline{S}_1$, $\underline{S}_2$, and α that apply to the entire quadrilateral. Equations E2a, E2b, and E2c are simplified by applying the angle-addition formula:

$$2/\underline{S}^2_{\underline{i}} = (1/\underline{S}^2_1 + 1/\underline{S}^2_2) + (1/\underline{S}^2_1 - 1/\underline{S}^2_2) \cos(2\alpha) \cos (2\theta'_{\underline{i}})$$

$$- (1/\underline{S}^2_1 - 1/\underline{S}^2_2) \sin (2\alpha) (\sin (2\theta'_{\underline{i}}). \qquad \text{(E8)}$$

We have an equation of the form:

$$\underline{z} = \underline{c} + \underline{c}_1\underline{x} + \underline{c}_2\underline{y}$$

in which

$$\underline{c} = (1/\underline{S}_1^2 + 1/\underline{S}_2^2),$$

$$\underline{c}_1 = (1/\underline{S}_1^2 - 1/\underline{S}_2^2) \cos (2\alpha),$$

and

$$\underline{c}_2 = -(1/\underline{S}_1^2 - 1/\underline{S}_2^2) \sin (2\alpha).$$

Applying standard methods for least squares results in three equations that can be solved for $\underline{c}$, $\underline{c}_1$, $\underline{c}_2$, and, hence, α, $\underline{S}_1$, and $\underline{S}_2$.

Appendix F

COMPUTER PROGRAMS

```
10 REM   PROGRAM TO PRINT CONTENTS OF DATA FILES
20 REM   STORED AS <PRINTDAT.BAS>
30 WIDTH LPRINT 100
40 LPRINT:LPRINT
50 INPUT "QUAD NUMBER ? ", Q$
60 OPEN "I", #1,Q$
70 LPRINT Q$
80 IF EOF (1) THEN END
90 INPUT#1,DT$,AZ
100 LPRINT DT$,AZ;
110 FOR J=1 TO 6:INPUT #1,A(J):LPRINT USING "####.###"; A(J);:NEXT J
120 FOR J=1 TO 3: INPUT #1,B(J):NEXT J
130 FOR J=1 TO 3:LPRINT USING "####.###";B(J);:NEXT J:LPRINT
140 GOTO 80
```

```
1 PRINT "PROGRAM TO PUT QUADRILATERAL DATA INTO FILES.  CONTAINS DATA"
2 PRINT "FROM ASPEN GROVE LANDSLIDE. STORED UNDER <TEMPDAT.BAS>."
5 PRINT:PRINT:INPUT "WHICH QUAD";FILE$
10 OPEN "O",#1,FILE$
20 READ QD$,DT$,AZ
22 PRINT QD$;DT$;
25 IF AZ>360 THEN CLOSE#1:RESTORE:GOTO 5
30 FOR J=1 TO 6:READ A(J):NEXT J
40 FOR J=0 TO 3:READ B(J):NEXT J
50 IF QD$<>FILE$ THEN 20
55 PRINT:PRINT "FOUND IT!",DT$
60 PRINT#1,DT$;",";AZ;
70 FOR J=1 TO 6:PRINT#1,A(J);:NEXT J
80 FOR J=1 TO 3:C(J)=B(J)-B(0):PRINT#1,C(J);:NEXT J
90 GOTO 20
1000 REM *****  INSTRUCTIONS FOR TYPING DATA LINES  **********
1001 REM FIRST LINE GIVES QUAD. NUMBER, DATE, AND AZIMUTH FROM A TO C
1002 REM PLUS ANGLE IS WEST OF NORTH, MINUS ANGLE IS EAST OF NORTH
1005 DATA Q-18,17 MAY 1984,113
1006 REM NEXT LINE IS SERIES OF SLOPE DISTANCES MEASURED BETWEEN STAKES IN THE
1007 REM SEQUENCE  A-B,B-C,C-D,D-A,A-C,B-D
1010 DATA 5.02,7.741,5.132,8.655,9.396,9.855
1012 REM NEXT LINE IS SERIES OF STADIA ROD INTERCEPTS OBTAINED BY LEVELING
1013 REM IN THE SEQUENCE  A,B,C,D
1015 DATA .15320,.53602,2.64744,2.39918
2262 DATA Q-2,2 AUG 1985,-5
2264 DATA 1.775,3.016,2.016,3.239,3.007,4.204
2266 DATA .8391,.8758,1.50428,1.34972
2538 DATA Q-7,2 AUG 1985,47
2540 DATA 1.738,1.584,1.457,1.886,2.419,2.28
2542 DATA 2.58548,2.6734,3.04528,3.03838
2564 DATA Q-2,12 SEP 1986,-5
2566 DATA 1.754,3.159,2.029,3.434,2.994,4.435
2568 DATA 1.21978,1.26150,1.82279,1.64406
2660 DATA Q-7,12 SEP 1986,47
2662 DATA 1.705,1.607,1.435,1.876,2.415,2.259
2664 DATA 2.73918,2.75162,3.13011,3.16102
10000 DATA Q-99,0 AUG 1999,999
```

```
100 PRINT "STORED UNDER NAME <QUADDSP.BAS> "
110 PI=3.141592653589796#:WIDTH LPRINT 80
120 DIM BC(2,10),B(2,10),D(6)
130 PRINT "PROGRAM FOR COMPUTATION OF DISPLACEMENTS AT SURFACE OF A"
140 PRINT " LANDSLIDE, USING QUADRILATERAL MEASUREMENTS."
150 PRINT: PRINT "TO RUN PROGRAM, TYPE IN QUADRILATERAL NUMBER, IN THE"
160 PRINT "FORM,  Q-13   AND PUSH <RETURN>"
170 PRINT "THEN TYPE IN DATE OF READINGS THAT ARE TO BE USED AS A REFERENCE"
180 PRINT "IN THE FORM,  2 JULY 1983  AND PUSH <RETURN>"
190 PRINT "FINALLY, TYPE IN DATE OF READINGS THAT ARE TO BE USED TO"
200 PRINT "COMPUTE DEFORMATION, IN THE SAME FORM, AND PUSH <RETURN>"
210 PRINT
220 INPUT "QUADRILATERAL NUMBER";Q$
230 PRINT "REFERENCE LINES ARE: AB; AD; BC; CD."
240 INPUT "REFERENCE LINE";L$
250 INPUT "DATE OF REFERENCE MEASUREMENTS";DAT$(0)
260 INPUT "DATE OF MEASUREMENTS TO BE USED TO COMPUTE DEFORMATION";DAT$(1)
270 LPRINT:LPRINT Q$,DAT$(0),DAT$(1)
280 REM                    ############
290 REM   ### SEARCH FILES FOR SPECIFIED DATA  ###########################
300 KK=0:OPEN "I",#1,Q$
310 INPUT#1,DT$,AZ:I=2
320 IF DT$=DAT$(0) THEN I=0:KK=KK+1
330 IF DT$=DAT$(1) THEN I=1:KK=KK+1
340 QUAD$(I,0)=Q$:DATE$(I,0)=DT$:AZIM(I,0)=AZ
350 FOR J=1 TO 6:INPUT#1, A(I,J):NEXT J
360 FOR J=1 TO 3:INPUT#1, C(I,J):NEXT J
370 IF I=2 THEN 310
380 IF KK=2 THEN 450 ELSE 310
390 REM                    ############
400 REM A(I,J) <I=0 FOR REFERENCE DATE,I=1 FOR LATER DATE,J=1 TO 6> IS SERIES
410 REM OF SLOPE DISTANCES,A-B=1,B-C=2,C-D=3,D-A=4,A-C=5,B-D=6
420 REM C(I,J) <I SAME AS ABOVE> IS SERIES OF DIFFERENCES IN ELEVATION BETWEEN
430 REM STAKES, A-B=1,A-C=2,A-D=3.
440 REM   ###    PRINT DATA   ############################################
450 LPRINT "ORIGINAL DATA"I:CLOSE#1
460 FOR I=0 TO 1:LPRINT:FOR J=1 TO 6:LPRINT A(I,J);:NEXT J,I:LPRINT
470 FOR I=0 TO 1:LPRINT:FOR J=1 TO 3:LPRINT C(I,J);:NEXT J,I:LPRINT
480 REM                    ############
490 REM COMPUTE HORIZONTAL DISTANCES BETWEEN STAKES. STORE AS BC(I,J)
500 FOR I=0 TO 1:BC(I,1)=SQR(A(I,1)^2-C(I,1)^2)
510 BC(I,5)=SQR(A(I,5)^2-C(I,2)^2):BC(I,4)=SQR(A(I,4)^2-C(I,3)^2)
520 TP=C(I,1)-C(I,2):BC(I,2)=SQR(A(I,2)^2-TP^2)
530 TP=C(I,3)-C(I,2):BC(I,3)=SQR(A(I,3)^2-TP^2)
540 TP=C(I,1)-C(I,3):BC(I,6)=SQR(A(I,6)^2-TP^2)
550 NEXT I
560 REM                    ############
570 REM   ### CHECK ANGLES IN QUADRILATERAL ###########################
580 FOR I=0 TO 1:FOR J=1 TO 6:D(J)=BC(I,J)
590 NEXT J
600 K=1:FOR J=1 TO 4:JP1=J+1:JJ=J+4:IF J=4 THEN JP1=1:JJ=6
610 IF J=3 THEN JJ=5
620 TP=(D(J)^2+D(JJ)^2-D(JP1)^2)/(2*D(J)*D(JJ))
```

```
630 BETA(K)=ATN(SQR(ABS(1-TP^2))/TP):K=K+1
640 TP=(D(JP1)^2+D(JJ)^2-D(J)^2)/(2*D(JP1)*D(JJ))
650 BETA(K)=ATN(SQR(ABS(1-TP^2))/TP):K=K+1:NEXT J
660 GOSUB 1530
670 W1=-2*PI:FOR K=1 TO 8:W1=W1+BETA(K):NEXT K
680 W2=BETA(1)+BETA(8)-BETA(4)-BETA(5)
690 W3=BETA(6)+BETA(7)-BETA(3)-BETA(2)
700 LPRINT "ERRORS IN ANGLES W1,W2,W3=";W1*180/PI;W2*180/PI;W3*180/PI
710 FOR K=1 TO 8:THETA(I,K)=BETA(K):NEXT K
720 NEXT I
730 REM  *** CHOOSE ROUTINE FOR APPRORIATE REFERENCE LINE  *********
740 IF L$="CD" THEN 1020
750 IF L$="AD" THEN 1210
760 IF L$="BC" THEN 1370
770 REM *** COMPUTATIONS OF DISPLACEMENTS FOR SHEAR ZONES****
780 REM XXD,ZZD ARE ORIGINAL AND XD AND ZD ARE FINAL POSITIONS OF PT D
790 REM  ********  REFERENCE LINE AB  ****************************
800 AN=THETA(0,1)+THETA(0,6):P$="D"
810 XXD=BC(0,4)*COS(AN)
820 ZZD=BC(0,4)*SIN(AN)
830 AN=THETA(1,1)+THETA(1,6)
840 XD=BC(1,4)*COS(AN)
850 ZD=BC(1,4)*SIN(AN)
860 U=XD-XXD:W=ZD-ZZD:V=C(1,3)-C(0,3)
870 DIR=ATN(W/U)
880 DIRAZ=180-AZ-(THETA(0,1)-DIR)*180/PI
890 GOSUB 1580
900 AN=THETA(0,3)+THETA(0,8):P$="C"
910 XXC=BC(0,1)-BC(0,2)*COS(AN)
920 ZZC=BC(0,2)*SIN(AN)
930 AN=THETA(1,3)+THETA(1,8)
940 XC=BC(1,1)-BC(1,2)*COS(AN)
950 ZC=BC(1,2)*SIN(AN)
960 U=XC-XXC:W=ZC-ZZC:V=C(1,2)-C(0,2)
970 DIR=ATN(W/U)
980 DIRAZ=180-AZ-(THETA(0,1)-DIR)*180/PI
990 GOSUB 1580
1000 GOTO 260
1010 REM *********  REFERENCE LINE CD  *************************
1020 AN=THETA(0,4)+THETA(0,7):P$="A"
1030 XXA=BC(0,4)*COS(AN)
1040 ZZA=BC(0,4)*SIN(AN)
1050 AN=THETA(1,4)+THETA(1,7)
1060 XA=BC(1,4)*COS(AN)
1070 ZA=BC(1,4)*SIN(AN)
1080 U=XA-XXA:W=ZA-ZZA:V=C(0,3)-C(1,3)
1090 DIR=ATN(W/U)
1100 DIRAZ=-AZ-(THETA(0,5)-DIR)*180/PI
1110 GOSUB 1580
1120 AN=THETA(0,5)+THETA(0,2):P$="B"
1130 XXB=BC(0,3)-BC(0,2)*COS(AN):ZZB=BC(0,2)*SIN(AN)
1140 AN=THETA(1,5)+THETA(1,2)
1150 XB=BC(1,3)-BC(1,2)*COS(AN):ZB=BC(1,2)*SIN(AN)
```

```
1160 U=XB-XXB:W=ZB-ZZB:V=C(1,1)-C(1,2)-(C(0,1)-C(0,2))
1170 DIR=ATN(W/U):DIRAZ=-AZ-(THETA(0,5)-DIR)*180/PI
1180 GOSUB 1580
1190 GOTO 260
1200 REM ********* REFERENCE LINE AD *************************
1210 AN=THETA(0,1)+THETA(0,6):P$="B"
1220 XXB=BC(0,1)*COS(AN):ZZB=BC(0,1)*SIN(AN)
1230 AN=THETA(1,1)+THETA(1,6)
1240 XB=BC(1,1)*COS(AN):ZB=BC(0,1)*SIN(AN)
1250 U=XB-XXB:W=ZB-ZZB:V=C(1,1)-C(0,1)
1260 DIR=ATN(W/U):DIRAZ=-AZ+(THETA(0,6)-DIR)*180/PI
1270 GOSUB 1580
1280 AN=THETA(0,4)+THETA(0,7):P$="C"
1290 XXC=BC(0,4)-BC(0,3)*COS(AN):ZZC=BC(0,3)*SIN(AN)
1300 AN=THETA(1,4)+THETA(1,7)
1310 XC=BC(1,4)-BC(1,3)*COS(AN):ZC=BC(1,3)*SIN(AN)
1320 U=XC-XXC:W=ZC-ZZC:V=C(1,2)-C(0,2)
1330 DIR=ATN(W/U):DIRAZ=-AZ+(THETA(0,6)-DIR)*180/PI
1340 GOSUB 1580
1350 GOTO 260
1360 REM ********* REFERENCE LINE BC *************************
1370 AN=THETA(0,3)+THETA(0,8):P$="A"
1380 XXA=BC(0,1)*COS(AN):ZZA=BC(0,1)*SIN(AN)
1390 AN=THETA(1,3)+THETA(1,8)
1400 XA=BC(1,1)*COS(AN):ZA=BC(1,1)*SIN(AN)
1410 U=XA-XXA:W=ZA-ZZA:V=C(1,1)-C(0,1)
1420 DIR=ATN(W/U):DIRAZ=-AZ+(THETA(0,2)+DIR)*180/PI
1430 GOSUB 1580
1440 AN=THETA(0,2)+THETA(0,5):P$="D"
1450 XXD=BC(0,2)-BC(0,3)*COS(AN):ZZD=BC(0,3)*SIN(AN)
1460 AN=THETA(1,2)+THETA(1,5)
1470 XD=BC(1,2)-BC(1,3)*COS(AN):ZD=BC(1,3)*SIN(AN)
1480 U=XD-XXD:W=ZD-ZZD:V=C(1,3)-C(1,1)-(C(0,3)-C(0,1))
1490 DIR=ATN(W/U):DIRAZ=-AZ+(THETA(0,2)+DIR)*180/PI
1500 GOSUB 1580
1510 GOTO 260
1520 REM ************* SUBROUTINE ****************************
1530 FOR II=1 TO 8:IF BETA(II)<0 THEN BETA(II)=BETA(II)+PI
1540 NEXT II
1550 RETURN
1560 REM ******** ********** *********** *********
1570 REM ******************* SUBROUTINE ***********************
1580 LPRINT "***********************************************************"
1590 LPRINT
1600 LPRINT "IF W IS NEGATIVE THEN MOVEMENT IS TOWARD THE REF. LINE."
1610 LPRINT "DISPLACEMENTS OF POINT ";P$;" : U -PARALLEL TO ";L$;" W -NORMAL"
1620 DISP=SQR(U^2+V^2+W^2)
1630 LPRINT "V VERTICAL":LPRINT "U";U;"    W";W;"    V";V;" DISPL";DISP
1640 PLG=V/SQR(U^2+W^2):PLG=ATN(PLG)*180/PI:LPRINT "PLUNGE(DOWNSLOPE) ";PLG
1650 LPRINT "ANGLE BETWEEN ";L$;" AND DISPL. DIR.= ";DIR*180/PI
1660 LPRINT "AZIMUTH OF DISPLACEMENT <NEG. ANGLE IS WEST OF NORTH>";DIRAZ
1670 RETURN
```

```
100 PRINT "STORED UNDER NAME <QUADSTR.BAS>"
110 PI=3.14159265358979#:WIDTH LPRINT 80
120 PRINT "PROGRAM FOR COMPUTATION OF DEFORMATIONS AT SURFACE OF "
130 PRINT " LANDSLIDES, USING QUADRILATERAL MEASUREMENTS."
140 PRINT " PROGRAM WRITTEN 1983 BY A. M. JOHNSON."
150 PRINT: PRINT "TO RUN PROGRAM, TYPE IN QUADRILATERAL NUMBER, IN THE"
160 PRINT "FORM,  Q-13   AND PUSH <RETURN>"
170 PRINT "THEN TYPE IN DATE OF READINGS THAT ARE TO BE USED AS A REFERENCE"
180 PRINT "IN THE FORM,  2 JULY 1983  AND PUSH <RETURN>"
190 PRINT "FINALLY, TYPE IN DATE OF READINGS THAT ARE TO BE USED TO"
200 PRINT "COMPUTE DEFORMATION, IN THE SAME FORM, AND PUSH <RETURN>"
210 PRINT
220 PRINT "IF YOU NEED TO ENTER NEW DATA USE THE PROGRAM NAMED <TEMPDAT.BAS>."
230 INPUT "QUADRILATERAL NUMBER";Q$
240 INPUT "DATE OF REFERENCE MEASUREMENTS";DAT$(0)
250 INPUT "DATE OF MEASUREMENTS TO BE USED TO COMPUTE DEFORMATION";DAT$(1)
260 LPRINT:LPRINT Q$,DAT$(0),DAT$(1)
270 REM                     ###############
280 REM #### SEARCH FILES FOR SPECIFIED DATA ####################
290 REM                     ###############
300 KK=0:OPEN "I",#1,Q$
310 INPUT#1,DT$,AZ:I=2
320 IF DT$=DAT$(0) THEN I=0:KK=KK+1
330 IF DT$=DAT$(1) THEN I=1:KK=KK+1
340 QUAD$(I,0)=Q$:DATE$(I,0)=DT$:AZIM(I,0)=AZ
350 FOR J=1 TO 6:INPUT#1, A(I,J):NEXT J
360 FOR J=1 TO 3:INPUT#1, C(I,J):NEXT J
370 IF I=2 THEN 310
380 IF KK=2 THEN 460 ELSE 310
390 REM                     ###############
400 REM A(I,J) (I=0 FOR REFERENCE DATE,I=1 FOR LATER DATE,J=1 TO 6) IS SERIES
410 REM OF SLOPE DISTANCES,A-B=1,B-C=2,C-D=3,D-A=4,A-C=5,B-D=6
420 REM C(I,J) (I SAME AS ABOVE) IS SERIES OF DIFFERENCES IN ELEVATION BETWEEN
430 REM STAKES, A-B=1,A-C=2,A-D=3.
440 REM                     ###############
450 REM #########   PRINT DATA   #######################################
460 LPRINT "ORIGINAL DATA"I:CLOSE#1
470 FOR I=0 TO 1:LPRINT:FOR J=1 TO 6:LPRINT A(I,J);:NEXT J,I:LPRINT
480 FOR I=0 TO 1:LPRINT:FOR J=1 TO 3:LPRINT C(I,J);:NEXT J,I:LPRINT
490 REM                     ###############
500 REM COMPUTE HORIZONTAL DISTANCES BETWEEN STAKES. STORE AS B(I,J)
510 FOR I=0 TO 1:H(I,1)=C(I,1):H(I,4)=C(I,3):H(I,5)=C(I,2)
520 B(I,1)=SQR(A(I,1)^2-C(I,1)^2)
530 B(I,5)=SQR(A(I,5)^2-C(I,2)^2):B(I,4)=SQR(A(I,4)^2-C(I,3)^2)
540 H(I,2)=C(I,2)-C(I,1):B(I,2)=SQR(A(I,2)^2-H(I,2)^2)
550 H(I,3)=C(I,2)-C(I,3):B(I,3)=SQR(A(I,3)^2-H(I,3)^2)
560 H(I,6)=C(I,3)-C(I,1):B(I,6)=SQR(A(I,6)^2-H(I,6)^2)
570 NEXT I
580 REM                     ###############
600 REM######   CHECK ANGLES OF QUADRILATERAL
```

```
610 FOR I=0 TO 1:FOR J=1 TO 6:D(J)=B(I,J):NEXT J
620 K=1:FOR J=1 TO 4:JP1=J+1:JJ=J+4:IF J=4 THEN JP1=1:JJ=6
630 IF J=3 THEN JJ=5
640 TP=(D(J)^2+D(JJ)^2-D(JP1)^2)/(2*D(J)*D(JJ))
650 BETA(K)=ATN(SQR(ABS(1-TP^2))/TP):K=K+1
660 TP=(D(JP1)^2+D(JJ)^2-D(J)^2)/(2*D(JP1)*D(JJ))
670 BETA(K)=ATN(SQR(ABS(1-TP^2))/TP):K=K+1:NEXT J
680 GOSUB 1700
690 W1=-2*PI:FOR K=1 TO 8:W1=W1+BETA(K):NEXT K:C1=W1/8
700 W2=BETA(1)+BETA(8)-BETA(4)-BETA(5):C2=W2/4
710 W3=BETA(6)+BETA(7)-BETA(3)-BETA(2):C3=W3/4
720 LPRINT "ERRORS IN ANGLES W1,W2,W3=";W1*180/PI;W2*180/PI;W3*180/PI
730 FOR K=1 TO 8:BTA(I,K)=BETA(K):NEXT K:REM ****NEW***
740 NEXT I
750 REM          #################
760 REM  *******  COMPUTE STRETCHES OF LINES  *******************
770 LPRINT:LPRINT "SLOPE STRETCHES":LPRINT "AB  BC  CD  AD  AC  BD"
780 FOR J=1 TO 6:S(J)=A(1,J)/A(0,J):LPRINT S(J);:NEXT J
790 LPRINT "*****************************************************"
800 LPRINT:LPRINT "STRAINS IN PERCENTAGES"
810 FOR J=1 TO 6:ST(J)=(S(J)-1)*100:LPRINT ST(J);:NEXT J
820 LPRINT
830 REM          ####################
840 REM  ****   COMPUTE ANGLES OF EACH TRIANGLE IN THE
850 REM  QUADRILATERAL, ANGLES ARE THETA (1) --- THETA (8)  ****************
860 FOR J=1 TO 6:D(J)=A(1,J):NEXT J
870 K=1:FOR J=1 TO 4:JP1=J+1:JJ=J+4:IF J=4 THEN JP1=1:JJ=6
880 IF J=3 THEN JJ=5
890 TP=(D(J)^2+D(JJ)^2-D(JP1)^2)/(2*D(J)*D(JJ))
900 THETA(K)=ATN(SQR(ABS(1-TP^2))/TP):K=K+1
910 TP=(D(JP1)^2+D(JJ)^2-D(J)^2)/(2*D(JP1)*D(JJ))
920 THETA(K)=ATN(SQR(ABS(1-TP^2))/TP):K=K+1:NEXT J
930 REM  **** COMPUTE DIRECTIONS OF LINES IN THE QUADRILATERAL,   ******
940 REM  **** USING AZIMUTH OF LINE AC AS REFERENCE  ********************
950 FOR I=0 TO 1:AM=AZ*PI/180
960 BITA(I,1)=-AM-BTA(I,1):BITA(I,2)=-AM+BTA(I,2):BITA(I,3)=-AM-BTA(I,5)
970 BITA(I,4)=-AM+BTA(I,6):BITA(I,5)=-AM:BITA(I,6)=-AM+BTA(I,2)+BTA(I,3)
980 LPRINT "POSITIVE AZIMUTHS ARE EAST OF NORTH, NEGATIVE ARE WEST OF NORTH."
990 LPRINT "AZIMUTHS OF LINES AB,BC,CD,AD,AC,BD",I
1000 FOR J=1 TO 6:LPRINT BITA(I,J)*180/PI;:NEXT J,I:LPRINT
1010 REM         ######################
1020 LPRINT:LPRINT "       %S1      %S2     %AREA CHANGE"
1030 LPRINT "S1          S2          DAREA"
1040 LPRINT "BMAX      GAMMA-MAX     PSI-MAX"
1050 REM         ###################
1060 REM *** COMPUTE PRINCIPAL STRETCHES AND DIRECTIONS ******
1070 FOR J=1 TO 4:JJ=J+4:IF J=3 THEN JJ=5
1080 LPRINT "TRIANGLE",J
1090 JP1=J+1:IF J=4 THEN JJ=6:JP1=1
1100 T0=1/S(J)^2-1/S(JP1)^2
```

```
1110 T1=T0/(1/S(J)^2-1/S(JJ)^2)
1120 IF J=1 THEN AG(5)=0:AG(1)=-THETA(1):AG(2)=THETA(2)-PI:GOTO 1160
1130 IF J=2 THEN AG(6)=0:AG(2)=-THETA(3):AG(3)=THETA(4)-PI:GOTO 1160
1140 IF J=3 THEN AG(5)=0:AG(4)=THETA(6):AG(3)=PI-THETA(5):GOTO 1160
1150 IF J=4 THEN AG(6)=0:AG(1)=THETA(8):AG(4)=PI-THETA(7):GOTO 1160
1160 T2=COS(2*AG(J))-COS(2*AG(JJ)):T3=COS(2*AG(J))-COS(2*AG(JP1))
1170 TP=T1*T2-T3
1180 T4=SIN(2*AG(J))-SIN(2*AG(JJ)):T5=SIN(2*AG(J))-SIN(2*AG(JP1))
1190 TP=TP/(T1*T4-T5):ALPHA(J)=(1/2)*ATN(TP)
1200 TV1=2*T0/(COS(2*ALPHA(J))*T3-SIN(2*ALPHA(J))*T5)
1210 TV2=2*(1/S(J)^2)-TV1*COS(2*(ALPHA(J)+AG(J)))
1220 T1=(1/2)*(TV1+TV2):T2=(1/2)*(TV2-TV1)
1230 REM *** S1=MAX. PRINCIPAL STRETCH; S2=MIN. PRINCIPAL STRETCH
1240 S1=SQR(1/T1):S2=SQR(1/T2)
1250 IF S2>S1 THEN ALPHA(J)=ALPHA(J)+PI/2:GOTO 1200
1260 AL1=ALPHA(J)*180/PI
1270 BMAX=ATN(S2/S1)
1280 GAMMAMAX=((S1/S2)-(S2/S1))/2:PSIMAX=ATN(GAMMAMAX)
1290 REM***  BMAX IS THE DIRECTION OF MAX. SHEAR STRAIN MEASURED FROM S1.
1300 REM***  GAMMAMAX IS THE MAXIMUM SHEAR STRAIN AND PSIMAX IS THE ANGLE
1310 REM*** OF MAX SHEAR STRAIN.
1320 IF JJ=5 THEN 1330 ELSE 1350
1330 LPRINT "ANGLE BETWEEN A-C AND MAX. STRETCH <NEG ANGLE CLOCKWISE>";AL1
1340 GOTO 1360
1350 LPRINT "ANGLE BETWEEN B-D AND MAX. STRETCH <NEG.ANGLE CLOCKWISE>";AL1
1360 LPRINT (S1-1)*100,(S2-1)*100,(S1*S2-1)*100
1370 LPRINT S1,S2,S1*S2
1380 LPRINT BMAX*180/PI,GAMMAMAX,PSIMAX*180/PI
1390 REM                    ##############
1400 REM *********   COMPUTE DIPS AND DIP DIRECTIONS  *****************
1410 FOR I=0 TO 1:DZDX1=H(I,J)/B(I,J):DZDX2=H(I,JJ)/B(I,JJ)
1420 DXDX1=COS(BITA(I,J)):DYDX1=SIN(BITA(I,J)):DXDX2=COS(BITA(I,JJ))
1430 DYDX2=SIN(BITA(I,JJ))
1440 IF ABS(DXDX2)<1E-10 THEN SWAP DZDX1,DZDX2:SWAP DXDX1,DXDX2:SWAP DYDX1,DYDX2
1450 R=DXDX2/DXDX1:BS=(DZDX2-R*DZDX1)/(DYDX2-R*DYDX1)
1460 AS=(DZDX2-BS*DYDX2)/(DXDX2):DIPDIR(I)=ATN(BS/AS)
1470 DIP(I)=AS*COS(DIPDIR(I))+BS*SIN(DIPDIR(I)):DIP(I)=ATN(DIP(I))
1480 IF DIP(I)<0 THEN DIPDIR(I)=DIPDIR(I)+PI:DIP(I)=-DIP(I)
1490 LPRINT:LPRINT I,"DIP DIRECTION",DIPDIR(I)*180/PI,"DIP",DIP(I)*180/PI
1500 NEXT I
1510 LPRINT "ROTATION",(DIPDIR(0)-DIPDIR(1))*180/PI,
1520 LPRINT "CHANGE IN DIP",(DIP(0)-DIP(1))*180/PI:LPRINT
1530 NEXT J
1540 LPRINT "************************************************************"
1550 LPRINT
1560 GOTO 240
1570 REM            #####################
1690 REM *********** SUBROUTINE *********************
1700 FOR II=1 TO 8:IF BETA(II)<0 THEN BETA(II)=BETA(II)+PI
1710 NEXT II
1720 RETURN
```

Appendix G

SOLUTION OF EQUATIONS DESCRIBING FORCED CIRCULATION

In this appendix I present some of the details of the solution of the equations for the mechanism of forced circulation.

Derivation of Pore Pressure Boundary Condition

The boundary, $z_{\underline{o}}$, is impermeable. Flow results from first-order perturbations of the boundary, no zero-order components of flow occur. Thus,

$$q_n = 0 = q_z\cos(\theta) - \tilde{q}_x\sin(\theta);$$

or,

$$\tilde{q}_z = \tilde{q}_x\tan(\theta), \tag{G1}$$

where,

$$\tan(\theta) = (A\ell)\cos(\ell x).$$

Because $q_{\underline{z}}$ is the product of two first-order quantities, it is a second-order quantity on the boundary. Consequently, $q_{\underline{z}}$ can be ignored. To relate the components of flow to the volumetric strains I use the continuity equation (Freeze and Cherry, 1979, p. 532, determined by combining their equations A2.9, A2.10, and A2.12):

$$-\vec{\nabla}\cdot\vec{q} = n\beta(DP/Dt) + \vec{\nabla}\cdot\vec{v}. \tag{G2}$$

In equation G2, β represents the compressibility of water, $\underline{n}$ represents the porosity of the soil, $\underline{q}$ is the Darcy velocity of the fluid relative to the grains, and the operator $\underline{D}/\underline{Dt}$ is the total-time or material-time derivative,

$$D/Dt = v_x(\partial/\partial x) + v_z(\partial/\partial z) + (\partial/\partial t).$$

I introduce Darcy's law,

$$q_x = -K^*(\partial P/\partial x); \quad q_z = -K^*(\partial P/\partial z). \tag{G3}$$

and substitute it into the continuity equation:

$$K^*\nabla^2 P = n\beta(DP/Dt) + \vec{\nabla}\cdot\vec{v}. \tag{G4}$$

I write out components of equation G4 and introduce the perturbation notation used in Chapter VII. Application of equation G1 helps to identify a second-order term on the left hand side of the equation. I retain only first-order terms:

$$K^*(\partial^2\bar{P}/\partial x^2) = n\beta[\bar{v}_x(\partial\bar{P}/\partial x) + (\partial\bar{P}/\partial t)] + \partial\bar{e}/\partial t. \quad \text{(G5)}$$

Making the change of coordinates, $\xi = x - \bar{v}_x t$, $t = \theta$, yields

$$K^*(\partial^2\bar{P}/\partial x^2) = n\beta[\bar{v}_x(\partial\bar{P}/\partial\xi) - \bar{v}_x(\partial\bar{P}/\partial\xi)] - \bar{v}_x(\partial\bar{e}/\partial\xi). \quad \text{(G6)}$$

The quantity in square brackets in equation G6 is zero; thus, the boundary condition for pore pressures simplifies to

$$[\partial^2\bar{P}/\partial\xi^2]_{z_o} = -(\bar{v}_x/K^*)[\partial\bar{e}/\partial\xi]_{z_o}. \quad \text{(G7)}$$

Equation G7 is equation (7.28) in Chapter VII.

<u>Solution for the Stresses and Velocities in the Porous Elastic Material</u>

I start with equations 7.34 and 7.35 from Chapter VII, making appropriate substitutions of ξ for <u>x</u>.

$$\bar{P} = \exp(-\ell z)[c_1 \cos(\ell\xi) + c_2 \sin(\ell\xi)] \quad (7.34)$$

$$\bar{\phi} = (c_3 + c_4\ell z)\exp(-\ell z)[c_5 \cos(\ell\xi) + c_6 \sin(\ell\xi)] \quad (7.35)$$

The free slip boundary condition (equation 7.21) in terms of $\bar{\phi}$ is:

$$[\partial^2\bar{\phi}/\partial\xi\partial z]_{z_o} = 0. \tag{G8}$$

where $\partial^2\bar{\phi}/\partial\xi\partial z$ is determined by

$$(\partial^2\bar{\phi}/\partial\xi\partial z) = -\ell^2[c_3 + c_4(\ell z - 1)]\ [(-c_5 \sin(\ell\xi)$$

$$+ c_6 \cos(\ell\xi)]. \tag{G9}$$

When equation G9 is substituted into equation G8, and $\underline{z}$ is set equal to zero, I determine that

$$c_3 = c_4 \tag{G10}$$

Thus, c_3 and c_4 can be set equal to unity.

To apply the velocity boundary condition, equation 7.3, I use the definition of $\underline{v_z}$ and transform coordinates; thus,

$$\bar{v}_z = (\partial\bar{u}_z/\partial t) \rightarrow \bar{v}_z = -\bar{v}_x(\partial\bar{u}_z/\partial\xi).$$

I compute $\underline{u}_{\underline{z}}$ by integrating the constitutive equation relating $\underline{T}_{\underline{zz}}$ and $\underline{E}_{\underline{zz}}$. After making the appropriate substitutions for the stress function into equation 7.25c, I integrate to get an expression for $\tilde{\underline{v}}_{\underline{z}}$:

$$\tilde{v}_z = (-\tilde{v}_x/2G) \frac{\partial}{\partial \xi} \int \{(\partial^2\tilde{\phi}/\partial\xi^2) - \nu\nabla^2\tilde{\phi} + (1-2\nu)\tilde{P}\} \, dz$$

$$+ f(\xi). \qquad \text{(G11)}$$

In equation G11, $\underline{f}(\xi)$ must be zero, because $\tilde{\underline{v}}_{\underline{z}} \to 0$ as $\underline{z} \to \infty$. When the operations in equation G11 are carried out, I determine an expression for $\tilde{\underline{v}}_{\underline{z}}$.

$$\tilde{v}_z = (-\tilde{v}_x/2G) \exp(-\ell z)\{-\ell[\ell(2 + \ell z)c_5 - 2\ell\nu c_5$$

$$- (1 - 2\nu)c_1/\ell] \sin(\ell\xi) + \ell[\ell(2 + \ell z)c_6$$

$$- 2\ell\nu c_6 - (1 - 2\nu)c_2/\ell] \cos(\ell\xi)\} \qquad \text{(G12)}$$

In equation G12, $\underline{z}$ is set equal to zero, and the velocity boundary condition (equation 7.20) is used to solve for the constants; Thus,

$$0 = 2\ell c_5 - 2\ell\nu c_5 - (1 - 2\nu)c_1/\ell, \qquad \text{(G13a)}$$

and

$$\bar{v}_x A\ell = (-\bar{v}_x \ell/2G)\ [2\ell c_6 - 2\ell\nu c_6 - (1 - 2\nu)c_2/\ell] \qquad \text{(G13b)}$$

Equations G13a and G13b simplify to

$$c_1 = 2\ell^2(1 - \nu)\ c_5/(1 - 2\nu) \qquad \text{(G14a)}$$

and

$$c_2 = [2GA\ell + 2\ell^2(1 - \nu)c_6\ell]/(1 - 2\nu) \qquad \text{(G14b)}$$

Now we use the boundary condition given by equation G7 to solve for $\underline{c}_5$ and $\underline{c}_6$. To compute $\underline{\bar{e}}$, I use equations 7.25a and 7.25c, and the definition of $\underline{e}$:

$$e = E_{\xi\xi} + E_{zz}.$$

Thus,

$$\bar{e} = [(1 - 2\nu)/2G]\ (\nabla^2\bar{\phi} + 2\bar{P}), \qquad \text{(G15)}$$

and

$$(\partial \bar{e}/\partial \xi) = [(1 - 2\nu)/2G] \{-2\ell^3 \exp(-\ell z) [-c_5 \sin(\ell\xi)$$

$$+ c_6 \cos(\ell\xi)] + 2\ell \exp(-\ell z) [-c_1 \sin(\ell\xi)$$

$$+ c_2 \cos(\ell\xi)]\}. \tag{G16}$$

I differentiate equation 7.34 to get an expression for $(\partial^2\bar{P}/\partial\xi^2)$:

$$(\partial^2\bar{P}/\partial\xi^2) = -\ell^2 \exp(-\ell z) \{c_1 \cos(\ell\xi) + c_2 \sin(\ell\xi)\}. \tag{G17}$$

Equations (G16) and (G17) are substituted into equation (G7), the no-flow condition at the boundary, to obtain two more equations relating the unknown constants. When z is set equal to zero and the sine and cosine terms are collected, the following expressions are obtained.

$$\ell c_1 = [\bar{v}_x(1 - 2\nu)/K{*}G][-\ell^2 c_6 + c_2] \tag{G18}$$

$$\ell c_2 = [\bar{v}_x(1 - 2\nu)/K{*}G] [\ell^2 c_5 - c_1]. \tag{G19}$$

Equations (G14a), (G14b), (G18) and (G19) constitute a system of four algebraic equations that can be solved simultaneously for the unknown constants, c_1, c_2, c_5, and c_6. An expression for c_5 is given in the text as equation (7.38).

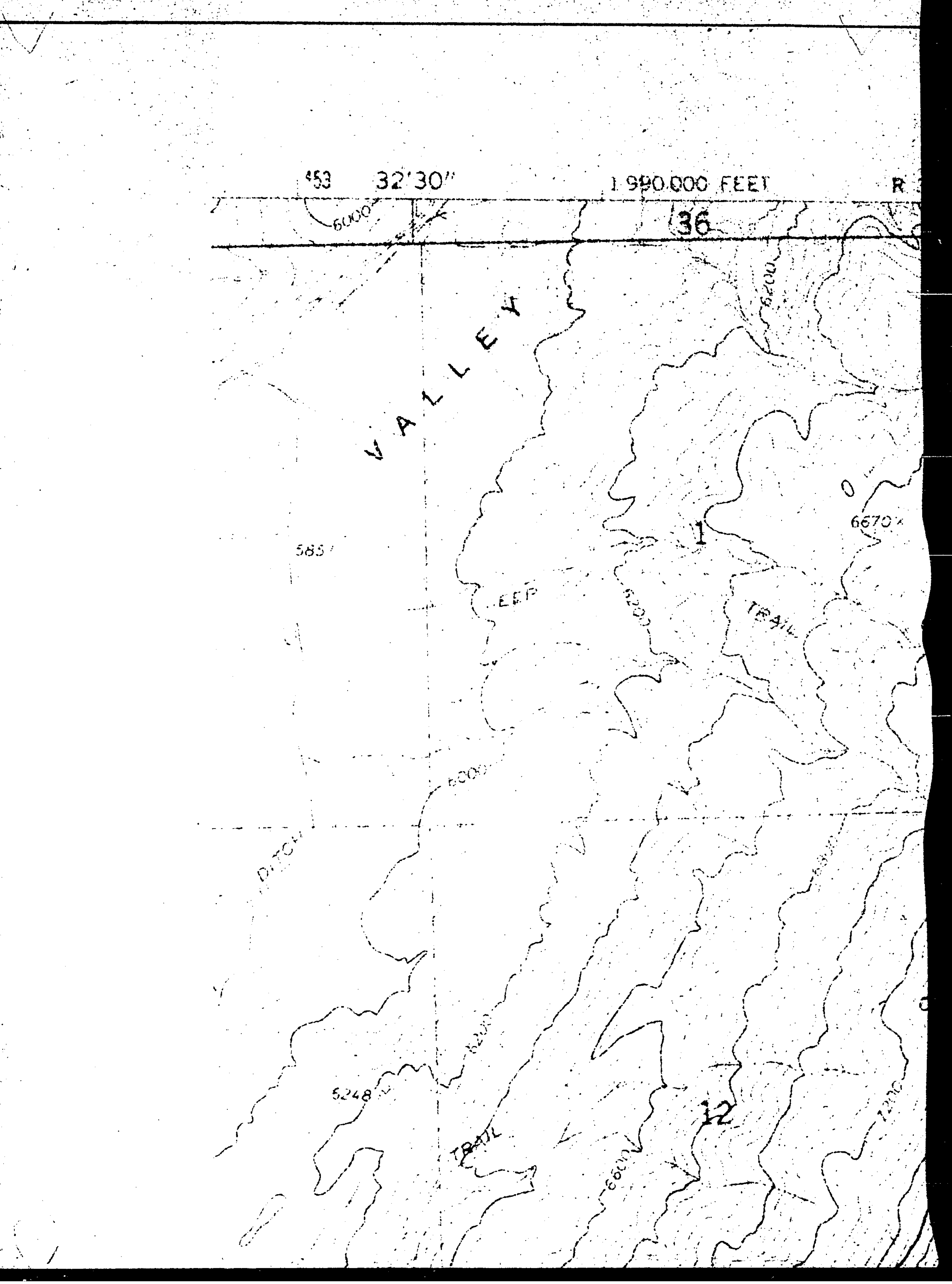
453
32'30"
1 990 000 FEET
R
36
6000
6200
VALLEY
0
6670
1
585
EEP
TRAIL
6000
DITCH
6200
5248
12
TRAIL
6600
7200

EPHRAIM QUADRANGLE
UTAH—SANPETE CO.
7.5 MINUTE SERIES (TOPOGRAPHIC)

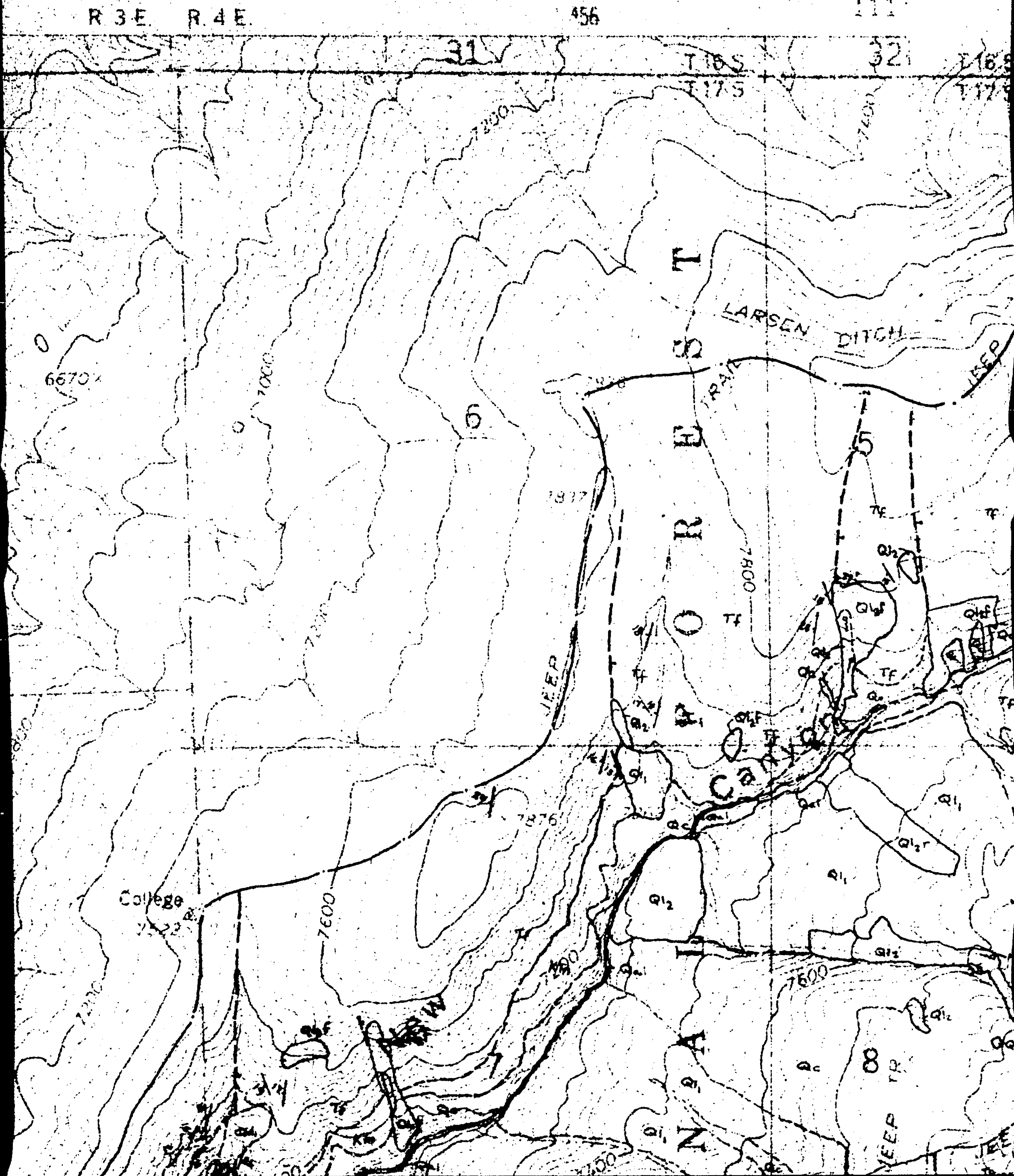

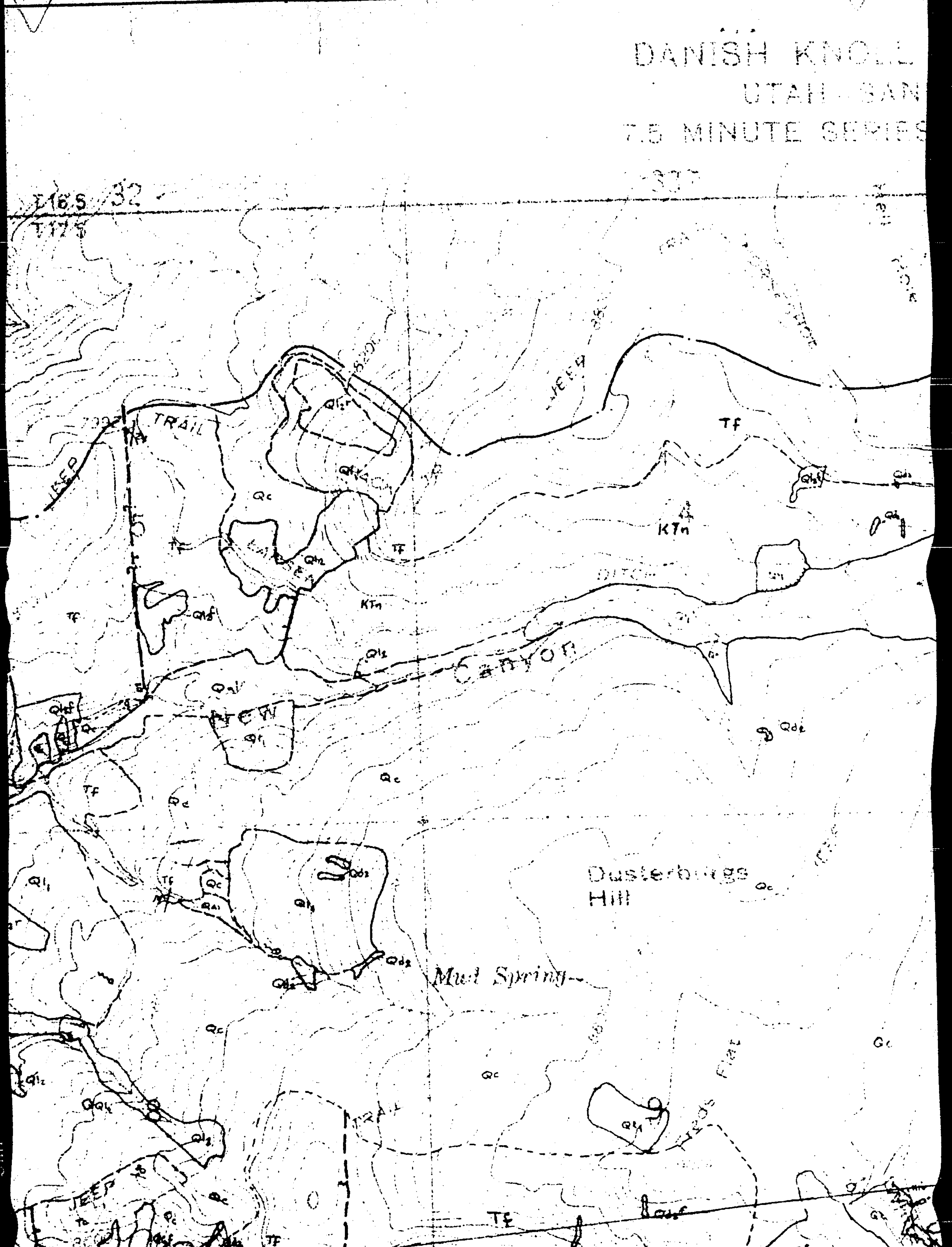
DANISH KNOLL
UTAH
7.5 MINUTE
T16S
T17S
JEEP TRAIL
DITCH
Canyon
Hill
Mud Spring
TRAIL
JEEP
TF
KTn
Qc

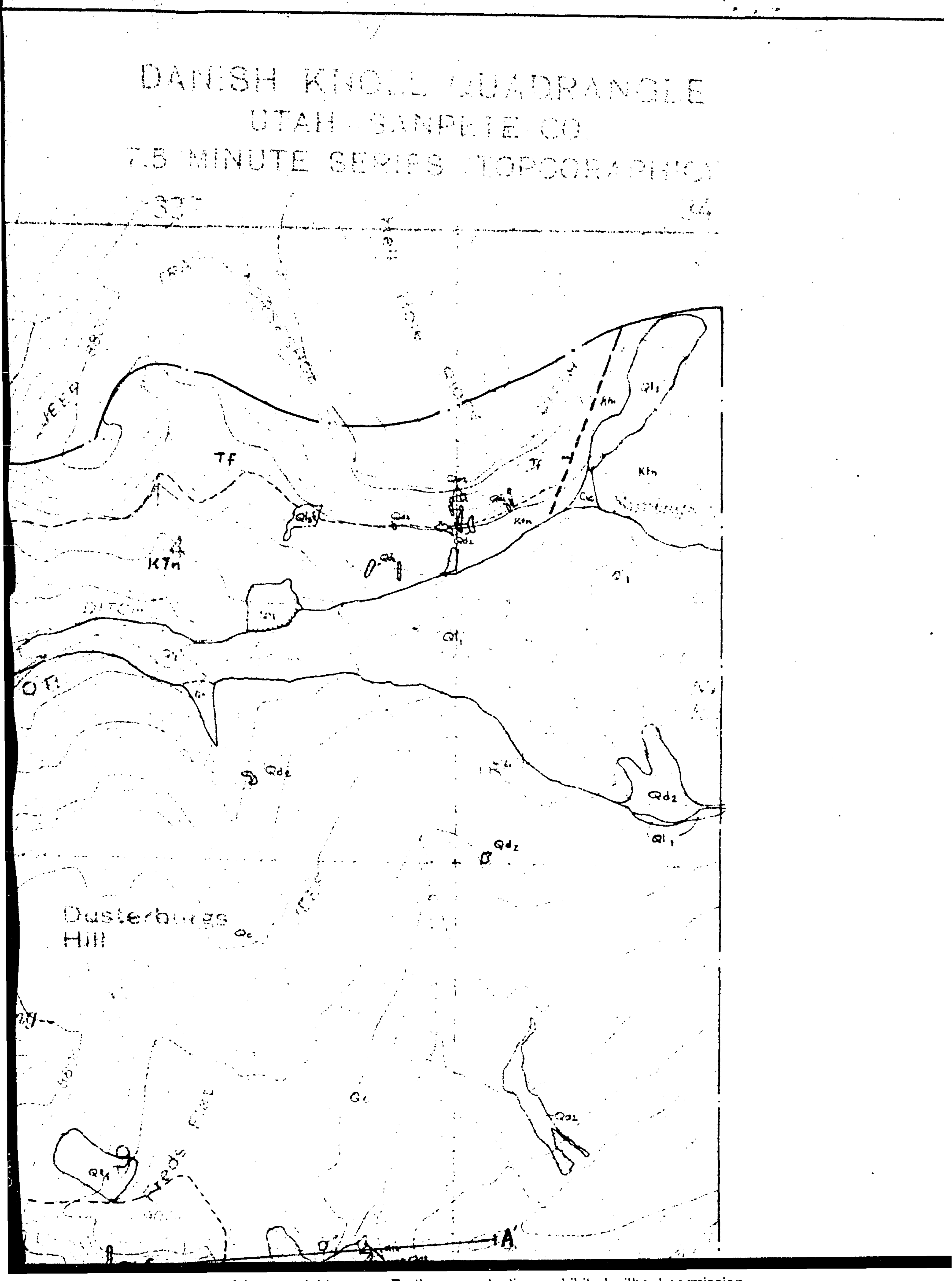
DANISH KNOLL QUADRANGLE
UTAH - SANPETE CO.
7.5 MINUTE SERIES (TOPOGRAPHIC)
Tf
KTn
Qd2
Qt1
Kfn
Ql1
Dusterburgs
Hill
A'

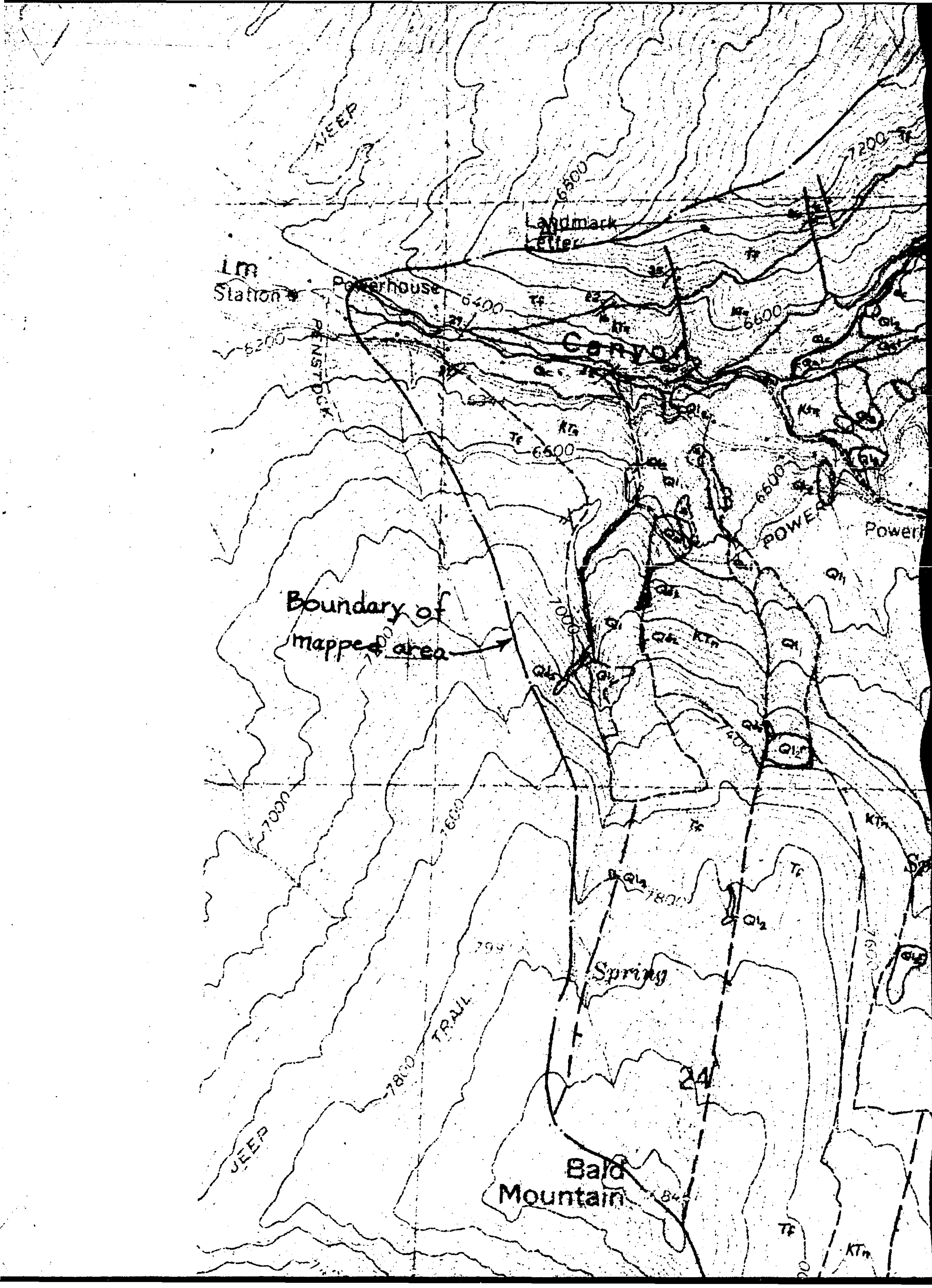

Landmark
Letter
Powerhouse
Station
PENSTOCK
Canyon
Boundary of
mapped area
POWER
Spring
24
Bald
Mountain
JEEP
TRAIL
6500
6400
6200
6600
7200
7000
7400
7800
7600

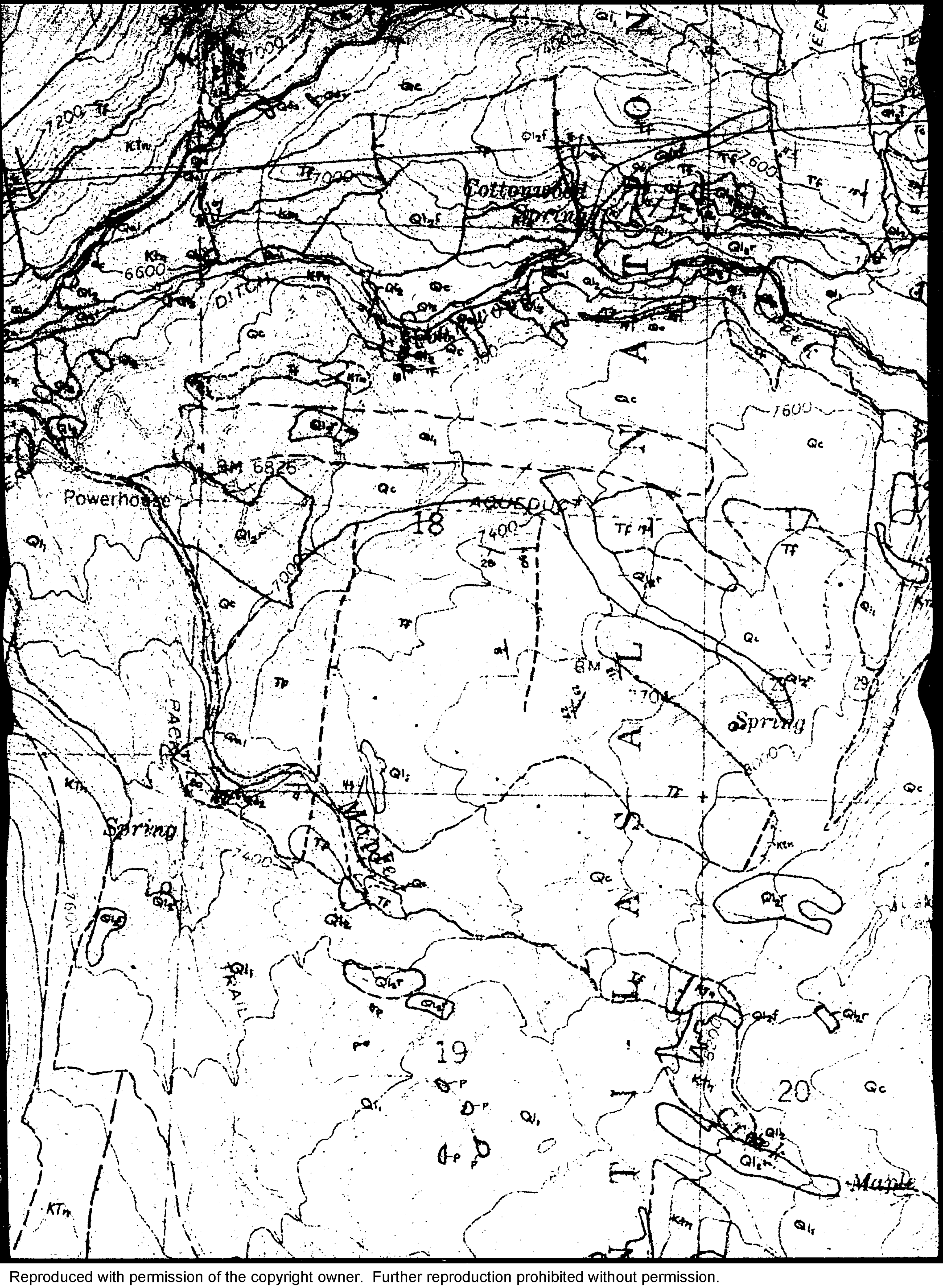

Cottonwood
Spring
DITCH
Powerhouse
BM 6826
AQUEDUCT
18
PACK
TRAIL
Spring
Maple
19
20
Spring
Maple

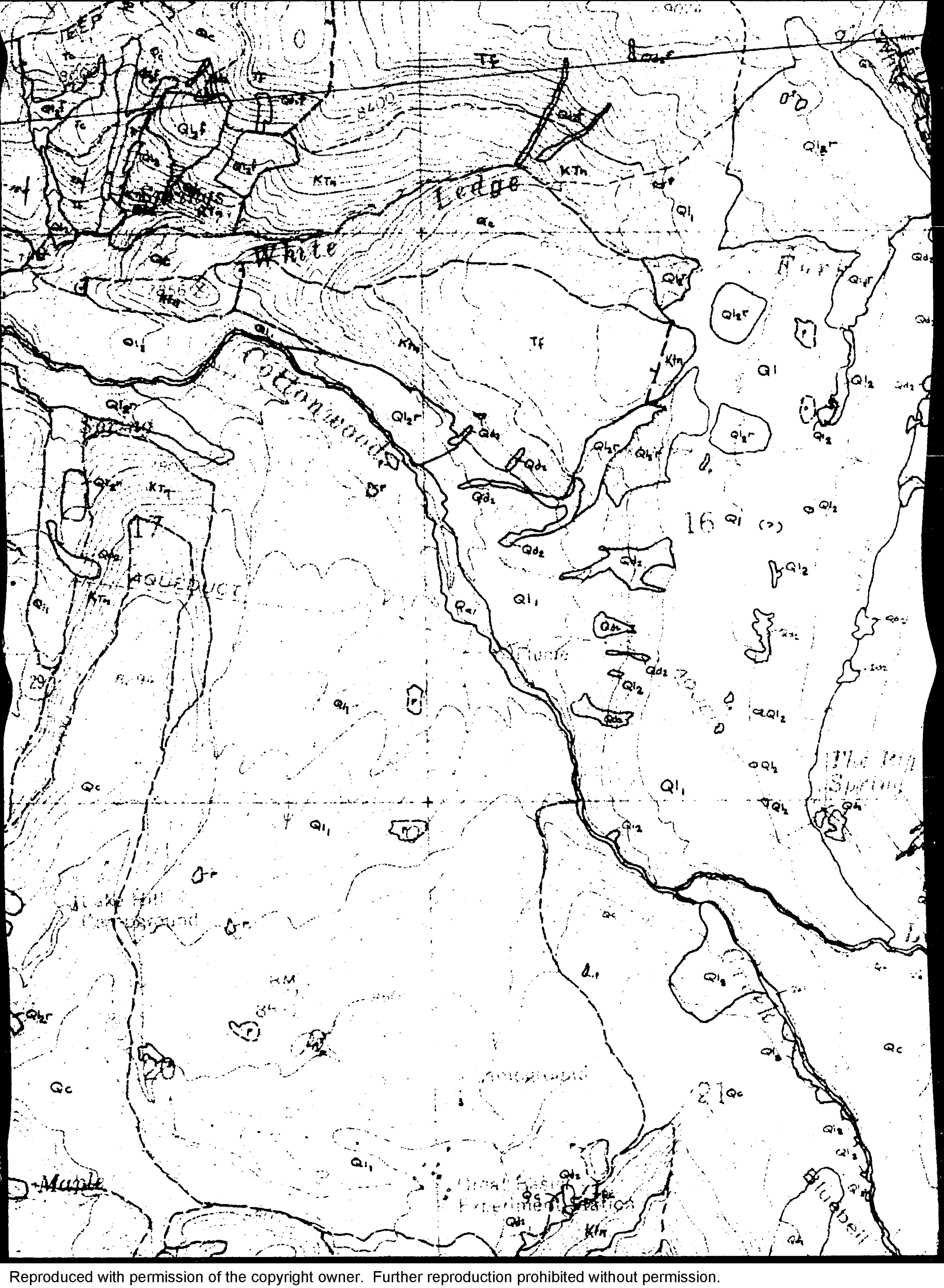

White
Ledge
Cottonwood
AQUEDUCT
16
17
21
Maple
8400
Tf
KTn
Qc
Ql1
Ql2r
Qd2

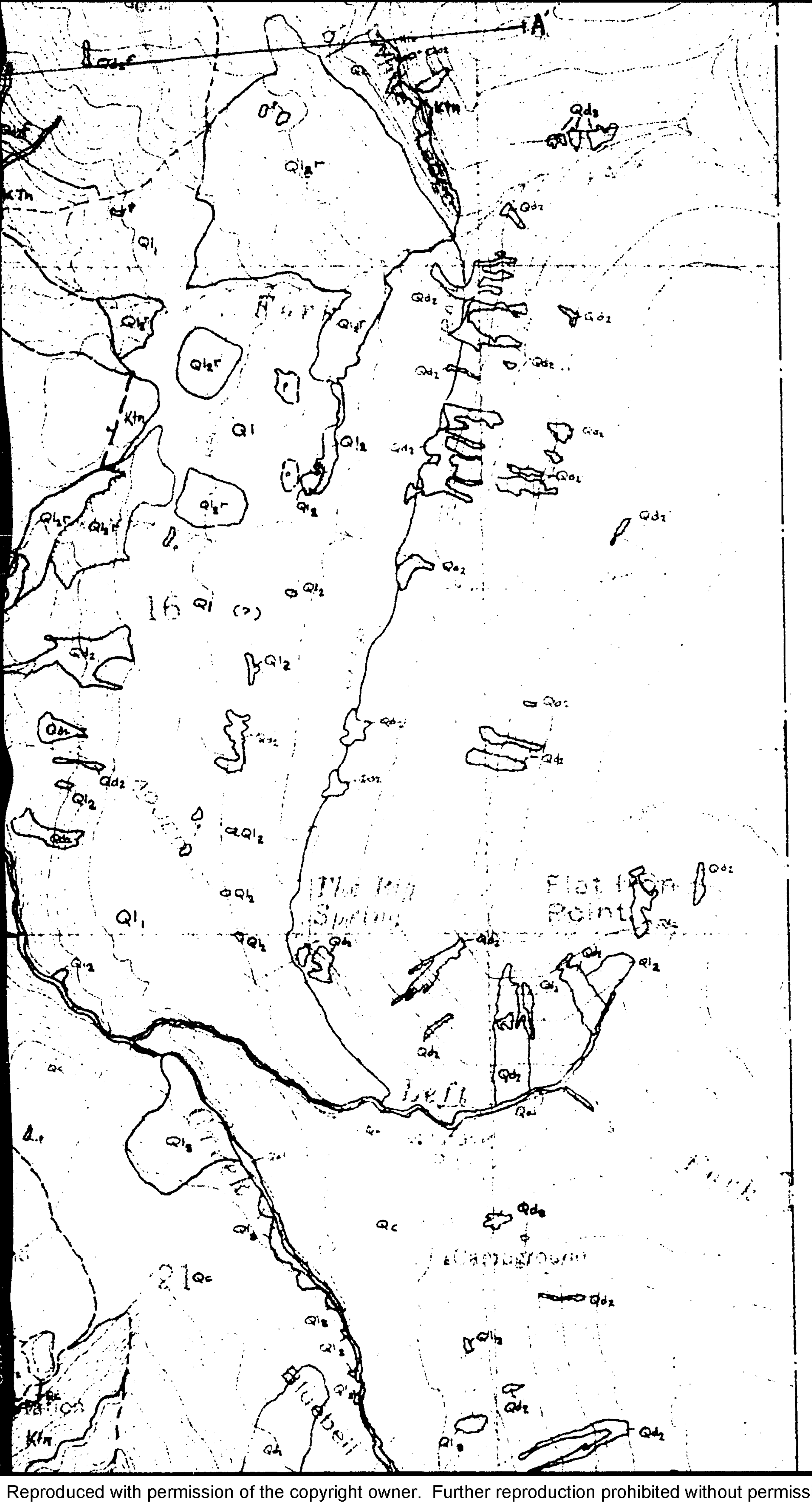
A'
Ktn
Qd2
Ql2r
Ql1
Ql
Ql2
16
Ql (?)
Flat Iron
Point
Qc
21

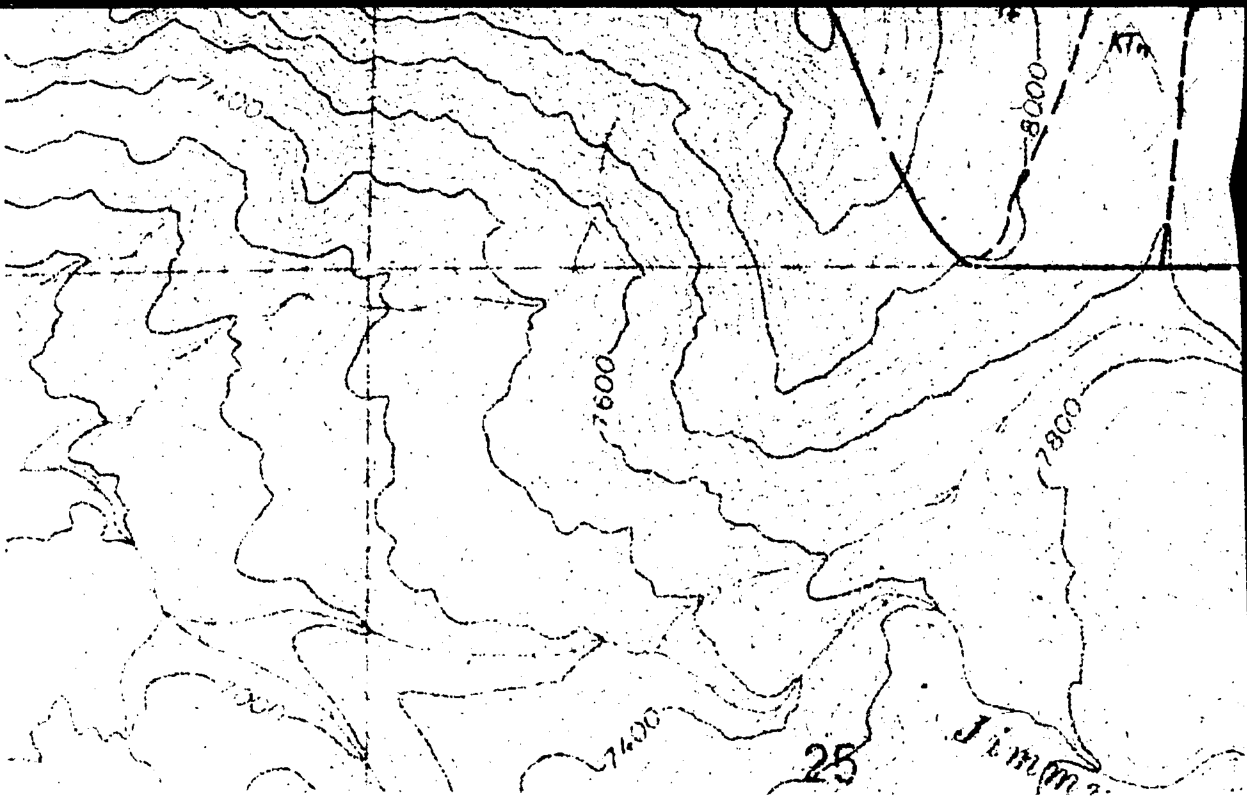
KTn
8000
7400
7600
7800
7400
25
Jimm

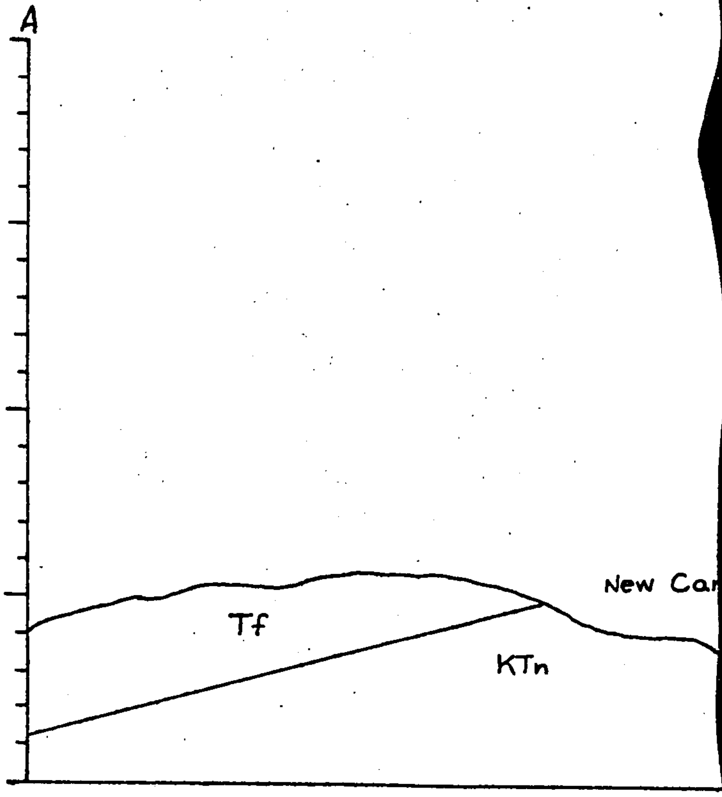
A
Tf
KTn
New Ca

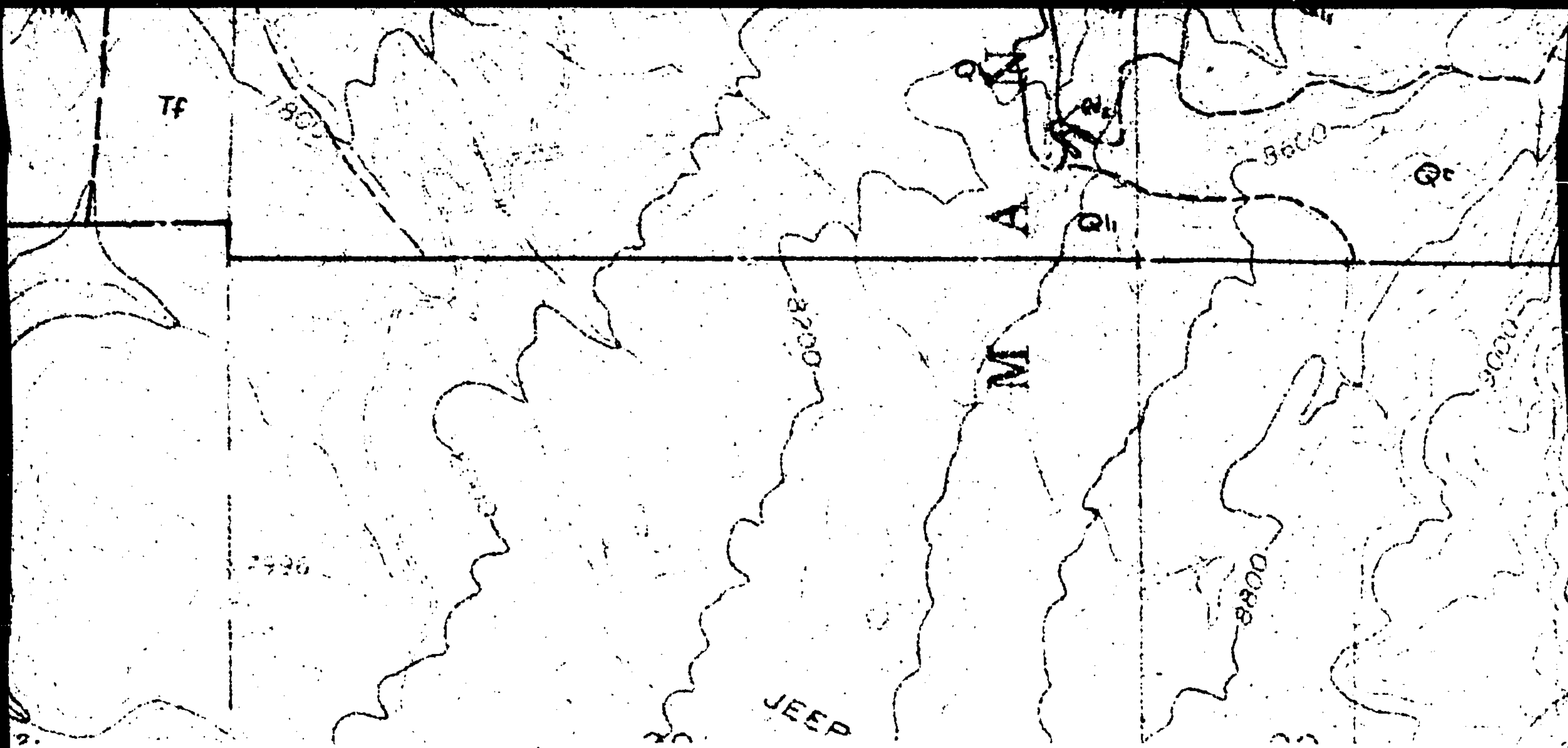

Geologic Map of part of Ephraim Ca

0

Scale

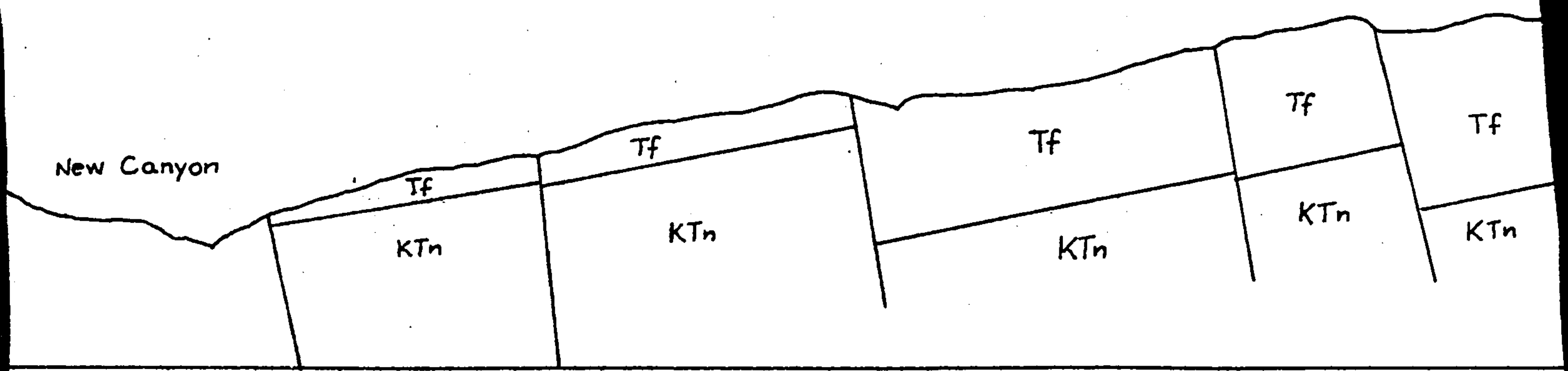

Section A-A′

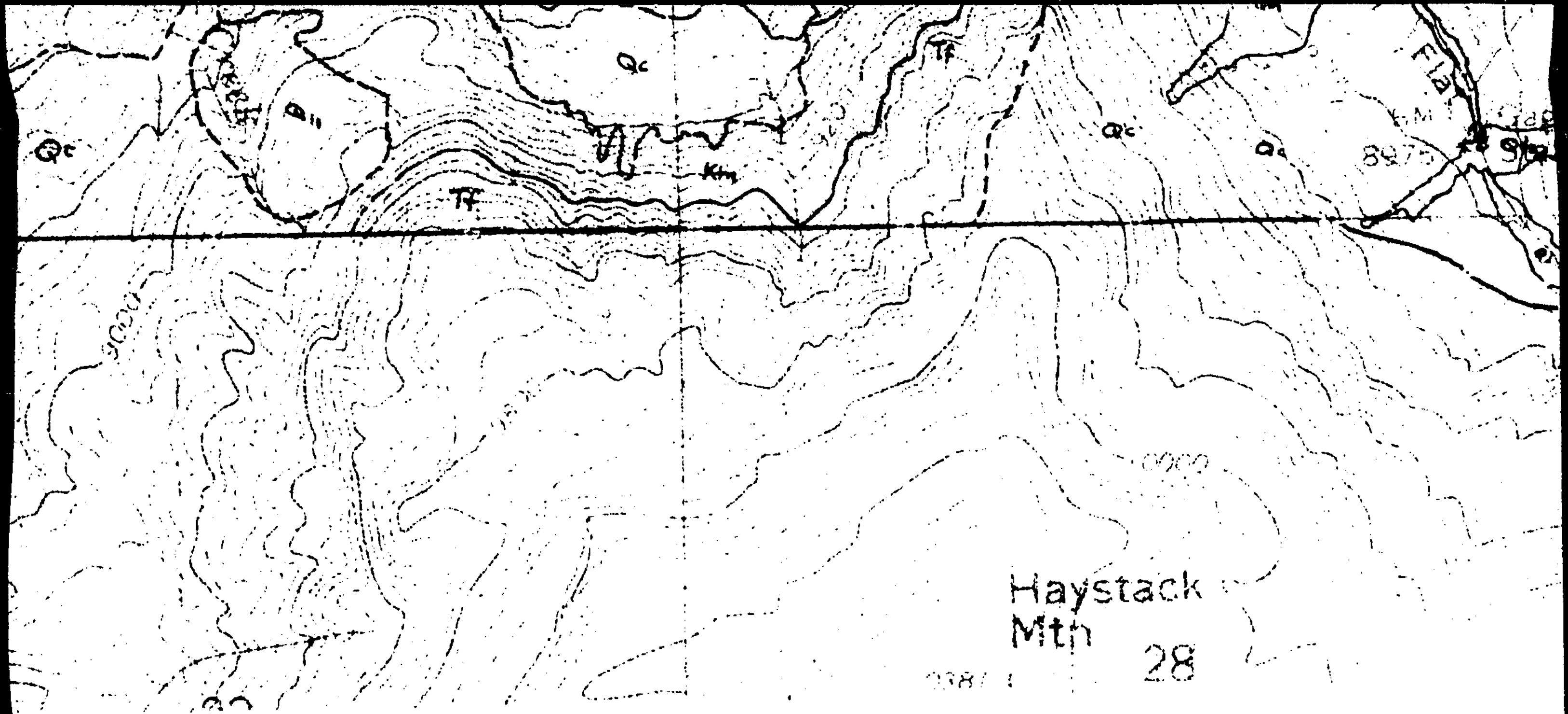

aim Canyon, central Utah

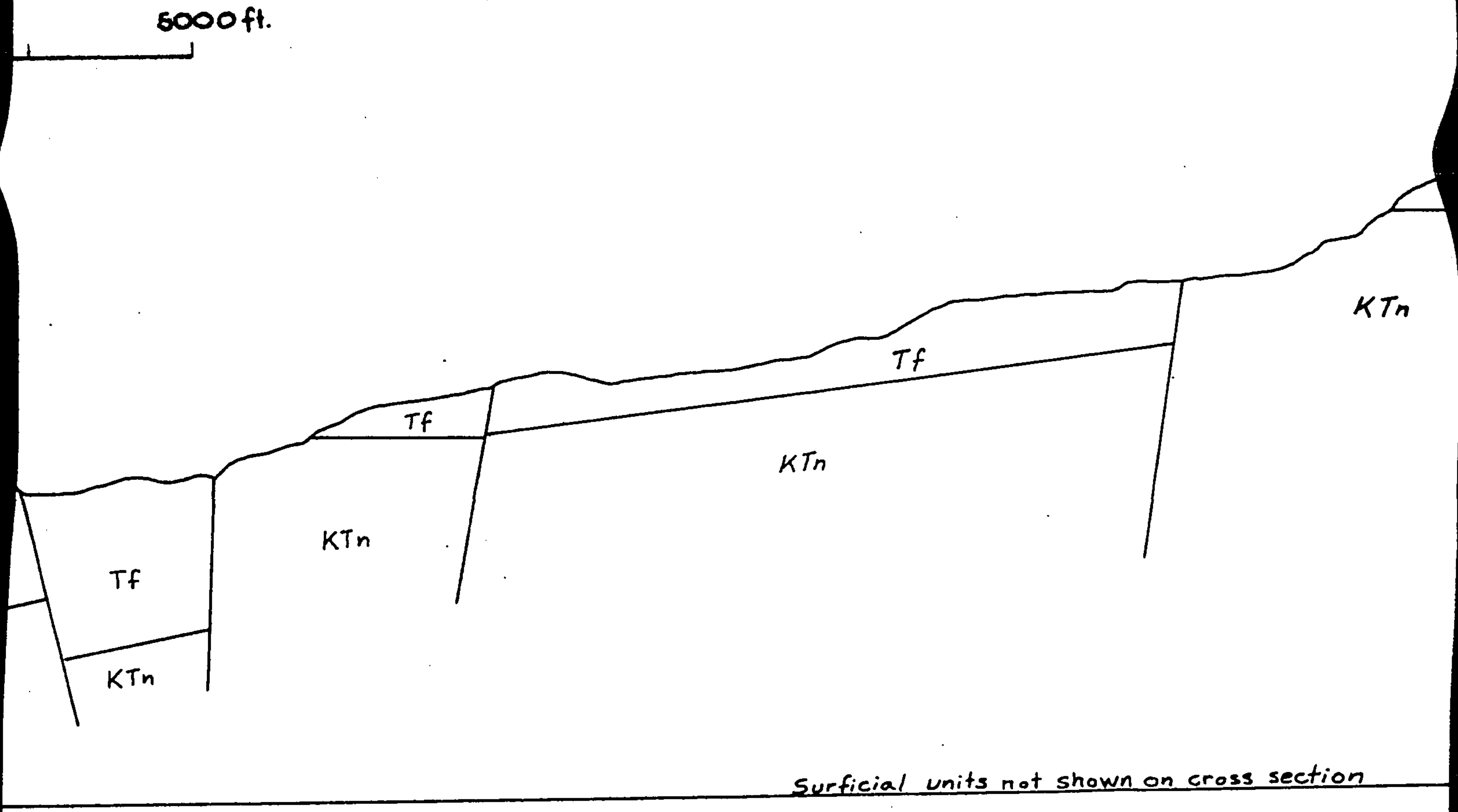

A-A′

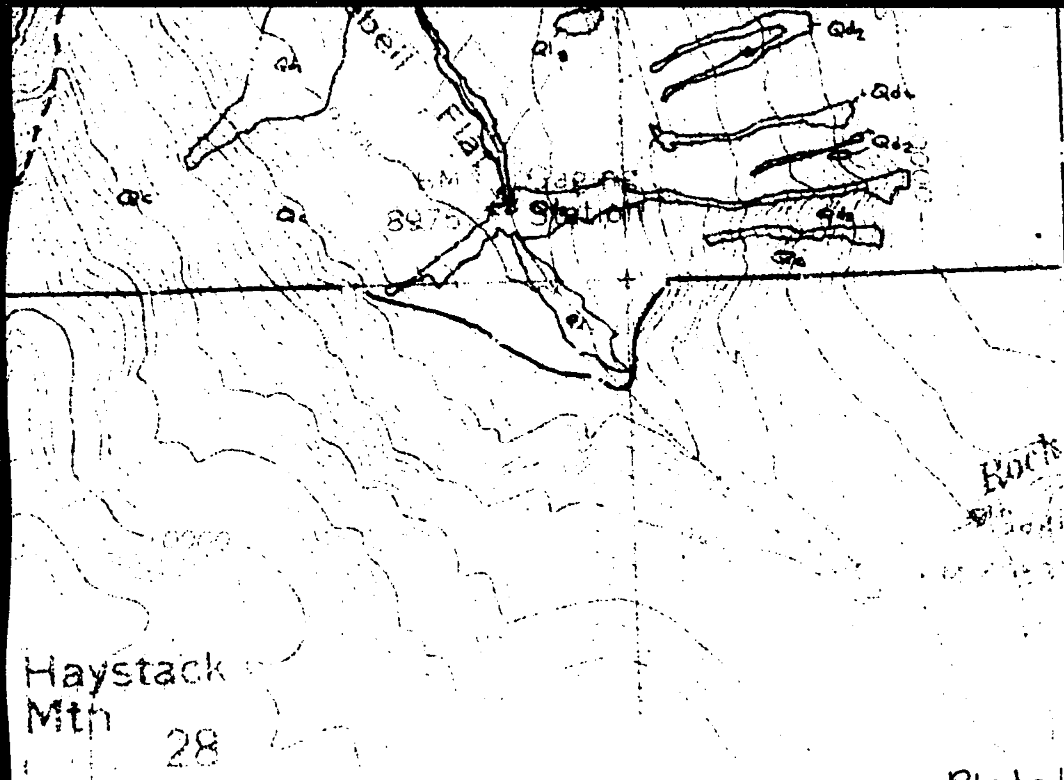

Qd2
Station
8975
Rock
Haystack
Mtn
28

Plate I.

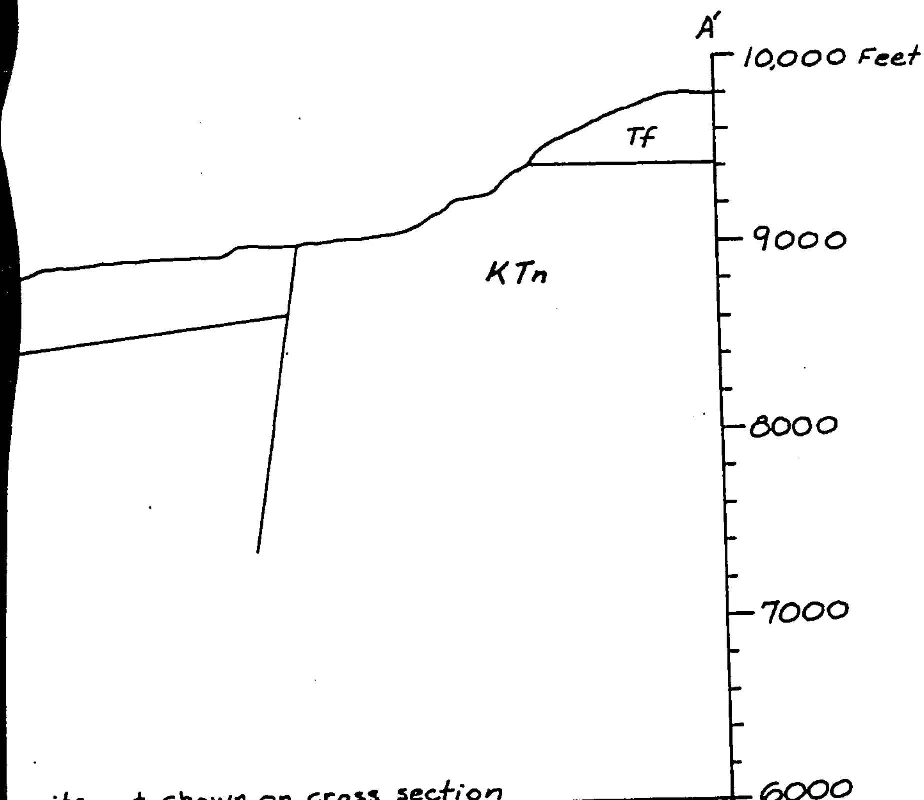

A′
10,000 Feet
Tf
9000
KTn
8000
7000
6000
units not shown on cross section

DESCRIPTION OF MAP UNITS

QUATERNARY DEPOSITS

Ql_2 **Younger landslide deposits, undivided**--Brown, reddish-brown, and gray, unconsolidated, unsorted debris: boulder-, cobble-, and pebble-size clasts of limestone and sandstone, supported by a matrix of sandy clay. Deposits made by earthflows, slumps, and similar landslides that occurred in older landslide debris sometime between 1983 and 1986. Surfaces of deposits are cracked and deformed. Heads of landslides slope gently, bodies slope parallel to neighboring ground, and toes slope more steeply than neighboring ground. Thickness ranges up to about 30 m

Ql_2f **Younger landslide deposits, first-time failures**--Deposits made by rockslides and earthflows that occurred in previously unfailed materials sometime between 1983 and 1986. Gray or reddish-brown porous rubble consisting of blocks and cobble- and pebble-size clasts mixed with clay. Upper parts of deposits clast supported, lower parts matrix supported. Earthflow deposits resemble those of Ql_2 in lithology, color, and texture. Thickness ranges up to about 15 m. Locally includes areas of bedrock

Qd_2 **Younger debris flow deposits**--Brown, unconsolidated, unsorted, unstratified debris; angular boulder-, cobble-, and pebble-size clasts of limestone and sandstone in a matrix of sandy or silty clay. Deposits left by debris flows that were active between 1983 and 1986. Deposits form long, narrow strips in and adjacent to gullies on steep slopes. Thickness ranges up to about 2 m

Qd_2f **Younger debris flow deposits, first-time failures**--Brown, unconsolidated, unstratified, unsorted debris; angular boulder-, cobble-, and pebble-size clasts of limestone and sandstone in a matrix of sandy clay or silty clay. Primarily matrix supported. Unit was deposited by debris flows during 1983-1986. The flows mobilized from bedrock or weathered-bedrock that had not previously failed and moved downslope

Qal **Alluvium**--Brown, sorted, stratified, unconsolidated deposits of clay, silt, sand, pebbles, cobbles, and boulders. Alluvium occurs in and adjacent to channels of Ephraim Creek and its tributaries. Upper few decimeters of terrace deposits (older alluvium above beds of active channels) commonly weathered to dark brown. Thickness of deposits ranges up to a few meters

reddish-
debris:
of
trix of
slumps,
der
1986.
med.
lope
lope more
s ranges

s--
that
sometime
own porous
d pebble-
of
x
se of Ql_2
s ranges
f bedrock

ated,
der-,
e and
y.
ive
narrow
slopes.

es--
ed
le-size
ix of

ows
bedrock
y failed

dated
bles, and
to
es.
lder
monly
sits

Qc **Colluvium, residuum, and slope wash, undifferentiated**--Poorly sorted, unstratified or locally stratified, unconsolidated deposits of boulder-, cobble-, and pebble-size clasts of limestone and sandstone in a gray or brown matrix of sandy clay or silty clay. Upper few decimeters commonly is a brown or dark brown topsoil. Material derived from local bedrock and transported downslope by gravity or sheet flow. Includes talus deposit at base of White Ledge (SE1/4 sec. 9, T. 17 S., R. 4 E.), fan- and cone-shaped deposits at the base of steep slopes, and sheetlike deposits that mantle gentle to steep slopes. Deposits typically 1 to 10 m thick. Locally includes area of bedrock and alluvium

Ql_1 **Older landslide deposits**--Unsorted, unstratified, unconsolidated debris; boulder-, cobble-, and pebble-size clasts of sandstone and limestone supported by a brown or gray matrix of sandy clay. A dark brown soil 50 to 100 cm thick is developed in this unit. Toes, benches, ridges, closed depressions, and other morphologic features characteristic of landsliding are subdued on these deposits. Thickness ranges up to 50 (?) m

Qd_1 **Older debris or mud-flow deposits**--Gray or brown, weathered, crudely stratified debris. Angular boulder-, cobble- and pebble-size clasts of limestone or sandstone supported by matrix of silty clay or clay. Deposits result from single debris-flow events and occur in and near channels, and have subdued levees and tonguelike terminations. Dark brown soil, 10 to 40 cm thick, is developed on these deposits. Thickness ranges up to about 2 m

TERTIARY DEPOSITS

Tc **Colton Formation** (Eocene)--Green, variegated and brown claystones interbedded with gray limestones and fine- to medium-grained yellow or brown sandstones. Conformable with and interfingers with the underlying Flagstaff Limestone. Only the lower 20 to 30 m exposed in study area. (Spieker, 1946; Bonar, 1948; Zawiskie and others, 1982)

Tf

TKn

Tf **Flagstaff Limestone (Eocene and Paleocene), undivided**--White, gray, and light-brown limestones interbedded with gray, green, and black claystones. Conformably and gradationally overlies the North Horn Formation. Lower 80 to 90 m (Ferron Mountain Member): gray, bluish-gray, and light-brown carbonate rocks interbedded with dark gray, massive or laminated, 0.05- to 2.4-m-thick claystones. Carbonate beds are 0.1 to 1.9 m thick, fine grained or micritic. Mud cracks filled with dark micrite are common. Gastropods and pelecypods common in fine-grained, sparry carbonate beds. Middle 132 to 142 m (Cove Mountain Member): white, pale gray, and pale yellowish-brown micritic, massive carbonates in beds 0.1 to 8.0 m thick; white or gray, limy, medium-grained sandstones; gypsum nodules in gray, green, red, or orange claystone beds. Cove Mountain Member consists of, from bottom to top, 20 m of green and gray claystones containing abundant gypsum nodules; 15 m of thick, resistant, massive limestone with solution cavities; 20 to 25 m of red and gray claystones interbedded with limestones and lenticular, limy sandstones; and 72 to 87 m of alternating white, massive or laminated limestones, fissile, black or green claystones, and beds of chert nodules. The Cove Mountain Member does not contain fossil mollusks. Upper 50 m of Flagstaff Limestone (Musinia Peak Member): olive-green or light-brown claystones; laminated and massive, gray and light-gray, cherty, fossiliferous limestones; brown chert nodules; silicified fossiliferous limestones. Mollusk fossils abundant in Musinia Peak Member. Total thickness of Flagstaff Limestone in Ephraim Canyon is about 275 m (Spieker, 1946; Bonar, 1948; LaRocque, 1960; Stanley and Collinson, 1979)

TKn **North Horn Formation** (Paleocene to Upper Cretaceous)--Orange to buff sandstones and variegated mudstones. Only the upper 250 m exposed in Ephraim Canyon. Upper 150 m: evenly bedded, red, orange, brown, gray, green, purple, or variegated mudstones; thick, evenly bedded yellow, orange, or gray, well-cemented, fine- to coarse-grained, massive sandstones; and (uncommon) gray fossiliferous limestones. Lower 100 m: irregularly bedded, red, orange, brown, gray, green, purple, or variegated mudstones; yellow, orange, or gray, well-cemented, crossbedded, lenticular sandstones; green, fine-grained sandstones and nodular green siltstones (Bonar, 1948)

Contact
Fault—
dash
Strike
Strike
15
70
Seep or
Pond
Wet land

- Contact--Dashed where approximately located
- Fault—Bar and ball on downthrown side, dashed where approximately located
- 15 Strike and dip of beds
- 70 Strike and dip of fault
- Seep or spring
- Pond
- Wet lands

PLEASE NOTE:

Oversize maps and charts are filmed in sections in the following manner:

LEFT TO RIGHT, TOP TO BOTTOM, WITH SMALL OVERLAPS

The following map or chart has been refilmed in its entirety at the end of this dissertation (not available on microfiche). A xerographic reproduction has been provided for paper copies and is inserted into the inside of the back cover.

Standard 35mm slides or 17" x 23" black and white photographic prints are available for an additional charge.

University Microfilms International

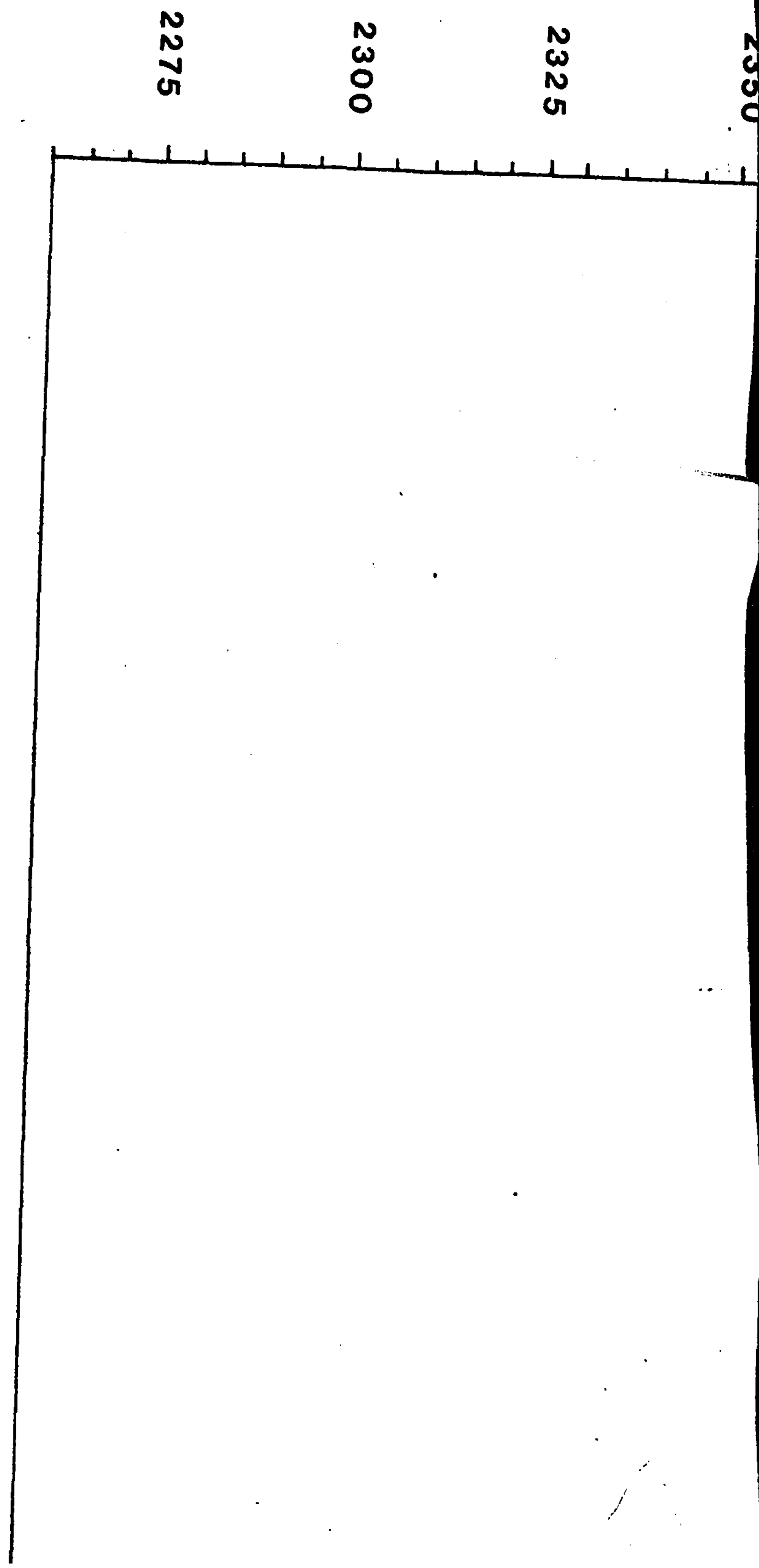
2275
2300
2325
2350

The Aspen Grove Landslide, Ephraim Canyon, Utah

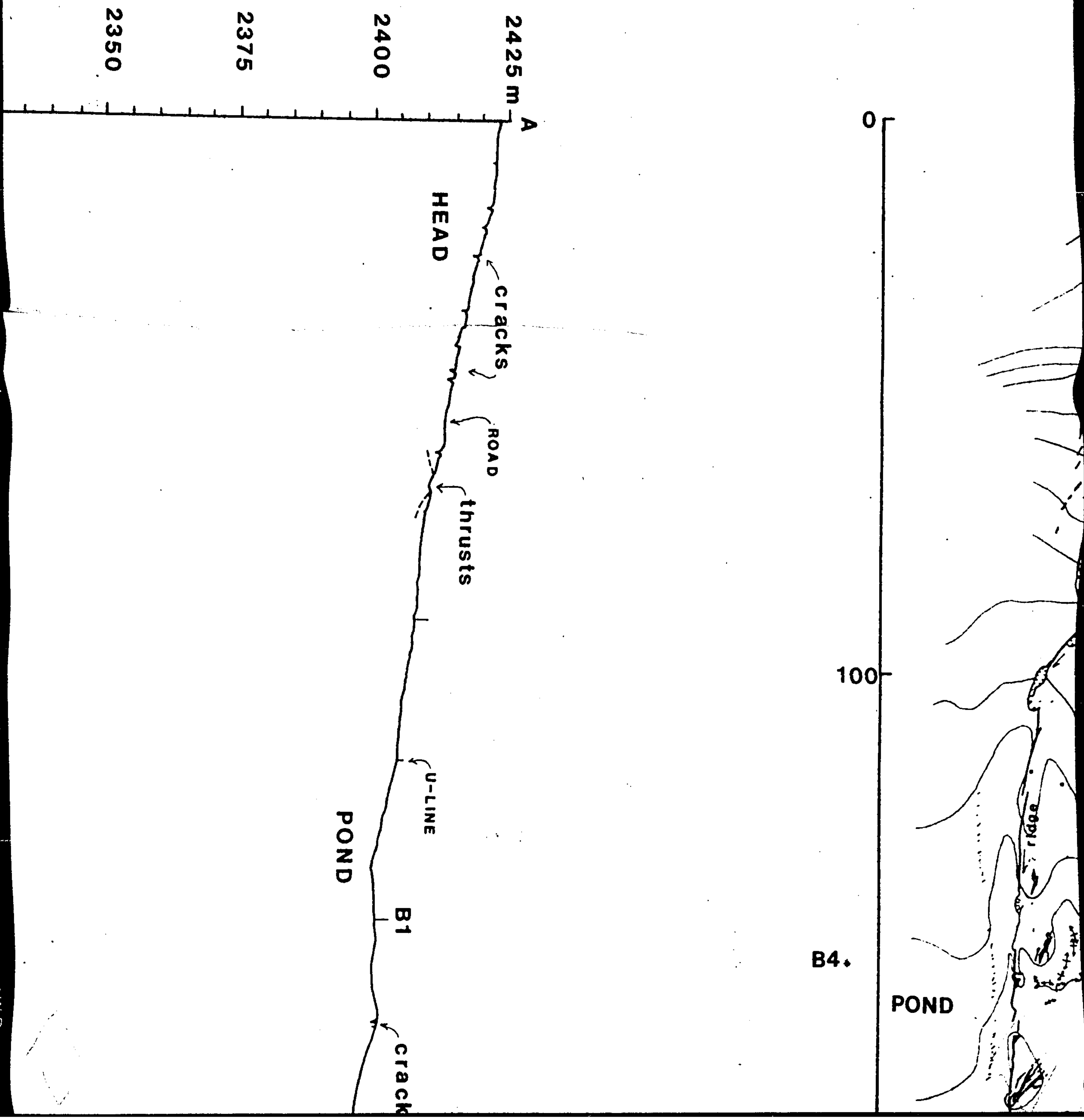

e,

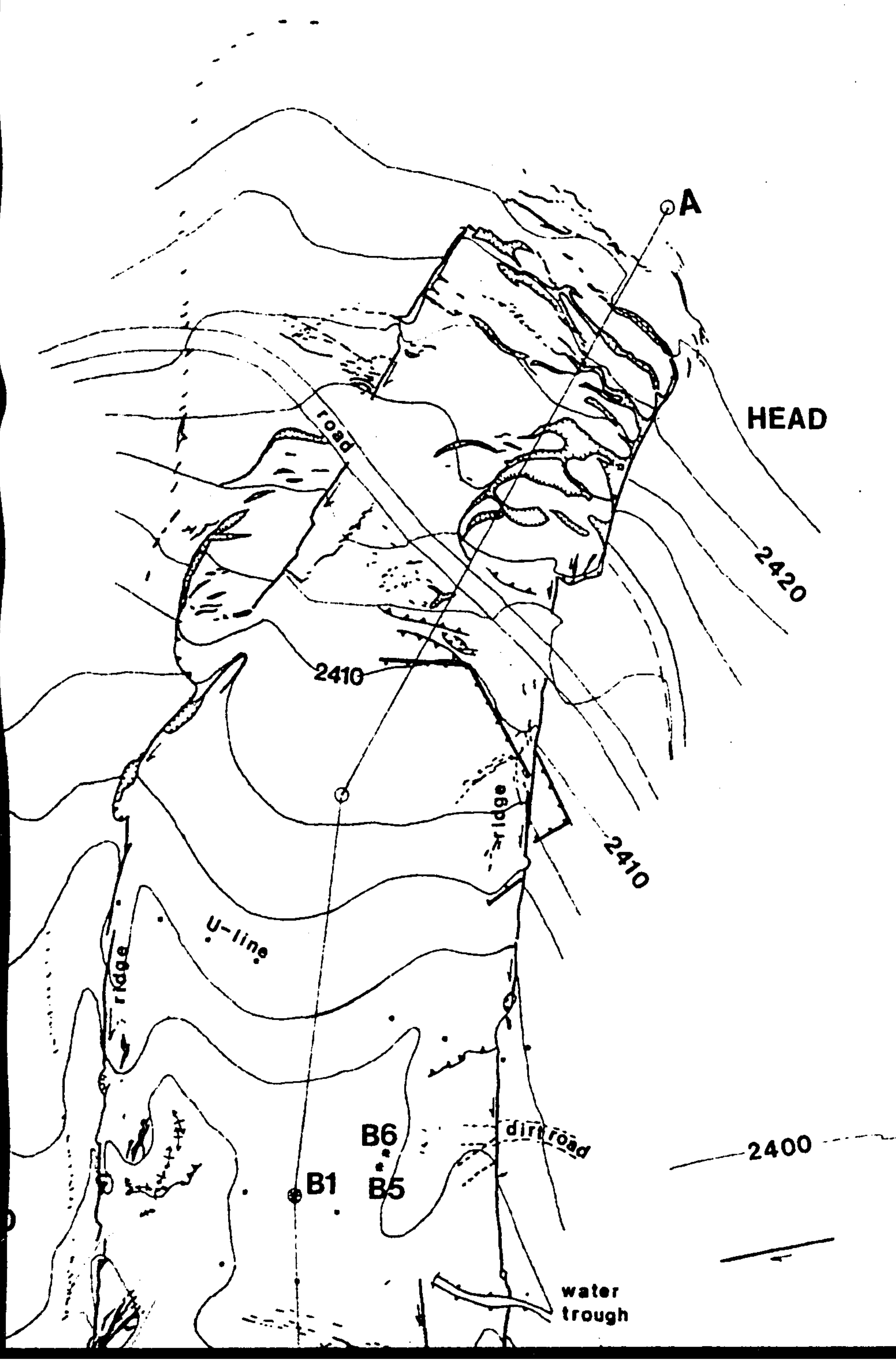

EXPLANATION

2400 Topographic contour

Strike-slip fault, showing direction of moveme

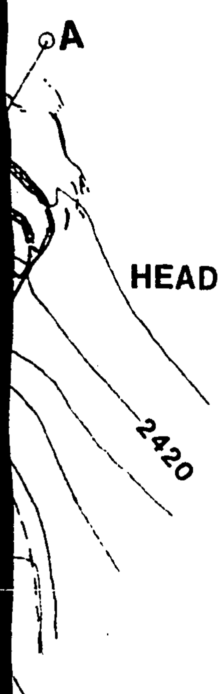

EXPLANATION

2400 — Topographic contour

Strike-slip fault, showing direction of movement

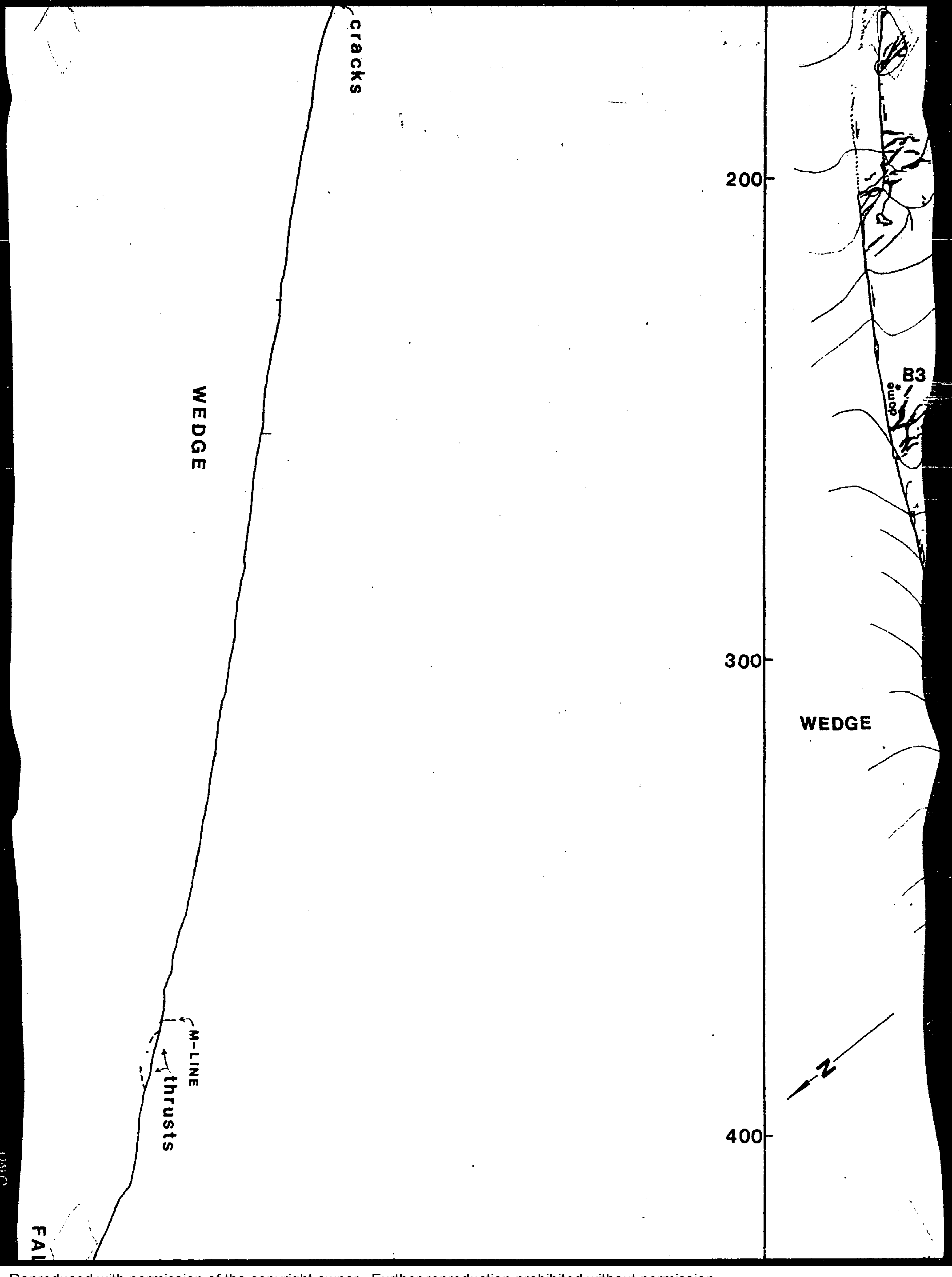
cracks
WEDGE
M-LINE
thrusts
FA
200
300
400
B3
dome
WEDGE
N

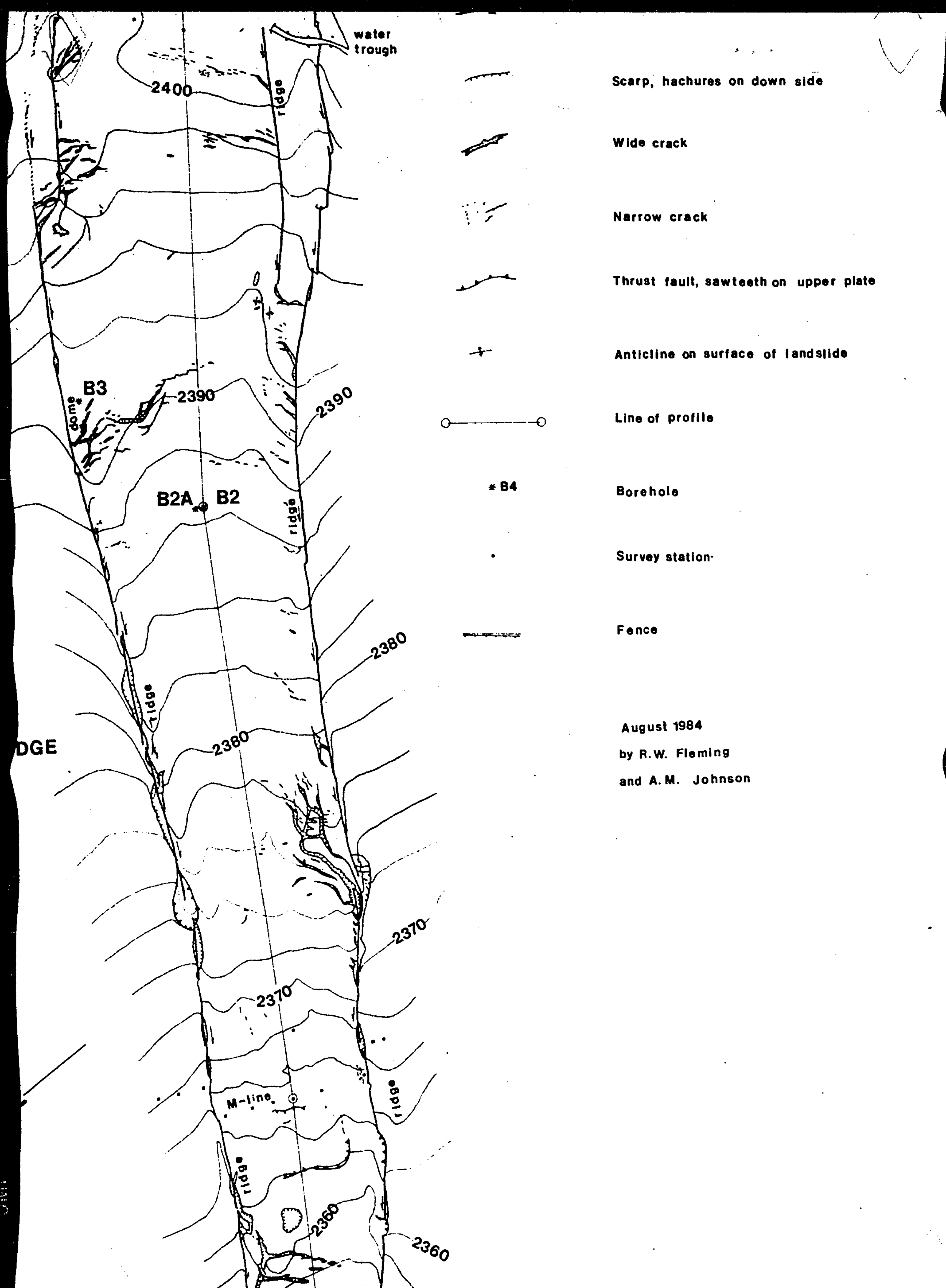
water trough
2400
ridge
B3
dome
2390
2390
B2A
B2
ridge
2380
2380
ridge
DGE
2370
2370
M-line
ridge
ridge
2360
2360
Scarp, hachures on down side
Wide crack
Narrow crack
Thrust fault, sawteeth on upper plate
Anticline on surface of landslide
Line of profile
B4
Borehole
Survey station
Fence
August 1984
by R.W. Fleming
and A.M. Johnson

Scarp, hachures on down side

Wide crack

Narrow crack

Thrust fault, sawteeth on upper plate

Anticline on surface of landslide

Line of profile

* B4 Borehole

Survey station

Fence

August 1984

by R.W. Fleming

and A.M. Johnson

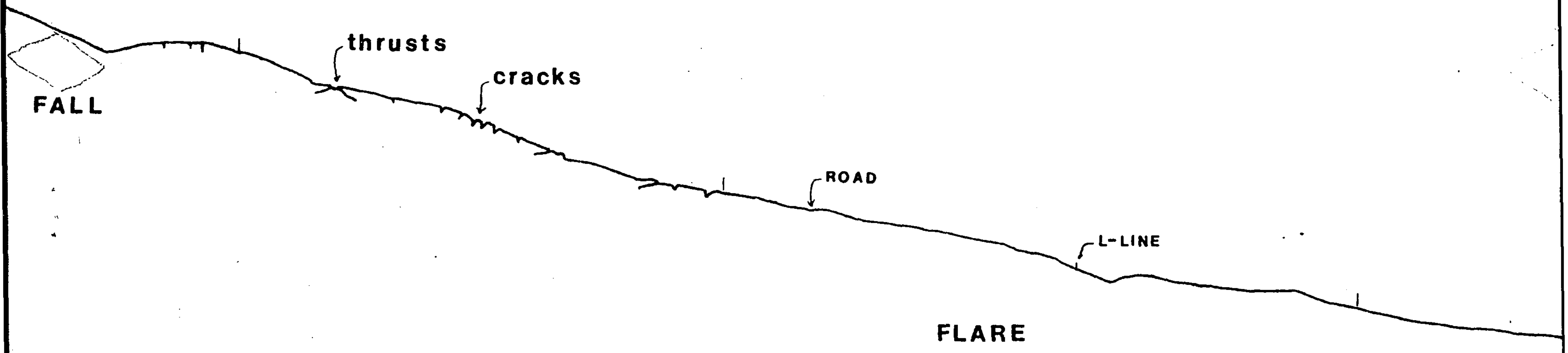

Profile A–A'

(no vertical exageration)

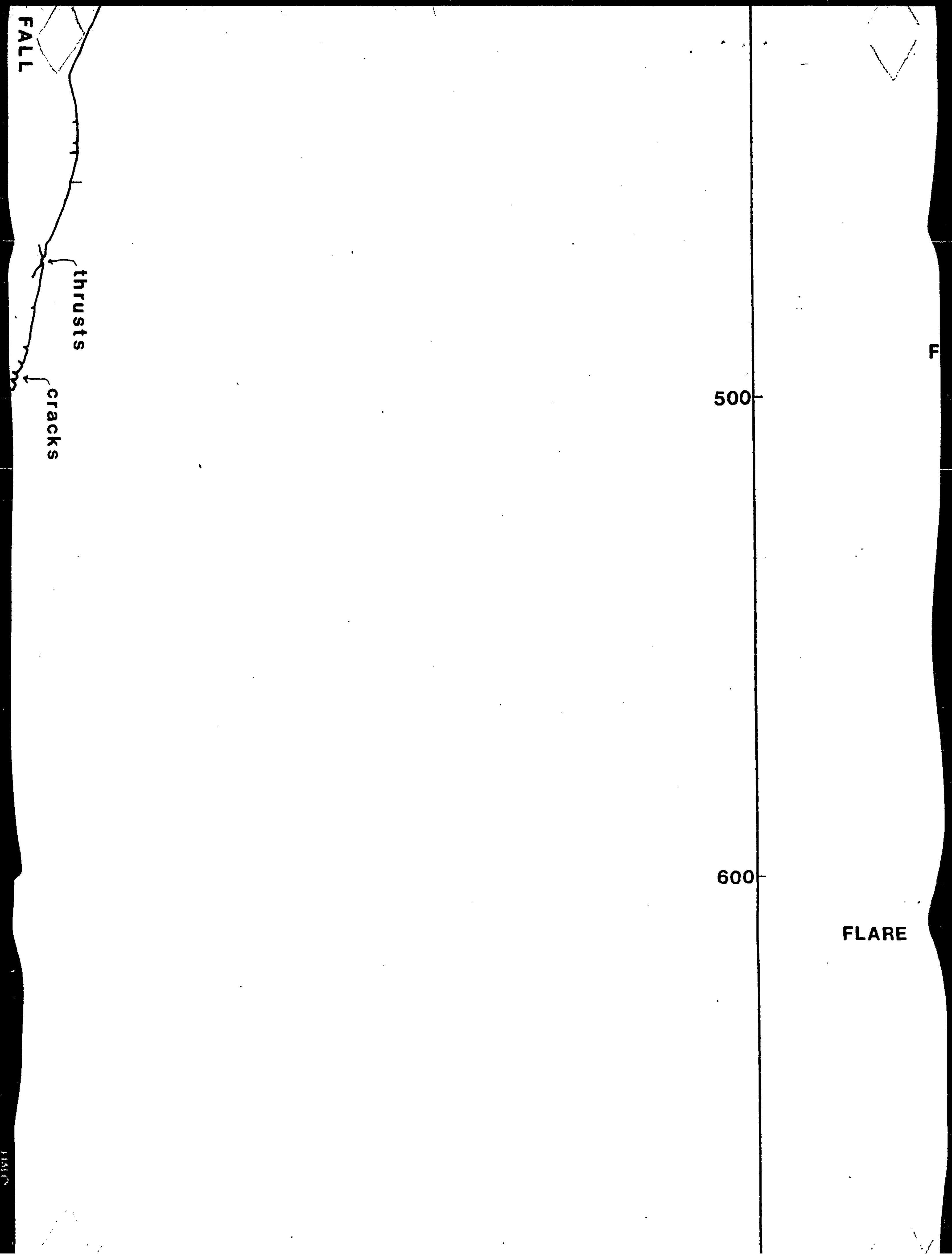
FALL
thrusts
cracks
500
600
FLARE

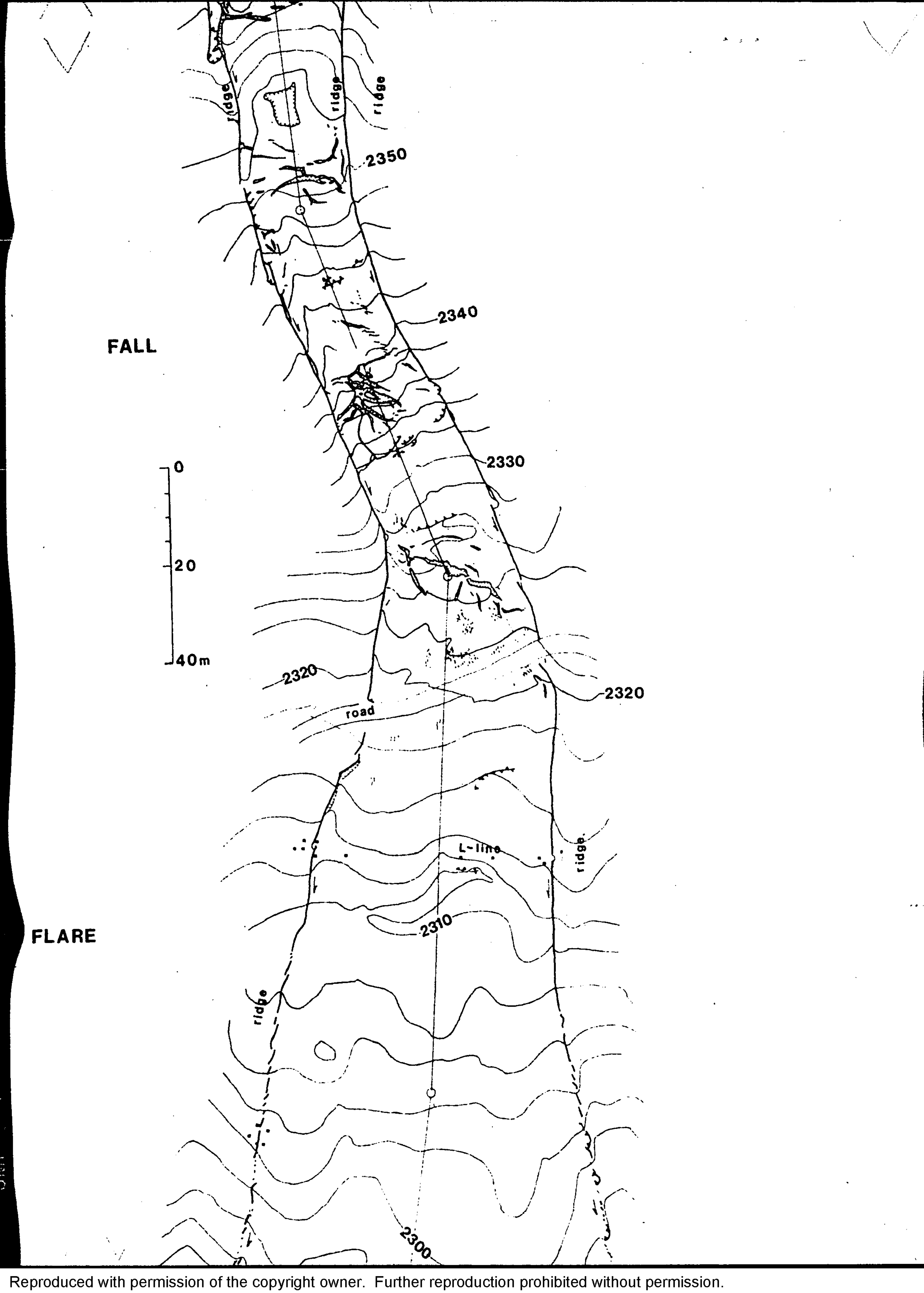

ridge
ridge
ridge
2350
2340
FALL
2330
0
20
40m
2320
2320
road
L-line
ridge
FLARE
2310
ridge
2300

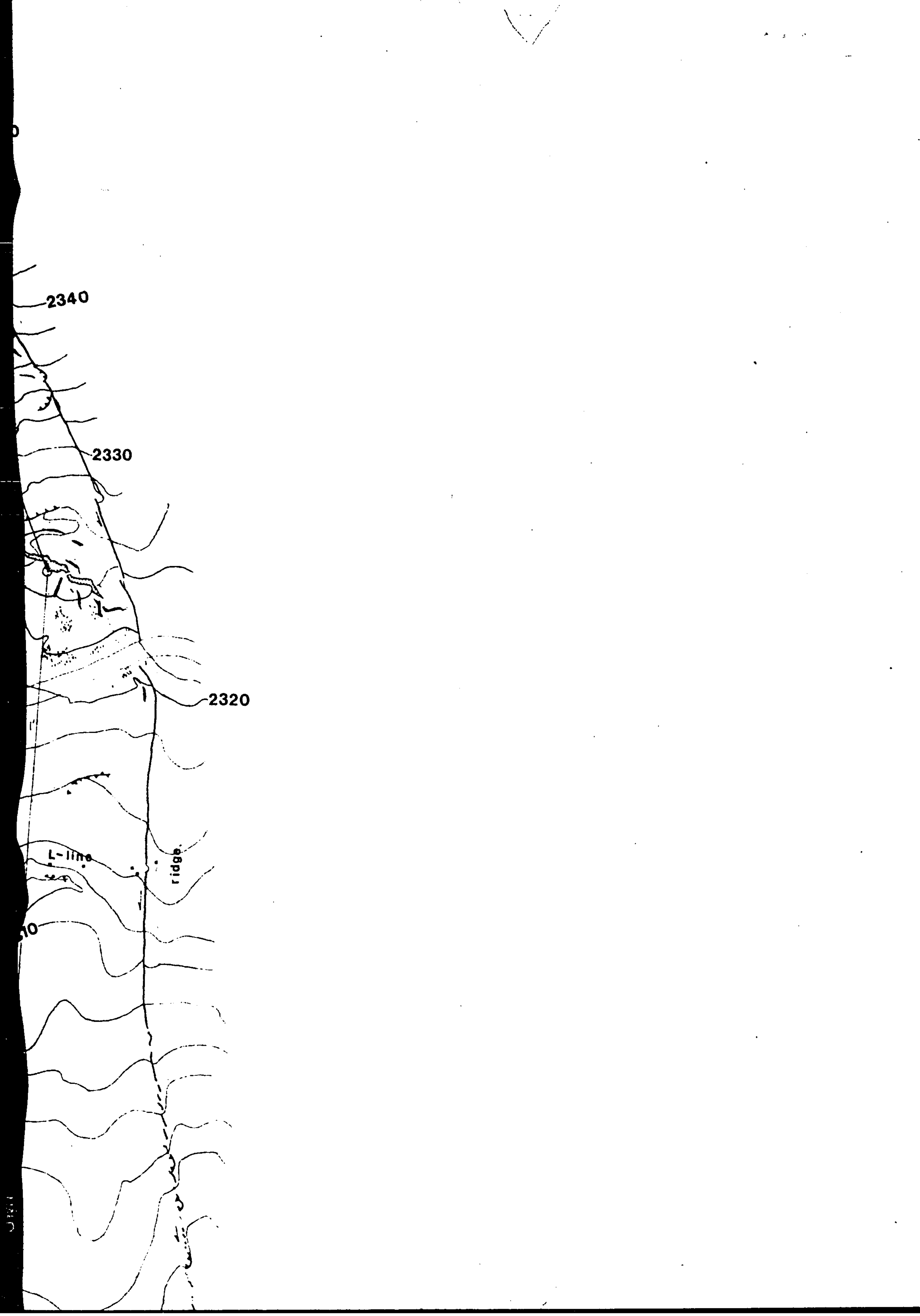
2340
2330
2320
L-line
ridge

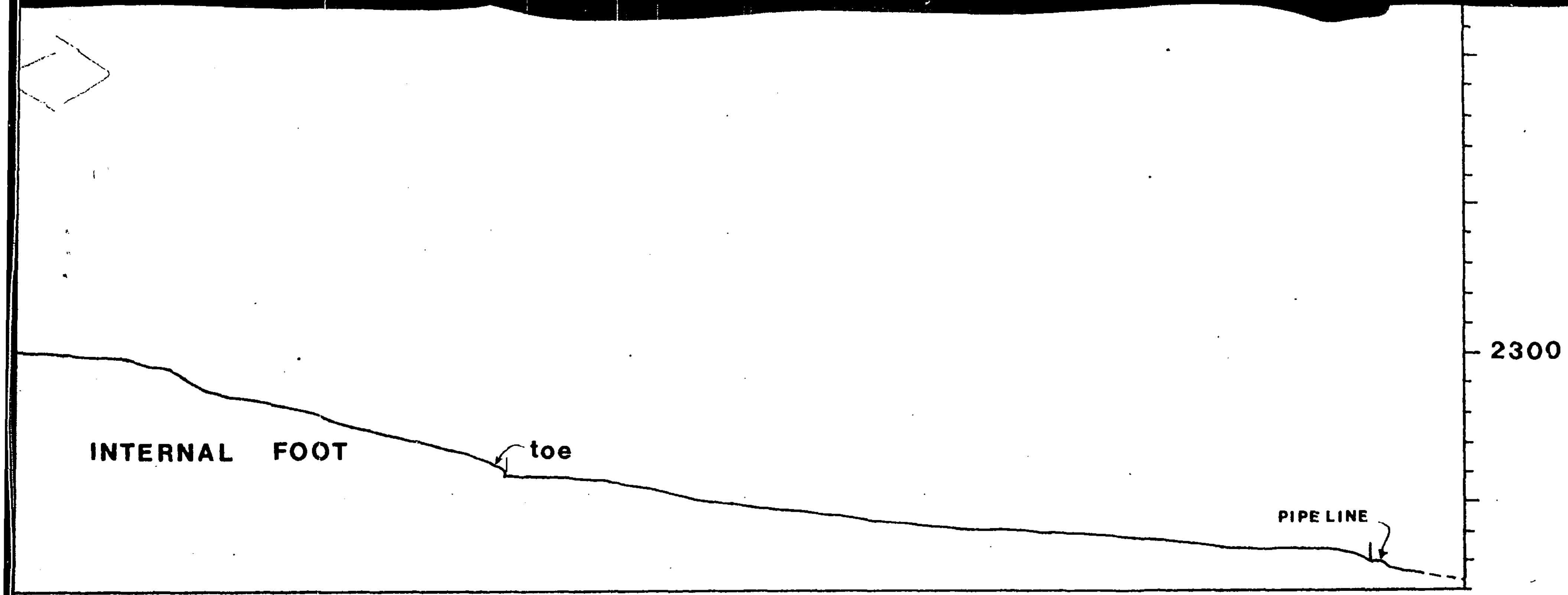
INTERNAL FOOT
toe
PIPE LINE
2300

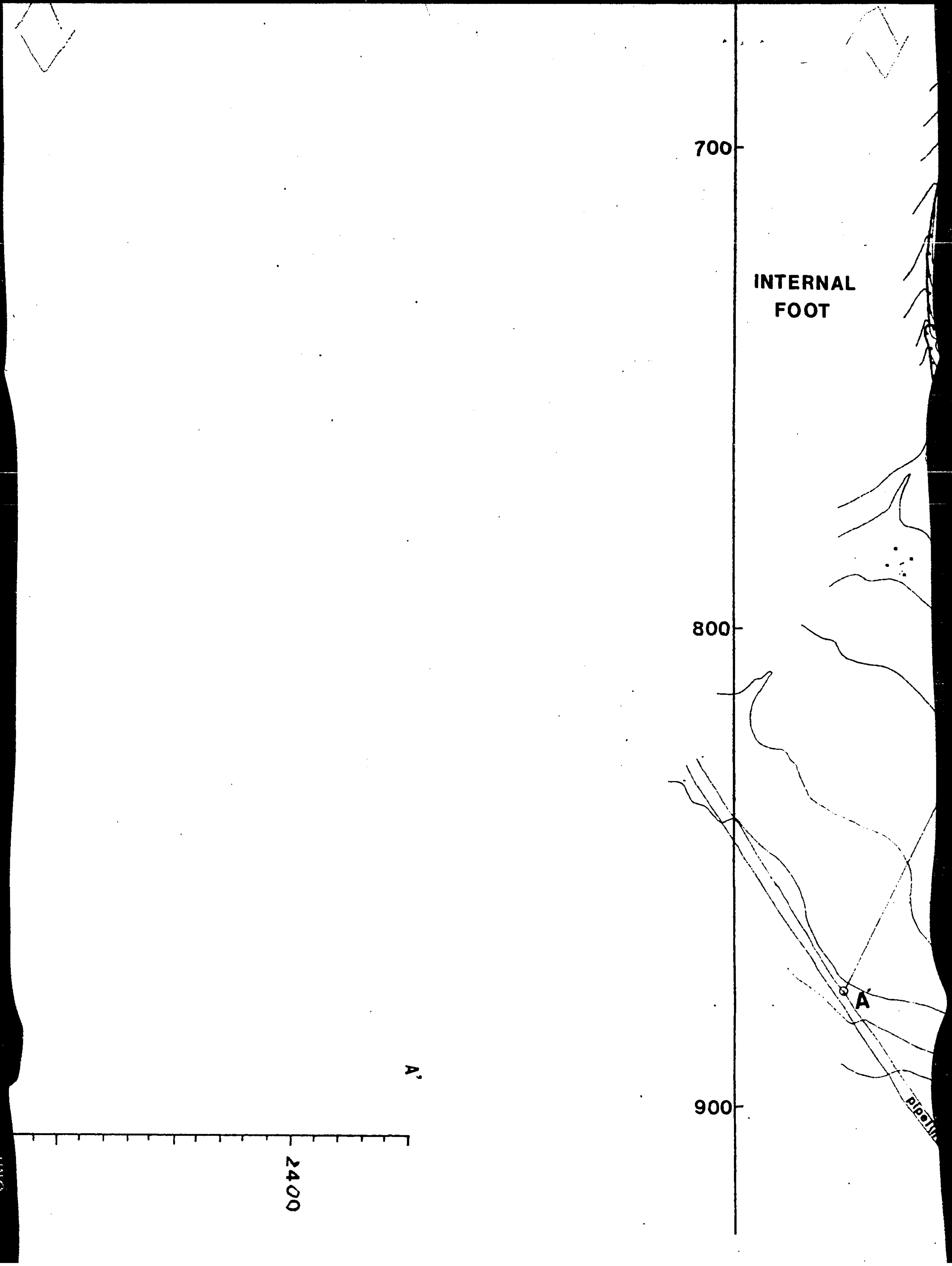
700
INTERNAL
FOOT
800
A'
900
A'
2400

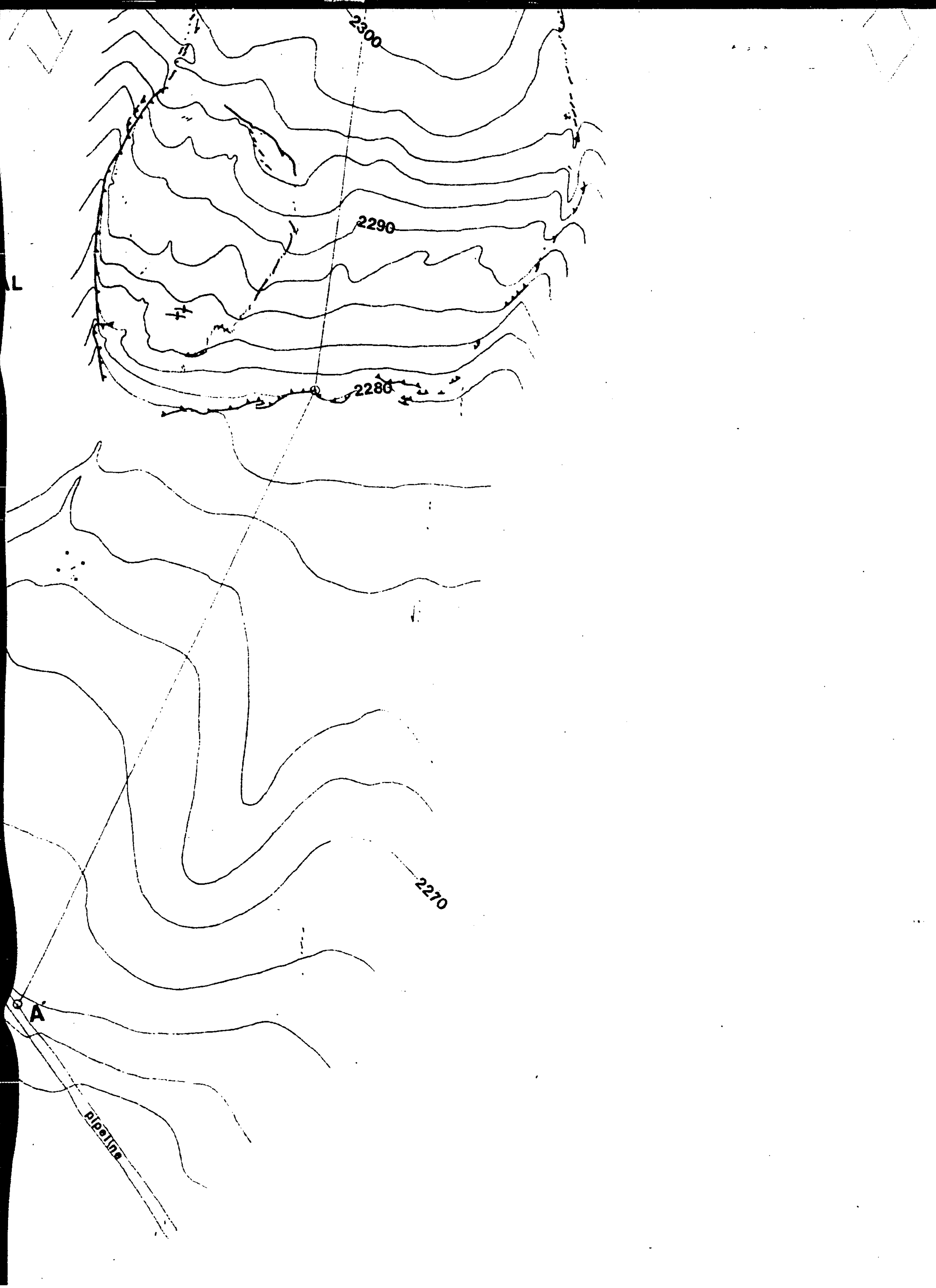
2300
2290
2280
2270
A
L
pipeline

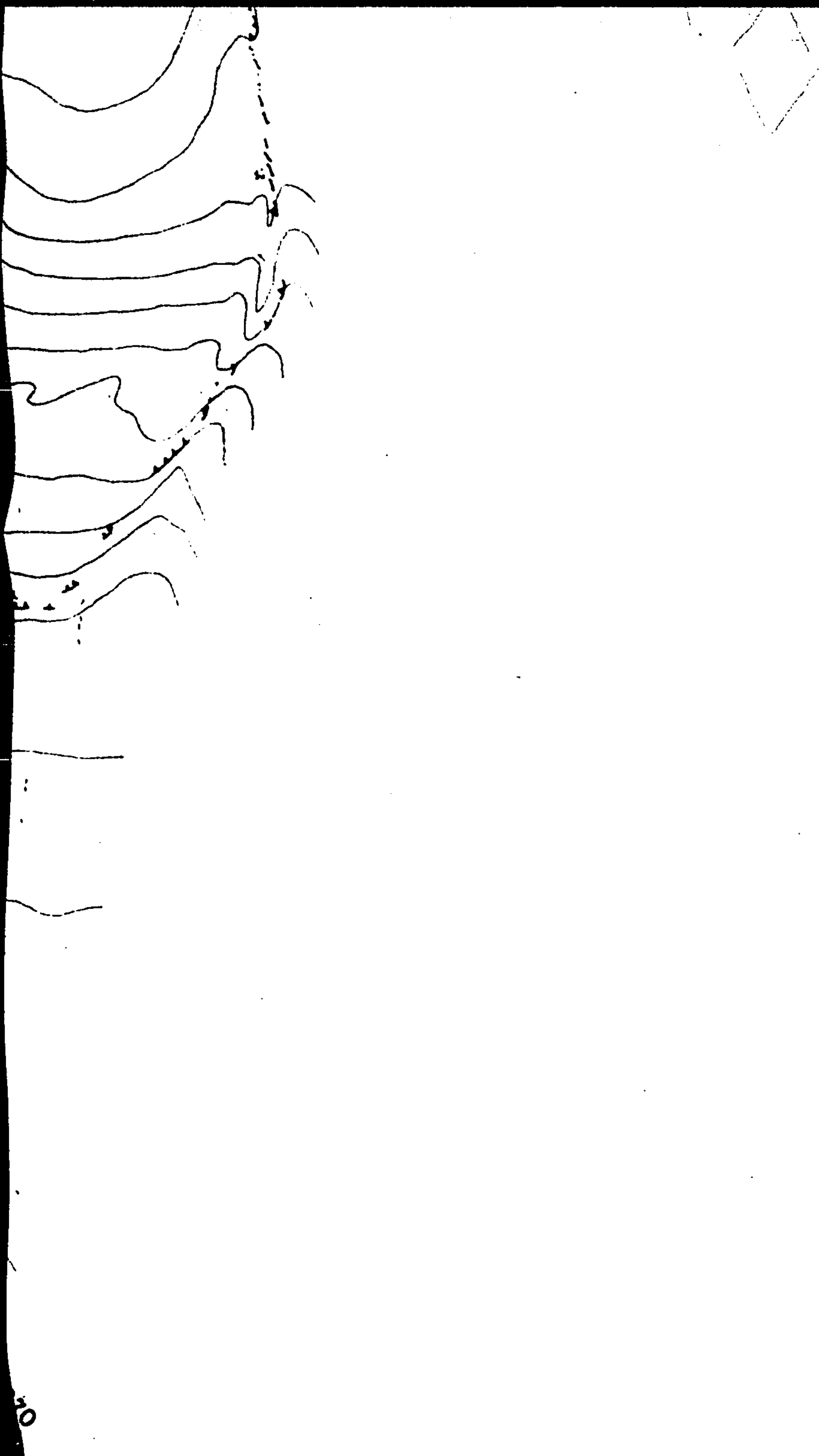

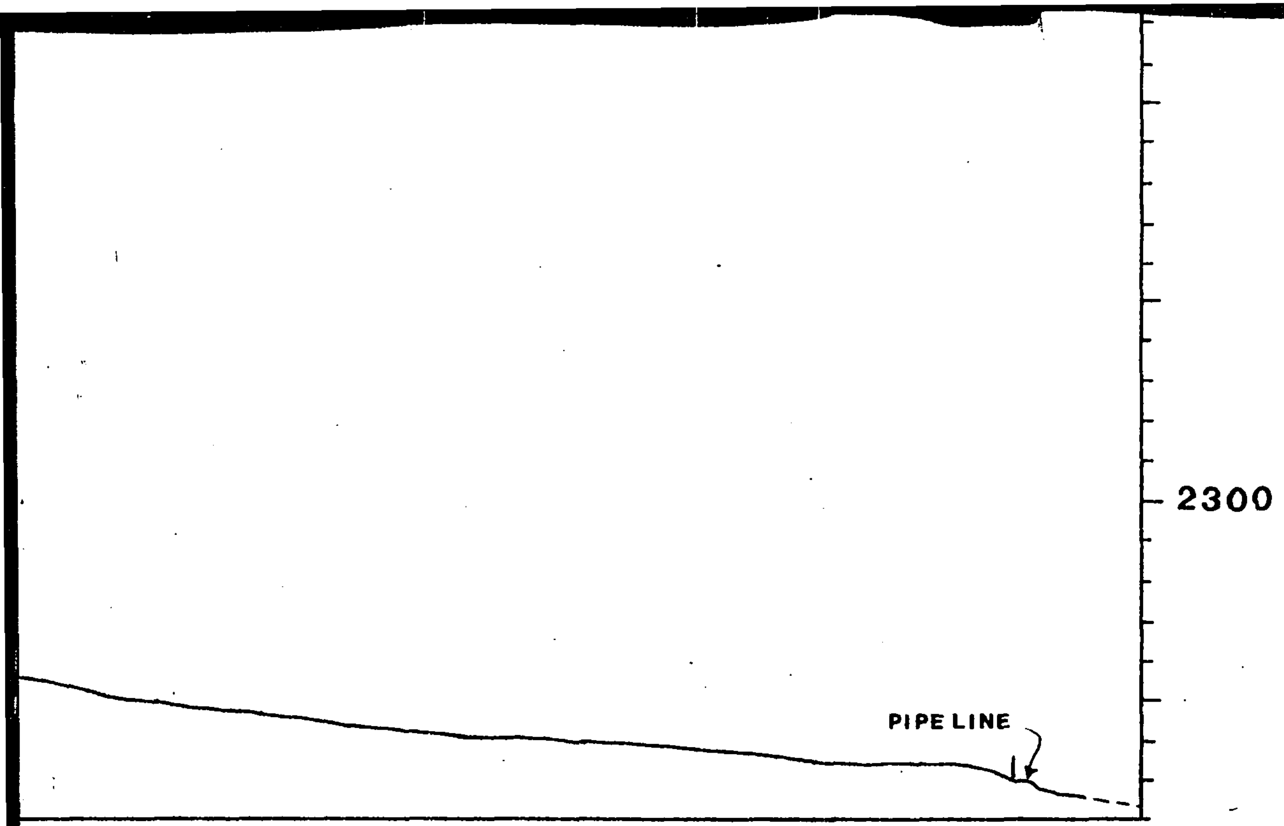

Plate 2

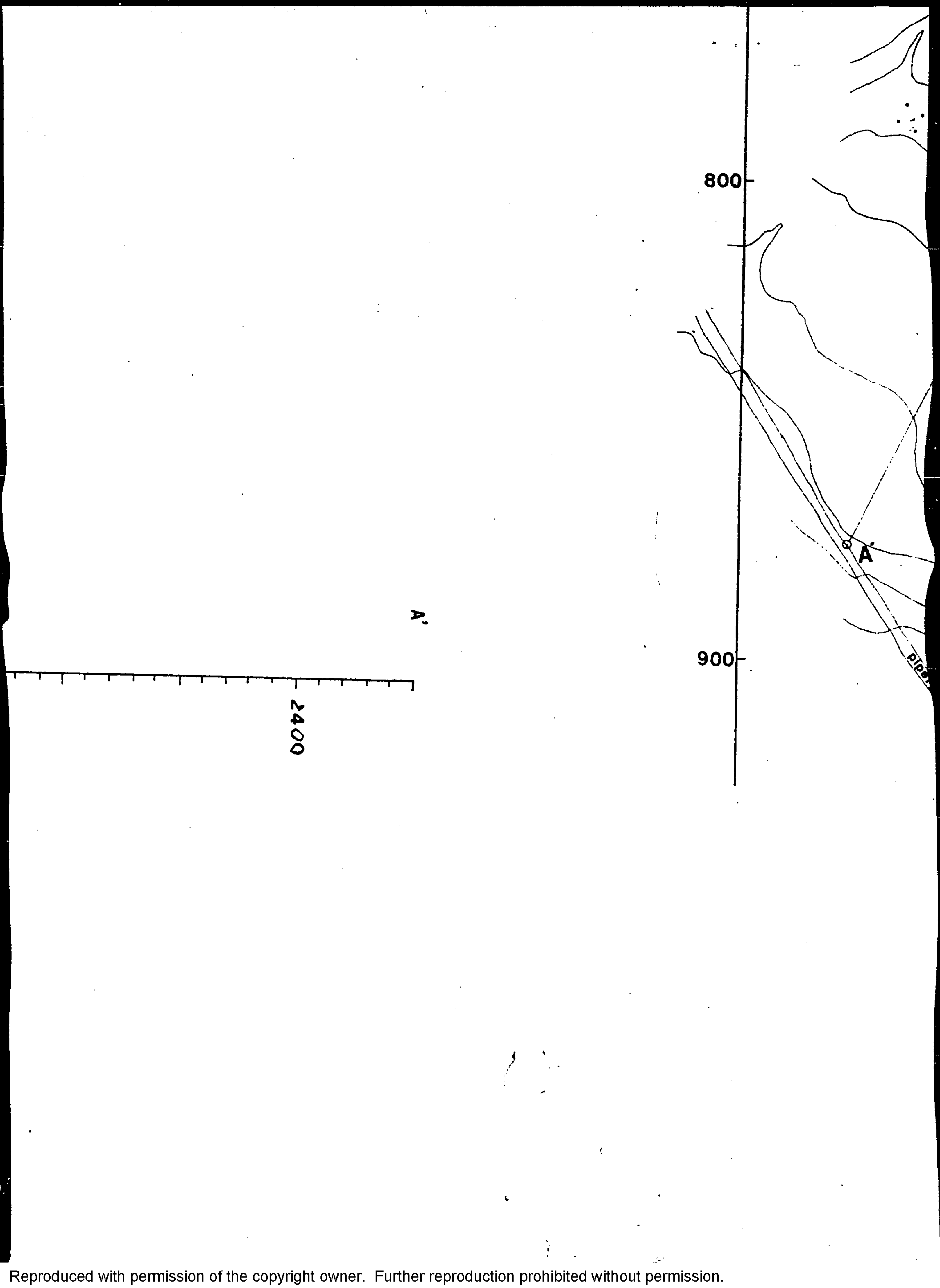
800
900
A'
A'
2400
pipe

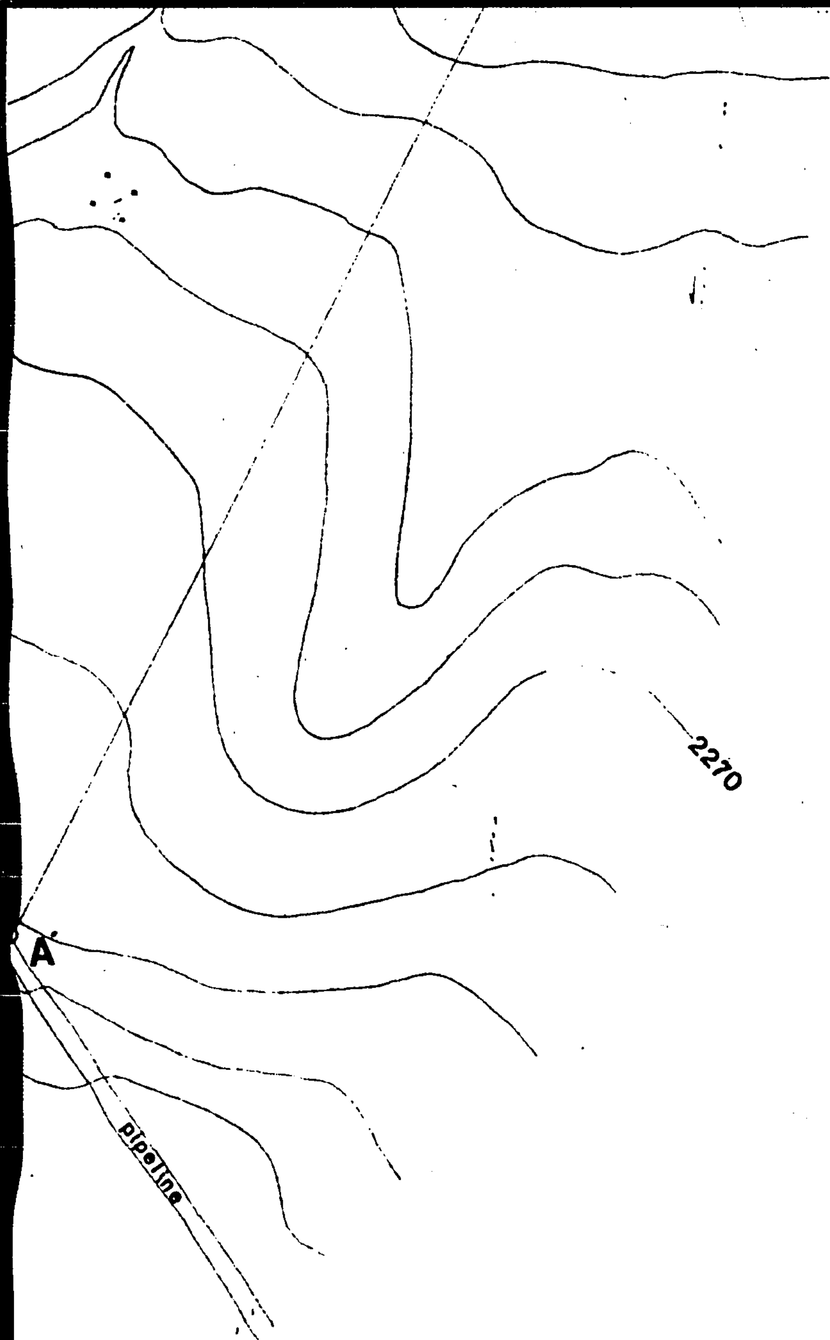
2270
A'
pipeline

PLEASE NOTE:

Oversize maps and charts are filmed in sections in the following manner:

LEFT TO RIGHT, TOP TO BOTTOM, WITH SMALL OVERLAPS

The following map or chart has been refilmed in its entirety at the end of this dissertation (not available on microfiche). A xerographic reproduction has been provided for paper copies and is inserted into the inside of the back cover.

Standard 35mm slides or 17" x 23" black and white photographic prints are available for an additional charge.

University Microfilms International

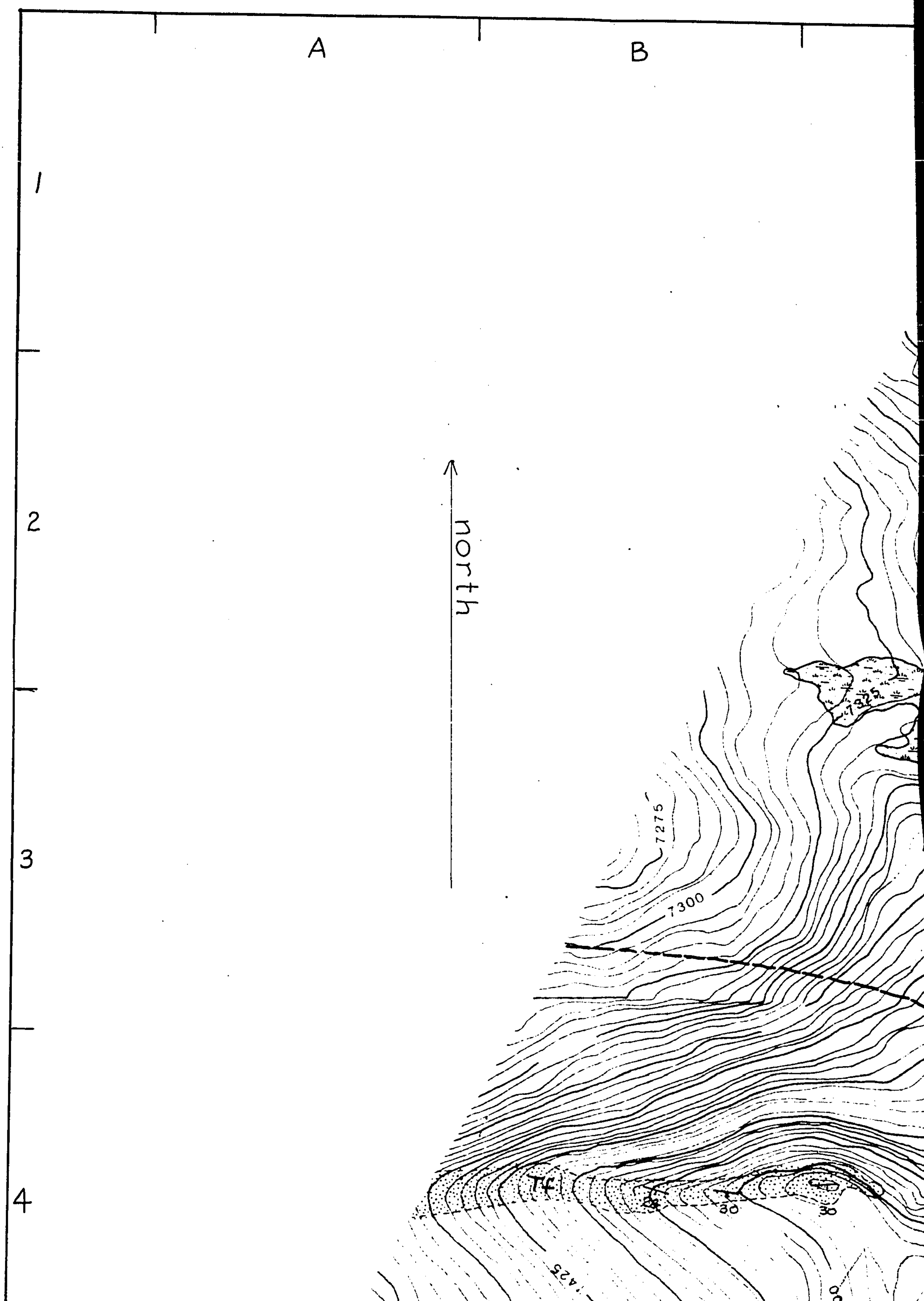
A
B
1
2
3
4
north
7275
7300
7325
Tf
30
30
30

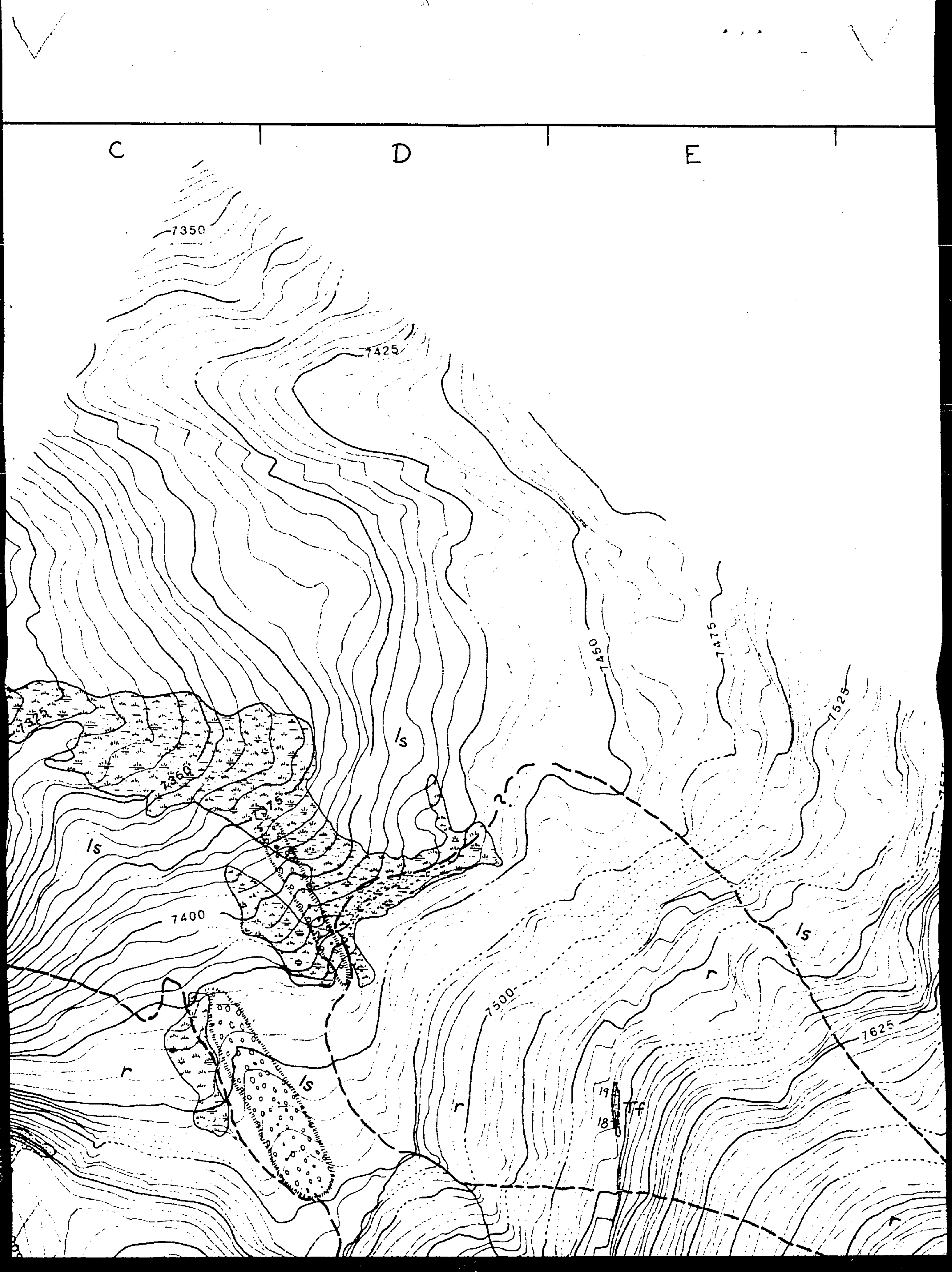
C
D
E
7350
7425
7325
7360
7375
7400
ls
ls
ls
ls
7450
7475
7525
7500
7625
r
r
r
r
19
18
Tf
?

F G H

Explanation

ls landslide debris

r residuum, weathered from the Flagstaff limestone

Tf bedrock outcrops of the Flagstaff Limestone

boundaries of the active landslide in 1984

contact between residuum and landslide debris

strike and dip of bedding

ridge - low topographic ridge in landslide debris, studded with boulders

wet land

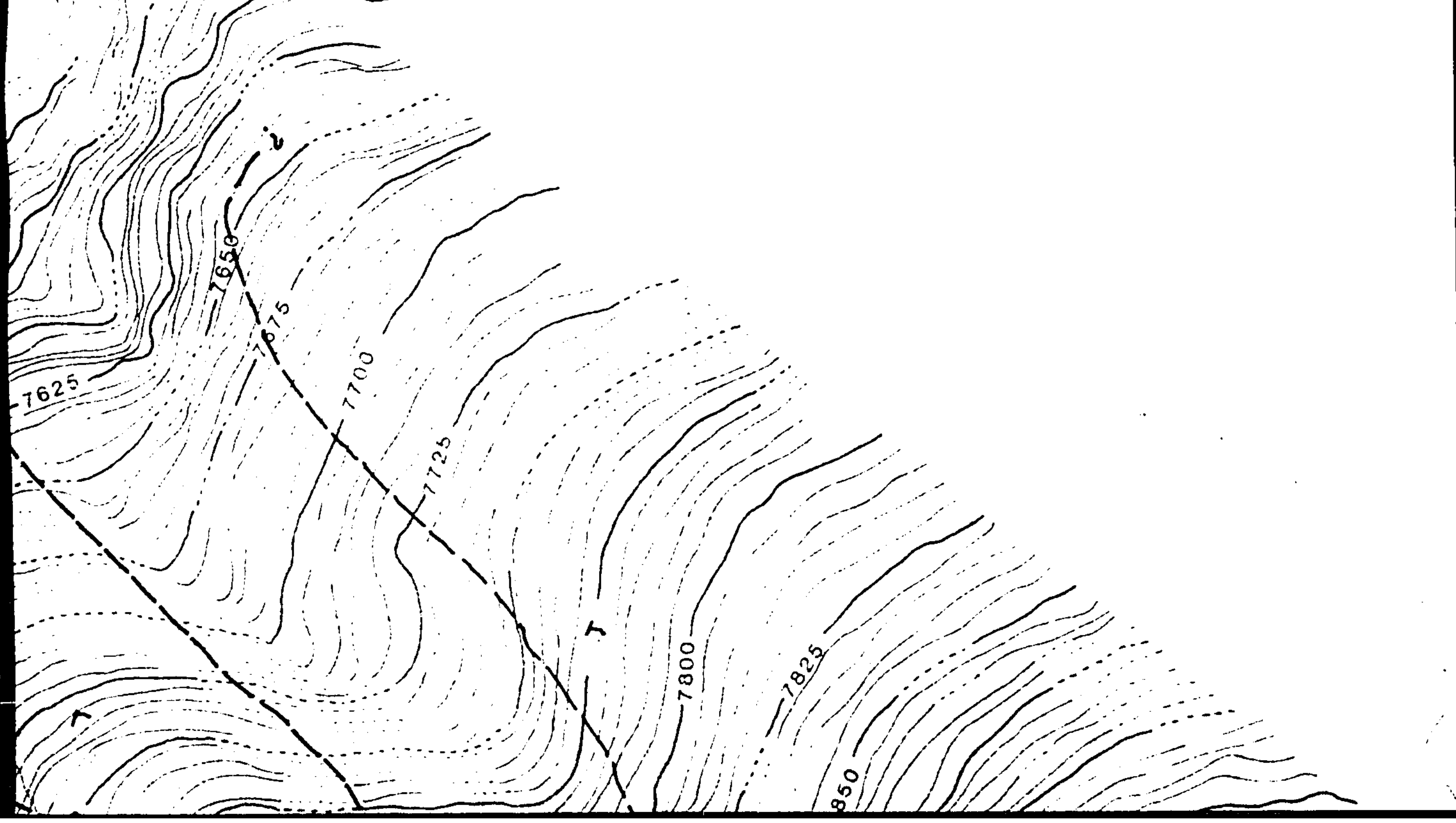

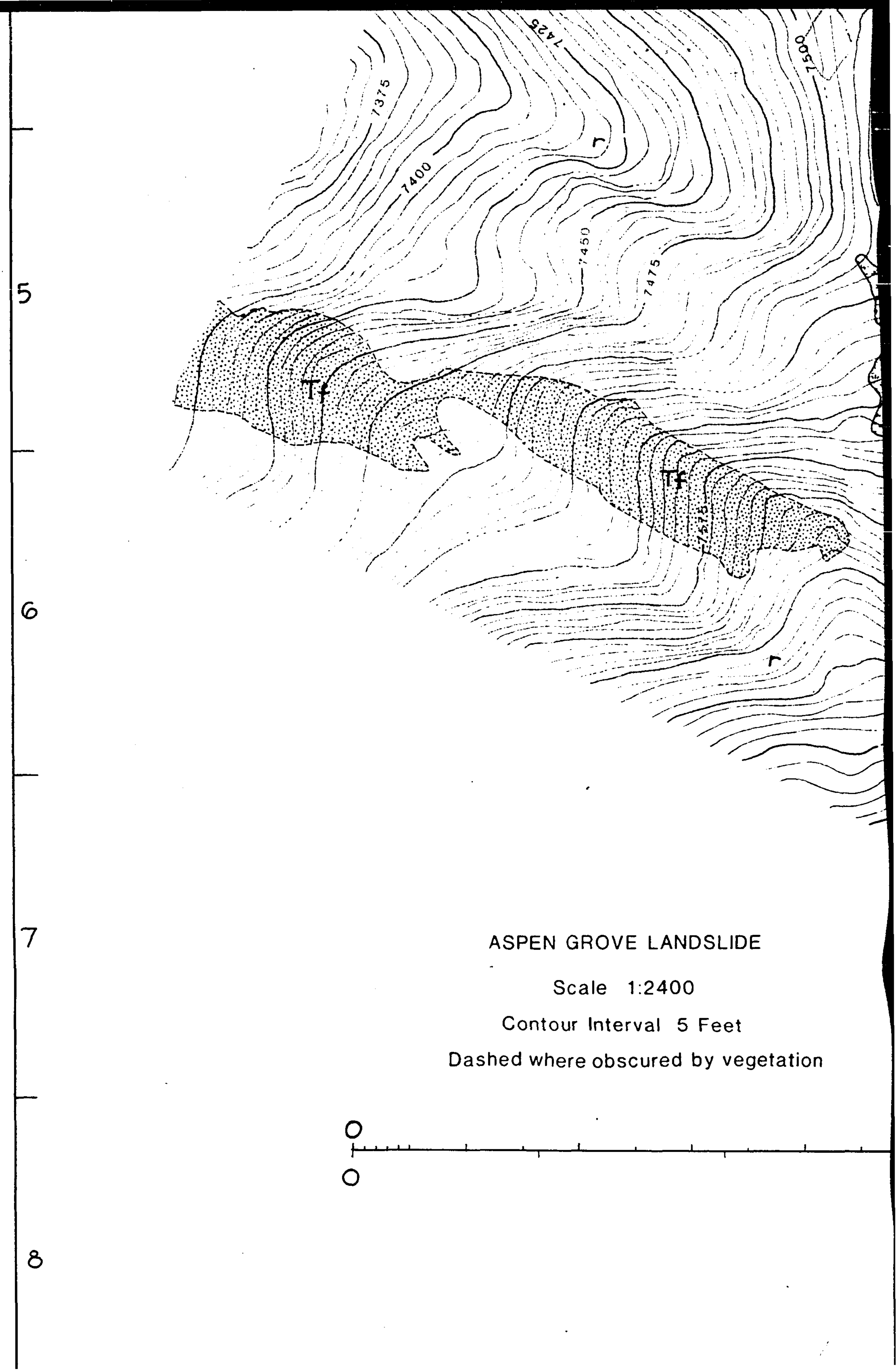
7375
7400
7425
7450
7475
7500
Tf
Tf
5
6
7
8
ASPEN GROVE LANDSLIDE
Scale 1:2400
Contour Interval 5 Feet
Dashed where obscured by vegetation
0
0

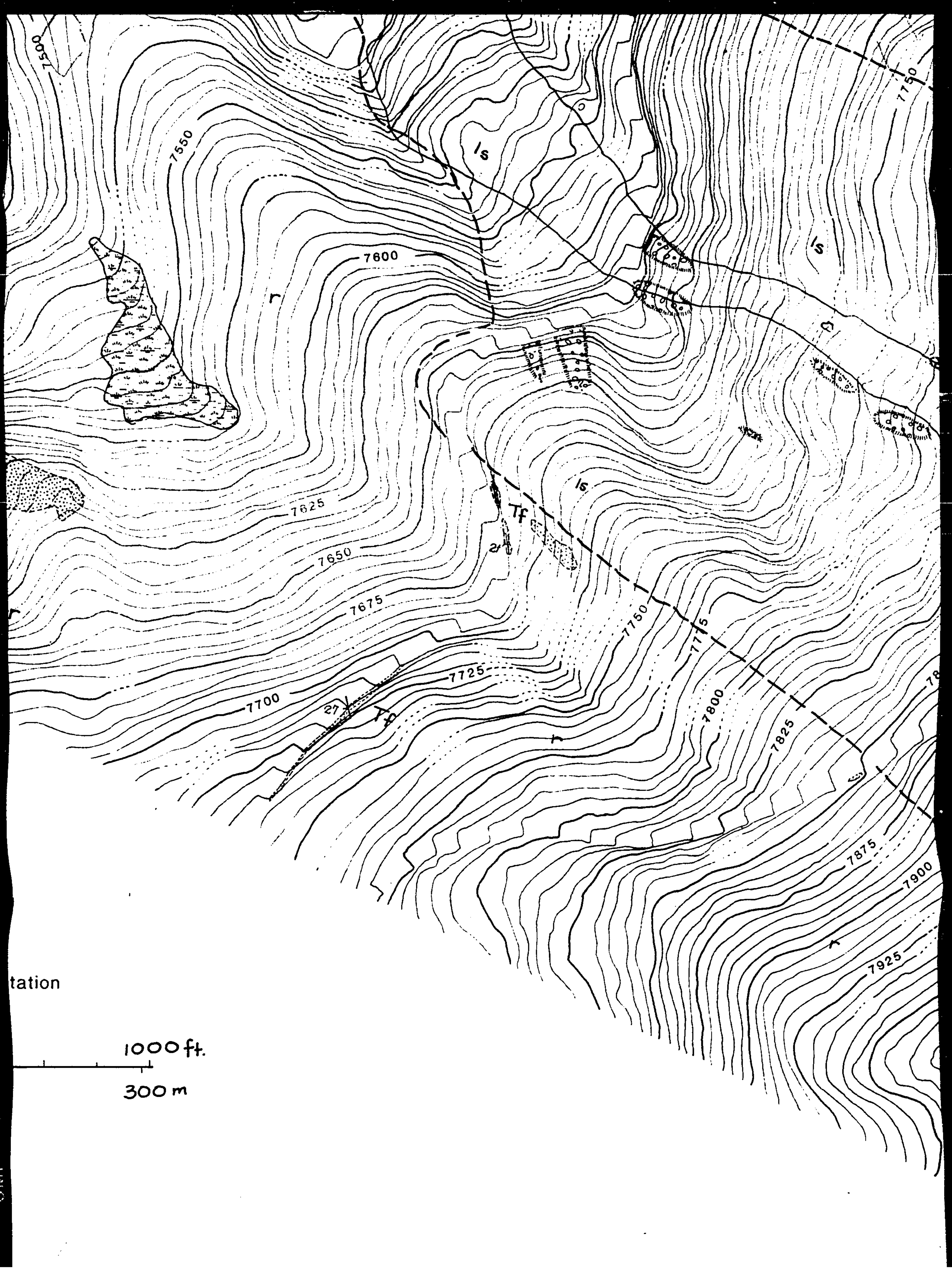
7500
7550
7600
7625
7650
7675
7700
7725
7750
7775
7800
7825
7875
7900
7925
ls
ls
ls
r
r
r
Tf
Tp
21
27
tation
1000 ft.
300 m

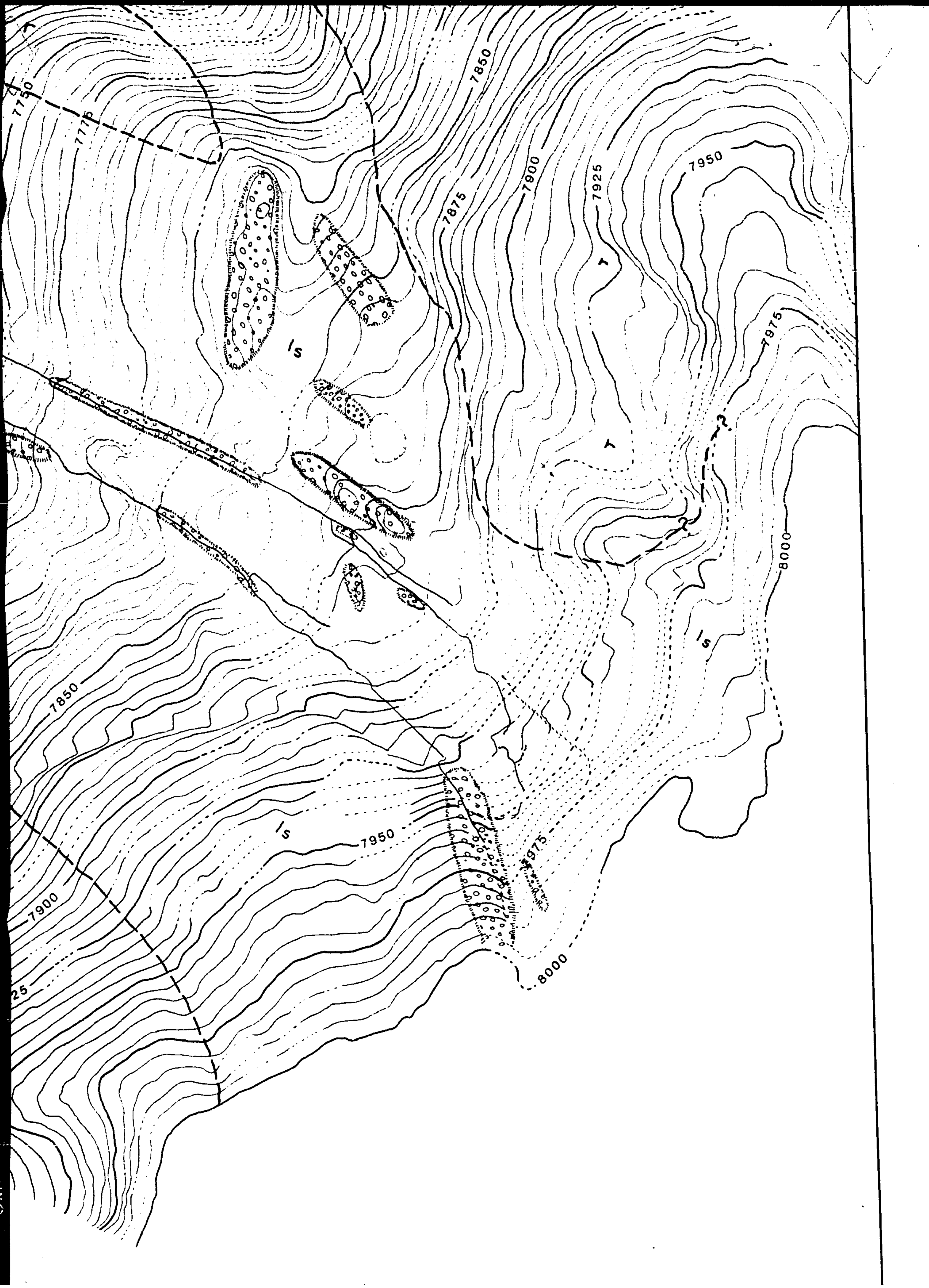
7750
7775
7850
7875
7900
7925
7950
7975
8000
ls
T
?
7850
7900
7950
7975
8000
25

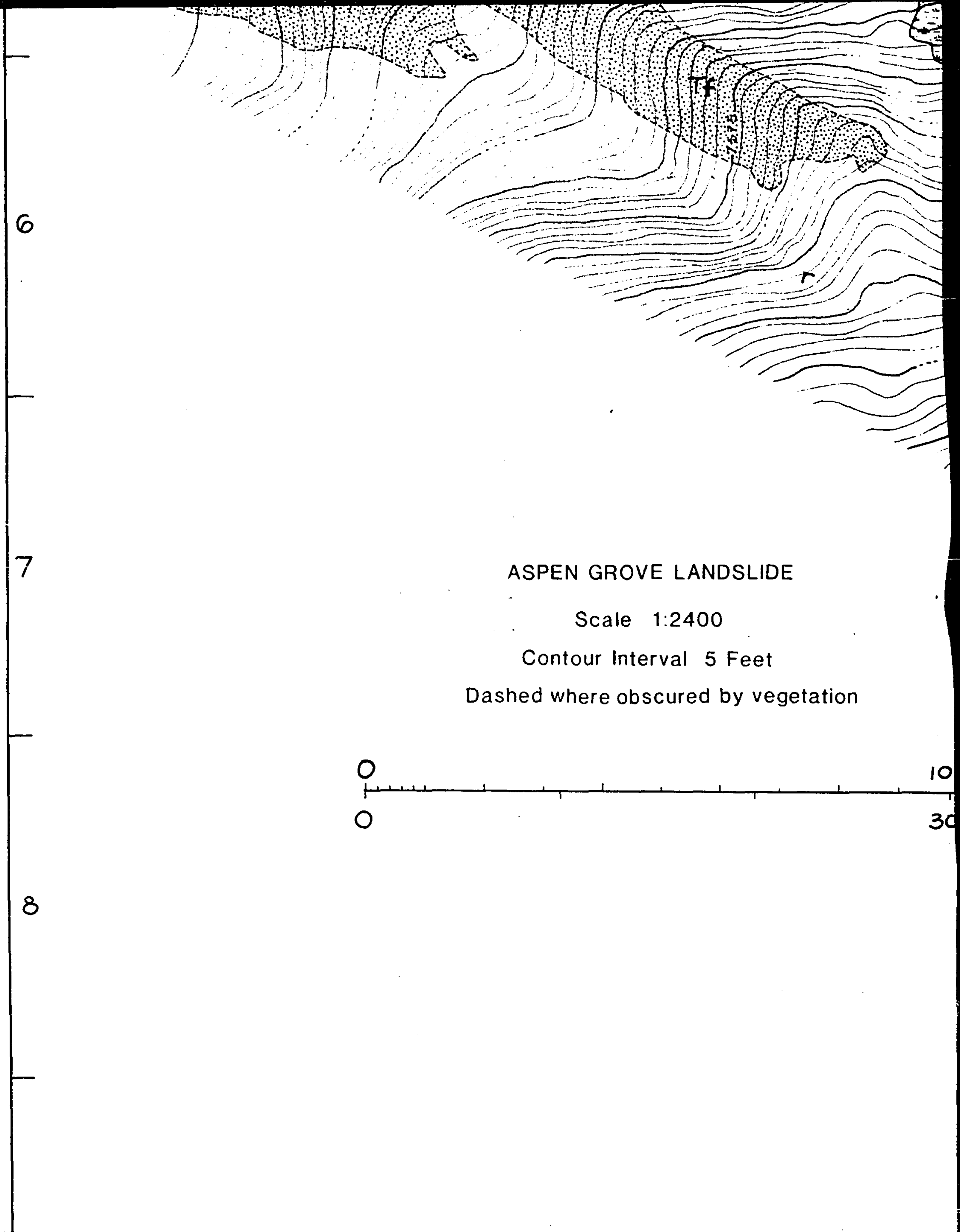

Tf
6
7
ASPEN GROVE LANDSLIDE
Scale 1:2400
Contour Interval 5 Feet
Dashed where obscured by vegetation
0
0
8

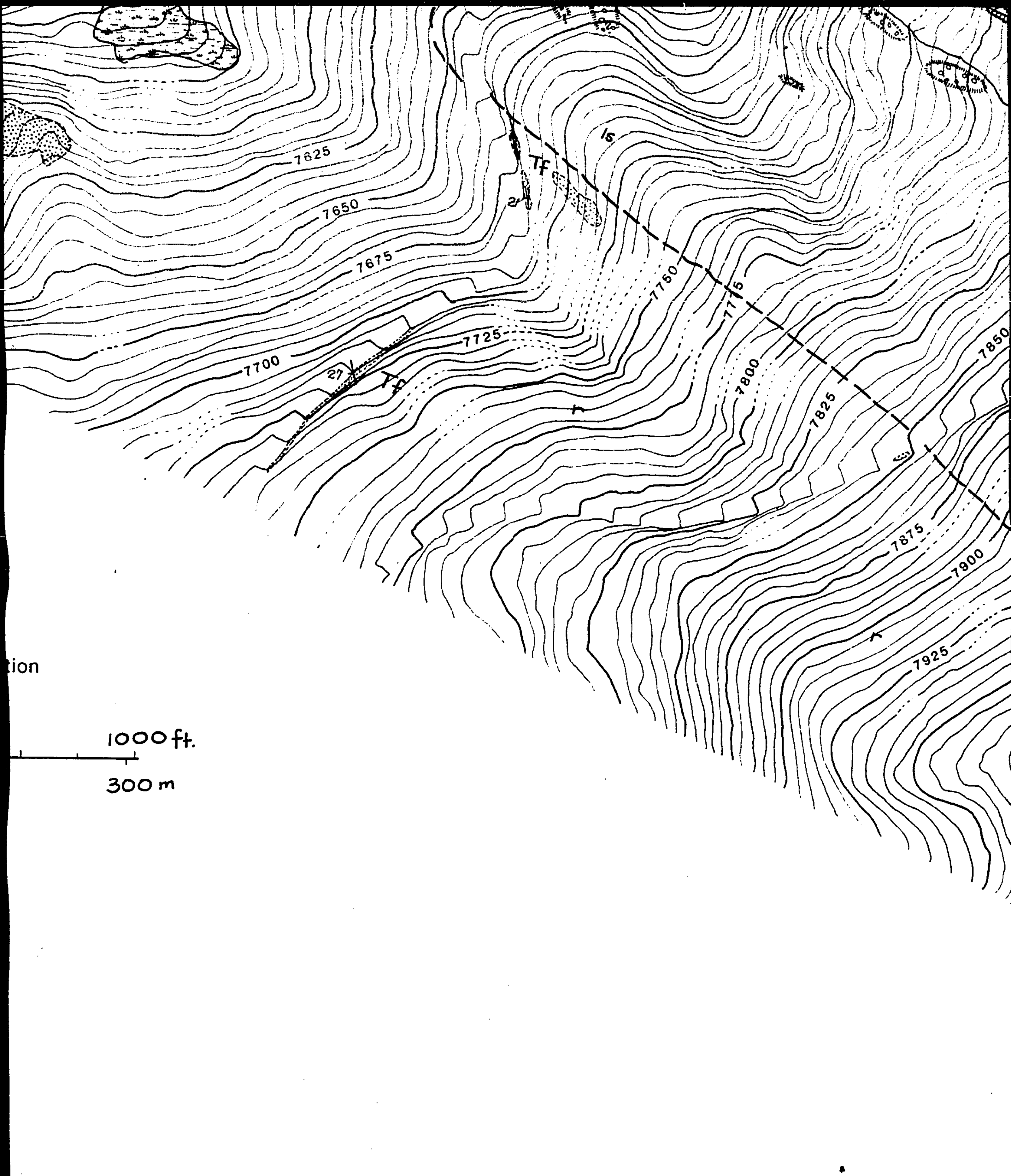
7625
7650
7675
7700
7725
7750
7775
7800
7825
7850
7875
7900
7925
Tf
27
tion
1000 ft.
300 m

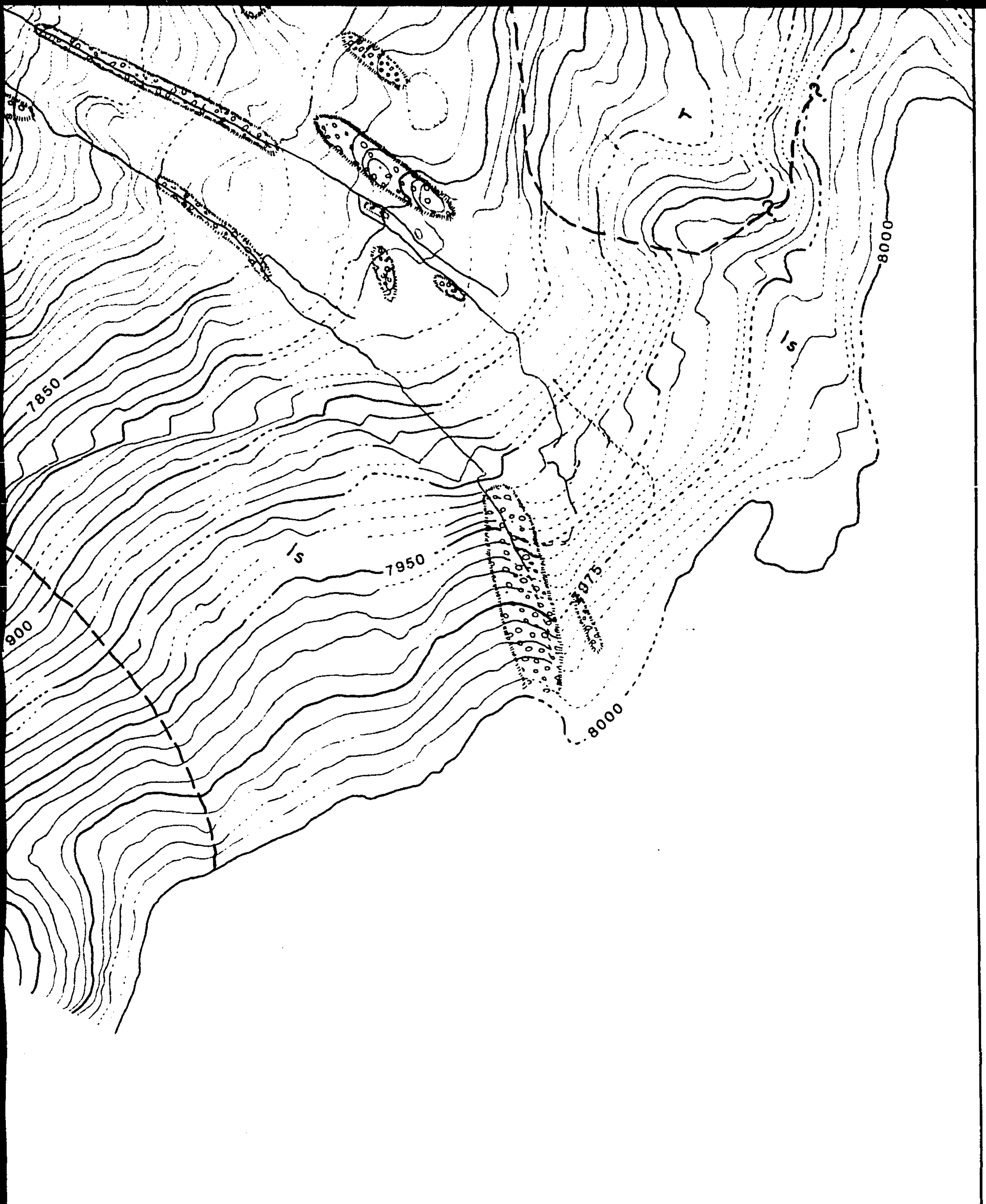

geology mapped 1985 by Rex L. Baum
Compiled by Diana Fair from aerial photographs of June 14, 1983

Plate 3

PLEASE NOTE:

Oversize maps and charts are filmed in sections in the following manner:

LEFT TO RIGHT, TOP TO BOTTOM, WITH SMALL OVERLAPS

The following map or chart has been refilmed in its entirety at the end of this dissertation (not available on microfiche). A xerographic reproduction has been provided for paper copies and is inserted into the inside of the back cover.

Standard 35mm slides or 17" x 23" black and white photographic prints are available for an additional charge.

University Microfilms International

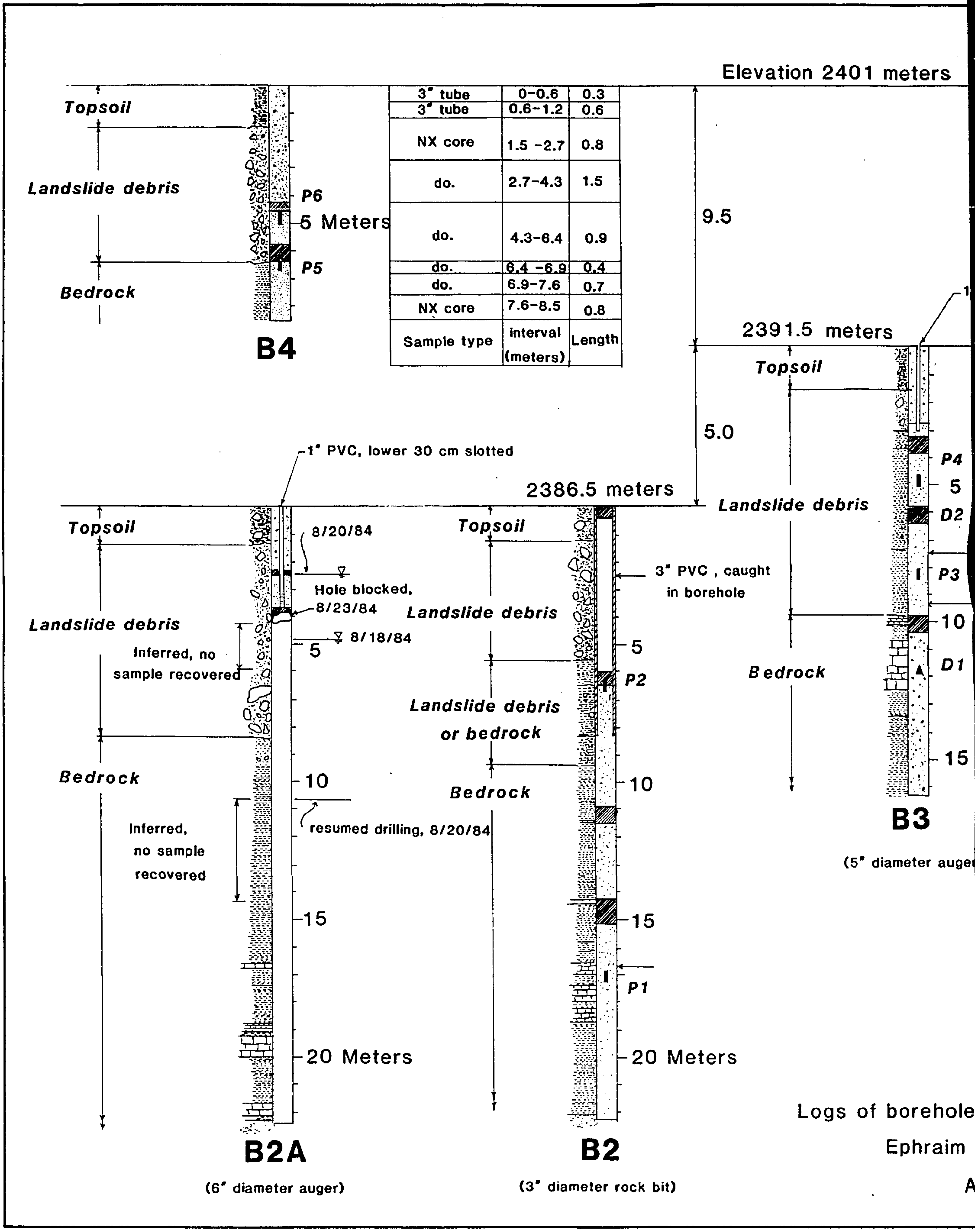

Sample type	interval (meters)	Length
3" tube	0-0.6	0.3
3" tube	0.6-1.2	0.6
NX core	1.5 -2.7	0.8
do.	2.7-4.3	1.5
do.	4.3-6.4	0.9
do.	6.4 -6.9	0.4
do.	6.9-7.6	0.7
NX core	7.6-8.5	0.8

Logs of borehole

Ephraim

A

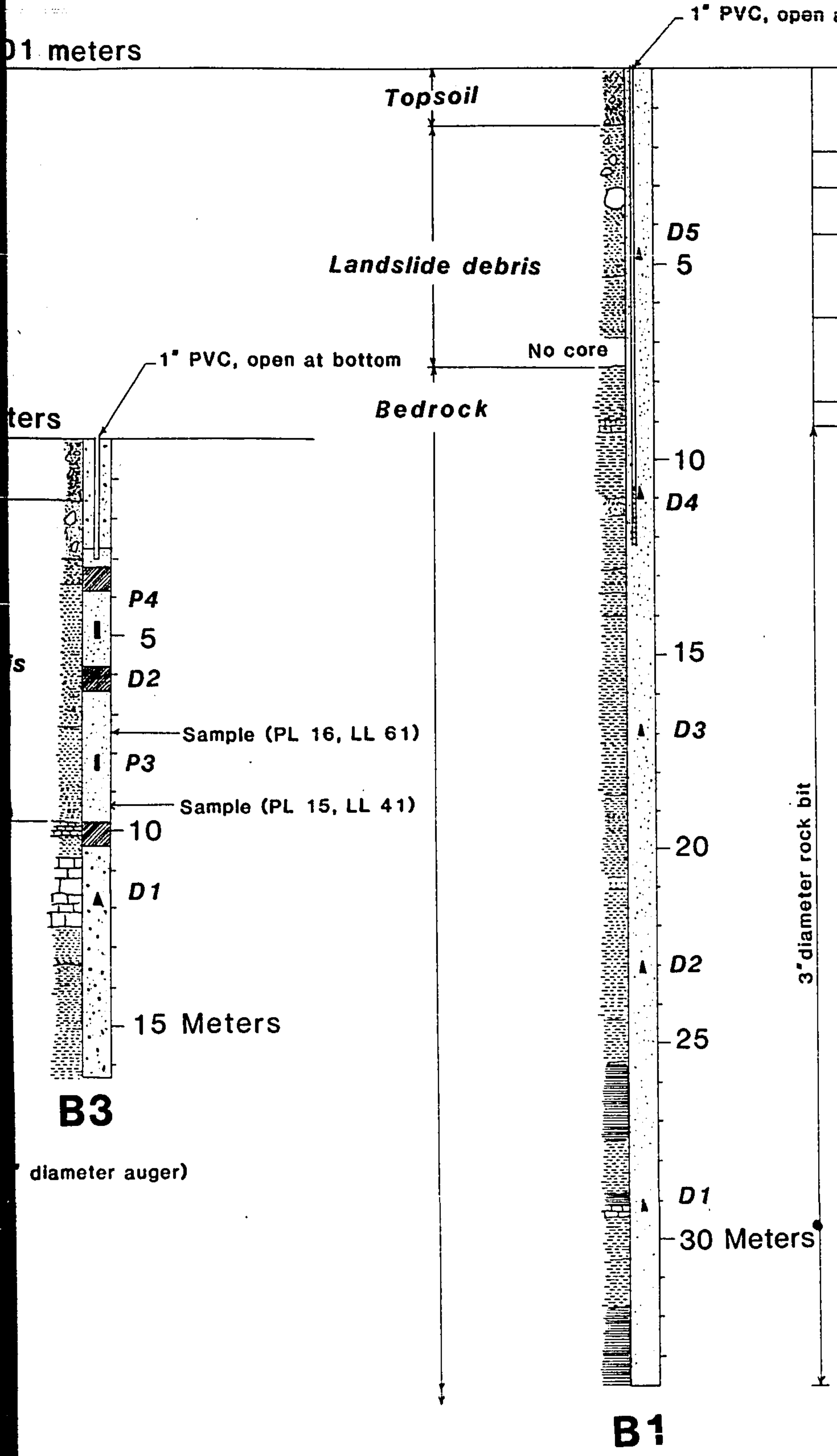

3"tube	0-0.6	un-known
	0.6-1.2	
	1.2-1.8	
5" Auger	2.2-3.0	N/A
NX core	3.0-4.3	0.4
do.	4.3-6.4	0.9
do.	6.4-8.5	1.2
NX core	8.5-9.1	0.3

EXPLANATION

- Organic sandy clay with sandstone clasts
- Medium sand with sandstone clasts
- Sandy clay with sandstone clasts
- Silt
- Plastic clay
- Claystone
- Shale
- Limestone
- Cherty limestone
- Sandstone
- D5 Displacement gauge
- P5 Piezometer
- Bentonite seal
- Cuttings
- Sand
- Water level

)f boreholes in the Aspen Grove landslide,
Ephraim Canyon central Utah
August 1984

Locations of boreholes shown on Plate

Plate 4

PLEASE NOTE:

Oversize maps and charts are filmed in sections in the following manner:

LEFT TO RIGHT, TOP TO BOTTOM, WITH SMALL OVERLAPS

The following map or chart has been refilmed in its entirety at the end of this dissertation (not available on microfiche). A xerographic reproduction has been provided for paper copies and is inserted into the inside of the back cover.

Standard 35mm slides or 17" x 23" black and white photographic prints are available for an additional charge.

University Microfilms International

Map showing displacement and ch

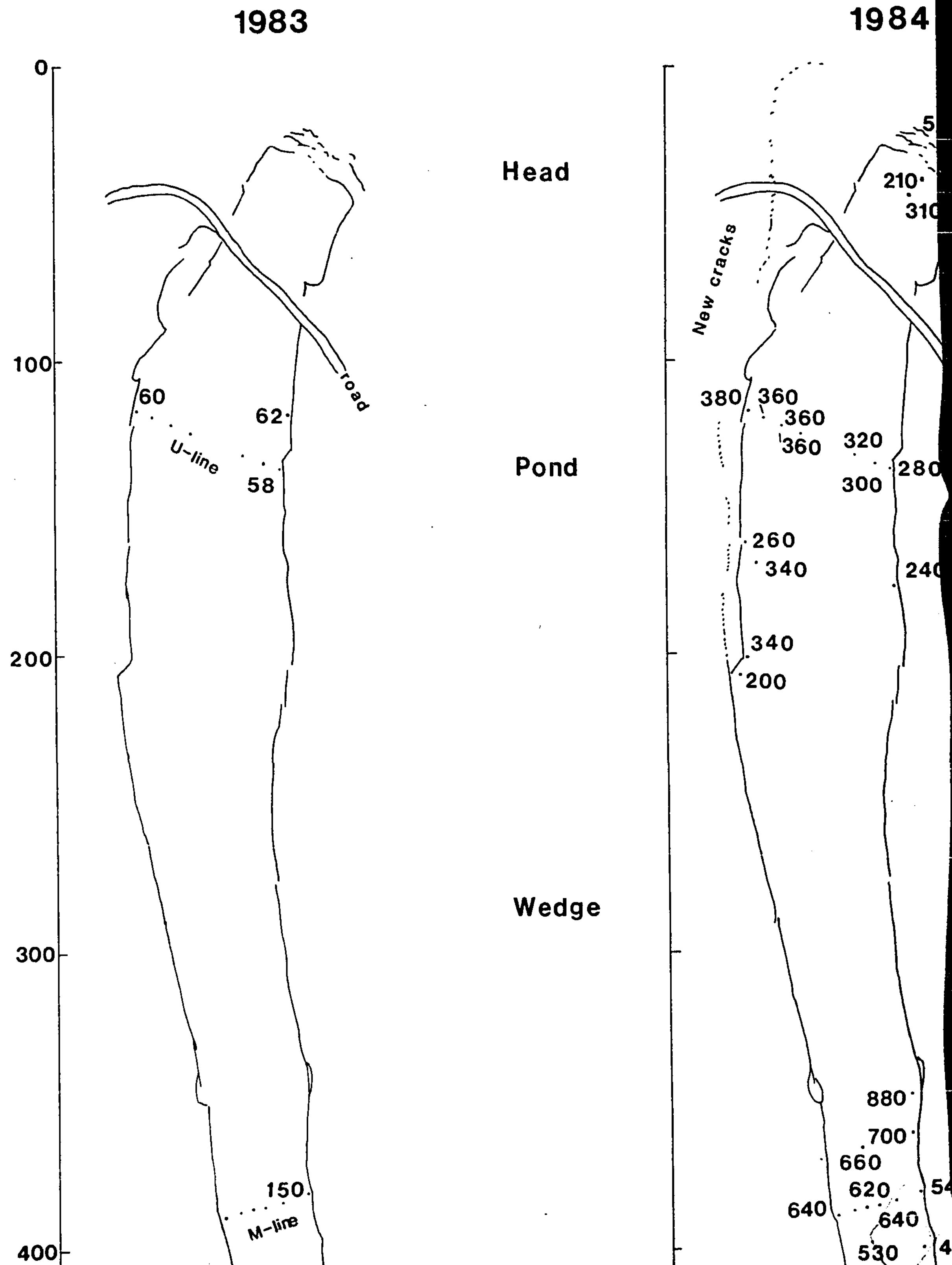

and change in boundaries of the Aspen Grove landslide, Ephraim Ca

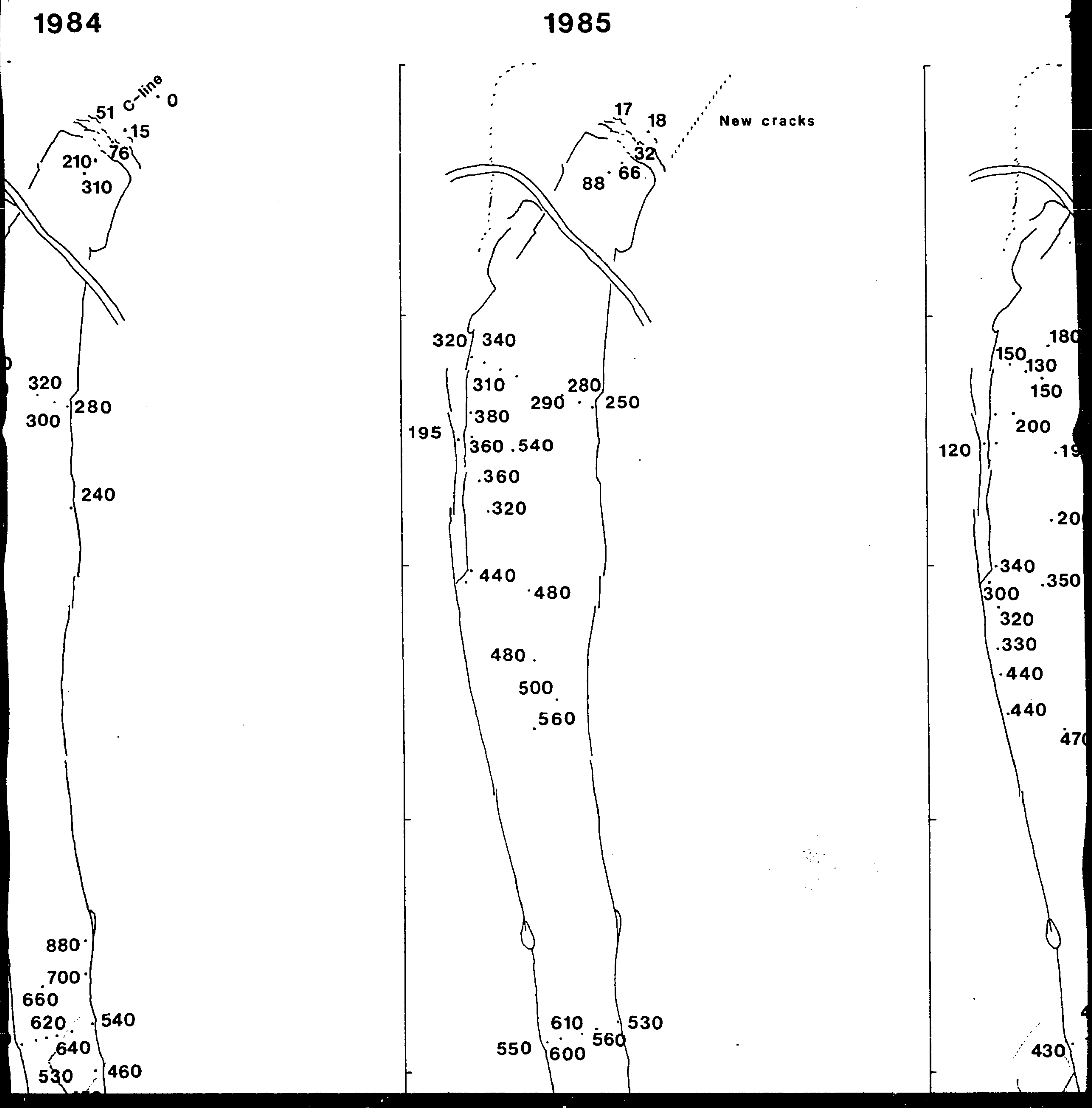

Ephraim Canyon, central Utah

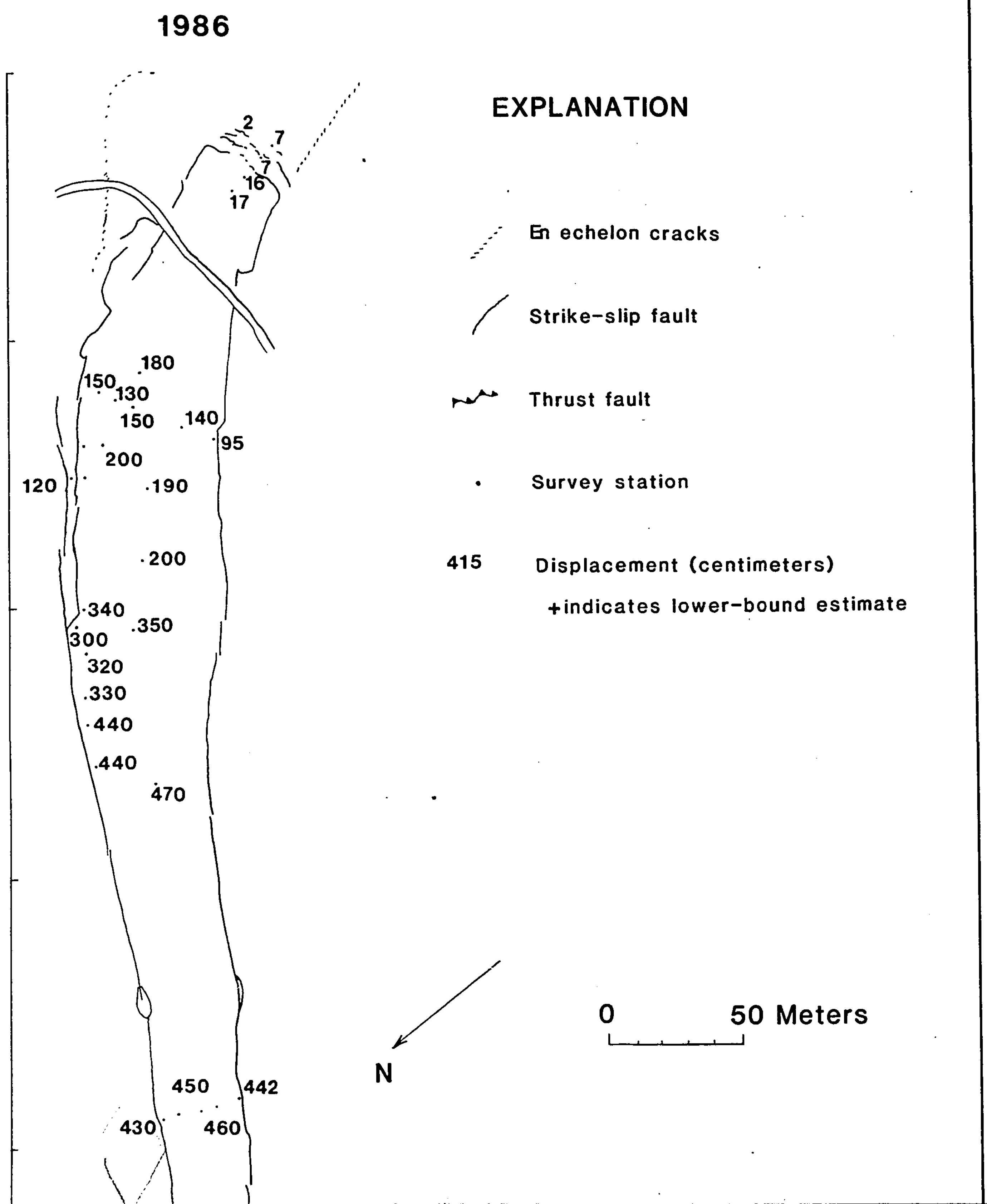

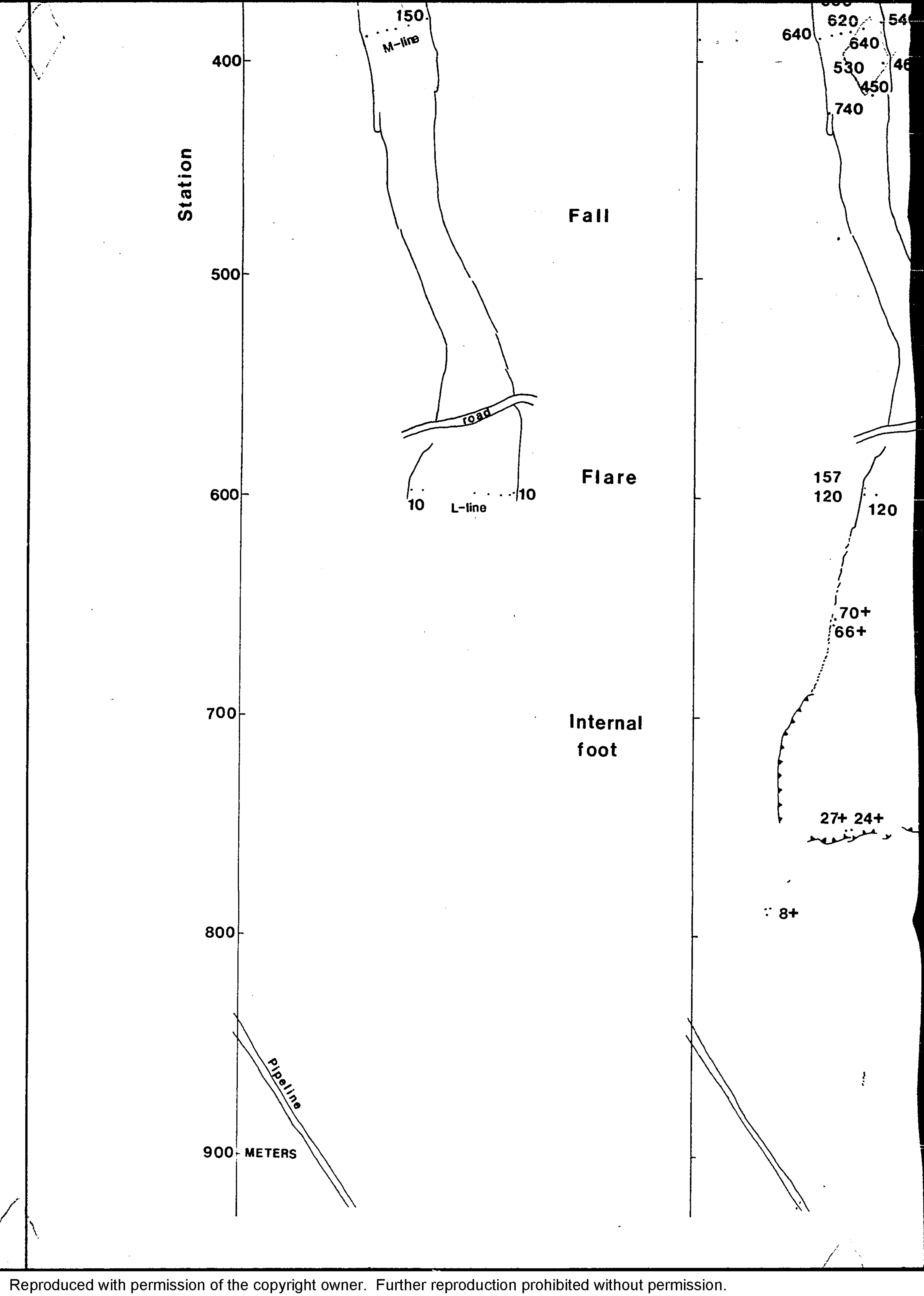

Station
400
500
600
700
800
900
METERS
150
M-line
road
10
L-line
10
Fall
Flare
Internal
foot
Pipeline
620
640
640
530
450
740
157
120
120
70+
66+
27+ 24+
8+

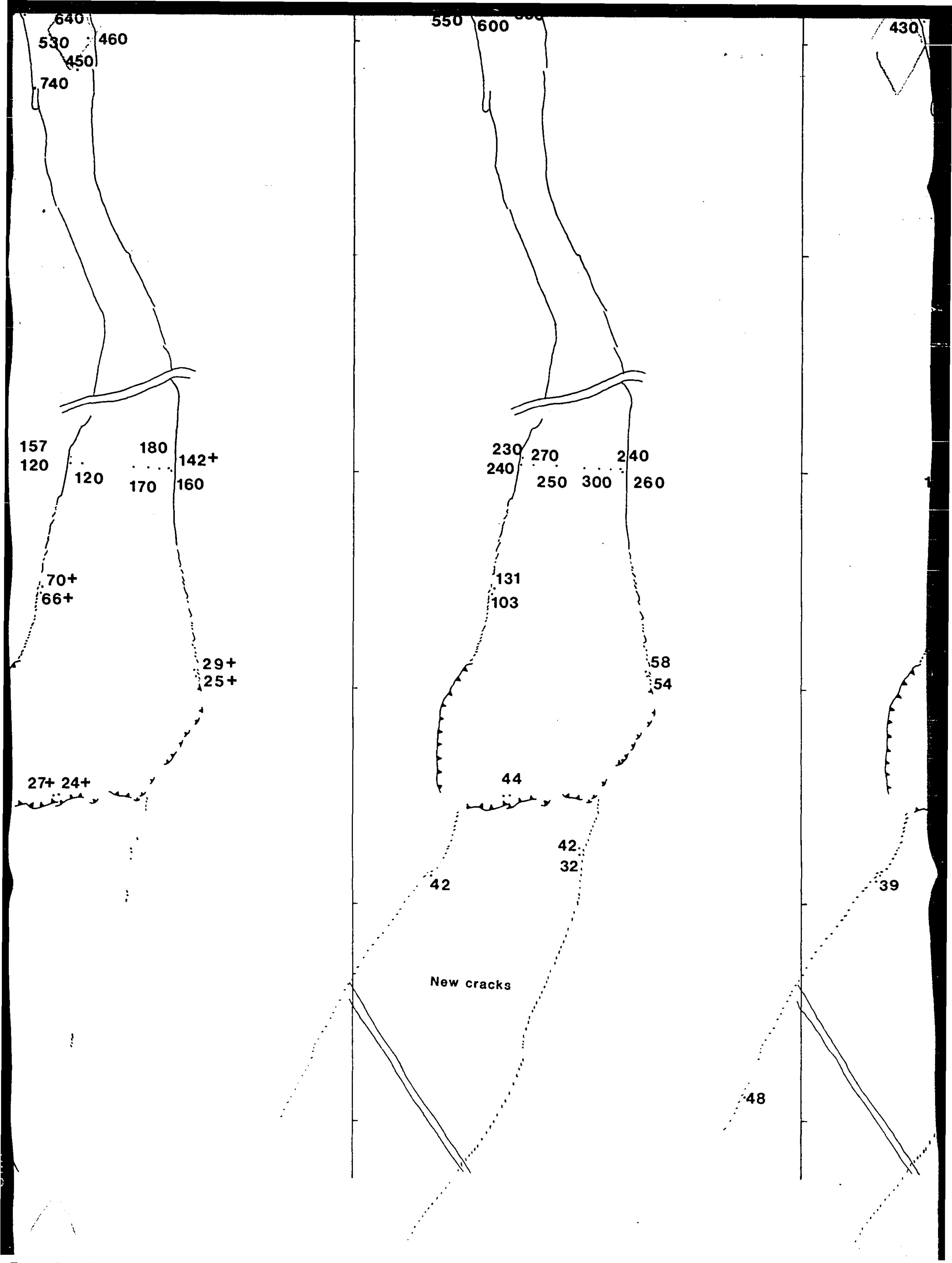
640
530
460
450
740
157
120
120
180
142+
170
160
70+
66+
29+
25+
27+ 24+
550
600
230
240
270
250
300
240
260
131
103
58
54
44
42
32
42
New cracks
48
430
39

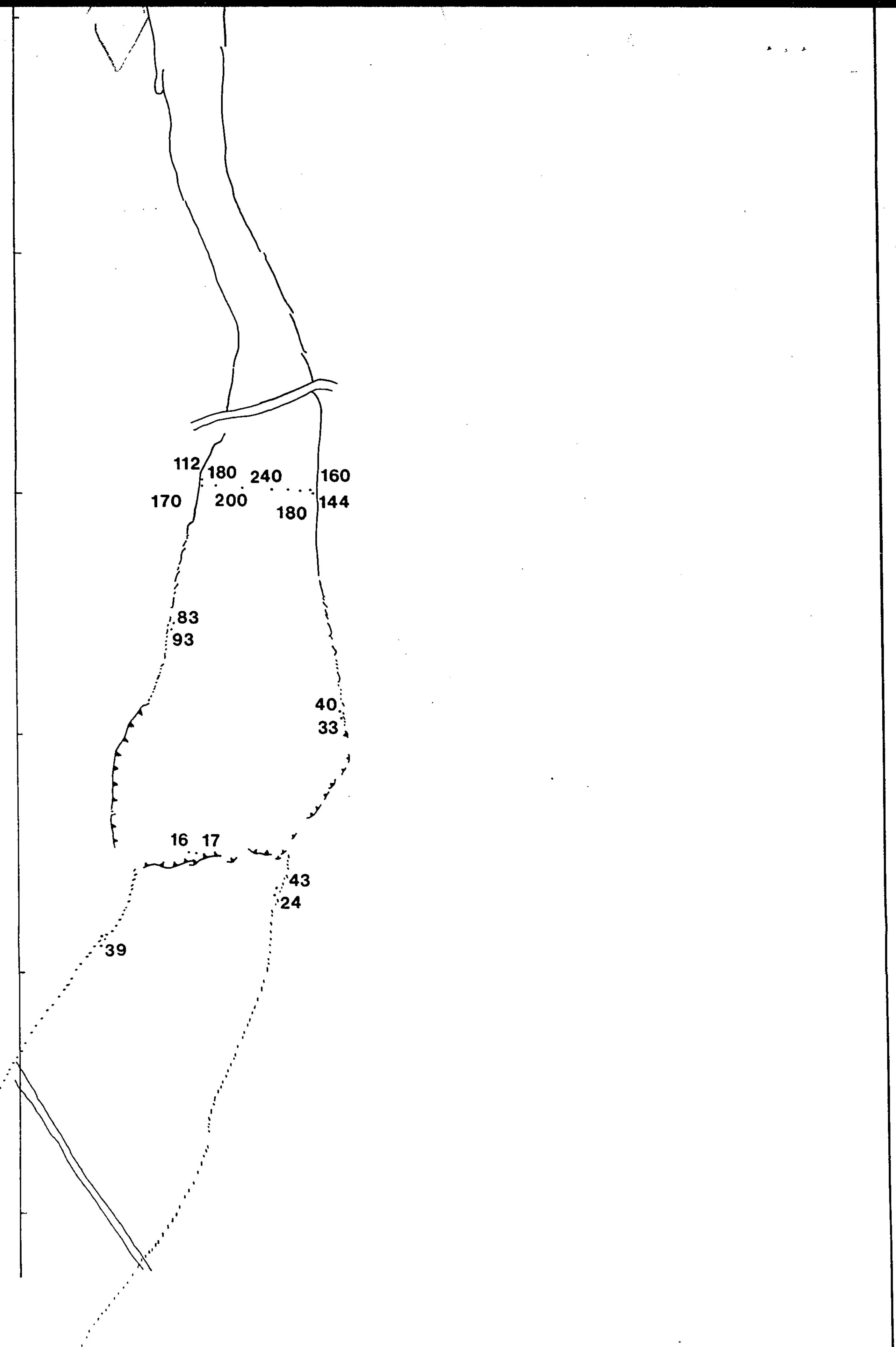
112
180
240
160
170
200
180
144
83
93
40
33
16
17
43
24
39

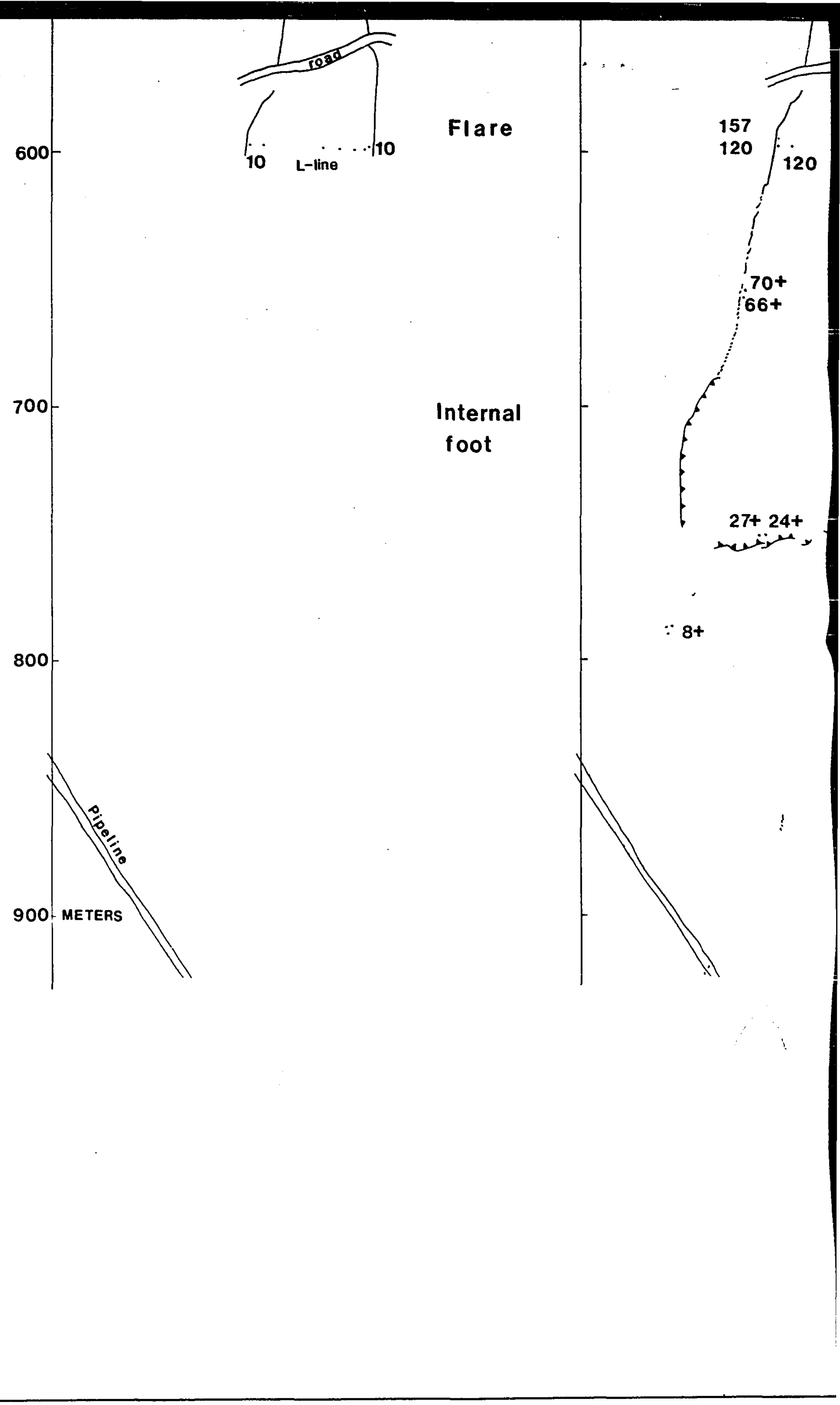
road
Flare
157
120
120
10
L-line
10
600
700
800
900
METERS
Internal
foot
70+
66+
27+ 24+
8+
Pipeline

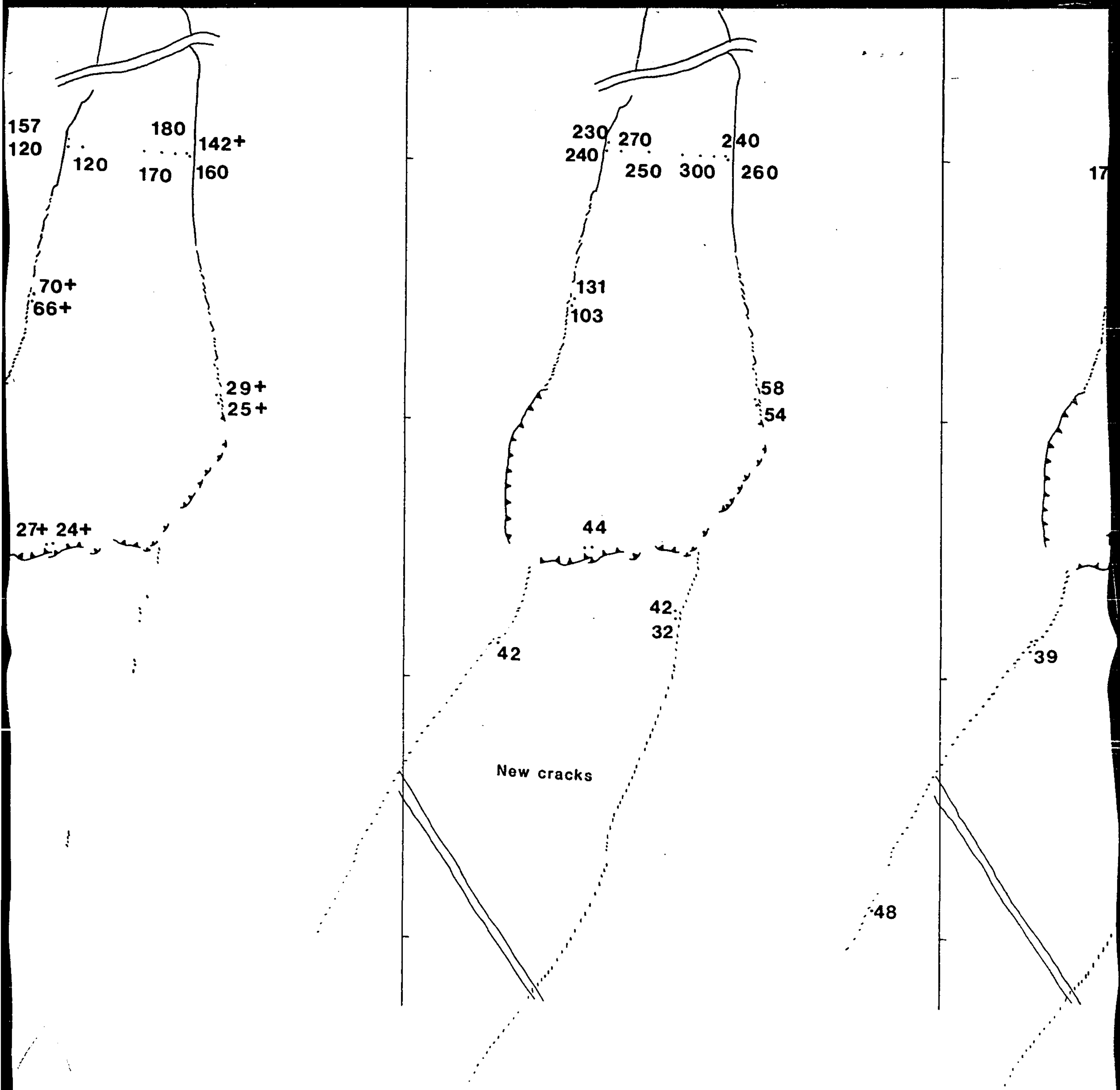

Base maps reduced and modified from origina

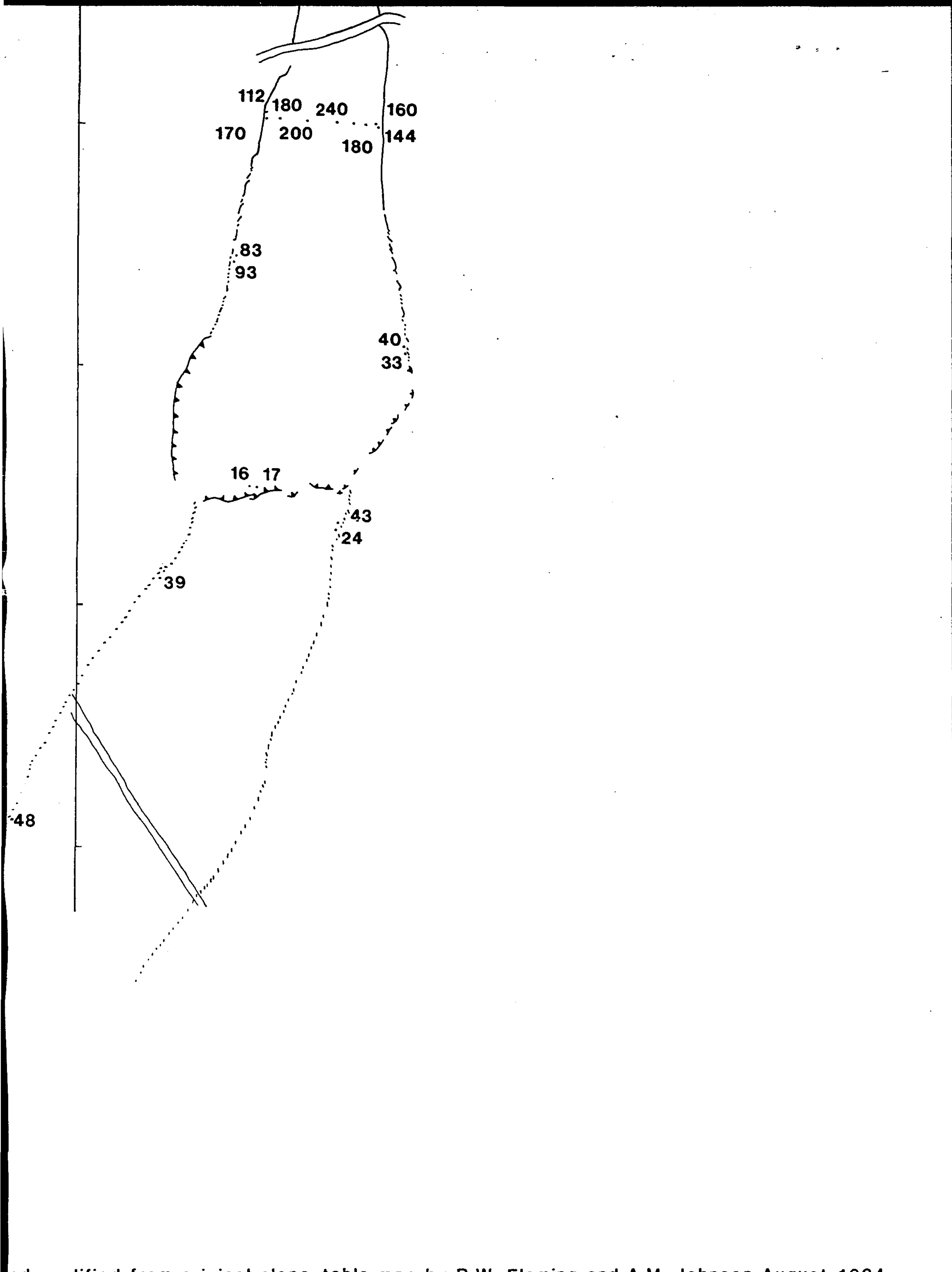

nd modified from original plane-table map by R.W. Fleming and A.M. Johnson, August 1984

Plate 5

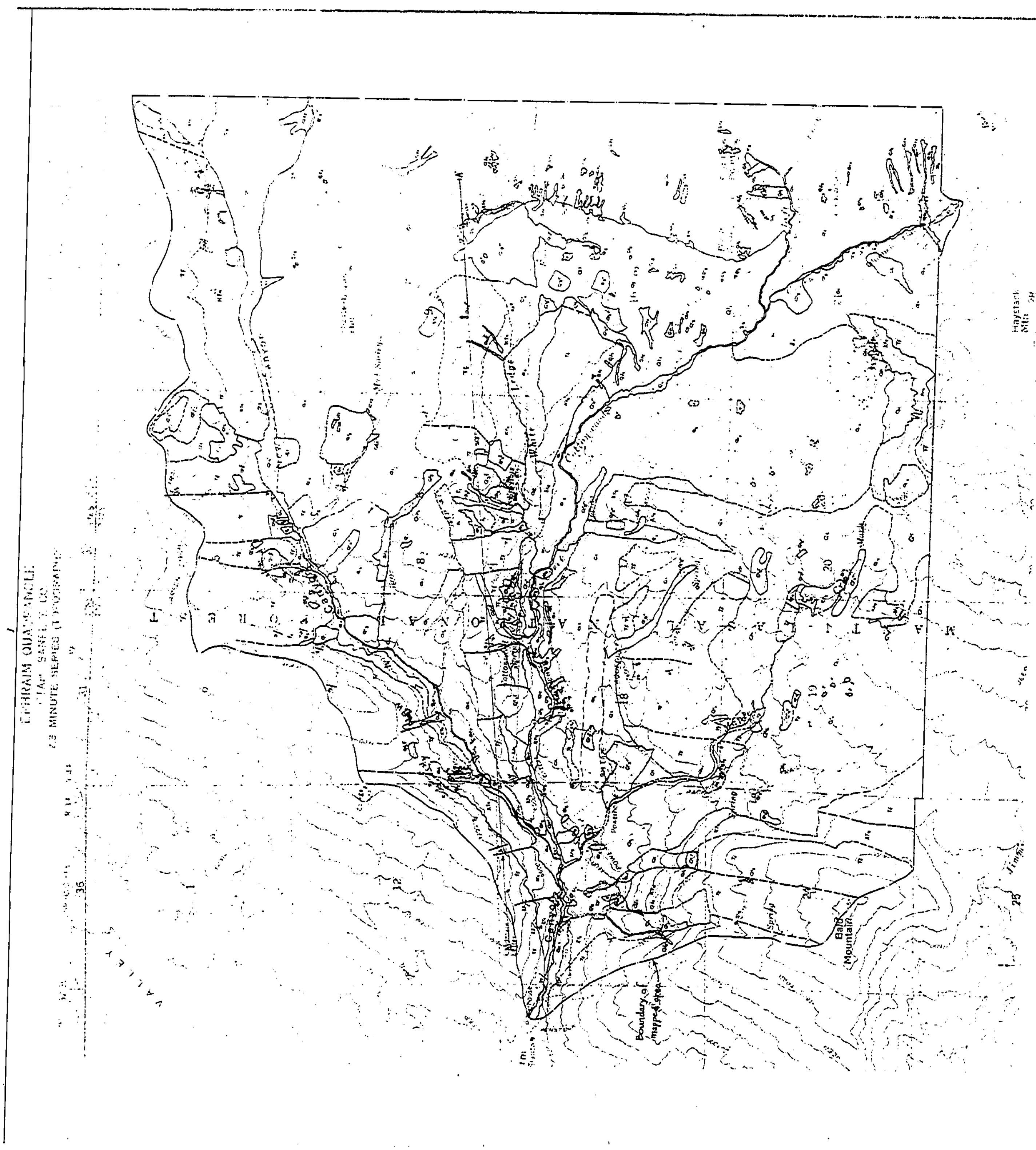
EPHRAIM QUADRANGLE
Bald Mountain

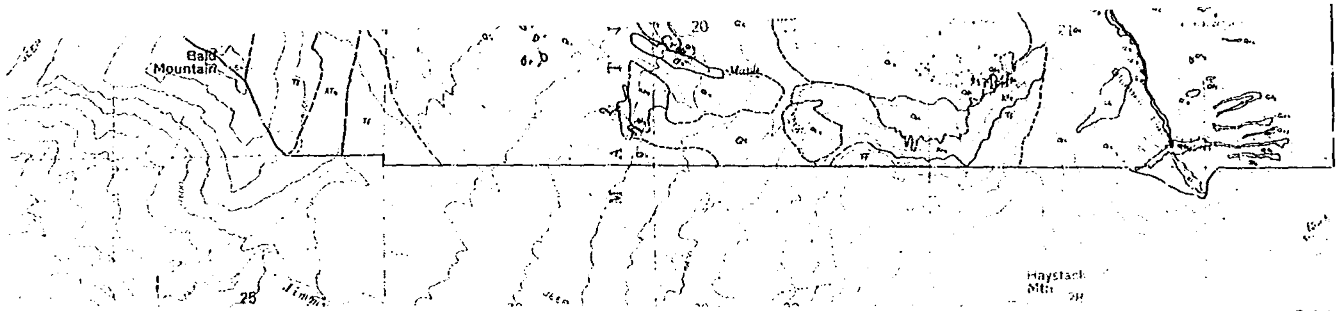

Plate I

Geologic Map of part of Ephraim Canyon, central Utah

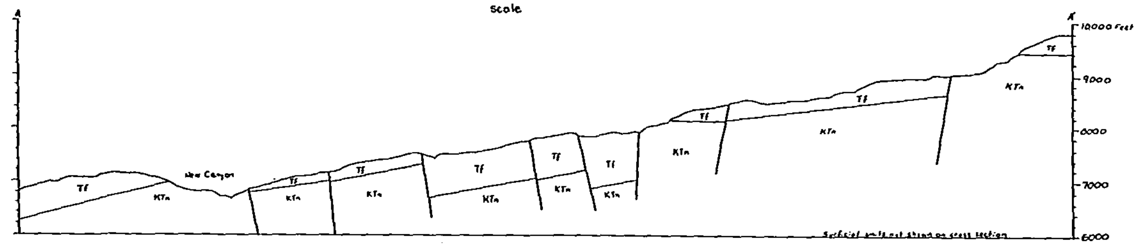

Section A-A'

The Aspen Grove Landslide,
Ephraim Canyon, Utah

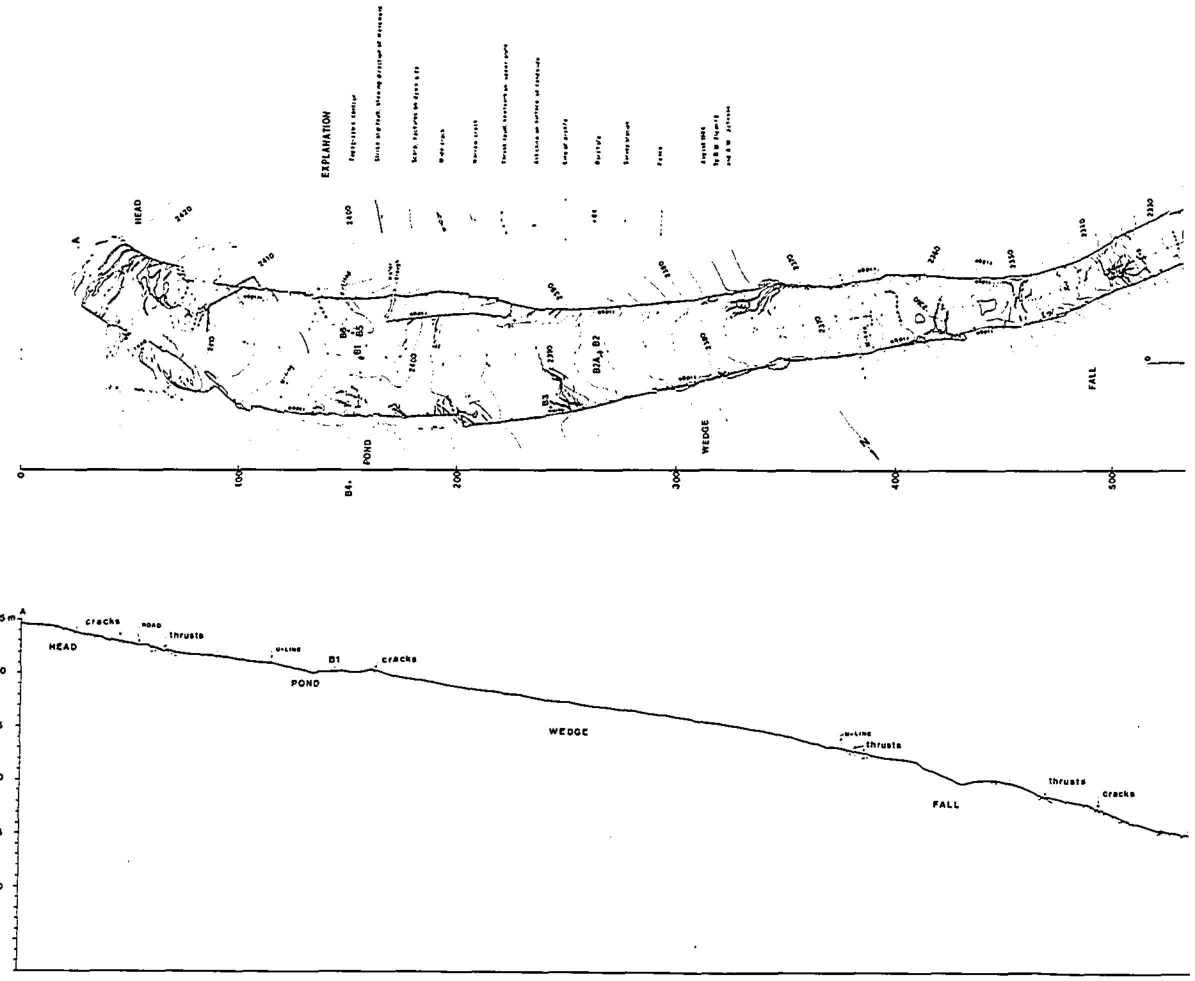

Profile A–A'

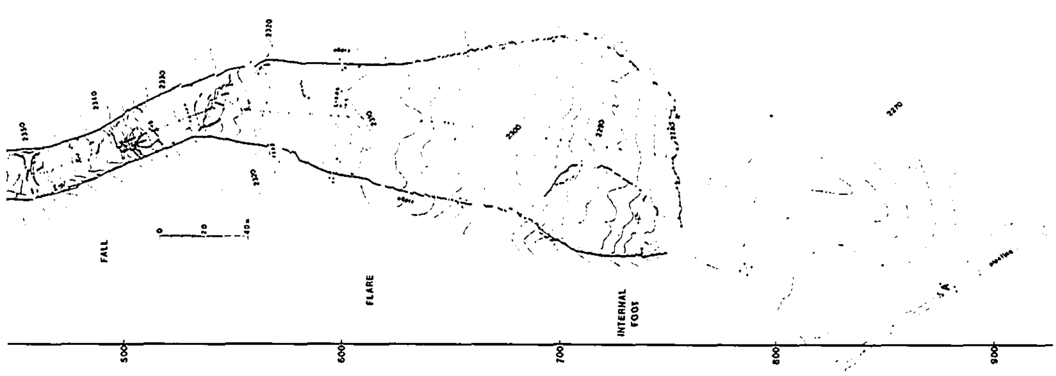

FALL
FLARE
INTERNAL FOOT
500
600
700
800
900

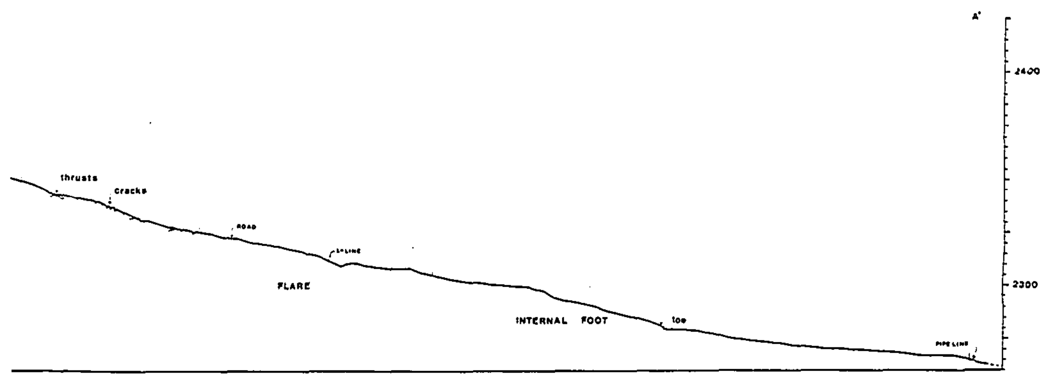

A'
2400
2300
thrusts
cracks
FLARE
INTERNAL FOOT
toe

A–A'

2

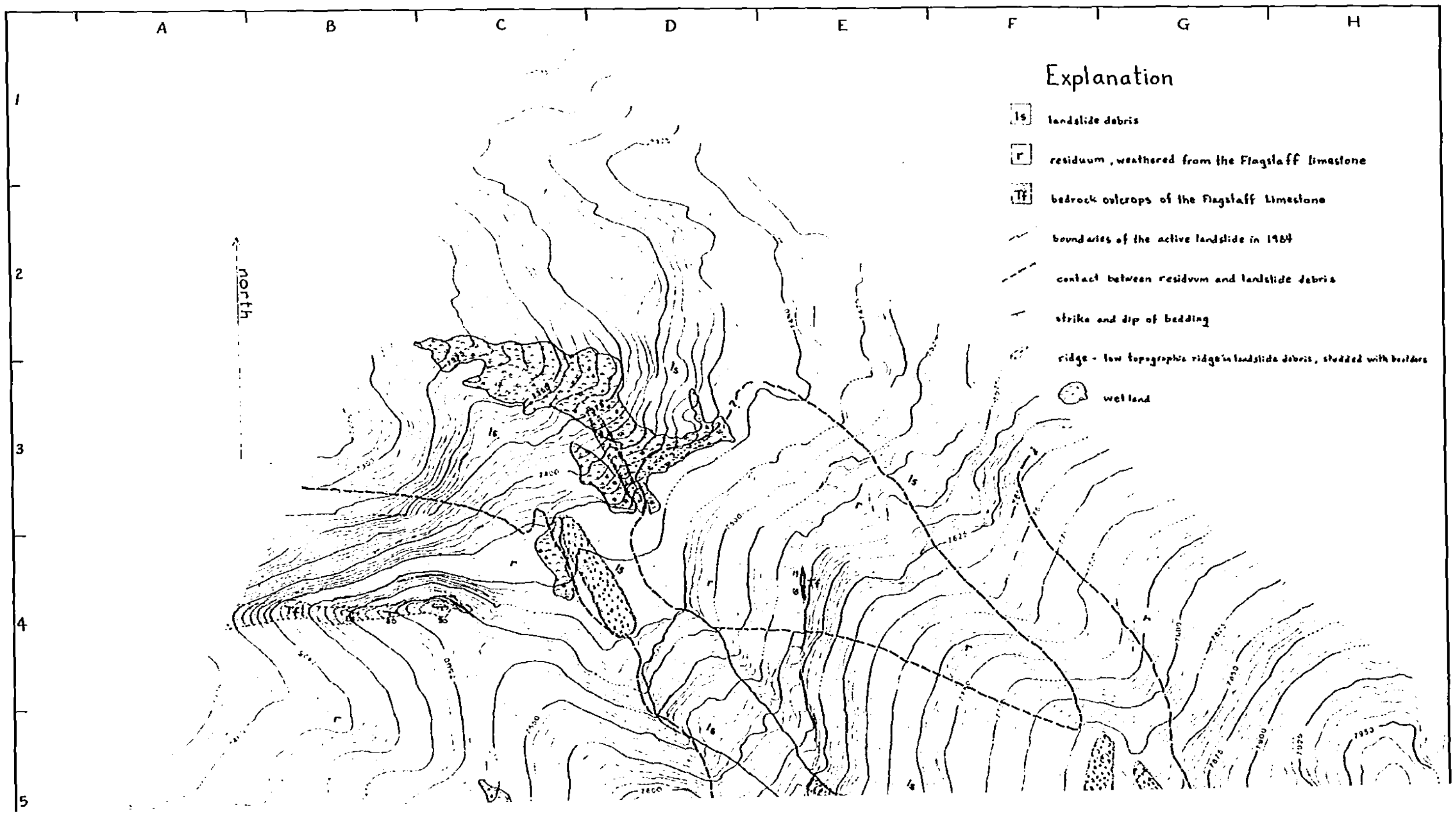
Explanation
ls landslide debris
r residuum, weathered from the Flagstaff limestone
Tf bedrock outcrops of the Flagstaff limestone
boundaries of the active landslide in 1984
contact between residuum and landslide debris
strike and dip of bedding
ridge - low topographic ridge in landslide debris, studded with boulders
wetland
north
A
B
C
D
E
F
G
H
1
2
3
4
5

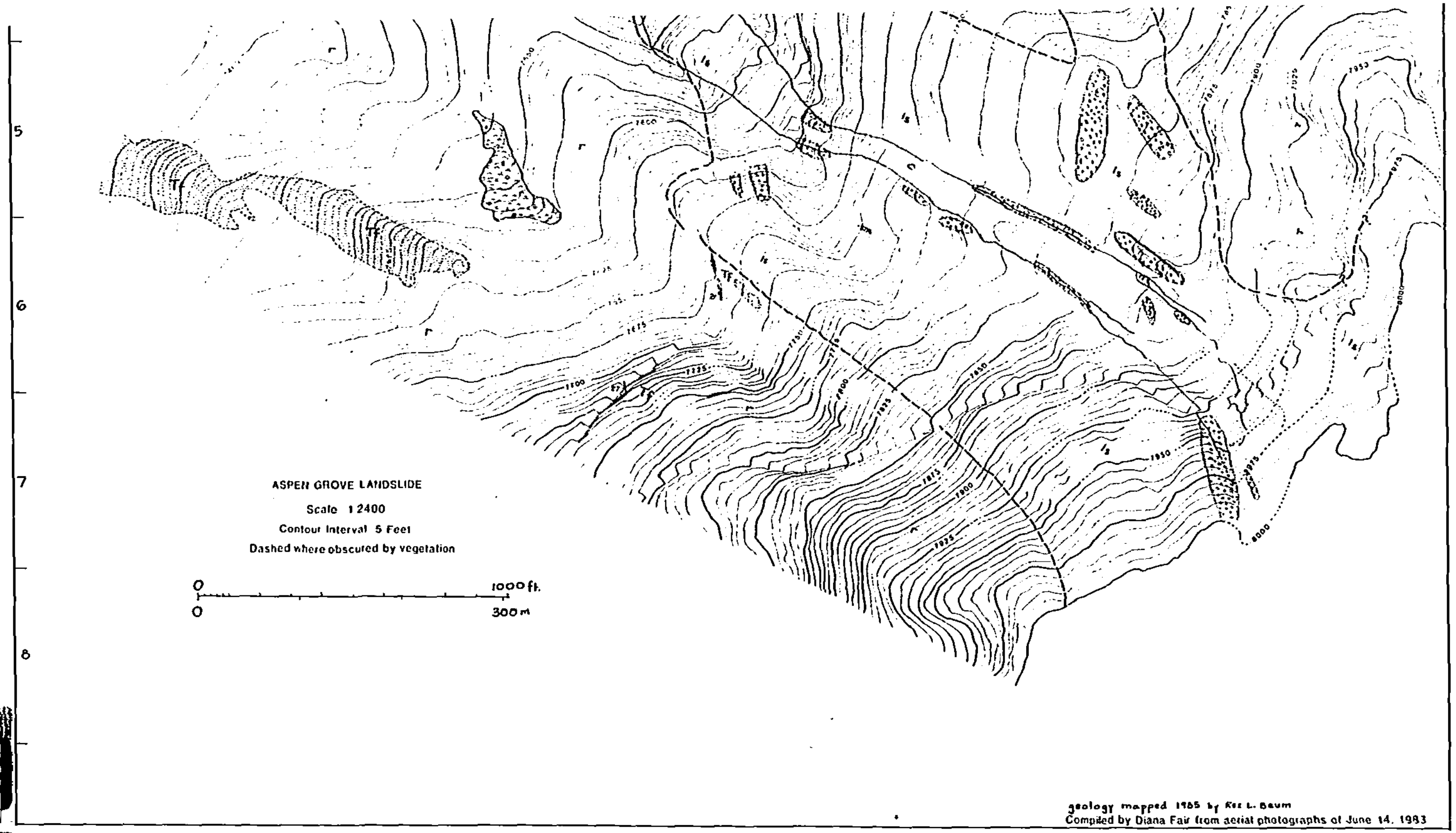
ASPEN GROVE LANDSLIDE
Scale 1:2400
Contour Interval 5 Feet
Dashed where obscured by vegetation
0 1000 ft.
0 300 m
5
6
7
8
geology mapped 1985 by Rex L. Baum
Compiled by Diana Fair from aerial photographs of June 14, 1983

Plate 3

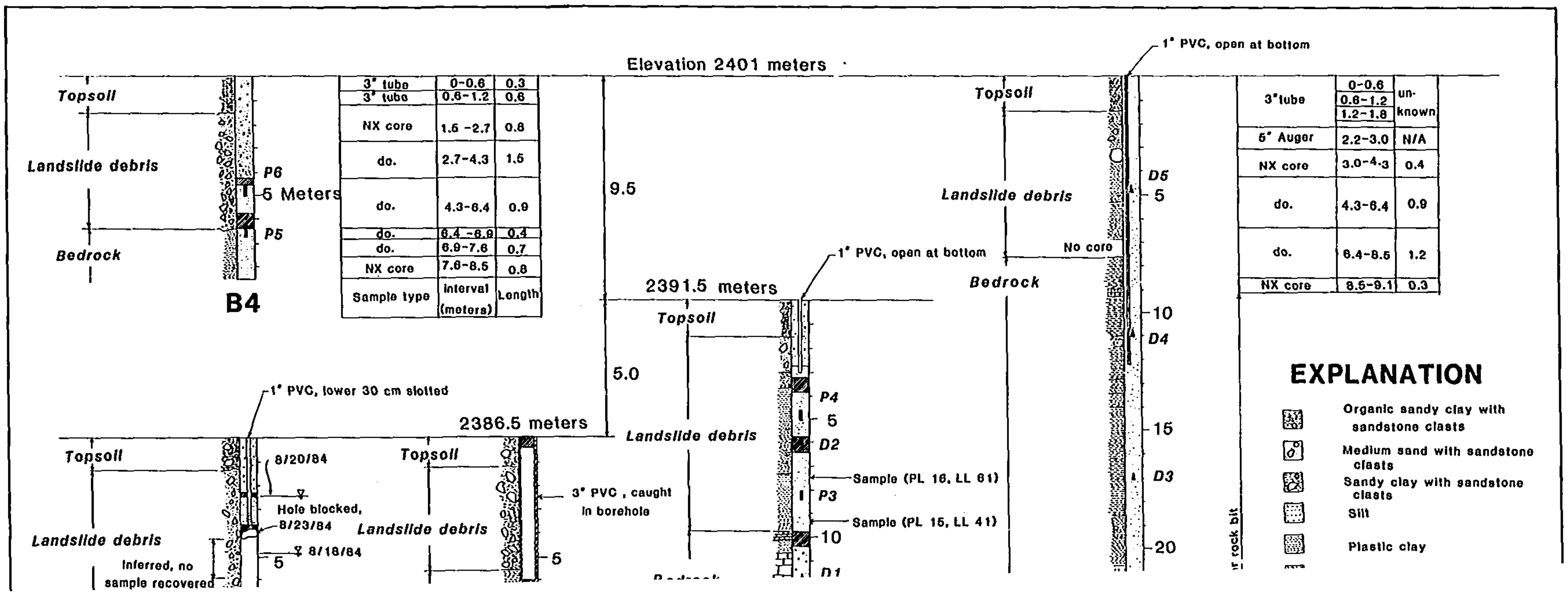
Elevation 2401 meters
Topsoil
Landslide debris
Bedrock
P6
5 Meters
P5
B4
3" tube 0-0.6 0.3
3" tube 0.6-1.2 0.6
NX core 1.5-2.7 0.8
do. 2.7-4.3 1.5
do. 4.3-6.4 0.9
do. 6.4-6.9 0.4
do. 6.9-7.6 0.7
NX core 7.6-8.5 0.8
Sample type
Interval (meters)
Length
9.5
5.0
2391.5 meters
2386.5 meters
1" PVC, open at bottom
1" PVC, lower 30 cm slotted
8/20/84
Hole blocked, 8/23/84
8/18/84
Inferred, no sample recovered
3" PVC, caught in borehole
P4
D2
P3
D1
D5
D4
D3
Sample (PL 16, LL 61)
Sample (PL 15, LL 41)
No core
3"tube 0-0.6 0.6-1.2 1.2-1.8 un-known
5" Auger 2.2-3.0 N/A
NX core 3.0-4.3 0.4
do. 4.3-6.4 0.9
do. 6.4-8.5 1.2
NX core 8.5-9.1 0.3
EXPLANATION
Organic sandy clay with sandstone clasts
Medium sand with sandstone clasts
Sandy clay with sandstone clasts
Silt
Plastic clay

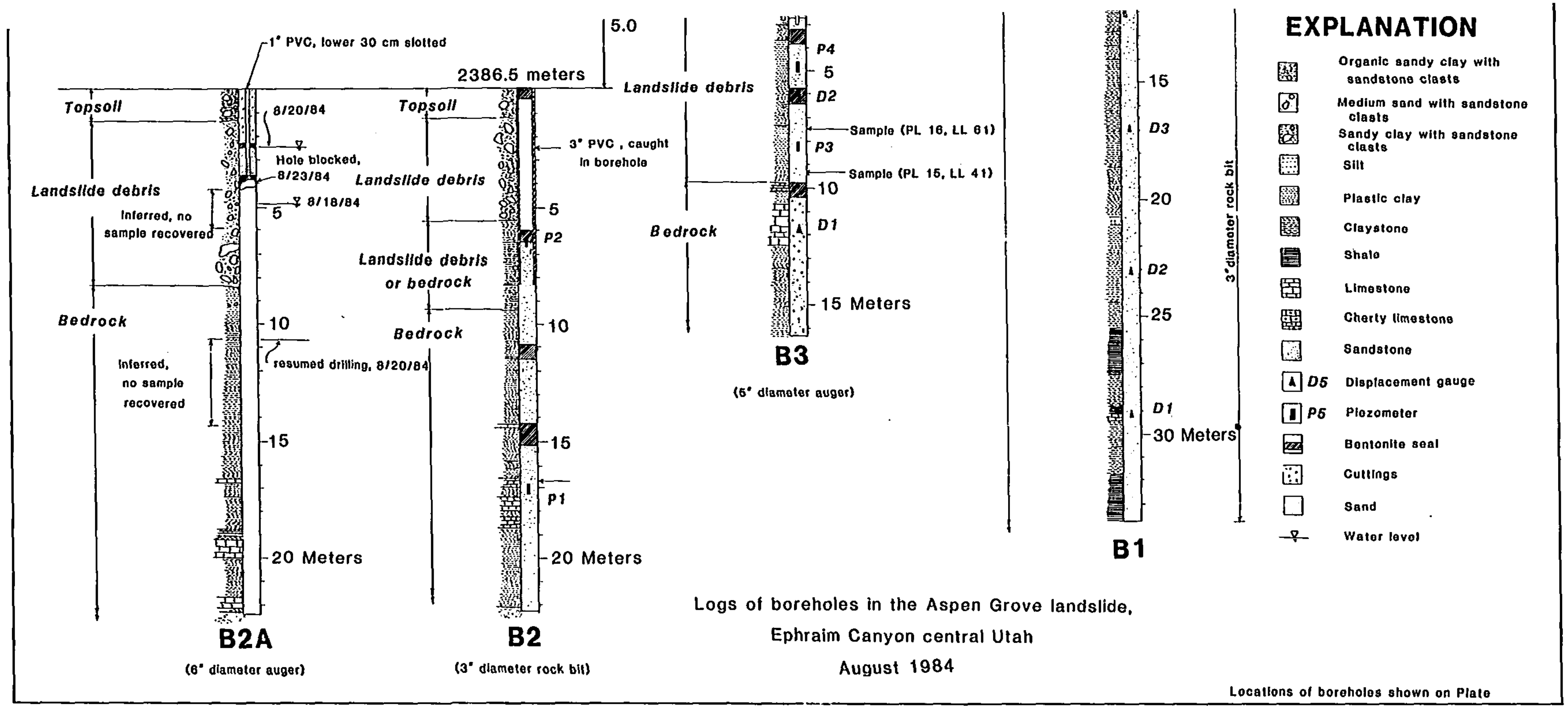

Logs of boreholes in the Aspen Grove landslide,
Ephraim Canyon central Utah
August 1984

Locations of boreholes shown on Plate

Plate 4

Map showing displacement and change in boundaries of the Aspen Grove landslide, Ephraim Canyon, central Utah

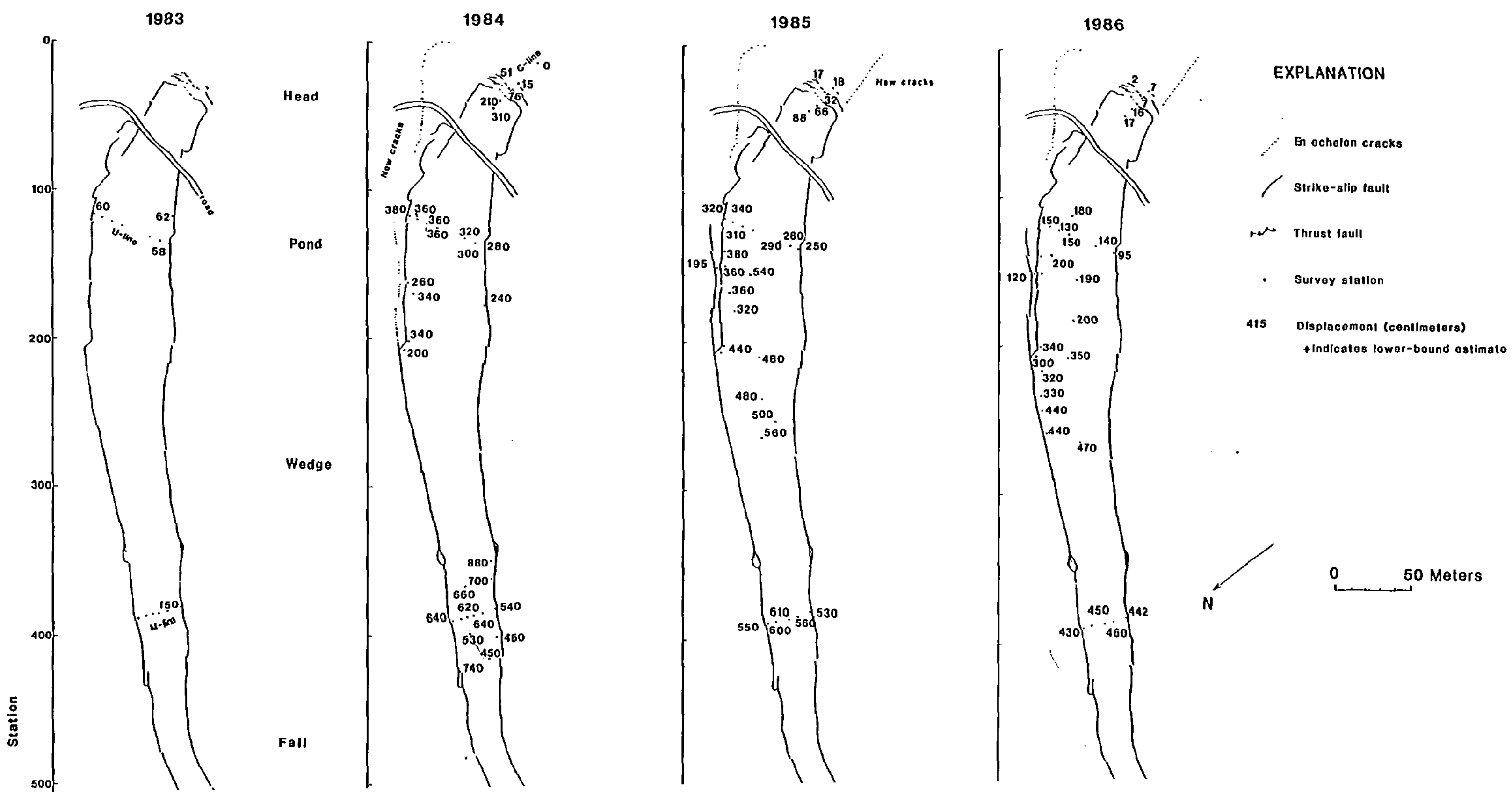

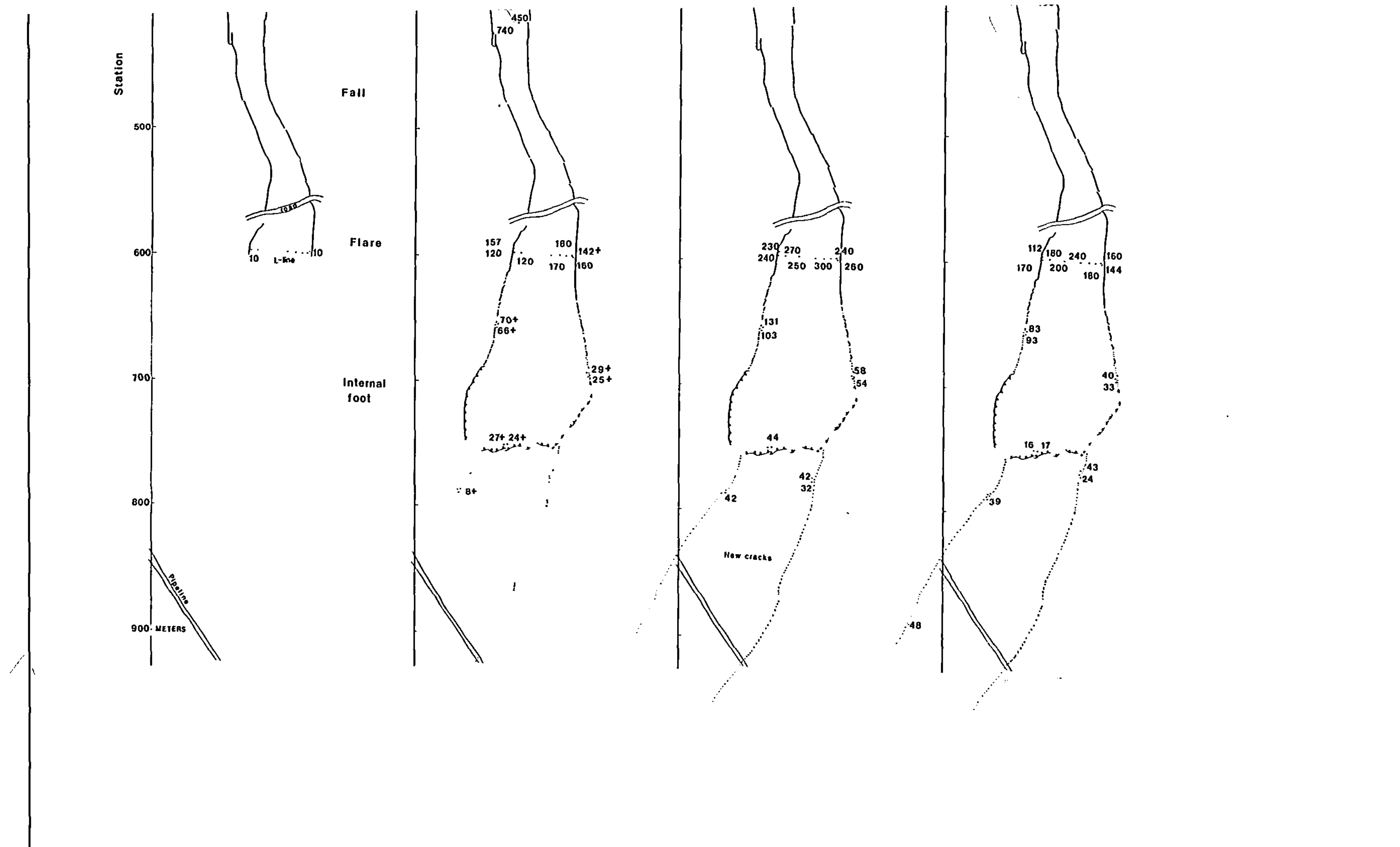

Base maps reduced and modified from original plane-table map by R.W. Fleming and A.M. Johnson, August 1984

Plate 5